

Aim and Scope

The objective of the *Journal of Residuals Science & Technology* (JRS&T) is to provide a forum for technical research on the management and disposal of residuals from pollution control activities. The Journal publishes papers that examine the characteristics, effects, and management principles of various residuals from such sources as wastewater treatment, water treatment, air pollution control, hazardous waste treatment, solid waste, industrial waste treatment, and other pollution control activities. Papers on health and the environmental effects of residuals production, management, and disposal are also welcome.

Editor-in-Chief

P. Brent Duncan
Department of Biology
University of North Texas
Denton, TX, USA
pduncan@unt.edu

Editorial Advisory Board

Muhammad Abu-Orf
AECOM, USA
mohammad.abu-orf@aecom.com

Steve Dentel
University of Delaware, USA
dentel@udel.edu

Richard Dick
Cornell University, USA
rid1@cornell.edu

Guor-Cheng Fang, Ph.D.
Hungkuang University, Taiwan
gcfang@sunrise.hk.edu.tw

Robert Hale
Virginia Institute of Marine Science, USA
hale@vims.edu

Paul F. Hudak
University of North Texas, USA
hudak@unt.edu

Blanca Jimenez Cisneros
Inst. de Ingenieria, UNAM, Mexico
bjc@mumas.iingen.unam.mx

Julia Kopp
Technische Universitat
Braunschweig, Germany
j.kopp@tu-bs.de

Uta Krogmann
Rutgers University, USA
krogmann@aesop.rutgers.edu

D. J. Lee
National Taiwan University, Taiwan
djlee@ntu.edu.tw

Giuseppe Mininni
Via Reno 1, Italy
mininni@irsa.rm.cnr.it

John Novak
Virginia Tech, USA
jtnov@vt.edu

Nagaharu Okuno
The University of Shiga Prefecture,
Japan
okuno@ses.usp.ac.jp

Jan Oleszkiewicz
University of Manitoba, Canada
oleszkie@ms.umanitoba.ca

Banu Örmeci
Carleton University, Canada
banu_ormeci@carleton.ca

Ian L. Pepper
University of Arizona, USA
ipepper@ag.arizona.edu

Ioana G. Petrisor
Co-Editor-in-Chief
Environmental Forensics Journal, USA
Environmental.Forensics@gmail.com

Bob Reimers
Tulane University, USA
reimers@tulane.edu

Dilek Sanin
Middle East Technical University,
Turkey
dsanin@metu.edu.tr

Mike Switzenbaum
Professor Emeritus
Marquette University, USA
michael.switzenbaum@marquette.edu

Heidi Snyman
Golder Associates Africa (Pty) Ltd.,
South Africa
hsnyman@golder.co.za

Ludovico Spinosa
Consultant at Commissariat
for Env. Energ. in Region,
Puglia, Italy
ludovico.spinosa@fastwebnet.it

P. Aarne Vesilind
Bucknell University, USA
aarne.vesilind@gmail.com


Doug Williams
California Polytechnic State
University, USA
wmsengr@thegrid.net

JOURNAL OF RESIDUALS SCIENCE & TECHNOLOGY—Published quarterly—January, April, July and October by DEStech Publications, Inc., 439 North Duke Street, Lancaster, PA 17602.

Indexed by Chemical Abstracts Service. Indexed/abstracted in Science Citation Index Expanded. Abstracted in Current Contents/Engineering, Computing & Technology. Listed in ISI Master Journal.

Subscriptions: Annual \$219 per year. Single copy price \$60. Foreign subscriptions add \$45 per year for postage.

(ISSN 1544-8053)

 DEStech Publications, Inc.

439 North Duke Street, Lancaster, PA 17602-4967, U.S.A.

©Copyright by DEStech Publications, Inc. 2016—All Rights Reserved

Jerry J. Wu, Ph.D., P.E.

Feng Chia University, Department of Environmental Engineering and Science
100 Wenhwa Road, Seatwen District, Taichung 407, Taiwan

E-mail: jjwu@fcu.edu.tw; Phone: +886-4-2451-7250 Ext. 5206; Fax: +886-4-2451-5332



EDUCATION

- B.S.; National Cheng Kung University, Environmental Engineering, Taiwan, 1985–1989
- M.S.; National Taiwan University, Environmental Engineering, Taiwan, 1989–1991
- Ph.D.; Michigan State University, Civil and Environmental Engineering, USA, 1991–1998

POSITIONS

- Vice Dean, (2013.8–) Office of Industry-Academia Cooperation, Feng Chia University, Taichung, Taiwan
- Distinguished Professor, (2012.8–) Department of Environmental Science and Engineering, Feng Chia University, Taichung, Taiwan
- Professor, (2007.8–2012.7) Department of Environmental Science and Engineering, Feng Chia University, Taichung, Taiwan
- Visiting Professor, (2011.6–2014.8) Department of Civil and Environmental Engineering, Michigan State University, E. Lansing, USA
- Associate Professor, (2002.8–2007.7) Department of Environmental Science and Engineering, Feng Chia University, Taichung, Taiwan
- Assistant Professor, (1999.2–2002.7) Department of Environmental Science and Engineering, Feng Chia University, Taichung, Taiwan

PUBLICATIONS

(Reviewed, Archival Journal Papers)

1. Jerry J. Wu, Sung-hee Park, Susan M. Hengemuehle, Melvin T. Yokoyama, Howard L. Person, and Susan J. Masten, "The Effect of Storage and Ozonation on the Physical, Chemical, and Biological Characteristics of Swine Manure Slurries", *Ozone Science & Engineering*, Vol. 20, pp. 35–50, 1998.
2. Jerry J. Wu, Sung-hee Park, Susan M. Hengemuehle, Melvin T. Yokoyama, Howard L. Person, John B. Gerrish, and Susan J. Masten, "The Use of Ozone to Reduce the Concentration of Malodorous Metabolites in Swine Manure Slurry", *Journal of Agricultural Engineering Research*, Vol. 72, pp. 317–327, 1999.
3. C.C. Wu and J.J. Wu, "Effect of Charge Neutralization on the Dewatering Performance of Alum Sludge by Polymer Conditioning", *Water Science and Technology*, Vol. 44, No. 10, pp. 315–319, 2001.
4. Jerry J. Wu and Susan J. Masten, "Mass Transfer of Ozone in a Semi-Batch Stirred Reactor", *Journal of Environmental Engineering-ASCE*, Vol. 127, No. 12, pp. 1089–1099, 2001.
5. Jerry J. Wu and Susan J. Masten, "Oxidation Kinetics of Phenolic and Indolic Compounds by Ozone: Application to Synthetic and Real Swine Manure Slurry", *Water Research*, Vol. 36, No. 6, pp. 1513–1526, 2002.
6. C.C. Wu, Jerry J. Wu, and R.Y. Huang, "Effect of Floc Strength on Sludge Dewatering by Vacuum Filtration", *Colloids and Surfaces A: Physicochem. Eng. Aspects*, Vol. 221, pp. 141–147, 2003.
7. C.C. Wu, Jerry J. Wu, and R.Y. Huang, "Floc Strength and Dewatering Efficiency of Alum Sludge", *Advances in Environmental Research*, Vol. 7, pp. 617–621, 2003.
8. Jerry J. Wu, C.C. Wu, H.W. Ma, and C.C. Chang, "Treatment of Landfill Leachate by Ozone-based Advanced Oxidation Processes", *Chemosphere*, Vol. 54, pp. 997–1003, 2004.
9. Jerry J. Wu, M. Muruganandham, J.S. Yang, and S.S. Lin, "Oxidation of DMSO on Goethite Catalyst in the Presence of H₂O₂ at Neutral pH", *Catalysis Communications*, Vol. 7, No. 8, pp. 901–906, 2006.
10. Pon Yu Liu, Jerry J. Wu and Chih Chao Wu, "Control of disinfection byproduct formation in Feng-Shan reservoir by the traditional treatment processes plus O₃—pilot-plant test", *Water Science & Technology*, Vol. 55, pp. 127–131, 2007.
11. M. Muruganandham and Jerry J. Wu, "Granular a-FeOOH—A Stable and Efficient Catalyst for the Decomposition of Dissolved Ozone in Water", *Catalysis Communications*, Vol. 8, No. 5, pp. 668–672, 2007.

12. M. Muruganandham J.S. Yang, and Jerry J. Wu, "Effect of Ultrasonic Irradiation on the Catalytic Activity and Stability of Goethite Catalyst in the Presence of H₂O₂ at Acidic Medium", *Industrial & Engineering Chemistry Research*, Vol. 46, Issue 3, pp. 691–698, 2007.
13. M. Muruganandham, S.H. Chen, and J.J. Wu, "Evaluation of Water Treatment Sludge as a Catalyst for Aqueous Ozone Decomposition", *Catalysis Communications*, Vol. 8, No. 8, pp. 1609–1614, 2007.
14. Jerry J. Wu, M. Muruganandham, L.T. Chang, J.S. Yang, and S.H. Chen, "Ozone-based Advanced Oxidation Processes for the Decomposition of N-Methyl-2-Pyrrolidone in Aqueous Medium", *Ozone: Science and Engineering*, Vol. 29, No. 3, pp. 177–183, 2007.
15. M. Muruganandham, S.H. Chen, and J.J. Wu, "Mineralization of N-methyl-2-pyrrolidone by Advanced Oxidation Processes", *Separation and Purification Technology*, Vol. 55, pp. 360–367, 2007.
16. J.J. Wu, M. Muruganandham, and S.H. Chen, "Degradation of DMSO by Ozone-based Advanced Oxidation Processes", *Journal of Hazardous Materials*, Vol. 149, No. 1-2, pp. 218–225, 2007.
17. M. Muruganandham and J.J. Wu, "Synthesis, Characterization and Catalytic Activity of Easily Recyclable Zinc Oxide Nanobundles", *Applied Catalysis B: Environmental*, Vol. 80, pp. 32–41, 2008.
18. J.J. Wu, J.S. Yang, and M. Muruganandham, "Kinetics and Modeling of IPA Oxidation Using Ozone-based Advanced Oxidation Processes", *Industrial & Engineering Chemistry Research*, Vol. 47, pp. 1820–1827, 2008.
19. J.J. Wu, S.H. Chen, and M. Muruganandham, "Catalytic Ozonation of Oxalic Acid Using Carbon Free Rice Husk Ash Catalysts", *Industrial & Engineering Chemistry Research*, Vol. 47, pp. 2919–2925, 2008.
20. J.J. Wu, J.S. Yang, M. Muruganandham, and C.C. Wu, "The Oxidation Study of 2-Propanol Using Ozone-based Advanced Oxidation Processes", *Separation and Purification Technology*, Vol. 62, pp.39–46, 2008.
21. J.J. Wu, M. Muruganandham, L.T. Chang, and S.H. Chen, "Oxidation of Propylene Glycol Methyl Ether Acetate (PGMEA) Using Ozone Based Advanced Oxidation Processes", *Ozone: Science and Engineering*, Vol. 30, No. 5, pp.332-338, 2008.
22. J.J. Wu, M. Muruganandham, and Y.S. Chen, "Effect of Temperature on the Formation of Macroporous ZnO Bundles and Its Application in Photocatalysis", *Journal of Hazardous Materials*, Vol. 172, No. 2-3, pp. 700–706. 2009.
23. S. Anandan and J.J. Wu, "Microwave Assisted Rapid Synthesis of Bi₂O₃ Short Nanorods", *Material Letters*, Vol. 63, No. 27, pp. 2387–2389, 2009.
24. J.J. Wu, R. Amutha, M. Muruganandham, G.J. Lee, and G. Mokrousov, "Flux Assisted Shape Tunable Synthesis of Zinc Oxide Microflowers", *Advanced Science Letters*, Vol. 3, No. 4, pp. 491–495, 2010.
25. S. Anandan, G.J. Lee, P.K. Chen, C. Fan, and J.J. Wu, "The Removal of Orange II Dye in Water by Visible Light Assisted Photocatalytic Ozonation Using Bi₂O₃ and Au/Bi₂O₃ Nanorods", *Industrial & Engineering Chemistry Research*, Vol. 49, No. 20, pp. 9729–9737, 2010.
26. J.J. Wu, M. Muruganandham, G.J. Lee, V.N. Batalova, and G. Mokrousov, "Catalytic Ozonation of Oxalic Acid Using SrTiO₃ Catalyst", *Ozone: Science and Engineering*, Vol. 33, No. 1, pp. 74–79, 2011.
27. T.L. Hu, J.Z. Hwa, W.F. Chang, and J.J. Wu, "The Anti-bacterial Study Using Nano Silver-doped High Density Polyethylene Pipe", *Sustainable Environment Research*, Vol. 22, pp. 153–158, 2011.
28. R. Amutha, M. Muruganandham, G. J. Lee, V.N. Batalova, G.M. Mokrousov, and J.J. Wu, "Solvent Free Synthesis, Characterization and Catalytic Activity of a-Fe₂O₃ Nanomaterial", *Advanced Science Letters*, Vol. 4, No. 2, pp. 496–500, 2011.
29. P. Sathishkumar, R. Sweena, J.J. Wu, and S. Anandan, "Synthesis of CuO-ZnO Nanophotocatalyst for Visible Light Assisted Degradation of a Textile Dye in Aqueous Solution", *Chemical Engineering Journal*, Vol. 171, pp. 136–140, 2011.
30. S. Anandan, G.J. Lee, S.H. Hsieh, M. Ashokkumar, and J.J. Wu, "Amorphous Titania-Coated Magnetite Spherical Nanoparticles: Sonochemical Synthesis and Catalytic Degradation of Nonylphenol Ethoxylate", *Industrial & Engineering Chemistry Research*, Vol. 50, No. 13, pp. 7874–7881, 2011.
31. R. Amutha M. Muruganandham, G.J. Lee, and J.J. Wu, "Facile Microwave-combustion Synthesis of Wurtzite CdS Nano/micro Materials", *Journal of Nanoscience and Nanotechnology*, Vol. 11, No. 11, pp. 1–5, 2011.
32. A.V. Shabalina, G.M. Mokrousov, T.I. Izaak, E.D. Fakhrutdinova, and J.J. Wu, "Highly Porous Cellular Copper as a Catalyst for Ozone Oxidation of Organic Water Pollutants", *Russian Journal of Applied Chemistry*, Vol. 84, No. 12, pp. 2046–2050, 2011.
33. L.N. Skvortsova, L.N. Chukhlomina, G.M. Mokrousov, V.N. Batalova, and J.J. Wu, "Catalytic Oxidation of Phenol in the Presence of Iron-containing Composites Based on Silicon and Boron Nitrides", *Russian Journal of Applied Chemistry*, Vol. 85, No. 1, pp. 44–48. 2012.
34. C.Y. Chen, J.C. Weng, J.H. Chen, S.H. Ma, T.L. Horng, J.J. Wu, and C.Y. Tsay, "Preparation of Spray Pyrolyzed Bismuth Oxide and its Application in Inhibition of Ultraviolet from Light-emitting Diode (LED)", *Advanced Materials Research*, Vol. 509, pp. 147–149, 2012.
35. P.K. Chen, G.J. Lee, S. Anandan, and J.J. Wu, "Synthesis of ZnO and Au Tethered ZnO Pyramid-like Microflower for Photocatalytic Degradation of Orange II", *Material Science and Engineering: B*, Vol. 177, No. 2, pp. 190–196, 2012.
36. S. Anandan, G.J. Lee, C.K. Yang, M. Ashokkumar, and J.J. Wu, "Sonochemical Synthesis of Bi₂CuO₄ Nanoparticles for Catalytic Degradation of Nonylphenol Ethoxylate", *Chemical Engineering Journal*, Vol. 183, pp. 46–52, 2012.
37. M. Muruganandham, R. Amutha, M.S.M. Abdel Wahed, B. Ahmmad, Y. Kuroda, R.P.S. Suri, J.J. Wu, and M. Sillanp, "Controlled Fabrication of a-GaOOH and a-Ga₂O₃ Self-Assembly and Its Superior Photocatalytic Activity", *Journal of Physical Chemistry C*, Vol. 116, No.1, pp. 44–53, 2012.
38. S. Anandan, G.J. Lee, and J.J. Wu, "Sonochemical Synthesis of CuO Nanostructures with Different Morphology", *Ultrasonics Sonochemistry*, Vol. 19, No. 3, pp. 682–686, 2012.
39. T.L. Hu*, J.Z. Hwa, W.F. Chang, and J.J. Wu, "The Anti-bacterial Study Using Nano Silver-doped High Density Polyethylene Pipe", *Sustainable Environment Research*, Vol. 22, No. 3, pp. 153–158, 2012.
40. S.H. Hsieh, G.J. Lee, C.Y. Chen, J.H. Chen, S.H. Ma, T.L. Horng, and J.J. Wu, "Synthesis of Ru Doped Bi₂O₃/Pt Nanophotocatalysts for Hydrogen Production from Water Splitting under Visible Light Irradiation", *Journal of Nanoscience and Nanotechnology*, Vol. 12, No. 7, pp. 5930–5936, 2012.
41. M. Muruganandham, R. Amutha, G.J. Lee, S.H. Hsieh, and J.J. Wu*, "Facile Fabrication of Tunable Bi₂O₃ Self-assembly and its Solar Photocatalytic Activity", *Journal of Physical Chemistry C*, Vol. 116, pp. 12906–12915, 2012.
42. A.V. Shabalina, G.M. Mokrousov, E.D. Fakhrutdinova, T.I. Izaak, and J.J. Wu, "Water Ozonation with Copper Catalyst for Organic Pollutants Removal", *Eurasian ChemTech Journal*, Vol. 14, pp. 219–226, 2012.
43. V. Batalova, L. Skvortsova, G. Mokrousov, L. Naumova, and J.J. Wu, "Photocatalytic Degradation of Organic Water Pollutants Using Fe-Containing Natural and Synthetic Materials", *Butlerov Communications*, Vol. 31, No.7, pp. 73–84, 2012.
44. C.Y. Chen, J.C. Weng, J.H. Chen, S.H. Ma, T.L. Horng, J.J. Wu and C.Y. Tsay, "Preparation of Spray Pyrolyzed Bismuth Oxide and Its Application in Inhibition of Ultraviolet from Light-Emitting Diode (LED)", *Advanced Materials Research*, Vol. 509, pp. 147–149, 2012.
45. J.J. Wu, G.J. Lee, Y.S. Chen, and T.L. Hu, "The Synthesis of Nano-silver/ Polypropylene Plastics for Antibacterial Application", *Current Applied Physics*, Vol. 12, pp. 89–95, 2012.
46. S. Anandan, N. Pugazhenthiran, T. Selvamani, S.H. Hsieh, G.J. Lee, and J.J. Wu, "Investigation on Photocatalytic Potential of Au-Ta₂O₅ Semiconductor Nanoparticle by Degrading Methyl Orange in Aqueous Solution by Illuminating with Visible Light", *Catalysis Science & Technology*, Vol. 2, No. 12, pp. 2502–2507, 2012.
47. R. Amutha, M. Muruganandham, G.J. Lee, J.J. Wu, and M. Sillanpaa "Large Scale Fabrication of Wurtzite CdS Self-Assembly Using Single Source Molecular Precursor", *Advanced Science, Engineering and Medicine*, Vol. 5, No. 1, pp. 161–165, 2013.
48. M. Muruganandham, M.E.T. Sillanpaa, R.P.S. Suri, G.J. Lee, J.J. Wu*, B. Ahmad, and Y. Kuroda, "Fabrication and Photocatalytic Properties of Self-Assembled In(OH)₃ and In₂O₃ Nano/Micro-Cubes", *Journal of Nanoscience and Nanotechnology*, Vol. 13, pp.1639-1648, 2013.

49. M. Muruganandham, G.J. Lee, J.J. Wu, I. Levchuk, and M. Sillanpaa, "By-product Assisted Hydrothermal Synthesis of InOOH Microflower Composed of Nanosheets", *Materials Letters*, Vol. 98, pp. 86–89, 2013.
50. P.K. Chen, G.J. Lee, S.H. Davies, S.J. Masten, R. Amutha, and J.J. Wu, "Hydrothermal Synthesis of Coral-like Au/ZnO Catalyst and Photocatalytic Degradation of Orange II Dye", *Materials Research Bulletin*, Vol. 48, No. 6, pp. 2375–2382, 2013.
51. S.H. Hsieh, G.J. Lee, S.H. Davies, S.J. Masten, and J.J. Wu, "Synthesis of Cr₂O₃ and Pt doped RuO₂/Bi₂O₃ Photocatalysts for Hydrogen Production from Water Splitting", *American Journal of Environmental Engineering*, Vol.3, No. 3, pp. 115–120, 2013.
52. R. Amutha, G.J. Lee, E. Repo, M. Sillanpaa, and J.J. Wu, "Low Temperature Synthesis of Single Crystal ZnO Microflower Composed of Hexagonal Nanorods", *Materials Letters*, Vol. 107, pp. 64–67, 2013.
53. S.H. Hsieh, G.J. Lee, C.Y. Chen, J.H. Chen, S.H. Ma, T.L. Horng, K.H. Chen, and J.J. Wu, "Hydrothermal Synthesis of Mesoporous Bi₂O₃/Co₃O₄ Microsphere and Photocatalytic Degradation of Orange II Dyes by Visible Light", *Topics in Catalysis*, Vol. 56, No. 9-10, pp. 623–629, 2013.
54. S. Anandan, B.G. Sundara Raj, G.J. Lee, and J.J. Wu, "Sonochemical Synthesis of Manganese (II) Hydroxide for Supercapacitor Applications", *Materials Research Bulletin*, Vol. 48, No. 9, pp. 3357–3361, 2013.
55. S.H. Hsieh, A. Manivel, G.J. Lee, and J.J. Wu, "Synthesis of Mesoporous Bi₂O₃/CeO₂ Microsphere for Photocatalytic Degradation of Orange II Dye", *Materials Research Bulletin*, Vol. 48, No. 10, pp.4174–4180, 2013.
56. R. Amutha, G.J. Lee, J.J. Wu, M. Sathish, and M.E.T. Sillanpaa, "Synthesis and Electrochemical Properties of Biporous alpha Fe₂O₃ Superstructures", *Journal of Nanoscience and Nanotechnology*, Vol. 13, pp. 6635–6643, 2013.
57. S. Anandan, N. Pugazhenthiran, T. Lana Villarreal, G.J. Lee, and J.J. Wu, "Catalytic Degradation of a Plasticizer, Di-ethylhexyl Phthalate, Using NxTiO_{2-x} Nanoparticles Synthesized via Co-precipitation", *Chemical Engineering Journal*, Vol. 231, pp. 182–189, 2013.
58. G.J. Lee, A. Manivel, V. Batalova, G. Mokrousov, S. Masten, and J.J. Wu, "Mesoporous Microsphere of ZnS Photocatalysts Loaded with CuO or Mn₃O₄ for the Visible-Light-Assisted Photocatalytic Degradation of Orange II Dye", *Industrial & Engineering Chemistry Research*, Vol. 52, pp. 11904–11912, 2013.
59. Y.C. Chu, G.J. Lee, C.Y. Chen, S.H. Ma, J.J. Wu, T.L. Horng, K.H. Chen, and J.H. Chen, "Preparation of Bismuth Oxide Photocatalyst and Its Application in White-light LEDs", *Journal of Nanomaterials*, 2013/ ArticleID596324, 2013.
60. G.J. Lee, C.L. Hong, V. Batalova, G. Mokrousov, and J.J. Wu, "Synthesis of Nitrogen-Doped ZnS with Camellia Brushfield Yellow Nanostructures for Enhanced Photocatalytic Activity under Visible Light Irradiation", *International Journal of Photoenergy*, Vol. 2013, Article ID 801846, pp. 1–7, 2013.
61. R. Amutha, M. Sillanpaa, G.J. Lee, J.C. Lin, C.K. Yang, and J.J. Wu, "Catalytic Ozonation of 2-Ethoxy Ethyl Acetate Using Mesoporous Nickel Oxalates", *Catalysis Communications*, Vol. 43, pp. 88–92, 2014.
62. M. Muruganandham, R.P.S. Suri, Sh. Jafari, M. Sillanpaa, G.J. Lee, J.J. Wu, and M. Swaminathan, "Recent Developments in Homogeneous Advanced Oxidation Processes for Water and Wastewater Treatment", *International Journal of Photoenergy*, Vol. 2014, Article ID 821674, pp. 1–21, 2014.
63. M. Muruganandham, R. Suri, M. Sillanpaa, J.J. Wu, B. Ahmmad, S. Balachandran, and M. Swaminathan, "Recent Developments in Heterogeneous Catalyzed Based Environmental Remediation Processes", *Journal of Nanoscience and Nanotechnology*, Vol. 14, pp. 1898–1910, 2014.
64. A. Manivel, S. Ramkumar, J.J. Wu, A.M. Asiri, and S. Anandan, "Exploration of (S)-4,5,6,7 Tetrahydrobenzo[d]thiazole-2,6-diamine as Feasible Corrosion Inhibitor for Mild Steel in Acidic Media", *Journal of Environmental Chemical Engineering*, Vol. 2, pp. 463–470, 2014.
65. E.D. Fakhrutdinova, A.V. Shabalina, G.M. Mokrousov, A.N. Salanov, and J. J. Wu, "Copper Containing Photocatalyst Based on F-TiO₂ for Hydrogen Production from Water and Water Organic Solution", *Russian Journal of Inorganic Chemistry*, Vol. 59, pp. 291–297, 2014.
66. S. Anandan and J.J. Wu, "Ultrasound Assisted Synthesis of TiO₂-WO₃ Heterostructures for the Catalytic Degradation of Tergitol (NP-9) in Water", *Ultrasonics Sonochemistry*, Vol. 21, pp. 1284–1288, 2014.
67. Ching-Sen Lin, Tzyy-Leng Horng, Jing-Heng Chen, Kun-Huang Chen, Jerry J. Wu, Chin-Yi Chen, and Shih-Hsin Ma, "Mechanical Properties Measurement of Polymer Films by Bulge Test and Fringe Projection", *Advances in Materials Science and Engineering*, Article ID 170279, 2014.
68. G.J. Lee, S. Anandan, S.J. Masten, and J.J. Wu, "Sonochemical Synthesis of Hollow Copper Doped Zinc Sulfide Nanostructures: Optical and Catalytic Properties for Visible Light Assisted Photosplitting of Water", *Industrial & Engineering Chemistry Research*, Vol. 53, pp. 8766–8772, 2014.
69. S. Anandan, C.Y. Chen, and J.J. Wu, "Sonochemical Synthesis and Characterization of Turbostratic MnNi(OH)₂ Layered Double Hydroxide Nanoparticles for Supercapacitor Applications", *RSC Advances*, Vol. 4, pp. 55519–55523, 2014.
70. B.G. Sundara Raj, A.M. Asiri, A.H. Qusti, J.J. Wu, and S. Anandan, "Sonochemically Synthesized MnO₂ Nanoparticles as Electrode Material for Supercapacitors", *Ultrasonics Sonochemistry*, Vol. 21, pp. 1933–1938, 2014.
71. S. Anandan and J.J. Wu, "Sonochemical Synthesis of Carbon Supported Sn Nanoparticles and its Electrochemical Application", *Ultrasonics Sonochemistry*, Vol. 21, pp. 1954–1957, 2014.
72. Chin-Yi Chen, Jui-Chung Weng, Jing-Heng Chen, Shih-Hsin Ma, Kun-Huang Chen, Tzyy-Leng Horng, Chien-Yie Tsay, Chi-Jung Chang, Chung-Kwei Lin, and Jerry J. Wu, "Photocatalyst ZnO-Doped Bi₂O₃ Powder Prepared by Spray Pyrolysis", *Powder Technology*, 272, pp. 316–321, 2015.
73. B.G. Sundara Raj, R.N. Radhika Ramprasad, A.M. Asiri, J.J. Wu, and S. Anandan, "Ultrasound Assisted Synthesis of Mn₃O₄ Nanoparticles Anchored Graphene Nanosheets for Supercapacitor Applications", *Electrochimica Acta*, Vol. 156, pp. 127–137, 2015.
74. A. Manivel, G.J. Lee, C.Y. Chen, J.H. Chen, S.H. Ma, T.L. Horng, and J.J. Wu, "Synthesis of MoO₃ Nanoparticles for Azo Dye Degradation by Catalytic Ozonation", *Materials Research Bulletin*, Vol. 62, pp. 184–191, 2015.
75. V. Vinoth, J.J. Wu, A.M. Asiri, and S. Anandan, "Simultaneous Detection of Dopamine and Ascorbic Acid Using Silicate Network Interlinked Gold Nanoparticles and Multi-walled Carbon Nanotubes", *Sensors and Actuators B: Chemical*, Vol. 210, pp. 731–741, 2015.
76. S. Anandan and J.J. Wu, "Effective Degradation of Fipronil Using Combined Catalytic Ozonation Processes", *Ozone: Science and Engineering*, Vol. 38, pp. 186–190, 2015.
77. S. Anandan, T. Lana-Villarreal, and J.J. Wu, "Sonochemical Synthesis of Mesoporous NiTiO₃ Ilmenite Nanorods for the Catalytic Degradation of Tergitol in Water", *Industrial & Engineering Chemistry Research*, Vol. 54, pp. 2983–2990, 2015.
78. S. Naveenraj, G.J. Lee, S. Anandan, and J.J. Wu, "Nanosized Tantalum Based Materials—Synthesis and Applications", *Materials Research Bulletin*, Vol. 67, pp. 20–46, 2015.
79. B.G. Sundara Raj, A.M. Asiri, J.J. Wu, and S. Anandan, "Synthesis of Mn₃O₄ Nanoparticles via Chemical Precipitation Approach for Supercapacitor Application", *Journal of Alloys and Compounds*, Vol. 636, pp. 234–240, 2015.

C O N T E N T S

Research

- Effective Adsorption of Pb(II) Ions by Gel Beads of Sodium Alginate and Polyethylene Glycol**S1
DAOJI WU, ZHIMIN GAO, HUIXUE REN, JIAHUI JIANG, FENGXUN TAN and BING XU
- Total Nitrogen Removal of Effluent from a Municipal Sewage Treatment Plant via a Composite Biofilter**S9
YUANHONG DING, QING WANG, HONGQIANG REN, YI QIAN and GUIZHONG ZHOU
- Chemical Fractions and Mobility of Cd, Cu, Pb and Zn in Soil Profile of a Sewage Irrigation Area, Northwest China**S13
BAILIN LIU, SHIWEI AI, RUI GUO, LIANG REN, WENYA ZHANG and YINGMEI ZHANG
- The Input and Characteristics of Exotic Uranium in the Soils Around a Uranium Waste Rock Dump in South China**S21
ZHI-GANG FENG, XIAO-LONG WANG, RONG CHEN, XIAN-ZHE DUAN, QIANG MA and SHI-LI HAN
- Influence of Temperature and pH on Methanogenic Digestion in Two-phase Anaerobic Co-digestion of Pig Manure with Maize Straw**S27
LEI ZHANG, KEQIANG ZHANG, WENXUAN GAO, ZHONGWEI ZHAI, JUNFENG LIANG, LIANZHU DU and XINMEI FENG
- Removal of Streptomycin from Honey by Cation-exchange Resin**S33
QIONG HE, YIZHU YAN, NI CHENG, XIAOFENG XUE, LIMING WU and WEI CAO
- Effects of Chlorine and Phosphor on Zinc Transformation Behavior During Sewage Sludge Combustion**S39
YANLONG LI, RUNDONG LI, LEI WANG, WEIYUN WANG and TIANHUA YANG
- Study on Nonlinear Model Predictive Control of Activated Sludge Process**S45
LI HONGLU, FENG YUZHAO, ZHANG XIAOQIN, YU HAIBO, ZHANG HENG and SUN RONGJI
- Addition of Calcium Compounds Improve the Yield of Hydrogen and Retention of Chromium Metal during the Gasification of Simulated Waste**S51
LIN CHIOU-LIANG, WU MIN-HAO and HSU TZU-PIN
- Crystallization Behaviour of Chromium in Stainless Steel Slag: Effect of Feo and Basicity**S57
XINGRONG WU, XIAOMIN DONG, RUNTAO WANG, HUIHONG LÜ, FABIN CAO and XINGMEI SHEN
- Coal Dust Reduce the Rate of Root Growth and Photosynthesis of Five Plant Species in Inner Mongolian Grassland**S63
WANG ZHAN-YI, HOU JIA, GUO JIAN-YING, WANG CHENG-JIE and WANG MING-JIU
- Application of Vacuum Distillation to Treat Wastewater Coming from Hot Rolling Process**S75
LV ZI-QIANG, CAI JIU-JU, SUN WEN-QIANG and LIU CHAO
- Thermal Recirculation and Efficiency of Phenolic Resin as Building Insulation**S81
TING-YU CHEN, WEN-PEI SUNG and YU-KUANG ZHAO
- The Study on the Operating Characteristics of Algae-Contaminated Reservoir Water Using GAC-sand Dual Media Filter Flofilter**S93
YONG LEI WANG, KEFENG ZHANG, WENJUAN CHEN, HONGBO WANG, MEI LI and RUIBAO JIA

Contents

Adsorption Thermodynamics of Metronidazole on the Conjugated Microporous Polymers	S101
CHUNLI ZHENG, SHANSHAN FENG, QIAORUI WANG and MIAOMIAO DU	
Characteristics of Nitrogen and Phosphorus Removal in Multiple Post-Denitrification Process with Different Aeration Rates	S107
REN-JIAN DENG, JIN-SONG ZHANG and ZHI-JUN QU	
Analyses of Polycyclic Aromatic Hydrocarbon in Aerosol of a Lead-zinc Concentrator	S119
AI GUANG-HUA and LIU YAN-FEI	
Detection of Pesticide Residues in Mulberry Leaves Using Vis-Nir Hyperspectral Imaging Technology	S125
SUN JUN, JIANG SHUYING, ZHANG MEIXIA, MAO HANPING, WU XIAOHONG and LI QINGLIN	
The Remediation of Petroleum Contaminated Soils Using Microwave Irradiation: A Laboratory Study	S133
HUAYI JIANG, MEIYING LI, HONGYUAN QI and YULONG WANG	
Removal of Toxic Organic Pollutants from Coke Plant Wastewater by UV-Fenton	S143
YANGYANG LIANG, SUQIN LI and BIN LI	
The Strength and Durability Studies of Cement Mortar Blended with Solar PV Cells	S149
SUNG-CHING CHEN, RAN HUANG, HUI-MI HSU and LI-WEI TENG	
Separating and Recycling of Fe, Cu, Zn from Dumped Copper Slag by Microwave Irradiation Assisted Carbothermic Method	S155
YALONG LIAO, JUAN ZHOU and FEIRONG HUANG	
Research on the Feces-Bearing Capacity of the Farmland in Anhui Province of China	S161
CAILIN ZHANG, XIAOLONG CHEN, DONGFU FAN, TONGQIAN KANG and SHUYUN YANG	
Facile Synthesis of Fe₃O₄-N-[(3-Trimethoxysilyl)propyl]ethylenediamine Triacetic Acid Trisodium Salt and Adsorption of Sr²⁺	S169
YAOQIANG HU, CHAOMING QUAN, MIN GUO, XIUSHEN YE and ZHIJIAN WU	
Characteristics of Mercury Emissions from a Coal-fired Power Plant	S175
LIU QI-ZHEN, SUN YI, BAI YONG, XU XIAO-YU, TIAN YING-MING and LU JINMEI	
Extraction of Aluminum from Coal Fly Ash by Alkali Activation with Microwave Heating	S181
NENGSHENG LIU, JINHUI PENG, LIBO ZHANG, SHIXING WANG, SHAOJUN HUANG and SUFANG HE	
Effects of Two Kinds of Herbage Crops on the Removal of High Molecular Weight Polycyclic Aromatic Hydrocarbons in Sludge	S189
FENG SHENG-DONG, WANG WEI, SHI WEI, ZHANG XUE, JIA HAI-BIN, ZHANG XUE-NA, LI YU-LING, CHANG RUI-XUE and YANG ZHI-XIN	
Study on Anaerobic Digestion of Kitchen Waste for Biogas Production	S195
FENG LEI, GAO YUAN, KOU WEI, LI RUNDONG, YU MEILING, SHAO LIJIE and WANG XIAOMING	

Effective Adsorption of Pb(II) Ions by Gel Beads of Sodium Alginate and Polyethylene Glycol

DAOJI WU^{1,2}, ZHIMIN GAO^{1,2}, HUIXUE REN^{1,2,*}, JIAHUI JIANG^{1,2}, FENGXUN TAN^{1,2} and BING XU^{1,2}

¹School of Municipal and Environmental Engineering, Shandong Jianzhu University, Jinan 250101, P. R. China

²Co-Innovation Center of Green Building, Jinan, 250101, P. R. China

ABSTRACT: Novel gel beads were prepared using sodium alginate and polyethylene glycol to remove Pb(II) ions from aqueous solutions. The biopolymeric beads were characterized through scanning electron microscopy and energy-dispersive spectroscopy analyses. Effects of experimental parameters including initial pH, adsorbent dosage, reaction temperature, contact time, and initial metal ion concentration were discussed. The adsorption of Pb(II) ions followed the pseudo-second-order kinetics and fitted the Freundlich adsorption isotherm. Thermodynamic study also suggested that the adsorption reaction was spontaneous and exothermic. Chemical adsorption was found to be the main mechanism of Pb adsorption. The fabricated biosorbent exhibits potential for removal of Pb(II) ions.

INTRODUCTION

LEAD is a heavy metal found widespread in industrial effluents [1,2]. This element causes various diseases and disorders even at low concentrations because of physiologically toxic and non-biodegradable properties [3]. Bioadsorbents have recently gained wide attention for Pb removal because of their high efficiency, relatively low cost, and simplicity [4].

Sodium alginate (SA), a negatively charged polysaccharide, is composed of β -D-mannuronic acid (M units) and α -L-guluronic acid (G units) [5]. SA features formability, hydrophilicity, biocompatibility, biodegradability, and efficiency and exhibits high activity with the carbonyl and hydrogen groups on the chain [6]. However, the natural property of SA is unstable in several cases. SA preserved for long periods demonstrates severe thermal degradation and poor water resistance, thereby requiring modification [7,8].

Polyethylene glycol (PEG), a linear or branched polyether, is formed through ring-opening polymerization of ethylene oxide [9]. PEG presents a special structure and is usually used as a grafting agent, cosolvent, and porogen [10, 11]. PEG also exhibits stability, hygroscopicity, dispersibility, biocompatibility, non-toxicity, and non-irritability [12].

SA and PEG can be feasibly combined to be suitable for significant applications. Siddaramaiah *et al.* [13] studied the miscibility of SA and PEG. Moreover, Chen [14] investigated Cr(III) ion adsorption by using SA-based porous membrane adsorbents prepared with PEG as porogen.

In this study, we combined SA with PEG to synthesize SA-PEG-Ca gel beads (hereinafter referred to as SA-PEG) with excellent performance and reduced cost. The composite was characterized through scanning electron microscopy (SEM) and energy-dispersive spectroscopy (EDS) analyses. The optimum adsorption conditions were determined by experiments. The performance of the developed gel beads for Pb(II) adsorption were assessed by determining adsorption isotherms, kinetics, thermodynamics, and mechanism.

MATERIALS AND METHODS

Materials

SA (chemically pure), PEG (chemically pure), lead nitrate (analytically pure), and sodium hydroxide (analytically pure) were purchased from National Pharmaceutical Group Chemical Reagent Co., Ltd. Anhydrous calcium chloride (analytically pure) was provided by Tianjin BoDie Chemical Co., Ltd. Concentrated hydrochloric acid (analytically pure) was purchased from Laiyang Kant Chemical Co., Ltd.

*Author to whom correspondence should be addressed.
E-mail: renhx138@163.com; Tel: +86-531-86361570; Fax: +86-531-86361273

SA-PEG Preparation

SA and PEG (1:1) was mixed, stirred, and mixed uniformly to prepare 2 wt% mixed solution. The mixture was added transferred using a 10 mL syringe into 100 mL of 1 wt% calcium chloride solution under magnetic stirring. The produced beads were allowed to harden for 24 h, filtered, washed, and then dried to obtain the desired adsorbents. A photograph of the obtained beads is shown in Figure 1. The diameter of the SA-PEG bead is about 4 cm. Stock metal ion solutions were prepared with a final concentration of 1 gL⁻¹.

Bead Characterization

Polymer surface morphologies were recorded using a JSM-6380LASEM (Japan Electronics Co., Ltd.) at an accelerating voltage of 20 kV. Elemental analysis of the beads was conducted through EDS with an electron beam under 15 kV acceleration voltage and 15 mmWD.

Adsorption

Pb(II) ion sorption experiments were performed in an SHZ-B water bath equipped with a constant temperature vibrator (110rmin-1). Simulated wastewater with different Pb(II) concentrations (i.e., 1.0, 5.0, 10.0, 15.0, and 20.0 mgL⁻¹) were prepared by diluting the stock Pb(NO₃)₂ standard solution. The effects of experimental conditions were investigated by adjusting pH, adsorbent dosage, temperature, and time. The beads were separated through centrifugation, and the supernatant was analyzed by atomic absorption spectrometry. Removal rate was calculated as follows [15].

$$\text{Removal rate (\%)} = \frac{(C_0 - C) \times 100}{C_0} \quad (1)$$

Where C_0 and C are the initial and final concentrations of Pb(II) ions, respectively.



Figure 1. Photograph of SA-PEG.

RESULTS AND DISCUSSION

Structural Characterization of SA-PEG

SEM Analysis

SEM images of fabricated beads are presented in Figure 2. Surface morphology of beads shows a relatively homogeneous porous structure conducive to adsorption reaction from theoretical and practical aspects.

EDS Analysis

Specific images and quantitative elemental composition of the composites are listed in Figure 3. The EDS spectrum shows that the main elements are C, O, Ca, and Pb. The amount of Pb(II) ions in the cross-section is higher than that on the surface. This finding may be ascribed to the intra-particle diffusion of Pb(II) ions

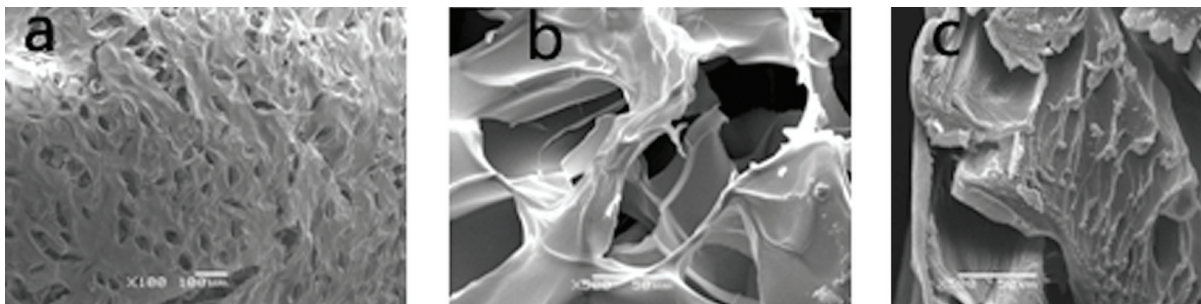


Figure 2. SEM micrographs of the bead surfaces (a) and (b) and cross-sectional image (c).

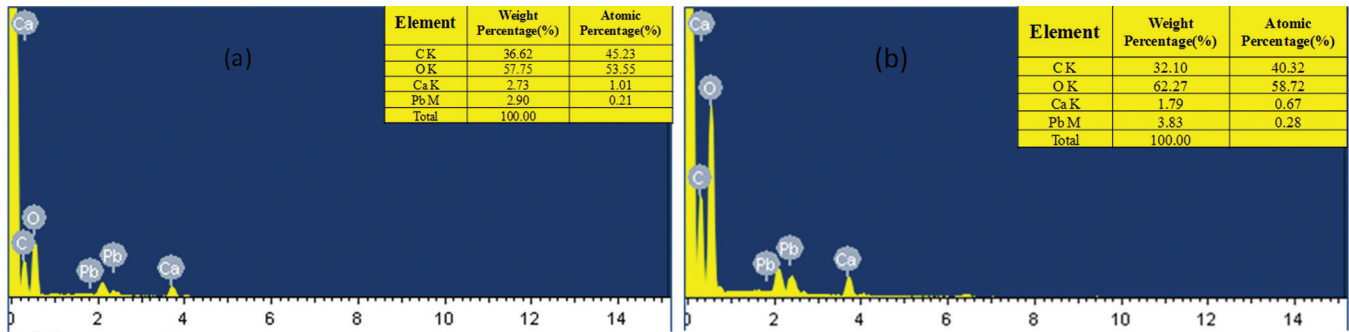


Figure 3. EDS spectrum of a surface and b cross-section of the beads.

into the adsorbent, thereby inducing the formation of a network structure of gel beads.

Factors Affecting Pb(II) Ion Adsorption

Effect of pH on Pb(II) Ion Adsorption

As illustrated in Figure 4, the removal rate for Pb(II) increased as the pH increased from 2 to 5. This finding can be attributed to two aspects. First, in acidic pH, the functional groups on the adsorbent surface are protonated, which results in considerable repulsion between the positively charged adsorbent surface and Pb(II) ions. Second, excess hydrogen ions in the solution may interact with the functional groups of SA-PEG, thereby occupying the active sites of the adsorbent. The maximum Pb²⁺ removal efficiency of approximately 100% was reached at pH 5.0, which is the closest pH to the pK of SA, the main component of SA-PEG. Pb²⁺ removal efficiency decreased with further increase in solution pH. This result could be attributed to the for-

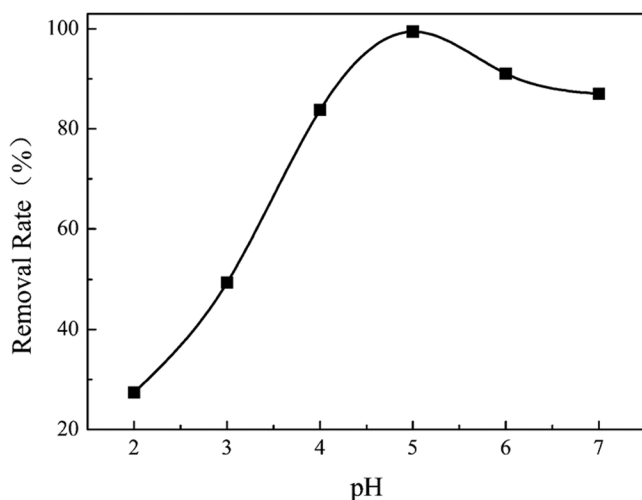


Figure 4. Effects on pH (experiment condition: put 0.8g SA-PEG gel beads into 100 mL 5 mg L⁻¹ lead solution, control the reaction time 7h at 298.15 K, change pH from 2 to 7).

mation of the hydroxyl species of Pb. Thus, adsorption was performed at the optimal pH of 5.0 in the following experiments.

Effect of Adsorbent Dosage on Pb(II) Ion Adsorption

Adsorbent dosage was varied from 0.2 g to 1.6 g in 100 mL sample volume. As shown in Figure 5, the removal efficiency increased with increasing adsorbent dosage. This phenomenon can be explained by the increased number of functional groups and active sites on the SA-PEG surface. Adsorption was mild and gradual at adsorbent dosages higher than 0.8 g, which could be due to the fixed amount of Pb(II) ions in the solution. As such, sample solutions with the optimal adsorbent dosage of 0.8 g were used for further adsorption experiments.

The effects on initial adsorbent concentration and temperature on Pb(II) adsorption are shown in following Figure 6 and 7, respectively.

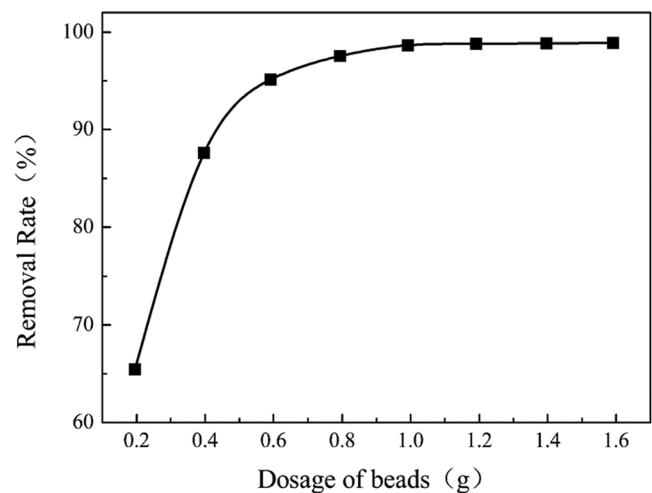


Figure 5. Effects on dosage of beads (experiment condition: put a certain amount SA-PEG gel beads into 100 mL 5 mg L⁻¹ lead solution, adjust pH to 5.0 and control the reaction time 7 h at 298.15 K).

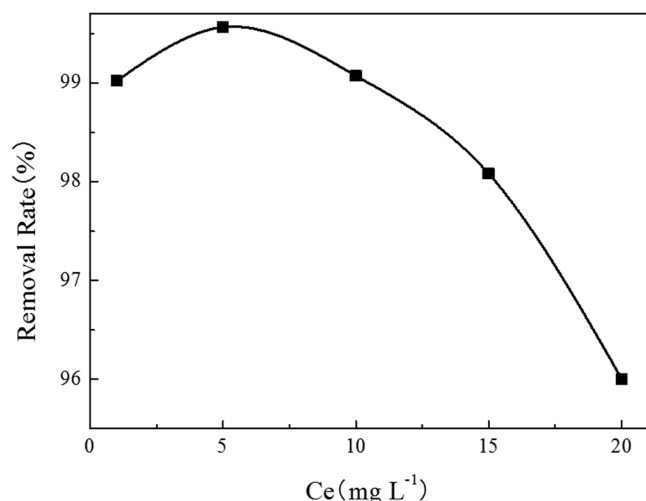


Figure 6. Effects on initial concentration (experiment condition: put 0.8 g SA-PEG gel beads into 100 mL lead solution with the concentration ranging from 1 mg L⁻¹ to 20 mg L⁻¹, adjust pH to 5.0 and control the reaction time 7 h at 298.15 K).

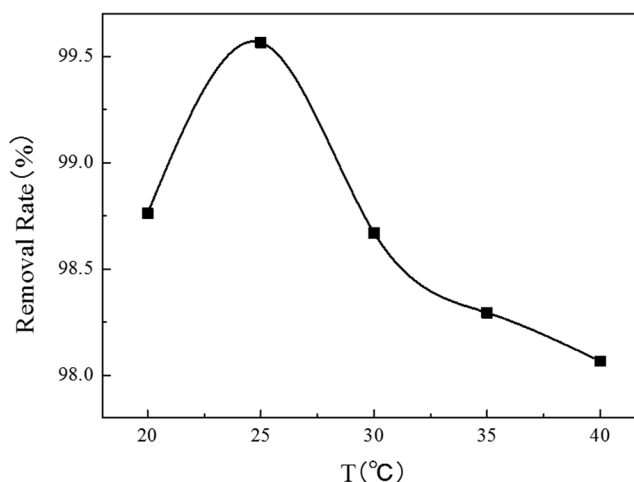


Figure 7. Effects on temperature (experiment condition: put 0.8 g SA-PEG gel beads into 100 mL 5 mg L⁻¹ lead solution, adjust pH to 5.0 and control the reaction time 7 h, changing temperature from 293.15 K to 313.15 K).

Adsorption Isotherms

Empirical models such as Langmuir, Freundlich, and Dubinin–Radushkevich (D–R) were applied to test the experimental data [16–18].

The parameters and correlation coefficients of the isotherm equations for Pb(II) ions adsorbed on SA-PEG are summarized in Table 1. All the coefficient R^2 values of the Freundlich model at different temperatures were higher than 0.99. Results suggest that the adsorption of Pb(II) ions on the prepared adsorbent is a heterogeneous process.

Essential characteristics of Langmuir, Freundlich, and D–R models can be expressed by the dimensionless constant (R_L), linear fitting value of n , and free energy of adsorption (E), respectively. The significance of these parameters is discussed in the literature. In the Langmuir model, the R_L ($R_L = 1/(1 + K_L C_0)$) values were all less than 1.0, implying that Pb(II) adsorption on SA-PEG is a favorable process. In the Freundlich model, the n values of the linear fitting were between

0 and 1, which indicates that Pb(II) adsorption easily occurred. From the linear plot of the D–R isotherm, the calculated E values were within the range of 8.45 kJ mol⁻¹ to 9.13 kJ mol⁻¹. This finding could be attributed to the chemisorption between the adsorbent and Pb.

Adsorption Kinetics

The uptake–time curves at different concentrations are shown in Figure 8. Results suggest adsorption of Pb(II) ions rapidly increased during the initial 3 h and reached about 85% of the equilibrium value. Subsequently, the adsorption rate gradually increased and remained in equilibrium after 7 h. Several empirical models were applied to test the experimental data and evaluate the adsorption mechanism [16–18].

The fitting curves and parameter values of the kinetic equations for Pb(II) ions adsorbed on the SA-PEG surface are listed in Table 1 and Figure 9, respectively. The R^2 values of the pseudo-second-order model at different adsorbent concentrations were closer to 1.0 and

Table 1. Adsorption Constant of the Four Isotherm Models.

T (°C)	Langmuir			Freundlich			D-R		
	q_m (mg g ⁻¹)	K_L	R^2	n	K_F	R^2	β (mol ² kJ ⁻²)	q_m (mg g ⁻¹)	R^2
20	17.5039	0.0058	0.9357	1.0310	0.1014	0.9996	-0.0076	82.21899	0.9994
25	21.3038	0.0048	0.9419	1.0253	0.1018	0.9997	-0.0074	85.72389	0.9994
30	26.0213	0.0039	0.9520	1.0210	0.1021	0.9998	-0.0071	88.39295	0.9993
35	30.5530	0.0034	0.9645	1.0182	0.1026	0.9999	-0.0069	90.37930	0.9992
40	35.4359	0.0029	0.9384	1.0158	0.1031	0.9999	-0.0067	92.45699	0.9991

q_m is saturation adsorption capacity (mg g⁻¹); K_L is Langmuir adsorption constant; K_F is Freundlich adsorption constant; n is empirical constant; β is adsorption constant representing free energy adsorption in D-R model (mol²/J²).

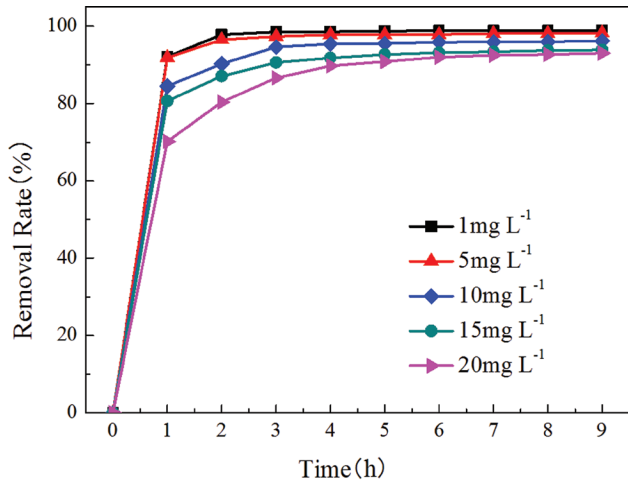


Figure 8. Effects on adsorption time on Pb(II) ion removal (initial adsorbent concentration and volume = 5 mg L^{-1} and 100 mL , respectively; mass of SA-PEG gel beads = 0.8 g ; $\text{pH} = 5.0$; and temperature = 298.15 K).

higher than those of the other models. These results demonstrate that the pseudo-second-order model is the best-fitting model to describe the adsorption process of Pb(II) on the gel bead adsorbent. Hence, chemical

adsorption is considered the rate-limiting step of the adsorption mechanism.

The intra-particle diffusion curve of Pb(II) did not pass through the origin. Hence, intra-particle diffusion was not the only rate-limiting step. External particle diffusion (such as surface adsorption and liquid film diffusion) may also limit the reaction rate.

In summary, the mechanism of Pb(II) ion sorption with SA-PEG consisted of three parts: (1) rapid adsorption, dominated by chemical adsorption; (2) gradual adsorption, controlled by intra-particle diffusion; and (3) general equilibrium.

Adsorption Thermodynamics

Thermodynamic experiments were conducted by varying the solution temperature between 293 and 313 K. Parameters including standard free energy change (ΔG° , kJ mol^{-1}), standard entropy change (ΔS° , $\text{kJ mol}^{-1} \text{K}^{-1}$), and standard enthalpy change (ΔH° , kJ mol^{-1}) were calculated using the Van't Hoff equation [16–18].

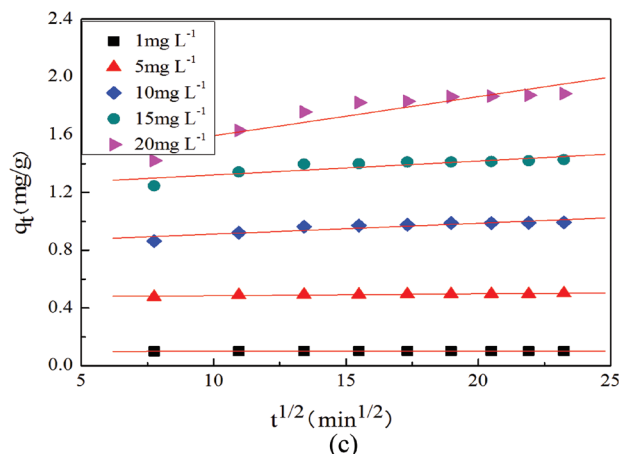
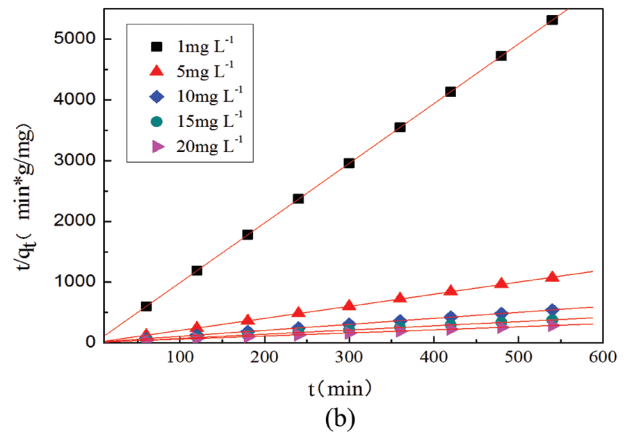
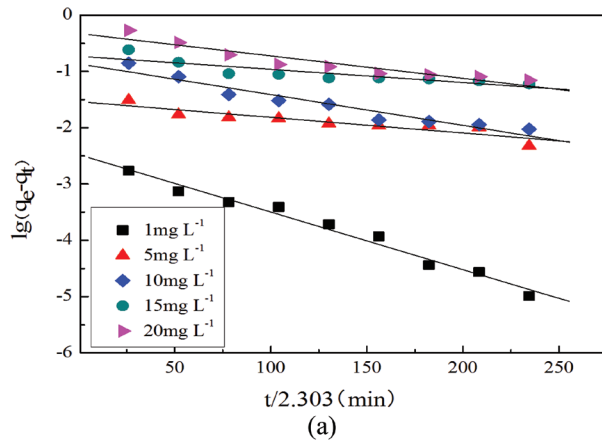


Figure 9. Linear fitting graphs of pseudo-first-order (a), pseudo-second-order (b) and intra-particle diffusion (c).

Table 2. Kinetic Parameters for Pb²⁺ Adsorption.

C_0 (mg·L ⁻¹)	Pseudo-first-order			Pseudo-second-order			Intra-particle Diffusion		
	q_{e1} (mg g ⁻¹)	k_1 (min ⁻¹)	R^2	q_{e2} (mg g ⁻¹)	k_2 (g mg ⁻¹ min ⁻¹)	R^2	C (mg g ⁻¹)	k_f	R^2
1	0.0033	0.0102	0.9797	0.1019	7.9901	0.9999	0.0996	0.0001	0.8217
5	0.0289	0.0029	0.8352	0.5035	0.4820	0.9998	0.4725	0.0013	0.8306
10	0.1361	0.0055	0.9338	1.0128	0.0942	0.9999	0.8362	0.0076	0.8211
15	0.1860	0.0023	0.7677	1.4477	0.0795	0.9999	1.2249	0.0096	0.7511
20	0.4705	0.0040	0.8926	1.9654	0.0231	0.9998	1.3228	0.0270	0.8271

q_e is the equilibrium adsorption capacity (mgg⁻¹); k_1 is the pseudo-first-order kinetic rate constant (min⁻¹); k_2 is the pseudo-second-order kinetic constant (g(mg·min)⁻¹); k_f is the intraparticle diffusion rate constant.

The parameters of the thermodynamic equations for Pb(II) ions adsorbed on SA-PEG are summarized in Table 3. The linear fitting graph of the thermodynamic model is shown in Figure 10. Negative ΔG° indicates that the adsorption process is spontaneous. The results showed that ΔG° values slightly decreased with increasing temperature; hence, adsorption was not favorable at high temperatures. Negative ΔS° reflects that the adsorption reaction reduces the randomness of the solid–solution interface. The obtained negative ΔH° value confirmed that the adsorption process is exothermic. According to other similar studies, the negative value of ΔH° (–26.57 kJ mol⁻¹) suggests that the main mechanism of Pb(II) ion adsorption on gel beads is chemical adsorption; this finding is in good agreement with the result of the D–R isotherm.

CONCLUSION

This study shows that SA-PEG is an excellent adsorbent for effective removal of Pb(II) ions from aqueous solutions. Summarizing, first, SEM and EDS techniques were applied to characterize SA-PEG. The results indicate that the main components of the biosorbent exhibit good miscibility. The adsorbent also presents a homogeneous porous structure, which is conducive for the adsorption reaction. Second, the maximum adsorption of Pb on SA-PEG was attained under the optimized conditions of 25°C, pH 5.0, 5 mg/L initial Pb concentration, and 0.8 g of the sorbent. Finally, Adsorption isotherms, kinetics, and thermodynamics were used to study the adsorption mechanism of SA-PEG. The results best fitted the Freundlich and

pseudo-second-order models; hence, the adsorption mechanism is a chemical adsorption process, as confirmed by the E value derived from the D–R model. Furthermore, the thermodynamic study indicated the spontaneous and exothermic nature of Pb(II) adsorption.

ACKNOWLEDGEMENTS

This study was financially supported by Chinese National Science and Technology Project of Water Pollution and Governance (2012ZX07404-003-006C), Science and Technology Project of MOHURD and BOHURD of ShanDong Province (2015-K7-005,KY006), Research Funds for the Doctoral Program of Shandong Jianzhu University (XNBS1309), and scholarship from Shandong provincial government for going abroad as an academic visitor.

REFERENCES

1. W. Wei, L. Xiangzhi, S. Peiqing, W. Xin, Z. Hong, H. Mei, M. Zongwan and Z. Jing, “Simple Whole-Cell Biodetection and Bioremediation of Heavy Metals Based on an Engineered Lead-Specific Operon”, *Environ. Sci. Technol.*, Vol. 48, No. 6, 2014, pp. 3363–3371. <http://dx.doi.org/10.1021/es4046567>
2. N.V. Suc and H.T.Y. Ly, “Lead (II) removal from aqueous solution by chitosan flake modified with citric acid via crosslinking with glutaraldehyde”, *J. Chem. Technol. Biot.*, Vol. 88, No. 9, 2013, pp. 1641–1649. <http://dx.doi.org/10.1002/jctb.4013>
3. W. Yin, W. Xuejiang, W. Xin, L. Mian, Y. Lianzhen, W. Zhen, X. Siqing and Z. Jianfu, “Adsorption of Pb (II) in aqueous solutions by bamboo charcoal modified with KMnO₄ via microwave irradiation”, *Colloid. Surface. A*, Vol. 414, 2012, pp. 1–8. <http://dx.doi.org/10.1016/j.colsurfa.2012.08.007>
4. Z. Yiming, F. Shiyu, Z. Liangliang, Z. Huaiyu and M.V. Levit, “Use of carboxylated cellulose nanofibrils-filled magnetic chitosan hydrogel

Table 3. Thermodynamic Parameters for Adsorption of Pb²⁺.

ΔG° (kJmol ⁻¹)					ΔS° (kJ mol ⁻¹ ·K ⁻¹)	ΔH° (kJ mol ⁻¹)
293.15 K	298.15 K	303.15 K	308.15 K	313.15 K		
-17.2721	-17.0481	-16.8589	-16.7069	-16.6453	-0.031	-26.57

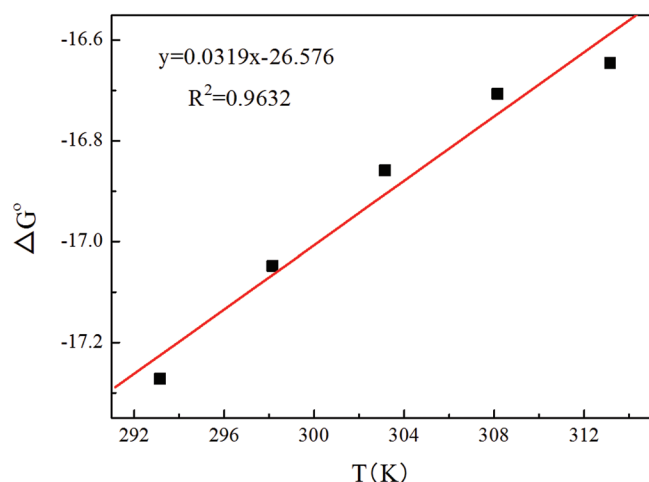


Figure 10. Linear fitting graph of thermodynamic model.

beads as adsorbents for Pb (II)", *Carbohydr. Polym.*, Vol. 101, 2014, pp.75–82. <http://dx.doi.org/10.1016/j.carbpol.2013.08.055>

5. N. Khuathan and T. Pongjanyakul, "Modification of quaternary poly-methacrylate films using sodium alginate: Film characterization and drug permeability", *Int. J. Pharmaceut.*, Vol. 460, No. 1, 2014, pp. 63–72. <http://dx.doi.org/10.1016/j.ijpharm.2013.10.050>
6. M. M. Lakouraj, F. Mojerlou and E.N. Zare, "Nanogel and superparamagnetic nanocomposite based on sodium alginate for sorption of heavy metal ions", *Carbohydr. Polym.*, Vol. 106, 2014, pp. 34–41. <http://dx.doi.org/10.1016/j.carbpol.2014.01.092>
7. H. Zhen, Y. Xiaoxu, P. Xi, Z. Yulong, F. Meifen and Z. Qiang, "Thermal degradation study of sodium alginate-zeolite 4A composites", *Proc. 17th LAPRI World Conf. on Packag.*, Tianjin, China, Scientific Research Publishing, USA, 2010, pp.406–409.
8. Z. Ruping and D. Matai, "Preparation properties and characterization of the blend film of sodium alginate and polyvinyl alcohol", *J. Funct. Mater.*, Vol. 40, No. 2, 2009, pp. 295–297(Ch).
9. F.M. Veronese and G. Pasut, "PEGylation, successful approach to drug delivery", *Drug Discov. Today*, Vol. 10, No. 21, 2005, pp.1451–1458. [http://dx.doi.org/10.1016/S1359-6446\(05\)03575-0](http://dx.doi.org/10.1016/S1359-6446(05)03575-0)
10. A.B. Hegge, T. Andersen, J.E. Melvik, E. Bruzell, S. Kristensen and H.H. Tønnesen, "Formulation and bacterial phototoxicity of curcumin loaded alginate foams for wound treatment applications: studies on curcumin and curcuminoides XLII", *J. Pharmacol. Sci.*, Vol. 100, No. 1, 2011, pp. 174–185. <http://dx.doi.org/10.1002/jps.22263>
11. M. Mishra and J.E. Andersen, "Design and evaluation of microporous membrane coated matrix tablets for a highly water soluble drug", *Chem. Pharm. Bull.*, Vol. 58, No. 7, 2010, pp. 995–1000. <http://dx.doi.org/10.1248/cpb.58.995>
12. M. Davidovich-Pinhas and H. Bianco-Peled, "Alginate–PEGAc: A new mucoadhesive polymer", *Acta Biomater.*, Vol. 7, No. 2, 2011, pp. 625–633. <http://dx.doi.org/10.1016/j.actbio.2010.09.021>
13. Siddaramaiah and T.M. Mruthunjaya Swamy, "Studies on miscibility of sodium alginate/polyethylene glycol blends", *J. Macromol. Sci.*, Vol. 44, No. 3, 2007, pp. 321–327. <http://dx.doi.org/10.1080/10601320601077492>
14. C. Jianhua, "Preparation and investigation on the adsorption behavior of polyethylene glycol modified sodium alginate porous membrane adsorbent for Cr (III) ions", *Adv. Mater. Res.*, Vol. 455, 2012, pp. 786–795.
15. A.K. Vipin, B. Hu and B. Fugetsu, "Prussian blue caged in alginate/calcium beads as adsorbents for removal of cesium ions from contaminated water", *J. Hazard. Mater.*, Vol. 258, 2013, pp. 93–101. <http://dx.doi.org/10.1016/j.jhazmat.2013.04.024>
16. A.S.K. Kumar, T. Gupta, S.S. Kakan, S. Kalidhasan, V. Rajesh and N. Rajesh, "Effective adsorption of hexavalent chromium through a three center (3c) co-operative interaction with an ionic liquid and biopolymer", *J. Hazard. Mater.*, Vol. 239, 2012, pp. 213–224. <http://dx.doi.org/10.1016/j.jhazmat.2012.08.065>
17. V. Rajesh and N. Rajesh, "Adsorption isotherms, kinetics and thermodynamic studies towards understanding the interaction between a microbe immobilized polysaccharide matrix and lead", *Chem. Eng. J.*, Vol. 248, 2014, pp. 342–351. <http://dx.doi.org/10.1016/j.cej.2014.03.022>
18. R.K. Gautam, A. Mudhoo, G. Lofrano and M.C. Chattopadhyaya, "Biomass-derived biosorbents for metal ions sequestration: Adsorbent modification and activation methods and adsorbent regeneration", *J. Environ. Chem. Eng.*, Vol. 2, No. 1, 2014, pp. 239–259. <http://dx.doi.org/10.1016/j.jece.2013.12.019>

Total Nitrogen Removal of Effluent from a Municipal Sewage Treatment Plant via a Composite Biofilter

YUANHONG DING^{1,*}, QING WANG², HONGQIANG REN^{2,*}, YI QIAN¹ and GUIZHONG ZHOU¹

¹*School of environment, Qingdao University of Science and Technology, Qingdao 266000, China.*

²*State Key Lab. of pollution control and resources reuses, Nanjing University, Nanjing 210093, China*

ABSTRACT: A pilot-scale Composite Biofilter was applied to treat the effluent of secondary sediment tank from a Sewage Treatment Plant, which Total Nitrogen (TN) was mainly composed of nitrate, sodium acetate was added into it as external carbon source, and the results indicated that, the optimal conditions for Composite Biofilter was about at, HRT of 2 h and sodium acetate of 100 mg/L, the concentrations of ammonia, TN and TP of treated effluent was averagely about at 0.95 mg/L, 9.2 mg/L and 0.05 mg/L respectively, which was measured up to strict local standards, in addition, the Composite Biofilter had the advantage on phosphorous removal either, and a good performance of denitrification was achieved on low temperature (5–15°C).

INTRODUCTION

TOTAL NITROGEN (TN) and ammonia is regarded as important pollutants to lead to water eutrophication [1,2] maximizing emission concentration is strictly restricted by China Integrated Wastewater Discharge Standard (First class A, GB18918-2002), when “Cyanobacteria break-out Incident in Taihu Lake” happened in 2007, about 20,000 chemical factories surrounding the Taihu Lake had been shut down by Wuxi Governments, then a more strict local standards “Water Pollutants Discharge Standard for Municipal Sewage Plant and Industrial Factories surrounding the Taihu Lake DB32/1072-2007” has been carried out since Jan 1, 2008, therefore all those operating wastewater treatment facilities were confronted with challenges of upgrade or reconstruction to achieve deep denitrification, many post-treatment facilities were used to treat the emission effluent, such as absorbance system [3], anaerobic/anoxic/aerobic (A2/O)-biological aerated filter (BAF) [4], flocculation-coagulation-filtration system, sand filter [5] and constructed wetlands [6], however, the treated discharge effluent cannot reach the local standards effectively, Such factors as flocculation of temperature and C/N(CODcr/TN) ratio, made the treating process much complicated.

Deep-bed Filter is an effective way for deep denitrification [7]. Owing to its small covers, ease of auto-

mation and steady removal efficiency for low content of NO_x^- , it may be an ideal way for nitrogen removal in sewage effluent [8]. Quartz sand, with the diameter range from 2 to 4 millimeter, was commonly used as the packing of Deep-bed Filter, the denitrification bacterium, attached on the quartz sand can transform nitrate-nitrite to nitrogen gas [9], during this process, the generated nitrogen gas accumulated and released intermittently out gap of filter sand, thus contact oxidation between sewage effluent and microbe was increased, and the removal efficiency of nitrogen was promoted [10].

But little was known about the nitrogen removal efficiency to sewage effluent by Deep-bed Filter under the condition of low temperature and aerobic water, in this study, a pilot-scale Composite Biofilter (5~10 m³/d), was designed according to the operational principal of Deep-bed Filter, to investigate the influence of nitrogen removal by low temperature, normal DO (dissolved oxygen) and HRT (Hydraulic Retention Time), which filling materials was mainly composed of sea sand, quartz and oyster shell.

EXPERIMENTAL

Pilot-Scale Composite Biofilter Set-Up

An integrated pilot-scale Composite Biofilter, set up in Wuxi Donggang Sewage Treatment Plant, was carried out to treat effluent from secondary sedimentation tank, the main body of Composite Biofilter was a stain-

*Author to whom correspondence should be addressed.
E-mail: yhding@nju.edu.cn; hqren@nju.edu.cn; +86-138-5164-1868

less steel cylinder with height of 4.93 m (abbreviation of meters) and diameter of 0.63 m and packing thickness of 1.83 m, which treatment scale is 5~10 m³/d. External carbon source, necessary for denitrification, was provided continuously by addition of sodium acetate, on the other hand, external nitrogen source, necessary for rapid acclimation of denitrifying bacterium, was provided only by addition of urea and potassium nitrate for one month, then stopped.

The sand components of Composite Biofilter is listed in Table 1. The main components of the media is sea sand (another kind of quartz) with diameter of 1~4 mm, density of 1385 kg/m³ and sphericity degree of 0.8~0.9. All the medium parameters, including with uniformity, Mohs hardness, specific density and acid-solubility, measured up to specifications of American Water Works Association. The filtration blocking was resolved by online backwashing of wash water and air scour every 24 hour, and the accumulated nitrogen gas was released periodically by wash water every 2 hour. The Temperature ranged from 8.6~33.8°C, the HRT was determined as: 1.5 h; 2.0 h; 3.0 h respectively; The concentrations of added sodium acetate was determined as: 0; 0.05; 0.10; 0.35; 0.37; 0.69 g/L respectively.

Water Quality

The raw water treated by Composite Biofilter, was effluent from secondary sediment in Wuxi Donggang Sewage Treatment Plant, its water quality was as followings: COD (chemical oxygen demands) 13.50~912.98 mg/L, TN 0.90~57.64 mg/L, TP (total phosphorus) 0.00~0.68 mg/L, pH 7.28~9.10 mg/L, NO₃-N 0.25~23.04 mg/L, NO₂-N 0.00~5.82 mg/L, NH₃-N 0.00~4.25 mg/L, TOC (total organic carbon) 7.1~1026.0 mg/L, DO 0.39~10.93 mg/L, SS (suspended solid) 0~57 mg/L, the water sample components indicated that TN was composed mainly about NO₃-N.

The Plant, with treatment capacity of 1000 m³/d, located on Donggang Town in China Wuxi city, run since Nov 26, 2011, its main treatment process was Anaerobic-Anoxic-Oxic reacting tanks and Biologi-

cal Aerated Filter, and its influent was from the mixed municipal wastewater and industrial wastewater. The quality of COD, ammonia and TP in effluent measured up to strict local standard "DB32/1072-2007", but that of TN exceeded frequently over this strict criteria.

Analytical Method

The measurements of COD, NH₄-N, NO₂-N, NO₃-N, TN, TP, SS and TOC were conducted according to the Standard Methods [11], The temperature and DO were determined by PB-10 (Sartorius, Germany), a Japan Shimadzu spectrophotometer UV1700 and a Japan Shimadzu TOC-5000 analyzer were used.

RESULTS AND DISCUSSION

Effect of Temperature on TN Removal

When wastewater temperatures lower 15°C, the enzymatic activity of denitrifying bacterium usually would be weakened or even completely inhibited, that would cause low efficiency of denitrification, but that was not observed obviously in Composite Biofilter, as shown in Figure 1, although the wastewater temperatures lowered 15°C for 3 months, the TN removal efficiency was still maintained at 40~60%, occasionally even more than 80~90%. The results indicated that, a good performance of nitrogen removal could be obtained by Composite Biofilter, even under low temperature (5~15°C).

Effect of DO on TN Removal

When oxygen is adequate, the electron could be

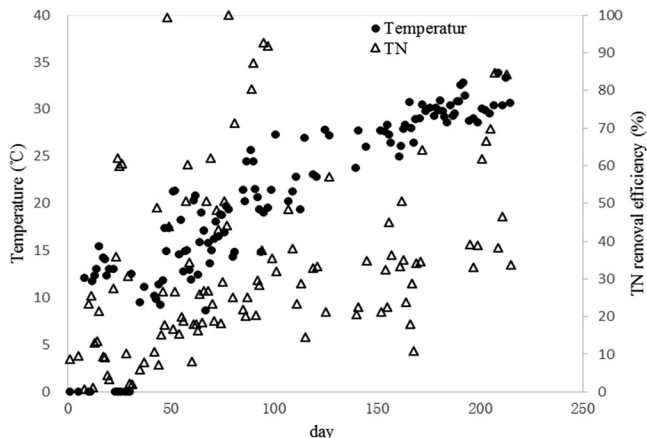


Figure 1. Effects of wastewater temperature on TN removal efficiency.

Table 1. Sand Components in the Composite Biofilter.

Components	Producing Area	Granularity, mm	Height, cm
Pebble	Nanjing Yuhua Stone	3~6	30
		6~12	20
Quartz sand	Shantou sea sand	12~16	10
		16~32	10

transferred from carbohydrates to oxygen by aerobic bacteria, while oxygen was lacking, the electron could be transferred from carbohydrates to nitrate by anoxic bacterium [12]. The DO concentration was decreased from top to bottom of Composite Biofilter, at the top, the DO concentrations was high, thus ammonia could be nitrified to nitrite and nitrate, at the bottom, the DO was scarce, nitrite and nitrate would be transformed to nitrogen gas by denitrifying bacterium, The effect of DO on TN removal is presented in Figure 2. It seemed that, the TN removal efficiency was not affected obviously by DO concentrations, The results demonstrated that, there happed aerobic denitrification in Composite Biofilter that was different from the conventional Deep-Bed Filter.

Effect of HRT on TN Removal

Contact time between wastewater and bacterium attached on the sand, could be affected by HRT, at low HRT, the residence time of pollutants in wastewater was very long, enough to biological degradation of nitrogen, but it was negative for treatment capacity, on the other hand, an high HRT could result in incomplete biological degradation of nitrogen and scour out a little of biofilm. As seen in Figure 3, when the HRT was fixed at 1.5 h, the TN removal efficiency was low, about 20% at early stage, after twenty days, the TN removal efficiency was increased to 40–60%, as HRT was set at 2.0 h, that was maintained at 50–80%.

Effect of Sodium Acetate on TN Removal

As the raw water of Composite Biofilter was from effluent of secondary sediment tank of Donggang Sewage Treatment Plant, there was insufficient available

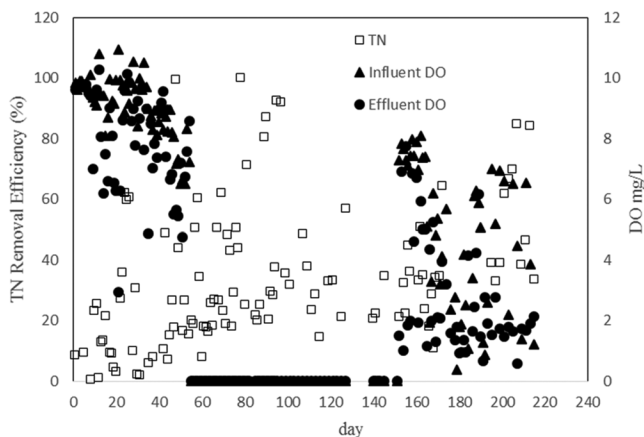


Figure 2. Effects of wastewater DO on TN removal efficiency.

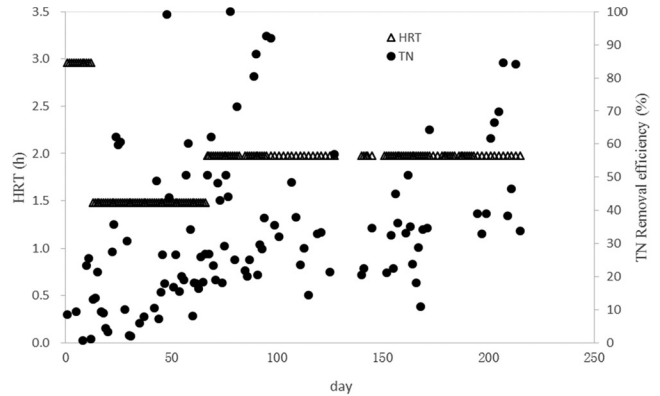


Figure 3. Effects of wastewater HRT on TN removal efficiency.

carbon source for bacterium to assimilate residual nitrogen in wastewater, therefore, it was necessary to add some external carbon source to maintain a normal C/N ratio, such as methanol, sodium acetate and glucose, in this experiment, sodium acetate was added continuously as external carbon source, because of some advantages of rapid assimilation and low cost [13], as Figure 4 showed, when the concentrations of added sodium acetate was 690 mgg/L, the TN removal efficiency was at 40–50%, and the treated effluent had anaerobic smell. When the concentrations of sodium acetate was decreased to 350 mg/L, the TN removal efficiency was 20–40% and the odor got weaker. when the concentrations of sodium acetate was adjusted to 50 mg/L, the TN removal efficiency was declined rapidly to zero, Based on the above results, 100 mg/L was regarded as optimal concentration of sodium acetate.

Removal Efficiency of Ammonia and TP by Composite Biofilter

Removal efficiencies of ammonia and TP was also

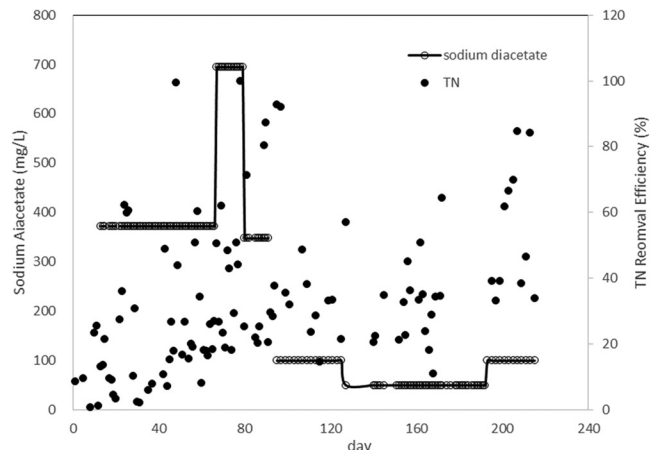


Figure 4. Effects of sodium acetate on TN removal efficiency.

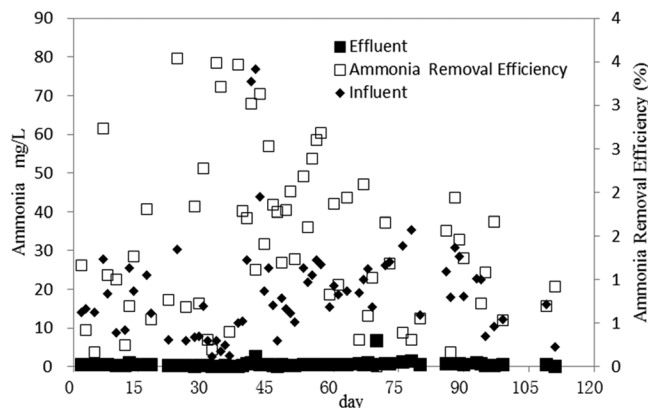


Figure 5. Removal efficiency of Composite Biofilter for ammonia.

examined in detail. As seen in Figures 5 and 6, the averaged concentrations of ammonia and TP in treated effluent, was 0.95, 0.05 mg/L respectively, it seemed that, ammonia was changed into nitrite and nitrate by nitrifying bacterium in aerobic conditions, while phosphorous was possibly adsorbed onto sand.

CONCLUSIONS

The pilot-scale experiments indicated that, as a single facilities, the Composite Biofilter could be used to achieve deep nitrogen removal of effluent in Sewage Treatment Plant, different from the conventional Deep-Bed Filter, it could be run well on the condition of low temperature (5–15°C) and aerobic water, perhaps there happened aerobic denitrification to maintain a good nitrogen removal, and had an advantage of phosphorous removal either, while Deep-Bed Filter was usually run under anoxic environment and normal temperature to achieve a good denitrification. The treated water was

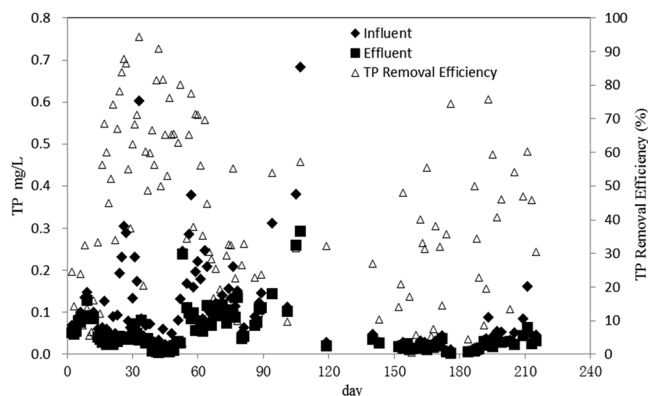


Figure 6. Removal efficiency of Composite Biofilter for TP.

measured up to strict local standards, the treated concentrations of ammonia, TN, TP and SS was less than 5 mg/L, 15 mg/L, 0.5 mg/L and 10 mg/L respectively. The optimal conditions for Composite Biofilter was HRT of 2 h and sodium acetate of 100 mg/L.

ACKNOWLEDGEMENT

Authors wish to thank the Foundation of Jiangsu Science and Technology Project (No 2012011) to support the research, focusing on deep nitrogen removal of Sewage wastewater.

REFERENCES

1. N. Qzturk, "Nitrate removal from aqueous solution by adsorption onto various materials", *J. Hazard. Mater.*, 112, 2004, 155–162. <http://dx.doi.org/10.1016/j.jhazmat.2004.05.001>
2. A. Fkhami, "Adsorption and electrosorption of nitrate and nitrite on high-area carbon cloth: An approach to purification of water and waste-water samples", *Carbon*, 41, 2003, 1320–1322. [http://dx.doi.org/10.1016/S0008-6223\(03\)00068-X](http://dx.doi.org/10.1016/S0008-6223(03)00068-X)
3. M.S. Amit, "A review of emerging adsorbents for nitrate removal from water", *Chem. Eng. J.*, 168, 2011, 493–504. <http://dx.doi.org/10.1016/j.cej.2011.01.103>
4. Y.Z. Chen, B.K. Li, L. Ye and Y.Z. Peng, "The combined effects of COD/N ratio and nitrate recycling ratio on nitrogen and phosphorus removal in anaerobic/anoxic/aerobic (A2/O)-biological aerated filter (BAF) systems", *Biochem. Eng. J.*, 93, 2015, 235–242. <http://dx.doi.org/10.1016/j.bej.2014.10.005>
5. T. Daniele, L. Adriano and B. Tonetti, "Wastewater treatment by anaerobic filter and sand filter: Hydraulic loading rates for removing organic matter, phosphorus, pathogens and nitrogen in tropical countries", *Eco. Eng.*, 82, 2015, 583–589. <http://dx.doi.org/10.1016/j.ecoeng.2015.05.018>
6. J.H. Park, S.H. Kim, D.R. Delaune, J.S. Choc, J.S. Heo, Y.S. Okd and D.C. Seo, "Enhancement of nitrate removal in constructed wetlands utilizing a combined autotrophic and heterotrophic denitrification technology for treating hydroponic wastewater containing high nitrate and low organic carbon concentrations", *Agri. Wat. Manag.*, 162, 2015, 1–14. <http://dx.doi.org/10.1016/j.agwat.2015.08.001>
7. X.B. Yang and W.L. Kan, "Application of Deep Bed Denite Filter for Upgrading and Retrofitting", *Chin. water. wastewater*, 12, 34–36.
8. J. Sun, 2003. *Nitrogen-containing wastewater treatment technology and application*, Chemical Industry Press, Beijing, 2003.
9. D. Kulikowska, T. Jozwiak, P. Kowal and S. Ciesielski, 2010. "Municipal landfill leachate nitrification in RBC biofilm-process efficiency and molecular analysis of microbial structure", *Bior. Technol.*, 101, 2011, 3400–3405. <http://dx.doi.org/10.1016/j.biortech.2009.12.050>
10. S.I. Abou, M.E. Fawzy and A.S. Gendy, "El Potential of using biological aerated filter as a post treatment for municipal wastewater", *Eco. Eng.*, 84, 2015, 53–57. <http://dx.doi.org/10.1016/j.ecoeng.2015.07.022>
11. S.E.P.A.O. China, 2002. *Monitoring and Analysis Method of Water and Wastewater* (Fourth Edition), China Environmental Science Press, Beijing.
12. G.B. Li, 2005. *Water Quality Engineering*, China Architecture & Building Press, Beijing, 2005.
13. Q.Q. Xia, X.Q. Yi, X.Y. Zhang, "Advanced Treatment Characteristics of Biofilter with Different External Carbon Sources and Its Techno-economic Analysis", *Water. Wastewater*, 15, 2011, 91–94.

Chemical Fractions and Mobility of Cd, Cu, Pb and Zn in Soil Profile of a Sewage Irrigation Area, Northwest China

BAILIN LIU, SHIWEI AI, RUI GUO, LIANG REN, WENYA ZHANG and YINGMEI ZHANG*
*Gansu Key Laboratory of Biomonitoring and Bioremediation for Environmental Pollution, School of Life Sciences,
Lanzhou University, Lanzhou 730000, China*

ABSTRACT: The Chinese government recently planned to supply financial support for comprehensive prevention and control of heavy metal pollution in 30 cities nationwide, among which Baiyin city took the first place. The present study aimed to investigate the chemical fractions and mobility of Cd, Pb, Cu and Zn in the soil profile (0–60 cm depth) of cornfields in the Dongdagou region, Baiyin city, Northwest China. The modified BCR (now the Standards, Measurement and Testing Programme of the European Community) method was employed to analyse the chemical fractions of heavy metals, and mobility index used to assess heavy metal mobility. Besides, Pearson correlation matrix was adopted to study the effects of soil properties (depth, total organic matter and pH) on heavy metal mobility. Results show that the soils are seriously polluted with heavy metals, especially by Cd. Cadmium is particularly presented in the acid soluble fraction, while Pb is mainly in the reducible fraction. As for Cu and Zn, they are likely to be retained in the residual fraction. With few exceptions, heavy metal concentrations in non-residual fractions generally decrease with the deepening of soil depth. Heavy metal pollution in soils has reached at least 60 cm deep, and the main pollution is found in the soils of 0–30 cm depth. In soil profile, heavy metal mobility is in the order of Cd > Cu > Pb > Zn; meanwhile, total organic matter has a significant role in retaining heavy metals in soils. Immediate measures should be taken to prevent the potential risk of heavy metals for local agro-ecosystem and the public.

INTRODUCTION

In the last decade, several heavy metal pollution events have taken place in China [1]. Heavy metal pollution in farmlands not only decreases crop yield and quality, but also threatens ecosystem safety and human health, especially for those near mining and smelting sites [2]. In China, about 12.1% of farmlands showed heavy metal concentrations over relevant standards [3], where Cd, Ni, Cu, As, Hg and Pb were deemed as the dominating pollutants [4]. For comprehensive prevention and control of heavy metal pollution, in May 2015, the Chinese government planned to strengthen management and provide special financial support for 30 cities nationwide, amongst which Baiyin city took the first place.

Baiyin city was a famous base of non-ferrous metal mining and smelting in Gansu province, Northwest China. It is also well known as a sewage irrigation region. Due to lack of strict supervision system, acid

mine drainage and poorly-treated industrial effluents had been discharged into Dongdagou stream (a local drain ditch) and severely contaminated the river ecosystem. Even worse, sewage from the stream had been utilized to irrigate the surrounding farmlands for years. It is reported that farmlands here have been contaminated by several heavy metals [5,6]. For the sake of mitigating pollution in Baiyin city, the Dongdagou region should be on the top of the agenda. However, data of heavy metal status in local farmlands is very limited, especially for these regarding chemical fractions and mobility in the soil profile.

Total metal content is a poor indicator that cannot provide sufficient information on heavy metal bioavailability [7,8]. Heavy metals in soils can be categorized into different chemical fractions [9,10], and only those in particular fractions are bioavailable for plants [11]. Accordingly, many studies have been developed to figure out the chemical fractions of heavy metals, and the BCR (now the Standards, Measurement and Testing Programme of the European Community) method has been widely adopted [12]. It divides heavy metals into four operationally defined geochemical fractions, i.e.,

*Author to whom correspondence should be addressed.
Email: ymzhang@lzu.edu.cn. Tel.: +86-13919123067. Fax: +86-931-8913631

the acid soluble fraction (F1), reducible fraction (F2), oxidizable fraction (F3) and residual fraction (F4) [10]. Heavy metals in F1 are bioavailable, while heavy metals in F2 and F3 may become bioavailable, when soil pH or redox potential changes [12]. These three fractions are also called as the non-residual fraction (NRF) versus F4 which is thought to be inactive.

The primary objective of the present study is to investigate the status of Cd, Pb, Cu and Zn in the soil profile of cornfields in the Dongdagou region, Baiyin city, Northwest China. To the best of our knowledge, there are scarce reports on chemical fractions and mobility of heavy metals in soil profile. The data produced here will provide significant guidance for local pollution prevention and control.

MATERIALS AND METHODS

Study Area and Sampling

Baiyin city has an arid and semi-arid climate with average annual precipitation and temperature of 220 mm and 6–9°C. Because of high yield and economic benefit, maize which serves as food both for human being and live stocks becomes the staple crop here.

The study area, the Dongdagou region, is located in the vicinity of Baiyin city and named after Dongdagou stream. Acid mine drainage and industrial effluents had severely contaminated the aquatic environment of Dongdagou stream which originates in the mining and smelting sites and drained into the Yellow River, and further polluted the surrounding farmlands as a result of flooding irrigation with sewage from the stream.

In November 2014, five sampling sites were chosen in the cornfields along Dongdagou stream from upstream to downstream (Figure 1). In our previous study, we collected soil samples every 20 cm in soil profile; however, we found this sampling method sometimes is not very accurate and may conceal some useful information. Thus, in the present study, we collected the soil samples every 10 cm. At each site, soil samples with five replicates were collected using a stainless drill at the depths of 0–10, 10–20, 20–30, 30–40, 40–50 and 50–60 cm in sequence. *In situ*, subsamples at the same depth were thoroughly mixed for a composite one. In total, 30 composite samples (6 samples per site × 5 sites) were collected. They were then stored in sealed bags and transported to the lab immediately for further analysis.

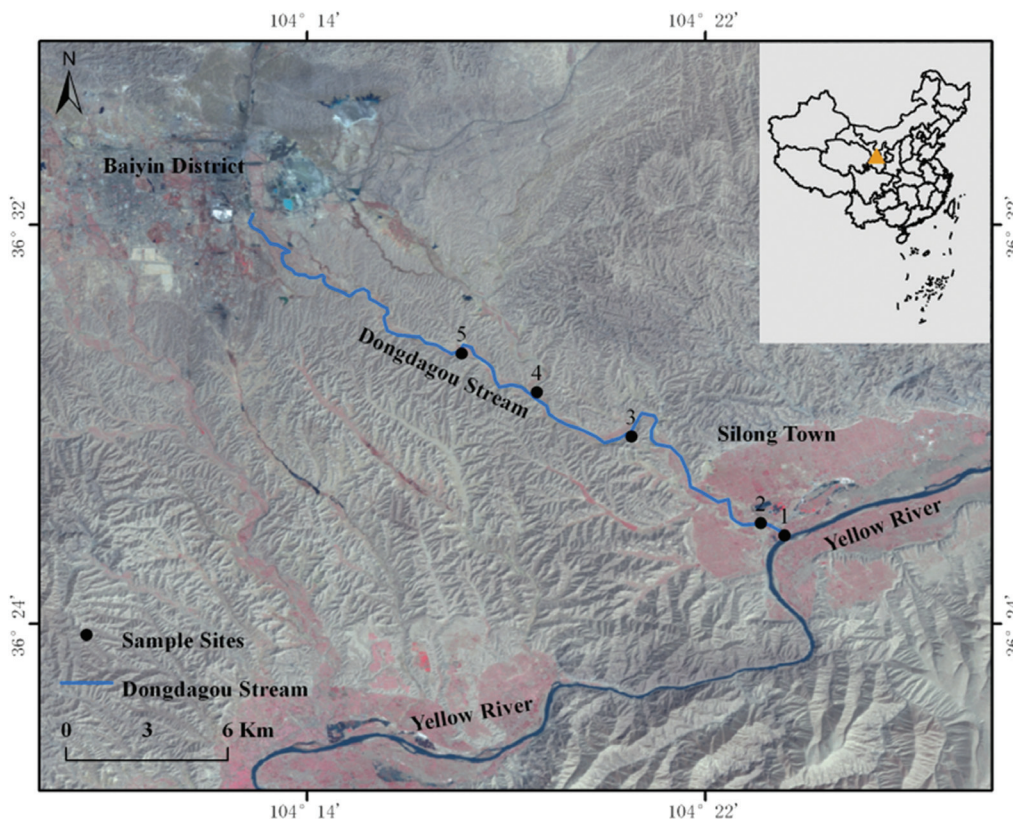


Figure 1. Map of the study area and sampling sites.

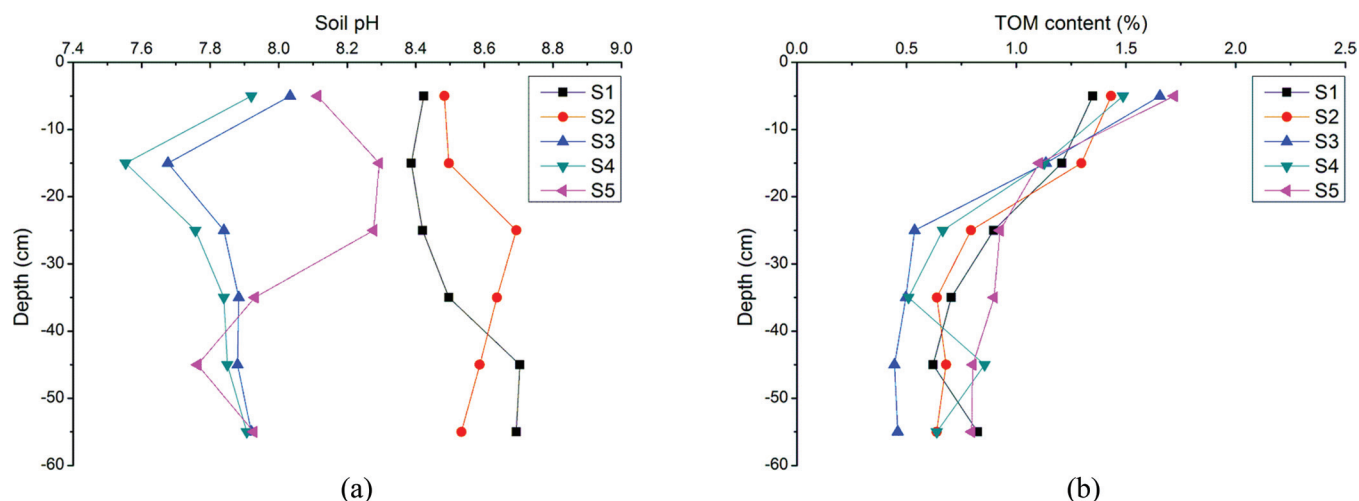


Figure 2. Variation distributions of soil pH and TOM in soil profile of cornfields in the Dongdagou region.

Analysis

In lab, all soil samples were air-dried, ground and sieved as required before analysis. Soil pH was measured in a 1:2.5 (w/v) solid-to-water ratio with a pH electrode (PB-10, Sartorius, Germany). Total organic matter of soils (TOM) was determined with the method of potassium dichromate oxidation. The results of soil pH and TOM are shown in Figure 2. As shown, soil pH varies greatly with sampling sites and soil depth, while TOM decreases along the soil depth gradient. Overall, the study area has slight-alkaline soils (pH 7.5–8.7) with low TOM content (1.72–0.44%).

Chemical fractions of heavy metals were determined by the BCR method with some modifications, and the detailed procedures were described elsewhere [13]. In the present study, F1, F2, F3 and F4 are used to represent the four chemical fractions obtained from the modified BCR method, respectively. For total digestion, 0.30 g soil (fine particle < 2 mm) was accurately weighed into a teflon crucible. It was primarily digested with concentrated HCl (5 ml), and further digested with a mixed acid system of “HNO₃ (5 ml) + HF (4 ml) + HClO₄ (2 ml)”. Finally, the digestion solution was diluted with deionized water to a volume of 50 ml. The concentrations of Cd, Pb, Cu and Zn in solutions were detected by the flame atom absorption spectrophotometer (FAAS, ZEEnit700P, Analytik Jena, Germany) at the experiment center in the school of life science, Lanzhou University.

Heavy Metal Mobility in Soil Profile

To compare the mobility of heavy metals in soil pro-

file, the mobility index (*MI*) was calculated [14,15]. The formula is as follows:

$$MI = (C_{\text{topsoils}} - C_{\text{deep soils}}) / \Delta h \quad (1)$$

where C_{topsoils} and $C_{\text{deep soils}}$ are total contents (the sum of heavy metal concentrations in all four chemical fractions) in the topsoils and deep soils, respectively; Δh is the height difference. The lower the *MI* value, the stronger the heavy metal mobility is.

Statistical Analysis

Statistical analysis was made with SPSS16.0 software package (SPSS Inc., Chicago, Illinois, USA), and variation distributions of heavy metals in soil profile were constructed by OriginPro 8.0 software (Origin-Lab Inc., Hampton, Massachusetts, USA).

RESULTS AND DISCUSSION

Accuracy of the Modified BCR Method

To check the accuracy of the modified BCR method, the topsoils were chosen as standard materials which were subjected to both methods of modified BCR and total digestion. The recovery was calculated as follows [16]:

$$\text{Recovery (\%)} = (C_{F1} + C_{F2} + C_{F3} + C_{F4}) / C_T \times 100 \quad (2)$$

where C_{F1} , C_{F2} , C_{F3} and C_{F4} are heavy metal concentrations in F1, F2, F3 and F4, respectively; C_T is heavy metal content obtained from the total digestion.

The recovery in the present study is in the range of 74.51–139.3%, which agrees with the results of 75.53–136.5% obtained by [17]. This indicates that the method used in this study is reliable and repeatable.

Variation Distributions of Heavy Metals in Soil Profile

To determine the accurate soil depth that heavy metals have reached is difficult and costly, because it is generally far deeper than the actual sampling depth [14,15]. In the current study, the soils of 0–60 cm depth are taken into account. Variation distributions of heavy metals in each chemical fraction are shown in Figures 3 and 4. As shown, much higher concentrations and greater NRF proportions of heavy metals are found at S3 and S4 (the middle reaches of Dongdagou stream), while S2 and S1 (the downstream of Dongdagou stream) are relatively less polluted.

Cadmium

In general, Cd concentration in each chemical fraction arranges as follows: F1 > F2 > F3 > F4. At S1 and S2, Cd concentrations are low and change little with depth. However, at S3, S4 and S5, Cd levels in NRF decrease from the surface to 30-cm depth, and then remain stable. Surface enrichment of Cd may be due to the fact that exogenous Cd initially deposits in topsoils, and then sinks into deeper positions [16]. Pollution becomes increasingly slight along the depth gradient, and Cd concentrations in soils deeper than 40 cm are similar among all sampling sites, indicating that the distribution of heavy metals mainly depends on the soils itself in deep soils [18]. A similar vertical variation of Cd is also found in agricultural soils near a lead-acid battery factory in Baoding city (China) [13].

Compared to the background (0.116 mg kg⁻¹), Cd pollution in soils has reached at least 60-cm depth (deeper position was not considered in the current study), and the main pollution is found in the soils of 0–30 cm depth. High heavy metal concentrations in NRF reflect great bioavailability [7]. In the study area, Cd is the most labile metal pollutant which may be easily assimilated by biota.

Lead

In the soil profile at S1 and S2, Pb concentrations are relatively stable, while it decreases with depth at S3. Contrastingly, Pb displays distinct distribution pat-

terns at S4 and S5, where Pb levels in all fractions reach peak concentrations at the depth of 50-cm and 40-cm, for each. As shown, Pb concentrations in F1 are usually less than 20 mg kg⁻¹ (representing less than 10% of the total content), and Pb levels in F3 are slightly greater than those in F1. For F4, its proportions are nearly stable at all sites, occupying about 30%. Lead is mainly bound with the reducible fraction. Pb in F2 has an average concentration of 277.3 mg kg⁻¹ (about 47%) at S5, 210.3 mg kg⁻¹ (about 58%) at S4, and 163.4 mg kg⁻¹ (56%) at S3, respectively. With regard to S1 and S2, the proportions reach 49% and 33%, respectively.

The findings of previous reports also support our results that Pb is more likely to be enriched in F2 (i.e., the reducible fraction) as a consequence of combining with Fe-Mn oxides and hydroxides [8,19]. This suggests that Pb should be managed cautiously because of its potential bioavailability.

Copper

With few exceptions, Cu concentrations usually change little along the depth gradient at S1, S2 and S5, where it is mainly retained in F4 (more than 50% of total content). At S3 and S4, Cu concentrations in all fractions decrease from surface to 60-cm depth, whilst the proportions in F4 increase from 30–70%. Heavy metals in F4 are incorporated into aluminosilicate and unlikely to be released [18]. In the study area, dominant Cu presented in F4 indicates that it has limited bioavailability. Even so, both S3 and S4 show more than 60% and 143 mg kg⁻¹ of Cu in NRF in the soils of 0–20 cm depth, indicating a considerable potential risk. Besides, about 13% of the total Cu is presented in F3 at all sites, whereas only 3–10% of Cu is found in F1.

Zinc

Variation distribution of Zn in soil profile is similar among these five sampling sites: fluctuating little from surface to 20-cm depth, then decreasing dramatically (20–40 cm depth), and finally remaining stable at a low level in deep position (40–60 cm depth). The highest Zn concentration seems to be accumulated in F4, followed by F2 and F3, while Zn in F1 is very low. In the soils of 0–20 cm depth at S3 and S4, however, both the F1 concentrations of Zn are about 140 mg kg⁻¹ and account for more than 26% of the total content, comparable to those in F2. For other sites, the F1 proportions of Zn vary with depth within the range of 0–20%, while

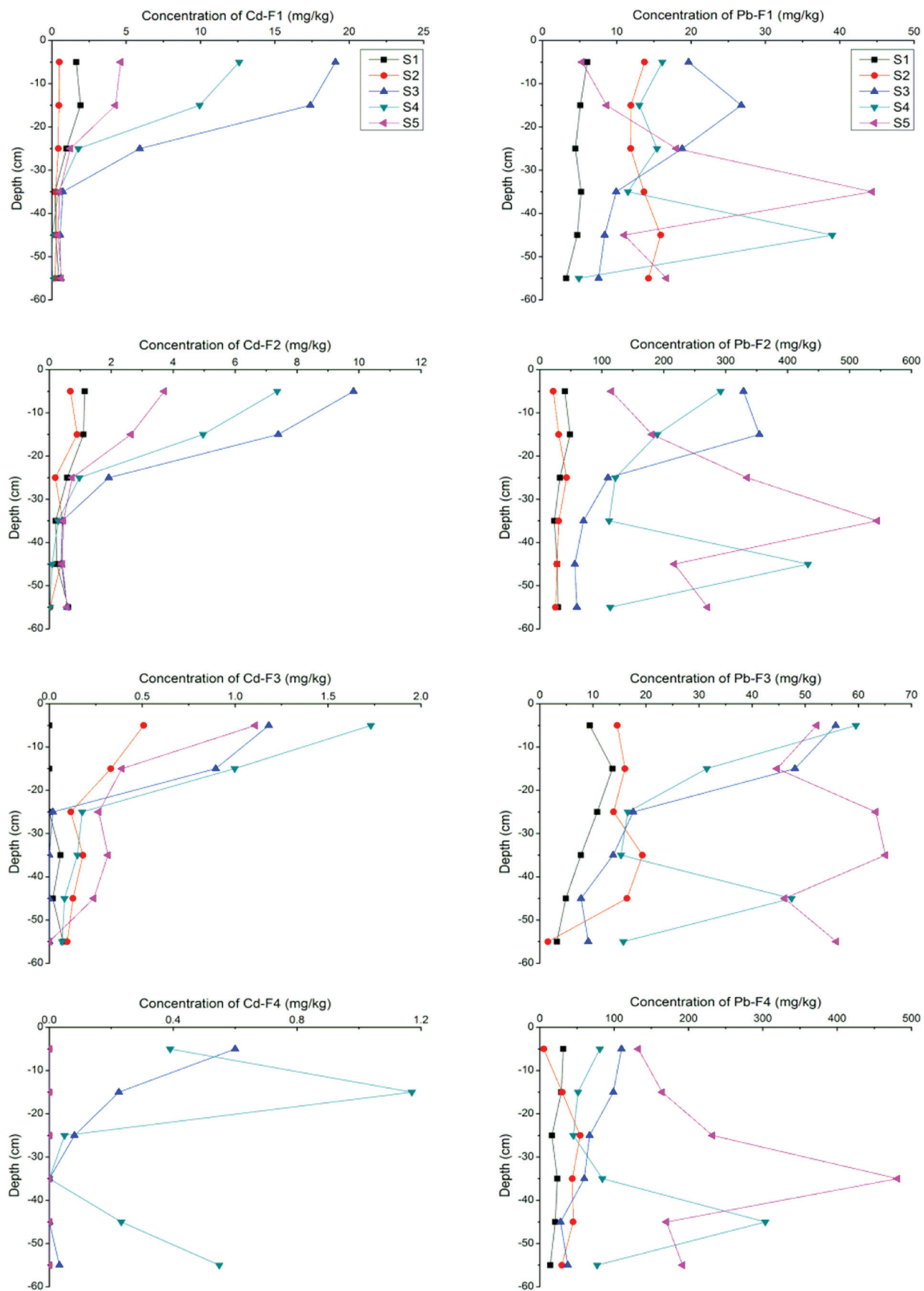


Figure 3. Variation distributions of Cd and Pb in each chemical fraction in soil profile of cornfields in the Dongdagou region.

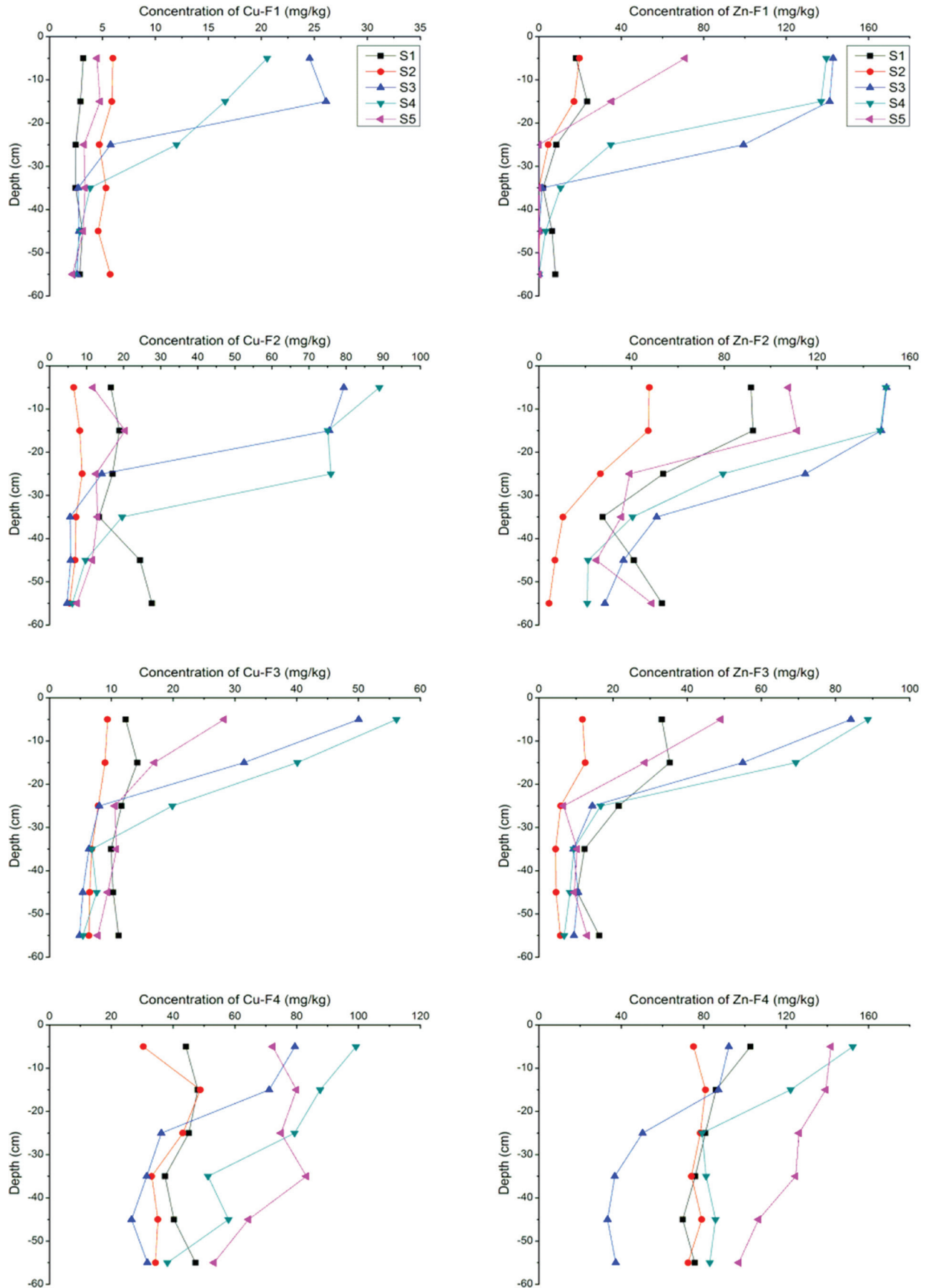


Figure 4. Variation distributions of Cu and Zn in each chemical fraction in soil profile of cornfields in the Dongdagou region.

Table 1. The Mobility Indexes of Heavy Metals in Soil Profile at All Sampling Sites.

	S1	S2	S3	S4	S5
Cd	0.03	0.02	0.58	0.43	0.16
Pb	0.75	—	8.00	4.73	—
Cu	—	0.01	3.79	4.25	0.92
Zn	1.85	1.43	7.88	8.39	4.22

—Abnormal vertical distribution of heavy metals is not considered.

F2 proportions are generally in the range of 20–40%, and F3 proportions are about 10%.

Heavy Metal Mobility in Soil Profile

The MI values for heavy metals roughly arrange in a decreasing order of Zn > Pb > Cu > Cd (Table 1). According to MI, Cd has the strongest mobility in the soil profile. Similar results are also found in other areas worldwide [14,15,20]. This is interpreted as the fact that Cd mainly exists in F1 which shows a high potential of exchangeability and mobility. However, the mobility of Cu at S2 is somehow stronger than Cd. Lead has stronger mobility than Zn, except for at S3. Overall, heavy metal mobility in the soil profile of cornfields in the Dongdagou region is in the order of Cd > Cu > Pb > Zn.

Once getting into the soils, soil properties (soil depth, pH and TOM, etc.) are important internal factors affecting heavy metal mobility in soil profile [15].

The relationships between soil properties and heavy metals in the soil profile of cornfields in the Dongdagou region are shown in Table 2. Heavy metal concentrations generally decrease with the deepening of soil depth [18], while TOM plays a fundamental role in retaining heavy metals [21]. In the present study, with few exceptions, strong and negative correlations are observed between soil depth and heavy metal concentrations (Table 2), while TOM is positively correlated with Cd, Zn, and partially with Cu and Pb ($p < 0.05$). Thus, increasing TOM content in soils may be an effective measure to prevent heavy metal from moving down in the soil profile. Comparatively, soil pH has a poor relationship with heavy metals, and significant correlation is only observed between soil pH and Pb at S2. This may be due to the narrow interval of soil pH value [22].

CONCLUSIONS

Heavy metal pollution in cornfield soils varies greatly with the sampling site and soil depth in the Dongdagou region, Baiyin city, Northwest China. The most polluted area is found at the middle reaches of Dongdagou stream, while the lightest pollution is at the downstream region. Cadmium is the priority pollutant in local cornfield soils. The analysis of chemical fractions indicates that Cd mainly in the acid soluble fraction has the greatest bioavailability, and Pb shows a high potential ecotoxicity in the reducible fraction,

Table 2. Relationships Between Soil Properties (Depth, TOM and pH) and Heavy Metal Concentrations in the Soil Profile of Cornfields in the Dongdagou Region.

Site	Soil Property	Depth	TOM	pH	Cd	Pb	Cu	Zn
S1	Depth	1			-0.813*	-0.891*	0.200	-0.819*
	TOM	-0.854*	1		0.968**	0.871*	0.251	0.983**
	pH	0.892*	-0.706	1	-0.703	-0.763	0.292	-0.648
S2	Depth	1			-0.903*	0.233	-0.445	-0.928**
	TOM	-0.896*	1		0.934**	-0.564	0.393	0.972**
	pH	0.300	-0.678	1	-0.569	0.892*	0.018	-0.534
S3	Depth	1			-0.906*	-0.903*	-0.878*	-0.947**
	TOM	-0.866*	1		0.965**	0.928**	0.973**	0.899*
	pH	0.040	0.201	1	-0.038	-0.169	-0.029	-0.118
S4	Depth	1			-0.882*	0.100	-0.967**	-0.917*
	TOM	-0.760	1		0.931**	0.327	0.803	0.900*
	pH	0.356	-0.083	1	-0.268	0.228	-0.361	-0.362
S5	Depth	1			-0.888*	0.319	-0.893*	-0.878*
	TOM	-0.846*	1		0.915*	-0.463	0.623	0.915*
	pH	-0.721	0.397	1	0.580	-0.216	0.605	0.566

*Correlation is significant at the 0.05 level (2-tailed).

**Correlation is significant at the 0.01 level (2-tailed).

while dominant Cu and Zn are retained in the residual fraction. Heavy metal concentrations generally decrease with the deepening of soil depth, and then remain stable at relatively low levels in deep position. Total organic matter plays a fundamental role in retaining heavy metal mobility in soil profile. Heavy metal pollution in soil profile of local cornfield soils has reached the depth of 60 cm, and the main pollution is found in the soils of 0–30 cm depth. We suggest that further pollution prevention and control in the Dongdagou region should pay specially attentions to Cd in the soils of 0–30 cm depth.

ACKNOWLEDGEMENTS

This work was financially supported by the National Natural Science Foundation of China (Grant No. 41171391). The first author was particularly grateful to Dr. Jin Baocheng and Ms. Du Ping for their technical assistances and writing help, respectively.

REFERENCES

1. Lu Y, Song S, Wang R *et al.* Impacts of soil and water pollution on food safety and health risks in China. *Environ Int*, 77, 2015. 5–15. <http://dx.doi.org/10.1016/j.envint.2014.12.010>
2. Bai J, Xiao R, Gong A *et al.* Assessment of heavy metal contamination of surface soils from typical paddy terrace wetlands on the Yunnan Plateau of China. *Phys Chem Earth* Vol. 36 No. 9. 2011. 447–450. <http://dx.doi.org/10.1016/j.pce.2010.03.025>
3. MEP (Ministry of Environment Protection of the People's Republic of China). Report on the state of the Environment in China. 2000. (In Chinese)
4. MEP&MLR (Ministry of Environment Protection and Ministry of Land Resources of the People's Republic of China). Nationwide Soil Pollution Survey Report. 2014. http://www.zhb.gov.cn/gkml/hbb/qt/201404/t20140417_270670.htm. (In Chinese)
5. Nan ZR, Zhao CY. Heavy metal concentrations in gray calcareous soils of Baiyin region, Gansu province, PR China. *Water Air Soil Poll Vol. 118*, No. 1. 2000. 131–142. <http://dx.doi.org/10.1023/A:1005135618750>
6. Si WT, Ji WH, Yang F *et al.* The function of constructed wetland in reducing the risk of heavy metals on human health. *Environ Monit Assess*, Vol. 118 No. 1. 2011. 531–537. <http://dx.doi.org/10.1007/s10661-010-1847-z>
7. Zhong XL, Zhou SL, Zhu Q *et al.* Fraction distribution and bioavailability of soil heavy metals in the Yangtze River Delta—A case study of Kunshan City in Jiangsu Province, China. *J Hazard Mater*, 198. 2011. 13–21. <http://dx.doi.org/10.1016/j.jhazmat.2011.10.003>
8. Jiang M, Zeng GM, Zhang C *et al.* Assessment of heavy metal contamination in the surrounding soils and surface sediments in Xiawangang River, Qingshitang District. *PLoS One* Vol. 8 No. 8. 2013. e71176. <http://dx.doi.org/10.1371/journal.pone.0071176>
9. Tessier A, Campbell PG, Bisson M. Sequential extraction procedure for the speciation of particulate trace metals. *Anal Chem* Vol. 51 No. 7. 1979. 844–851. <http://dx.doi.org/10.1021/ac50043a017>
10. Ure A, Quevauviller P, Muntau H *et al.* Speciation of heavy metals in soils and sediments. An account of the improvement and harmonization of extraction techniques undertaken under the auspices of the BCR of the Commission of the European Communities. *Int J of Environ An Ch* Vol. 51 No. 1. 1993. 135–151. <http://dx.doi.org/10.1080/03067319308027619>
11. Walter I, Martínez F, Cala V. Heavy metal speciation and phytotoxic effects of three representative sewage sludges for agricultural uses. *Environ Pollut* Vol. 139 No. 3. 2006. 507–514. <http://dx.doi.org/10.1016/j.envpol.2005.05.020>
12. Rodríguez L, Ruiz E, Alonso-Azcárate J *et al.* Heavy metal distribution and chemical speciation in tailings and soils around a Pb–Zn mine in Spain. *J Environ Manage* Vol. 90 No. 2. 2009. 1106–1116. <http://dx.doi.org/10.1016/j.jenvman.2008.04.007>
13. Liu GN, Yu YJ, Hou J *et al.* An ecological risk assessment of heavy metal pollution of the agricultural ecosystem near a lead-acid battery factory. *Ecol Indic* 47. 2014. 210–218. <http://dx.doi.org/10.1016/j.ecolind.2014.04.040>
14. Sterckeman T, Douay F, Proix N *et al.* Vertical distribution of Cd, Pb and Zn in soils near smelters in the North of France. *Environ Pollut* Vol. 107 No. 3. 2000. 377–389. [http://dx.doi.org/10.1016/S0269-7491\(99\)00165-7](http://dx.doi.org/10.1016/S0269-7491(99)00165-7)
15. Liu GN, Xue W, Tao L *et al.* Vertical distribution and mobility of heavy metals in agricultural soils along Jishui river affected by mining in Jiangxi Province, China. *CLEAN—Soil Air Water* Vol. 42 No. 10. 2014. 1450–1456. <http://dx.doi.org/10.1002/clen.201300668>
16. Yuan CG, Shi JB, He B *et al.* Speciation of heavy metals in marine sediments from the East China Sea by ICP-MS with sequential extraction. *Environ Int* Vol. 30 No. 6. 2004. 769–783. <http://dx.doi.org/10.1016/j.envint.2004.01.001>
17. Sow AY, Ismail A, Zulkifli SZ. Geofractionation of heavy metals and application of indices for pollution prediction in paddy field soil of Tumpat, Malaysia. *Environ Sci Pollut R* Vol. 20 No. 12. 2013. 8964–8973. <http://dx.doi.org/10.1007/s11356-013-1857-9>
18. Nemati K, Bakar NKA, Abas MR *et al.* Speciation of heavy metals by modified BCR sequential extraction procedure in different depths of sediments from Sungai Buloh, Selangor, Malaysia. *J Hazard Mater* Vol. 192 No. 1. 2011. 402–410. <http://dx.doi.org/10.1016/j.jhazmat.2011.05.039>
19. He ZL, Yang XE, Stoffella PJ. Trace elements in agroecosystems and impacts on the environment. *J Trace Elem Med Bio* Vol. 19 No. 2. 2005. 125–140. <http://dx.doi.org/10.1016/j.jtemb.2005.02.010>
20. Nannoni F, Protano G, Riccobono F. Fractionation and geochemical mobility of heavy elements in soils of a mining area in northern Kosovo. *Geoderma* Vol. 161 No. 1. 2011. 63–73. <http://dx.doi.org/10.1016/j.geoderma.2010.12.008>
21. Bhuiyan MA, Parvez L, Islam M *et al.* Heavy metal pollution of coal mine-affected agricultural soils in the northern part of Bangladesh. *J Hazard Mater* Vol. 173 No. 1. 2010. 384–392. <http://dx.doi.org/10.1016/j.jhazmat.2009.08.085>
22. Micó C, Recatalá L, Peris M *et al.* Assessing heavy metal sources in agricultural soils of an European Mediterranean area by multivariate analysis. *Chemosphere* Vol. 65 No. 5. 2006. 863–872. <http://dx.doi.org/10.1016/j.chemosphere.2006.03.016>

The Input and Characteristics of Exotic Uranium in the Soils Around a Uranium Waste Rock Dump in South China

ZHI-GANG FENG^{1,*}, XIAO-LONG WANG^{1,2}, RONG CHEN^{1,2}, XIAN-ZHE DUAN¹, QIANG MA¹ and SHI-LI HAN¹

¹*School of Nuclear Resource Engineering, University of South China, Hengyang 421001, China*

²*Key Discipline Laboratory for National Defense for Biotechnology in Uranium and Hydrometallurgy, University of South China, Hengyang 421001, China*

ABSTRACT: Five soil profiles were sampled around a uranium waste rock dump in South China, which included two unpolluted and three potentially uranium-polluted profiles. Through the comparison of the uranium distribution characteristics and the analysis of the uranium chemical forms of these profiles, the following conclusions can be drawn: (1) significant uranium pollution to the surrounding soils was caused by the dump, and the average uranium in these soils, such as the profiles WP1, WP2 and WP3, was 633.6, 9 and 2.7 times more enriched than the background value; (2) the exotic uranium, which was preferentially aggregated in the upper layer of the soils near the pollution source, would be gradually precipitated in the lower layer of the soils away from the pollution source; (3) the input flux of the exotic uranium of each chemical form would be larger in the soils closer to the pollution source.

INTRODUCTION

URANIUM, which is a toxic and radioactive element, can cause potential threats to human health and ecological security when it is accumulated in the supergene environment, in which the soil is an important uranium-hosted medium [1–3]. Generally, the uranium anomalies in soils are mainly considered as a result of human activities, e.g., nuclear test, mining, phosphate fertilizer application and nuclear fuel cycle [1–4]. The uranium pollution of the soils in uranium mining and metallurgy regions has attracted considerable interests [5–8]. In China, there are about 200 sites for the storage of waste rocks and tailings, with the total weight of approximately 58 million tons, which were produced by uranium mining operation [9], and the regions around such sites have become the main targets of recent remediation of uranium polluted soils [9–10]. However, there is still lack of studies on the quantitative assessment and chemical forms of the exotic uranium in soils, which is an important basis for objectively assessing the soil quality and effectively remediating uranium polluted soils.

In this study, we reported the uranium distribution characteristics of five soil profiles around a waste rock

dump of a granite-type uranium mine in South China. On this basis, we quantitatively estimated the input flux of exotic uranium and its variation along the depth of the uranium polluted soils and along the downstream runoff direction of the waste rock dump, and characterized the chemical forms of exotic uranium by sequential chemical extraction procedure.

MATERIALS AND METHODS

Sampling

The studied region is located in a granite-type uranium mine that was exploited underground in northern Guangdong Province, South China. Large amounts of waste rocks produced by mining operation were open-air stacked in a valley with gentle side slopes in the mine area, and thus became a waste rock dump with an area of about 3000 km² and a mean thickness of 20 m. This dump, whose waste rocks have uranium contents of 1-2 orders of magnitude higher than bedrocks in this region, is a potential pollution source of uranium. In this study, five soil profiles were collected as follows: two soil profiles (i.e., BP1 and BP2), which were regarded as the profiles unpolluted by uranium, were located in the upstream of the dump, and were 20 m and 10 m away from the dump, respectively. The other three soil profiles (i.e., WP1, WP2 and WP3), which

*Author to whom correspondence should be addressed.
Email: feng_zg@sina.com; Tel. +86 131 7034 0655

were located in the downstream and were 50 m, 100 m and 180 m away from the dump, respectively, were considered as the profiles potentially polluted by uranium. Each profile, which grew on granites, was a natural occurrence generally with a thickness of a few tens of centimeters. The bottom-up notching of these profiles was sampled, and each sampling length was 10 cm or 5 cm.

Sequential Chemical Extraction

A modified sequential chemical extraction procedure was adopted, which was based on previous studies on the analysis of the chemical forms of radionuclides in soils and sediments [11]. In this procedure, six chemical forms (i.e., six fractions) were obtained. They were exchangeable (including water-soluble) (Fraction I), associated with carbonates (Fraction II), co-precipitated with amorphous ferromanganese oxyhydroxides (Fraction III), associated with crystalline ferromanganese oxyhydroxides (Fraction IV), organic matter-bound (Fraction V) and associated with residue phases (Fraction VI), respectively.

Measurement Methods

The trace elements of the bulk samples were measured by ELAN DRC-e quadrupole inductively coupled plasma mass spectrometer (Q-ICP-MS) at the State Key Laboratory of Ore Deposit Geochemistry, Chinese Academy of Sciences. The analytical accuracies monitored by the two soil standards (GSS-4 and GSS-6) showed that the relative deviations between the measurements and the recommended values of Zr and Hf were < 15% and that of uranium was < 10%, respectively. Uranium of various chemical forms in the soils was analyzed using a WGJ-III type trace uranium analyzer at the University of South China, with a detection limit of 0.02 ng/mL, and a relative deviation < 5% controlled by uranium standard solution. All the reagents used in this study were analytical grade.

RESULTS AND DISCUSSION

Homogeneity Test of the Soil Parent Materials

During weathering of rocks, both Zr and Hf are co-variant and considerably inert elements [12–13]. All the Zr-Hf correlation diagrams of the samples in each soil profile showed good linear relationships (Table 1 and Figure 1), indicating that the profiles were produced by weathering of homogeneous granites.

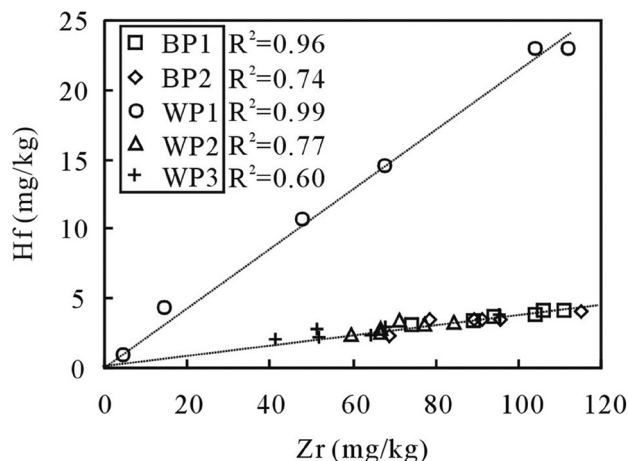


Figure 1. The correlation diagrams between Zr and Hf of the five soil profiles. The contents of Zr in the profile WP1 were expressed as $Zr \times 10^{-1}$.

Uranium Distribution Characteristics in the Soil Profiles

The uranium distribution characteristics in the soil profiles were determined. The uranium contents of BP1 and BP2 were 7.95 mg/kg and 7.32 mg/kg on average (i.e., sample length-weighted average value except bedrock, hereafter), respectively, which displayed no obvious variation in depth and were close to each other. In addition, the uranium contents of the bedrocks (i.e. granites) of the five soil profiles generated by weathering of homogeneous parent rocks were relatively uniform, ranging from 10.2 mg/kg to 12.9 mg/kg (Table 1 and Figure 2). These profiles, whose distance from the bedrock surface were ≤ 45 cm, were weakly

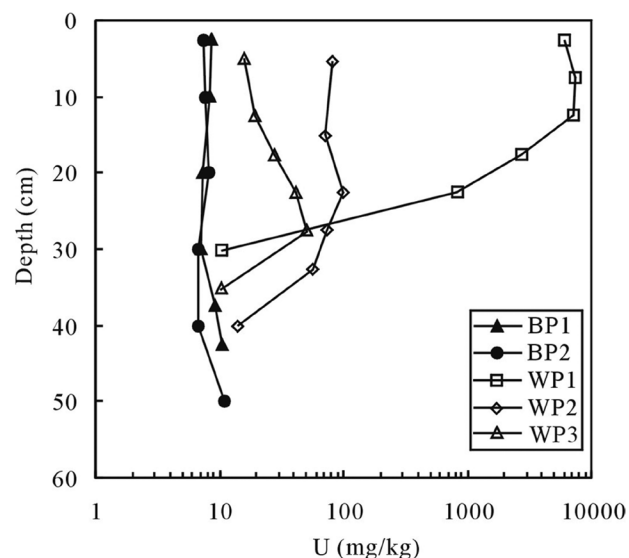


Figure 2. Variation of uranium contents in the five soil profiles along the depths.

Table 1. The Contents (mg/kg) of the Elements U, Zr and Hf in the Five Soil Profiles Studied in Depth.

Sample No.*	Depth (cm)	Zr	Hf	U	Sample No.*	Depth (cm)	Zr	Hf	U
BP1-T5	0~5	94.2	3.73	8.72	WP1-T2	15~20	476	10.6	2730
BP1-T4	5~15	106	4.13	8.35	WP1-T1	20~25	142	4.24	820
BP1-T3	15~25	74.4	3.09	7.41	WP1-Y	25~35	44.5	0.92	10.2
BP1-T2	25~35	89.2	3.4	6.99	WP2-T5	0~10	77.6	3.03	80.6
BP1-T1	35~40	104	3.92	9.34	WP2-T4	10~20	59.6	2.35	71.6
BP1-Y	40~45	111	4.1	10.5	WP2-T3	20~25	84.8	3.2	99.2
BP2-T5	0~5	95.8	3.51	7.46	WP2-T2	25~30	66.7	2.52	74.8
BP2-T4	5~15	115	4.12	7.66	WP2-T1	30~35	71.3	3.32	56.1
BP2-T3	15~25	89.4	3.45	8.15	WP2-Y	35~45	66.6	2.86	12.9
BP2-T2	25~35	91	3.55	6.73	WP3-T5	0~10	41.5	2.02	15.6
BP2-T1	35~45	78.4	3.56	6.68	WP3-T4	10~15	67.8	3.01	19
BP2-Y	45~55	68.7	2.36	11.2	WP3-T3	15~20	51.4	2.87	27.8
WP1-T5	0~5	675	14.5	6010	WP3-T2	20~25	95.6	3.81	41.1
WP1-T4	5~10	1120	23	7420	WP3-T1	25~30	52	2.28	49.5
WP1-T3	10~15	1040	23	7260	WP3-Y	30~40	64.5	2.32	10.4

*BP1-Y, BP2-Y, WP1-Y, WP2-Y and WP3-Y stand for the bedrocks of the profiles BP1, BP2, WP1, WP2 and WP3, respectively; BP1-T1~BP1-T5, BP2-T1~BP2-T5, WP1-T1~WP1-T5, WP2-T1~WP2-T5 and WP3-T1~WP3-T5 denote the soil samples of the profiles BP1, BP2, WP1, WP2 and WP3, respectively.

weathered and similar to each other in pedogenesis features, so the distribution characteristics of the uranium in BP1 and BP2 could reflect the background condition of the soils in the region.

Concerning WP1, WP2 and WP3, their uranium contents (excluding the bedrocks) were 820–7420 mg/kg, 56.1–99.2 mg/kg and 15.6–49.5 mg/kg, respectively, with average values of 4848 mg/kg, 76.36 mg/kg and 28.1 mg/kg, respectively, which were respectively 633.6, 9 and 2.7 times higher than the average uranium content (i.e., 7.64 mg/kg) of BP1 and BP2. This indicated that these profiles underwent significant uranium pollution. Moreover, the soil closer to the pollution source was more severely polluted by uranium.

Input of Exotic Uranium in the Soils

Assuming that the average uranium content of BP1 and BP2 is regarded as the background value of uranium in the studied soils, excess uranium of the profiles WP1, WP2 and WP3 relative to the background value was attributed to the input of exotic uranium. The uranium contents of WP1, WP2 and WP3 at different depths were higher than those of BP1 and BP2 (Figure 2), indicating that there is an input of exotic uranium in their whole profiles. The input fluxes of uranium of WP1, WP2 and WP3 were 4840.36 mg/kg, 68.72 mg/kg and 20.46 mg/kg, respectively, which were calculated by subtracting the background value from the average uranium content of the soil profiles. These results indicated that the soil profile closer to the waste

rock dump along its downstream runoff direction had a larger input flux of exotic uranium. In addition, in the soil profile closer to the dump, a larger amount of exotic uranium was mainly aggregated in the upper layer (e.g., WP1), while the exotic uranium was gradually precipitated in the lower layer (e.g., WP3) when the profile was away from the dump.

Chemical Forms of Uranium in the Soils

The uranium contents of various chemical forms in the profiles BP2, WP1, WP2 and WP3 were listed in Table 2. The absolute values of the deviations between the total uranium contents of all chemical forms and the bulk sample were < 10% for most samples, and 10–20% for the rest samples, indicating that analytical results of the sequential chemical extraction of uranium were reliable.

The uranium of each chemical form in WP1, WP2, and WP3 was more enriched than that of BP2 at different depths, with an exception of the Fraction I of WP3, which was below the detection limit (Figure 3). This indicated that uranium was introduced to the whole profiles from the pollution source. In addition, the uranium of each chemical form of BP2 was very low (< 5 mg/kg) and even cannot be detected (e.g., Fraction I and Fraction IV), so the characteristics of uranium distribution of various chemical forms in WP1, WP2 and WP3 might reflect the variation trends of the uranium pollution degree. Concerning Fraction I [Figure 3(a)], its uranium contents in WP1 and WP2 showed

Table 2. The Uranium Contents (mg/kg) of Various Chemical Forms in the Four Soil Profiles (i.e. BP2, WP1, WP2 and WP3) and Their Deviations (%) to the Analytical Results of Bulk Samples.

Sample No.*	Fraction						Sun of I to VI	Deviation**
	I	II	III	IV	V	VI		
BP2-T5	–	2.14	0.9	–	2.04	1.65	6.73	–9.79
BP2-T4	–	1.9	0.39	–	2.88	1.65	6.82	–10.97
BP2-T3	–	4.93	0.19	–	2.43	1.4	8.95	9.82
BP2-T2	–	2	0.16	–	2.01	1.89	6.06	–9.96
BP2-T1	–	2.05	0.35	–	2.16	2.35	6.91	3.44
BP2-a	–	2.66	0.34	–	2.33	1.8		
WP1-T5	89.47	1642.81	374.29	34.3	3914.41	11.03	6066.31	0.94
WP1-T4	354.44	2935.47	1058.86	56.67	3616.52	19.83	8041.79	8.38
WP1-T3	134.6	2275.79	493.54	32.4	3130.76	21.94	6089.03	–16.13
WP1-T2	15.97	1447.25	140.23	17.97	833.42	4.89	2459.73	–9.9
WP1-T1	2.24	450.61	73.86	15.71	335.25	2.54	880.21	7.34
WP1-a	119.34	1750.39	428.16	31.41	2366.07	12.05		
WP2-T5	11.11	32.48	4.97	0.25	23.39	2.98	75.18	–6.72
WP2-T4	8.47	39.4	4.43	0.21	23.36	7.11	82.98	15.89
WP2-T3	4.73	57.74	5.77	0.34	31.5	7.09	107.17	8.03
WP2-T2	3.66	48.62	4.2	0.36	21.82	3.63	82.29	10.01
WP2-T1	0.12	42.74	3.75	0.19	14.92	2.74	64.46	14.9
WP2-a	6.81	41.84	4.65	0.26	23.11	4.81		
WP3-T5	–	7.94	0.92	–	3.28	2.55	14.69	–5.83
WP3-T4	–	10.94	0.99	0.11	4.11	2.67	18.82	–0.95
WP3-T3	–	16.42	1.46	0.18	5.52	1.64	25.22	–9.28
WP3-T2	–	29.18	2	0.24	10.64	3.19	45.25	10.1
WP3-T1	–	35.29	2.3	0.25	13.18	3.75	54.77	10.65
WP3-a	–	17.95	1.43	0.13	6.67	2.73		

*Sample No. is the same as that shown in Table 1 except BP2-a, WP1-a, WP2-a and WP3-a, which denote the sample length-weighted average values of the profiles BP2, WP1, WP2 and WP3, respectively.

**Deviation = [(Sum of I to VI) – (bulk sample)]/(bulk sample)×100%, where the analytical result of the bulk sample is shown in Table 1. In addition, in the data of the table, “–” denotes below the detection limit.

increasing tendencies from the bottom to the top; the uranium contents of Fractions II–VI [Figures 3(b)–3(f)] displayed increasing tendency in WP1, but no obvious change in WP2 and decreasing tendency in WP3 from the bottom to the top. On the other hand, the input fluxes of various chemical forms of uranium in WP1, WP2 and WP3, in which Fraction II and Fraction V were more prominent, showed the same trend as WP1 > WP2 > WP3 (Figure 4).

Uranium Pollution Mechanism in the Soils

The above results demonstrated that exotic uranium could exist in all the six chemical forms in the soils polluted by uranium, implying that the transfer of uranium from the pollution source into the surrounding soils might be mainly in three ways including water-soluble, colloidal and clastic states. In these states, the uranium transferred into the soils in water-soluble state

might occur in Fractions I–II through direct precipitation or redistribution; the uranium into the soils in colloidal state might occur in Fraction III and Fraction V by coagulation; the uranium into the soils in clastic state might occur in Fraction VI. For the exotic uranium of Fraction IV in the soils, it might be mainly derived from the crystallization of Fraction III. In addition, the input fluxes of the exotic uranium that was associated with carbonates (Fraction II) and organic matter-bound (Fraction V) were obvious larger than those of the other Fractions (Figure 4), implying that the uranium might be transferred preferentially into water-soluble state and organic colloid from the pollution source.

CONCLUSIONS

1. The uranium waste rock dump generated significant uranium pollution to the surrounding soils,

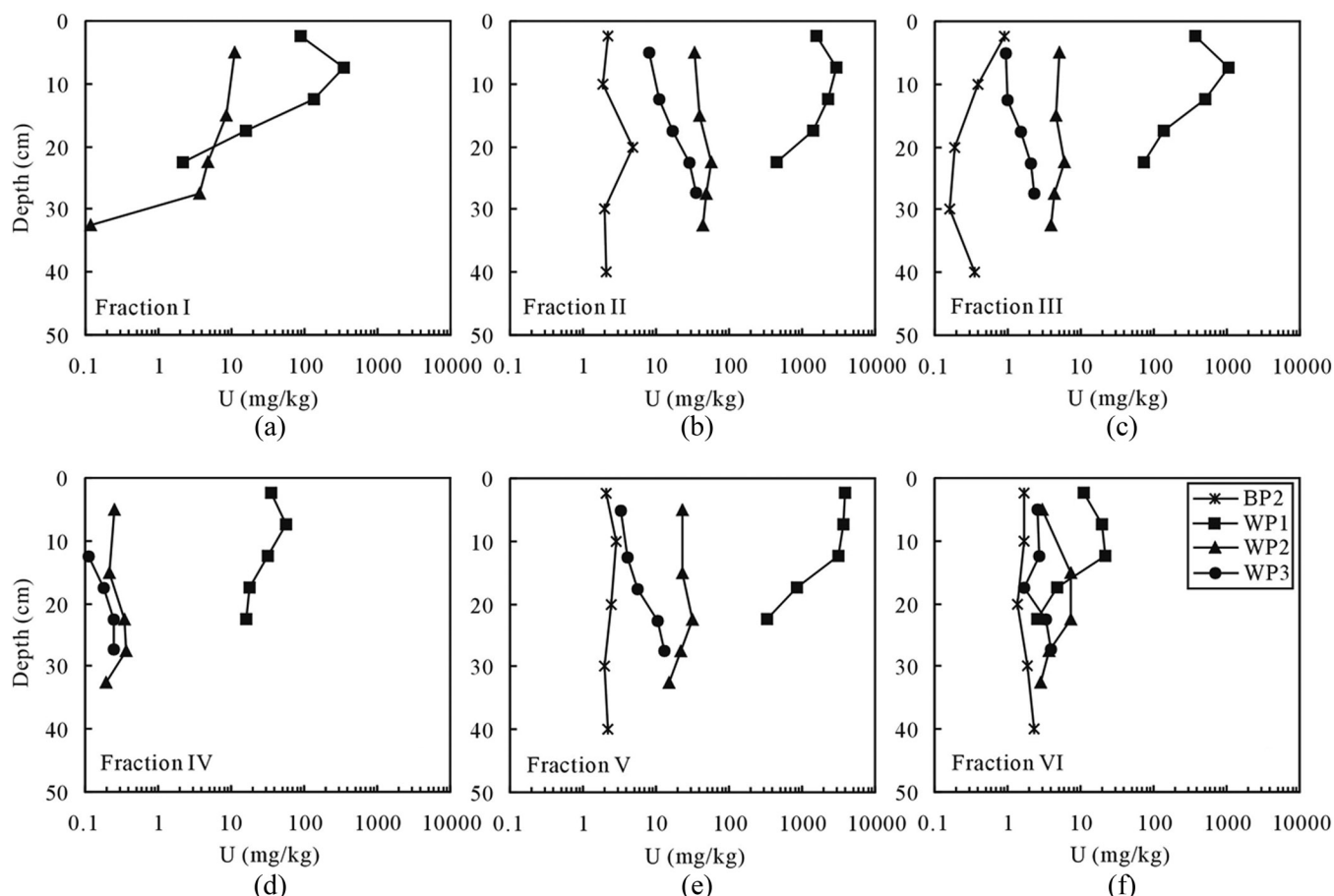


Figure 3. The content variation of various chemical forms of uranium in the profiles BP2, WP1, WP2 and WP3 along the depths. (a) exchangeable (including water-soluble); (b) associated with carbonates; (c) co-precipitated with amorphous ferromanganese oxyhydroxides; (d) associated with crystalline ferromanganese oxyhydroxides; (e) organic matter-bound; (f) associated with residue phases.

and the soils closer to the pollution source had more severe uranium pollution.

2. The exotic uranium was preferentially aggregated in the upper layer of the soils near the pollution source, while it would be gradually precipitated in the lower layer of the soils away from the pollution source.
3. The input flux of exotic uranium of each chemical

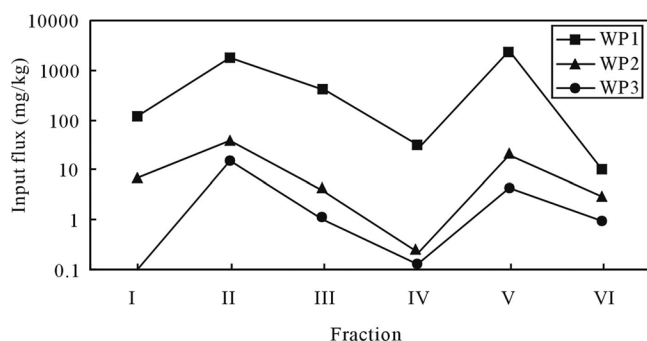


Figure 4. The input fluxes of various chemical forms of uranium in the profiles WP1, WP2 and WP3.

form would be larger in the soils closer to the pollution source.

ACKNOWLEDGEMENTS

This work was supported by the National Natural Science Foundation of China (NSFC, grant no. 40973070, 41373115) and Zhengxiang Scholar Program of the University of South China.

REFERENCES

1. Abed, A. M., and Sadaqah, R. M., "Enrichment of uranium in the uppermost Al-Hisa Phosphorite Formation, Eshidiyya basin, southern Jordan", *Journal of African Earth Sciences*, Vol. 77, 2013, pp. 31–40. <http://dx.doi.org/10.1016/j.jafrearsci.2012.09.009>
2. El-Taher, A., and Althoyaib, S. S., "Natural radioactivity levels and heavy metals in chemical and organic fertilizers used in Kingdom of Saudi Arabia", *Applied Radiation and Isotopes*, Vol. 70, 2012, pp. 290–295. <http://dx.doi.org/10.1016/j.apradiso.2011.08.010>
3. Mortvedt, J. J., "Plant and soil relationships of uranium and thorium decay series radionuclides—A review", *Journal of Environmental Quality*, Vol. 23, 1994, pp. 643–650. <http://dx.doi.org/10.2134/jeq1994.00472425002300040004x>

4. Bagherifam, S., Lakzian, A., Ahmadi, S. J., *et al.*, “Uranium removal from aqueous solutions by wood powder and wheat straw”, *Journal of Radioanalytical and Nuclear Chemistry*, Vol. 283, 2010, pp. 289–296. <http://dx.doi.org/10.1007/s10967-009-0348-4>
5. Gavrilescu, M., Pavel, L. V., and Cretescu, I., “Characterization and remediation of soils contaminated with uranium”, *Journal of Hazardous Materials*, Vol. 163, 2009, pp. 475–510. <http://dx.doi.org/10.1016/j.jhazmat.2008.07.103>
6. Carvalho, I. G., Cidu, R., Fanfani, L., *et al.*, “Environmental impact of uranium mining and ore processing in the Lagoa Real District, Bahia, Brazil”, *Environmental Science & Technology*, Vol. 39, 2005, 8646–8652. <http://dx.doi.org/10.1021/es0505494>
7. Wang, L., Luo, X., Peng, F., *et al.*, “Changes of microbial activity and functional diversity of contaminated soil microbes community in uranium tailings”, *Environmental Science & Technology*, Vol. 37, No. 3, 2014, pp. 25–31. (in Chinese)
8. Du, Y., Zhu, X. J., Gao, B., *et al.*, “Distribution characteristics of uranium in typical sites of tailings pond in uranium mine”, *Nonferrous Metals (Mine Section)*, Vol. 66, No. 1, 2014, pp. 5–9. (in Chinese)
9. Zha, Z., Wang, D., Feng, X., *et al.*, “Evaluation on remediation of uranium contaminated soils by brassica mustard”, *Chemical Research and Application*, Vol. 26, No. 2, 2014, pp. 223–229. (in Chinese)
10. Sun, S. Y., and Zhou, Q., “Ecological effect and bioremediation of radioactive contaminated soils”, *Chinese Journal of Eco-Agriculture*, Vol. 16, No. 2, 2008, pp. 523–528. (in Chinese). <http://dx.doi.org/10.3724/SP.J.1011.2008.00523>
11. Feng, Z. G., Zhang, B., Duan, X. Z., *et al.*, “Uranium mobility in waste materials generated by uranium mining and hydrometallurgy: implications for its in-situ immobilization”, *Journal of Residuals Science & Technology*, Vol. 12, No. Suppl. 1, 2015, pp. S159–S163.
12. Nesbitt, H. W., Markovics, G., and Price, R. C., “Chemical processes affecting alkalis and alkaline earths during continental weathering”, *Geochimica et Cosmochimica Acta*, Vol. 44, 1980, pp. 1659–1666. [http://dx.doi.org/10.1016/0016-7037\(80\)90218-5](http://dx.doi.org/10.1016/0016-7037(80)90218-5)
13. Nesbitt, H. W., and Markovics, G., “Weathering of granodioritic crust, long-term storage of elements in weathering profiles, and petrogenesis of siliciclastic sediments”, *Geochimica et Cosmochimica Acta*, Vol. 61, 1997, pp. 1653–1670. [http://dx.doi.org/10.1016/S0016-7037\(97\)00031-8](http://dx.doi.org/10.1016/S0016-7037(97)00031-8)

Influence of Temperature and pH on Methanogenic Digestion in Two-phase Anaerobic Co-digestion of Pig Manure with Maize Straw

LEI ZHANG¹, KEQIANG ZHANG², WENXUAN GAO², ZHONGWEI ZHAI², JUNFENG LIANG², LIANZHU DU^{2,*}
and XINMEI FENG³

¹*School of Environmental Science and Engineering, Tianjin University, Tianjin 300191, China*

²*Agro-Environmental Protection Institute, Ministry of Agriculture, Tianjin 300191, China*

³*JTI-Swedish Institute of Agricultural and Environmental Engineering, Uppsala, SE-75007, Sweden*

ABSTRACT: The objective of this work was to investigate the performance and archaeal community of methanogenic digester under different temperatures (35°C, 55°C) and pH values (6.5, 7.0, 7.5, 8.0 and 8.5) in two-phase anaerobic digestion of pig manure and maize straw. The specific CH₄ yields decreased by 22.6%, 60.0% and 94.1% for pH 7.5, 8.0 and 8.5 compared with pH 7.0 (277 N mL·g⁻¹ COD_{add}) at 35°C, and decreased by 31.6%, 70.9% and 95.0% compared with pH 7.0 (253 N mL·g⁻¹ COD_{add}) at 55°C. The methane productions of mesophilic digestion at five pH levels were 13.6%, 9.7%, 24.1%, 50.8% and 30.0% higher than that of thermophilic digestion. Terminal restriction fragment length polymorphism (T-RFLP) analyses combined with clone library indicated that Methanosaeta and Methanosarcina were the dominant genus at 35°C and 55°C, respectively, and the relative abundance decreased significantly with the pH increasing from 7.5 to 8.5.

INTRODUCTION

ANAEROBIC DIGESTION (AD) process has been reported more and more for treating organic wastes and produce renewable energy. Wide range of organic waste including municipal, agricultural, and food industry wastes were used as feedstock for AD [1–3].

The production of plant residual and breeding waste were in large quantities in China. The crop straw and manure productions are more than 700 million and 3.0 billion tons, respectively [4]. These wastes caused serious environmental problems, because much of them were discharged without any treatment and resulted in organic pollution and microbial loads increasing. The energy production from these agriculture wastes by means of AD was a valuable alternative for fossil energy resources, especially in rural area [4]. However, conventional anaerobic digestion exhibits some disadvantages related to feedstock characteristics, such as the imbalance of C/N [5], the inhibition of VFAs in rich carbon waste digestion [6] due to the rapid acidification, drop of pH and succedent inhibition of metha-

nogens activity. For the feedstock rich of nitrogen, ammonia inhibition which induced by high ammonia concentrations were considered to be destructive for AD [7]. What's more, the pollution induced by large quantity effluent from low solid digestion processes was very common. Thus, the application of the conventional AD is limited. Many processes have been applied to upgrade AD in order to overcome the limitations above-mentioned.

Co-digestion of different substrates has become more and more popular since it can increase the biogas production and improve the stability which was necessary for the process. Many researches have focused on co-digestion of different wastes [8–10]. Compared with manure alone, the feedstock including 30% of energy crops increased methane production by 16–65% per digester volume [8]. Furthermore, two-phase AD has obvious advantages over the single phase AD since they (1) screening and enrichment of completely different microbial in each phase, (2) protection methanogens from substantial VFAs, and (3) reduce the amount of effluent through the recycling of methanogenic effluent to solid feedstock in acidogenic digestion [11,12].

In AD, no matter single or two-phase digestion,

*Author to whom correspondence should be addressed.
Email: dulianzhu99@163.com, Tel.: +86 22 23616673

many factors influence the performance of the process, among which temperature and pH value are two important ones. Some researches showed that the thermophilic temperature was favorable for AD compared with mesophilic process, especially for the co-digestion process [13–15]. Compared with 35°C, anaerobic digestion of livestock manure at 55°C showed a kinetic advantage [16]. Meanwhile, many studies revealed the influence of pH on AD, especially on ammonia inhibition in the digestion for nitrogen-rich feedstock [13,17]. Although the influence of pH and temperature on AD has been studied widely, the relevant researches on methanogenic digestion in two-phase anaerobic digestion, especially in co-digestion of pig manure with maize straw has not been reported.

The aim of this work was to investigate the influence of temperature and pH values on methanogenic digestion of effluent from acidification digester in laboratory scale. In addition, their influence on archaeal community structure was also explored.

MATERIAL AND METHODS

Design and Operation of Semi-continuous Laboratory Scale Reactors

The solid acidogenic fermentation reactor of two-phase AD was fed with mixture of fresh pig manure, maize straw and inoculum. The characteristics of feedstock and inoculum such as total solid, volatile solid, total Kjeldahl nitrogen, total carbon are given in Table 1. The ratio of fresh pig manure to maize straw was 10:17 on a dry weight basis to obtain a suitable C/N. The TS of the feedstock in acidogenic fermentation reactors was 24–30%. These reactors were performed under mesophilic condition (30°C). The solid acidogenic fermentation reactor was as same as that used in the previous work [18]. The laboratory-scale methanogenic reactors were processed semi-continuously and fed daily with acidogenic leachate taking from the two-phase digestion system. The characteristics of the acidogenic leachate are showed as follow: pH 5.8–7.2, COD 19125–31241 mg·L⁻¹, alkalinity 5237–7079 mg·L⁻¹, total ammonia 992–1316 mg·L⁻¹, VFA 2.57–4.34 g·L⁻¹. The high concentration of alkalinity can be explained by the ammonium salt generated by ammonia and dissolved CO₂ which produced during the acidogenic digestion [19]. The semi-continuous methanogenic digestion was performed in 500 mL bottles (effective volume 200 mL) in triplicate. Before starting this experiment, the inoculum was incubated for 2

weeks at 35°C and 55°C respectively to acclimatize the microorganisms to experimental conditions. The second phase reactor at different pH (6.5, 7.0, 7.5, 8.0 and 8.5) was incubated in water bath at temperature 35°C or 55°C, respectively. The COD loading rate was 2.5 g·L⁻¹·d⁻¹ and the HRT was 10 d. The pH was adjusted daily to the setting value with a mixture of HCl (4.5%) and H₃PO₄ (12.5%) after feeding. Recorded the biogas yield and withdrew the samples from methanogenic reactors before feeding. The pH, ammonia, COD, VFA, alkalinity and content of CH₄ were analyzed every two days. The homogenized samples taken from every reactor were kept at -80°C for DNA extraction and archaeal community structure analysis.

Chemical Analysis

The pH, COD and ammonia were performed with standard methods [20]. Free ammonia (FA) was calculated by Equations (1) and (2) [13]:

$$FA = \frac{TAN}{1 + 10^{(pKa-pH)}} \quad (1)$$

$$pKa = 0.09018 + \frac{2729.92}{T + 273.15} \quad (2)$$

TAN is total ammonia, mg·L⁻¹; pKa is the dissociation constant of ammonium ion, and *T* is the temperature in °C.

For VFAs, samples were frozen at -20°C, and centrifuged at 3000 r·min⁻¹ for 5 min after unfrozen. The supernatant was filtered with 0.45 μm membrane and then analyzed with liquid chromatography (LC-10AVP, Shimadzu, Japan). 0.005 mol·L⁻¹ H₂SO₄ aqueous solution was use as mobile phase at a flow rate of 0.8 mL·min⁻¹. The temperature of column oven was 30°C, and injection volume was 25 μL.

Biogas production was recorded by a wet-tip counter with liquid displacement [13]. The composition of biogas was analyzed using a gas chromatograph [21].

Table 1. Characteristics of Substrates and Inoculum.

Material	TS, %	VS, %	pH	TC/TS, %	TKN/TS, %
Pig Manure	27.8	78.3	6.5	43.20	3.72
Maize Straw	86.2	91.3	—	56.01	1.09
Inoculum	5.4	81.7	7.9	—	—

Dry basis.

DNA Extraction

Samples were centrifuged at 14,000 g for 10 min. After removing the supernatants, the Fast DNAs Spin Kit for soil (Mpbio, USA) were used to extract DNA. The genomic DNA was kept at -20°C for the following T-RFLP analysis, archaeal 16S rRNA gene library construction and sequencing.

T-RFLP Analysis

Labeled the 5' end of the Arc912R primer with 6-carboxy fluorescein (FAM). PCR products were digested with enzyme HhaI at 65°C for 3 h [22]. Details of other treatment and data analysis have been described elsewhere [23].

Cloning and Sequencing

The extracted DNA from different reactors were mixed and used as templates. The primer pair described elsewhere [24] was used to amplify the archaeal 16S rRNA gene. PCR products were cloned into a pGEM-T Easy plasmid (Promega, USA). 147 colonies were picked up and sequenced by Sangon Biotech (Shanghai). The obtained 16S rDNA gene sequences were aligned on the website of NCBI.

RESULTS AND DISCUSSION

FA in Semi-continuous Methanogenic Reactors

Total ammonia concentration under different conditions reached to $1.1\text{--}1.3\text{ g}\cdot\text{L}^{-1}$, and the values at lower pH were higher than those at higher pH, no matter mesophilic or thermophilic digestion. Normally, the inhibition of ammonia, mainly attributed to FA (NH_3), is very common in digestion with manure as the feedstock [25]. Figure 1 shows that FA concentrations in these reactors operating at 55°C were higher than those at 35°C , and it increased rapidly with the pH increasing. Many researches have proved the inhibition of FA on methanogens [26,27], but these results often conflicted with each other about the threshold concentration of FA because the inhibitory threshold concentration depended on temperature, pH and inoculum greatly [28]. At higher temperature, the biogas process became more sensitive to ammonia when pH values increased [29]. According to the early findings, FA concentration ranging from $80\text{--}150\text{ mg}\cdot\text{L}^{-1}$ at pH 7.5 induced inhibitory in mesophilic digestion, but the

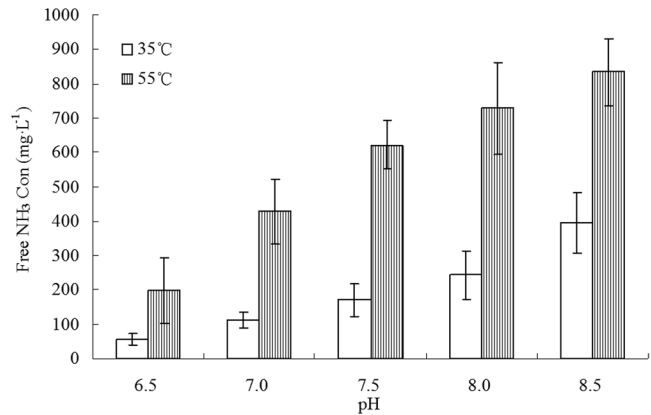


Figure 1. Un-ionized ammonia (NH_3 , as N) profiles under different temperatures and pH values.

inhibitory concentration could increase to $700\text{ mg}\cdot\text{L}^{-1}$ if the inoculum was well acclimated under high ammonia level. In this study, the inoculum was taken from well operating anaerobic reactors digested with pig manure at the total ammonium between $1200\text{--}1600\text{ mg}\cdot\text{L}^{-1}$ (FA concentration was from $130\text{--}550\text{ mg}\cdot\text{L}^{-1}$), which might not lead to the inhibition of biogas and methane production at the pH 7.0 and 55°C (about $425\text{ mg}\cdot\text{L}^{-1}$ free NH_3). However, the inhibition might happen when pH was higher than 7.0 at thermophilic digestion. Thus, thermophilic digestion was unsuitable to treat protein-rich wastes such as manure, even though the kinetic rate was more favorable compared with mesophilic digestion.

Biogas Production

The biogas production (Calculated to be at 0°C and 1 atm) during the digestion under different conditions is showed in Figure 2.

It shows that the daily specific biogas yields at 35°C were a little higher than that at 55°C at the same pH level. It decreased with the increase of pH in thermophilic, and the same trend could be observed in mesophilic digestion except at pH 7.0. The maximum average specific biogas yield at 35°C was $428\text{ N mL}\cdot\text{g}^{-1}\text{ COD}_{\text{add}}$ at pH 7.0, while that obtained at 55°C digestion was $398\text{ N mL}\cdot\text{g}^{-1}\text{ COD}_{\text{add}}$ at pH 6.5.

Figure 3 shows that the average specific methane yields at 35°C digestion were 265, 277, 215, 111 and $16\text{ N mL}\cdot\text{g}^{-1}\text{ COD}_{\text{add}}$ at these five pH levels, respectively. The largest decrease (by 94.1%) in methane production was from $277\text{ N mL}\cdot\text{g}^{-1}$ (pH 7.0) to $16\text{ N mL}\cdot\text{g}^{-1}$ (pH 8.5). The average specific methane yields at 55°C were 233, 253, 173, 74 and $13\text{ N mL}\cdot\text{g}^{-1}\text{ COD}_{\text{add}}$, and it decreased by 31.6%, 70.9% and 95.0% with pH in-

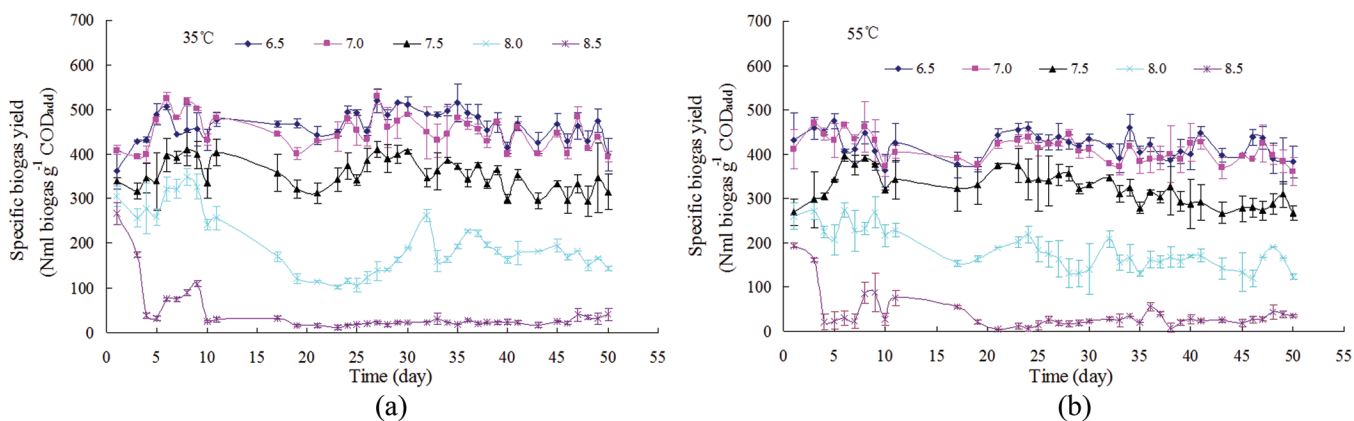


Figure 2. Daily specific biogas yields under different temperatures and pH values.

creasing from 7.0 to 7.5, 8.0 and 8.5, respectively. This drastic reduction in methane yield may be caused by the sharp increase of un-ionized ammonia (Figure 1). Angelidaki and Ahring [30] have reported that FA concentration at $700 \text{ mg} \cdot \text{L}^{-1}$ caused 50% inhibition of anaerobic digestion. In this work, the methane production decreased by 60.0% (35°C) and 70.9% (55°C) when pH increased from 7.0 to 8.0. The methane yields at five pH levels (pH from 6.5 to 8.5) at 35°C were 13.6%, 9.7%, 24.1%, 50.8% and 30.0% higher than that at 55°C. No matter mesophilic or thermophilic digestion, the maximum specific methane yields could be achieved at pH 7.0, and it had an increase by 9.7% at mesophilic digestion than that at thermophilic digestion. Compared with pH 7.0, the specific methane yields at pH 6.5 decreased by less than 8.0% at 35°C and 55°C. This semi-continuous experiment clearly demonstrated that reduction of pH enhanced the methane production effectively and pH 7.0 was most suitable pH for anaerobic digestion of acidogenic leachate, which was consistent with the results of digestion with piggery wastewater as feedstock [31]. Hashimoto also confirmed that lowering pH to 6 was responsible for the lowest digestion efficiency [32].

Archaeal Community Structure

Methane production is apparently correlated to the methanogenic microorganisms. The environmental factors, e.g., pH and temperature, usually impact on the microbial growth and metabolism, and finally affect the biogas yield.

The results of T-RFLP showed that Methanosaeta and Methanosarcina were the dominant methane-producing genus in the thermophilic and mesophilic digestion, respectively. Although they are attributed to the same order, Methanosaeta has a relatively higher

conversion rate for acetate compared with Methanosarcina, but Methanosarcina preferred higher temperature compared with Methanosaeta, which led to higher methane production at 35°C and higher Methanosarcina relative abundance at 55°C digestion.

Methanosarcina and Methanosaeta are attributed to Methanosarcinales, which was the dominant order in anaerobic digestion, the relative abundances were higher than 50% except that at pH 8.5 under 35°C, which was consistent with the previous reported results [23,33]. Moreover, at both 35°C and 55°C, the relative abundance of Methanosarcinales first increased and then decreased as the pH elevated. At 55°C, the relative abundance achieved the maximum value at pH 7.0, which was in accordance with the change of the specific CH_4 yield (Figure 3). However the relative abundance of methanosarcinales at pH 7.5 under 35°C was slightly higher than that at pH 7.0, although the specific methane yield was lower. These results showed that Methanosarcinales was inhibited severely at pH higher than 7.5 at both mesophilic and thermophilic digestion. As a consequence of that, the methane production decreased greatly.

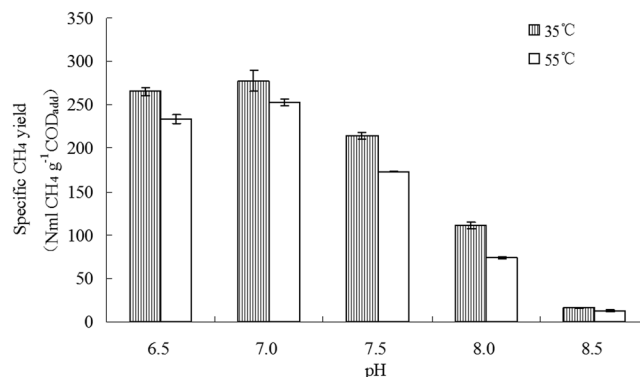


Figure 3. Specific CH_4 yield under different temperatures and pH values.

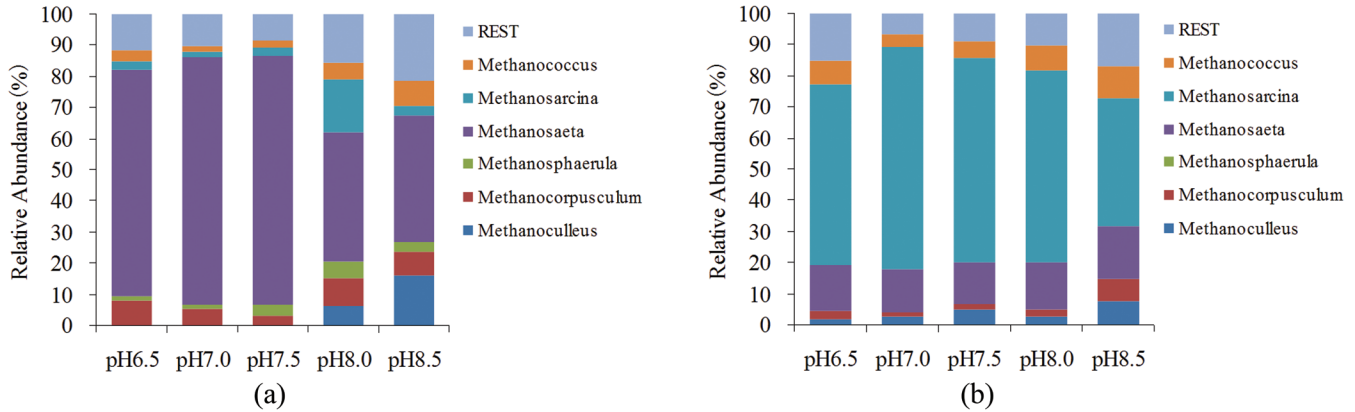


Figure 4. (a) Relative abundance of main archaeal families at mesophilic digestion. (b) Relative abundance of main archaeal families at thermophilic digestion.

CONCLUSIONS

Anaerobic digestion process is subjected to the inhibitions due to the sensitivity of archaeal community to environmental factors. The influence of temperature and pH value on co-digestion of pig manure with maize straw was firstly studied in detail and the main conclusions are as follows:

1. pH levels have significant effect on the specific CH₄ yields, regardless of mesophilic or thermophilic digestion.
2. The relatively lower pH was more appropriate for the co-digestion process. Compared with pH, temperature was more prominent factor which affected the community of methanogens.

ACKNOWLEDGMENTS

This research was supported by the National Natural Science Foundation of China (51008163) and Project in the National Science and Technology Pillar Program (2012BAD15B02).

REFERENCES

1. Cuetos, M. J., Gómez, X., Otero, M., Morán, A., “Anaerobic digestion of solid slaughterhouse waste (SHW) at laboratory scale: Influence of co-digestion with the organic fraction of municipal solid waste (OFMSW)”, *Biochemical Engineering Journal*, Vol. 40, No.1, 2008, pp. 99–106. <http://dx.doi.org/10.1016/j.bej.2007.11.019>
2. Callaghan, F. J., Wase, D. A. J., Thayanithy, K., Forster, C. F., “Continuous co-digestion of cattle slurry with fruit and vegetable wastes and chicken manure”, *Biomass Bioenergy*, Vol. 27, No. 1, 2002, pp. 71–77. [http://dx.doi.org/10.1016/S0961-9534\(01\)00057-5](http://dx.doi.org/10.1016/S0961-9534(01)00057-5)
3. Recktenwald, M., Dey, E. S., Norrlöw, O., “Improvement of industrial-scale anaerobic digestion by enzymes combined with chemical treatment”, *Journal of Residuals Science & Technology*, Vol. 12, No. 4, pp. 205–214.
4. Luo, J., Dong, B. C., Chen, L., “Experiments on aerogenesis character-

- istics of anaerobic digestion of animal manure and corn straw”, *Transactions of the Chinese Society of Agricultural Engineering*, Vol. 28, No. 10, 2012, pp. 219–224.
5. Ward, A. J., Hobbs, P. J., Holliman, P. J., Jones, D. L., “Optimisation of the anaerobic digestion of agricultural resources”, *Bioresour. Technology*, Vol. 99, 2008, pp. 7928–7940. <http://dx.doi.org/10.1016/j.biortech.2008.02.044>
6. Rincón, B., Sánchez, E., Raposo, F., Borja, R., Travieso, L., Martín, M. A., Martín, A., “Effect of the organic loading rate on the performance of anaerobic acidogenic fermentation of two-phase olive mill solid residue”, *Waste Management*, Vol. 28, No. 5, 2008, pp. 870–877. <http://dx.doi.org/10.1016/j.wasman.2007.02.030>
7. Chen, Y., Cheng, J. J., Creamer, K. S., “Inhibition of anaerobic digestion process: A review”, *Bioresour. Technology*, Vol. 99, No. 10, 2008, pp. 4044–4064. <http://dx.doi.org/10.1016/j.biortech.2007.01.057>
8. Martínez, E.J., Redondas, V., Fierro, J., Gómez, X. Morán, A., “Anaerobic digestion of high lipid content wastes: FOG co-digestion and milk processing FAT digestion”, *Journal of Residuals Science & Technology*, Vol. 8, No. 2, 2011, pp. 53–60.
9. Lehtomäki, A., Huttunen, S., Rintala, J. A., “Laboratory investigations on co-digestion of energy crops and crop residues with cow manure for methane production: Effect of crop to manure ratio”, *Resources, Conservation and Recycling*, Vol. 51, No. 3, 2007, pp. 591–609. <http://dx.doi.org/10.1016/j.resconrec.2006.11.004>
10. Ren, J. W., Yuan, X. F., Li, J., Ma, X. G., Zhao, Y., Zhu, W. B., Wang, X. F., Cui, Z. J., “Performance and microbial community dynamics in a two-phase anaerobic co-digestion system using cassava dregs and pig manure”, *Bioresour. Technology*, Vol. 159, 2014, pp. 80–87. <http://dx.doi.org/10.1016/j.biortech.2013.12.120>
11. Wang, Z. J., Banks, C. J., “Evaluation of a two stage anaerobic digester for the treatment of mixed abattoir wastes”, *Process Biochemistry*, Vol. 38, No. 9, 2003, pp. 1267–1273. [http://dx.doi.org/10.1016/S0032-9592\(02\)00324-2](http://dx.doi.org/10.1016/S0032-9592(02)00324-2)
12. Feng, C. P., Shimada, S., Zhang, Z., Maekawa, T., “A pilot plant two-phase anaerobic digestion system for bioenergy recovery from swine wastes and garbage”, *Waste Management*, Vol. 28, No. 10, 2008, pp. 1827–1834. <http://dx.doi.org/10.1016/j.wasman.2007.08.009>
13. Cavinato, C., Fatone, F., Bolzonella, D., Pavan, P., “Thermophilic anaerobic co-digestion of cattle manure with agro-wastes and energy crops: comparison of pilot and full scale experiences”, *Bioresour. Technology*, Vol. 101, No. 2, 2010, pp. 545–550. <http://dx.doi.org/10.1016/j.biortech.2009.08.043>
14. Ahring, B. K., Ashraf, A. I., Mladenovska, Z., “Effect of temperature increase from 55 to 65°C on performance and microbial population dynamics of an anaerobic reactor treating cattle manure”, *Water Research*, Vol. 35, No. 10, 2001, pp. 2446–2452. [http://dx.doi.org/10.1016/S0043-1354\(00\)00526-1](http://dx.doi.org/10.1016/S0043-1354(00)00526-1)
15. Angelidaki, I., Chen, X., Cui, J., Kaparaju, P., Ellegaard, L., “Thermophilic anaerobic digestion of source-sorted organic fraction of house-

- hold municipal solid waste: start-up procedure for continuously stirred tank reactor”, *Water Research*, Vol. 40, No.14, 2006, pp. 2621–2628. <http://dx.doi.org/10.1016/j.watres.2006.05.015>
16. Chen, Y. R., Varel, V. H., Hashimoto, A. G., “Effect of temperature on methane fermentation kinetics of beef-cattle manure”, *Biotechnology Bioengineering Symposium*, Vol. 10, 1980, pp. 325–339.
 17. Strik, D.P.B.T.B., Domnanovich, A. M., Holubar, P., “A pH-based control of ammonia in biogas during anaerobic digestion of artificial pig manure and maize silage”, *Process Biochemistry*, Vol. 41, 2006, pp. 1235–1238. <http://dx.doi.org/10.1016/j.procbio.2005.12.008>
 18. Du, L. Z., Chen, L., Yang, P., Zhang, K. Q., “Effects of different ratios of pig manure and straw on solid acidogenic fermentation”, *Transactions of the Chinese Society of Agricultural Engineering*, Vol. 26, No.7, 2010, pp. 272–276.
 19. Niu, Q. G., Hojo, T., Qiao, W., Qiang, H., “Characterization of methanogenesis, acidogenesis and hydrolysis in thermophilic methane fermentation of chicken manure”, *Chemical Engineering Journal*, Vol. 244, 2014, pp.587–596. <http://dx.doi.org/10.1016/j.cej.2013.11.074>
 20. Wang, X. F., 2002. *Standard methods of water and wastewater analysis and detection*, the fourth edition. Beijing.
 21. Du, L. Z., Liang, J. F., Yang, P., Gao, W. X., Zhang, K. Q., “Influence of total solid content on anaerobic digestion of swine manure and kinetic analysis”, *Transactions of the Chinese Society of Agricultural Engineering*, Vol. 30, No.24, 2014, pp. 246–251.
 22. Xu, K. W., Liu, H., Du, G. C., Chen, J., “Real-time PCR assays targeting formyltetrahydrofolate synthetase gene to enumerate acetogens in natural and engineered environments”, *Anaerobe*, Vol. 15, No.5, 2009, pp. 204–213. <http://dx.doi.org/10.1016/j.anaerobe.2009.03.005>
 23. Padmasiri, S. I., Zhang, J., Fitch, M., Norddahl, B., Morgenroth, E., Raskin, L., “Methanogenic population dynamics and performance of an anaerobic membrane bioreactor (AnMBR) treating swine manure under high shear conditions”, *Water Research*, Vol. 41, No.1, 2007, pp. 134–144. <http://dx.doi.org/10.1016/j.watres.2006.09.021>
 24. Peng, J., Lü, Z., Rui, J., Lu, Y., “Dynamics of the methanogenic archaeal community during plant residue decomposition in an anoxic rice field soil”, *Applied and Environmental Microbiology*, Vol. 74, No.9, 2008, pp. 2894–2901. <http://dx.doi.org/10.1128/AEM.00070-08>
 25. Sawayama, S., Tada, C., Tsukahara, K., Yagishita, T., “Effect of ammonium addition on methanogenic community in a fluidized bed anaerobic digestion”, *Journal of Bioscience and Bioengineering*, Vol. 97, No.1, 2004, pp. 65–70. [http://dx.doi.org/10.1016/S1389-1723\(04\)70167-X](http://dx.doi.org/10.1016/S1389-1723(04)70167-X)
 26. Aymerich, E., Garcia-Mina, J. M., Esteban-Gutiérrez, M., Garcia-Heras, J. L., “Dry anaerobic digestion of agro-food waste in a batch system”, *Journal of Residuals Science & Technology*, Vol. 9, No. 1, 2012, pp. 1–7.
 27. Steinhaus, B., Garcia, M. L., Shen, A. Q., Angenent, L. T., “A portable anaerobic microbioreactor reveals optimum growth conditions for the methanogen *Methanosaeta concilii*”, *Applied and Environmental Microbiology*, Vol. 73, No. 5, 2007, pp. 1653–1658. <http://dx.doi.org/10.1128/AEM.01827-06>
 28. Garcia, M. L., Angenent, L. T., “Interaction between temperature and ammonia in mesophilic digesters for animal waste treatment”, *Water research*, Vol. 43, No. 9, 2009, pp. 2373–2382. <http://dx.doi.org/10.1016/j.watres.2009.02.036>
 29. Calli, B., Mertoglu, B., Inanc, B., Yenigun, O., “Methanogenic diversity in anaerobic bioreactors under extremely high ammonia levels”, *Enzyme and Microbial Technology*, Vol. 37, No. 4, 2005, pp. 448–455. <http://dx.doi.org/10.1016/j.enzmictec.2005.03.013>
 30. Angelidaki, I., Ahring, B. K., “Anaerobic thermophilic digestion of manure at different ammonia loads: effect of temperature”, *Water Research*, Vol. 28, No. 3, 1994, pp. 727–731. [http://dx.doi.org/10.1016/0043-1354\(94\)90153-8](http://dx.doi.org/10.1016/0043-1354(94)90153-8)
 31. Ho, L., Ho, G., “Mitigating ammonia inhibition of thermophilic anaerobic treatment of digested piggery wastewater: Use of pH reduction, zeolite, biomass and humic acid”, *Water Research*, Vol. 46, No.14, 2012, pp. 4339–4350. <http://dx.doi.org/10.1016/j.watres.2012.05.016>
 32. Hashimoto, K., Doi, T., Okuda, T., Nishijima, W., Nakai, S., Nishimura, K., “Function of wood chips for composting of sewage sludge by thermophilic and aerobic digestion”, *Journal of Residuals Science & Technology*, Vol. 12, No. 2, 2015, pp. 53–59. <http://dx.doi.org/10.12783/issn.1544-8053/12/2/3>
 33. Klocke, M., Nettmann, E., Bergmann, I., Mundt, K., Souidi, K., Mumme, J., Linke, B., “Characterization of the methanogenic Archaea within two-phase biogas reactor systems operated with plant biomass”, *Systematic and Applied Microbiology*, Vol. 31, No. 3, 2008, pp. 190–205. <http://dx.doi.org/10.1016/j.syapm.2008.02.003>

Removal of Streptomycin from Honey by Cation-exchange Resin

QIONG HE¹, YIZHU YAN¹, NI CHENG¹, XIAOFENG XUE², LIMING WU^{2,*} and WEI CAO^{1,*}

¹Department of Food Science and Engineering, School of Chemical Engineering, Northwest University, 229 North TaiBai Road, Xi'an City, China 710069

²Institute of Apiculture Research, Chinese Academy of Agricultural Science, Beijing, China 100093

ABSTRACT: The presence of streptomycin (STR) in honey has potentially undesirable effects on humans. This study evaluated the effect of conventional processing on STR levels and investigated a new approach to further removing STR using various types of resins. The use of cation-exchange resin (LS-904) after conventional processing, significantly reduced STR residues, with loss rate of approximately 100%. The optimal adsorption time and temperature were 60 min and 45°C, respectively. Moreover, compared with an anion-exchange resin (LS-905) or macroporous-adsorption resins (LS-200, NKA-9), LS-904 was more effective in removing STR from honey. The processed honey can be widely used as natural sweeteners.

INTRODUCTION

An antibiotic is a type of pharmaceutical that has the ability to kill or inhibit the growth of microorganisms. Antibiotics are extensively used in agriculture. In the field of apiculture, bees are treated with antibiotics to fight diseases such as American and European foulbrood diseases [1]. In the European Union, it is illegal to treat honeybees with antibiotics. However, in some developing countries, antibiotics are still used for this purpose; therefore, antibiotic-contaminated honey products can be found in the global marketplace [2].

Streptomycin (STR) is an aminoglycoside antibiotic which is produced by *Streptomyces griseus*. It can effectively inhibit gram-positive and gram-negative bacteria by causing codon misreading, which thus inhibits protein synthesis and leads to the death of the microbial cells [3]. Due to its inhibitory effects, STR has numerous applications in a wide range of human therapies and animal husbandry and agricultural practices, including apiculture (keeping honeybees) [4]. However, when this antibiotic is overused, STR residues may appear in many foodstuffs, e.g., meat products, animal livers, milk and, above all, in honey. Although it is debatable whether STR residues have a direct impact on human health, many cases of allergic attacks have occurred in recent years, and STR can induce severe skin rashes [3,5]. Furthermore, certain other negative effects

of this antibiotic, such as increasing the risk of hearing loss and toxicity to the kidneys, have also been claimed [6]. The long-term use of STR can induce bacterial resistance, and some studies have shown that *E. coli*, *Salmonella* and *Shigella* may carry this resistance [7].

Therefore, to protect human health against the dangers of STR residues, maximum residue limits (MRLs) for some food products were established by certain organizations. For example, the European Commission stipulated that the MRLs for STR in milk, porcine kidney and porcine muscle are 200, 1,000 and 500 mg kg⁻¹, respectively [7]. Moreover, Switzerland and Germany imposed a regulation that the MRL in honey is 20 µg kg⁻¹. Due to concerns for human health, many countries have banned the use of STR in natural products such as honey [7–8].

Honey is a sweet substance, produced from the nectar of flowers by honeybees. From ancient times, honey has been favored for its nutritional and medicinal qualities such as antibacterial and dermatological disorders [9–10]. Moreover, the antioxidant activity of honey can reduce the risk of degenerative diseases of aging [11]. Unfortunately, honey is vulnerable to contamination with antibiotics, such as STR, which are applied to treat honeybee diseases. Generally, once the amount of STR residues reaches the MRL, the tainted honey should be discarded. However, this practice may result in great waste because tainted honey still contains valuable substances that are underutilized. Considering these reasons, controlling the level of STR residues in honey is extremely urgent.

*Authors to whom correspondence should be addressed.
Email: apiswu@126.com (L.M. Wu), caowei@nwu.edu.cn (W. Cao),
Tel.: +86 29 88302632; FAX: +86 29 88302213 (W. Cao)

It is gratifying that several studies have shown that the processing of honeys is highly effective in reducing the detrimental effects of organophosphorus compounds and antibiotics [12–14]. However, few studies have investigated the effect of honey processing on the level of STR residues in honey. And there is little research on removing STR from honey. The present study aimed to determine how the honey processing steps, such as preheating, filtration, vacuum concentration, and pasteurization, affect the level of STR residues and to explore a simple, highly efficient, economical and safe method to remove STR from honey.

MATERIALS AND METHODS

Chemicals

Analytical grade STR and phosphoric acid were obtained from Sigma-Aldrich (St. Louis, MO, USA).

An STR quantification kit (batch number HE09024) was provided by Huaan Magnech Co., Ltd. (Beijing, China) and was used to conduct the enzyme-linked immunosorbent assay (ELISA), which utilized a specific rabbit anti-streptomycin antibody. The STR kit included all of the solvents and reagents necessary for the ELISA.

Adsorbents

The following resins were prepared for the study: the cation-exchange resin LS-904, the anion-exchange resin LS-905, and the macroporous adsorption resins LS-200 and NKA-9. The LS-904, LS-905 and LS-200 resins were provided by Xi'an Lanshen Exchange and Adsorbent Material, Ltd. (Xi'an, China), and the NKA-9 resin was purchased from Tianjin Nanda Adsorbent Material, Ltd. (Tianjin, China).

Honey Samples

Preparation of Raw Honey Samples

The raw honey samples were provided by beekeepers and were confirmed to be antibiotic-free.

Preparation of Spiked Honey Samples

The spiked honey samples were prepared according to the following steps. First, defined amounts of the STR standard were introduced into the raw honey

samples (200 g); next, the mixtures were homogenized in a water bath for 4 h at 25°C; the samples were then stored in the refrigerator until use.

ELISA Procedure

The concentration of STR in the honey samples was determined with an ELISA according to the manufacturer's instructions. The procedure was as follows: the spiked honey sample (2 g) and purified water (2 mL) were mixed to prepare the diluted honey sample. Then, phosphoric acid (0.04 mol L⁻¹, 4 mL) was added to the diluted honey sample, and the mixture was thoroughly homogenized. The pH value of the sample was adjusted to approximately 8.0 using sodium hydroxide (1 mol L⁻¹, 350 µL). After that, the STR-containing diluent was prepared by mixing the concentrated STR sample diluent and purified water at a ratio of 1:1 (v:v). The homogenates were centrifuged at 4,800 rotations/min (rpm) for 10 min, and the supernatants (100 µL) were removed and added to the STR-containing diluent, the samples were thoroughly mixed.

The absorbance of a 50 µL aliquot of the aqueous layer at 450 nm was measured with an ELISA Reader (Infinite M200 Pro, Tecan Austria GmbH, Grödig, Austria). The STR levels were calculated using a calibration curve. The concentration of STR was expressed in the form of µg kg⁻¹ honey. In this study, the limit of quantification of STR was 4 µg kg⁻¹. The average recovery rates ranged from 95.6–97.3% for all of the samples.

Processing of the Spiked Honey Sample

The procedure for processing the honey was organized into 4 consecutive steps according to the conventional method [15], including preheating, filtration, vacuum concentration, and pasteurization. After each step, the samples were collected, and the concentration of STR was determined using the ELISA.

Static Adsorption Experiments

Pretreatment of the Resins

Four different resins, i.e., the LS-904, LS-905, LS-200, and NKA-9 resins, were selected for the study, which required different pretreatments before use.

The cation-exchange resin (LS-904) and the anion-exchange resin (LS-905) were soaked in HCl (4%) and

NaOH (4%), respectively, for 2 h using a volume of the corresponding solvent that was three times greater than that of the resin volume. The macroporous adsorption resins (LS-200, NKA-9) were first soaked in ethanol (95%) for 24 h and then rinsed with purified water until the resins were ethanol-free; finally, these resins were soaked in a mixture of HCl (5%) and NaOH (5%) at a ratio of 1:1 to eliminate porogenic agents and monomers that had been trapped within the pores during the synthesis process. Eventually, all of the resins were rinsed using purified water until the resins were chemically neutral.

Screening the Adsorption Resins

To determine the optimal resin among the LS-904, LS-905, LS-200 and NKA-9 resins, the following experiment was conducted. Pre-weighed hydrated resins were added to a diluted honey sample (25 g) [honey:purified water (m:m) at 1:1.5] containing a certain concentration of STR, and the mixtures were stirred in a water-bath at the rate of 120 rpm at 25°C for 1 h. Then, the percentage of STR remaining in the honey was determined using the ELISA.

STR-adsorption Experiment

In this experiment, the influence of resin dose, contact time and temperature on adsorption process were explored. The diluted honey sample containing a certain concentration of STR (25 g) was added to the selected resin and swirled in a water-bath shaker at 120 rpm at 25°C. The amount of the resin was increased from 0.5–3.0 g. After 90 min, 4 g of honey sample was removed to determine the STR content. To study the effect of time, the adsorption time was increased from 30–90 min (in increments of 30 min), while the water-bath temperature and amount of resin were maintained at 25°C and 2 g, respectively. Similar methods were applied to assess the effect of temperature on STR adsorption by increasing the temperature from 25–65°C (in increments of 10°C).

Statistical Analysis

The assays were performed in triplicate, and the results were expressed as the mean values with the standard deviation (SD). The differences between values with $P < 0.05$ were considered significant. The statistical analyses were performed using Origin software, version 8.0 and Microsoft Office Excel 2010.

RESULTS AND DISCUSSION

Effect of the Processing Procedures on the Streptomycin Level

The effect of the processing procedures on the reduction of the STR level was determined by performing an ELISA, and the results are presented in Figure 1. The spiked honey samples were preheated at 45°C for 60 min to make them liquid. After the preheating processing, the STR level was decreased by 34.84%, indicating that STR is a thermally unstable antibiotic. A similar result was obtained in a previous study by Landerkin and Katznelson [16].

The preheated honey samples were then filtered to remove the suspended particles, including the bodies of honeybees, beeswax particles, and pollens. The decrease of STR content that occurred during the filtration process was not significant. Nevertheless, it has been shown that filtration significantly contributes to removing other types of antibiotics and organophosphorus insecticides from honey. This occurrence appears to depend on the degree of lipophilicity of the antibiotics (e.g., chloramphenicol) and parathion, which favors the association of these compounds with the fatty fractions [14]. However, STR does not tend to be retained in pollen or beeswax due to the hydrophilicity of STR. Therefore, the STR concentration had nearly no reduction after the filtration processing, which is consistent with the results of a study by Chen *et al.* [17].

Next, vacuum preconcentration was conducted at 55°C and 0.08 MPa for 45 min. Vacuum preconcentration plays a vital role in eliminating microorganisms and reducing the moisture content to a degree that retards fermentation [14]. In addition, vacuum precon-

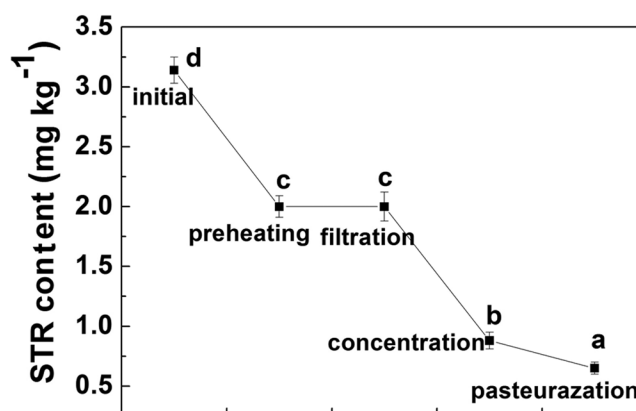


Figure 1. Changes of the streptomycin (STR) content in honey during conventional processing. Different lower case letters indicate significant differences at $P < 0.05$.

centration contributes to maintaining the honey in a liquid state for a long period due to melting the invisible crystals in honey [15]. After this procedure was performed, the STR residue was decreased by 54.9%.

For honey to become a commodity, it must be pasteurized at 85°C for 15 min. The mean loss of STR caused by pasteurization process was 28.54%, indicating that STR is unstable at high temperatures.

Screening to Determine the Optimal Resin

Despite being effective, the normal processing procedures did not completely remove the STR from honey. The level of STR residues after the 4 procedures were performed was 651 $\mu\text{g kg}^{-1}$, which far exceeded the MRL. Therefore, using absorption resins may be an efficient method to remove STR from honey. In the static adsorption tests, the performance of the 4 resins in removing STR was determined, as shown in Figure 2. The adsorption rates of the LS-905, NKA-9, LS-904, and LS-200 resins were 26.76%, 21.29%, 65.77%, 24.09%, respectively. Obviously, the LS-904 resin had the highest adsorption rate.

Compared with the macroporous adsorption resins (LS-200, NKA-9), the performance of ion-exchange resin is related to the properties of the exchange groups. Ion-exchange resins generally carry cations or anions that are exchanged with similarly charged ions in solution via electrostatic interactions. Hence, the ionic groups in a solution migrate to the resins and the other ion groups migrate in the opposite direction until electroneutrality is achieved. The LS-904 resin is a cation-exchange resin, whereas the LS-905 resin is an anion-exchange resin. The highest adsorption rate caused by

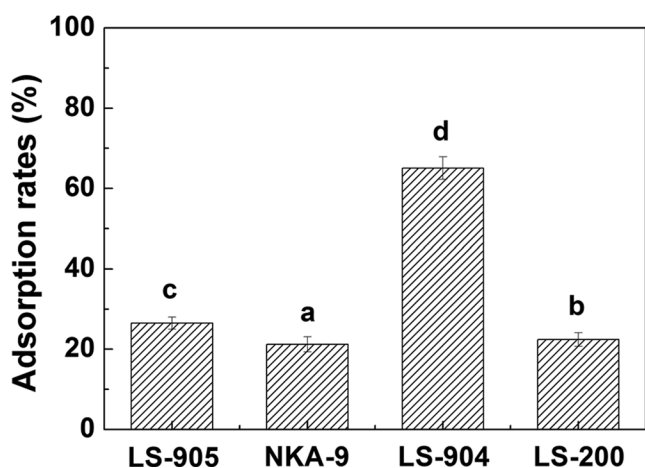


Figure 2. Rates of streptomycin (STR) adsorption by four types of resins. Different lower case letters indicate significant differences at $P < 0.05$.

the LS-904 resin could be attributed to the fact that the STR became Str-H_3^{3+} in the honey sample, which had a pH of 3.2–4.5, so that the H^+ ions produced by the LS-904 resin would be exchanged with Str-H_3^{3+} . The schematic diagram of this process is illustrated in Figure 3. Therefore, considering its adsorption capacity, the LS-904 resin was selected as the optimal resin to remove STR from honey.

Effect of the Adsorption by the Cation-exchange Resin on the STR Levels

In the static adsorption assay, the amount of LS-904 resin, the adsorption time and the temperature were varied to determine the optimal conditions. The results were depicted in Figure 4.

As shown in Figure 4(a), the optimal amount of LS-904 resin was determined. The STR content in honey samples decreased with an increase in the amount of resin and finally attained an equilibrium above 80 g LS-904 resin kg^{-1} honey, at which the STR residue was nearly zero. The efficiency of STR-residue removal using this method was satisfactory, reducing the STR content from 76.8 $\mu\text{g kg}^{-1}$ to nearly 0. The final STR content was far below the MRL, which indicated that the LS-904 resin is highly suitable for removing STR.

The effect of time on the adsorption of STR by the LS-904 resin was observed, and the results are shown in Figure 4(b). The STR level, which was initially at 68 $\mu\text{g kg}^{-1}$, decreased sharply within the first 30 min, then stabilized between 30 and 60 min. The STR level eventually remained unchanged after approximately 60 min, demonstrating that the maximum adsorption efficiency had been attained. More significantly, the reduction rate was approximately 100%. Based on these results, the optimum adsorption period is 60 min.

Figure 4(c) illustrates the effect of temperature on the adsorption of STR residues in honey by the LS-

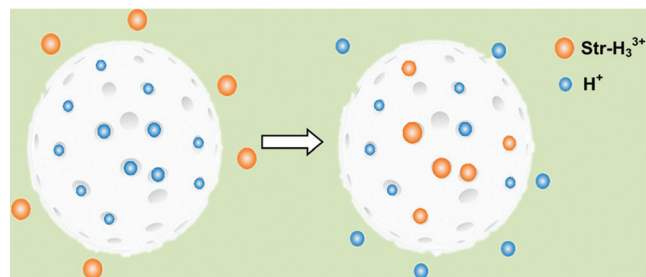


Figure 3. Process of streptomycin (STR) adsorption using a cation-exchange resin.

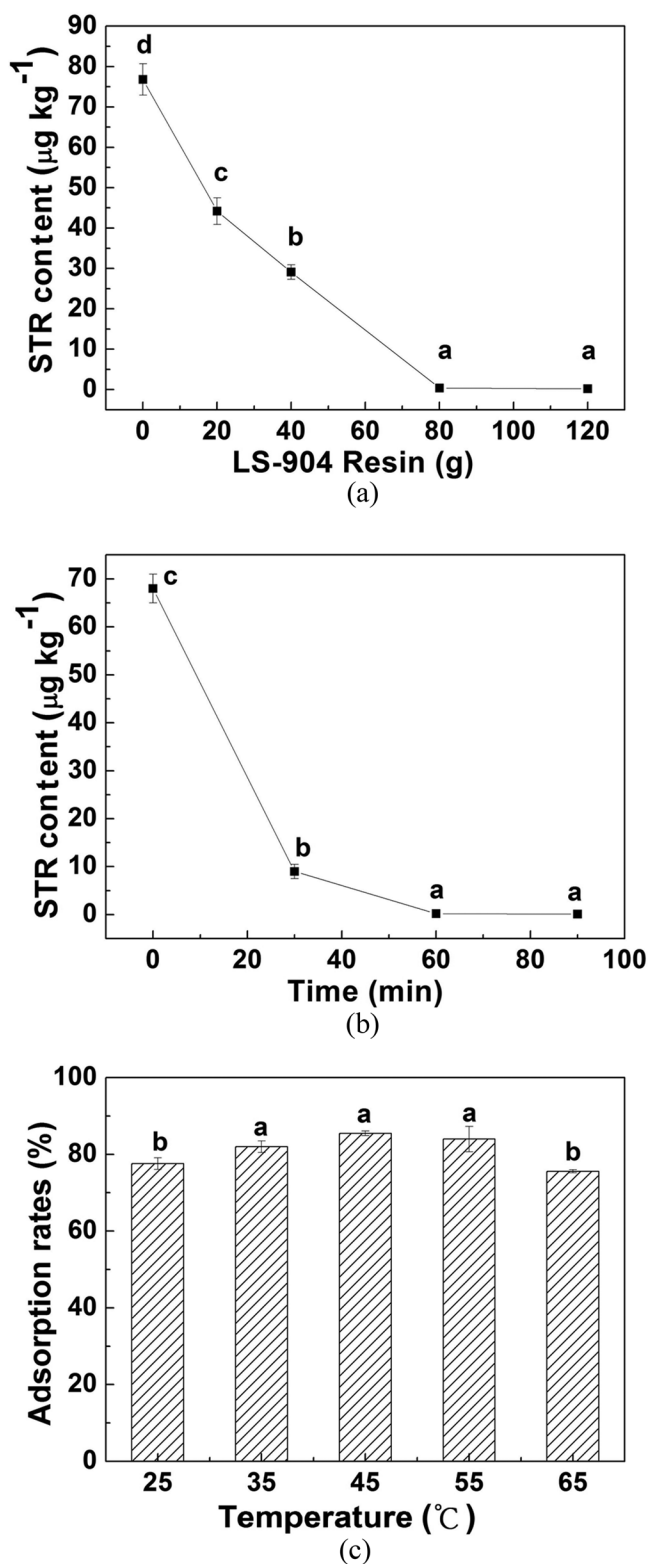


Figure 4. (a) Effect of LS-904 resin dose; (b) adsorption time; and (c) adsorption temperature on the removal of streptomycin (STR) from contaminated honey. Different lower case letters indicate significant differences at $P < 0.05$.

904 resin. When the temperature was increased from 25–45 $^{\circ}\text{C}$, the rate of STR adsorption increased to 86.72%. It is noteworthy that the adsorption rate was apparently greatest at 45 $^{\circ}\text{C}$, at which the STR content was approximately 10 $\mu\text{g kg}^{-1}$, lower than the MRL. However, after this point, the adsorption rate began to decrease with increasing temperature. Moreover, an unadvisable adsorption process is likely to impair the quality of the honey. As reported by Turkmen *et al.* [18], both high-temperature and a long exposure directly affect the bioactivities and qualities of honey, particularly some of the antioxidant properties. Therefore, although the STR content in honey was reduced by increasing the temperature, taking all the facts into consideration, 45 $^{\circ}\text{C}$ was chosen as the most appropriate adsorption temperature.

CONCLUSIONS

This study investigated the effect of conventional honey processing on the removal of STR residues from honey and explored an efficient method of further reducing the STR concentration using ion-exchange resins. The results indicated that vacuum concentration was the most efficient process for removing STR residues from honey. In addition, among the four candidate resins (LS-904, LS-905, LS-200 and NKA-9), the LS-904 resin had the highest adsorptive capacity for STR in honey, and the best adsorption time and temperature were determined to be 60 min and 45 $^{\circ}\text{C}$, respectively. By leveraging the method proposed in this paper, tainted honey could be widely used in food industry as a safe and acceptable natural sweetener.

ACKNOWLEDGEMENTS

This study was funded by the grants from the Agricultural Science & Technology of Shaanxi Province (No. 2012NKC01-21) and the Science & Technology of Xi'an (No. NC1405(1)).

REFERENCES

- Bogdanov, S., "Contaminants of bee products", *Apidologie*, Vol. 37, No. 1, 2005, pp. 1–18. <http://dx.doi.org/10.1051/apido:2005043>
- Michaud, V., "Antibiotic residues in honey—The FEEDM view", *Apicultura*, Vol. 40, 2005, pp. 52–54.
- Liu, B. Q., Zhang, B., Cui, Y. L., Chen, H. F., Gao, Z. Q. and Tang, D. P., "Multifunctional gold-silica nanostructures for ultrasensitive electrochemical immunoassay of streptomycin residues", *ACS Appl. Mater. Inter.*, Vol. 3, No.12, 2011, pp. 4668–4676. <http://dx.doi.org/10.1021/am201087r>
- Bohm, D. A., Stachel, C. S. and Gowik, P., "Confirmatory method for

- the determination of streptomycin in apples by LC-MS/MS”, *Anal. Chim. Acta*, Vol. 672, No. 1-2, 2010, pp. 103–106. <http://dx.doi.org/10.1016/j.aca.2010.03.056>
5. Edder, P., Cominoli, A. and Corvi, C., “Determination of streptomycin residues in food by solid-phase extraction and liquid chromatography with post-column derivatization and fluorometric detection”, *J. Chromatogr. A*, Vol. 830, No. 2, 1999, pp. 345–351. [http://dx.doi.org/10.1016/S0021-9673\(98\)00917-0](http://dx.doi.org/10.1016/S0021-9673(98)00917-0)
 6. Bignall, J. R., Crofton, J. W. and Thomas, J. A. B., “Effect of streptomycin on vestibular function”, *Brit. Med. J.*, Vol. 1, No. 4706, 1951, pp. 554–559. <http://dx.doi.org/10.1136/bmj.1.4706.554>
 7. Granja, R. H. M. M., Ni-o, A. M. M., Zucchetti, R. A. M., Ni-o, R. E. M., Patel, R. and Salerno, A. G., “Determination of streptomycin residues in honey by liquid chromatography-tandem mass spectrometry”, *Anal. Chim. Acta*, Vol. 637, No. 1-2, 2009, pp. 64–67. <http://dx.doi.org/10.1016/j.aca.2009.01.006>
 8. Bruijnsvoort, M. V., Ottink, S. J., Jonker, K. M. and Boer, E., “Determination of streptomycin and dihydrostreptomycin in milk and honey by liquid chromatography with tandem mass spectrometry”, *J. Chromatogr. A*, Vol. 1058, No. 1-2, 2004, pp. 137–142. [http://dx.doi.org/10.1016/S0021-9673\(04\)01307-X](http://dx.doi.org/10.1016/S0021-9673(04)01307-X)
 9. Gomes, S., Dias, L. G., Moreira, L. L., Rodrigues, P. and Estevinho, L., “Physicochemical, micro-biological and antimicrobial properties of commercial honeys from Portugal”, *Food Chem. Toxicol.*, Vol. 48, No. 2, 2010, pp. 544–548. <http://dx.doi.org/10.1016/j.fct.2009.11.029>
 10. Katiraei, F., Mahmodi, R., Mardani, K. and Babaei, E., “Antifungal activity of Iranian honeybees against candida, *aspergillus* species and *trichophyton rubrum*”, *J. Food Process. Pres.*, Vol. 38, No. 5, 2014, pp. 2078–2082. <http://dx.doi.org/10.1111/jfpp.12187>
 11. Gacche, R. N., Shinde, B. T., Dhole, N. A., Pund, M. M. and Jadhav, A. D., “Evaluation of floral honey for inhibition of polyphenol oxidase-mediated browning, antioxidant and antimicrobial activities”, *J. Food Biochem.*, Vol. 33, No. 5, 2009, pp. 693–706. <http://dx.doi.org/10.1111/j.1745-4514.2009.00245.x>
 12. Shakila, R. J., Vyla, S. A. P., Kumar, R. S., Jeyasekaran, G. and Jasmine, G. I., “Stability of chloramphenicol residues in shrimp subjected to heat processing treatments”, *Food Microbiol.*, Vol. 23, No. 1, 2006, pp. 47–51. <http://dx.doi.org/10.1016/j.fm.2005.01.012>
 13. Xu, R. H., Cheng, N., Huang, W., Gao, H., Deng, J. J. and Cao, W., “Effects of the processing steps on parathion levels during honey production and parathion removal by macroporous adsorption resins”, *Food Control*, Vol. 23, No. 1, 2012, pp. 234–237. <http://dx.doi.org/10.1016/j.foodcont.2011.07.020>
 14. Zhu, Q., Cao, W., Gao, H., Chen, N., Wang, B. N. and Yu, S. F., “Effects of the processing steps on chlorpyrifos levels during honey production”, *Food Control*, Vol. 21, No. 11, 2010, pp. 1497–1499. <http://dx.doi.org/10.1016/j.foodcont.2010.04.022>
 15. Subramanian, R., Hebbar, U. H. and Rastogi, N. K., “Processing of honey: a review”, *Int. J. Food Prop.*, Vol. 10, No. 1, 2007, pp. 127–143. <http://dx.doi.org/10.1080/10942910600981708>
 16. Landerkin, G. B. and Katznelson, H., “Stability of antibiotics in honey and sugar syrup as affected by temperature”, *Appl. Microbiol.*, Vol. 5, No. 3, 1957, pp. 152–154.
 17. Cheng, N., Gao, H., Deng, J. J., Wang, B. N., Xu, R. H. and Cao, W., “Removal of chloramphenicol by macroporous adsorption resins in honey: A novel approach on reutilization of antibioticscontaminated honey”, *J. Food Sci.*, Vol. 77, No. 9, 2012, pp. 169–172. <http://dx.doi.org/10.1111/j.1750-3841.2012.02868.x>
 18. Turkmen, N., Sari, F., Poyrazoglu, E. S. and Velioglu, Y. S., “Effects of prolonged heating on antioxidant activity and colour of honey”, *Food Chem.*, Vol. 95, No. 4, 2006, pp. 653–657. <http://dx.doi.org/10.1016/j.foodchem.2005.02.004>

Effects of Chlorine and Phosphor on Zinc Transformation Behavior During Sewage Sludge Combustion

YANLONG* LI, RUNDONG LI*, LEI WANG, WEIYUN WANG and TIANHUA YANG
The Key Laboratory of Clean Energy Liaoning Province, Shenyang Aerospace University, Shenyang, China

ABSTRACT: Effects of chlorine and phosphor on the transformation of zinc during combustion of sewage sludge (SS) was investigated by two approaches: combustion experiment and thermodynamic simulation. The result of thermodynamic simulation predicted that zinc existed as $ZnSO_4$ (s) below 400°C, while mainly as phosphate in solid phase when the combustion temperature was in the range from 500–1200°C but was released as metallic vapor at higher temperatures (>1300°C). $NaZnPO_4$ and $Zn(PO_3)_2$ were experimentally detected by X-ray diffraction in sewage sludge slag (SSA) at 900°C. The volatilization rate of zinc was below 10.00% in all cases, and increased slowly along with the combustion time and temperature. However, this volatilization rate significantly increased with chlorine addition through the formation of metal chloride, while phosphor additives restrained the volatilization of zinc.

INTRODUCTION

THE sewage sludge (SS) contains vast inorganic pollutants and abundant nutrients [1,2] that must be treated properly. Combustion of sewage sludge (SS) has significant advantages over landfill and composting. For example, it could decrease the volume of SS obviously, reduce organic pollution, save energy and land resources [3,4]. But the removal of heavy metals, the key pollutants, cannot be achieved during SS combustion, since some of them will volatilize in the flue gas or be adsorbed by the fine particles, and release into the environment eventually [5]. Zinc is the main heavy metal in SS in China [6,7], so it is important to research the migration and transformation of zinc during combustion of SS.

Thermodynamic simulations have been widely used in the research of the behavioral characteristics of heavy metals during waste combustion [8,9]. However, it must be pointed out that these thermodynamic simulations were based on the equilibrium of chemical reaction, not paying attention to the reaction time, which is important to the reaction. For example, Fraissler simulated the behavioral characteristics of zinc during combustion of SS, studying the influence of $CaCl_2$ and found that calculated and experimental data differed one from each other due to the dynamic effect [10].

Therefore, the results of thermodynamic simulations should be corrected by the experiment test results. The aim of this article was to experimentally evaluate the effects of chlorine and phosphor on the distribution of zinc during SS combustion and to analyze the chemical speciation of zinc by thermodynamic simulations.

MATERIALS AND METHODS

Materials

The SS samples were collected from Kunshan city, which was near to Shanghai city. The principal elements of the SS, such as C, H, O, N, S, Cl, were analyzed by an X-ray fluorescence spectrometer (ZSX100e, Japan). The content of P in the SS was measured by a SMT program for phosphorus fractionation, which was described elsewhere [11,12]. The contents of heavy metals were measured by an atomic absorption spectrometer (AAS 200, Perkin Elmer, US). The measured results are reported in Table 1. SS samples with the chlorine addition of 2.00 wt%, 4.00 wt% and 8.00 wt% were prepared using NH_4Cl , while SS samples with the phosphor addition of 5.00 wt%, 10.00 wt% and 15.00 wt% were obtained using $(NH_4)_3PO_4$.

Experimental Methods

The experimental setup used in this work included a tubular resistance furnace (high-temperature tube at-

*Authors to whom correspondence should be addressed.
Email: rdlee@163.com (Rundong Li); liyanlong1982@mail.dlut.edu.cn (Yanlong Li)

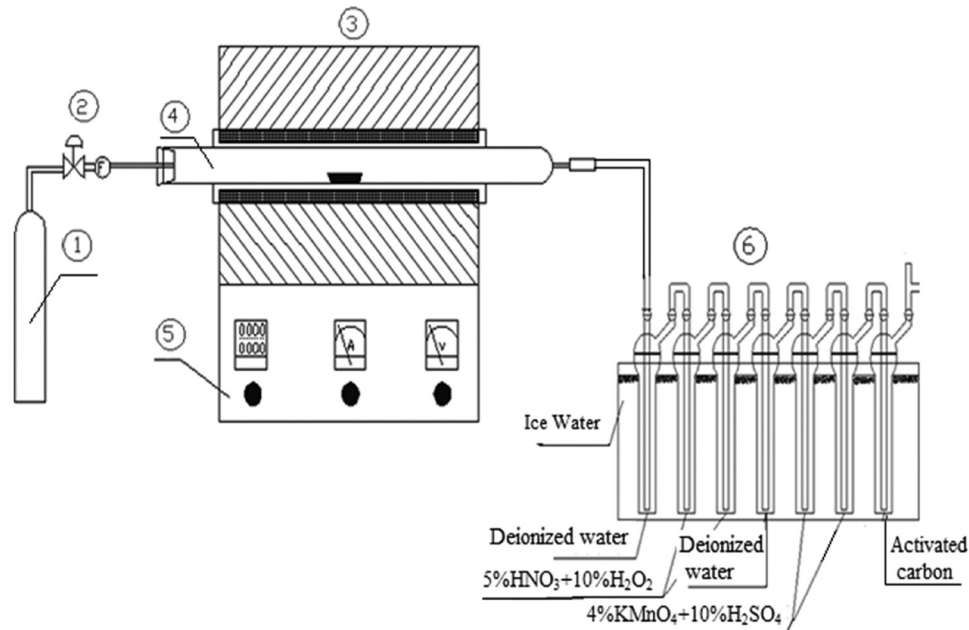


Figure 1. Scheme of the experimental apparatus. 1-gas bottle, 2-gas valve, 3-tubular resistance furnace, 4-quartz glass tube, 5-temperature controller, 6-the impinger train for gas adsorption.

mosphere furnace SGQ-6-12 type, diameter = 72 mm, length = 1000 mm) and an impinger train (Figure 1) which was made to adsorb the zinc present in the flue gas.

For the research of the combustion time and temperature effects on the volatilization of zinc, a series of combustion experiments of SS was carried out at 900°C with varied combustion time (20, 40, 60, 90 and 120 min), and a series of combustion experiments for 60 min at varied combustion temperatures (900, 950 and 1000°C). For the research of the chlorine and phosphorus effects on the volatilization of zinc, SS with three levels of chlorine addition (2.00%, 4.00% and 8.00%) and phosphorus addition (5.00%, 10.00% and 15.00%) were then combusted to study their impacts on the zinc volatilization at 900°C during 60 min. All these combustion experiments were carried out in air with a gas flow of 3.00 L/min (0°C, 101KPa).

After those combustion experiments, the residues in the quartz glass tube were collected as SSA, and the zinc volatilized into the flue gas was adsorbed by the impinger train. The contents of zinc in the SSA and the impingers train were then analyzed by the atomic

absorption spectrometer (AAS 200, Perkin Elmer, US) after digestion, as described elsewhere [13]. X-ray diffraction (XRD-X Pert PRO, Holland) was used to analyze the combined form of zinc in SSA over a range of 2θ angles between 10° and 80° using Cu $K\alpha$ radiation at 40 KV and 30 mA setting.

The volatilization rate of zinc was calculated according to the following formula:

$$\text{Volatility} = \left(1 - \frac{C_{slag} M_{slag}}{C_{sludge} M_{sludge}} \right) \times 100\% \quad (1)$$

where C_{slag} and C_{sludge} are the contents of zinc in SSA and SS, respectively; M_{slag} and M_{sludge} are the masses of SSA and SS, respectively.

THERMODYNAMIC EQUILIBRIUM SIMULATION

A conventional thermodynamic calculation was carried out by HSC-Chemistry 5.0 software [14,15] based on the free Gibbs energy minimization in order

Table 1. Elemental Analysis of the SS and the Contents of Heavy Metals in SS (dry basis).

Element	C	H	O	N	Cl	S	p	Si
Content (wt%)	12.36	1.80	13.30	2.05	0.03	0.59	0.92	5.01
Element	Zn	Cu	Pb	Ni	Cd	Cr		
Content (mgt/kg)	1580.92	648.60	15.93	89.97	1.32	444.79		

to simulate the chemical speciation of zinc in SS combustion. The calculations were performed in air atmospheres (79.00% N₂ and 21.00% O₂), considering an air excess number (α) of 1.4 in SS combustion. Then, the main elements considered were C, H, O, N, Si, S, P, Cl and Zn with the input value of 10.30, 18.00, 34.37, 99.50, 7.85, 0.19, 0.30, 8.60×10^{-3} and 2.42×10^{-2} mol in the HSC-Chemistry 5.0 software, respectively, which were calculated from the real elemental contents of SS and air. The calculations were performed in a temperature range between 100°C and 1600°C under atmospheric pressure. In the results of the calculations, “s” represented the solid phase and “g” represented the gas phase.

RESULTS AND DISCUSSION

Impacts of Combustion Time and Temperature

Figure 2(a) and 2(b) show that the volatilization

rates of zinc of all samples were below 10.00%, and most of the zinc was solidified in the SSA. The volatilization rate of zinc rises gradually with the increase of combustion time and temperature, but the impact of both factors was small. The results of experimental mass balances of zinc are shown in Figure 2(b), in which “Slag” represents the percentage of zinc in SSA; “Adsorbent” represents the percentage of zinc in the impinger train; “Cleaning solution” represents the percentage of zinc remained in the quartz burner tube, which was washed by 3% HNO₃; and “Loss” represents the percentage of zinc that could not be measured. The result of the experimental mass balances of zinc showed that the loss of zinc was slight [Figure 2(b)]. According to thermodynamic equilibrium data, the dominant chemical speciation of zinc below 400°C was ZnSO₄(s) [Figure 2(c)]; however, it was mainly in the form of phosphate in the solid phase when the combustion temperature increased from 500–1200°C, which was experimentally detected by XRD in SSA

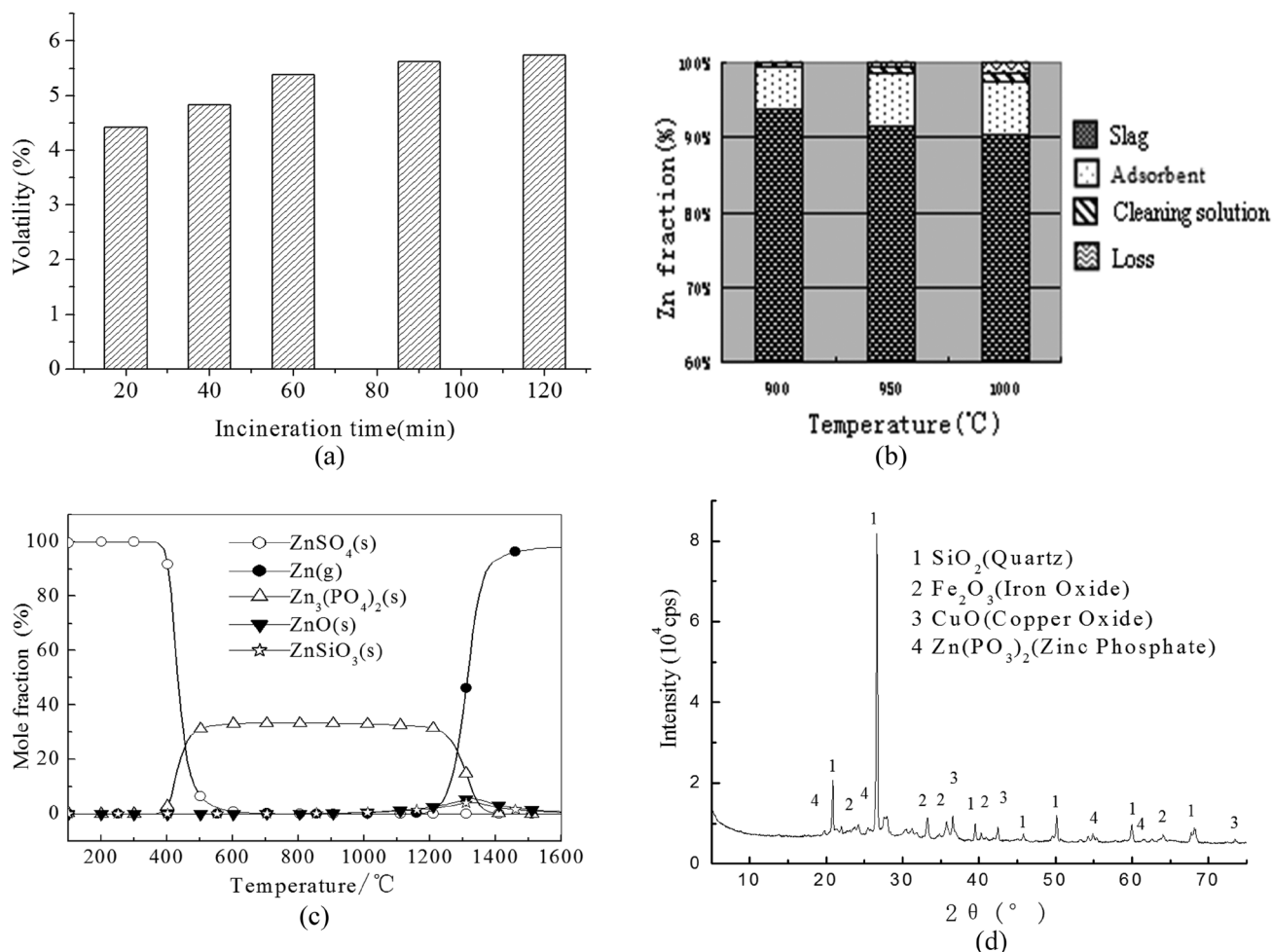


Figure 2. The effects of combustion time and temperature on the distribution of zinc: (a) volatility of zinc; (b) mass balance of zinc; (c) thermodynamic simulation results; (d) XRD results of a representative sample of SSA (900°C, 60 min).

at 900°C [Figure 2(d)]. According to thermodynamic equilibrium data, at temperatures above 1300°C, zinc was released as metallic vapor. Comparing the theoretical and experimental results, it could be found that the thermodynamic equilibrium simulation could describe the tendency of the chemical reaction and the speciation of the reaction products, but the prediction of the volatilization rate of zinc greatly varied from the experimental results due to chemical reaction dynamics.

Impact of Chlorine

To determine the effects of chlorine on Zn distribution, different samples of SS were combusted with the addition of 2.00–8.00% chlorine. As shown in Figure 3(a), it could be found that the volatilization rate of zinc increased significantly with chlorine addition. In addition, the volatilization rate of heavy metals zinc in the treated SSA appeared in the trend of increased then decreased, and the increasing speed is fast, the volatilization rate of zinc had been increased from 6.37% without chlorinating addition to 45.7% with chlorinating addition 8%.

As seen in Figure 3(b), zinc was mainly in $\text{ZnSO}_4(\text{s})$ at lower temperature, and with the increasing of temperature, $\text{ZnSO}_4(\text{s})$ transforms gradually to $\text{Zn}_3(\text{PO}_4)_2(\text{s})$, and then, transformed to $\text{Zn}(\text{g})$ and $\text{ZnCl}_2(\text{g})$ with the presence of NH_4Cl . The comparison of Figure 3(a) and 3(b) proved that the presence of the chlorine promotes zinc volatilization in chloride form.

As shown in Figure 3(c), the main crystal component of SSA were SiO_2 and Fe_2O_3 , and $\text{Zn}(\text{PO}_3)_2$ also was detected in the SSA by XRD analysis with chlorine addition of 2.00%, which also could prove the result of thermodynamic calculation that the main form of zinc at 900°C was phosphate.

Impact of Phosphorus

To demonstrate the influence of the phosphor addition (added in the form of $(\text{NH}_4)_3\text{PO}_4$) on the volatilization rate of zinc, some similar experiments were exerted. The results in Figure 4(a) show that the volatilization rate of zinc in the treated SSA appears in the trend of first decreased then increased (V-shape). The volatilization rate of zinc declined from 6.37–4.05% when phosphor addition increased from 5.00% to 10.00%, and then, increased to 5.65% when phosphor addition was 15%. According to the equilibrium data, phosphor addition in the form of $(\text{NH}_4)_3\text{PO}_4$ could inhibit the volatilization of zinc.

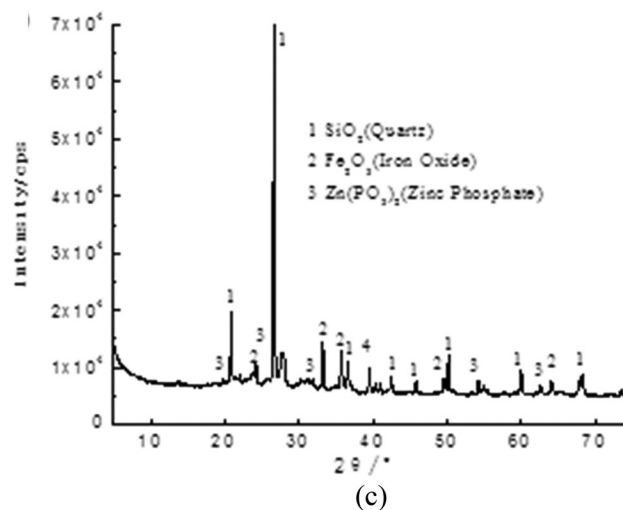
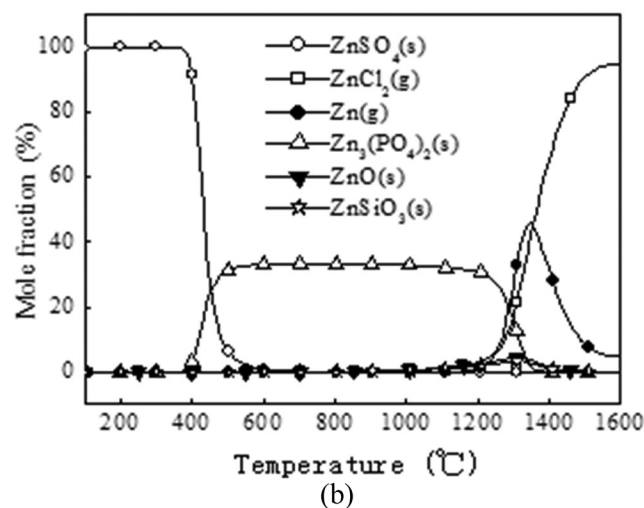
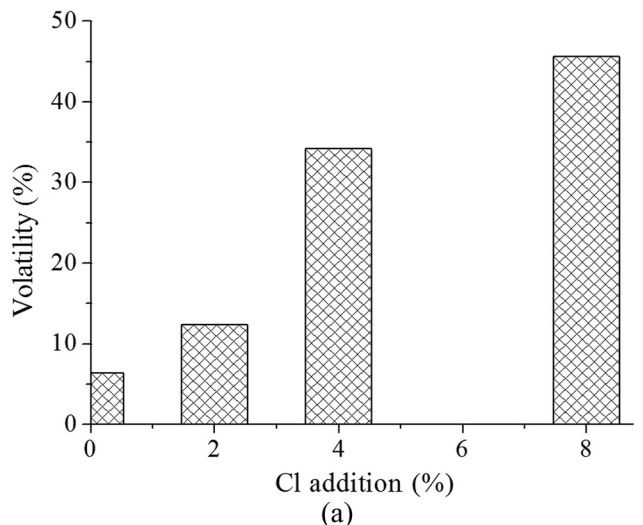


Figure 3. Effects of chlorine on the distribution of zinc: (a) volatility of zinc; (b) results of the thermodynamic calculation with the addition of 2.00% chlorine; (c) XRD results of a representative sample of SSA with the addition of 2.00% chlorine.

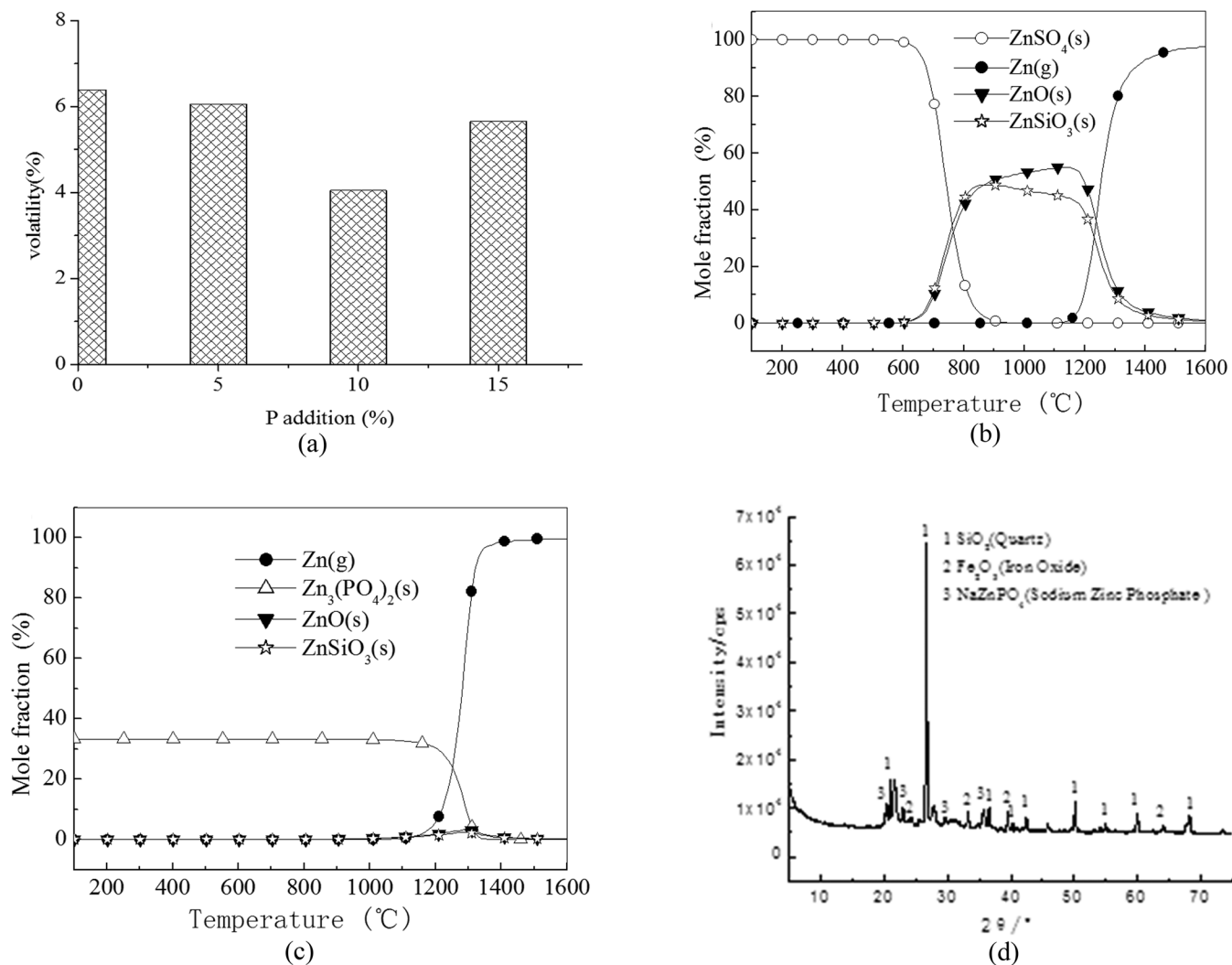


Figure 4. Effects of phosphor on the distribution of zinc: (a) volatility of zinc; (b) results of the thermodynamic calculation without phosphor; (c) results of the thermodynamic calculation with the phosphor addition of 10.00%; (d) XRD results of a representative sample of SSA with the phosphor addition of 10.00%.

As seen in Figure 4(b), ZnSO₄(s) was the main chemical speciation below 700°C without phosphorus. With the increase of temperature, ZnSO₄(s) transformed to ZnO(s) and ZnSiO₃(s), and when the temperatures was above 1100°C, zinc volatilized in the form of Zn(g). However, in the presence of phosphorus, when the temperatures was below 1100°C, the main form of zinc was Zn₃(PO₄)₂(s). Compared with Figure 4(a), it can be proved that phosphorus addition in the form of (NH₄)₃PO₄ could inhibit the volatilization of zinc through formation of Zn₃(PO₄)₂, which was identified by the XRD analysis of the SSA with phosphorus addition of 10.00% as shown in Figure 4(d).

CONCLUSIONS

According to the results of experiments, the phos-

phorus addition could raise the proportion of zinc in SSA through the formation of NaZnPO₄ and Zn(PO₃)₂. However, zinc volatilization during SS combustion significantly increased after chlorine addition, reaching 45.70% when the chlorine addition in the SS was 8.00%.

The results of thermodynamic calculations indicated that ZnSO₄(s) was the main chemical speciation at the lower combustion temperature. However, zinc was mainly in the form of phosphate in solid phase at higher temperatures (up to 1200°C) and it existed as gaseous substance above 1200°C. In addition, the fraction of ZnCl₂(g) obviously increased with chlorine addition and the fraction of Zn₃(PO₄)₂(s) obviously increased with phosphorus addition.

Comparing the thermodynamic calculation results with those combustion experiment results, it could be

found that the volatilization rate of zinc increased with chlorine addition significantly through the formation of metal chloride. However, phosphor additive restrained the volatilization of zinc.

ACKNOWLEDGEMENT

Thanks for the supports of National Basic Research Program of China (2011CB201500), and National Natural Science Foundation of China (51276119).

REFERENCES

1. K. Hashimoto, T. Doi, T. Okuda, W. Nishijima, S. Nakai, K. Nishimura. "Function of Wood Chips for Composting of Sewage Sludge by Thermophilic and Aerobic Digestion," *Journal of Residuals Science & Technology*, Vol. 12, No. 2, 2015, pp. 53–59. <http://dx.doi.org/10.12783/issn.1544-8053/12/2/3>
2. M. Aneta, S. Werle. "Analysis of the combustion and pyrolysis of dried sewage sludge by TGA and MS," *Waste management*, Vol. 34, No. 1, 2014, pp.174–179.
3. F. Zsabokorszky. "Present and Future Sewage Sludge Treatment in Hungary and its Energetic Utilisation," *Journal of Residuals Science & Technology*, Vol. 10, No. 4, 2013, pp.161–164.
4. A. Davidsson, E. Eriksson, F. Jerker. "Ozonation and thermal pre-treatment of municipal sewage sludge-implications for toxicity and methane potential," *Journal of Residuals Science & Technology*, Vol. 10, No. 2, 2013, pp. 85–91.
5. M.Pazos, G.M. Kirkelund, L.M. Ottosen. "Electrodialytic treatment for metal removal from sewage sludge ash from fluidized bed combustion," *Journal of Hazardous Materials*, Vol. 176, No. 1, 2010, pp. 1073–1078. <http://dx.doi.org/10.1016/j.jhazmat.2009.11.150>
6. J. Yang, G.H. Guo, T.B. Chen. "Concentrations and variation of heavy metals in municipal sludge of China," *China Water and Wastewater*, Vol. 25, No. 13, 2009, pp. 122–124. (In Chinese).
7. Z.S. Liu. "Control of heavy metals during incineration using activated carbon fibers," *Journal of Hazardous Materials*, Vol.142, No.1, 2007, pp. 506–511. <http://dx.doi.org/10.1016/j.jhazmat.2006.08.055>
8. Y. Zhang, and Y. Chi. "An Experiment Study on Distribution of Heavy Metals in the Incineration of Sludge," *Power System Engineering*, Vol. 21, No. 3, 2005, pp. 27–29. (In Chinese)
9. Chang-Hwan Jung, Masahiro Osako. "Thermodynamic behavior of rare metals in the melting process of municipal solid waste (MSW) incineration residues," *Chemosphere*, Vol. 69, No. 2, 2007, pp. 279–288. <http://dx.doi.org/10.1016/j.chemosphere.2007.03.071>
10. G. Fraissler, M. Joller, and T. Brunner. "Thermodynamic equilibrium calculations concerning the removal of heavy metals from sewage sludge ash by chlorination," *Chemical Engineering and Processing: Process Intensification*, Vol. 48, No. 1, 2009, pp. 152–164. <http://dx.doi.org/10.1016/j.cep.2008.03.009>
11. C. Xie, J. Zhao, J. Tang, J. Xu, X. Lin, X. Xu. "The phosphorus fractions and alkaline phosphatase activities in sludge," *Bioresource Technology*, Vol. 102, No. 3, 2011, pp. 2455–2461. <http://dx.doi.org/10.1016/j.biortech.2010.11.011>
12. M. Garcia-Albacete, A. Martín, M. C. Cartagena. "Fractionation of phosphorus biowastes: characterisation and environmental risk," *Waste management*, Vol. 32, No. 6, 2012, pp. 1061–1068.
13. U.S. Environmental Protection Agency (USEPA).1996. "Method 29-Determination of Metal Emissions from Stationary Sources," Office of Air Quality Planning and Standards, Washington, D.C.
14. Huan-Liang Tsai, Chi-Sheng Wang. "Thermodynamic equilibrium prediction for natural gas dry reforming in thermal plasma reformer," *Journal of the Chinese Institute of Engineers*, Vol. 31, No. 5, 2008, pp. 891–896. <http://dx.doi.org/10.1080/02533839.2008.9671444>
15. J. Kakumazaki, K. Takahiro, S. Katsuyasu. "Recovery of gold from incinerated sewage sludge Ash by chlorination," *ACS Sustainable Chemistry & Engineering*, Vol. 2, No. 10, 2014, pp. 2297–2300. <http://dx.doi.org/10.1021/sc5002484>

Study on Nonlinear Model Predictive Control of Activated Sludge Process

LI HONGLU¹, FENG YUZHAO^{2,*}, ZHANG XIAOQIN³, YU HAIBO¹, ZHANG HENG¹ and SUN RONGJI¹

¹Dept. of Environmental Engineering, Chongqing Logistics Engineering University, Chongqing, China

²Dept. of Engineering Management, Chongqing Logistics Engineering University, Chongqing, China

³National Research Centre, Chongqing Logistics Engineering University, Chongqing, China

ABSTRACT: The model predictive control (MPC) with a nonlinear back propagation (BP) was used to design activated sludge process control system, and then a new improved dynamic matrix controller (IDMC) design method was proposed. The method was tested with the digital simulation analysis in a small-scale wastewater treatment plant based on benchmark simulation model No.1 (BSM1). The results showed that IDMC designed by the method has good dynamic characteristics and strong adaptability to stock load, and thus improves stability of the control system.

INTRODUCTION

ACTIVATED SLUDGE process is widely applied in wastewater treatment [1–6]; many wastewater treatment methods are based on it, such as oxidation ditch, sequencing batch reactors (SBR) [7], anaerobic-anoxic-oxic process (A²/O process) [8]. To improve effluent quality and reduce energy consumption, a combination of activated sludge process and excellent control technology is needed.

The mechanism of wastewater treatment is complicated and difficult to model. The treatment process is strongly nonlinear and severely interfered by many factors. Therefore, common control techniques are not effective [9–12].

Activated sludge process is too complicated for a precise model to be built and it is strongly nonlinear with severe interference. Model predictive control (MPC) can work without a precise model. It has good stability and anti-interference ability. The understanding of MPC has significant implications in the area of wastewater treatment. In this paper, the model predictive control (MPC) with a nonlinear back propagation (BP) was used to design activated sludge process control system, and then a new design method improved dynamic matrix controller (IDMC) method was proposed.

SIMULATION MODEL

Benchmark Simulation Model No.1 (BSM1) is a simulation environment developed by the European Cooperation in the field of Scientific and Technical Research (COST) [13]. It defines a wastewater treatment plant layout, process models, influent data, simulation procedure and performance index [14]. BSM1 provides a reliable, convenient, perfect simulation environment, and it is an ideal tool for researchers to design, debug and compare control algorithms.

Plant Layout

The BSM1 plant is composed of 5 biological reactors and a secondary settling tank. Its layout is shown in Figure 1. The biological reactors include two 1000-m³ anoxic tanks and three 1333-m³ aerated tanks. For the first two aerated tanks, the default value of oxygen transfer coefficient (K_{La}) is 10/h. For the third aerated tank, K_{La} is 3.5/h without control action. The secondary settling tank is divided into ten 0.4-m-high layers. After the biological treatment, part of the wastewater returns to the first anoxic tank at a default flow rate of 55338 m³/d to go through the reactions again, which is called the internal recycle. The left flows into the secondary settling tank from the 6th layer and precipitates. After settling, clean water flows out from the 10th layer. Muddy water flows out from the 1st layer and returns to the first anoxic tank as well, which is called the external recycle. The waste sludge is discharged at a rate of 385 m³/d.

*Author to whom correspondence should be addressed.

Email: 1297345332@qq.com or 741767660@qq.com; Tel.: +862368731208; Fax: +862368581977

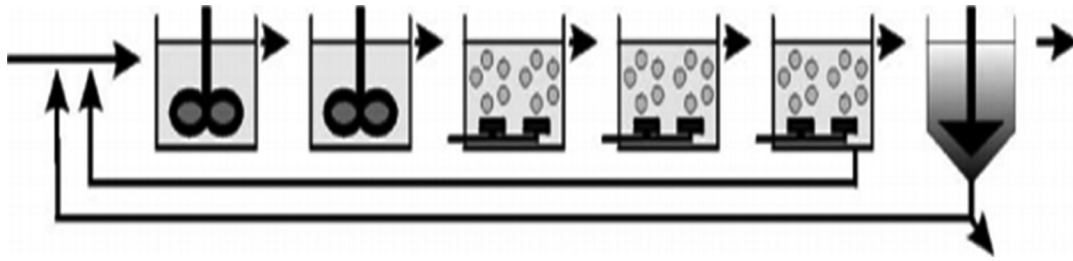


Figure 1. BSM1 plant layout.

Process Models

The above biological process is simulated using the Activated Sludge Model No.1 (ASM1) developed by the International Association of Water Quality (IAWQ). The above settling process is modeled using the double-exponential settling velocity function. Both models are recognized worldwide.

Influent Data

The influent data designed by the IAWQ for BSM1 are based on a large amount of actual data [15]. The data include 3 weather conditions, i.e., dry, rainy and stormy weather. For each weather condition, data over 14 days are included and the sample time for each day is 15 minutes. There are 15 data for each sampling point: t , S_I , S_S , X_I , X_S , $X_{B,H}$, $X_{B,A}$, X_P , S_O , S_{NO} , S_{NH} , S_{ND} , X_{ND} , S_{ALK} and Q . The influent S_{NH} concentration in dry weather is shown in Figure 2.

Control Variable

S_{NH} is one of the main wastewater pollutants, and denitrification is an important step in wastewater treatment. In this paper, K_{La} for the last aerated tank is cho-

sen as a manipulated variable to control the effluent S_{NH} .

DESIGN OF A NONLINEAR DYNAMIC MATRIX CONTROL (DMC) ALGORITHM

MPC was introduced in the 1970s. It has been developing with the rapid development of computer technology and successfully applied in industry practice. MPC is not only a kind of control algorithm but also a generalized method of control, including model algorithmic control (MAC), DMC, generalized predictive control (GPC).

This paper focuses on DMC. According to its principle [16], DMC is a control algorithm based on an approximate linear model which can be obtained by the step response of the controlled object. DMC can achieve the desired control effect when the controlled object is linear or a weakly nonlinear system. However, if the controlled object is a strongly non-linear system, linear model-based DMC would lead to model mismatch, resulting in poor control performance and big errors in control results.

Artificial neural network (ANN) is a kind of intelligent algorithm [17]. It can establish a mathematical model of the object by learning the historical informa-

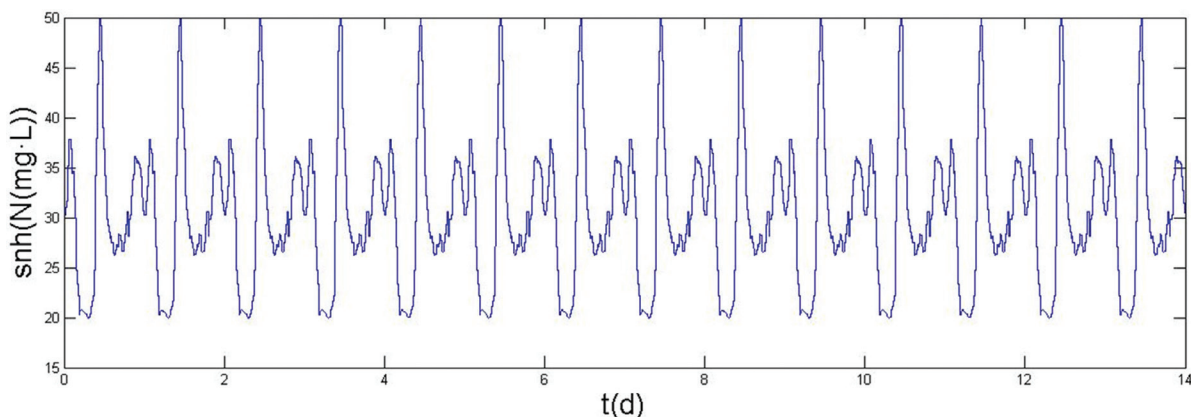


Figure 2. Influent S_{NH} concentration in dry weather.

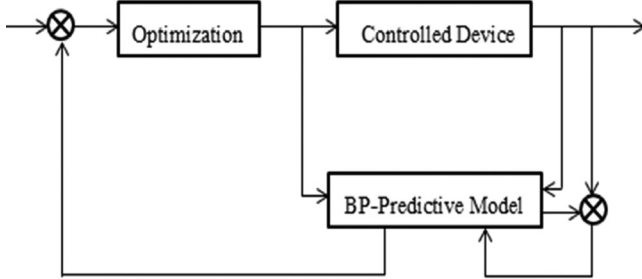


Figure 3. The principle of nonlinear DMC.

tion of the object. In this paper, back propagation (BP), which is the most widely applied in neural network modeling, is used to establish a nonlinear model of the controlled object. And the model is then used as a prediction model in DMC to improve predictive accuracy.

The Principle of Nonlinear DMC Algorithm

The principle of nonlinear DMC algorithm is shown in Figure 3. The method to improve DMC is to replace the linear model with the nonlinear model built with BP:

$$\tilde{y}(k+1) = \hat{f} \begin{bmatrix} y(k), y(k-1), \dots, y(k-n+1), \\ u(k), u(k-1), \dots, u(k-m+1) \end{bmatrix}$$

$y(k)$ is the output of the controlled object at moment k ; $u(k)$ is the manipulated variable at moment k . $\tilde{y}(k+1)$ is the predictive output at moment $k+1$. Here, $m = n = 2$.

It is worth noting that the prediction model should predict P output: $\tilde{y}(k+i)$, $i = 1 \dots P$; when $i = 1$, all the dependent variables of $\hat{f}(\cdot)$ take their real values, but when $i > 1$, $y(k+1)$, will be replaced by the predictive value of $\tilde{y}(k+i)$.

In order not to increase computational complexity, the part of rolling optimization remains the same as that in general DMC.

In order to deal with interference and avoid model mismatch, feedback calibration is performed.

Simulation and Analysis

Figure 4 shows the simulation results of DMC and BP-DMC.

As shown in Figure 4, BP-DMC was superior at some times but inferior at the other times to the general DMC. The mean deviation of general DMC was 1.2488 while that of BP-DMC was 1.2565. Overall, BP-DMC was inferior because: There were errors in the model; the training information was incomplete, and the errors of the model at some times were too large; except for the predictive output at moment $k+1$, those at moments $k+2, \dots, k+P$ used the predictive value of last moment as one of the dependent variables, which caused rapid increase in error.

In conclusion, BP-DMC needs further improvement.

IMPROVEMENT OF NONLINEAR DMC ALGORITHM

According to the conclusion of the previous section, because of large errors at some times, BP-DMC is not better than general DMC. In this section, BP-DMC is to be supplemented by DMC to improve predictive accuracy.

Specifically, BP-DMC and general DMC were put in parallel and the predictive outputs of the two algorithms were compared to the real output at each moment. Then the algorithm with a smaller difference was used to obtain the manipulated variable u at the

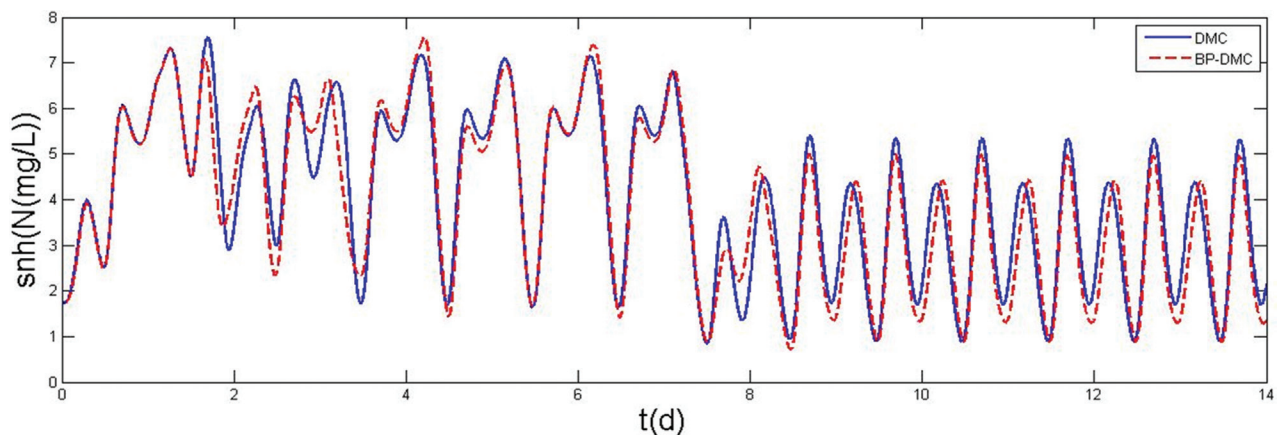


Figure 4. Comparison between DMC and BP-DMC simulation results.

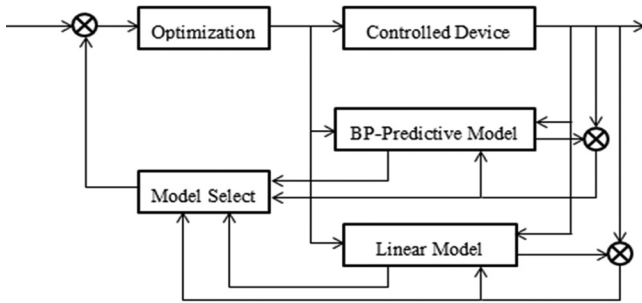


Figure 5. Principle of the improved BP-DMC.

moment. The principle of the improved BP-DMC is shown in Figure 5.

The simulation result is shown in Figure 6.

As shown in Figure 6, the improved BP-DMC had an ideal effect with a mean deviation of 1.0673, decreasing by 14.5 percent.

CONCLUSION

The improved BP-DMC takes the advantage of the high accuracy at some times of BP-DMC and the supplementation of general DMC at the other times. Simulation experiments on benchmark simulation model No.1 (BSM1) were conducted. The results showed that the improved DMC predicted more accurately and had an ideal effect with a mean deviation of 1.0673, decreasing by 14.5 percent. The improved BP-DMC has practical value in modeling of activated sludge process.

In the future, how to choose representative training data to make BP-DMC useful in more areas is worth exploring.

ACKNOWLEDGEMENTS

This work was supported by the National Water Pol-

lution Control and Management Scientific Major Project (Grant No. 2008ZX07315-003).

REFERENCES

1. Henze, M., Gujer, W., Mino, T., *et al.*, Activated sludge model No.1, IAWPRC, London, 1987.
2. Henze, M., Gujer, W., Mino, T., Matsuo, T. and Wentzel, MC., "Activated sludge model No.2d (ASM2D)", *Journal of Water Science & Technology*, Vol. 39, No. 1, 1999, pp.165–182. [http://dx.doi.org/10.1016/S0273-1223\(98\)00829-4](http://dx.doi.org/10.1016/S0273-1223(98)00829-4)
3. Gujer, W., Henze, M., Mino, T., and Loosdrecht, MV., "Activated sludge model No. 3", *Journal of Water Science & Technology*, Vol. 39(98), No. 1, 1999, PP. 183–193.
4. Henze, M., Gujer, W., Mino, T., *et al.*, Activated sludge models ASM1, ASM2, ASM2d and ASM3, IAWPRC, London, 2006.
5. Wang, D.S., Xu, X.Z., Liu, Z.Q., Gu, X.L. and Xu, G.R., "Optimized Coagulation on a Municipal Wastewater Treatment: Competitive and Synergetic Effect Among Different Pollutants," *Journal of Residual Science & Technology*, Vol. 6, No. 3, 2009, pp. 157.
6. Aimin, A., Qi, L.C., Zhang, H. and Chou, Y.X., "The Analysis of Impact Factors for Dissolved Oxygen Concentration in Wastewater Treatment System Using an Adaptive Modeling Method," *Journal of Residuals Science & Technology*, Vol. 06, No. 12, 2015, pp. S25–S30.
7. Tian, Y, Li, ZP, Zhang, J and Wu, D. "Investigation into the Fate of a Metabolic Uncoupler, 2,6-dichlorophenol in the Sequence Batch Reactor System," *Journal of Residual Science & Technology*, Vol. 06, No. 3, 2009, pp. 129.
8. Wang, C.W., Li, J., Zhao, B.H., Yue, Y.D. and Wang, Y.L., "Effect of Long Sludge Retention Time on Biological Phosphorus Removal in A²O Process," *Journal of Residuals Science & Technology* Vol. 06, No. 12, 2015, pp. S67–S73.
9. Lee, B.K., Sung, S.W., Chun, H.D. and Koo, JK., "Automatic control for DO and pH in the activated sludge process in a coke wastewater treatment plant," *Journal of Water Science & Technology*, Vol. 37, No. 12, 1985, pp. 142–148.
10. Olsson, G., Rundqwist, L., Eriksson, L. and Hall, L., 1985, Self-tuning control of the dissolved oxygen concentration in activated sludge systems, Oxford, Pergamon Press.
11. Machado, V.C., Tapia, G., Gabriel, D., Lafuente, J. and Baeza, JA., "Systematic identifiability study based on the Fisher Information Matrix for reducing the number of parameters calibration of an activated sludge model," *Journal of Environmental Modelling & Software*, Vol. 24, No. 11, 2009, pp. 1274–1284. <http://dx.doi.org/10.1016/j.envsoft.2009.05.001>
12. Kim, S., Lee, H., Kim, J., Kim, C and Ko, J., "Genetic algorithms for the

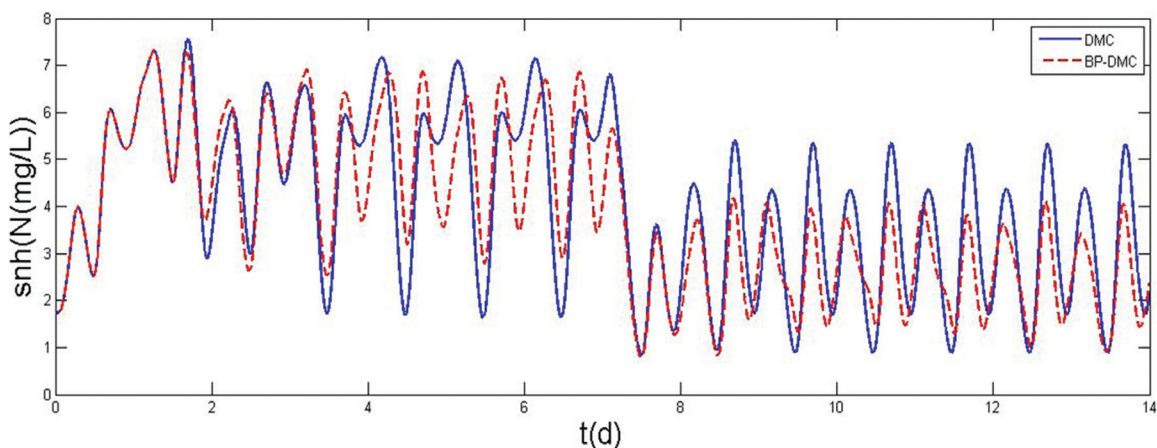


Figure 6. Comparison between DMC and improved BP-DMC simulation results.

- application of Activated Sludge Model No.1," *Journal of Water Science & Technology*, Vol. 45, No. 4, 2002, pp. 405–411.
13. Corpp, J. 2001. The COST simulation benchmark: Description and Simulator Manual, Luxembourg: Official Publications of the European Community.
 14. Alex, J., Benedetti, L., Corpp, J., *et al.*, Benchmark simulation model no. 1 (BSM1), IWA, 2008.
 15. M. N. Pons., Benchmark 1, Oct. 15, 2007: Office for Official Publications of the European Communities, <http://www.ensic.u-nancy.fr/COSTWWTP>.
 16. Xi, Y.G. 1993. Predictive Control. Beijing: National Defense Industry Press.
 17. Fu, H.X., Zhao, H. 2010. MATLAB ANN application and design, Beijing: China Machine Press.

Addition of Calcium Compounds Improve the Yield of Hydrogen and Retention of Chromium Metal during the Gasification of Simulated Waste

LIN CHIOU-LIANG, WU MIN-HAO* and HSU TZU-PIN

Department of Civil and Environmental Engineering, National University of Kaohsiung, 700, Kaohsiung University Rd., Nanzih District, 811, Kaohsiung, Taiwan, R.O.C.

ABSTRACT: This study explored the constituents of syngas and the distribution of chromium metal when different calcium compounds ($\text{Ca}(\text{NO}_3)_2$, CaCO_3 and CaO) were used as additives. In this experiment, artificially simulated waste was taken as the biomass for gasification and chromium metal was used as the heavy metal in the simulated waste. The syngas composition, the yield of H_2 and the retention of chromium metal were analyzed. Results showed that all the three calcium compounds could increase the proportion of H_2 , but that there was no significant difference between them. The contents of chromium in the bed materials with different particle size were measured and displayed that the concentrations of chromium were higher in the bed materials with particle diameters above 1.00 mm and below 0.35 mm. Under the operation temperature of 700°C , the calcium compounds retained the highest content of chromium metal, for it evaporated only a little under this low temperature. Therefore, adding calcium compounds into the fluidized bed during the gasification of the waste could enhance the yield of H_2 in the syngases and increase the content of retained chromium metal in the sand bed.

INTRODUCTION

CURRENTLY, there are 24 large incineration plants in Taiwan, which treat over 6 million tons of waste and generate about 1 million tons of combustion residue and about 300,000 tons of fly ash. According to the statistics released by Taiwan Environmental Protection Bureau, the disposal rate of urban solid waste has been 99.9% since 2008, and 97% of the waste (excluding the recycled one) is incinerated [1]. After recycling, most of the rest waste is organic. If the waste is gasified rather than incinerated, the waste can be decomposed and re-usable energy is generated, which creates positive effects on the sustainable development of the resources on the earth. In gasification, carbon materials (e.g., biomass and coal) are partly gasified under a high temperature into compound gases (H_2 , CO and CH_4). In general, the frequently-seen operation parameters in gasification include feeding material, temperature, pressure, feeding particle diameter, the particle diameter of bed material, the type of gas, equivalence ratio (ER), and steam/biomass ratio [2,3]. Many researches

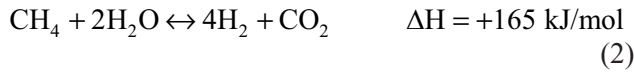
have shown that operation temperature and ER have major influences.

Luo *et al.* [4] pointed out that the carbon conversion efficiency would increase from 61.96–92.59% and the yield of gases would rise from $1.15 \text{ Nm}^3/\text{k}$ to $2.53 \text{ Nm}^3/\text{kg}$ when the operation temperature climbed up from $600\text{--}900^\circ\text{C}$. According to Alauddin *et al.* [3], temperature had significant impact on thermal transmission, as a higher temperature inside the gasifier would enhance the thermal transmission rates of the bed materials and the feeding materials and then influence the constituents of the generated gases. Schuster *et al.* [5] proposed that a high temperature would quicken dissociation, generate more gases, increase the thermal energy for the water gas shift reaction, and promote the endothermic reaction. Luo *et al.* [4] found that a higher operation temperature would accelerate the methane-steam reforming, the water-gas shift reaction and the Boudouard reaction, and thus create more H_2 and CO . These relative reaction mechanisms show as follows:

Methane-steam reforming



*Author to whom correspondence should be addressed.
Email: cllin0407@nuk.edu.tw



Water-gas shift reaction



Boudouard reaction



Another important parameter is ER, which is defined as “actual air fuel ratio/stoichiometric air fuel ratio”. Lv *et al.* [6] explored the influence of the adjustment of ER on the constituents of generated gases in gasification and found that when ER rose from 0.19 to 0.27, the CO₂ in the generated gases increased while CO and H₂ slightly decreased, for a higher ER led to more oxygen in the reaction and fasten carbon conversion. Li *et al.* [7] indicated that in the gasification procedure of a fluidized-bed gasifier, the content of H₂ and CO declined when the ER increased from 0.31 to 0.47. According to Basu [8], an ER lower than 0.2 would result in inadequate oxygen in the gasifier and the dissociation of gasification, which would generate more char, while an ER higher than 0.4 would lead to excessive fully combusted materials like CO₂ and H₂O in the gasifier, which would result in a low heating value of syngases. Therefore, Alauddin *et al.* [3] found that an appropriate ER range was from 0.2 to 0.4 in a gasifier. Maglinao *et al.* [9] suggested that the typical ER ratio in a pilot scale bubbling fluidized bed biomass gasifier was from 0.20 to 0.50. Therefore, ER parameter controlled at 0.3 seems to be a suitable value.

Currently, two kinds of gasifiers (the fluidized bed gasifier and the fixed bed gasifier) are widely used in business and various researches. The fluidized bed gasifier features an effective mass and thermal transmission, a good mixture of bed materials, an even bed temperature, and high flexibility of feeding. It is suitable for developing technologies to generate more syngas from biomass, which makes it very popular. Another advantage of the fluidized bed is that adsorbents can be added into the furnace to increase the yield of syngas or adsorb heavy metals in waste or biomass. In general, there is 0.22–0.34% of non-iron metals in waste when the gasification temperature stays in the range of 700–900°C, so it is possible that some heavy metals will emit into the environment and cause secondary pollu-

tion or harm to human body [10]. Under a high temperature, heavy metals cannot be destroyed and would become metal vapor or small particles, which would be emitted with flue gas or attach to the bed materials [11], so it is very important to control the heavy metals in gasification.

According to Ho *et al.* [12], heavy metals could be controlled through inhibiting the evaporation of metal compounds and adding solid adsorbents. The reactor of the fluidized bed allows effective contact between adsorbents and metal compounds as well as a mixed reaction, so it is the best reactor to control the evaporation of heavy metals by adding adsorbents. The frequently-used adsorbents include calcium-based and silica alumina adsorbents. Ho *et al.* [13] took adsorbents such as limestone, bauxite and zeolite as the bed materials of the fluidized bed and added heavy metals like Cr, Pb and Cd into the stimulated wastes to investigate the effects of the adsorbents on controlling the heavy metals. The research results showed that limestone was the best to adsorb the three heavy metals. Liu *et al.* [14] used CaO and CaCO₃ as additives to control heavy metal emission during waste incineration. The results showed that the defluidization time was prolonged and the emission of heavy metals was decreased. For waste thermo treatment, the control of heavy metal emission is an important problem. If adding calcium compounds can decrease the emission of heavy metals in the gasification of waste and may increase the content of H₂ in the syngases at the same time, it will greatly enhance the popularity of the waste gasification. Hence, this study focused on the influences of different calcium compounds (CaO, CaCO₃, Ca(NO₃)₂) on the syngas generation and the chromium metal distribution in the bed materials in a gasifier with fluidized bed, so as to provide references for the future development of waste gasification technologies.

METHODS

Experimental Materials

Most of the gasification biomass in the experiment was artificially stimulated waste, including sawdust, polypropylene (PP), polyethylene (PE) plastic bags and chromium metal solution. Table 1 showed the ultimate analysis. Table 2 listed the results of heating value and proximate analysis of the artificially stimulated waste. The main operation parameters of the experiment were gasification temperature (700°C, 800°C, 900°C) and types of added calcium compounds (Ca(NO₃)₂, CaCO₃

Table 1. The Ultimate Analysis of Artificial Waste.

Species	Polypropylene (wt%)	Polyethylene (wt%)	Sawdust (wt%)
C	86.16	85.71	43.12
H	12.20	13.04	5.80
O	0.52	0.39	46.0
N	1.12	0.86	5.01

and CaO). Three calcium compounds and the chromium metal solution were added into the PE plastic bags with PP plastic particles and sawdust. In the gasification, the parameters were set unchanged, including gas velocity ($1.3 U/U_{mf}$), particle diameter of silica sand bed material (0.775 mm) and ER (0.3).

Experimental Procedures

The bubbling fluidized bed gasifier was employed in this research, which had been reported in a previous paper [15]. This gasifier is made of stainless steel (AISI 310), with gasifier walls of about 0.3 cm, height of 120 cm and inner diameter of 10 cm. The heating system is based on electricity, and there is a 3-inch layer of heat insulation fiber on the external wall of the gasifier, which is used to prevent heat dissipation. In the gasifier, there are three thermocouples used to record the temperature in the gasifier and report to the temperature control system to control the operating temperature of the gasifier. Under the sand bed is a stainless steel dispersion board, and the silica sand was used as bed material with a fixed particle diameter of 0.775 mm. The density of silica sand was about 2,600 kg/m³. To prevent the gases generated in the gasification from emitting and prevent external air from entering the gasifier during the process of feeding, the feeding part is equipped with a double-valve device.

As for the sampling of the gases generated in the gasification, the sampling gases passed through a glass

Table 2. The Heating Value and Proximate Analysis of Artificial Waste.

Species	Polypropylene (wt%)	Polyethylene (wt%)	Sawdust (wt%)
Proximate Analysis			
Moisture	0.01	0.01	0.74
Volatile matter	99.99	99.99	81.60
Fixed carbon	0.00	0.00	16.60
Ash	0.00	0.00	1.07
Heating Value Analysis			
LHV (MJ/kg)	45.63	44.92	15.10

fiber filter and an impinger (with 100 ml of heavy metal absorption solution containing 33 ml of H₂O₂, 7.67 ml of HNO₃, and 100 ml of deionized water) in a low-temperature water tank. Then, the gases were cooled and the heavy metals in them were absorbed. Subsequently, the GF/A filter paper and silica gel were used to filter the remaining ash and water vapor, and an active pump was adopted to collect the sample which was then put into a sampling bag. After that, a gas chromatography (GC) with a thermal conductivity detector (TCD) was used to analyze the constituents of the syngases. After the gasifier was cooled, the bed material was collected after the experiment. An ASTM standard sieve was adopted to collect bed materials with different particle diameters, which were digested by a microwave digester. After that, the concentration of chromium metal was detected by a flame atomic absorption spectroscopy (FAAS).

RESULTS AND DISCUSSION

Influence of Different Calcium Compounds on the Constituents of the Generated Gases

As shown in Figure 1, before the addition of calcium compounds, there was about 10 mol% of H₂ in the syngas, while the proportion of H₂ increased after the calcium compounds were added. After 19 minutes at the operation temperature, there was more significant increase in the proportion of H₂ which climbed up to about 20 mol% (Figure 1). Chiang *et al.* [16] added 10% of CaO as an additive into the biomass and found that the proportion of CO₂ decreased by 7.5% while the proportion of H₂ slightly increased, for CaO could adsorb the CO₂ generated in the gasification. Except the first minute of sampling, the proportion of CO₂ in the gases declined along with the operation time. The results also showed that different types of the calcium compounds had no significant difference though they could increase the proportion of H₂. With the drastically growing impact of climate changes in recent years, all countries around the world have paid attention to the issues about CO₂ emission. According to this study, calcium-based additives can help reduce CO₂ emission and generate more H₂. This could be taken as a reference for practical operation of factories.

Influence of Different Calcium Compounds on the Distribution of the Chromium Metal in the Bed Materials

After the gasification and the gasifier cooled down

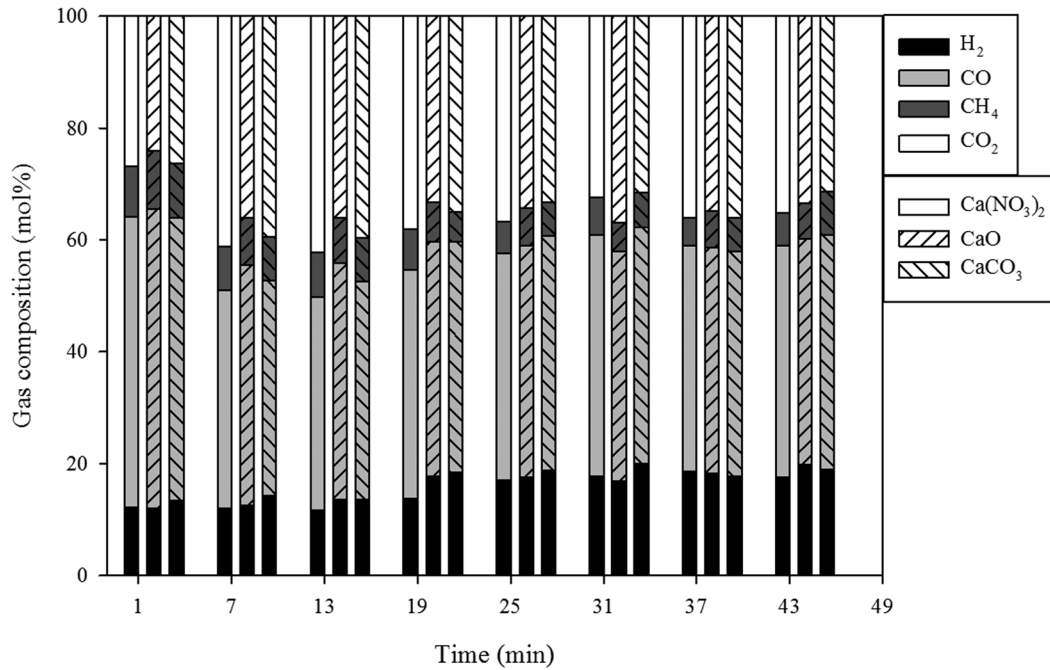


Figure 1. The constituents of syngas in the gasification with different calcium compounds under an operation temperature of 800°C.

to the room temperature, the silica sands were taken out and divided into eight groups according to their particle diameters. After they were digested in a microwave digester, FAAS was used to detect the concentration of the chromium metal. Of the eight bed material samples, the ones with particle diameters above 1.00 mm and below 0.35 mm contained high concentrations of chromium metal (Figure 2).

The possible reason for the higher concentrations of chromium metal in the bed material with a particle diameter above 1.00 mm might be agglomeration or sintering. Al-Otoom *et al.* [17] illustrated that agglomeration included relatively high proportions of calcium after fluidized bed combustion. Additionally, the im-

purities of some bed materials may become a liquid featuring with a low melting point and high viscosity [18]. Therefore, the bed material and calcium additives may agglomerate or sinter to increase the diameter. The chromium metal may attach to or be covered by the sintered liquid material on the bed material.

The possible reason for a high concentration of chromium metal in the bed material with a particle diameter lower than 0.35 mm may be that there is attrition between the particles and the gasifier wall during the fluidization, so that the particles gradually become smaller. Ayazi Shamlou *et al.* [19] suggested that the attrition in the fluidized bed combustor was caused by thermal stress, static stress, chemical stress and kinetic

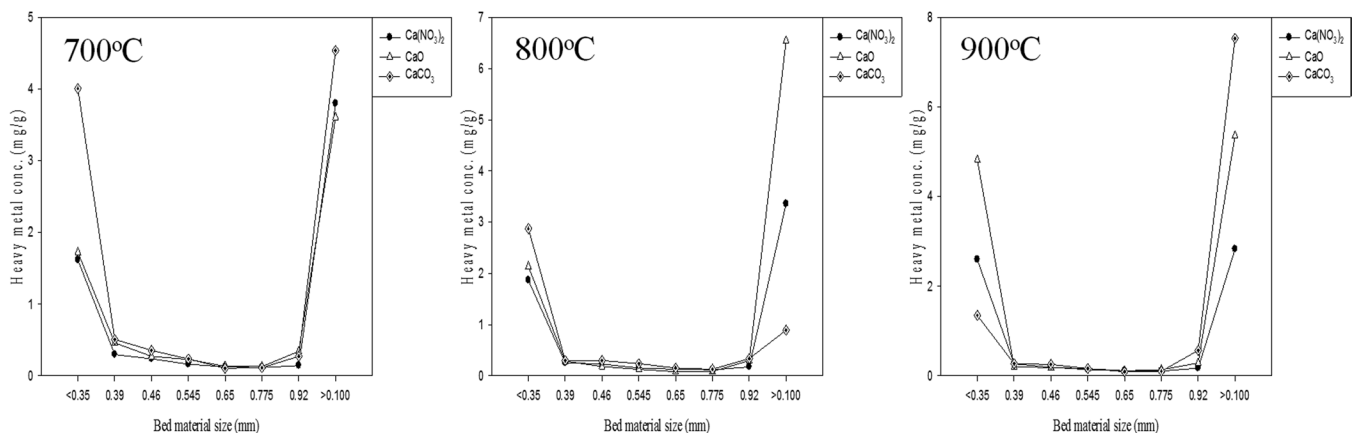


Figure 2. The chromium metal distribution in silica sand with different particle diameters.

stress. Lee *et al.* [20] also showed that many parameters, such as particle size, porosity, density and shape, could affect attrition during fluidization. Aside from the attrition among the bed materials, Lin and Wey [21] illustrated that the thermal and chemical stresses in the high-temperature incineration could create significant impact on the abrasion of the particles of bed materials because of the complicated constituents of the waste. The high temperature and the thermal shock might greatly wear the particles and thus increase the proportion of the bed material with a small particle diameter, whose greater surface area would adsorb more chromium metal. According to Kuo *et al.* [22], for the adsorption of chromium metal in the bed material with a small particle diameter, chemical adsorption plays a dominant role. Its adsorption reaction is as follows:



In an exploration into the distribution of heavy metals with bed materials with different particle diameters, Lin [23] also noticed the high concentration of heavy metals in the bed material with a larger or smaller particle diameter. Whether heavy metals are distributed in the bed materials or evaporated with the gases depends on their boiling points. Clark [24] indicated that most of the heavy metal compounds with high boiling points existed in the residue or thick ash, whereas most of the highly evaporable ones were in the ash or gases. Chromium metal has a high boiling point (2672°C), so most of them were retained in the bed materials.

The Proportion of Retained Chromium Metal in the Gasifier

In this study, the bed materials made of silica sand could adsorb heavy metals, which was similar to the research of Chen *et al.* [25] that many heavy metals were adsorbed by the silica sand during the operation, with an adsorption efficiency of “Cr > Pb > Cd”. Therefore, silica sand plays a highly important role in adsorbing heavy metals during the fluidized bed combustion process. However, there is close relationship between the adsorption rate and the boiling points of heavy metals, so the retentions of chromium metal in the bed materials under different operation temperatures were compared. There was a higher proportion of retained chromium metal under the temperature of 700°C, because chromium metal evaporated less at a lower temperature (Figure 3).

Additionally, Chen *et al.* [26] and Yao and Naruse

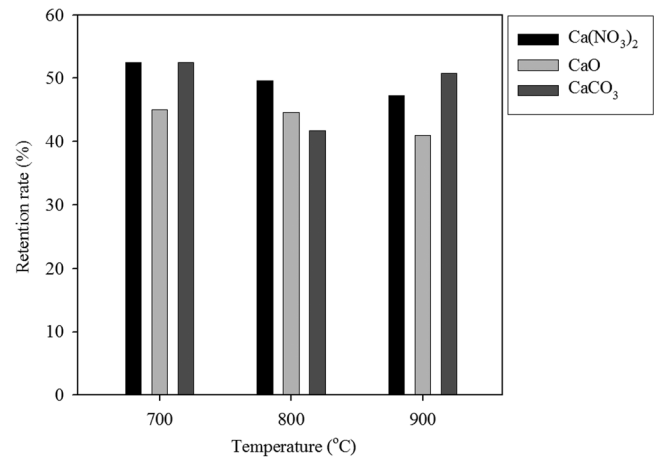


Figure 3. The influence of operation temperatures and calcium compounds on the retention of chromium metal in the bed materials.

[27] indicated that calcium-based additives could be used to adsorb heavy metals (Pb, Cd and Cr) during combustion procedure. Before calcium compounds were added, the proportion of retained Cr was about 20% under different operation temperatures in the bed material made of silica sand, but there was significant increase in the proportion (over 40%) of retained chromium metal in the bed materials after the calcium compounds were added. The retention of chromium metal by the three calcium compounds ranked as “Ca(NO₃)₂ > CaCO₃ > CaO”. However, in general, there was no significant difference between Ca(NO₃)₂ and CaCO₃ in term of the retention of Cr.

CONCLUSIONS

This study explored the constituents of syngases and the distribution of chromium metal when different calcium compounds (Ca(NO₃)₂, CaCO₃ and CaO) were used as additives under different gasification temperatures. The results showed that all the three calcium compounds could increase the proportion of H₂, but that there was no significant difference between them. The chromium was mainly distributed in the bed materials with particle diameters above 1.00 mm and below 0.35 mm. Under the operation temperature of 700°C, the calcium compounds retained the highest content of chromium metal, for the chromium metal evaporated only a little under such a low operation temperature. In conclusion, adding calcium compounds into the fluidized bed during gasification could enhance the proportion of H₂ in the syngases and increase the content of retained chromium metal in the sand bed.

REFERENCES

- Taiwan's Environmental Protection Administration (EPA). 2014. Yearbook of Environmental Protection Statistics, Taipei, Taiwan.
- Kumar, A., K. Eskridge, D. D. Jones, and M. A. Hanna. 2009. "Steam-air uidized bed gasification of distillers grains: Effects of steam to biomass ratio, equivalence ratio and gasification temperature," *Bioresour. Technol.*, 100:2062–2068. <http://dx.doi.org/10.1016/j.biortech.2008.10.011>
- Alauddin, Z. A. B. Z., P. Lahijani, M. Mohammadi, and A. R. Mohamed. 2010. "Gasification of lignocellulosic biomass in fluidized beds for renewable energy development: A review," *Renew Sust. Energ. Rev.*, 14:2852–2862. <http://dx.doi.org/10.1016/j.rser.2010.07.026>
- Luo, S., B. Xiao, Z. Hu, S. Liu, X. Guo, and M. He. 2009. "Hydrogen-rich gas from catalytic steam gasification of biomass in a fixed bed reactor: Influence of temperature and steam on gasification performance," *Int. J. Hydrogen Energy*, 34:2191–2194. <http://dx.doi.org/10.1016/j.ijhydene.2008.12.075>
- Schuster, G., G. Löffler, K. Weigl, and H. Hofbauer. 2001. "Biomass steam gasification—An extensive parametric modeling study," *Bioresour. Technol.*, 77:71–79. [http://dx.doi.org/10.1016/S0960-8524\(00\)00115-2](http://dx.doi.org/10.1016/S0960-8524(00)00115-2)
- Lv, P. M., Z. H. Xiong, J. Chang, C. Z. Wu, Y. Chen, and J. X. Zhu. 2004. "An experimental study on biomass air-steam gasification in a fluidized bed," *Bioresour. Technol.*, 95:95–101. <http://dx.doi.org/10.1016/j.biortech.2004.02.003>
- Li, K., R. Zhang, and J. Bi. 2010. "Experimental study on syngas production by co-gasification of coal and biomass in a fluidized bed," *Int. J. Hydrogen Energy*, 35:2722–2726. <http://dx.doi.org/10.1016/j.ijhydene.2009.04.046>
- Basu, P. 2006. Combustion and gasification in fluidized beds, CRC Press in Taylor & Francis Group, Florida, USA, p. 86. <http://dx.doi.org/10.1201/9781420005158>
- Maglinao, A. L., S. C. Capareda, and H. Nam. 2015. "Fluidized bed gasification of high tonnage sorghum, cotton gin trash and beef cattle manure: Evaluation of synthesis gas production," *Energy Convers. Manage.*, 105:578–587. <http://dx.doi.org/10.1016/j.enconman.2015.08.005>
- Jia, J., Y. Wu, L. Yang, P. Wu, X. Li, and X. Sun. 2015. "Human Health Risk Assessment of Harmful Trace Elements in Coal Gasification Residues," *J. Residuals Sci. Tech.*, 12(S1):S97–S104. <http://dx.doi.org/10.12783/issn.1544-8053/12/S1/15>
- Sun, J. Y., Y. F. Yang, and M. Zheng. 2015. "Double Consolidation Technology for the Stabilization of Heavy Metal Ions in the Fly Ash Generated by the Incineration of Municipal Solid Waste," *J. Residuals Sci. Tech.*, 12(S1):S31–S37.
- Ho, T. C., T. Tan, C. Chen, and J. R. Hopper. 1991. "Characteristics of metal capture during fluidized bed incineration," *AIChE Symp. Ser.*, 281(87):118–126.
- Ho, T. C., T. C. Chuang, S. Chelluri, Y. Lee, and J. R. Hopper. 2001. "Simultaneous capture of metal, sulfur and chlorine by sorbents during fluidized bed incineration," *Waste Manage.*, 21:435–441. [http://dx.doi.org/10.1016/S0956-053X\(00\)00135-5](http://dx.doi.org/10.1016/S0956-053X(00)00135-5)
- Liu, Z. S., T. H. Peng, and C. L. Lin. 2014. "Impact of CaO and CaCO₃ addition on agglomeration/defluidization and heavy metal emission during waste combustion in fluidized-bed," *Fuel Process. Technol.*, 118, 171–179. <http://dx.doi.org/10.1016/j.fuproc.2013.09.001>
- Wu, M. H., C. L. Lin, and W. Y. Zeng. 2014. "Effect of waste incineration and gasification processes on heavy metal distribution," *Fuel Process. Technol.*, 125:67–72. <http://dx.doi.org/10.1016/j.fuproc.2014.03.027>
- Chiang, K. Y., C. H. Lu, and K. L. Chien. 2011. "Enhanced energy efficiency in gasification of paper-reject sludge by a mineral catalyst," *Int. J. Hydrogen Energy*, 36:14186–14194. <http://dx.doi.org/10.1016/j.ijhydene.2011.05.024>
- Al-Otoom, A. Y., L. K. Elliott, B. Moghtaderi, and T. F. Wall. 2005. "The sintering temperature of ash, agglomeration, and defluidisation in a bench scale PFBC," *Fuel*, 84:109–114. <http://dx.doi.org/10.1016/j.fuel.2004.07.008>
- Lin, C. L., M. Y. Wey, and S. D. You. 2002. "The effect of particle size distribution on minimum fluidization velocity at high temperature," *Powder Technol.*, 126:297–301. [http://dx.doi.org/10.1016/S0032-5910\(02\)00074-8](http://dx.doi.org/10.1016/S0032-5910(02)00074-8)
- Ayazi Shamlou, P., Z. Liu, and J. G. Yates. 1990. "Hydrodynamic Influences on Particle Breakage in Fluidized Beds," *Chem. Eng. Sci.*, 45:809–817. [http://dx.doi.org/10.1016/0009-2509\(90\)85004-W](http://dx.doi.org/10.1016/0009-2509(90)85004-W)
- Lee, S. K., X. Jiang, T. C., Keener, and S. J. Khang. 1993. "Attrition of Lime Sorbents during Fluidization in a Circulating Fluidized Bed Absorber," *Ind. Eng. Chem. Res.*, 32:2758–2766. <http://dx.doi.org/10.1021/ie00023a044>
- Lin, C. L., and M. Y. Wey. 2003. "Effects of high temperature and combustion on fluidized material attrition in fluidized bed," *Korean J. Chem. Eng.*, 20(6):1123–1130. <http://dx.doi.org/10.1007/BF02706947>
- Kuo, J. H., C. L. Lin, and M. Y. Wey. 2010. "Mechanisms of particle agglomeration and inhibition approach in the existence of heavy metals during fluidized bed incineration," *Chem. Eng. Sci.*, 65:4955–4966. <http://dx.doi.org/10.1016/j.ces.2010.05.036>
- Lin, C. L. 2013. "Effects of fluidized parameters on capture of heavy metal in various bed-material size distributions," *Fuel Process. Technol.*, 106:149–159. <http://dx.doi.org/10.1016/j.fuproc.2012.07.015>
- Clarke, L. B. "The fate of trace elements during coal combustion and gasification: an overview," *Fuel*, 72:731–736. [http://dx.doi.org/10.1016/0016-2361\(93\)90072-A](http://dx.doi.org/10.1016/0016-2361(93)90072-A)
- Chen, J. C., M. Y. Wey, and M. H. Yan. 1997. "Theoretical and experimental study of metal capture during incineration process," *J. Environ. Eng.-ASCE*, 123:1100–1106. [http://dx.doi.org/10.1061/\(ASCE\)0733-9372\(1997\)123:11\(1100\)](http://dx.doi.org/10.1061/(ASCE)0733-9372(1997)123:11(1100))
- Chen, J. C., M. Y. Wey, and W. Y. Ou. 1999. "Capture of heavy metals by sorbents in incineration flue gas," *Sci. Total Environ.*, 228:67–77. [http://dx.doi.org/10.1016/S0048-9697\(99\)00030-3](http://dx.doi.org/10.1016/S0048-9697(99)00030-3)
- Yao, H., and I. Naruse. 2009. "Behavior of Lead compounds during municipal solid waste incineration," *Proc. Combust. Inst.*, 32(2):2685–2691. <http://dx.doi.org/10.1016/j.proci.2008.07.026>

Crystallization Behaviour of Chromium in Stainless Steel Slag: Effect of Feo and Basicity

XINGRONG WU*, XIAOMIN DONG, RUNTAO WANG, HUIHONG LÜ, FABIN CAO and XINGMEI SHEN
*Anhui Provincial Key Lab of Metallurgical Engineering & Resources Recycling, Anhui University of Technology,
Ma'anshan 243002, China*

ABSTRACT: The synthetic stainless steel slag systems with different basicity and different FeO contents were prepared using reagent powders, the crystallization of which was experimented by cooling from melt to 1400°C in N₂ atmosphere. The crystallization in the collected slag was studied using X-ray diffraction (XRD), scanning electron microscope (SEM) and energy dispersive spectrometer (EDS). It was found that an amorphous structure in slags with FeO was easier to be formed in low basicity (CaO/SiO₂) of 1.0 than the basic slags, while in slag systems with high basicity of 1.25 or 1.5, well crystalline phases including spinel and merwinite were formed, irrespective of FeO content. The results also showed that higher FeO content and lower basicity improved the precipitation of Cr₂O₃ into Mg(Al,Fe,Cr)₂O₄ spinel solid solution.

INTRODUCTION

DURING the smelting of ferrochromium and the refining of stainless steel, significant amount of slag is annually generated worldwide, which mainly consists of SiO₂, CaO, Al₂O₃, Fe₂O₃, FeO, Al₂O₃ and MgO. Different from ordinary steel slag, stainless steel slag also includes considerable amount of chromium oxide (typically as Cr₂O₃, 1.5–4.5 wt%). If it is not treated properly, even Cr³⁺ in the slag is gradually oxidized to Cr⁶⁺ over time when free lime and oxygen are available during or even after cooling [1,2]. Since Cr⁶⁺ is highly soluble in water, it would leach out from waste and cause the environmental pollution [3]. Therefore, researches on stainless steel slag have been receiving more and more attentions all around the world [4–5].

As all known, due to the complex of chemical compositions, solidified slag or chromium-containing residuals has a multicrystalline structure and consists of several different phases [6,7]. In order to recycle it efficiently, the stainless steel slag has to be further treated; therefore, it is important to figure out the physicochemical property and the crystallization behaviour of chromium in the slag. H. Shen *et al.* [6] collected two types of stainless steel slags from different factory and found that chromium was mainly precipitated in Fe–Cr–Ni alloys and Fe–Cr oxides. However, S. Mostafaei [8]

investigated the slags at three stages from seven EAF duplex stainless steel heats and found that all slag samples included molten oxides, magnesiochromite spinels and metallic droplets, while other solid phases formed depended on basicity. All these results demonstrated that the chemical components of factory slag were different and thus phase compositions varied dramatically.

In order to further investigate the effect of chemical composition on the crystallization characteristics, synthetic slag system was used. It was reported by Mundersbach *et al.* [9] that formation of the spinel phase was hindered in CaO–MgO–SiO₂–Cr₂O₃ synthetic slag with CaO/SiO₂ higher than 1.6. Hugo Cabrera-Real and *et al.* [10] investigated the effect of MgO and CaO/SiO₂ on the crystallization of CaO–SiO₂–Cr₂O₃–CaF₂–MgO synthetic slags and found that in slags with CaO/SiO₂ = 1 and high content of MgO, the only Cr-contained compound formed was MgCr₂O₄ spinel. In slag with CaO/SiO₂ = 2, MgCr₂O₄, CaCr₂O₄, CaCrO₄ and Ca₅(CrO₄)₃F were formed. Jian-li Li *et al.* [11] suggested that FeO could enhance the content of Cr of spinel phases in CaO–SiO₂–MgO–Al₂O₃–Cr₂O₃ system with the presence of low melting point CaF₂. Nevertheless, limited information is available for the effect of all the concerned slag compositions due to the complex of components in stainless steel slag systems.

So, in this paper, synthetic slags with different basicities (CaO/SiO₂) and contents of FeO were designed based on stainless steel slag with a view to study the

*Author to whom correspondence should be addressed.
Email: wuxingrong66@163.com

crystallization characteristics of slags and then to investigate the precipitation of chromium in the slag phases. This study would be helpful to properly treat the residual of chromium component in stainless steel slag further.

EXPERIMENTAL PROCESS

Selected slag compositions for present study were listed in Table 1. Reagent-grade powders of CaO, MgO, SiO₂, Al₂O₃, Cr₂O₃, Fe₂O₃ were used for slag synthesis. FeC₂O₄·2H₂O was used as FeO source in the batch. These powders were accurately weighed according to required proportions and then grounded well in an agate mortar. In this study, the mixtures have a basicity (CaO/SiO₂) of 1.0, 1.25 and 1.5, and FeO contents of 0.00, 3.00, 6.00 and 9.00 wt%. About 10 g powders for each batch in high pure MgO crucibles were heated to 1000°C to allow FeC₂O₄·2H₂O decomposed into FeO in N₂ atmosphere with a flow rate of 1L/min in a vertical electric furnace. Temperature was controlled and measured by a PtRh6-PtRh30 thermocouple. The overall error in the measurement and control of the temperature was less than ± 5°C. The mixtures were then heated to 1600°C and reserved at 1600°C for 30 min to ensure the formation of homogeneous melting. Then the slag samples were cooled at a rate of 3°C min⁻¹ to 1400°C and held isothermally at 1400°C for 300 min to ensure complete precipitation of minerals in the slag samples. At the end of holding time, the samples were rapidly taken out from the furnace and quenched in an oil pool.

After being dried, each slag sample was cut into two parts. One was grounded into fine powder for XRD (X'TRA, ARL Co.) characterization, using CuKα ra-

diation in 2θ range from 10° to 80° at a step of 0.02°, while the other was polished and sputter coated with a conductive layer of carbon. The mineralogy of the slag sample was analyzed by SEM (Quanta 450, FEI) in backscattering mode. SEM-energy dispersive spectrometer (Apollo X, EDAX Inc.) was also applied to determine the elemental composition of selected regions of the slag systems.

RESULTS AND DISCUSSION

XRD Characterization

XRD patterns of solid slags with different basicities and FeO contents were shown in Figure 1. As indicated in Figure 1(a), for the slag with basicity of 1.0 and no FeO, well crystalline structure was formed and spinel (MgCr₂O₄) and monticellite (CaMgSiO₄) have been identified as main phases. When FeO was added in the slag with basicity of 1.0, a certain amount of spinel phase was precipitated, and a broader hump between the 2θ angles of 25° and 35° is found. The amorphous hump showed the diffraction of glass phase, meaning that high temperature liquid at crystallization temperature of 1400°C existed. This result showed that the glass-crystalline structure was easier to be formed in slag with lower basicity with FeO of low melting point (1369°C). With increasing FeO content, the peaks of spinel were obviously enhanced, which meant more formation of spinel.

As seen from Figure 1(b) and 1(c), the slags with basicity of 1.25 and 1.5 exhibited similar crystallization behavior and included spinel (MgCr₂O₄) and merwinite (Ca₃MgSi₂O₈) as two main phases, regardless of FeO content. However, it was found that monticel-

Table 1. Mixture Compositions of The Experimental Slags, Wt %.

Slag No.	CaO	SiO ₂	MgO	Al ₂ O ₃	Cr ₂ O ₃	Fe ₂ O ₃	FeO	Basicity (CaO/SiO ₂)
S1	40.00	40.00	5.00	4.50	4.00	6.50	0.00	
S2	38.84	38.84	4.85	4.37	3.88	6.31	3.00	B = 1.0
S3	37.74	37.74	4.72	4.24	3.77	6.13	6.00	
S4	36.70	36.70	4.59	4.13	3.67	5.96	9.00	
S5	44.44	35.56	5.00	4.50	4.00	6.50	0.00	
S6	43.15	34.52	4.85	4.37	3.88	6.31	3.00	B = 1.25
S7	41.93	33.54	4.72	4.24	3.77	6.13	6.00	
S8	40.77	32.62	4.59	4.13	3.67	5.96	9.00	
S9	48.00	32.00	5.00	4.50	4.00	6.50	0.00	
S10	46.60	31.07	4.85	4.37	3.88	6.31	3.00	B = 1.5
S11	45.28	30.19	4.72	4.24	3.77	6.13	6.00	
S12	44.04	29.36	4.59	4.13	3.67	5.96	9.00	

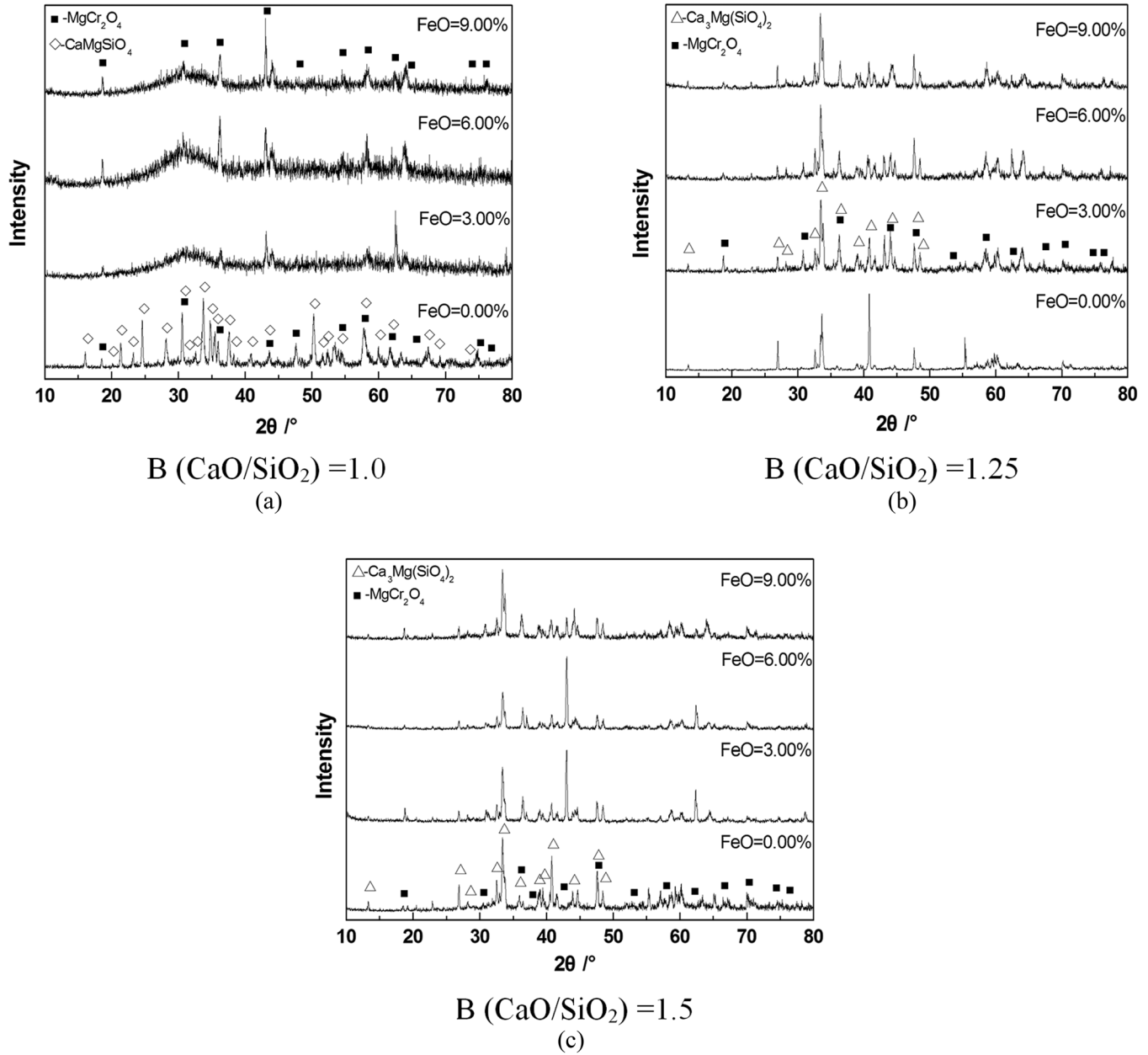


Figure 1. XRD patterns of slag samples with different basicity and different content of FeO. (a) $B(\text{CaO}/\text{SiO}_2) = 1.0$; (b) $B(\text{CaO}/\text{SiO}_2) = 1.25$; and (c) $B(\text{CaO}/\text{SiO}_2) = 1.5$.

lite (CaMgSiO_4) disappeared and merwinite ($\text{Ca}_3\text{MgSi}_2\text{O}_8$) developed, as the basicity increased.

Microscopic Investigation

Figure 2 was the typical backscattered SEM micrographs for the slag samples of different basicities and FeO contents. Seen from Figure 2(a) and combined with EDS analysis, we could find that a considerable part of the microstructure was bimodal with dark grey monticellite and bright spinel grains, surrounded by the

matrix. Furthermore, it was found that spinel was composed of Mg, Al, Fe, Cr and O, while few of Cr was existed in matrix. The spinel structure had a general formula of AB_2O_4 . A can be represented by Mg, Fe^{2+} , Mn or Zn and B by Al, Fe^{3+} or Cr^{3+} leading to spinel formulas as $(\text{Mg}, \text{Fe}^{2+}, \text{Mn}, \text{Zn})(\text{Al}, \text{Fe}^{3+}, \text{Cr}^{3+})_2\text{O}_4$ [12]. Thus, in this study, the spinel phase (MgCr_2O_4) characterized by XRD patterns was probably the $(\text{Mg}, \text{Fe})(\text{Al}, \text{Fe}, \text{Cr})_2\text{O}_4$ complex spinel.

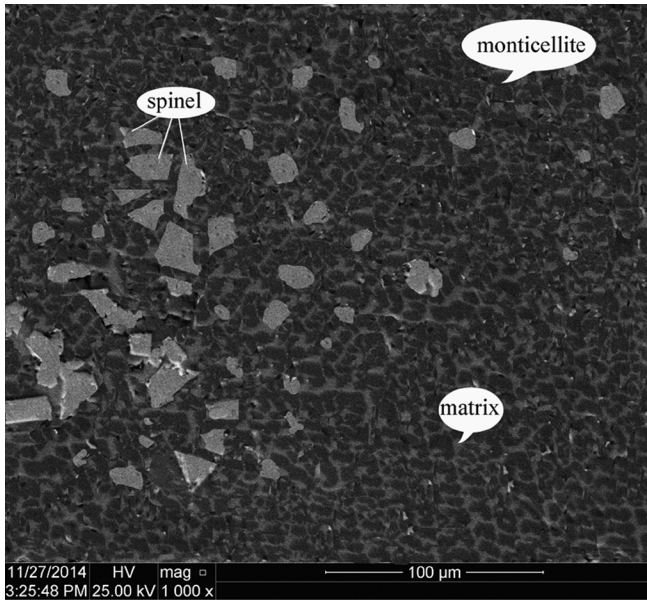
Figure 2(b) presented a typical microstructure of slag sample with $B = 1.0$ and $\text{FeO} = 6.00\%$. A homog-

enous glass phase was found throughout the microstructure while a large percentage of disseminated spinel was found in the matrix, which indicated that when slag included a relative FeO, spinel was the only phase crystallized from the slag with $B = 1.0$.

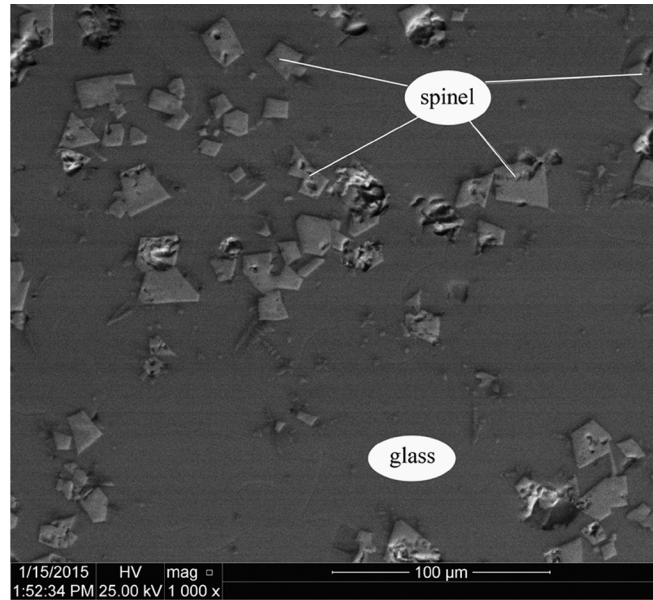
However, for slag samples with high basicity, spinel with block shape and merwinite with grey streaks of

irregular shape were observed, as shown in Figure 2(c) and 2(d). Chromium was mainly precipitated in spinel and few of chromium in matrix. All these investigations were consistent with XRD analysis above.

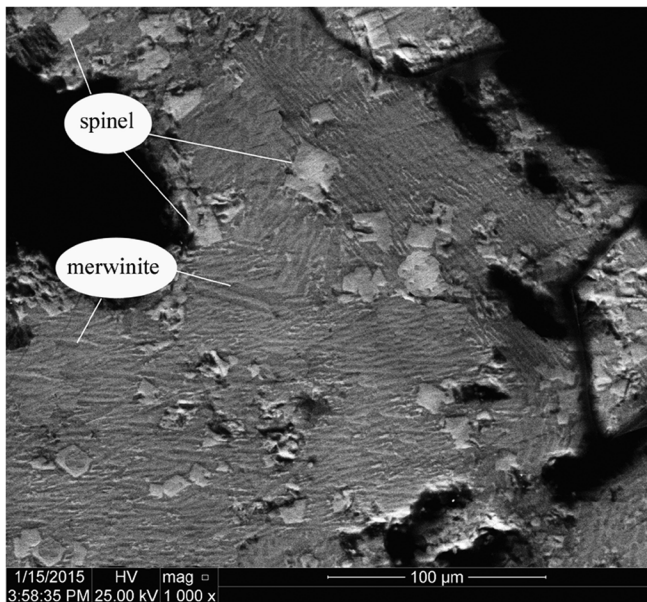
By the calculation based on EDS results, the content of Cr_2O_3 in spinel phase with different FeO contents and basicities was shown in Figure 3. In comparison,



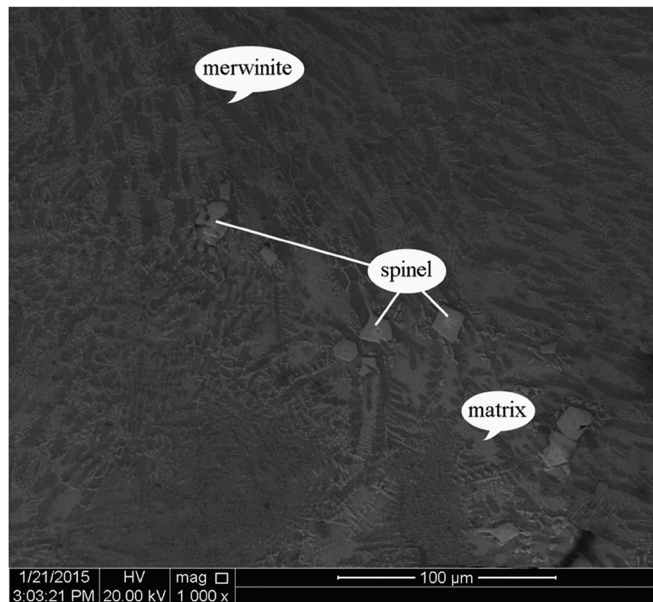
$B=1.0 \text{ FeO}=0.00\%$
(a)



$B=1.0 \text{ FeO}=6.00\%$
(b)



$B=1.25 \text{ FeO}=6.00\%$
(c)



$B=1.5 \text{ FeO}=6.00\%$
(d)

Figure 2. SEM micrographs for representative slag samples. (a) $B = 1.0 \text{ FeO} = 0.00\%$; (b) $B = 1.0 \text{ FeO} = 6.00\%$; (c) $B = 1.25 \text{ FeO} = 0.00\%$; (d) $B = 1.5 \text{ FeO} = 6.00\%$;

Cr_2O_3 content of spinel solid solution in slag with $B = 1.0$ and $\text{FeO} = 3.00\%$ was slightly lower than that in slag with $B = 1.0$ and $\text{FeO} = 0.00\%$. From XRD analysis above, in slag with $B = 1.0$, addition of FeO would form spinel crystalline-glass structure, therefore, at 1400°C , key major elements exchange between spinel and melt could be assessed by diffusion. Fluid activity during crystallization was largely responsible for carrying out this exchange. There was no clear variation in diffusion parameter (D) with the changing major element composition (Al , Cr , Fe^{3+}), however, there were some variations that were related to Al or Fe content. This was due to the low Cr content in slag may have a large effect on Cr_2O_3 content of spinel solid solution.

As seen in Figure 3, Cr_2O_3 content in spinel had the tendency to increase with the increasing FeO content in slag and showed a negative correlation with basicity of the slag. The spinel solid solutions formed by the $\text{MgFe}_x\text{Cr}_{2-x}\text{O}_4$ samples had different types of center-positive ions. The type of gap occupied by each ion could be determined based on the octahedral potential energy described in crystal field theory. The order of the potential energy was $\text{Cr}^{3+} > \text{Mg}^{2+} > \text{Fe}^{3+}$. The ion with a higher potential energy would have a higher priority for entering the octahedral gap. Compared with Mg^{2+} and Fe^{3+} , Cr^{3+} will be prioritized to occupy the octahedral gap. With more FeO in slag, higher Cr_2O_3 and lower Al_2O_3 were found due to a large Cr-Al exchange rate, which indicated that there was a distinct advantage for the chromium incorporated in spinel structure with high FeO content.

Whereas, high basicity of slag prevented Cr from

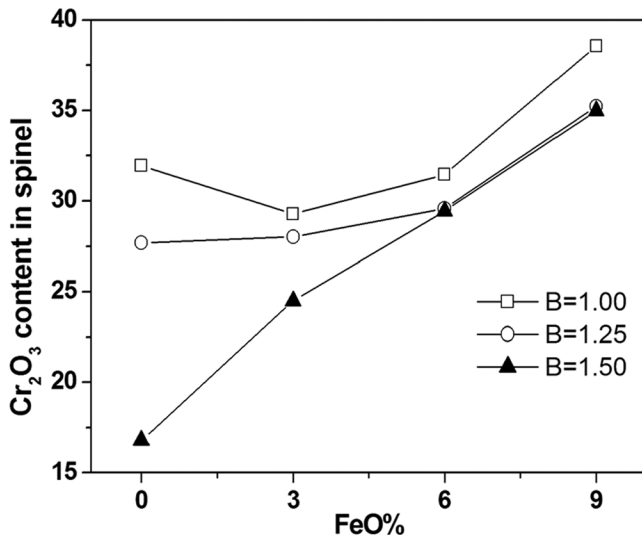


Figure 3. The variation of the content of Cr_2O_3 in spinel phase with FeO content in the slags under different basicity.

scavenging from the slag melt and then resulted in the chromium precipitation into spinel, which was consistent with the results by the previous report [13]. According to viewpoint of the coexistence theory of slag structure, stainless steel slag system was composed of Ca^{2+} , Mg^{2+} and O^{2-} as simple ions, SiO_4^{4-} as network-forming anions, molecules such as Al_2O_3 , Fe_2O_3 , and Cr_2O_3 etc. Therefore, we proposed that Cr_2O_3 might substitute for Al_2O_3 and/or Fe_2O_3 in spinel grains by diffusion. Meanwhile, the increase of slag basicity enhanced the melting temperature and viscosity of slag, which consequently diminished the diffusion flux or rate for the formation of spinel minerals, thus resulting in less Cr_2O_3 precipitating into spinel.

CONCLUSIONS

The effect of FeO content in synthetic slag with variable basicity (CaO/SiO_2) on crystallization behavior of chromium was investigated, the following findings were drawn.

1. When FeO was kept constant, with slag basicity increasing from 1.0 to 1.5, the crystallized phases were not the same, but complex spinel solid solution $(\text{Mg,Fe})(\text{Fe,Al,Cr})_2\text{O}_4$ was formed in all slag samples. In comparison, variation of FeO in slags with the same basicity did not change crystallized phases.
2. Higher FeO content were beneficial to increase the Cr_2O_3 content in spinel solid solution, especially when coupled with slag basicity of 1.5.

ACKNOWLEDGMENTS

The financial support of the National Natural Science Foundation of China (51274006, 51204004 and Anhui innovation team project of new technology in materialization of metallurgical solid wastes are appreciated.

REFERENCES

1. K. Pillay., H.V. Blotnitz., and J. Petersen., "Ageing of chromium(III)-bearing slag and its relation to the atmospheric oxidation of solid chromium(III)-oxide in the presence of calcium oxide," *Chemosphere*, 52(10), 2003:1771–1779.
2. C.R., Panda., K.K., Mishra., B.D., Nayak., D.S., Rao., and B.B., Nayak., "Release behaviour of chromium from ferrochrome slag," *Int. J. Environment Technology and Management*, 15(3-6), 2012: 273–278.
3. A. A., Ramezaniapour, M., Nikravan and R., Maknoon., "Characterization of bottom ash from petrochemical waste incinerator," *Journal of Residuals Science and Technology*, 8(4), 2011: 189–196.
4. H.W., Zhang, and X., Hong., "An overview for the utilization of wastes

- from stainless steel industries,” *Resources Conservation & Recycling*, 55(8), 2011:745–754.
5. B., Adamczyk, R., Brenneis, C., Adam, and D., Mundersbach., “Recovery of chromium from AOD-converter slags,” *Steel Research International*, 81(12), 2010 :1078–1083.
 6. H., Shen, E., Forsberg, and U., Nordström., “Physicochemical and mineralogical properties of stainless steel slags oriented to metal recovery,” *Resources Conservation & Recycling*, 40(3), 2004: 245–271.
 7. B. T., Alexander, T., James M, and H. F., Xu., “Quantification of mineralogical and amorphous species in chromium ore processing residue,” *Journal of Residuals Science and Technology*. 9(4), 2012:131–141.
 8. S., Mostafae, M., Andersson, and P. G., Jönsson., “Petrographical study of microstructural evolution of EAF duplex stainless steelmaking slags,” *Ironmak.Steelmak.*, 38(2), 2011: 90–99.
 9. G. J., Albertsson, L. D., Teng, F., Engström, and S., Seetharaman., “Effect of the heat treatment on the chromium partition in CaO–MgO–SiO₂–Cr₂O₃ synthetic slags,” *Metall. Mater. Trans. B*, 44(6), 2013: 1586–1597.
 10. H., Cabrera-Real, A., Romero-Serrano, B., Zeifert, A., Hernandez-Ramirez, M., Hallen-Lopez, and A., Cruz-Ramirez., “Effect of MgO and CaO/SiO₂ on the immobilization of chromium in synthetic slags,” *Journal of Material Cycles & Waste Management*, 14(4), 2012:317–324.
 11. J. L., Li, A. J., Xu, D. F., He, Q. X., Yang, and N.Y., Tian., “Effect of FeO on the formation of spinel phases and chromium distribution in the CaO–SiO₂–MgO–Al₂O₃–Cr₂O₃ system,” *International Journal of Mineral and Metallurgical. Materials.*, 20(3), 2013:253–258.
 12. D., Lenaz, H., Skogby, F., Princivalle, and U., Halenius., “The MgCr₂O₄-MgFe₂O₄ solid solution series: Effects of octahedrally coordinated Fe³⁺ on T–O bond lengths,” *Physics & Chemistry of Minerals.*, 33(7), 2006: 465–474.
 13. X. R., Wu, R. T., Wang, H. H., Lü, X. M., Shen, and L. S., Li. 2015. “Influence of Basicity and Fe₂O₃ on Crystallization Characteristics of CaO–MgO–SiO₂–Al₂O₃–Cr₂O₃–Fe₂O₃ System,” presented at International Workshop on Materials Science and Engineering, August 7–9, 2015.

Coal Dust Reduce the Rate of Root Growth and Photosynthesis of Five Plant Species in Inner Mongolian Grassland

WANG ZHAN-YI^{1,*}, HOU JIA², GUO JIAN-YING³, WANG CHENG-JIE¹ and WANG MING-JIU¹

¹College of Ecology and Environment, Inner Mongolia Agricultural University, Hohhot, China, 010019

²College of Vocation and Technology, Inner Mongolia Agricultural University, Baotou, China, 014109

³Institute of Water Resources in Pastoral Areas, Hohhot, China

ABSTRACT: Dust pollution is one of the major environmental problems in opencast mining, which has a significant impact on the surrounding ecosystem. Little is known about the effect of coal dust deposition on plant growth in grasslands, especially on root growth. In this study, we studied how coal dust deposition affected plant growth, with a focus on root growth. Five plants which commonly can be found in Inner Mongolian grassland were selected and cultured with hydroponics methods in greenhouse. Two kind of coal dust (coal powder and granite powder) were sprayed on the plant for 35 days. Root morphology parameters and photosynthesis parameter were determined. We found that among the six measured root morphological characters, root surface area and volume were negatively affected by coal dust in most species. Both coal powder and gangue powder inhibited root growth of four out of five species. *Lespedeza davurica* was the only species that was not affected by dust pollution. Coal dust can negatively affect the photosynthesis rate. Based on these results, we found that coal dust is harmful for plant growth. The growth of grass with long-term acceptance of coal dust pollution may be threatened, even can not be grow in the contaminated grassland.

INTRODUCTION

DUST POLLUTION is a major environmental problem occurred during the mining process of open-pit coal mines. This problem is common in six countries (USA, China, India, Russia, South Africa, Australia), which hold 84% of world hard coal reserves [1,2]. Dust pollution is serious in the arid areas of Inner Mongolia, China, where many open-pit coal mines have been established in recent years. During 2006–2010, Inner Mongolia was the biggest coal production province in China [3]. Eleven out of the 14 open-pit coal mines in China are located in Inner Mongolia [4]. Most of the open-pit coal mines are located in the Inner Mongolian grasslands. Meanwhile development of animal husbandry and livelihood of local people highly depend on the health of these grasslands. Thus, dust pollution may pose threats to the livelihood of local people via its damage on grassland health. For example, in the city of Xilinhote at least 106 km² of grasslands were polluted by coal dust, and 6.7 million Chinese Yuan was paid to compensate herdsmen during 2011–2013 [5].

Dust pollution has been documented to have significant effects on the health of ecosystems and plants. Coal dust increases soil surface temperature [6], and pH value and metal ion concentrations of water leaching from coal pits [7,8]. It contains toxic chemicals such as fluoride and sulfur compounds, which negatively affects vegetation growth [9]. Coal dust emission shades off sunlight, adversely affecting photosynthetically active radiation [10] and photosynthesis performance of *Avicennia marina* in South Africa [2]. Dust particles occlude stomata [11,12]. Coal dust from an Indian mine alters leaf morphology and leaf physiology of nearby garden plants [13]. Biomass of annual plants was significantly bigger on the coal dust plume than off the plume in Oregon, USA [14].

All the researches we have found focus on effects of coal dust pollution on plants' aboveground parts; no study has assessed its effects on plant belowground parts. Besides this, dust of different origin and nature should have a different influence on the plant growth. There are two sources of coal dust in open-pit coal mining in Inner Mongolia, and we suspect the two types of dust have different effects on plant growth, due to their differences in chemical composition. Coal powder, coming from the pit or coal yard, should have

*Author to whom correspondence should be addressed.
Email: zhanyiwang2006@163.com; TEL: +86 471 5193953

similar chemical composition as the coal itself. The most common coal in Inner Mongolia is lignite, which contains mainly C (63.73%), H (6.26%), O (28.12%), N (1.43%), and S (0.46%) [15]. Gangue powder, coming from digging, transporting, and heaping of waste soils (the soil covering the coal and need to be removed during mining), contains SiO_2 (76–77%), Na_2O and K_2O (7.75–8.15%), and CaO (0.20–0.22%) [16]. Wong *et al.* (1984) report that road dust from different sources have different impacts on plants, some inhibiting, while others promoting, plant root growth [17]. Coal dust from different sources may also affect plant root growth differently.

If the effects of coal powder and gangue powder on plant growth differ among species, then in the long-run some species would be threatened and may go extinct, while other species would increase in abundance. In other words, species composition in a grassland under long-term coal dust pollution may change significantly, leading to changes in grassland state and ecosystem services it can provide. This study examined the short-term effects of coal powder and gangue powder on plant growth of different species. Our questions were (1) how coal powder and gangue powder affect root growth, leaf photosynthesis, and plant biomass, (2) if coal powder and gangue powder affect the same species differently, and (3) if the effects differ among plant species.

MATERIALS AND METHODS

Monitoring the Deposition Rate of Coal Dust

Coal dust deposition rate was monitored at West #2 Coal Mine of Shengli Coal Field, located in west Xilinhot, Inner Mongolia, China. The type of coal is lignite. The dominant wind is west wind. The average annual rainfall was 350 mm [18].

Dust deposition rate was monitored by a gravimetric method during Apr–Sep of 2013. Dust was collected following the Chinese National Standard [19,20] during Apr–Sep of 2013 when local coal mines can only be working in this periods. Two collection sites were set up 500 m away from the coal mine, one to the east and the other, west. At each collection site, three collection cups (15 cm in diameter and 30 cm high) were set up 50 m apart, each placed on a 180 cm-tall cement column. The collection cup was filled with glass balls (1.2 cm in diameter).

The dust in each collection cup was washed with deionized water. The dust solution, filtered through 1

mm-sieve, was poured into a porcelain crucible. The porcelain crucible with dust solution was first heated dry on a hot plate, then baked in a drying oven at 105°C. After it was weighed (W2), the crucible was washed with deionized water and baked in the drying oven at 105°C, and its weight taken (W1). The difference in the two weight measures was the dust weight (W2 – W1).

Laboratory Experiment Design

Five common species in the region were selected for the experiment: *Agropyron cristatum*, *Chenopodium album*, *Lespedeza davurica*, *Leymus chinensis*, and *Melissilus ruthenicus*. Seeds were collected from the grassland far from the West #2 Coal Mine in September of 2012. During May–Jul of 2013 seeds were germinated and plants cultured hydroponically in a greenhouse. Seeds were placed in sand for 7 days to allow germination. On the 7th day plants were moved into hydroponic growing systems, each filled with 10 L of Hoagland nutrient solution. Three treatments were set up: control (CK), coal powder treated (CP), and gangue powder treated (GP). The coal powder and gangue powder were collected from West #2 Coal Mine. Each treatment included three replicates, each replicate a hydroponic growing system. Each hydroponic system held 10 plants, with 2 plants from each of the 5 species.

Under the CP or GP treatment, either coal powder or gangue powder was sprayed on the plants and added into the nutrient solution at the same time once every two days. The amount of the sprayed coal powder or gangue powder was equal to the coal dust deposition rate measured at the downwind site (0.59 g/m²/d). A cuboid cap (100 × 50 × 160 cm) was used to cover the plants of the same treatment during dust spraying. Since the aboveground and belowground part of plant were divided by the engraftment plate, dust sprayed can not come into the solution. The dust sprayed were added directly into the nutrients solution based on the area of the plate and dust deposition rate. Physical and chemical properties of coal powder and gangue powder from the coal mine were tested. The powder was sieved by a 0.149 mm and the heavy metal determined by Atomic Absorption Spectrometry). The pH value of powder was determined by a pH meter (Leici co., LTD, PHS-3C type) with a powder and water ratio of 1:5. All the determination was three replicates.

Roots of all plants were scanned with an Epson Perfection V700 Photo Scanner (Seiko Epson Corpo-

ration, Nagano, Japan) once every 7 days for 35 days (not includes the 7 days of germination). After the scan the plants were put back to their origin positions in the hydroponic growing systems. The scanned images were analyzed with a WinRHIZO Root Analysis System (Regent Instruments Inc., Canada). Measurements of six root morphological variables (volume, surface area, number of tips, length, numbers of forks, and diameter) were recorded. On the last sampling time (the 35th day), leaf temperature, stomata conductance, and net photosynthetic rate were measured with a portable Photosynthesis System (LI-6400XT, USA). Three measurements were taken on each plant during 9–11:30 A.M. under a LED light source, each on a healthy and fully mature leaf. Finally, all plants were harvested and put into a drying oven at 75°C. Root biomass and total plant biomass were weighed after the plants were dried for 24 hours.

Data Analysis

One-way analysis of variance was used to compare each variable among three treatments at a sampling time (SPSS 13.0 for Windows). The variables were six root morphological characters, leaf temperature, stomatal conductance, net photosynthetic rate, root biomass, and total plant biomass. Statistical significance was defined for $p = 0.05$.

RESULTS

Deposition Rate of Coal Dust and Chemical Properties of Coal Powder

Dust deposition rate was 0.26 g/m²/d at the upwind site ($N = 3$, $se = 0.06$) and 0.59 at the downwind site ($N = 3$, $se = 0.10$). Concentration of heavy metal in the powder was determined (Table 1). Concentration of chromium (Cr) and lead (Pb) were significantly smaller in coal powder than in gangue powder ($p = 0.0005$ and 0.0001, respectively).

Plant Root Morphology, Photosynthesis, and Biomass

Agropyron Cristatum

Measurements of all six root morphological variables in the dust treatments were smaller than those in the control, but the measurements were statistically the same between the two dust treatments (Figure 1). Between the dust treatments and the control, measurements of five variables in the CP and GP treatments, and root diameter in the GP treatment became significantly smaller than those in the control by the last sampling time (day 35). Root diameter in the CP treatment was statistically the same as that in the control throughout the experiment. Between the CP and GP treatments measurements of all six variables were the same throughout the experiment.

Leaf temperature was the same among the three treatments (Figure 2). Stomatal conductance was significantly smaller in the dust treatments than in the control ($p = 0.016$ for coal powder, and 0.011 for gangue powder); net photosynthetic rate in the dust treatments were significantly smaller than (CP) ($p = 0.018$) or the same as (GP) that in the control. Between the two dust treatments both stomatal conductance and net photosynthetic rate were statistically the same.

Both root and total biomass were smaller in the dust treatments than in the control (coal powder: $p = 0.035$ and 0.001, respectively; gangue powder: $p = 0.014$ and 0.001, respectively, Table 2). Between the two dust treatments there was no difference in both variables.

Chenopodium Album

Measurements of three out of six root morphological variables (root volume, surface area, and length) in the dust treatments were smaller than those in the control, while measurements of all six variables were statistically the same between the two dust treatments (Figure 3). Between the dust treatments and the con-

Table 1. Physical and Chemical Properties of the Two Types of Coal Dust.

Dust	pH	Heavy Metal (means \pm se, N = 3, mg/kg)				
		Cd	Cr	As	Cu	Pb
Coal powder	6.06	0.05 \pm 0.01a	22.14 \pm 1.56b	4.12 \pm 0.16a	13.36 \pm 0.74a	11.89 \pm 0.15b
Gangue powder	7.27	0.018 \pm 0.01b	51.07 \pm 1.07a	3.77 \pm 0.08a	15.13 \pm 0.45a	30.03 \pm 0.71a
Soil of the riginal site *	8.22	0.093	38.3	6.85	12.3	15.0

*According to the published data by Guo (2012) [21], the original grassland was the grassland before the coal mine was established.

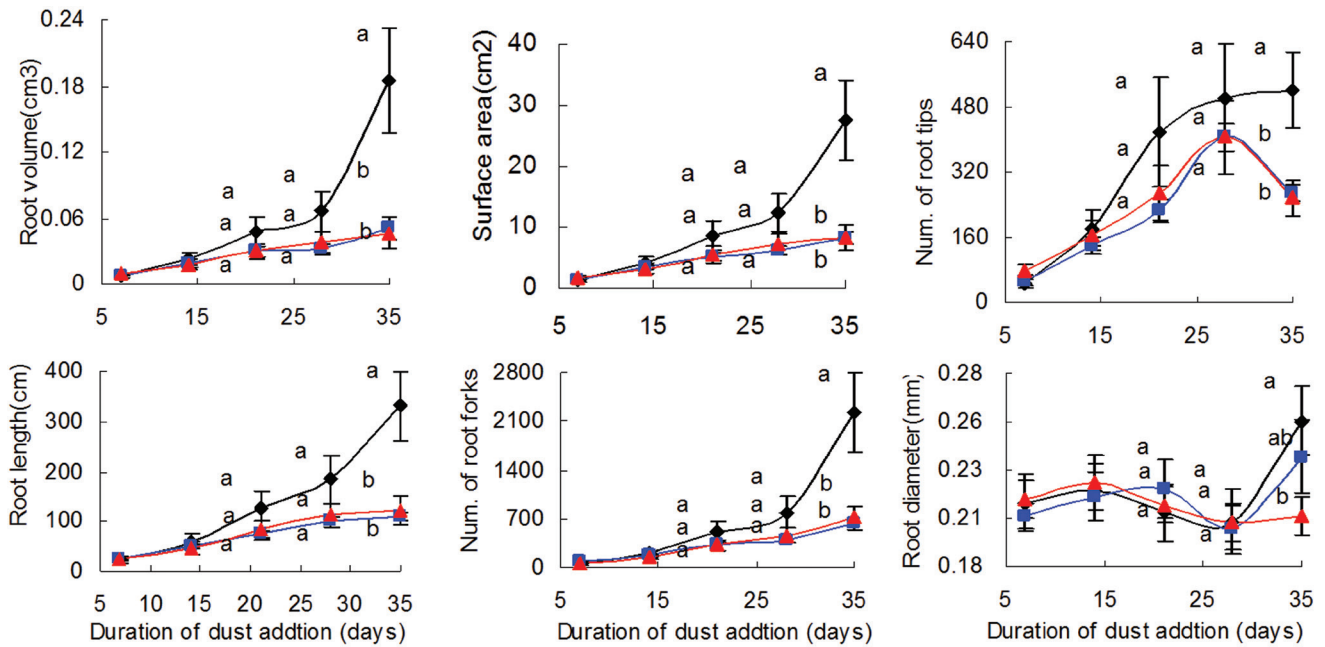


Figure 1. Comparison of temporal trends in six root morphology variables among three treatment groups, control (CK), coal powder (CP), and gangue powder (GP) for *Agropyron cristatum*. Different letters indicate significantly different means among treatments (◆—CK, ▲—GP, ■—CP).

control, root volume and surface area in the CP and GP treatments, and root length in the GP treatment became significantly smaller than those in the control by the last sampling time (day 35).

Although root diameter and number of root tips in the CP and/or GP treatments were significantly bigger than those in the control on the 3rd or 4th sampling time, the differences disappeared by the last sampling time. Between the CP and GP treatments measurements of five out of six variables were the same throughout the experiment. Although number of root tips was smaller in the CP treatment than in the GP treatment on the 4th sampling time, the difference disappeared by the last sampling time.

Leaf temperature in the two dust treatments were significantly bigger than that in the control, and it was smaller in the CP than in the GP treatment (Figure 2). However, stomatal conductance and net photosynthetic rate were statistically the same among the three treatment groups.

Root biomass was statistically the same among the three treatments (Table 2). Total biomass was significantly smaller in the dust treatments than in the control; while it was the same between the two dust treatments.

Lespedeza Davurica

The values of all six root morphological variables

Table 2. Comparison of Root and Total Biomass (G, Mean +/- Standard Error) on the Last Sampling Time (Day 35) Among the Three Treatments.

Plant Species	Biomass	Control	Coal Dust	Gangue Powder
<i>Agropyron cristatum</i>	Root	0.050 ± 0.009 a*	0.013 ± 0.002 b	0.014 ± 0.004 b
	Total	0.260 ± 0.055 a	0.060 ± 0.019 b	0.048 ± 0.010 b
<i>Chenopodium album</i>	Root	0.184 ± 0.027 a	0.123 ± 0.017 a	0.137 ± 0.022 a
	Total	3.157 ± 0.341 a	1.643 ± 0.184 b	1.775 ± 0.150 b
<i>Lespedeza davurica</i>	Root	0.024 ± 0.007 a	0.019 ± 0.005 a	0.028 ± 0.005 a
	Total	0.180 ± 0.050 a	0.187 ± 0.041 a	0.133 ± 0.047 a
<i>Leymus chinensis</i>	Root	0.024 ± 0.004 a	0.015 ± 0.003 ab	0.017 ± 0.002 b
	Total	0.204 ± 0.050 a	0.094 ± 0.018 b	0.106 ± 0.012 b
<i>Melissilus ruthenicus</i>	Root	0.027 ± 0.005 a	0.010 ± 0.001 b	0.014 ± 0.002 b
	Total	0.146 ± 0.027 a	0.079 ± 0.018 a	0.101 ± 0.018 a

*Different letters indicate significantly different means among the three treatments within a species.

were statistically the same among the three treatments by the last sampling time (day 35) (Figure 4). Although number of root tips on the 3rd and 4th sampling times, and root length on the 3rd sampling time were different among treatments, the differences disappeared by the last sampling time.

Leaf temperature in the dust treatments was the

same as (CP) or bigger than (GP) that in the control; and it was smaller in the CP than in the GP treatment (Figure 2). However, stomatal conductance and net photosynthetic rate were statistically the same among the three treatments.

Both root and total biomass were the same among the three treatments (Table 2).

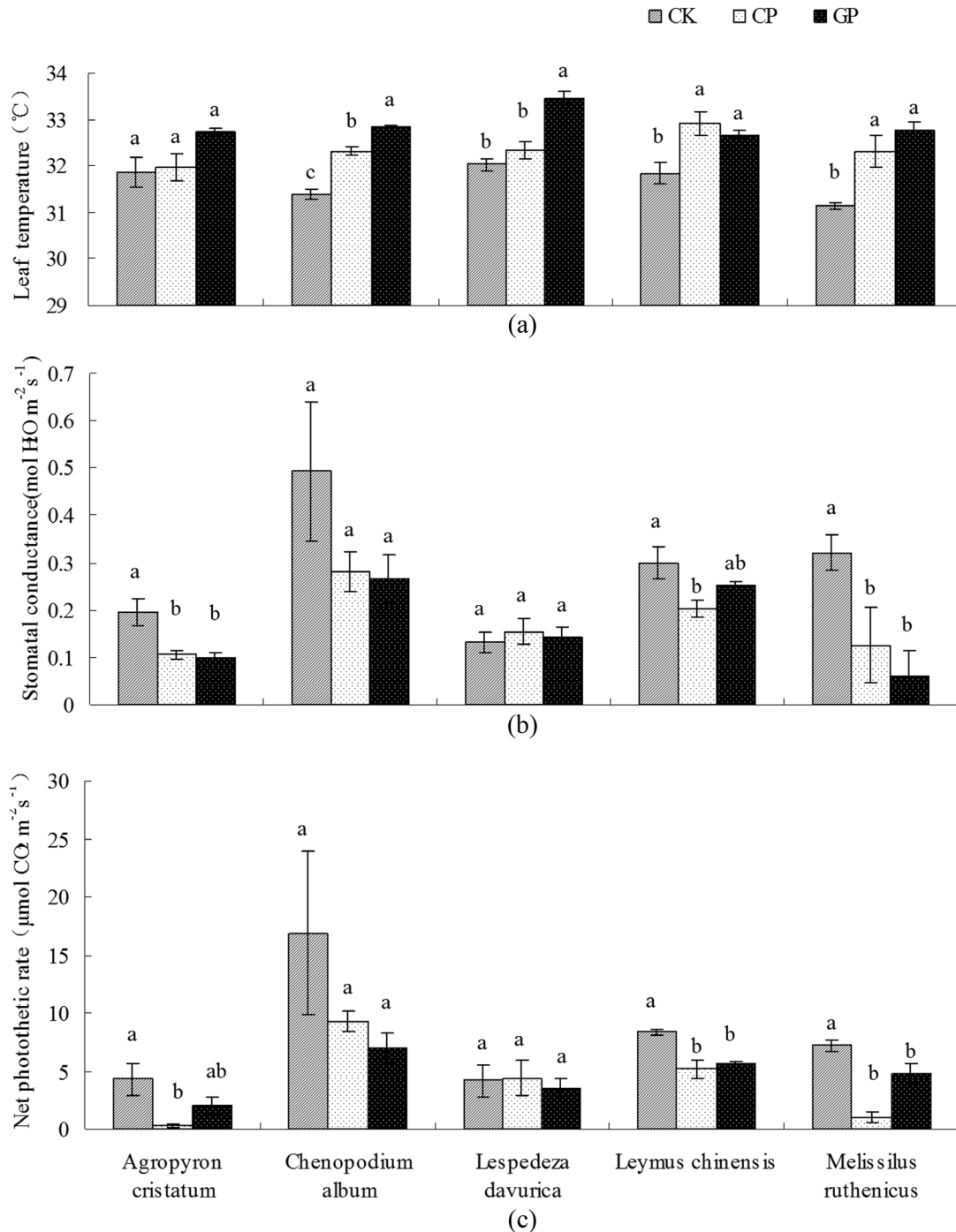


Figure 2. Comparison of three photosynthesis variables on the last sampling day (day 35) among three treatment groups: (a) control (CK); (b) coal powder (CP); and (c) gangue powder (GP) for all five species. Different letters indicate significantly different means among treatments within a species.

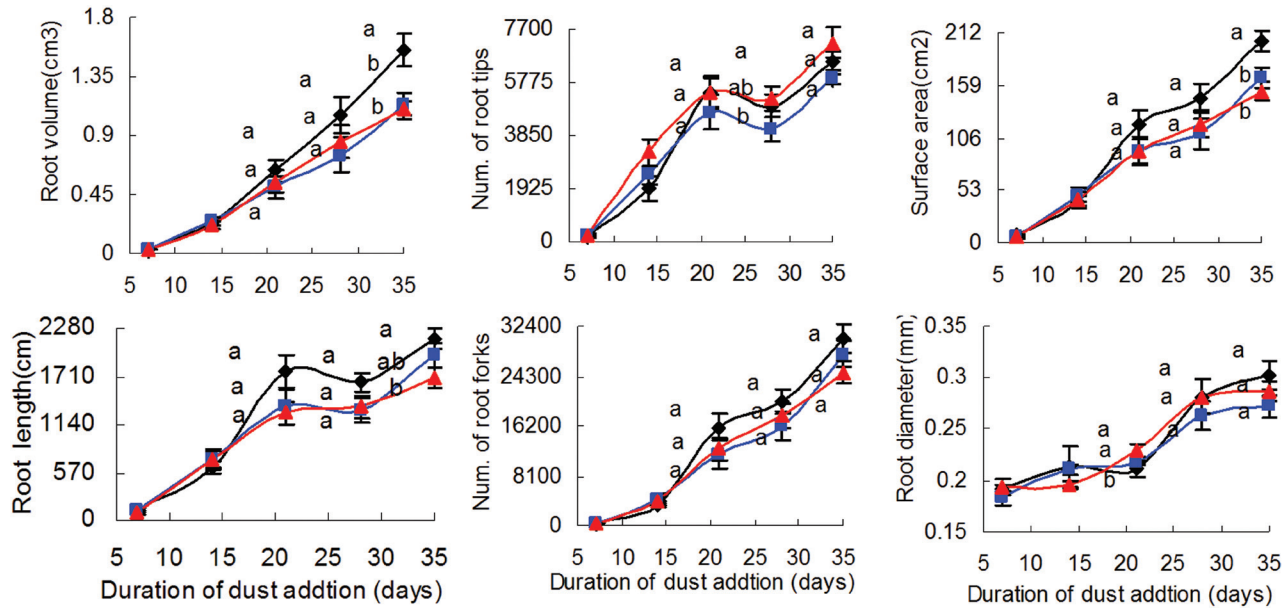


Figure 3. Comparison of temporal trends in six root morphology variables among three treatment groups, control (CK), coal powder (CP), and gangue powder (GP) for *Chenopodium album*. Different letters indicate significantly different means among treatments (◆—CK, ▲—GP, ■—CP).

Leymus Chinensis

Measurements of four out of six root morphological variables were statistically the same between the dust treatments and the control, while measurements of five variables were statistically the same between the two dust treatments (Figure 5). Between the dust treatments and the control, the two variables with different values

were root surface area (CP = GP > control) and root diameter (GP > CP = control) on the last sampling time. Between the CP and GP treatments, the one variable with different value was root diameter (CP < GP) on the last sampling time.

Leaf temperature was significantly bigger, stomatal conductance was either significantly smaller (CP) or the same (GP), and net photosynthetic rate was signifi-

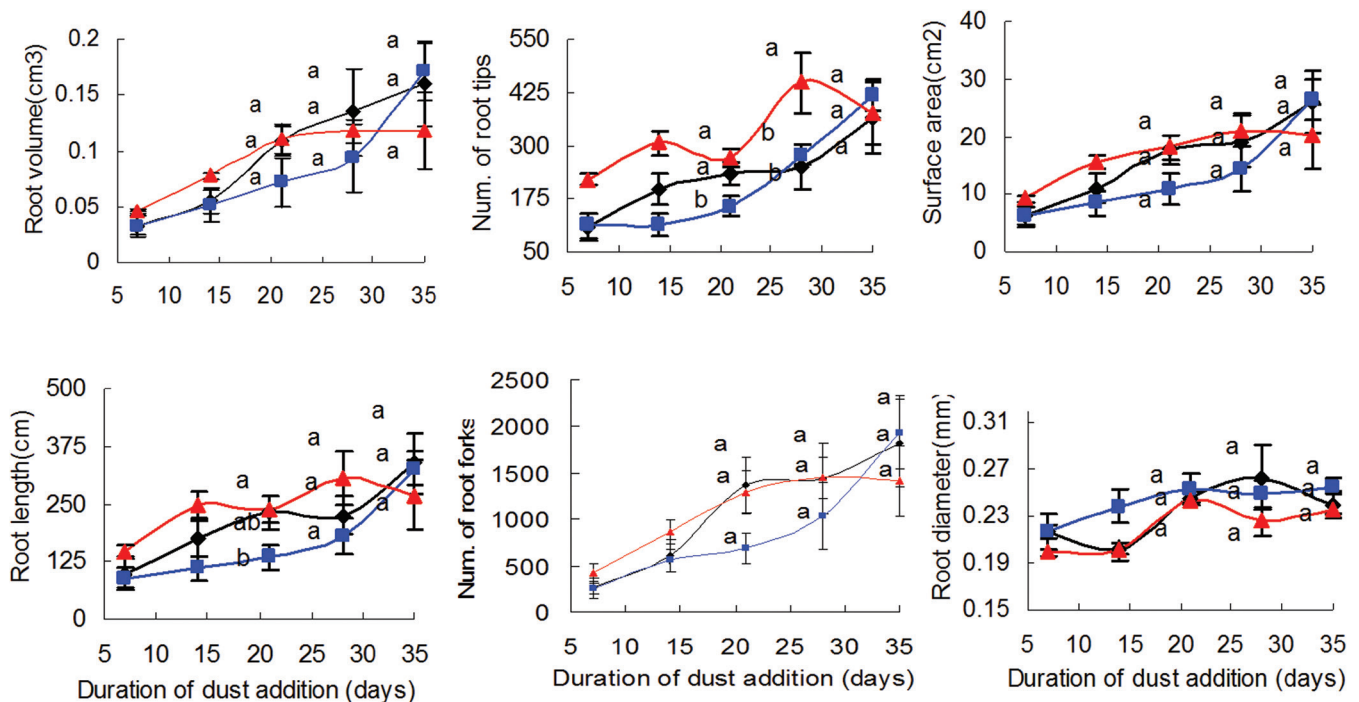


Figure 4. Comparison of temporal trends in six root morphology variables among three treatment groups, control (CK), coal powder (CP), and gangue powder (GP) for *Lespedeza davurica*. Different letters indicate significantly different means among treatments (◆—CK, ▲—GP, ■—CP).

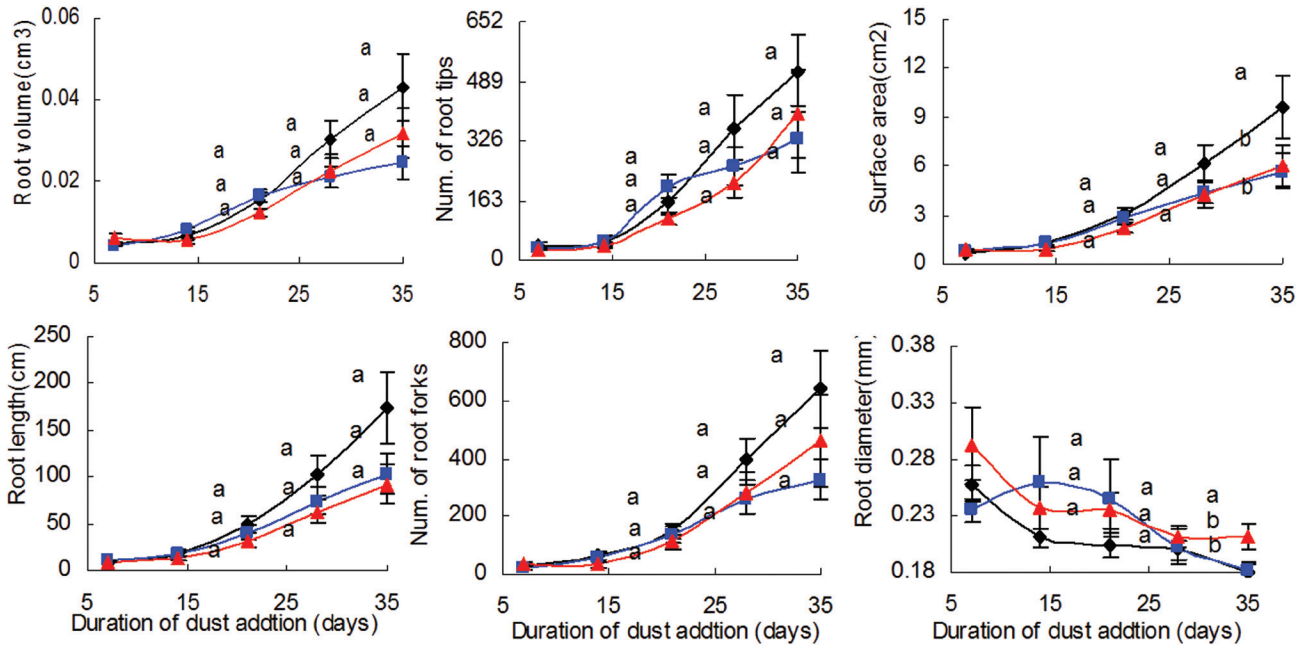


Figure 5. Comparison of temporal trends in six root morphology variables among three treatment groups, control (CK), coal powder (CP), and gangue powder (GP) for *Leymus chinensis*. Different letters indicate significantly different means among treatments (◆—CK, ▲—GP, ■—CP).

cantly smaller in the dust treatments, compared to that in the control (Figure 2). Between the two dust treatments there was no difference in all three variables.

Root biomass in the dust treatments was the same as (CP) or significantly smaller (GP) than that in the control (Table 2). Total biomass was significantly smaller in the dust treatments than in the control (Table 2). Be-

tween the two dust treatments there was no difference in the two variables.

Melissilus Ruthenicus

Measurements of four out of six root morphological variables were significantly smaller in the dust treat-

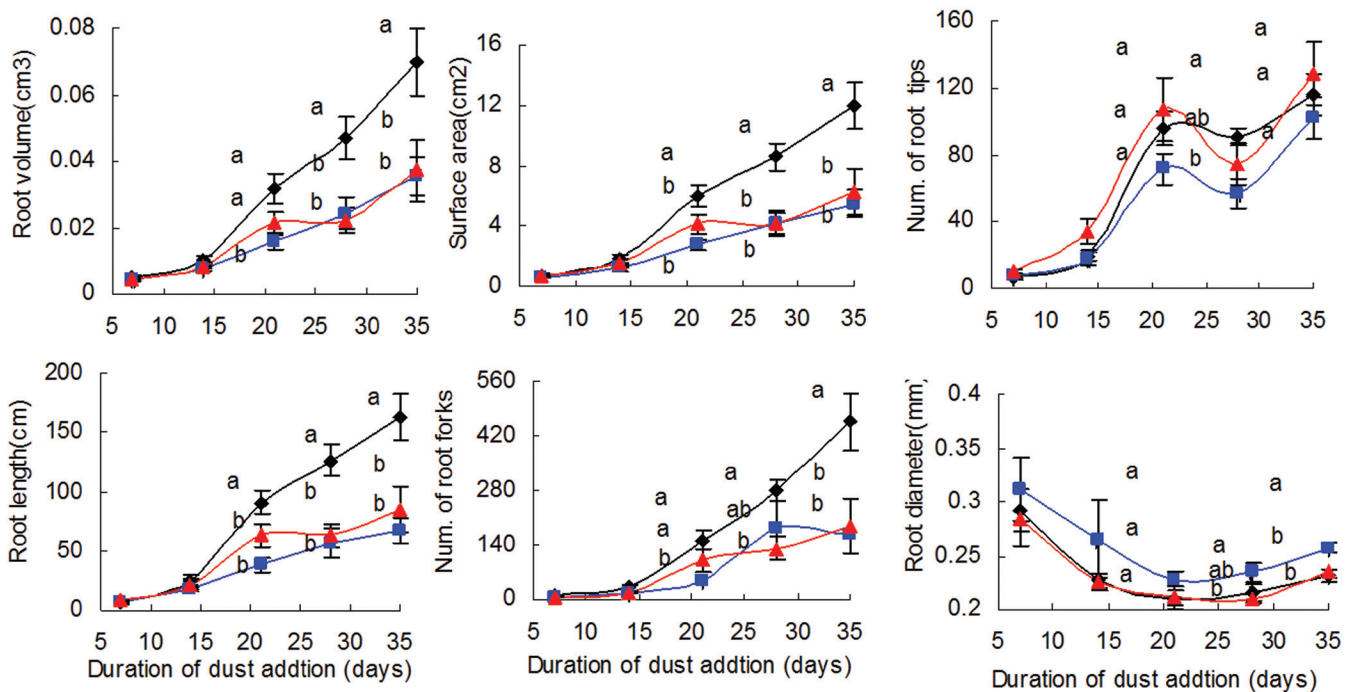


Figure 6. Comparison of temporal trends in six root morphology variables among three treatment groups, control (CK), coal powder (CP), and gangue powder (GP) for *Melissilus ruthenicus*. Different letters indicate significantly different means among treatments (◆—CK, ▲—GP, ■—CP).

ments than in the control, while measurements of five variables were the same between the two dust treatments (Figure 6). Between the dust treatments and the control, root volume, surface area, length, and number of root forks in the dust treatments became smaller than those in the control as early as on the 3rd sampling time. However, root diameter in the CP treatment was significantly bigger than that in the control. Between the CP and GP treatments, root diameter in the CP treatment was significantly bigger in the GP treatment by the last sampling time.

Leaf temperature was significantly bigger, while stomatal conductance and net photosynthetic rate were significantly smaller in the dust treatments than in the control (Figure 2). Between the two dust treatments there was no difference in all three variables.

Root biomass was significantly smaller in the dust treatments than in the control (Table 2), but total biomass was statistically the same between the dust treatments and the control. Between the two dust treatments there was no difference in both variables.

Comparison of Coal Dust Effects Among Species

After spraying coal powder or gangue powder on the plant, different plants have different reaction (Table 3 and 4). Effects of dust addition (CP and GP) on *Chenopodium album*, *Agropyron cristatum* and *Melissilus ruthenicus* contributed equally. Both dust have an strongest impact on *Agropyron cristatum* and *Melissilus ruthenicus*, while have no effect on *Lespedeza davurica* among the five plant species. *Leymus chinensis* was more affected by coal powder compared it to the gangue powder.

DISCUSSION

On the effects of coal dust, we have found studies on plant species composition [14,22] and plant photosynthesis [23,2], but we have found no study on plant root growth. This study examined the effects of coal dust on plant growth of five species. *Lespedeza davurica* was the only species whose root morphology was not affected by coal dust; the other four species were negatively affected to a varying degree.

Five out of six root morphological characters were negatively affected by coal dust, and one appeared to be positively affected. Among the negatively affected, root surface area were reduced by coal dust in most species (4 species), followed by root volume (3), root length (2 or 3), number of root forks (2), and number of

root tips (1). The one positively affected, root diameter, was increased by coal powder in *Melissilus ruthenicus*, and by gangue powder in *Leymus chinensis*.

The negative effects of coal dust on root morphology was likely caused by the reduced supply of carbohydrates to root, resulting from reduced photosynthetic efficiency by coal dust. Other people also found that coal dust can reduce photosynthetic performance of the mangrove, *Avicennia marina* [2]. In addition, the effects of gangue powder on root morphology may be caused by the high concentrations of toxic heavy metals, chromium and lead, in the powder. Root diameter is found to be increased in plants under chromium stress [24]. The soil in the coal mining region could be polluted by heavy metals [25,26].

Among the five species, *L. davurica* was the only species whose root morphology, photosynthesis, and biomass were not affected by coal powder or gangue powder. Our result is consistent with other findings that *L. davurica* or *Lespedeza* species is/are resistant to disturbances such as drought [27,28] and heavy metal contamination [29,30]. Coal dust pollution is likely to reduce light availability to plants, but *L. davurica* is known to have strong adaptation to different light intensities and can be cultivated widely across geographical regions [31].

Effect of coal dust pollution on photosynthetic efficiency varied by species: net photosynthetic rate was reduced by coal dust in three of the five species, but not affected in the other two species. The species-specific response is likely related to the capacity of leaf trapping dust particles. Naidoo and Naidoo (2005) observe that dust particles are trapped in between leaf hairs on pubescent leaves and species affected least by dust are the ones with glabrous leaves [32]. The three species whose photosynthesis were negatively affected were either with pubescent leaves (*A. cristatum* and *L. chinensis*) or with leaflets clustered together (*M. ruthenicus*). The two species whose photosynthesis were not affected were with glabrous leaves (*L. davurica* and *C. album*).

Leaf temperature was increased by coal dust in four of five species. We believe the cause for the increased leaf temperature is the same as that reported by Hirano *et al.* (1995) for cucumber and kidney bean plants: coal dust particles on the leaf surface absorb solar energy, leading to increase in leaf temperature [12].

In this study, we found that coal dust inhibited plant root growth and reduced photosynthetic rate of some species, but did not affect other species. The species with less resistance to coal dust pollution would gradu-

Table 3. Summary the Effects of Coal Powder on Plant Growth Based on the Results from the Last Sampling Time.

Plant Species	Root Morphology					Photosynthesis ¹			Biomass		
	Volume	Fork	Length	Surface Area	Tip	Diameter	LT	SC	NPR	Root	Total
<i>Agropyron cristatum</i>	-	-	-	-	-	-	-	-	-	-	-
<i>Chenopodium album</i>	-	-	-	-	-	-	+	-	-	-	-
<i>Lespedeza davurica</i>	-	-	-	-	-	-	+	-	-	-	-
<i>Leymus chinensis</i>	-	-	-	-	-	+	+	-	-	-	-
<i>Melissilus ruthenicus</i>	-	-	-	-	-	-	+	-	-	-	-

¹LT: leaf temperature; SC: stomatal conductance; NPR: net photosynthetic rate.

- Value of the coal powder group was significantly smaller than that of the control group.

+ Value of the coal powder group was significantly bigger than that of the control group.

Blank: Values of the coal powder group and the control group were statistically the same.

Table 4. Summary the Effect of Gangue Powder on Plant Growth Based on the Results from the Last Sampling Time.

Plant Species	Root Morphology					Photosynthesis ¹			Biomass		
	Volume	Fork	Length	Surface Area	Tip	Diameter	LT	SC	NPR	Root	Total
<i>Agropyron cristatum</i>	-	-	-	-	-	-	-	-	-	-	-
<i>Chenopodium album</i>	-	-	-	-	-	-	+	-	-	-	-
<i>Lespedeza davurica</i>	-	-	-	-	-	-	+	-	-	-	-
<i>Leymus chinensis</i>	-	-	-	-	-	+	+	-	-	-	-
<i>Melissilus ruthenicus</i>	-	-	-	-	-	-	+	-	-	-	-

¹LT: leaf temperature; SC: stomatal conductance; NPR: net photosynthetic rate.

- Value of the coal powder group was significantly smaller than that of the control group.

+ Value of the coal powder group was significantly bigger than that of the control group.

Blank: Values of the coal powder group and the control group were statistically the same.

ally decrease in abundance and may even disappear from the grasslands under long-term coal dust pollution, while the species with strong resistance to coal dust pollution are likely to stay and become dominant. Long-term field observations and experiments on the responses of grassland ecosystems to coal dust pollution are needed, so we can gain knowledge on the patterns and processes related to coal dust pollution, and apply the knowledge to manage the grasslands better so the ecosystem services can be optimized to meet the needs of multiple land users.

CONCLUSIONS

In this study five common plant species in an Inner Mongolian grassland were treated with coal dust to simulate the effects of coal dust deposition on plant growth. Our results showed that *L. davurica* was most resistant to coal dust deposition among the five species. Coal dust inhibited plant root growth. Among the six root morphological characters, root volume and surface area were reduced by coal dust in most species. More observations and experiments should be carried out to study the responses of grassland ecosystems to coal dust pollution.

ACKNOWLEDGEMENTS

This work was supported by Science and Technology Innovation Team (IRT1259) in Chinese Ministry of Education, program of China Postdoctoral Science Foundation (2015M572634XB) and scientific research program of Inner Mongolia Agricultural University (No. BJ2013C-3). The author would like to thank assistant Prof. Jin Yao in New Mexico State University for her revision on the manuscript.

REFERENCES

- Kavalov, B. and Peteves, S. D. 2007. The future of coal, <http://www.eirc-foundation.eu/Publications/Energy/EUR%2022744%20EN%20The%20Future%20of%20Coal.pdf>
- Naidoo, G. and Chirkoot, D., "The effects of coal dust on photosynthetic performance of the mangrove, *Avicennia marina* in Richards Bay, South Africa", *Environmental Pollution*, Vol. 127, No. 3, 2004, pp. 359–366. <http://dx.doi.org/10.1016/j.envpol.2003.08.018>
- Liao, H. and Wei, Y. M. "China's energy and CO₂ emission forecasting and perspective in the 12th Five-Year Plan", *Bulletin of the Chinese Academy of Sciences*, Vol. 26, No. 2, 2011, pp. 150–153.
- Geng, H.Q. "The environmental and social problems and countermeasures in China's large mine", *Science (Shanghai)*, Vol. 60, No. 3, 2008, pp. 33–37.
- Government of Xilinhot City. 2014. Compensation work for grassland polluted by dust of Victory Coal Mining was completed, http://www.xilinhaote.gov.cn/zwxw_1/.
- Sharratt, B.S. and Glenn, D.M., "Orchard floor management utilizing soil applied coal dust for frost protection: Part II. Seasonal microclimate effect", *China Agricultural Meteorology*, No. 43, 1988, pp. 147–154. [http://dx.doi.org/10.1016/0168-1923\(88\)90088-3](http://dx.doi.org/10.1016/0168-1923(88)90088-3)
- Carson, C.A. "Subsurface leachate migration from a reject coal pile in South Carolina", *Water, Air and Soil Pollution*, Vol. 53, No. 3, 1990, pp. 345–366.
- Anderson, M.A., Bertsch, P.M., Feldman, S.B. and Zelazny, L.W. "Interactions of acidic metal-rich coal pile runoff with a subsoil", *Environmental Science and Technology*, Vol. 25, No. 12, 1991, pp. 1038–1046. <http://dx.doi.org/10.1021/es00024a008>
- Rao, D. N., "A study of the air pollution problem due to coal unloading in Varanasi, India", *Proceedings of the Second International Clean Air Congress*, 1971. pp. 273–276. <http://dx.doi.org/10.1016/B978-0-12-239450-8.50060-5>
- Sharifi, M.R., Gibson, A.C. and Rundel, P.W., "Surface dust impacts on gas exchange in Mojave Desert shrubs", *Journal of Applied Ecology*, Vol. 34, No. 4, 1997, pp. 837–846. <http://dx.doi.org/10.2307/2405275>
- Ricks, G. R., Williams, R. J. H., "Effects of atmospheric pollution on deciduous woodland part 2: effects of particulate matter upon stomatal diffusion resistance in leaves of *Quercus petraea* (Mattuschka) Liebl", *Environmental Pollution*, Vol. 6, No. 2, 1974, pp. 87–109. [http://dx.doi.org/10.1016/0013-9327\(74\)90026-3](http://dx.doi.org/10.1016/0013-9327(74)90026-3)
- Hirano, T., Kiyota, M. and Aiga, I., "Physical effects of dust on leaf physiology of cucumber and kidney bean plants", *Environmental Pollution*, Vol. 89, No. 3, 1995, pp. 255–261. [http://dx.doi.org/10.1016/0269-7491\(94\)00075-0](http://dx.doi.org/10.1016/0269-7491(94)00075-0)
- Sarma, K.K.V., Kumari, C.S. and Prameela, K. "Observations on the impact of coal dust pollution on certain kitchen garden plants at and around strut pit mine, Yellandu", *Asian Journal of Plant Science*, Vol. 5, No. 1, 1993, pp. 43–46.
- Spencer, S. and Tinnin, R., "Effects of coal dust on plant growth and species composition in an arid environment", *Journal of Arid Environments*, Vol. 37, No. 3, 1997, pp. 475–485. <http://dx.doi.org/10.1006/jare.1997.0289>
- Ding, X.K., Zhang, Y.F., Zhang, T.K., Tang, J., Xu, Y. and Zhang, J. "Effect of operational variables on the hydrogasification of Inner Mongolian lignite semicoke", *Energy Fuels*, Vol. 27, No. 8, 2013, pp. 4589–4597. <http://dx.doi.org/10.1021/ef4007092>
- Shi, G.H., Miao, L.C., Zhang, F.Q., Jian, P., Fan, W.M. and Liu, D.Y., "Emplacement age and tectonic implications of the Xilinhot A-type granite in Inner Mongolia, China", *Chinese Science Bulletin*, Vol. 127, No. 3, 2004, pp. 723–729. <http://dx.doi.org/10.1007/BF03184272>
- Wong, M.H., Cheung, L.C. and Wong, W.C., "Effects of roadside dust on seed germination and root growth of *Brassica chinensis* and *B. parachinensis*", *Science of the Total Environment*, Vol. 33, No. 1–4, 1984, pp. 87–102. [http://dx.doi.org/10.1016/0048-9697\(84\)90383-8](http://dx.doi.org/10.1016/0048-9697(84)90383-8)
- Li, S.Y., Li, X.B., Ying, G. and Fu, N., "Vegetation indexes- biomass models for typical semi-arid steppe—A case study for Xilinhot in northern china", *Chinese Journal of Plant Ecology*, Vol. 31, No. 1, 2007, pp. 23–31. <http://dx.doi.org/10.17521/cjpe.2007.0004>
- GB/T 15265-94, Ambient air-determination of dustfall-gravimetric method, the national standard in the People's Republic of China. 1994.
- Qian, G. Q. and Dong, Z.B., "Discussions on different dust trapping methods and on some related topics", *Chinese Journal of Desert Research*, Vol. 24, No. 6, 2001, pp. 779–783.
- Guo, E.G., Zhang, S.L., Cai, Y. and Li, J. "Impact of the open-pit coal mine on soil environment quality in grassland", *Chinese Open Cast Mining Technology*, Vol. 1, 2012, pp. 93–98.
- Spencer, S. "Effects of coal dust on species composition of mosses and lichens in an arid environment", *Journal of Arid Environments*, Vol. 49, No. 4, 2001, pp. 843–853. <http://dx.doi.org/10.1006/jare.2001.0816>
- Thompson, J.R., Mueller, P.W., Flückiger, W. and Rutter, A. J. "The effect of dust on photosynthesis and its significance for roadside plants", *Environmental Pollution (Series A)*, Vol. 134, No. 2, 1984, pp. 171–190. [http://dx.doi.org/10.1016/0143-1471\(84\)90056-4](http://dx.doi.org/10.1016/0143-1471(84)90056-4)
- Das, P., Samantaray, S. and Rout, G. R., "Studies on cadmium toxicity in plants: A review", *Environmental Pollution*, Vol. 98, No. 1, 1997, pp. 2–36. [http://dx.doi.org/10.1016/S0269-7491\(97\)00110-3](http://dx.doi.org/10.1016/S0269-7491(97)00110-3)

25. Chen, Y., Zhao, H. X., Xie, Z. H., Huang, H. Y., Zang, S. Y. and Lian, B., "Heavy metal pollution characteristics in the Kaili Coal Mining region, Guizhou Province, China", *Journal of Residuals Science & Technology*, Vol. 12, No. S1, 2015, pp.123–131. <http://dx.doi.org/10.12783/issn.1544-8053/12/S1/18>
26. Yu, Y., Zhang, Y.X., Zhang, Q., Zhang, X.Q., Meng, X.J. and Lu, Z.H., "Improvement of Heavy Metal Resistant Bacteria on Phytoremediation of Reclaimed Land using Coal Gangue", *Journal of Residuals Science & Technology*, Vol. 12, No. S1, 2015, pp105–103. <http://dx.doi.org/10.12783/issn.1544-8053/12/2/11>
27. Zhao, X., Dong, K., Zhang, Y., Yang, W.D. and Liang, P.F., "Study on lamina anatomical structure of *Lespedeza daurica* (Laxm.) Schindl. from different populations", *Acta Agrestia Sinica*, Vol. 17, No. 4, 2009, pp. 445–451 .
28. Gao, Q., Chen, X.Y., Du, J.Y., Li, W. and Hao, X., "On variation of drought tolerance in species and provenances of *Lespedeza Michx*", *Journal of Beihua University (Natural Science)*, Vol. 6, No. 3, 2005, pp. 257–260.
29. Wang, Y.B., Zhang, L., Liu, D.Y., Xie, J.C., Chu, L. and Li, Y. "Analysis of vegetation state in the copper tailing yard in Tongling", *Chinese Journal of Ecology*, Vol. 23, No. 1, 2004, pp. 135–139.
30. Sun, Q.Y., Lan, C.Y., Wong, M.H. and Yang, L.Z., "Natural colonized plants on tailings of lead-zinc mine", *Acta Ecologica Sinica*, Vol. 21, No. 9, 2001, pp. 1457–1463.
31. Ma, Y.J., Ma, R., Cao, Z.Z. and Li, Y., "Analyzing of photosynthetic characteristics and influencing factors of 5 *Lespedeza* Species", *Journal of Arid Land Resources and Environment*, Vol. 26, No. 4 , 2012, pp. 166–171 .
32. Naidoo, G. and Naidoo, Y., "Coal dust pollution effects on wetland tree species in Richards Bay, South Africa", *Wetlands Ecology and Management*, Vol. 13, No. 5, 2005, pp. 509–515. <http://dx.doi.org/10.1007/s11273-004-3939-4>

Application of Vacuum Distillation to Treat Wastewater Coming from Hot Rolling Process

LV ZI-QIANG^{1,2}, CAI JIU-JU¹, SUN WEN-QIANG^{1,*} and LIU CHAO¹

¹State Key Laboratory of Eco-Industry, Northeastern University, Shenyang 110819, Liaoning, China

²University of Science and Technology Liaoning, Anshan 114051, Liaoning, China

ABSTRACT: Based upon the concepts of vacuum distillation and utilization of waste heat to treat wastewater, a vacuum distillation method has been put forward to be used for treatment of wastewater coming from hot rolling process. Experiments were conducted to study the dependence of pH, electrical conductivity (EC), chemical oxygen demand (COD) and suspended solids (SS) of treated water on operating pressure and evaporation rate. Based upon the analysis of the results, optimum values for the operating pressure and evaporation rate were determined. The results showed that treated water can meet the requirements set for the recycled water in iron and steel industries.

INTRODUCTION

DISTILLATION is a process to separate various liquid fractions based upon the differences in their boiling points. By heating the mixture to a certain temperature, low boiling components are evaporated and are condensed to complete the separation of these components. One of the advantages of the distillation is that it does not introduce any impurity to the system. The solvent is obtained directly from system components. Under low pressure conditions, separation can be achieved at lower temperatures. It indicates appropriate direction for the utilization of low temperature waste heat [1]. The process of handling domestic waste landfill leachate with the method of vacuum distillation has been studied and analyzed by Tongji University scientific research team, who thought that the process could solve the equipment corrosion problems in traditional processing technology. The process made efficient use of low grade heat source [2–4]. Vacuum distillation is usually applied in separation and refining of petrochemical and oil products, however the use of this technology is found to be scarce in the field of wastewater treatment [5–8]. Krings *et al.* reported a modified vacuum distillation apparatus to isolate volatiles from lipid food matrices and systematically evalu-

ated it using neutral synthetic oil (Miglyol 812) spiked with 14 flavor compounds [9]. Kurganova *et al.* have reported the possibility of using vacuum distillation in an open system for separating oxygen and hydrogen impurities from arsenic selenide glass melts [10]. Ni *et al.* studied vacuum distillation system used for treating paper mill wastewater under the function of additives and reported that the initial pH plays an important role in the COD removal [11]. However, to the best of our knowledge, study of the treatment and mechanism of vacuum distillation for iron and steel industry wastewater is still non-existent in the literature.

Improve the recycling rate of wastewater is the only way to realize water-saving targets in iron and steel industry. However, there are rich resources of low temperature flue gas waste heat in the steel industry, which have not been used efficiently [12–13]. Low temperature flue gas waste heat refers to the sensible heat of iron and steel industries' waste gas, which has a temperature of less than 230°C [14]. Based upon the symbiotic status of waste water and waste heat in iron and steel industries, we put forward a new wastewater treatment technology for iron and steel industries. The method is based upon vacuum distillation, which uses low temperature flue gas waste heat as a heat source. In the present work, experiments have been performed to study and analyze the wastewater treatment process (coming from hot rolling process in steel industry) using vacuum distillation and the corresponding optimum operating parameters.

*Author to whom correspondence should be addressed.
E-mail: neu20031542@163.com; Tel: +86-13889167436

Table 1. Characteristics of Wastewater Coming from Steel Industries.

Indicators	pH	EC $\mu\text{s}\cdot\text{cm}^{-1}$	COD $\text{mg}\cdot\text{L}^{-1}$	SS $\text{mg}\cdot\text{L}^{-1}$
Hot rolled comprehensive wastewater	7.91	1601.37	165.960	50

Table 2. Standards Set by the Government of China for Wastewater Quality.

Indicators	pH	EC $\mu\text{s}\cdot\text{cm}^{-1}$	COD $\text{mg}\cdot\text{L}^{-1}$	SS $\text{mg}\cdot\text{L}^{-1}$
Recycling water quality control values	6–9	450	80	20

MATERIALS AND METHODS

According to the water quality requirements of water circulation in enterprises, four indicators including the condensate pH, electrical conductivity (EC), chemical oxygen demand (COD) and suspended solids (SS) have been studied.

These indicators of the wastewater coming from the hot rolling process in steel industry and the corresponding standards set by the government of China are shown in Table 1 and Table 2 respectively.

Parameters Studied

While using low temperature waste heat as the distillation heating source, the operating pressure (vacuum) and the distillate flow rate are the main parameters which influence both the condensate water quality and quantity. Wastewater was evaporated under different operating pressures. For each group of experiments, the volume of wastewater used was 1500 ml. Samples were collected once the condensate volume reached 150 ml. Collected samples were stored in 500 ml beakers EC,

pH, COD and SS of the samples were measured. The relationships between the water quality indices and the operating pressure were analyzed by using appropriate graphical techniques. From these relationships the optimum operating parameters were obtained.

Experimental Setup

The vacuum distillation device has been shown in Figure 1. Figure 1(a) is the schematic of the experimental setup, while Figure 1(b) is the photograph of the experimental rig. The setup mainly consisted of a vacuum saturation cylinder (3L), electronic balance (having accuracy of 0.1 mg), heater with digital display (0–100°C), condensation cycle device (cooling water circulating pump, condensing coil and cooling water bucket), collection tank, buffer tank and vacuum pump. The vacuum saturation cylinder is equipped with vacuum gauge and a discharge valve.

Experimental Procedure

Various steps for the experimental procedure have

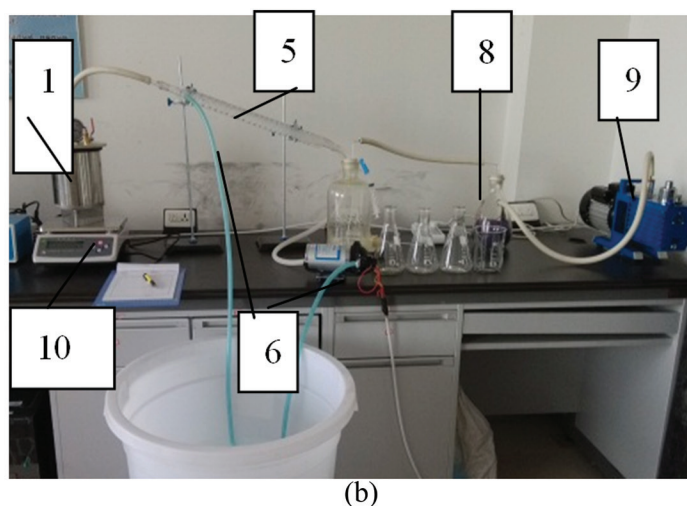
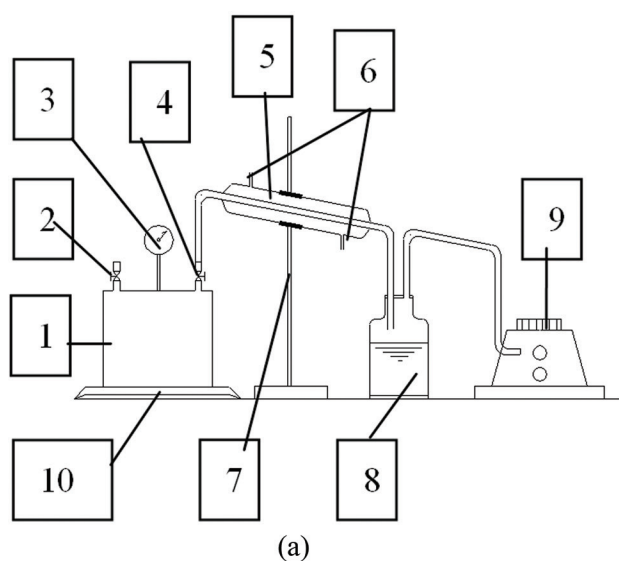


Figure 1. Photograph and the schematics of the experimental setup. 1: Vacuum saturation cylinder. 2: Intake valve. 3: Pressure gauge. 4: Exhaust valve. 5: Condensing coil. 6: Condensation cycle device. 7: Test tube rack. 8: Collection tank. 9: Vacuum pump. 10: Electronic balance.

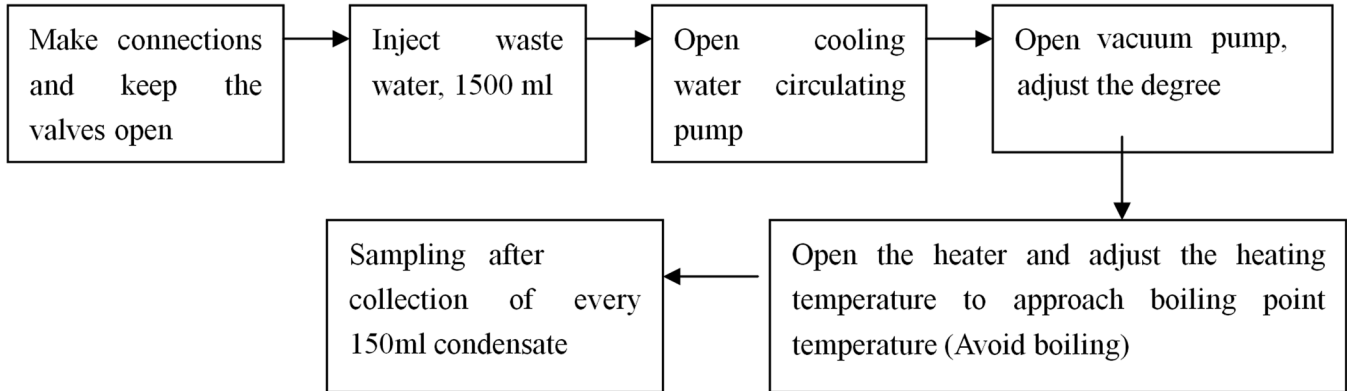


Figure 2. Experimental procedure followed in the current study.

been shown in Figure 2. In order to avoid drying of the heating reactor, it takes eight samples during each experiment.

RESULTS

Change in Condensed Fluid’s pH with Pressure and Evaporation Rate

Figure 3 shows the change in pH of condensate with different operating pressures and evaporation rates. Figure 3(a) shows the pH of condensed fluid changing with the evaporation rate under different operating pressures, while Figure 3(b) shows the pH values of condensed fluid changing with the operating pressure under different evaporation rates. It is clear that, under different operating conditions, the pH of condensed fluid always lies between 7.0–7.5, which meets the requirements shown in Table 2. Under a certain operating pressure, the pH value first decreases, and then rises

with an increase in the evaporation rate. In all studied cases, the pH value attains a minimum when the evaporation rate is about 50%. Similarly, at a certain evaporation rate, the pH value of the condensate first reduces and then rises with a decrease in the operating pressure. In all studied cases, the pH value attains a minimum when the operating pressure is higher than 0.02 MPa.

Change in Condensed Fluid’s EC with Pressure and Evaporation Rate

Figure 4 shows the change in EC of condensed fluid with pressure and evaporation rate. Figure 4(a) shows change in condensed fluid’s EC value with the evaporation rate under different operating pressures, while Figure 4(b) shows change in condensed fluid’s EC value with the operating pressure under different evaporation rates. It is clear that, under different operating conditions, EC values for all condensed fluid samples meet

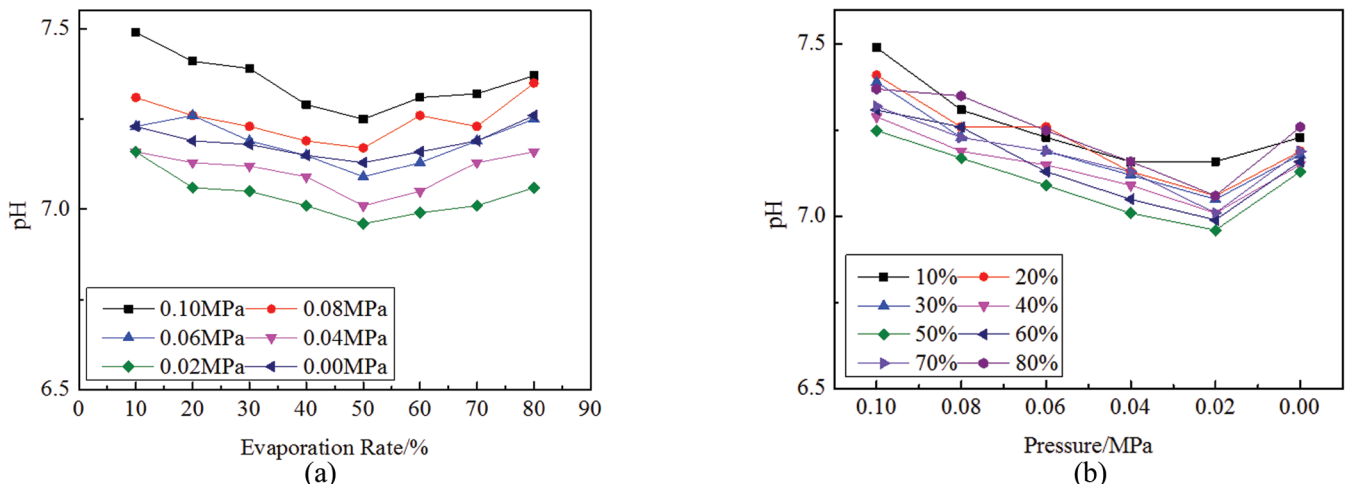


Figure 3. Graphs showing changes in condensed fluid pH with pressure and evaporation rate.

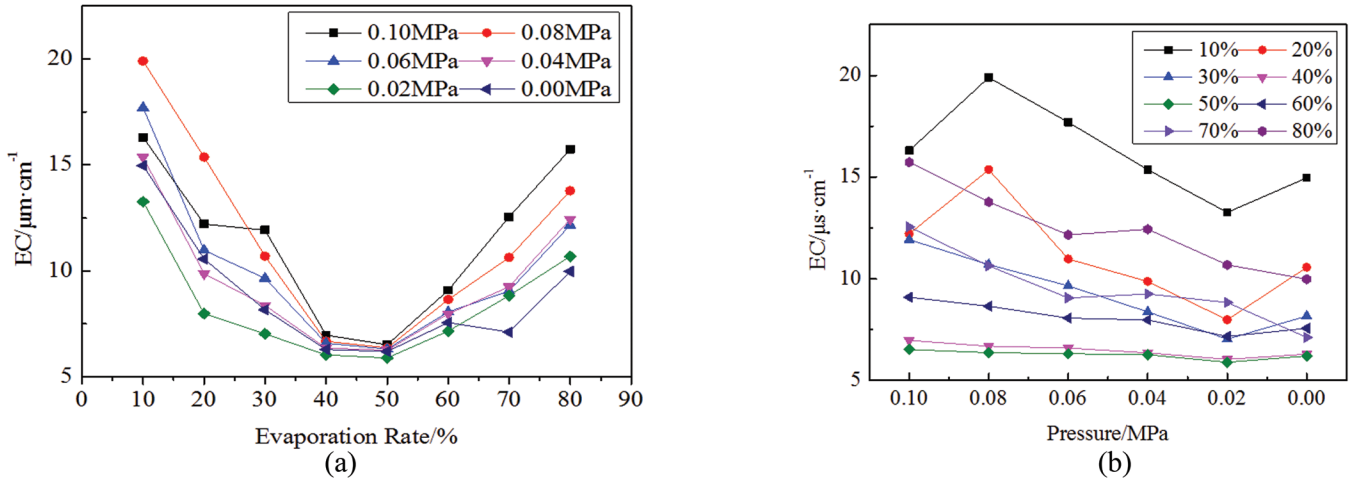


Figure 4. Graphs showing changes in condensed fluid EC with pressure and evaporation rate.

the requirements presented in Table 2. Under a certain operating pressure, the EC of condensed fluid first reduces and then rises with an increase in the evaporation rate. In all studied cases, the EC value attains a minimum when the evaporation rate is about 40–50%. For a certain evaporation rate, the EC value of the condensed fluid first reduces and then rises with a decrease in the operating pressure. In all studied cases, the EC value attains a minimum when the operating pressure is around 0.02MPa.

Change in Condensed Fluid’s COD with Pressure and Evaporation Rate

Figure 5 shows changes in condensed fluid’s COD values with pressure and evaporation rate. Figure 5(a) shows changes in condensed fluid’s COD values with

evaporation rate under different operating pressures, while Figure 5(b) shows changes in condensed fluid’s COD values with operating pressure under different evaporation rates. It is clear that, under different operating conditions, the COD values for all condensed fluid samples lies between 40–80 mg·L⁻¹, which meets the requirements stated in Table 2. Under a certain operating pressure, the value of condensed fluid’s COD reduces with an increase in evaporation rate. When the evaporation rate is higher than 50%, the decrease in COD value slows down. For a certain evaporation rate, the COD value of condensed fluid first reduces and then rises with a decrease in the operating pressure. In all studied cases, the COD value attains a minimum when the operating pressure is around 0.02 MPa. If the operating pressure is reduced further, the COD value begins to increase.

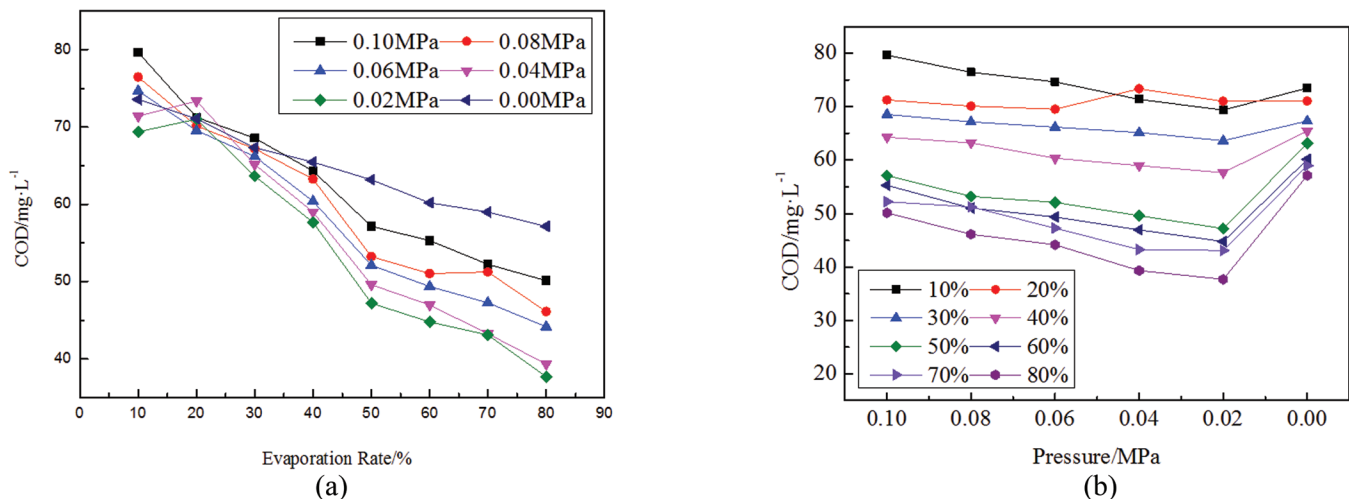


Figure 5. Graphs showing changes in condensed fluid’s COD with pressure and evaporation rate.

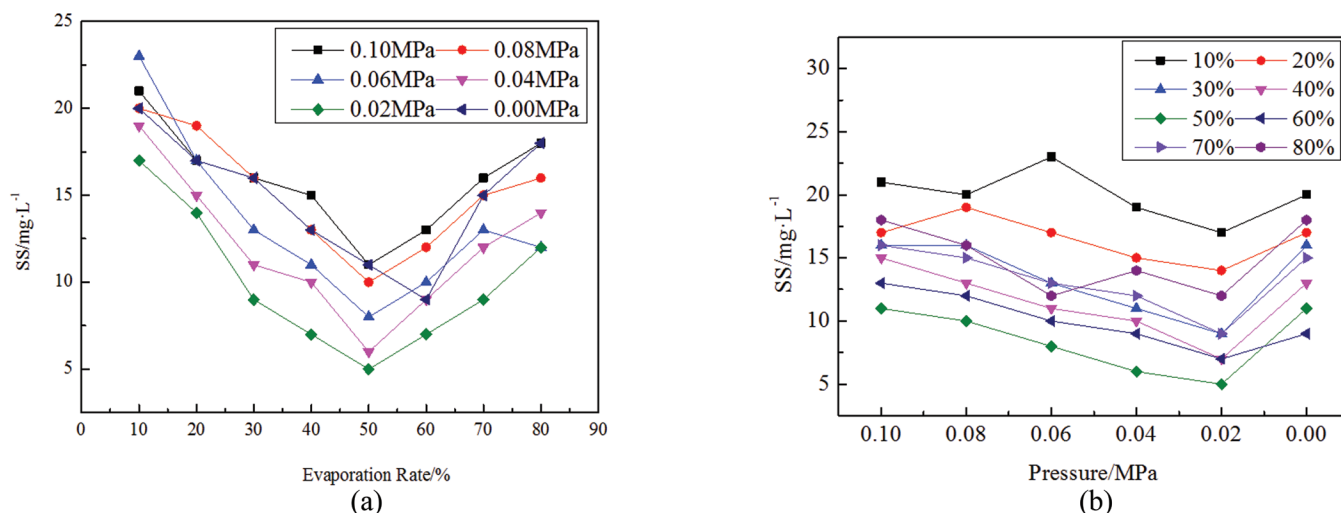


Figure 6. Graphs showing changes in condensed fluid's SS with pressure and evaporation rate.

Changes in Condensed Fluid's SS with Pressure and Evaporation Rate

Figure 6 shows the variation in condensed fluid's SS values with operating pressure and evaporation rate. Figure 6(a) shows change in condensed fluid's SS values with evaporation rate under different operating pressures, while Figure 6(b) shows change in condensed fluid's SS values with operating pressure under different evaporation rates. It is clear that, under different operating conditions, the SS values for all condensed fluid samples lie below 20 mg·L⁻¹, which meets the requirements stated in Table 2. The only exception to it is the condition, when operating pressure is between 0.06–0.1 MPa and the evaporation rate is between 10–20%. The SS values for the condensed samples under these conditions are higher than 20 mg·L⁻¹. For a certain operating pressure, the SS value of the condensed fluid achieved the minimum when the evaporation rate is 50%. At a certain evaporation rate, the SS value of the condensed fluid first reduces and then rises with a decrease in the operating pressure. In all studied cases, the SS value attains a minimum when the operating pressure is around 0.02 MPa.

DISCUSSION

Analysis of Changes in Condensed Fluid's pH and EC Values with Pressure and Evaporation Rate

Changes in the values of condensed fluid's pH and EC are mainly caused by the entrainment of steam from waste water at the beginning of the evaporation. With the increase in rate of evaporation, steam entrain-

ment is gradually reduced. But in the later stages of evaporation, evaporation conditions were significantly worse due to the poor quality of the wastewater, which in turn increases the steam entrainment. Changes in the values of condensed fluid's pH and EC with the pressure are mainly caused by the air flow rate and flow velocity of wastewater surface evaporation. When the operating pressure is high, large air flow going in and out of the cylinder under the effect of vacuum pump was observed. Since the degree of vacuum in vacuum saturation cylinder is very small, which forms a strong turbulent airflow above the liquid level in cylinder, and then the free particles on the surface of the liquid will be carried into the condensed fluid, which increases the volatility of other substances in the wastewater. The results lead to increased content of related substances in the condensed fluid. On the contrary, under the condition of vacuum or close to vacuum, only little or no air flow going into the vacuum saturation cylinder was observed. Therefore, there is lesser amount of related substances carried by the air. But when the pressure is too low, the boiling point of water is reduced. It becomes extremely prone to boiling evaporation. The observed violent boiling was the effect of increasing the concentration of the wastewater related substances, which flow into the condensed fluid with steam.

Analysis of Changes in Condensed Fluid's COD with Pressure and Evaporation Rate

Variation in COD values is due to the entrainment of organics (present in wastewater) in vapor phase. The variation of COD with evaporation rate is different from that observed for EC values. This is due to the

reason that most of the organisms are present in the top layer of the wastewater. In general, the COD values decline with an increase in the evaporation rate.

Analysis of Changes in Condensed Fluid's SS Values with Pressure and Evaporation Rate

The variation in SS values with operating pressure and evaporation rate is mainly due to the water quality in operation process and air flow of the water surface. At a particular operating pressure, when evaporation begins, part of insoluble, lighter impurities present in wastewater are carried to the condensed fluid by steam and air. Although, there are still some suspended solids in the condensate, however the contents of light weight insoluble impurities in wastewater decrease with an increase in the condensed fluid evaporation rate. When the evaporation rate is higher, the content of light weight insoluble impurities in the wastewater is not the main factor causing variations in SS values of the condensate. Instead, the main reason is that the concentration of insoluble impurities increases at the later stages of evaporation. By then, the wastewater evaporation becomes more intense, due to which the insoluble impurities in wastewater are entrained in vapors and are carried to the condensate. This in turn results in an increase in the SS value of the condensate sample.

CONCLUSIONS

Experiments have been conducted to study the treatment of wastewater coming from hot rolling process in iron and steel industries by vacuum distillation. The quality of the condensate (condensed fluid) has been analyzed. Following conclusions are drawn from the analysis.

1. Using vacuum distillation to process the wastewater coming from hot rolling process in iron and steel industries results in values of pH, electrical conductivity (EC), chemical oxygen demand (COD) and suspended solids (SS) for treated water, all of which lie within the standards set by the government of China.
2. For a certain operating pressure, the values of pH, EC and SS first decrease and then rise with an increase in evaporation rate. All three indicators

(pH, EC and SS) attain minimum values when the evaporation rate is about 40–50%. COD value reduces with an increase in the evaporation rate. When the evaporation rate is higher than 50%, the decreasing trend of COD slows down.

3. For a particular evaporation rate, the values of pH, EC, COD and SS first decrease and then increase with a decrease in the operating pressure. All four indicators (pH, EC, COD and SS) attain a minimum when the operating pressure is about 0.02MPa.

REFERENCES

1. Wang, D.X., Lu, F. and Zou, H.F., 2013. *Vacuum distillation*, Beijing, Chemical industry press, Inc.
2. Ahn, W.Y., Kang, M.S. and Yim, S.K., "Advanced landfill leachate treatment using integrated membrane process", *J. Desalination*, Vol. 12, No. 3, 2002, pp.109–114. [http://dx.doi.org/10.1016/S0011-9164\(02\)00740-3](http://dx.doi.org/10.1016/S0011-9164(02)00740-3)
3. Cecen, F. and Aktas, O., "Aerobic co-treatment of landfill leachate with domestic wastewater", *J. Environ. Eng.* Vol. 21, No. 3, 2004, pp. 303–312.
4. Yang, Q., He, P.J. and Shao, L.M., "Treatment of Leachate from Municipal Solid Waste Landfills by Evaporation in Vacuum", *J. Environmental Engineering*, Vol. 24, No. 2, 2006, pp.17–19.
5. Gu, W.G., Huang, Y.Q., Wang, K., Zhang, B.J., Chen, Q.L. and Hui, C.W., "Comparative analysis and evaluation of three crude oil vacuum distillation processes for process selection", *J. Energy*, Vol. 76, No. 5, 2014, pp.559–571. <http://dx.doi.org/10.1016/j.energy.2014.08.053>
6. Song, K., Park, S., Na, J. and Han, C.H., "Optimal operation strategy of batch vacuum distillation for sulfuric acid recycling process Jaehum", *J. Computers and Chemical Engineering*, Vol. 71, No. 5, 2014, pp. 104–115.
7. Lu, X.H., Wang, P.F., Zhang, Y.J. and Zhi, D., "Root Nitrogen Uptake in Wastewater-Irrigated Pepper Fields", *J. Journal of Residual Science and Technology*, Vol. 12, No. 4, 2015, pp. 241–247. <http://dx.doi.org/10.12783/issn.1544-8053/12/4/7>
8. Yang, Q.H., Zhao, X.X., Zhang, J., Wang, Y., Zou, W., Ming, H.M. and Zhao, C.Q., 2015. "Components of a Bioflocculant for Treating Tannery Wastewater", *J. Journal of Residual Science and Technology*, Vol. 12, No. 2, pp. 99–103. <http://dx.doi.org/10.12783/issn.1544-8053/12/2/9>
9. Ulrich, K., Dattatreya, S.B. and Ralf, G.B., "Thin layer high vacuum distillation to isolate the flavor of high-fat food", *J. Eur Food Res Technol*, Vol. 217, No. 2, pp. 70–73.
10. Kurganova, A.E. and Snopatin, G.E., 2012. "Churbanov . Purification of glass melts in the As-Se system with vacuum distillation", *J. Glass Physics and Chemistry*, Vol. 38, No. 3, 2003, pp. 300–306.
11. Li, N., Ma, H.Z. and Wang, B., "Treatment of industrial wastewater by vacuum distillation", *J. Journal of Shaanxi Normal University (Natural Science Edition)*, Vol. 39, No. 3, 2011, pp. 51–55.
12. Che, D.F. and Liu, Y.H., 2006. *Fluegases energy cascade use*, Chemical, Beijing, Industry Press, Inc.
13. Lian, H.K., Li, Y., Shu, G.Y. and Gu, C.W., "An Overview of Domestic Technologies for Waste Heat Utilization", *J. Energy Conservation Technology*, Vol. 29, No. 166, 2011, pp. 123–128.
14. Tang, J.J., Zhou, K.G. and Zhang, Q.X., "Sulfuric acid recovery from rare earth sulphate solutions by diffusion dialysis", *J. Trans Nonferrous Met. Soc. China*, Vol. 16, No. 4, 2006, pp. 951–955. [http://dx.doi.org/10.1016/S1003-6326\(06\)60358-0](http://dx.doi.org/10.1016/S1003-6326(06)60358-0)

Thermal Recirculation and Efficiency of Phenolic Resin as Building Insulation

TING-YU CHEN¹, WEN-PEI SUNG^{1,*} and YU-KUANG ZHAO²

¹*Department of Landscape Architecture, Integrated Research Center for Green Living Technologies, National Chin-Yi University of Technology, Taichung 41170, Taiwan*

²*Department of Refrigeration, Air Conditioning and Energy Engineering, Integrated Research Center for Green Living Technologies, National Chin-Yi University of Technology, Taichung 41170, Taiwan*

ABSTRACT: The objective of this research is to develop a comfortable living environment with energy-saving features. Two buildings insulated with phenolic resins were constructed according to experimental design to study variations of outdoor and indoor temperatures. The CFD program is used to simulate the large-scale environmental flow field analyses. Results of CFD simulation carried out for the five time intervals of a day show that (1) air current assists in carrying away heat from the wall surface, the indoor temperature drops faster and the indoor air flow becomes turbulent when the window is opened; (2) when the window is closed, the indoor air flow near the window varies the most; (3) phenolic resin insulation has good thermal property.

INTRODUCTION

MOST buildings with close environment are not capable of dissipating properly the thermal heat input; hence, the heat is accumulated to increase the building indoor temperature. Auxiliary air conditioning is needed in modern buildings to maintain a comfortable living or working environment at the cost of energy consumption. How to manage a comfortable environment with the minimum consumption of energy is a major concern and research topic for many nations [1–5]. Hence, heat preservation and insulation are discussed so that the thermal transport from outside environment into a closed building or environment can be reduced to alleviate the air conditioning loadings [6,7]. During ancient times, leaves and thatch were used as natural insulating materials to insulate buildings. In the 20th century, the modern science and technology leads to the development of many insulating materials with high thermal efficiencies including light-weight formed materials, materials inlaid with air pockets, and reflective materials. Modern building emphasizes the use of materials that is aesthetically natural, comfortable and healthy. In addition to providing effective insulation, the insulating material must be light-weight with strength, easy to process, durable, aesthetic, com-

fortable, healthy, easy to clean, and resistant to moisture and microbial growth. Other energy and pollution related features of the construction material include requiring low energy to produce, with low pollution potential and environmentally friendly. The new phenolic insulation material used in this research is environmentally friendly with high economic value; it is low in toxicity and efficient in insulation so that it can be considered as a green construction material [8–10].

In order to understand whether the phenolic resin is suitable for building insulation material, it is used to insulate the experimental building for monitoring outdoor and indoor temperatures across the roof and the walls on the four sides (east, south, west and north) to evaluate the insulation efficiency of phenolic resin as building insulation material. The experimental results show that during summer, phenolic plate has obvious insulation effect of reducing 5–10°C whereas during winter under northeastern monsoon, the temperature difference across the building wall is 4–7°C indicating the characteristics of phenolic plate to insulate against low temperature [11]. The computational fluid dynamics (CFD) program is used to simulate the large-scale environmental flow field analyses so that more realistic simulation results with fewer errors can be obtained. The CFD to simulate the building isolated with phenolic resin based on the experimental monitoring results obtained in previous years. The results thus obtained

*Author to whom correspondence should be addressed.
Email: wps@ncut.edu.tw

will provide valuable references to future relative base design, building construction, and landscape.

METHODOLOGY

During the first year of the research, phenolic resin was used to construct an experimental building in order to understand whether the phenolic resin is applicable for constructing a building to provide comfort living conditions with less energy consumptions. Two phenolic resin-insulated experimental buildings with 30 monitoring points as shown in Figure 1 were constructed to study thermal transportation and temperature variations.

The experimental results were used to identify parameters for conducting the simulation on solar radiation, thermal transportation between outdoor and indoor across phenolic resin board, and temperature variations using the CFD program. The computer model is shown in Figure 2. The underlying equation for this multiphysics CFD modeling in building envelopes is the energy equation shown in Equations (1)–(3). The energy equation allows considering the effect all of the following heat phenomena: convection in fluid, conduction in solids, thermal (solar) radiation, and external heat gains.

$$\rho \frac{\partial \vec{V}}{\partial t} + \rho(\vec{V} \cdot \nabla)\vec{V} = -\nabla P + \rho \vec{g} + \mu \nabla^2 \vec{V} \quad (1)$$

$$\rho C_p \frac{\partial T}{\partial t} + (\vec{V} \cdot \nabla)\rho C_p T = \nabla \cdot (k \nabla T) + \mu \Phi + \dot{q} \quad (2)$$

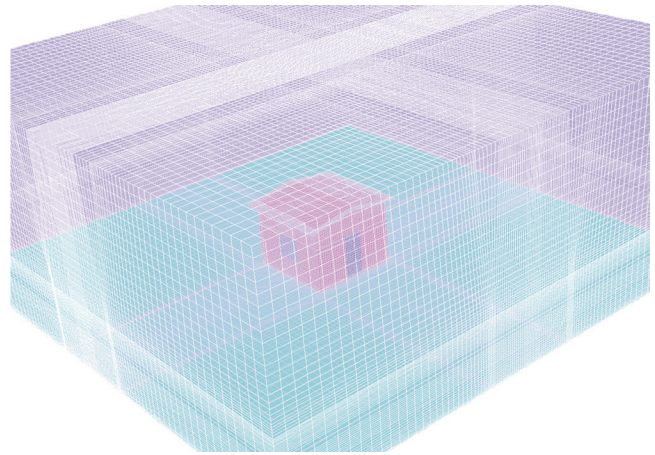


Figure 2. Simulated model of the experimental building.

$$\rho = \frac{p_{op} + p}{\frac{R}{M_w} T} \quad (3)$$

Where:

- T = Temperature
- ρ = Density
- C_p = Specific Heat
- q = Heat source (mean solar radiation)
- R = Gas constant
- M_w = molecular weight of gas
- $-\Delta P$ = is the pressure force
- $\rho \vec{g}$ = is the gravity force
- $\mu \nabla^2 \vec{V}$ = is the shearing force
- $\nabla \cdot (k \nabla T)$ = is the conduction dissipation
- $\mu \Phi$ = is the Viscous dissipation
- \dot{q} = is the Heat generation



(a)



(b)

Figure 1. Buildings equipped with phenolic resin insulation.

Weather variables (major influencing factors include: air temperature, air density, wind velocity etc.) considerably influence the hydrothermal performance of a building envelope. In site planning, buildings can then be reasonably positioned based on the analysis result of the wind environment, while other factors such as day lighting, noise, building coverage, height, orientation, spacing and configuration are addressed as well [12,13]. Therefore it is essential to incorporate these variables into this simulation methodology. Air temperature should not be the only parameter used to define the thermal climate, but indeed it is the most commonly used. In this paper the operative temperature [Equation (4)] is calculated, which includes the ambient air temperature (T_a), air velocity (v) and the mean radiation temperature [Equation (5)] that is as a function of the radiation intensity from each surface. [14]

$$T_{op} = \begin{cases} (M.R.T + T_a \sqrt{10v}) / (1 + \sqrt{10v}) & (v \geq 0.1 \text{ m/s}) \\ (M.R.T + T_a) / 2 & (v < 0.1 \text{ m/s}) \end{cases} \quad (4)$$

$$M.R.T. = \left(\frac{I_{rad} \cdot \pi}{\sigma} \right)^{0.25} \quad (5)$$

Where:

- $M.R.T.$ = Means radiation temperature (T_a)
- T_a = Ambient air temperature ($^{\circ}\text{C}$)
- T_{op} = Operative temperature ($^{\circ}\text{C}$)
- v = Velocity (m/s)
- σ = Stefan Boltzmann constant ($\text{kg}/(\text{s}^3 \text{K}^4)$)
- I_{rad} = radiation intensity ($\text{W}/(\text{m}^2 \text{sr})$)

The solar variables such as the sun direction vectors, sunshine fraction, and direct and diffuse solar irradiation necessary for the solar ray tracing algorithm computations are then calculated. The energy equation is show as Equations (6)–(8) [15].

$$E_{total} = E_{direct} + E_{diffuse, solar} + E_{reflect, ground} \quad (6)$$

$$E_{d, solar} = CE_{direct} \frac{1 + \cos \epsilon}{2} \quad (7)$$

$$E_{r, ground} = E_{direct} (C + \sin \beta) \rho_g \frac{1 + \cos \epsilon}{2} \quad (8)$$

Where:

E_{total} = total solar radiation

- E_{direct} = normal direct solar irradiation
- $E_{diffuse}$ = total diffuse irradiation
- $E_{d, solar}$ = diffuse solar irradiation
- $E_{r, ground}$ = ground reflected solar irradiation

The simulation was carried out based on various grids to perform grid independence test. First, one point in the model was selected as the reference point for selecting points with various heights to perform grid test analyses with the results shown in Figure 3. Seven sets of various grid numbers were evaluated for the grid range from 20w cells to 400w cells. The grid of 250w cells shows no tendency of diffusion or convergence; i.e. the analysis results carry no significant variations so that stable simulation and good analysis results are obtained (Figure 4). Hence, the grid of 250w cells was used for performing the subsequent simulation based on conditions of the actual site with comparisons of actually monitored experimental data and computer monitoring results for model calibration. The weather conditions for July (summer) in Taichung (Taiwan) were used for simulating the atmospheric space for evaluating the overall building indoor and outdoor thermal environments.

RESULTS AND DISCUSSIONS

Results of simulation on variations of the outdoor and indoor temperatures using data collected with the experimental building insulated with phenolic resin are shown in Figure 5 (window closed) and Figure 6 (windows opened). Under similar conditions, when the ambient wind speed is not high, the room with windows closed has more uniform temperature distribution than room with windows opened that reveals the insulating characteristics of phenolic resins. At 8:00 A.M., the east-side wall is exposed to solar irradiation; its temperature

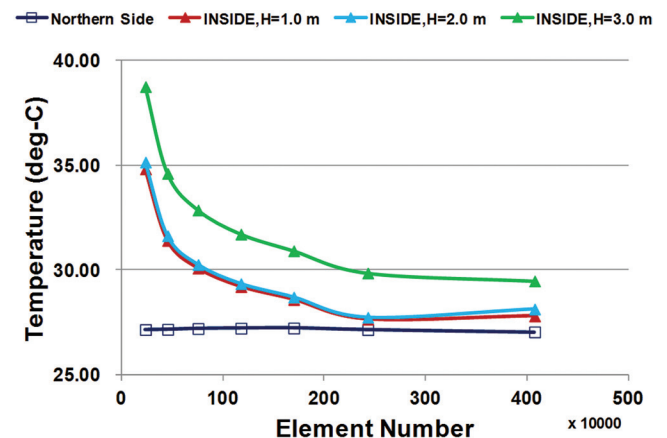


Figure 3. Simulated test of grid point.

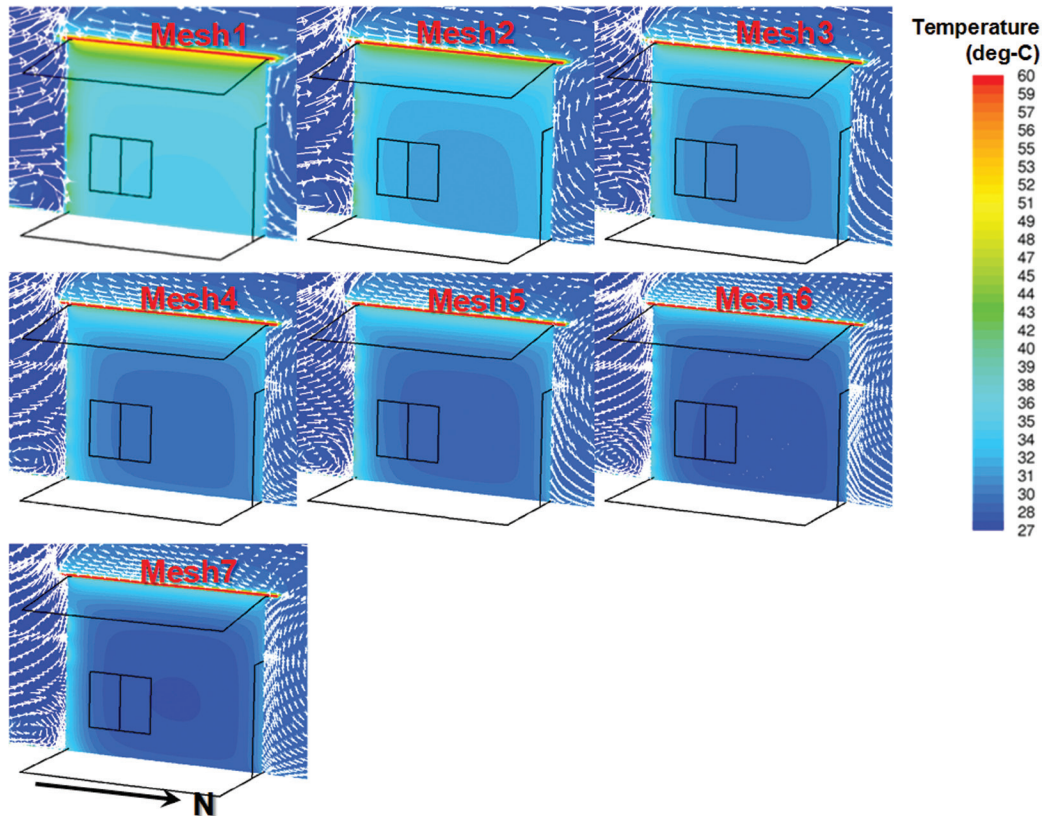


Figure 4. Results of analyzing indoor space using grids of various points.

gradually increases. At noon, the sun is directly over the building so that heat comes directly from the roof top. At 2:00 P.M., the west-side wall is exposed to solar irradiation, and breeze enters the building through the east-side window to carry some heat away from the wall. Hence, opening the window causes the room temperature to drop fast. The simulation results for the period between 8:00 A.M. and 10:00 A.M. indicate that the opened window causes the room temperature to rise. Additionally, when the window is opened, the heat comes from a fixed source but the movement of indoor air current leads to more uniform spatial temperature distribution but higher room temperature.

Results of flow analyses along the north-south directions are indicated in Figure 7 for closed window and Figure 8 for opened window. The window is located on the east-side wall; when the sun is above the horizon at a certain angle of inclination, a small floor area is exposed to the incident solar irradiation through the window. Hence, the simulated results for the period between 8:00 A.M. and 10:00 A.M. show a region of relatively higher temperature adjacent to the hot floor area. With the sun rises further, this floor area will gradually move from the center of the building toward the window.

When the window of the phenolic resin insulated building is closed, heat is easily transmitted through the window glass panes into the building. Hence, the area surrounding the windows experiences the generation of more vigorous speed field during all time intervals starting 8:00 A.M.. Figure 7 shows that the east-side wall is exposed to heat at 8:00 A.M., but the temperature is not obvious so that the speed field is weak. During other time intervals, the window shows obvious vigorous heat exchange; the speed field shows the direction from the east-wall window toward the west-side wall. After reaching the wall, it is diffused toward the room and the ground.

Simulation results for the insulated building with window opened (Figure 8) show that after entering the building through window, the air current diffuses to all directions until hitting the boundary wall; it is then reflected from the wall to form turbulent current. Because the experimental building has a single window, after the formation of turbulent air current, some air current may also flow out of the building. Hence, air flows of different directions, i.e. flowing into and out of the room, near the window cause weaken air current flowing into the building and poor indoor air circulation that indirectly affect the building heat dissipation.

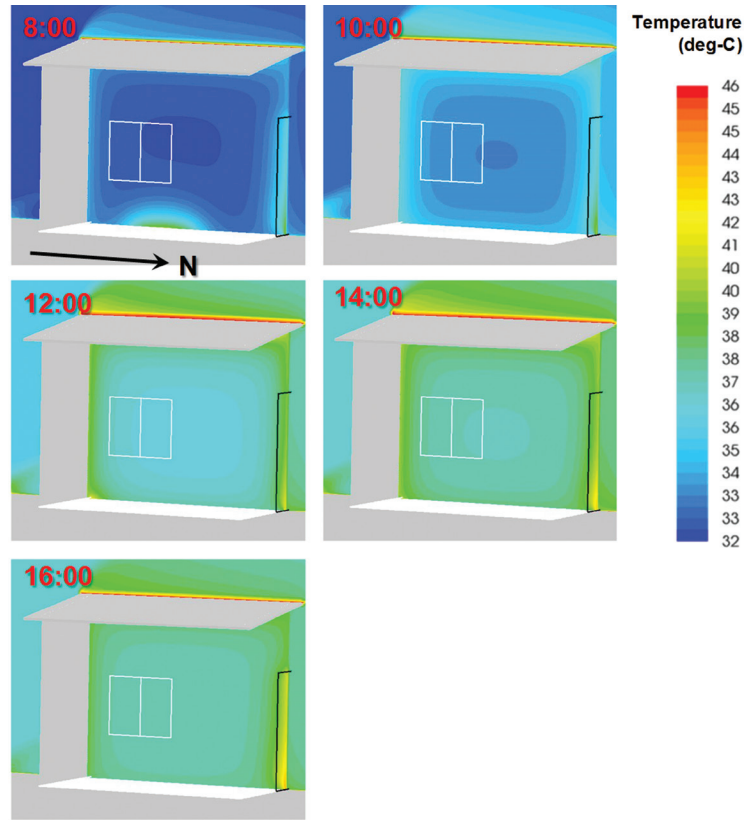


Figure 5. Simulated Room Temperature for Window Closed.

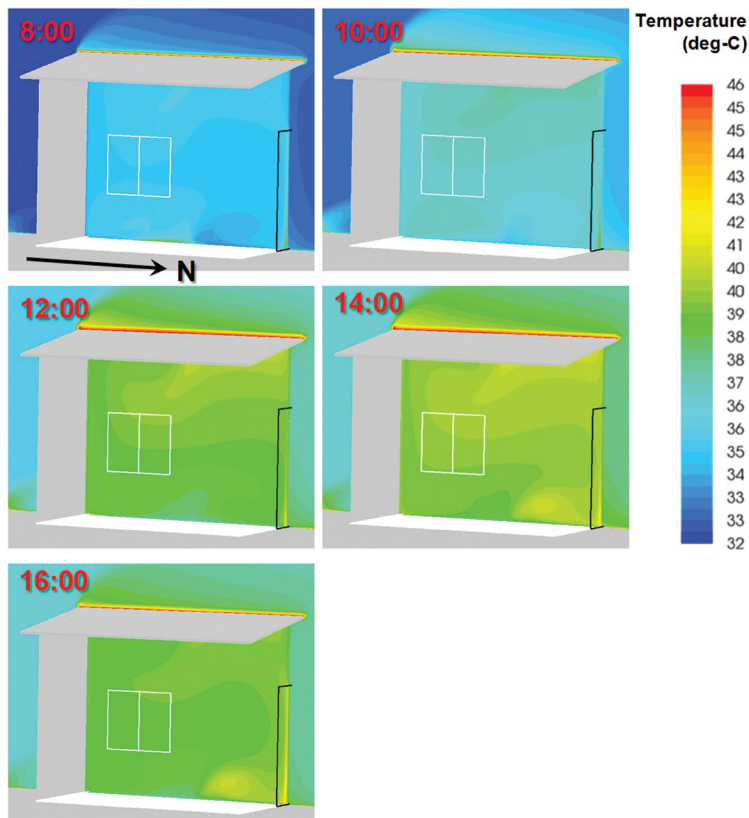


Figure 6. Simulated Room Temperature for Window Opened.

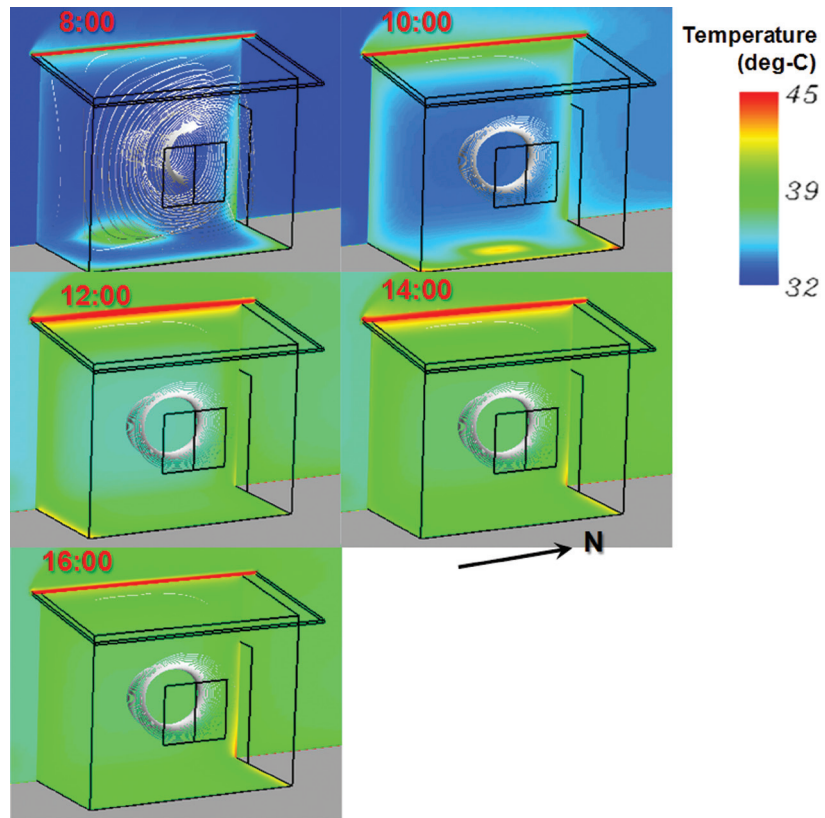


Figure 7. Simulated Variations of Air flow for Closed Window (North-South Direction).

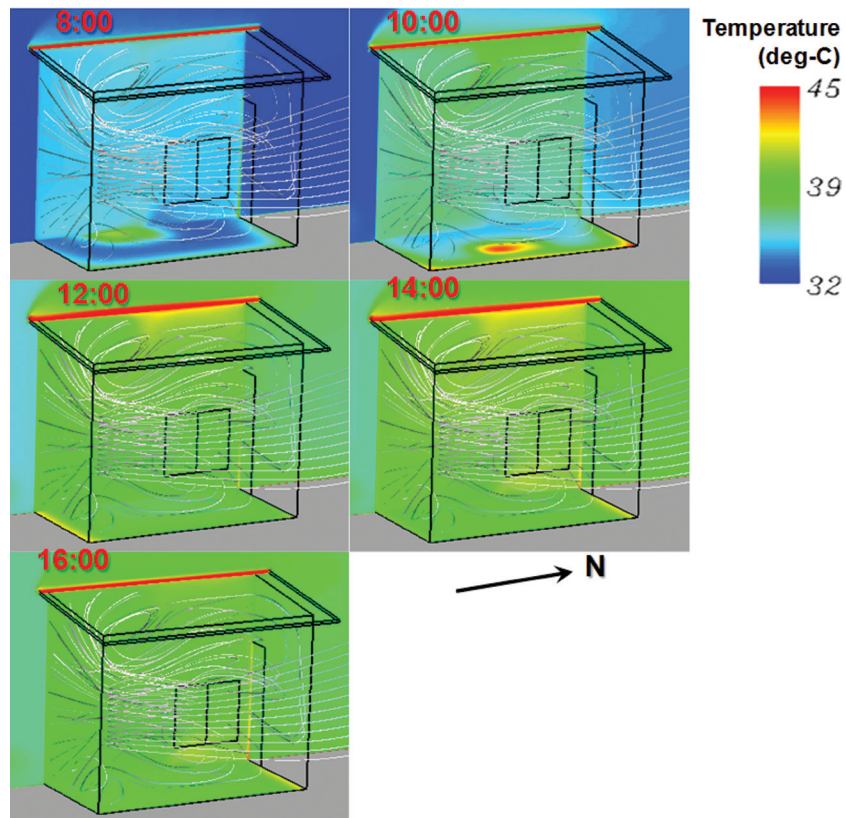


Figure 8. Simulated Variations of Air flow for Opened Window (North-South Direction).

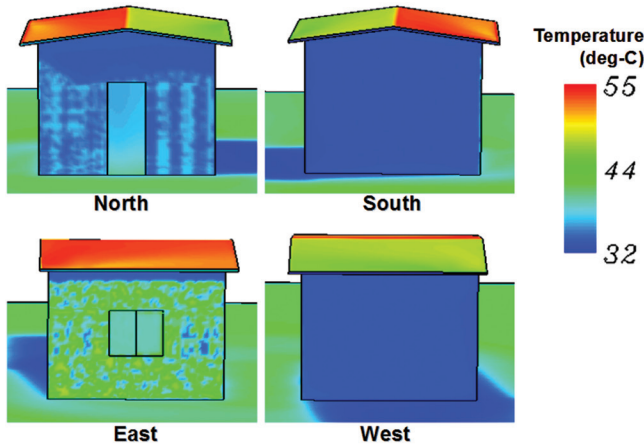


Figure 9. Simulated 8:00 A.M. Wall Surface Temperature (Window Closed).

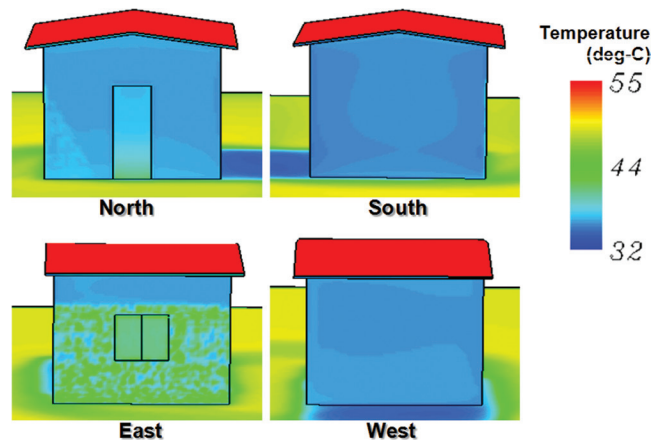


Figure 10. Simulated 10:00 A.M. Wall Surface Temperature (Window Closed).

Figures 9–13 show temperature distributions during the four time intervals between 8:00 A.M. and 4:00 P.M. on the roof and outside surface of the wall for closed window whereas Figures 14–18 show those for opened window. Among the five time intervals, at 8:00 A.M., the wall temperature is generally the lowest, and the east-side wall surface temperature is the highest among walls of other directions because the east-side wall is subject directly to the sun rising in the south-east direction. During the same time interval, the roof temperature rises gradually. At 10:00 A.M., the sun rises higher, the east-side wall is under the roof shadow, its heated surface is thus reduced but the temperature rises for the roof and the wall on other sides. At 12:00 noon, the sun is at the apex, and the building shadow is the smallest so that the indoor heat mainly comes from the roof.

At 2:00 P.M., the west-side wall is subject to solar irradiation so that its temperature rises whereas the roof temperature rises continuously to reach the highest

level of 55°C and then gradually decreases. When the sun moves to the 4:00 P.M. position, the area exposed to solar irradiation for the west-side wall increases, and the east-side roof temperature decreases. Because the sun rises from southwest to move toward northwest, the north-side wall surface experiences faster temperature decrease than the east-side and south-side walls.

The two experimental buildings have similar appearance, dimensions and features; they are subject to similar environmental and heating condition. The influence of window is the greatest because the window is the largest transparent structure in the experimental building. The solar radiation can easily penetrate the transparent window to bring the solar radiation heat into the building because the traditional window has lower heat transmittance of 6.40 W/(m²·K) than solid wall. Results of the model simulation for the building with opened window show that the outside wall surface temperature is always higher than indoor room

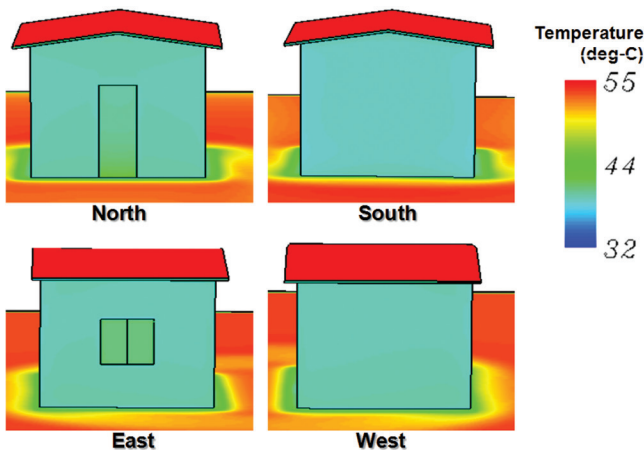


Figure 11. Simulated 12:00 Noon Wall Surface Temperature (Window Closed).

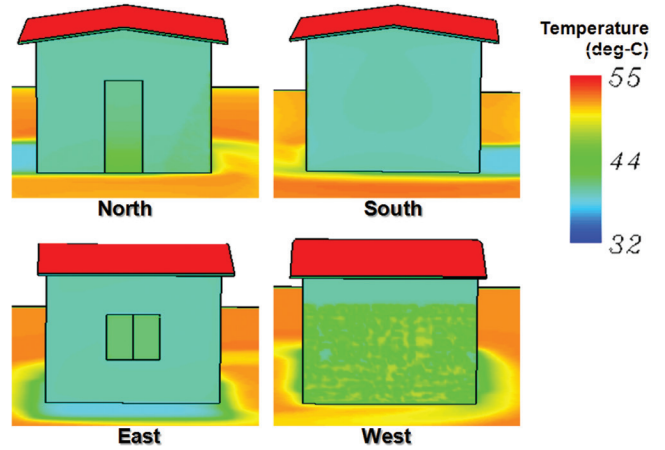


Figure 12. Simulated 2:00 P.M. Wall Surface Temperature (Window Closed).

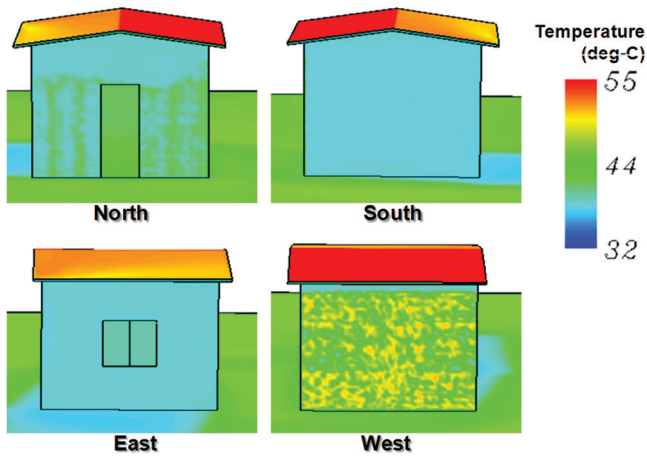


Figure 13. Simulated 4:00 P.M. Wall Surface Temperature (Window Closed).

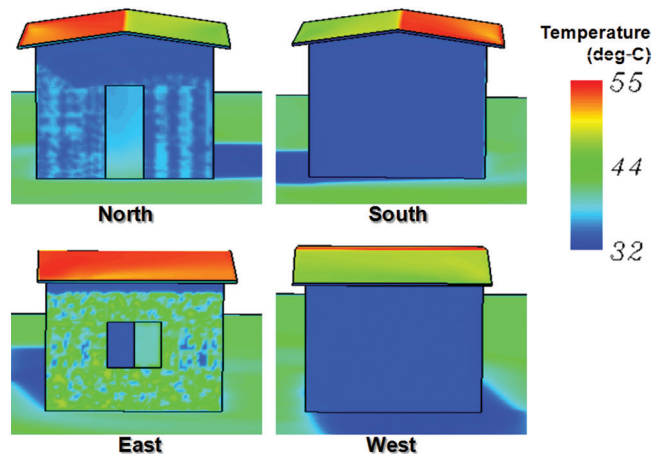


Figure 14. Simulated 8:00 A.M. Wall Surface Temperature (Window Opened).

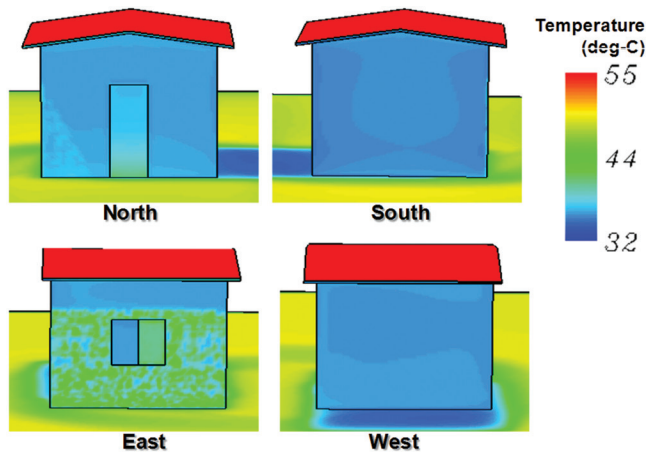


Figure 15. Simulated 10:00 P.M. Wall Surface Temperature (Window Opened).

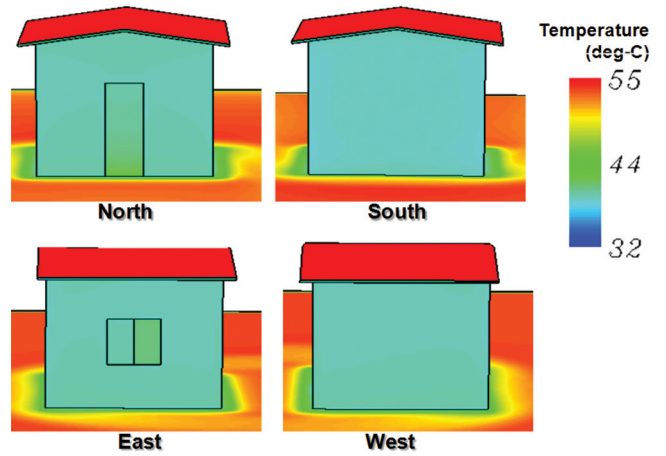


Figure 16. Simulated 12:00 noon Wall Surface Temperature (Window Opened).

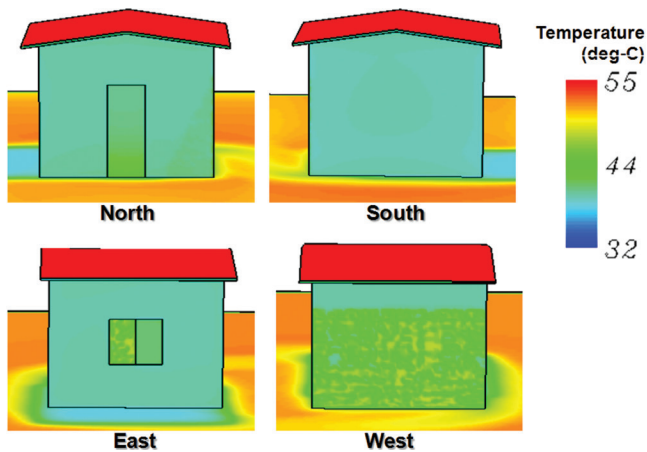


Figure 17. Simulated 2:00 P.M. Wall Surface Temperature (Window Opened).

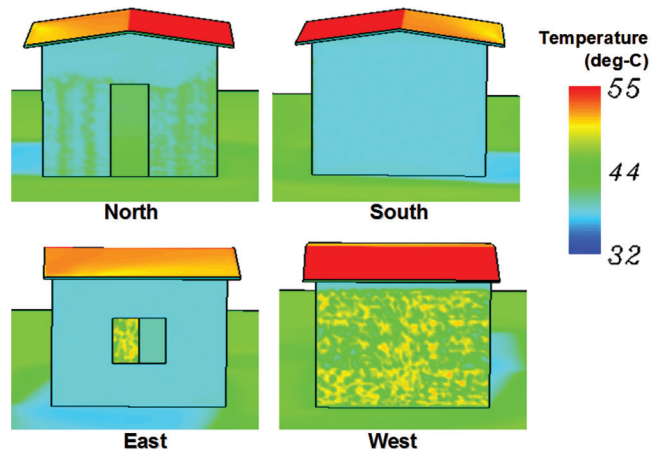


Figure 18. Simulated 4:00 P.M. Wall Surface Temperature (Window Opened).

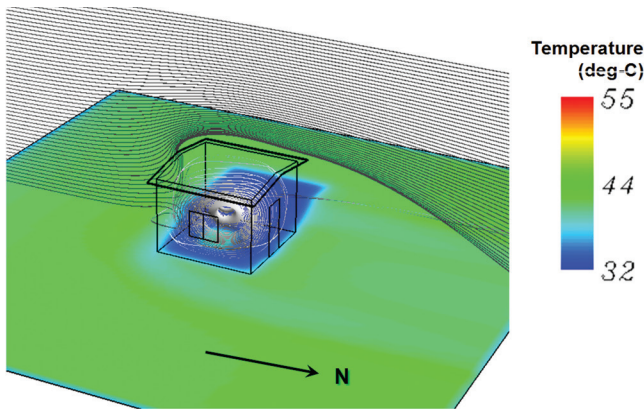


Figure 19. The 8:00 A.M. air field analyses for outdoor environment (window closed).

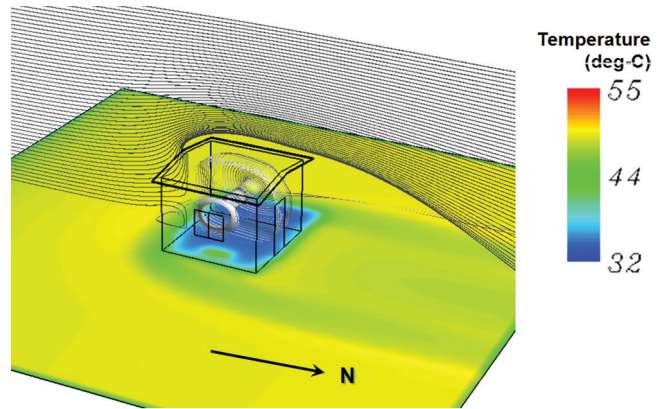


Figure 20. The 10:00 A.M. air field analyses for outdoor environment (window closed).

temperature. Hence, when the building is subject to poor ventilation or weak wind speed, heat can easily be transmitted indoors but cannot be dissipated easily so that the indoor temperature is raised.

Figures 19–23 shows the simulation of outdoor air field in this region and the resulting indoor air field; Figures 24–28 show the simulation results on the diffusions for both building sides and roof. Under full sunshine without shading, the building and surrounding ground show different temperature at various times; the temperatures are the highest at 12:00 noon and next highest at 2:00 P.M.. Simulation of the larger environment shows that air field influences the temperature variations for the building and the surrounding ground. Air current will bring heat away from the wall surface and ground so that the building north wall temperature has a tendency of being relatively low under the large environment. The building shade also causes temperature differences between wall surface and surrounding ground in addition to indicating the angle of solar irradiation.

As the natural reduction of building temperature is concerned, ventilation at nighttime is appropriate for regions where daytime outdoor air temperature is higher than indoor temperature; the outdoor cooler outdoor air enters the building to lower the indoor temperature or exhaust the heat stored in the building materials. Because the major objective of this research is to study the thermal insulation effect of phenolic resin used as building insulator, comparisons of outdoor and indoor temperatures of the building insulated with phenolic resin are important to show the satisfactory thermal insulation characteristics of phenolic reused. If natural ventilation is applied for lowering the indoor temperature, whether the window should be closed or opened depends on the natural environment. Under full sunshine with outside temperature greater than indoor temperature during daytime, the window should be closed but opened during nighttime when outside temperature is lower than indoor temperature. Additionally, if shading is provided at appropriate locations of the building, the indoor room temperature will be reduce effectively.

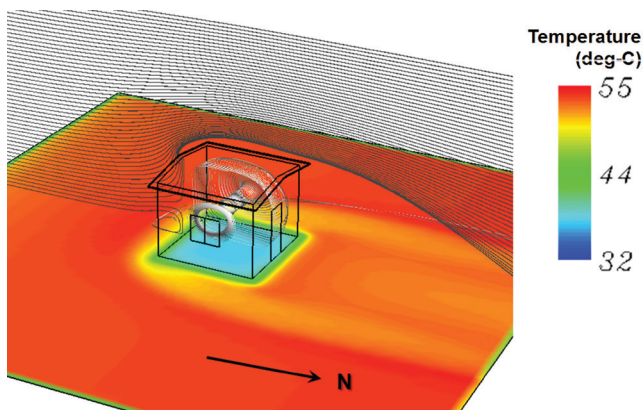


Figure 21. The 12:00 P.M. air field analyses for outdoor environment (window closed).

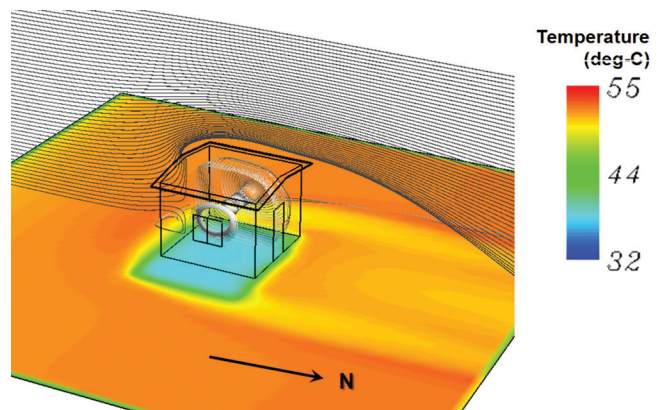


Figure 22. The 2:00 P.M. air field analyses for outdoor environment (window closed).

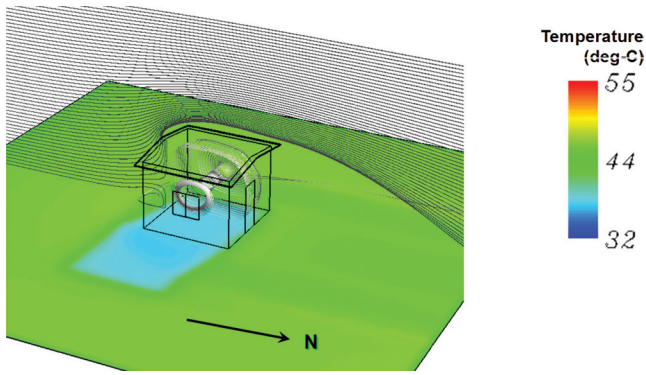


Figure 23. The 4:00 P.M. air field analyses for outdoor environment (window closed).

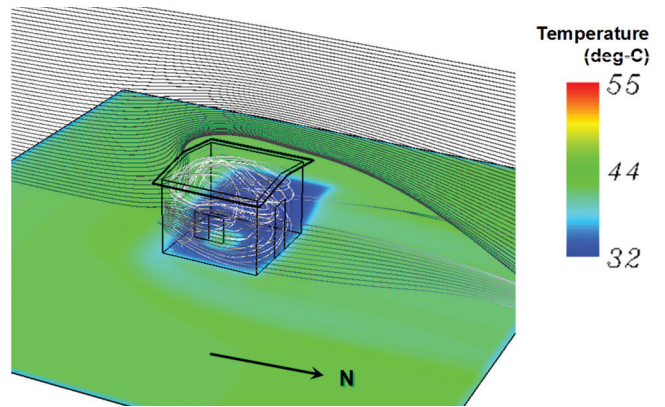


Figure 24. The 8:00 A.M. air field analyses for outdoor environment (window opened).

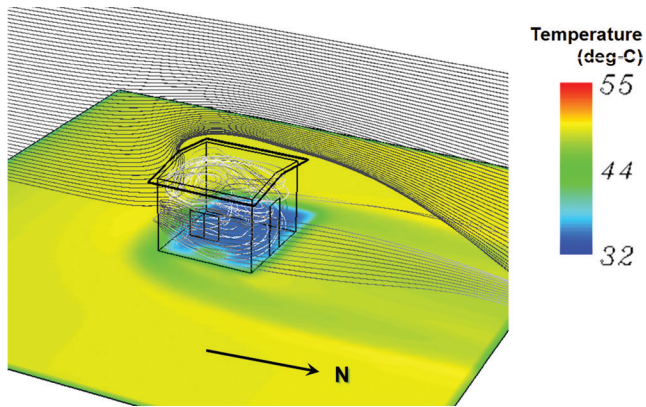


Figure 25. The 10:00 A.M. air field analyses for outdoor environment (window closed).

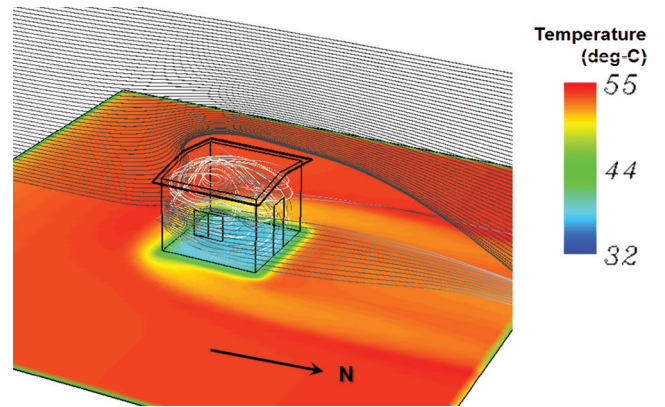


Figure 26. The 12:00 P.M. air field analyses for outdoor environment (window closed).

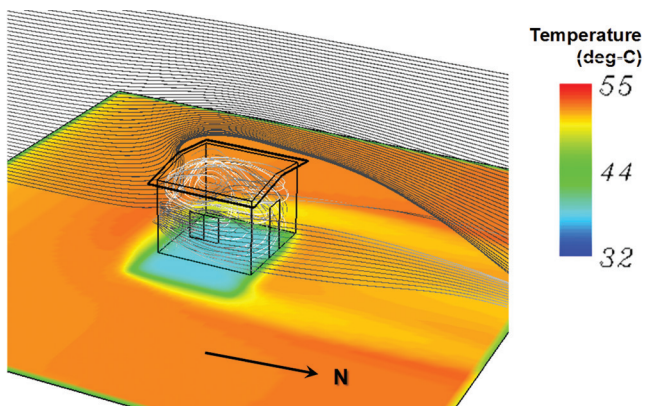


Figure 27. The 2:00 P.M. air field analyses for outdoor environment (window closed).

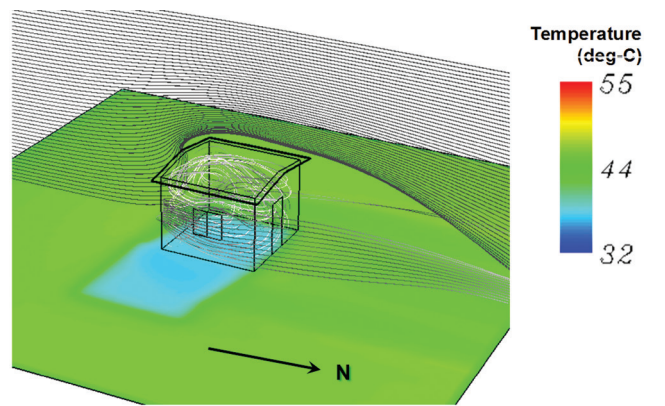


Figure 28. The 4:00 P.M. air field analyses for outdoor environment (window closed).

Frequently closing the window may affect the building permeability and aesthetic appearance, glass pane with good insulation property can be used to reduce solar irradiation and absorbance.

CONCLUSIONS

Mimicking nature to improve building design for reducing energy consumption, environmental pollution, and urban heat island effect has been seriously conserved in recent years. Improving building design to provide a comfortable indoor living environment without consuming excess energy is an important issue to energy-thirsty Taiwan that is located in subtropical region with hot and humid summer. In this research, the thermal insulation behavior of phenolic resin used as building insulation is studied using laboratory buildings insulated with phenolic resin. A computer model is developed using the CFD software to simulate the building thermal behavior. The solar irradiation, building, and the ambient and indoor thermal environments were simulated using the experimental data obtained earlier to result in more realistic simulated conclusions without significant errors.

Results of CFD simulation carried out for the five time intervals of a day show that air current assists in carrying away heat from the wall surface, and the indoor temperature drops faster when the window is opened. Temperature variations between 8:00 A.M. and 10:00 A.M. reveal that opening window will raise the indoor temperature during this time period. Results of simulating the indoor air flow show that when the window is closed, the indoor air flow near the window varies the most; the air speed velocity field is from the east-side wall to the west-side wall. When the window is opened, the indoor air flow becomes turbulent. After entering the room through the window, the air diffuses in all directions, and the speed field is compensate or weakened by air flow of the opposite direction leading to poor indoor ventilation. Simulation of the larger environment indicates that window is an important factor to influence the indoor thermal behavior. Phenolic resin insulation has good thermal property; if it is applied in cope with other means such as shading or improving window constructing materials, the room temperature will be effectively reduced. The environmental air flow will effectively assist in removing heat from the wall surface and floor. Under the experimental conditions, the daytime outdoor temperature is higher than indoor temperature so that ventilation can only be applied during nighttime when the outside temperature

becomes lower. This study offers quantitative scientific data to confirm a common practice for lowering indoor temperature. Results of this environmental air flow analysis will be valuable quantitative information to be referenced by engineers and planners for future base design or landscape design of energy-efficient green buildings.

ACKNOWLEDGEMENT

The National Science Council of Taiwan supported this research through grant No. NSC 101-3113-E-167-001 and NSC 103-2218-E-167-003-MY2. These supports are gratefully acknowledged.

REFERENCES

- Warren, L. P.; Taylor, P. A., "A comparison of occupant comfort and satisfaction between a green building and a conventional building", *Building and Environment*. Vol. 43, No. 11, 2008, pp. 1858–1870. <http://dx.doi.org/10.1016/j.buildenv.2007.11.006>
- Rahman, M. M.; Rasul, M. G.; Khan, M. M. K., "Energy conservation measures in an institutional building in sub-tropical climate in Australia", *Applied Energy*. Vol. 87, No. 10, 2011, pp. 2994–3004. <http://dx.doi.org/10.1016/j.apenergy.2010.04.005>
- Zhao, D. X., He, B. J., Johnson, C., & Mou, B., "Social problems of green buildings: From the humanistic needs to social acceptance", *Renewable and Sustainable Energy Reviews*, Vol. 51, 2015, pp. 1594–1609. <http://dx.doi.org/10.1016/j.rser.2015.07.072>
- Bluyssen, P. M., "Towards new methods and ways to create healthy and comfortable buildings", *Building and Environment*, Vol. 45(4), pp. 808–818. <http://dx.doi.org/10.1016/j.buildenv.2009.08.020>
- Song, W.C.; Li, X.; Sun, S. H.; Yang, Y. L.; Jia, R.B., 2015. "Test study of enhanced Coagulation for conventional treatment with low temperature and low turbidity", *Journal of Residuals Science and Technology*, Vol. 12, S1, 2010, pp. S39–S46.
- Sadineni, S. B.; Madala, S.; Boehm, R.F., "Passive building energy savings: A review of building envelope components", *Renewable and Sustainable Energy Reviews*. Vol. 15, No. 8, 2011, pp. 3617–3631. <http://dx.doi.org/10.1016/j.rser.2011.07.014>
- Mohammad, S.; Al, H., "Performance characteristics and practical applications of common building thermal insulation materials", *Building and Environment*. Vol. 40, No. 3, 2005, pp. 353–366. <http://dx.doi.org/10.1016/j.buildenv.2004.05.013>
- Chen, T. Y.; Sung, W. P.; Shih, M. H.; Zhao, Y. K., "Evaluating the Effectiveness of Applying Phenolic Resin as Thermal Barrier in Buildings During Summer and Winter", *Applied Mechanics and Materials*. Vol. 44–47, 2010, pp. 2040–2044. <http://dx.doi.org/10.4028/www.scientific.net/AMM.44-47.2040>
- Jwo, C.S.; Jeng, L.Y.; Cheng, H.; Chen, S.L., "Research of water-base nano-PU paint for heat insulation", *Proceedings of SPIE—The International Society for Optical Engineering*, 2008, pp. 7130.
- Sung, W. P.; Cheng, T. J.; Chang, C. I., "Application of 6-Sigma methodology to improve process capability of multiple characteristics of fireproof resin products", *Practice Periodical of Hazardous, Toxic, and Radioactive Waste Management*. ASCE, Vol. 13, No. 2, 2009, pp. 82–89. [http://dx.doi.org/10.1061/\(ASCE\)1090-025X\(2009\)13:2\(82\)](http://dx.doi.org/10.1061/(ASCE)1090-025X(2009)13:2(82))
- Chen, T. Y.; Sung, W. P.; Shih, M. H.; Zhao, Y. K., "Evaluating the Effectiveness of Applying Phenolic Resin as Thermal Barrier in Buildings During Summer and Winter", *Applied Mechanics and Materials*, Vol. 44–47, 2010, pp. 2040–2044. <http://dx.doi.org/10.4028/www.scientific.net/AMM.44-47.2040>

12. Guo, W.; Liu, X.; Yuan, X., "Study on Natural Ventilation Design Optimization Based on CFD Simulation for Green Buildings", *Procedia Engineering*, Vol. 121, 2015, pp. 573–581. <http://dx.doi.org/10.1016/j.proeng.2015.08.1036>
13. Hu, X.; Wu, L.; Dong, C., "Thermodynamic analysis of sludge drying and incinerating process system", *Journal of Residuals Science and Technology*, Vol. 12, S1, 2015, pp. S61–S66.
14. Daniel, R.; Mikael, R.; Lars, W., "CFD modelling of radiators in buildings with user defined wall functions", *Applied Thermal Engineering*, In Press, Accepted Manuscript, 2015, pp. 2–16.
15. Chadi, Y.; Caesar, A. S., "A methodology for 3-D multiphysics CFD simulation of air leakage in building envelopes", *Energy and Building*, Vol. 65, 2013, pp.146–158. <http://dx.doi.org/10.1016/j.enbuild.2013.05.050>

The Study on the Operating Characteristics of Algae-Contaminated Reservoir Water Using GAC-sand Dual Media Filter Flofilter

YONG LEI WANG^{1,2,*}, KEFENG ZHANG^{1,2}, WENJUAN CHEN³, HONGBO WANG^{1,2}, MEI LI^{1,2} and RUIBAO JIA⁴

¹College of Environmental and Municipal Engineering, Shandong Jianzhu University, 250101

²Co-Innovation Center of Green Building, 250101

³China Everbright Water (Ji'nan) Co., Ltd., 250032

⁴Shandong Province City Water Supply and Drainage Water Quality Monitoring Center, 250101, Jinan, China

ABSTRACT: The problem of reservoir water quality caused by massive algae pollution keeps going serious, and the traditional solid-liquid separation technology generally fails to meet water quality standards. In the present study, GAC-sand-double-filtration flofilter was built to treat reservoir water derived from the Yellow River that has been polluted by high levels of algal biomass, with the running characteristics and operating results specifically investigated. The experimental results showed that, running effect was relatively superior when the dosage of PAFC was 4 mg/L (Al^{3+}), the pressure of dissolved air was 0.4 Mpa, and the reflux ratio was 8%. Algal biomass fixed onto GAC and sand filter layer was mainly found in the carbon layer, which accounted for 97.4% of the total biomass (the highest value was 50.2 nmol p/g), and the biomass fixed onto carbon layer was 16.7 times of that fixed onto the sand layer (3.0 nmol p/g). Clearly, the removal of pollutants mainly occurred in the carbon layer. Also, the removal efficiency of particulate matter such as blue-green algae, turbidity, COD_{Mn} , UV_{254} , NPOC, ammonia nitrogen was 96.48%, 92.40%, 92.56%, 57.40%, 52.50%, 51.60% and 75.67%, respectively. The odor was reduced from 4 to 0, and the content of geosmin and methylisoborneol was less than their detection limit, with the removal efficiency of chloroform and chlorodibromomethane as 60% and 55.1%, respectively. In general, the results showed that the flofilter process had imposed an efficient effect on the removal of algal biomass, odor substances and disinfection byproducts precursors.

INTRODUCTION

THE problem of reservoir water pollution has become increasingly worse, with algae pollution as a typical culprit. Since the Yellow River is continuously polluted, the plain reservoirs has generally displayed characteristics of shallow depth, with high levels of algal biomass found during the summer, and algal density would decline during the winter due to low levels of temperature and turbidity. With the acute exacerbation of water eutrophication problem, algal reproduction has posed a serious threat to aquatic ecosystems, especially during the spring and autumn when temperature changes dramatically and algae outbreaks occur frequently and such phenomenon could pose a severe threat to water treatment plant operation and water safety. Due to the fact that the density of algal community is usually small, the removal efficiency of algae by

using the traditional solid-liquid separation technology is not satisfactory, ensued by a series of problems, such as filter blockage, backwash cycle shortage, soaring processing cost and worsening water quality. Under certain circumstances, the safety of water supplies is under great threat of microcystins produced by some algae species [1~4]. The technology of flofilter with the process of flotation and filtration integrated seems promising, which could not only handle water quality problem with high levels of algal biomass present, but also display a good removal efficiency of water turbidity, odor and colour. Meanwhile, the operation mode is flexible in terms of reducing operating costs effectively [5]. Researchers have carried out numerous studies on the flotation and filtration process [6~8]. For example, Zhang et al. developed GAC-sand dual media with dissolved air flotation/ filtration technology to process water body with high levels of organic matter and algal biomass in MiYun Reservoir, and the overall result was satisfactory [9,10]. On the basis of water quality

*Author to whom correspondence should be addressed.
E-mail: wyl1016@sina.com; Tel: +86-531-86361857; Fax: +86-531-86361631

analysis of reservoir water samples collected from the Yellow River, the present study tests the coagulation conditions, reflux ratio, algal biomass and decontamination capability of carbon and sand filter layer when the technology of flofilter is implemented, with an in-depth analysis of the operational characteristics of flofilter being used. Therefore, the present study could provide new perspective and technical support regarding the development of water plant treatment technology.

MATERIALS AND METHODS

Raw Water Quality

Conventional Indicators

Raw water samples were collected from Jinan Queshan Yellow River reservoir, and the test period was between May and September. Water temperature was in the range of 19.2~27.0°C, pH value was in the range of 8.18~8.40, and the value of turbidity, COD_{Mn} and UV_{254} was in the range of 2.17~4.30 NTU, 2.63~3.28 mg/L and 0.039~0.045 cm^{-1} , respectively.

Algae Indicators

The dominant algal species found in Queshan reservoir is cyanobacteria, also known as blue-green algae, and it often blooms during the summer [11]. With an increasing water temperature since May, the content of algae began to rise, and the variation trend of chlorophyll A and cyanobacteria was generally consistent. Chlorophyll A content of raw water samples collected in September was in the range of 6.46~14.37 $\mu g/L$, with the average value as 9.35 $\mu g/L$. The density of blue-green algae was in the range of 1173~3398 cells/mL, with the average value as 2593.49 cells/mL. Algae content rose in line with the changes in the season or the temperature.

Test Equipment

The processing capacity of pilot testing device was about 5 m^3/h , with its dimensions as 2.6 m \times 0.8 m \times 4.3 m, and all structures such as the mixing tank, flocculation tank and floating flofilter were established together. The upper part of the floating filter was flotation zone, and the lower part was the filter area. After the flocculation process, water flew into the contact chamber, where water was mixed with pressurized water containing dissolved gas, and produced bubbles

would first adhere to the floc particles and then float to the separation zone. Generated scum on the surface was then removed by using scraping slag. After such flotation process, water would then flow down into the filtration area. Filter layer was filled with activated charcoal and quartz sand, and the height of activated carbon filter layer was 600 mm (the range of diameter was 0.8~1.2 mm). The height of quartz sand filter layer was 300 mm (the range of diameter was 0.8~1.2 mm), and the supporting layer filled with gravel of 400 mm was below the filter layer. Backwash of air and water was conducted with long-handled filter head, with coagulant dosed by the metering pumps. The schematic diagram of floating flofilter pilot plant was shown in Figure 1.

Analysis Method

The test items and methods of pilot test followed standard methods for the Examination of Water and Wastewater APHA/AWWA/WEF (2005).

All assays were carried out in triplicate, with the averages and corresponding standard deviations sta-

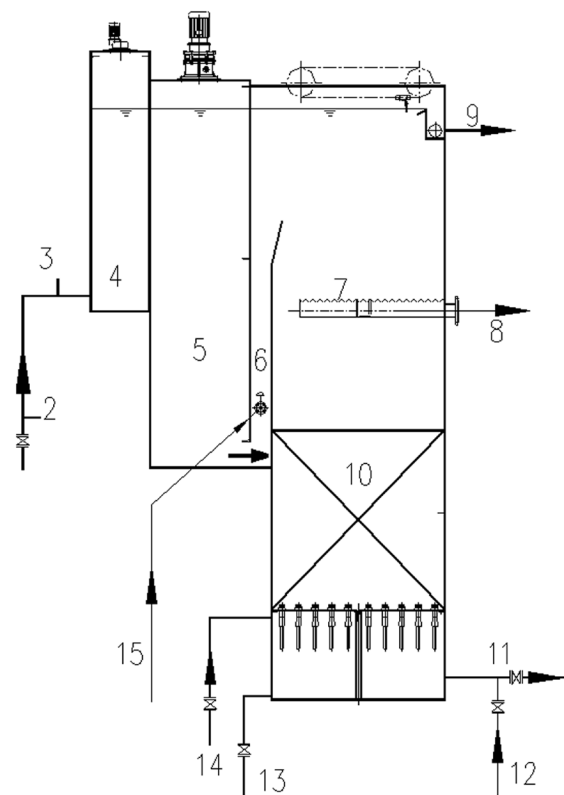


Figure 1. Testing device of flofilter. 1. Inlet pipe; 2. Dosage; 3. Dosage; 4. Mixing tank; 5. Flocculation tank; 6. Contact tank; 7. Flotation tank; 8. Backwashing drain pipe; 9. Scum; 10. Filter layer; 11. Outlet pipe; 12. Backwashing Inlet pipe; 13. Vent pipe; 14. Backwashing inlet pipe; 15. From dissolved gas cylinders.

tistically determined. All chemical reagents were of analytic reagent grade. All glassware and polyethylene tubes were soaked in 3% HCl overnight prior to use. Excel 2003 was used to produce figures and perform relevant statistical analyses.

EXPERIMENTAL RESULTS AND DISCUSSION

Optimization of Coagulant Dosage

Through the pre-experimental research, we chose PAFC (PAFC) as the flocculant [12], and the dosing method was used as the wet cast. The speed of mixing was 50 r/min, and the stirring rate of the reaction was 15 r/min, with PAFC dosage specifically optimized.

COD_{Mn}

As can be seen from Figure 2, when PAFC dosage was 4 mg/L, the removal rate of COD_{Mn} reached the highest point, during which stage the total removal rate reached $51.91\% \pm 4.26\%$, and the flotation removal rate was $33.33\% \pm 2.58\%$. When PAFC dosage was 5~7 mg/L, the total removal rate remained in the range of 33~45%, and it didn't increase with the addition of dosage. Meanwhile, the removal rate of flotation unit decreased slightly, and the removal rate was in the range of 10~30%. This is because the flotation process required flocs with relatively small size after the coagulation process. With an increase of dosage, the generated floc gradually grew bigger, and the amount of gas that contained in the floc would not provide sufficient buoyancy. As a result, the stability of the carrier gas floc went unsteady.

Turbidity

The removal of turbidity (by using flofilter) was sta-

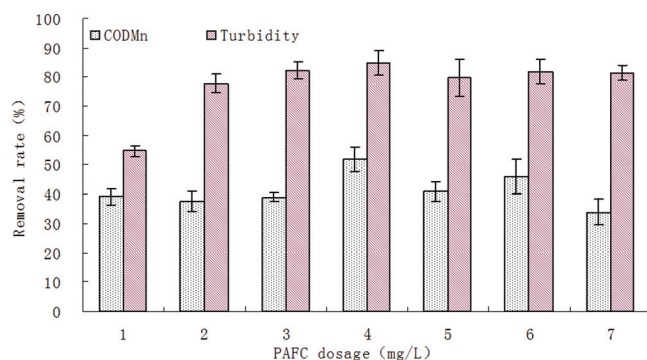


Figure 2. COD_{Mn} and Turbidity removal efficiency under different dosage.

ble when various amounts of dosage were used (Figure 2), and the total removal rate was about 80%. When PAFC dosage was 4 mg/L, the removal rate was up to $84.82\% \pm 4.85\%$, and the removal rate using flotation also reached $33.99\% \pm 3.21\%$. When the dosage was 5~7 mg/L, the average removal rate was approximately 80%. Although the removal effect was relatively good, the flotation efficiency actually declined during this stage. This is because the generated floc was becoming bigger, and the amount of adhesion bubble was insufficient, all of which led to the fact that the buoyancy declined, and the stability of bubble-floc went unsteady. With the addition of coagulant dosage, it would not only increase the operating costs, but also produce a large amount of metal ions due to the existence of excess amount of coagulant, resulting in aluminum residues in effluent [13]. Therefore, the optimum PAFC dosage was determined as 4 mg/L (account as Al^{3+}).

Optimized Reflux Flotation Ratio

When the dissolved air pressure was about 0.4 Mpa, the dissolved air system produced small but dense bubbles in milky white color. Therefore, the reflux ratio of the dissolved gas system was optimized under a stable operation pressure of 0.4 Mpa.

COD_{Mn}

It can be seen from Figure 3 that the maximum value of COD_{Mn} in filter effluent was 1.33 mg/L, the minimum value was 0.97 mg/L, and the average value was 1.08 mg/L during the test period. When the reflux ratio was in the range of 6~10%, the total removal rate of COD_{Mn} was relatively high, and it might reach $62.53\% \pm 4.20\%$. This indicated that the removal of organic matters using carbon-sand filter was not only related to the adsorption and interception of carbon-sand filter

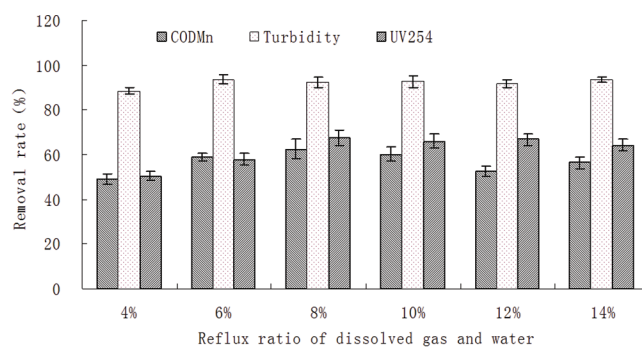


Figure 3. COD_{Mn} , Turbidity and UV_{254} removal under different reflux ratio.

layer on the suspended solids, but also to the growth of microorganisms attached to the filter. As a result, the formed biofilm attached to the filter layer would play a key role during the biodegradation process.

Turbidity

With an increase of reflux ratio, turbidity of flotation unit showed a decreasing trend (Figure 3), mainly because the adhesion chance of micro-bubbles with flocs was enhanced when the amount of dissolved gas increased. Under different operating conditions with varying reflux ratios, there were few differences in the removal rate of flofilter, and the average removal rate was maintained around 90%. The maximum turbidity value of filter effluent was 0.36 NTU, the minimum value was 0.27 NTU, and the mean value was 0.31 NTU.

UV₂₅₄

It can be seen from Figure 3 that the UV₂₅₄ value of influent was stable with the mean value as 0.040 cm⁻¹. The maximum UV₂₅₄ value of effluent was 0.022 cm⁻¹, the minimum value was 0.014 cm⁻¹, and the average value was 0.019 cm⁻¹. With an increase of reflux ratio, the total removal rate also increased. A relatively high level of removal rate was obtained when reflux ratio was between 8~12%, and the average removal rate was 66.5% ± 3.10%, beyond which the UV₂₅₄ value of effluent started to decrease.

According to the removal efficiency of COD_{Mn}, turbidity and UV₂₅₄, a relatively good removal effect could be achieved during the operation process when the reflux ratio was in the range of 8~10%. Therefore, 8% was chosen as the optimum reflux ratio when the economic cost was taken into account.

Research on the Filter Unit Characteristics

GAC-sand filter materials were used in the filter unit of flofilter device, and a certain amount of biofilm started to grow on the surface of the filter after some running time. The organic compounds in the raw water could provide nutrients for the development of biofilms. Meanwhile, microbial metabolism could effectively reduce the pollutant content in the water body. The quartz sand filter layer could effectively intercept the shedding biofilm, thus providing a protection mechanism for maintaining the quality of filtered water. After some running time, the distribution of microbial biomass and the removal efficiency of con-

taminants attached to different filter layer were investigated. Also, the characteristics of GAC-sand filter were analyzed during different flotation states.

The Distribution of Microbial Biomass in the Filter Layer

In order to investigate the growth conditions of biofilms attached to the surface of the filter, samples collected from different filter layers were used for biomass detection and analysis. Sampling points were described as following: the distance between the activated carbon top of sampling point 1, 2 and 3 was 100 mm, 200 mm and 500 mm, respectively, and sampling point 4 was at the distance of 150 mm from the top of the quartz sand. Also, the distribution patterns of microbial biomass from different carbon layers were studied. In order to quantify microbial biomass, filter samples were collected for four consecutive months. The results showed that microbial biomass mainly existed in the activated carbon filter, which could account for 97.4% ± 1.21% of the total biomass. The highest value of microbial biomass was 50.2 nmol p/g, 15.7 times that of the quartz sand (3.0 nmol p/g). Also, the particle size of activated carbon and quartz was 0.8~1.2 mm. Due to oxidation and activation process, the activated carbon formed a complex pore structure, with complex functional groups and hydrocarbons established on the carbon surface, which displayed following physical properties such as porous, light weight and larger specific surface area. As a result, the pore structure was capable of absorbing impurities in the water body due to its strong adsorption capacity [14].

Contributions of Filter Layers to the Removal of Pollutants

To further study the contributions of different filter layers to the removal of pollutants, pollutants removal efficiency at different filter layer depth was investigated, with test conditions shown as following: the reflux ratio was 8%, PAFC dosing was 4.0 mg/L, and the filter speed was 5 m/h. Simultaneously, water samples from the raw water were collected and analyzed to obtain parameters such as the DAF effluent, the effluent of carbon filter layer 1, the effluent of carbon filter layer 2, the effluent of quartz sand layer and the effluent of supporting layer. Test results were shown in Figure 4, with sampling port numbers 1 to 6 representing the influent, and sampling points 1 to 4 representing the effluent.

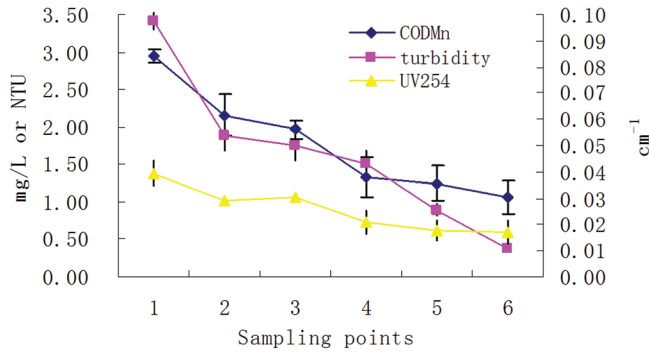


Figure 4. Removal efficiency curves of COD_{Mn}, Turbidity, and UV₂₅₄.

COD_{Mn}

As shown in Figure 4, the COD_{Mn} of flofilter influent was in the range of 3.13–3.44 mg/L, the COD_{Mn} of effluent was in the range of 3.13–3.44 mg/L, and the average total removal rate was 56%. The removal of COD_{Mn} mainly occurred in the activated carbon layer, and active carbon played a key role during the biodegradation process since microbes could attach to the surface and internal structure of the filter materials after a long running time. Meanwhile, raw water with high content of dissolved oxygen provided ideal conditions for biological metabolism. The removal rate of COD_{Mn} in the upper layer of active carbon was higher than that in the lower part due to the fact that most microorganisms were living in the upper layer, indicating an asymmetric distribution of microbial biomass within filter layers.

Turbidity

It can be seen from Figure 4 that the effluent turbidity reached 0.33–0.42 NTU when the turbidity of raw water was changed from 3.29 to 3.51 NTU with the average removal rate as 90.0%. Turbidity removal contribution rate of activated carbon layer reached 63% ± 1.0%, whereas sand filter layer accounted for 25% ± 1.6%. Since some small inorganic particles had penetrated carbon filter layer, sand filter layer still had a relatively large contribution to the turbidity removal

efficiency. Turbidity could be further reduced by 12% ± 2.5% when water flow through the supporting layer, suggesting that the supporting layer could not only play a key role in supporting filter media and preventing erosion, but also intercept some particulate matters.

UV₂₅₄

It can be seen from Figure 4 that UV₂₅₄ was mainly removed in the activated carbon layer, and the removal rate of UV₂₅₄ in the lower layer was higher than that in the upper. One possible explanation is that suspended biofilm debris had blocked the activated charcoal pore, resulting in a decline of adsorption capacity of the activated carbon. By contrast, the quartz sand filter layer and supporting layer contributed less to UV₂₅₄ removal.

The Removal Efficiency of Water Polluted by High-density Algae Using Floating Filter Technology

The Removal Efficiency of Conventional Pollutants

After a period of steady operation process, PAFC dosage was 4.0 mg/L, the reflux ratio was 8%, and the filtration rate was 8.0 m/h. The removal efficiency of COD_{Mn}, turbidity, UV₂₅₄, ammonia nitrogen, NPOC, particulate matters and blue-green algae by using flofilter technology were shown in Table 1.

Existing experimental results showed that flofilter technology generally displayed a high removal rate of conventional pollutants such as turbidity, particulate matter and blue-green algae, with the average removal rates above 90% for all cases. Although the removal rate of other indicators was lower than 60%, the effluent quality could meet the requirement of drinking water quality standards, and the removal rate of COD_{Mn} was significantly higher than that of common carbon sand filter. The blue-green algae, particulate matters and other organic pollutants were discharged with the scum. As a result, their content in flotation effluent was efficiently reduced. GAC-sand filter that integrated in the filtration unit was adopted for further processing

Table 1. The Removal Efficiency of Conventional Pollutants by Using Flofilter Technology.

Items	COD _{Mn} (mg/L)	Turbidity (NTU)	UV ₂₅₄ (cm ⁻¹)	Ammonia Nitrogen (mg/L)	NPOC (mg/L)	Particulate Matter (a/mL)	Blue-green Algae (10 ⁶ cells/L)
Raw water	3.24	4.30	0.040	0.185	2.81	24217	2.593
DAF effluent	2.45	1.81	0.022	0.129	2.16	—	—
Flofilter effluent	1.38	0.32	0.019	0.045	1.36	853	0.197
Removal rate	57.41	92.56	52.50	75.67	51.60	96.48	92.40

Table 2. Removal Efficiency of Unconventional Pollutants by Floating Filter Technology (Unit: Mg/L).

Items	Analytic Hierarchy Process (AHP) Odor	Soil Smelly	Dimethyl Borneol	Trichloromethane	Bromodichloromethane	Chlorodibromomethane	Tribromomethane
Raw water	Earthy taste, Level 4	$< 5 \times 10^{-6}$	$< 5 \times 10^{-6}$	0.035	0.0203	0.0207	0.0041
Flofilter effluent	Odorless, Level 0	$< 5 \times 10^{-6}$	$< 5 \times 10^{-6}$	0.014	0.0180	0.0093	0.0111
GB5749-2006	Odorless	0.00001	0.00001	0.02	0.06	0.01	0.01

of pollutants, and such filter not only played a key role in the interception and adsorption of inorganic and organic pollutants, but also degraded some organic substances. Moreover, the content of dissolved oxygen was increased to a sufficient amount after the flotation process. Therefore, the removal rate of GAC-sand filter was significantly higher than that of ordinary sand carbon filter.

Removal Efficiency of Odor Substances and Precursors of Disinfection Byproducts (DBPs)

Due to the growth of algae and actinomycetes, abnormal odor was disseminated from the surface water of reservoirs contaminated by massive algal species [15]. The smelly and dimethyl borneol was secreted by actinomycetes, and the smelly substances were produced by algae during the metabolism process. Trihalomethanes (THMs) is a representative of the volatile disinfection by-products, which displays some obvious carcinogenicity. Similarly, tribromomethane is also carcinogenic [16]. Therefore, it is necessary to study the removal efficiency of DBPs precursors since trichloromethane, bromodichloromethane and chlorodibromomethane are all directly related to the yield of DBPs. The removal efficiency of odor substances and precursors of DBPs by using flofilter technology was shown in Table 1 and Table 2.

As shown in Table 1 and Table 2, flofilter technology displayed a good purification effect regarding odor substances and precursors of DBPs. Also, it showed a strong capacity to remove precursors of trichloromethane and chlorodibromomethane. The odor level was lowered down from level 4 to level 0. Specifically, the earthy odor was removed completely, and the soil smelly and dimethyl borneol content was less than the detection limit. Also, the removal rate of trichloromethane and chlorodibromomethane was $60\% \pm 4.50\%$ and $55.1\% \pm 3.8\%$, respectively.

CONCLUSIONS

1. Through the optimization of relevant technology

parameters such as coagulation conditions, reflux ratio and dosage, the right type of flocculant was determined, PAFC was selected, the dosage was chosen as 4.0 mg/L (Al^{3+}), the dissolved air pressure was 0.4 Mpa, and the reflux ratio was 8%. Under such test conditions, an excellent removal efficiency was achieved.

- Through studies of the distribution patterns of microbial biomass in the filter, it was evident that biomass mainly existed in the activated carbon filter, which accounted for $97.4\% \pm 1.21\%$ of the total biomass, with the highest value of biomass as 50.2 nmol p/g, which was about 15.7 times that of the quartz sand (3.0nmol p/g). Therefore, maximum amount of COD_{Mn} , turbidity, UV_{254} , ammonia nitrogen and NPOC was efficiently removed in the activated carbon layer.
- The removal rate of particulate matters, blue-green algae, turbidity, COD_{Mn} , UV_{254} , ammonia nitrogen and NPOC was 96.48%, 92.40%, 92.56%, 57.40%, 52.50%, 75.67% and 51.60%, respectively when algal density in the water reached the peak. Odor level was lowered down from level 4 to level 0, and the effluent content of geosmin and methylisoborneol was less than the detection limit. Specifically, the removal efficiency of chloroform and chlorodibromomethane reached 60% and 55.1%, respectively. The results thus showed that flofilter technology had generally displayed an excellent removal efficiency of odor substances and disinfection byproducts precursors.

ACKNOWLEDGEMENTS

This work was financially supported by the Natural Water Pollution Control and Treatment Technology Major Projects (2012ZX07404-003-006), Ministry of Housing and Urban-Rural Development Technology Projects (2014-K5-026), Department of housing and Urban-Rural Construction Department Technology Projects (KY022), Shandong province key development projects (2015GSF117003), Dr. Fund of

Shandong Jianzhu University in 2015(XNBS1511) and Universities Innovation Programme of Jinan City (201303076), Natural Science Foundation of Shandong Province (ZR2014EEM009) and A Project of Shandong Province Higher Educational Science and Technology Program (J13LC01).

REFERENCES

- Masu, S., "Removal of Dissolved Organic Carbon by Processes of Coagulation", *J. Journal of Environmental Protection and Ecology*, Vol. 14, No. 1, 2013, pp. 49–54.
- Henderson, R. and Jefferson, B., "The impact of algal Properties and Pre-oxidation on solid-liquid separation of algae", *J. Water Research*, Vol. 3, No. 42, 2008, pp. 1827–1845. <http://dx.doi.org/10.1016/j.watres.2007.11.039>
- Wang, Z.S. and Liu, W.J. *Slightly polluted source water treatment*, Beijing, PA: China Building Industry Press.
- Chen, J.J. and Hsuan, H. Y., "The mechanisms of potassium permanganate on algae removal", *J. Water Research*. Vol. 18, No. 39, 2005, pp. 4420–4428. <http://dx.doi.org/10.1016/j.watres.2005.08.032>
- Wang, Y.L., *The study on the treatment of reservoir water derived from yellow river by the technology of micro-flocculation and GAC sand dual filtration flofilter*, master's degree thesis, PA: Shandong Jianzhu University.
- Lundh, M. and Lennart, J., "Experimental studies of the fluid dynamics in the separation zone in dissolved air flotation", *J. Water Research*, Vol. 34, No. 1, 2000, pp. 21–30. [http://dx.doi.org/10.1016/S0043-1354\(99\)00136-0](http://dx.doi.org/10.1016/S0043-1354(99)00136-0)
- Maens, L., Lennart, J. and Jan, D., "Experimental studies of the fluid dynamics in the separation zone in dissolved air flotation", *J. Water Research*, Vol. 34, No. 10, 2000, pp. 21–30.
- Chen, J. and Yeh, H., "Effect of ozone and permanganate on algae coagulation removal-Pilot and bench scale tests", *J. Chemosphere*, Vol. 74, 2009, pp. 840–846. <http://dx.doi.org/10.1016/j.chemosphere.2008.10.009>
- Liu, Y., Zhang, S. and Zhang, X.J., "A study of treatment of water from Miyun reservoir by dissolved air flotation process", *J. Industrial Water & Wastewater*, Vol. 35, No. 6, 2004, pp. 17–20.
- Zhang, S., Liu, Y. and Zhang X.J., "Treating of algae-laden raw water with GAC-Sand dual media deep bed Dissolved air flotation/ filtration", *J. Environmental Science*, Vol. 25, No.5, 2004, pp. 52–56.
- Malollari, I., Bacu, A., Bekteshi, A., Babani, F., and Uku, S., "Bekteshi and etc. Nutrition factors of the shkodra lake Waters and their Distribution", *J. Journal of Environmental Protection and Ecology*, Vol. 13, No. 2, 2012, pp. 532–540.
- Wang, Y.L., Jia, R.B. and Zhang, K.F., "Study of novel filtration flofilter water treatment equipment water diversion Huanghe reservoir", *J. Water Technology*, Vol. 35, No. 6, 2009, pp. 67–70.
- Song, W. C., Li, X., Sun, S. H., Yang, Y. L. and Jia, R. B., "Test Study of Enhanced Coagulation for Conventional Treatment with Low Temperature and Low Turbidity". *Journal of Residuals Science & Technology*, Vol. 12, supplement 1, 2015, pp. 39–46. <http://dx.doi.org/10.12783/issn.1544-8053/12/S1/6>
- Li J, Cui Y, Zhang W, Dong, Y. and Jia S., "Biological Toxicity of Sewage Sludge Stabilized by Reed Bed on the Luminescent Bacteria", *Journal of Geoscience & Environment Protection*, Vol. 3, 2015, pp. 1–6. <http://dx.doi.org/10.4236/gep.2015.31001>
- Shen Lijuan. *Study on the distribution of odourous compounds in eutrophic water body and the products of anaerobic metabolizing of algae*, Nanjing, PA: Nanjing University.
- Cosma, C., Nicolau, M., Patroescu, V., Stefanescu, M., Ballo, A., and Florescu, S., "The Incidence of By-products (THMs) Disinfection in Drinking Water", *Journal of Environmental Protection and Ecology*, Vol. 10, No. 1, 2009, pp. 14–22.

Adsorption Thermodynamics of Metronidazole on the Conjugated Microporous Polymers

CHUNLI ZHENG*, SHANSHAN FENG, QIAORUI WANG and MIAOMIAO DU

Department of Environmental Science and Engineering, Xi'an Jiaotong University, Xi'an 710049, China

ABSTRACT: Conjugated microporous polymers (CMPs) now attract extensive interests in water treatment as a kind of ideal porous absorbent with tunable porosity, large surface areas, excellent thermal and chemical stability. In this work the adsorption of metronidazole (MNZ) by CMPs was studied. Two kinds of CMPs were used and named as HCMP-1 and HCMP-2, respectively. The adsorption characteristics of MNZ by the two CMPs under different temperatures were investigated. Adsorption kinetics of MNZ on HCMP-1 and HCMP-2 under all tested temperatures fitted the pseudo-second-order model well, and adsorption quantity of MNZ by the two CMPs decreased with the increase in temperature. Adsorption thermodynamics demonstrated that adsorption of MNZ by HCMP-1 and HCMP-2 was spontaneous and exothermic in nature. This work may provide fundamental guidance for the removal of antibiotics by CMPs.

INTRODUCTION

METRONIDAZOLE (MNZ) is a most commonly used antibiotics to treat infections stemming from various anaerobic microbes and protozoans [1]. The wide usage of MNZ leads to its continuous input into aquatic environments. Since MNZ has high solubility, low biodegradability and high toxicity, it is persistent in water and can easily bioaccumulate in organisms. According to the International Agency for Research on Cancer, MNZ is considered as a potential carcinogen and mutagen [2]. Thus efficient removal of MNZ from water is necessary. Unfortunately, bio-treating methods cannot fully decompose MNZ. Therefore, other technological alternatives such as photo-catalysis, UV/H₂O₂ system, ozonation, etc., were suggested. Especially, the adsorption process has recently received much attention by taking the advantages of easy operation, high reliability, design flexibility, and regenerability [3]. Various adsorbents such as clinoptilolite [4], soil [5], several forms of activated carbon [6–8], calcium phosphate materials [9], and core-shell magnetic nanoparticles [10] were utilized and their adsorption performance were investigated.

Conjugated microporous polymers (CMPs) have long been considered as ideal absorbents for gas adsorption since they are of fine tuned microporosity,

large surface areas and good stability [11]. Recently, CMPs has begun to be used in liquid-liquid separation. Li *et al.* found that CMPs exhibit significant surface superhydrophobic so that they efficiently extracted oils, nonpolar organic solvents and even polar organic solvents from water but no any water molecular were adsorbed, which suggested an ideal adsorption selectivity [11]. However, studies on the removal of hydrophilic contaminants such as MNZ from water by CMPs are very few.

Based on this background, in this paper we applied two kinds of CMPs, named HCMP-1 and HCMP-2, to the adsorption of MNZ. The adsorption characteristics of MNZ by the two CMPs under different temperatures were investigated. Adsorption kinetic and thermodynamic parameters were calculated, which may offer fundamental guidance for the removal of antibiotics by CMPs.

EXPERIMENTAL METHODS

Materials

Metronidazole with a purity of 99%, 1,3,5-triethynylbenzene, 1,4-diethynylbenzene (98% of purity), bis-(triphenylphosphine) palladium (II) dichloride (98% of purity) and copper (I) iodide (98% of purity) were purchased from Sigma-aldrich. Methods for the synthesis of HCMP-1 and HCMP-2 were shown in Ref. [11]. All other chemicals were of analytical grade.

*Author to whom correspondence should be addressed.
E-mail: clzheng@mail.xjtu.edu.cn; Tel: +86-29-82668571; Fax: +86-29-82668571

Ultrapure water was produced from a Sartorius Arium 611VF system (Göttingen, Germany).

Adsorption Experiments

0.0030 g of powder HCMP-1 and HCMP-2 were placed in a 50-mL flask, respectively. Then 10 ml of MNZ solution (25 mg/L) was added. The flasks were covered by parafilm and rocked in the dark under 125 rpm and different temperatures. At a certain time interval, the sample was withdrawn and then filtered by a 0.45 μm membrane. The filtrate was analyzed to determine the residual concentration of MNZ. Blanks and controls were conducted under the identical conditions. Each sample was repeated three times and the mean value was used.

Measurement

Scanning electron microscope characterization of the synthesized CMPs was performed on JSM-6701F (JEOL, Ltd.) after coating the surfaces of HCMP-1 and HCMP-2 with Au film, respectively. Brunauer-Emmett-Teller (BET) surface areas of the HCMP-1 and HCMP-2 were characterized with nitrogen sorption measured at -196°C using physisorption analyzer (ASAP 2020, Micromeritics). Residual concentration of MNZ in filtrate was recorded with an UV-Visible Spectrophotometer (Shimadzu 2100S) at the wavelength of 320 nm [6]. In order to calculate the concentration retained in the adsorbent phase, the following equation is used.

$$q_t = \frac{C_0 - C}{M} \times V \quad (1)$$

where C_0 and C are the initial concentration and residual concentration of MNZ (mg/L) at time t , respectively. V is the volume of solution (L) and M is the mass of sorbent (g).

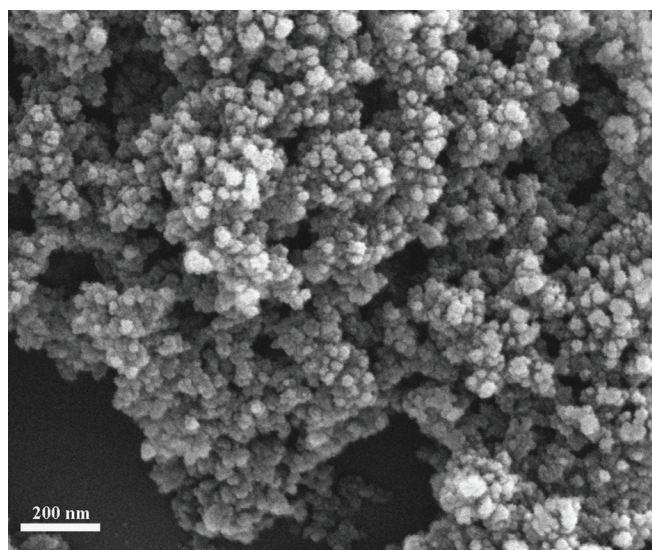
RESULTS AND DISCUSSION

Characterization of the CMPs

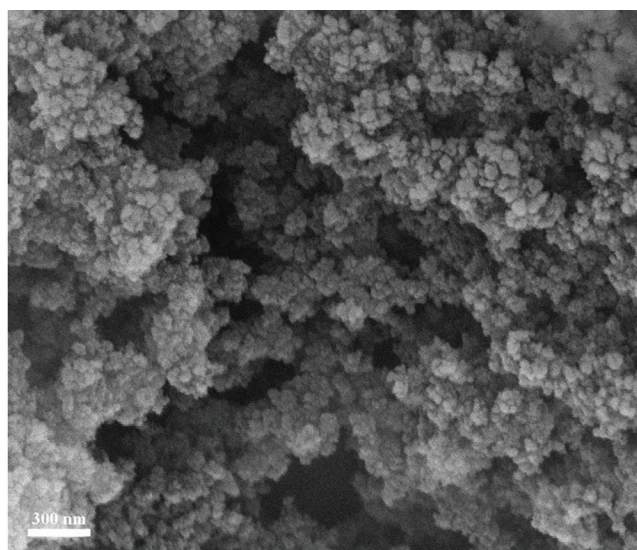
The SEM images of HCMP-1 and HCMP-2 surfaces were shown in Figure 1. Both HCMP-1 and HCMP-2 had a similar morphology composed of agglomerated microgel particles. HCMP-1 had an average particle size of 20 nm in diameter [Figure 1(a)], while HCMP-2 was composed of relatively larger particles with a size of 30 nm in diameter [Figure 1(b)], which might be contributed to the different “strut” length in the CMPs network. Brunauer-Emmett-Teller (BET) surface areas equaled to 710 m^2/g and 690 m^2/g for HCMP-1 and HCMP-2, respectively. Taking advantages of their high surface area, the two CMPs could be applied as porous adsorbents for the removal of MNZ from water.

Adsorption Kinetics

Figure 2(a) and 2(b) display the relationship between contact time and the adsorption of MNZ on the two CMPs, respectively. Under all temperatures, the adsorption amount of MNZ by HCMP-1 increased rap-



(a)



(b)

Figure 1. SEM pictures of (a) HCMP-1 and (b) HCMP-2. Scale bar: 500 nm.

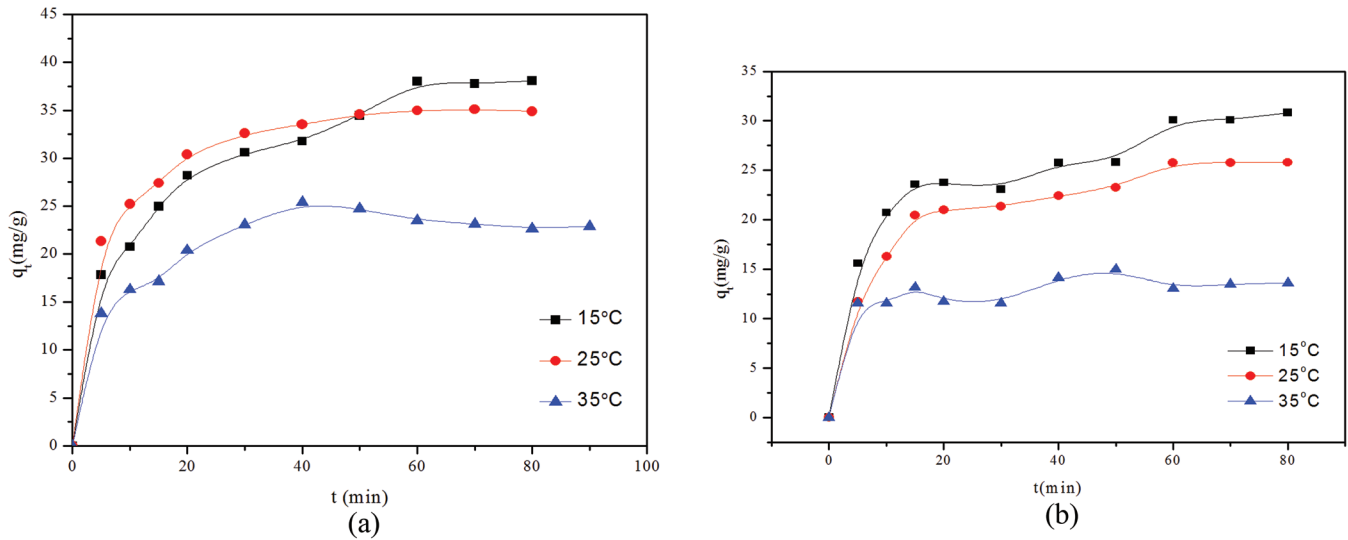


Figure 2. Effects of contact time on the adsorption of MNZ by the CMPs at different temperatures. The initial concentration of MNZ was set at 25 mg/L: (a) HCMP-1, and (b) HCMP-2.

idly within 40 min, and then became flattened from 40 min to 80 min. The curves which described the adsorption of MNZ in HCMP-2 demonstrated the same trend. It was observed that when temperature increased, both adsorption amounts and adsorption velocities of MNZ on the two CMPs increased. These results suggested that low temperature was beneficial to adsorption of MNZ on the two CMPs. Blanks and controls showed that no loss on MNZ concentration during whole 80 min.

For further investigating adsorption of MNZ on the two CMPs, the kinetic data were expressed by both the pseudo-first-order and pseudo-second-order models [12]. The pseudo-first-order model fit the experi-

mental data well during the beginning 40 min only (data not shown). However, data of correlation coefficients R^2 for the linear plots of t/q_t versus time based on the pseudo-second-order model were consistent and close to 1 during whole 80 min (Figure 3), which suggested that the pseudo-first-order model was not an appropriate one. Moreover, values of $q_{e, cal}$ well agreed with $q_{e, exp}$ further indicating that the adsorption was confirmed to the pseudo-second-order model (Table 1). These results demonstrated that adsorption of MNZ on HCMP-1 and HCMP-2 was a chemisorption process, involving valency forces such as sharing or exchange of electrons between sorbent and sorbate [13].

The pseudo-first-order and pseudo-second-order

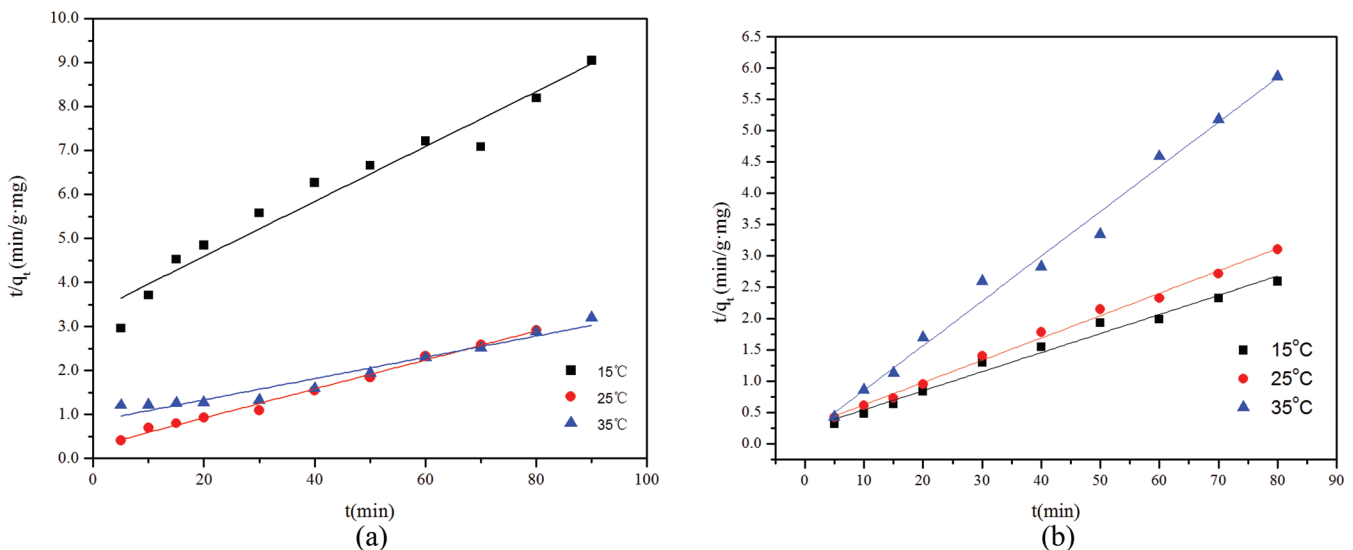


Figure 3. Plots of experimental data expressed by the pseudo-second-order kinetic model. (a) HCMP-1, and (b) HCMP-2.

models are written by Equations (2) and (3) [12]:

$$\ln(q_e - q_t) = \ln(q_e) - K_1 t \quad (2)$$

$$\frac{1}{q_t} = \frac{1}{K_2 q_e} + \frac{1}{q_e} t \quad (3)$$

where q_e and q_t (mg/g) are the amounts of solute sorbed at equilibrium and time t , and K_1 is the rate constant of the pseudo-first order sorption (1/min). K_2 is the rate constant of the pseudo-second-order sorption (g/mg·min).

When temperature went up from 15–35°C, adsorption equilibrium capacity, q_e , decreased from 43.48–24.21 mg/g for HCMP-1. The same trend was also observed for HCMP-2. Table 1 shows that adsorption quantity of MNZ on HCMP-1 was higher than those of HCMP-2, which may be attribute to the fact that HCMP-1 possesses a larger surface area. Since the surface area of CMPs can be tuned by employing different monomers with various molecular lengths [11], further improvement in the adsorption of MNZ on CMPs would be anticipated.

Adsorption Thermodynamics

To confirm the thermodynamics adsorption process, standard free energy change (ΔG^θ), enthalpy change (ΔH^θ), and entropy change (ΔS^θ) are determined using the following equations:

$$K_c \propto \frac{q_e}{C_e} \quad (4)$$

$$\Delta G^\theta = -RT \ln K_c \quad (5)$$

$$\ln K_c = \frac{\Delta S^\theta}{R} - \frac{\Delta H^\theta}{RT} \quad (6)$$

where K_c is the equilibrium constant and T is the solution temperature (°C); R is the gas constant (8.314 J/mol·K). The apparent enthalpy of adsorption (ΔH^θ) and entropy of adsorption (ΔS^θ) are calculated from adsorption data at different temperatures.

These thermodynamic parameters were given in Table 2. As for HCMP-1, the values of ΔG^θ increased from –2.78, –2.29 to –0.73 kJ/mol at 15, 25 and 35°C, respectively, which suggested that the adsorption process of MNZ on HCMP-1 was spontaneous and lower temperature was beneficial to the adsorption of MNZ.

Table 1. Pseudo-second Order Kinetic Parameters at Different Temperatures.

Sorbent	T (°C)	K_2	$q_{e, cal}$	R^2	$q_{e, exp}$
HCMP-1	15	0.0022	43.48	0.9930	38.08
	25	0.0061	37.04	0.9994	35.08
	35	0.013	24.21	0.9914	22.89
HCMP-2	15	0.004	32.80	0.983	30.83
	25	0.005	28.06	0.995	25.77
	35	0.036	14.02	0.989	13.63

The obtained ΔH^θ value (–0.85 kJ/mol) revealed the exothermic process of MNZ adsorption on the CMPs. The positive value of ΔS^θ reflected the affinity of HCMP-1 for MNZ, as well as structural changes in sorbate and sorbent happened during the adsorption process. The similar trend was also found in HCMP-2 except the value of ΔS^θ . It can be seen from Table 2, the value of ΔS^θ for HCMP-2 was negative, which suggested a randomness decrease at sorbate-solution interface during the adsorption process.

CONCLUSIONS

In this paper, two conjugated microporous polymers, HCMP-1 and HCMP-2, were applied to the adsorption of metronidazole from aqueous solution under different temperatures. Under all temperatures, the adsorption kinetics of MNZ on HCMP-1 and HCMP-2 fitted the pseudo-second-order model, and adsorption amount of MNZ by the two CMPs decreased with the increase in temperature. Adsorption thermodynamic study showed that adsorption of MNZ on the two CMPs was spontaneous and exothermic. Compared to HCMP-2, HCMP-1 possessed a higher adsorption capacity towards MNZ, which should be due to the larger surface area of HCMP-1. Based on this study, it can be concluded that low temperature was beneficial to the adsorption of MNZ on CMPs.

Table 2. Thermodynamic Parameters.

Sorbent	T(°C)	Thermodynamic Parameters				
		K_c	ΔG^θ (kJ/mol)	ΔH^θ (kJ/mol)	ΔS^θ (J/mol·K)	R^2
HCMP-1	15	3.19	–2.78			
	25	2.52	–2.29	–0.85	6.58	0.856
	35	1.33	–0.73			
HCMP-2	15	3.19	–2.78			
	25	2.52	–2.29	–37.784	–135.167	0.877
	35	1.33	–0.73			

ACKNOWLEDGEMENT

This work was supported by the National Natural Science Foundation of China (Grant No. 21307097), Industrial research project of Science and Technology Department of Shaanxi Province (Grant Nos. 2014K10-02), and the Fundamental Research Funds for the Central Universities (Grant No. 2012jdhz39).

REFERENCES

1. Lanzky, P. F., Halling-Sorensen, B., "The toxic effect of the antibiotic metronidazole on aquatic organisms", *Chemosphere*, Vol. 35, No. 11, 1997, pp. 2553–2561. [http://dx.doi.org/10.1016/S0045-6535\(97\)00324-X](http://dx.doi.org/10.1016/S0045-6535(97)00324-X)
2. Lam, A., Rivera, A., Rodríguez-Fuentes, G., "Theoretical study of metronidazole adsorption on clinoptilolite", *Microporous Mesoporous Materials*, Vol. 49, No. 1-3, 2001, pp. 157–162. [http://dx.doi.org/10.1016/S1387-1811\(01\)00413-9](http://dx.doi.org/10.1016/S1387-1811(01)00413-9)
3. Sogancioglu, M., Yel, E., "Sludge Using a Marble Processing Wastewater Treatment Method", *Journal of Residuals Science & Technology*, Vol. 11, No. 4, 2014, pp. 137–141.
4. Rabolle, M., Spliid, N. H., "Sorptions and mobility of metronidazole, olaquinox, oxytetracycline and tylosin in soil", *Chemosphere*, Vol. 40, No. 7, 2000, pp. 715–722. [http://dx.doi.org/10.1016/S0045-6535\(99\)00442-7](http://dx.doi.org/10.1016/S0045-6535(99)00442-7)
5. Çaliskan, E., Goktürk, S., "Adsorption Characteristics of Sulfamethoxazole and Metronidazole on Activated Carbon", *Separation Science and Technology*, Vol. 45, No. 2, 2010, pp. 244–255. <http://dx.doi.org/10.1080/01496390903409419>
6. Rivera-Utrilla, J., Prados-Joya, G., Sánchez-polo, M., *et al.*, "Removal of nitroimidazole antibiotics from aqueous solution by adsorption/bioadsorption on activated carbon", *Journal of Hazardous Materials*, Vol. 170, No. 1, 2009, 2009, pp. 298–305. <http://dx.doi.org/10.1016/j.jhazmat.2009.04.096>
7. Ocampo-Pérez, R., Orellana-García, F., Sánchez-polo, M., *et al.*, "Adsorption-from theory to practice", *Journal of Colloid And Interface Science*, Vol. 401, No. 1, 2013, pp. 116–124. <http://dx.doi.org/10.1016/j.jcis.2013.03.038>
8. Queiroz, A. C., Santos, J. D., Monteiro, F. J., "Development of a system to adsorb drugs onto calcium phosphate materials", *Journal of Materials Science-Materials in Medicine*, Vol. 16, No. 7, 2005, pp. 641–646. <http://dx.doi.org/10.1007/s10856-005-2535-3>
9. Chen, D., Deng, J., Liang, J., Xie, J., Huang, K., "Core-shell magnetic nanoparticles with surface-imprinted polymer coating as a new adsorbent for solid phase extraction of metronidazole", *Analytical Methods*, Vol. 5, No. 3, 2013, pp. 722–728. <http://dx.doi.org/10.1039/C2AY25897H>
10. Li, A., Sun, H. X., Tan, D. Z., Fan, W. J., Wen, S. H., "Superhydrophobic conjugated microporous polymers for separation and adsorption", *Energy & Environmenta. Science*, Vol. 4, No. 7, 2011, pp. 2062–2065. <http://dx.doi.org/10.1039/c1ee01092a>
11. Ho, Y. S., McKay, G., "Pseudo-second order model for sorption processes", *Process Biochemistry*, Vol. 34, No. 5, 1999, pp. 451–465. [http://dx.doi.org/10.1016/S0032-9592\(98\)00112-5](http://dx.doi.org/10.1016/S0032-9592(98)00112-5)
12. Fan, X.D., Zhang, X.K., 2015. "Adsorption of heavy metal by adsorbents from food waste residue", *Journal of Residuals Science & Technology*, Vol. 12, No. 1, pp. S155–S158. <http://dx.doi.org/10.12783/issn.1544-8053/12/S1/22>
13. Fernandez, C. A., Liu, J., Thallapally, P. K., Strachan, D. M., "Switching Kr/Xe Selectivity with Temperature in a Metal-Organic Framework", *Journal of The American Chemical Society*, Vol. 134, No. 22, 2012, pp. 9046–9049. <http://dx.doi.org/10.1021/ja302071t>

Characteristics of Nitrogen and Phosphorus Removal in Multiple Post-Denitrification Process with Different Aeration Rates

REN-JIAN DENG^{1,2}, JIN-SONG ZHANG^{1,3,*} and ZHI-JUN QU³

¹Environmental Science and Engineering Research Center, Harbin Institute of Technology Shenzhen Graduate School 518055, China

²School of Civil Engineering, Hunan University of Science and Technology, Xiangtan Hunan 411201, China

³Shenzhen Water (Group) Co.Ltd., Shenzhen 518030, China

ABSTRACT: The nutrient (nitrogen and phosphorus) removal from municipal wastewater was investigated by sequencing batch reactor (SBR) with different aeration rates. The results indicated that the removal performances of nitrogen and phosphorus both increased first and then decreased with increasing aeration rates, and that the aeration rate should be controlled at 25 L.h⁻¹ (dissolved oxygen = 2.7 mg.L⁻¹) in order to achieve ideal removal efficiencies of total nitrogen (TN) and total phosphorus (TP). Aeration rate had a prominent effect on the occurrence of nitrification and denitrification (SND), and excessive aeration would weaken nitrogen removal during SND process. In contrast, excessive aeration had no effect on the release rate of the anaerobic phosphorus, and the decrease of these polyhydroxyalkanoates (PHAs) could significantly influence phosphorus uptake, which was very essential for controlling the biological phosphate removal.

INTRODUCTION

RECENTLY, much research has been carried out to develop a biological nitrogen removal (BNR) process in wastewater treatment system. In order to enhance the efficiency of BNR, the intensification of denitrification process is necessary. BNR can be achieved through denitrification process (including pre-denitrification and post-denitrification process) in wastewater treatment plants (WWTPs). The post-denitrification process, referred as Anaerobic-Oxic-Anoxic and Dephanox process, has been proposed by many researchers [1,2]. Its advantages mainly include lower energy consumption by no use of internal circulation flow, less sludge production for endogenous decay and higher efficiency for total nitrogen (TN) removal. In post-denitrification process without carbon source [3], the denitrification can be approximated as endogenous denitrification. Therefore, many researchers [1,4,5] mainly devote themselves to improving the post-denitrification rate in order to enhance BNR, but pay little attention to surveying the relationship between aeration rates and nutrient removal performance in post-denitrification process.

Nitrogen and phosphorus removal performance are

closely related with aeration rates or dissolved oxygen (DO). Hence, DO concentration is considered as one of the most important parameters for the BNR process. General, lower DO concentration is more conducive to the denitrification process. But too high DO concentration may lead to inefficient sludge settle-ability and bad nitrogen removal. As a consequence, lots of studies on aeration optimization [6–8] and low DO technology [9] had been done recently for cutting energy consumption. In southern China, most of WWTPs lack the automatic control and regulation devices, so that DO concentration in aeration tank always keeps high condition during the rainy season when influent wastewater characteristics are defined as the low concentrations of pollutants and flow fluctuation [8–10]. Some researchers reported that excessive aeration could inhibit TP removal performance [11–13], but the mechanism was not clearly stated. Moreover, it was not studied how excessive aeration affected the nitrogen removal in the post-denitrification process. Therefore, it is of great necessity to propose methods to evaluate how excessive aeration affects BNPR, especially in the post-denitrification process.

The main aim of this study was to investigate the SBR reactor operated as anaerobic/aerobic1/anoxic/aerobic2/drainage/pre-anoxic mode (defined as multiple post-denitrification process), for understanding the mechanisms of treatment performance and nutrient

*Author to whom correspondence should be addressed.
E-mail: zhangjinsong@waterchina.com

removal under different aeration rates. Some insights into this post-denitrification behavior, as well as the involved mechanisms, were also proposed.

MATERIALS AND METHODS

Test Setup

The lab batch experiments were carried out in reactor with an active volume of 5 L and dimensions of 18 cm in diameter and 25 cm in height, as shown in Figure 1. The reactor content was stirred mechanically with a propeller on a vertical axis of 25~75 rpm. The room temperature was kept at $25 \pm 1^\circ\text{C}$. Two peristaltic pumps were used for both feeding and drawing. A diffused aeration system with a blower capacity of $250 \text{ L}\cdot\text{h}^{-1}$ was connected to the bottom of the reactor. The anaerobic, anoxic or aerobic environment was achieved by aeration or stirring. The system was controlled by the programmable logic controller (PLC).

Operational Conditions

The experimental procedures and operational conditions lasted for nearly 5 months at $25 \pm 1^\circ\text{C}$, defined as Runs I–IV. In order to investigate the role of post-denitrification and pre-anoxic operation for nutrient removal in this SBR system, the anoxic mixing sequence for the sludge was also viewed as a parameter in the SBR operational conditions after drainage se-

quence [14]. Hence, the SBR was conducted with the sequences of fill, anaerobic, aerobic 1, anoxic, aerobic 2, sediment, drainage, pre-anoxic and idle, with the retention times of 5 min, 90 min, 210 min, 50 min, 30 min, 30 min, 5 min and 60 min, respectively. Then, the sequence times for the aerobic 1, anoxic, aerobic 2 and pre-anoxic sequences were changed in Run IV, with the retention times of 5 min, 120 min, 300 min, 90 min, 50 min, 30 min, 5 min and 120 min, respectively. The cycling time of Runs I–III and Run IV was 8 h and 12 h, respectively. In Runs I–IV, the aeration rates were kept at 15, 25, 35 and $40 \text{ L}\cdot\text{h}^{-1}$, respectively. The water filled ratios was 0.50 during the operational period. Mixed liquor suspended solids (MLSS) was kept at $2082 \pm 276 \text{ mg}\cdot\text{L}^{-1}$, and MLVSS was $1286 \pm 197 \text{ mg}\cdot\text{L}^{-1}$ during the experiment. The solid retention time (SRT) was kept 12 ± 2 days by controlling sludge wastage. The test duration of each period lasted for at least 32 days.

Wastewater Characteristics and Seed Sludge

The SBR reactor was installed in Yantian WWTPs employing modified sequencing batch reactor (MSBR) [10] in Shenzhen, China. The wastewater fed to the SBR reactor was collected from the primary sedimentation tank of Yantian WWTP. The specific characteristics were detailed in the Table 1. The seed sludge was taken from the aerobic tank of the full-scale WWTPs with sludge volume index (SVI) of $40 \text{ mL}\cdot\text{g}^{-1}$. After operation of 25 days, the process performance was stable and then the experiments were conducted according to the procedure which show in Run I.

Analysis Methods

Influent flow rate, temperature, pH and DO were measured daily, COD, TP, TN, ammonia nitrogen ($\text{NH}_4^+\text{-N}$), nitrate ($\text{NO}_3^-\text{-N}$) and MLSS in both influent and effluent were analyzed for two or three times every week. All the indexes were measured according to the standard methods in [15]. The sludge sample mixed with water was centrifuged for 3 min (3000 r/min) before the determination of the supernatant liquid. The DO was measured with a portable DO meter (HACH HQ30d). The oxidation reduction potential (ORP) and pH were monitored using a portable meter (HACH-sension2). The quantitative analysis of PHAs and Glycogen in biofilm could refer to the methods described in Refs. [16–18].

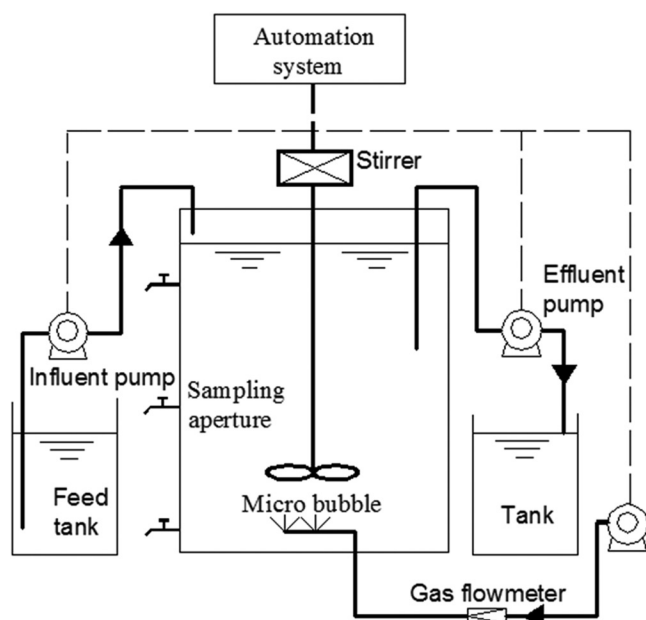


Figure 1. Experimental setup.

Table 1. Characteristics of the Influent.

Indexes	COD (mg.L ⁻¹)	TN (mg.L ⁻¹)	NH ₄ ⁺ -N (mg.L ⁻¹)	NO ₃ ⁻ -N (mg.L ⁻¹)	TP (mg.L ⁻¹)	pH
Average	329 ± 104a	35.8 ± 6.6	30.4 ± 7.1	1.1 ± 0.4	4.6 ± 1.1	7.0 ± 0.6

^aAverage ± standard deviation

Calculation Methods for TN Transformation

In order to investigate the relationship between SND intensity and aeration rate, the SND ratio can be calculated according to Equation (1) [17]:

$$\text{SND}\% = \left(1 - \frac{\text{NO}_X^- \text{ produced}}{\text{NH}_4^+ \text{ removal}} \right) \times 100\% \quad (1)$$

Here, NH₄⁺_{removal} can be calculated according to the Equation (2):

$$\text{NH}_4^+ \text{ removal} = \text{NH}_4^+ \text{ infl} + \text{NH}_4^+ \text{ decay} - \text{NH}_4^+ \text{ assi} \quad (2)$$

Where NH₄⁺_{infl} is the ammonia in initial anaerobic phase, NH₄⁺_{decay} is the ammonia produced by cell autolysis and hydrolysis reactions, NH₄⁺_{eff} is the effluent ammonia, and NH₄⁺_{assi} is the ammonia removal by assimilation. All the above units are mg-N.L⁻¹.

The NH₄⁺ increment (NH₄⁺ produced by cell death subtracts that removed by assimilation) can be calculated by the drainage amount of the excess sludge, as shown in Equation (3):

$$\text{NH}_4^+ \text{ decay} - \text{NH}_4^+ \text{ assi} = (\text{MLSS} \times f_{\text{vss/ss}} \times V_{\text{waste}} \times f_{\text{N/biomass}}) / Q \quad (3)$$

Where MLSS is the excessive sludge concentration, mg.L⁻¹; fvss/ss is the ratio of MLVSS/MLSS, which is dimensionless; Vwaste is the excessive sludge daily discharge amount, L; and f_{N/biomass} = 12.39 % is nitrogen ratio of the total biomass [19].

The (NO_X⁻_{produced} as the difference of NO_X⁻ between the anaerobic end and aerobic end in the process, and then it can be calculated according to Equation (4):

$$\text{NO}_X^- \text{ produced} = (\text{NO}_2^- + \text{NO}_3^-)_{\text{Aerobic}} - (\text{NO}_2^- + \text{NO}_3^-)_{\text{Anaerobic}} \quad (4)$$

RESULTS AND DISCUSSION

DO Concentration Profile

Figure 2 presents the variation of average DO lev-

els in the aerobic 1 during test. In Run I, the average DO value was 1.4 mg.L⁻¹ during the aerobic1 when the aeration rate was 15 L.h⁻¹. In Runs II and III, the average DO values were 2.7 mg.L⁻¹ and 4.1 mg.L⁻¹, respectively. In Run, Owing to much more total aeration time with 370 min, although the aeration rate was only 40 L/h, the average DO value increased to 6.4 mg.L⁻¹. The increasing trend of DO confirmed that DO control technology was successfully applicable for the purpose of this study.

Performance of COD Removal

As shown in Figure 3(a), although COD of the influent fluctuated in the range of 128~542 mg.L⁻¹, high COD removal efficiency (about 92%) always be achieved under different aeration rate in experiment period, and the average effluent concentration could be decreased to 22.6 mg.L⁻¹, which met the standard requirement. The results indicated that aeration rates had no obvious effect on COD removal in the multiple post-denitrification system, which agreed with the results of Wu *et al.* [20]

As shown in Figure 3(b), most influent COD was consumed in the anaerobic phase (including chemical removal, physical adsorption, etc.). This phenomenon was considered to be disadvantageous to the post-denitrification because no residual COD was left for

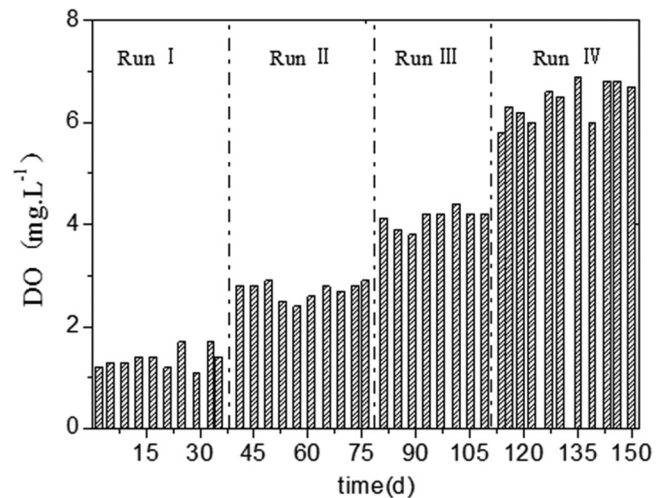


Figure 2. The variation of average DO concentration in the aerobic1 during the four operational periods.

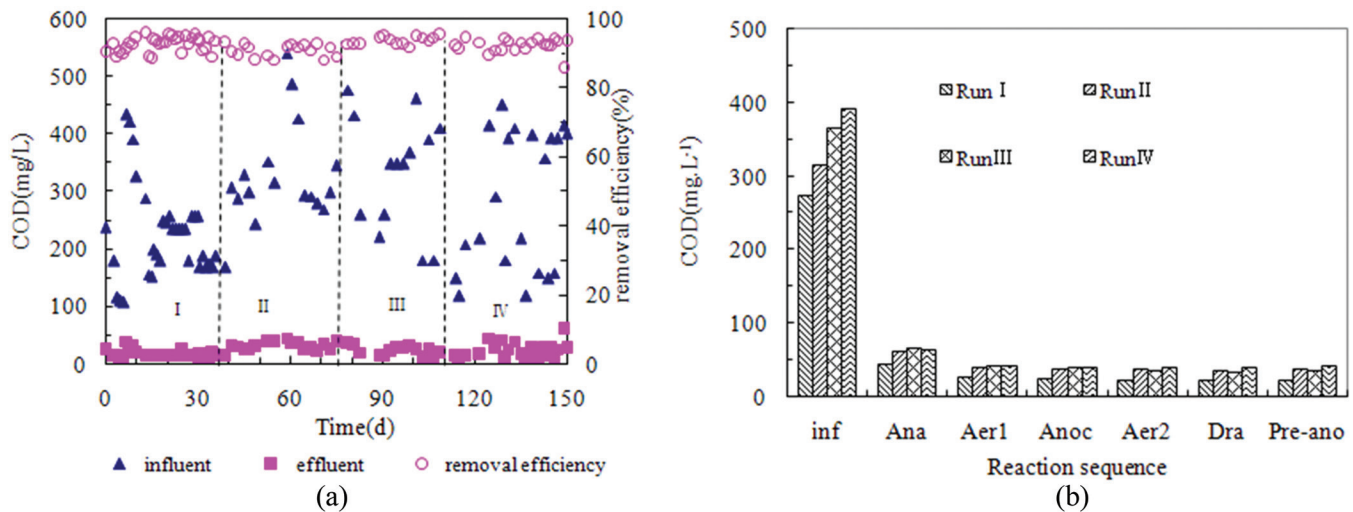


Figure 3. COD removal characteristics under different aeration rates. Note: *inf*: influent, *Ana*: anaerobic, *Aer1*: aerobic1, *Anoc*: anoxic, *Aer2*: aerobic2, *Dra*: drainage, *Pre-ano*: pre-anoxic.

denitrification in the anoxic phase. In addition, since many microorganisms would produce some refractory organics in high sludge concentration conditions, COD concentration increased slightly during the pre-anoxic phase. Similar phenomenon was also observed in the literature [21]. In general, the COD removal performance was not affected by the aeration rate or DO concentration.

PERFORMANCE AND CHARACTERISTICS OF NITROGEN REMOVAL

Performance of Nitrogen Removal

Details for nitrogen variations during the four operational Runs are described in Figure 4(a). As can be seen, almost complete nitrification was accomplished during the experimental period except Run 1. In Run 1, owing to low DO concentration, ammonia oxidation was not completely accomplished, with the maximum effluent $\text{NH}_4^+\text{-N}$ of 8.45 mg.L^{-1} , which could not meet the first-A wastewater discharge in China ($\text{NH}_4^+\text{-N} < 5 \text{ mg.L}^{-1}$). In Runs I–IV, there was enough DO and HRT for nitrification, so that the average effluent $\text{NH}_4^+\text{-N}$ concentration could be decreased to 1.5 ± 2.05 , 0.40 ± 0.42 and $0.32 \pm 0.44 \text{ mg.L}^{-1}$, respectively. The results showed that the effluent $\text{NH}_4^+\text{-N}$ concentration decreased with the increase of aeration rate and time. Thereby the main nitrogen components of the effluent changed from $\text{NH}_4^+\text{-N}$ and $\text{NO}_3^-\text{-N}$ to $\text{NO}_3^-\text{-N}$. For the entire experimental period, $\text{NO}_2^-\text{-N}$ concentration of the end of aerobic1 was also repeatedly monitored for many times (data were not shown here), all of which

less than 1.0 mg.L^{-1} . This revealed that nitrite accumulation was not obvious in this study owing to low influent $\text{NH}_4^+\text{-N}$ concentration and high DO concentration. In contrast, under high $\text{NH}_4^+\text{-N}$ concentration and low DO concentration, nitrite accumulation phenomenon was very easy to occur [22].

Figure 4(b) shows the variation of TN removal performance during experimental periods. The results revealed that there were obvious difference in TN removal in response to different aeration rates. In Run I, only 52.7% of influent TN was removed. The average removal efficiency increased to 60.5% in Runs II–III, but decreased to 50.3% in Run IV. For A²/O process, good TN removal performance could be obtained at the anaerobic/anoxic/oxic retention time ratio of 1:1.4:1.6 [23]. However, in this study, the ratios were 1:0.6:2.7 in Runs I–III and 1:0.75:2.9 in Run IV. That was to say, there was insufficient time for denitrification reactor. Consequently, TN removal efficiency was not excellent. Moreover, the results also revealed that excessive aeration had a significant effect on TN removal performance. The possible reasons were as follows: although the almost complete nitrification was almost accomplished in Run IV, excessive aeration not only affected the anoxic environment for denitrification, but also consumed PHAs which was an internal carbon source for denitrifying. As a result, the post-denitrification efficiency was reduced with the decrease of TN removal efficiency [17]. Therefore, it was critical to select an optimum aeration rate or DO concentration for the multiple post-denitrification process. Furthermore, both insufficient and excessive aeration had an adverse impact on the nitrogen removal.

Table 2. The Decrement TN of Anoxic and Pre-anoxic Under Different Aeration Rates.

Reaction Phase	The Decrement of TN (mg.L ⁻¹)			
	Run I	Run II	Run III	Run IV
Anoxic	1.30	1.50	1.23	0.48
Pre-anoxic	2.41	2.19	2.60	0.33

Note: inf-influent, Ana-anaerobic, Aer1-aerobic1, Anoc-anoxic, Aer2-aerobic2, Drainage, Pro-ano-pre-anoxic.

Characteristics of Nitrogen Removal

Figure 5 shows the transformation of nitrogen-form with the sequences under the four operational Runs. The lowest effluent concentration of TN appeared in Runs II–III. After filling, TN and NH₄⁺-N concentrations in the reactor declined sharply due to the dilution effect, the adsorption by microorganisms, the denitrification, and so on. During the aerobic1, NH₄⁺-N concentration decreased rapidly, and NO₃⁻-N concentration raised rapidly. Moreover, TN concentration also decreased in the aerobic1 phase during four operational Runs and the nitrite accumulation was not found. In Runs II–III, the average decrement of TN was around 1.23~1.50 mg.L⁻¹ in anoxic phase and 2.19~2.60 mg.L⁻¹ (Table 2 and Figure 5) in the pre-anoxic phase, respectively. Unfortunately, the average decrement of TN decreased to 0.48 mg.L⁻¹ in anoxic phase and 0.33 mg.L⁻¹ in pre-anoxic phase, respectively. Therefore, poor TN removal performance (an average of 50.3%) was obtained under excessive aeration conditions.

According to the mass balance and Equations (1)–(4), trace analysis was carried out on the transforma-

tion of nitrogen under different aeration conditions, as shown in Figures 6(a)–(d). In Runs I–IV, TN removal percentages by SND were 17.61%, 12.02%, 11.07% and 2.90% respectively, and those by denitrification were 38.89%, 44.07%, 43.23% and 46.52%, respectively. It was indicated that TN removal percentage by SND decreased with the increasing of aeration rate. Moreover, it was found that the nitrogen removal percentage by SND in this study was lower than those of other reports [24–26]. There were several reasons as follows. Firstly, the occurrence of the SND phenomenon in SBR process requires a low DO of below 1.0 mg.L⁻¹, but the lowest average of DO in this study was 1.4 mg.L⁻¹. Secondly, the SND phenomenon occurs easy with lack of carbon source and DO, but the carbon source in this study was sufficient (average C/N was 8.1). Thirdly, Morgenroth *et al.* [27] reported that the SND phenomenon was easy to occur when the average particle size of sludge was over 100 μm, but it was less than 100 μm in this study (date not shown here). In Run I, nitrogen removal rate in anaerobic phase was only 28.78%, but in Runs II–IV, it increased to 34.82%, 35.56% and 40.42%, respectively. Therefore, the COD for denitrifying in anaerobic phase increased correspondingly, while that for the growth of PAOs would reduce, which might affect the phosphorus removal performance.

In Runs I–IV, SND ratios calculated by Equation (1) were 28.56%, 20.69%, 13.37% and 2.79% respectively, indicating that SND ratio decreased gradually with the increase of aeration rate. This was destructive to the nitrogen removal, mainly due to the large change of pH value for the system. Based on the above results

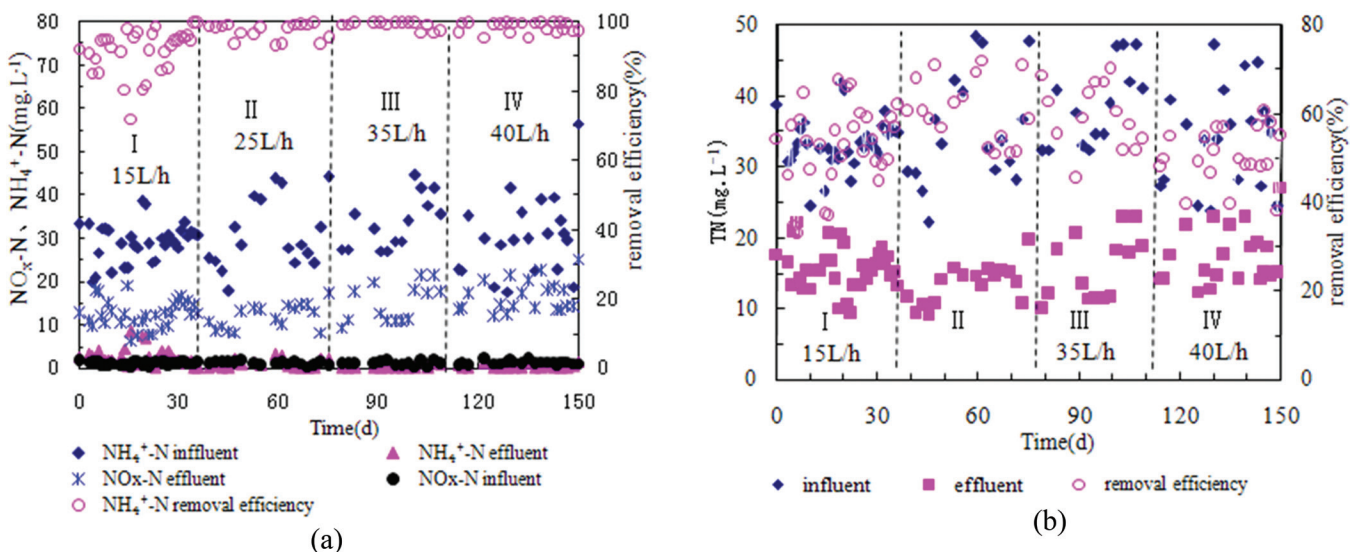


Figure 4. Nitrogen removal characteristics under different aeration conditions.

and analysis, the optimum DO concentration for the first aerobic stage should be controlled at 2.7 mg.L⁻¹ in this study.

Performance and Characteristics of Phosphorus Removal

Performance of Phosphorus Removal

Details for TP variations in Runs I-IV are described in Figure 7. The influent TP concentrations of Runs I-IV were identical (about 4.6 mg.L⁻¹). On the first 30 days in Run I, only (67.1 ± 11.0)% of influent TP was removed. In Run II, the aeration rate was kept at 25 L.h⁻¹, and the effluent TP decreased slightly to below 1.5 mg.L⁻¹, with an average removal efficiency of (74.6 ± 6.1) %. In Run III, DO concentration increased to 4.1 mg.L⁻¹, resulting in a higher TP removal rate as much as 78.2 ± 4.2 %. In Run IV, the aeration rate was kept at 40 L.h⁻¹ (DO=6.4 mg.L⁻¹) for a duration

of 350 min, but TP removal efficiency fell to (44.9 ± 42.8)% sharply, which agreed with the results of other researchers [12,13]. Consequently, higher DO concentration for the aerobic sequences would not be beneficial to phosphorus removal, and the optimum aeration rate for phosphorus removal should be kept at 25–35 L.h⁻¹ (DO = 2.7~4.1 mg.L⁻¹) in this study.

Characteristics of Phosphorus Removal

Wu *et al.* [28] and Ge *et al.* [29] reported that the influent COD/TP ratio was a critical parameter for biological phosphorus removal. Besides, phosphorus removal efficiency would not be inhibited by influent carbon source with the COD/TP ratio over 60 [30]. In Runs I-IV, COD/TP ratios showed little difference relative to the mean the COD/TP ratios of 63.9, 69.0, 66.8 and 62.6, respectively. Therefore, the carbon source was not the main reason why the phosphorus removal performance decreased drastically in Run IV.

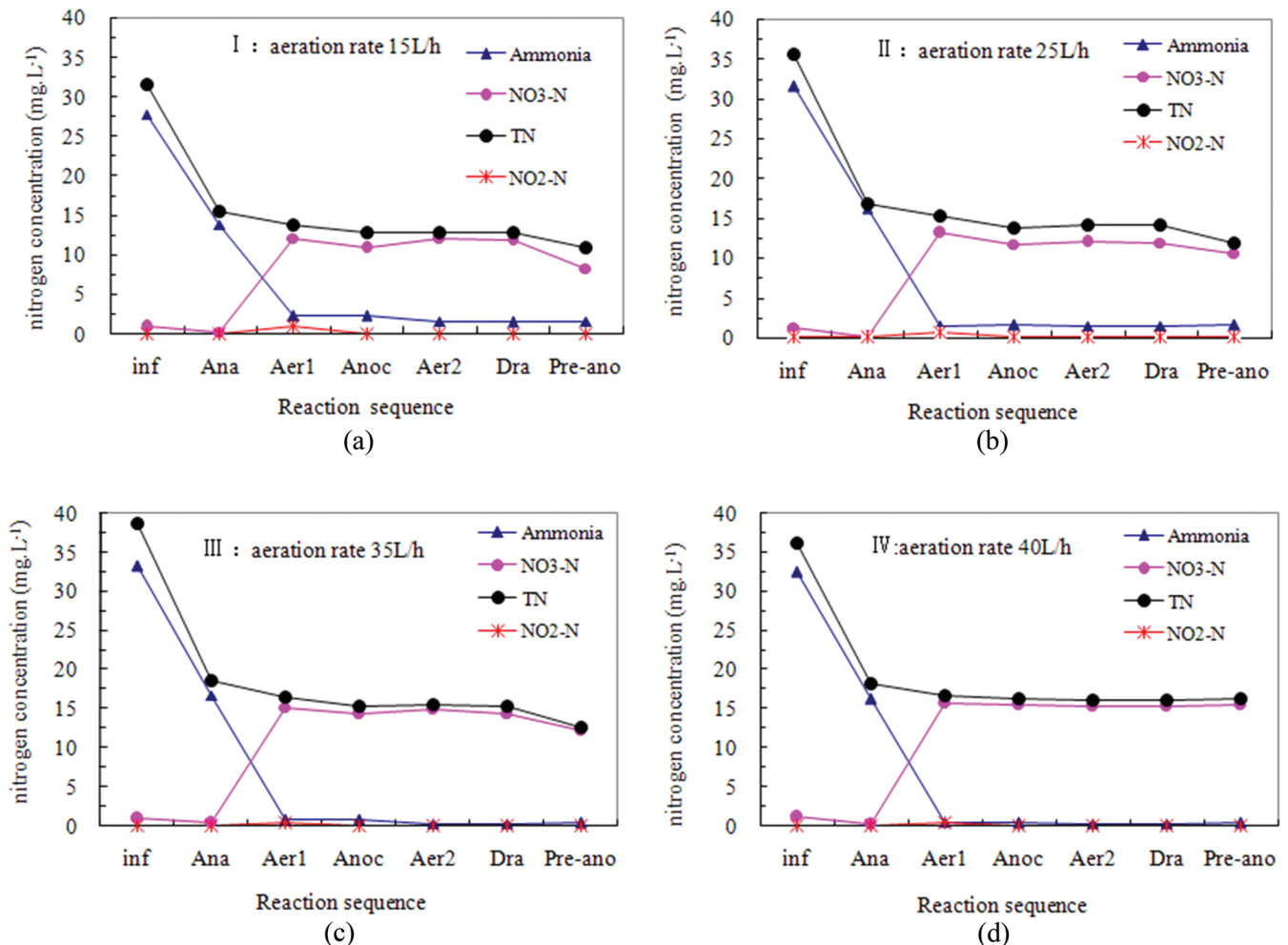


Figure 5. Variation of nitrogen concentration of SBR under different aeration rates.

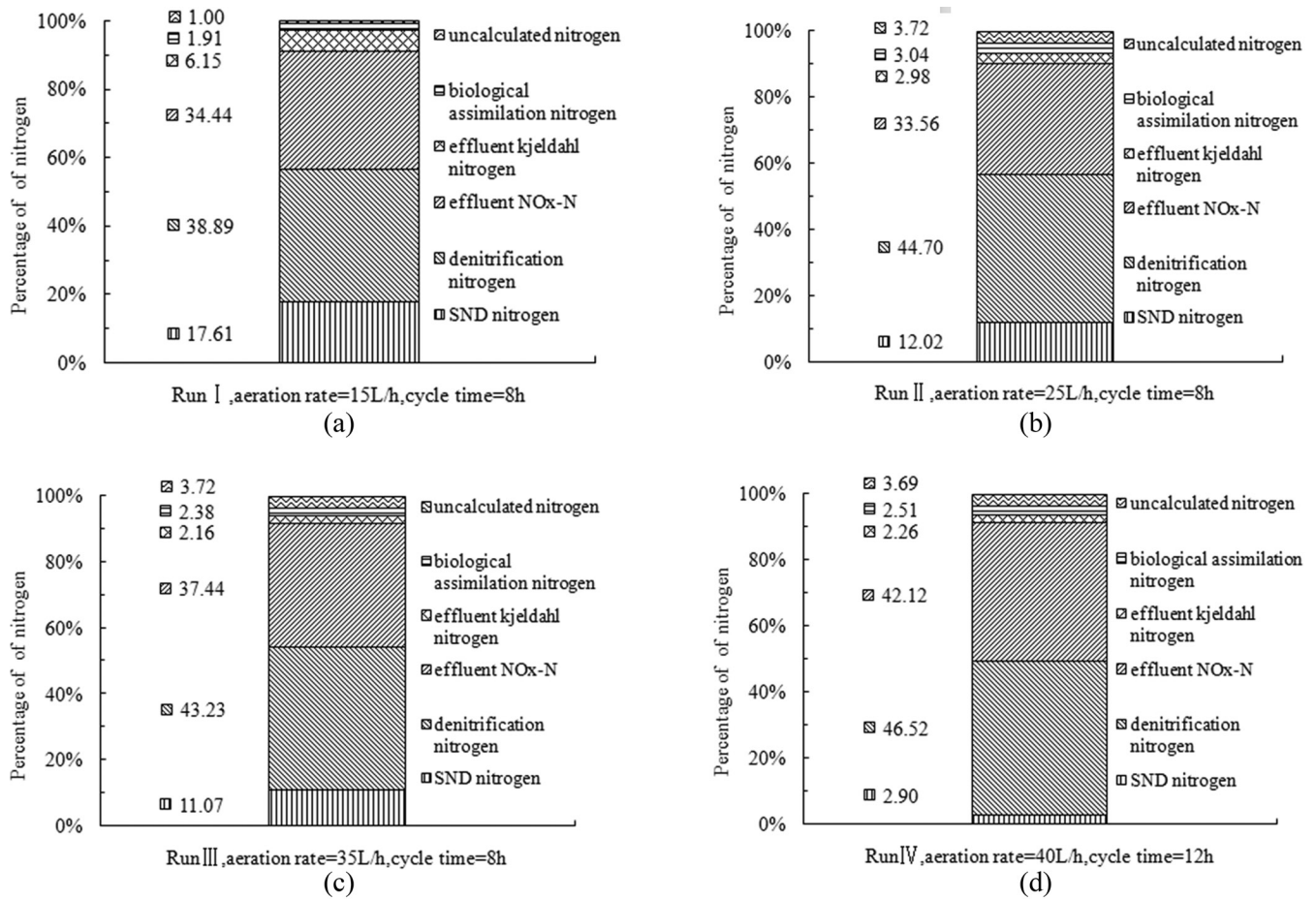


Figure 6. The nitrogen mass balance under different aeration rates.

In order to find the reasons why the phosphorus removal performance drastically decreased in Run IV, the variations of TP, PHA and glycogen in a single operating circle were analyzed, as shown in Figure 8. Although the aeration rates were different in Runs I–IV, TP, PHA and glycogen profiles in a single operating circle showed the same variation trend. In addition, Table 3 also compared the corresponding phosphorus removal parameters with those of several similar NBR process.

In anaerobic phase, the polyphosphate accumulating organisms (PAOs) could absorb influent organic substrates, such as volatile fatty acids (VFAs), to synthesize poly- β -hydroxyalkanoates (PHAs) with the stored polyphosphate as an energy source, and release phosphate from the cell. During the four operational Runs, the anaerobic phosphate release amount was 6.07~7.21 mg.L⁻¹ (Table 3), which showed little difference relative to the corresponding anaerobic phosphorus release rates in the range of 0.083~0.093 kg PO₄³⁻-P·(kg VSS.d)⁻¹ (Table 3). The results revealed that anaerobic phosphate release amount was not affected by aeration

rate, which agreed with the results of Fan [30]. In contrast, Matt Winkler *et al.* [1] reported that phosphorus release rates were different under different aeration conditions, which maybe cause by due to the sludge concentrations, but the total phosphate release amounts were similar (Table 3).

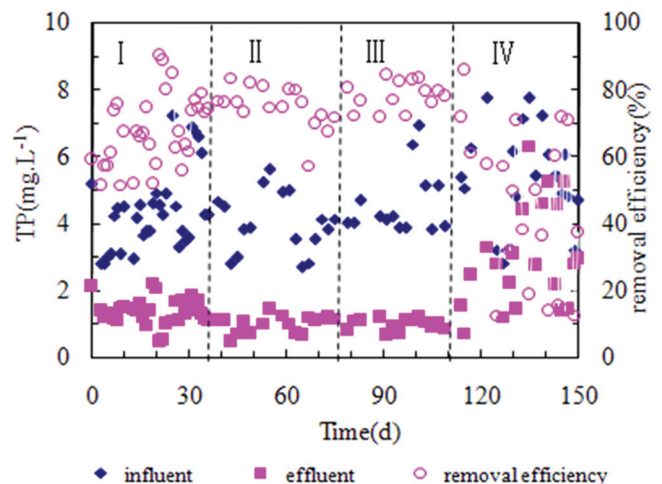


Figure 7. TP removal characteristics under different aeration rates.

In aerobic phase, PAOs used their stored PHAs as the energy source for biomass growth, glycogen replenishment, P uptake, polyphosphate storage, and so on. As shown in Figure 8, obvious different consumption rates of PHAs and aerobic phosphorus uptake rates were observed during the four operational Runs. In Runs I-IV, both of the consumption rate of PHAs and aerobic phosphorus uptake rate exhibited an increasing trend with aeration rate increasing, ranging from 0.100-0.125 mg-PHA.(mg-vss.d)⁻¹ and 0.045 to 0.047 mg-PHA.(mg-vss.d)⁻¹, respectively. But in Run IV, the consumption rate of PHAs increased to 0.160 mg-PHA.(mg-vss.d)⁻¹. Meanwhile the aerobic phosphorus uptake rates dropped to 0.038 kg PO₄³⁻-P.(kg VSS.d)⁻¹, and TP removal efficiency decreased obviously to (44.9±42.8)% (Figure 7). As a result, there was a negative correlation between the aerobic phosphorus uptake rates and the PHAs consumption rate, which agreed with the results of other researchers. Both Brd-

janovic *et al.*[11] and Takabatake *et al.*[31] found that aerobic phosphate uptake rate could be affected by the stored PHAs and polyphosphate in PAOs, and the content of PHAs in the sludge would decrease under excessive aeration conditions. Furthermore, Third's *et al.* [32] reported that high oxygen supply rates were potentially wasteful and allowed higher biomass growth at the expense of lower PHB production. Consequently, bad nitrogen and phosphate removal was obtained.

In addition, both Figure 8 and Table 3 showed that, during the four Runs, the average phosphate uptake amounts were only 0.12~0.38 mg.L⁻¹ in anoxic phase and 0.1 mg.L⁻¹ in pre-anoxic phase. This indicated that the denitrifying phosphorus accumulation was not obvious. After the long-term aeration (210 min), the useful external carbon source was very scarce, and the PHA in cell was also very low.

In this study, the carbon source was adequate, but anaerobic phosphate release amount and phospho-

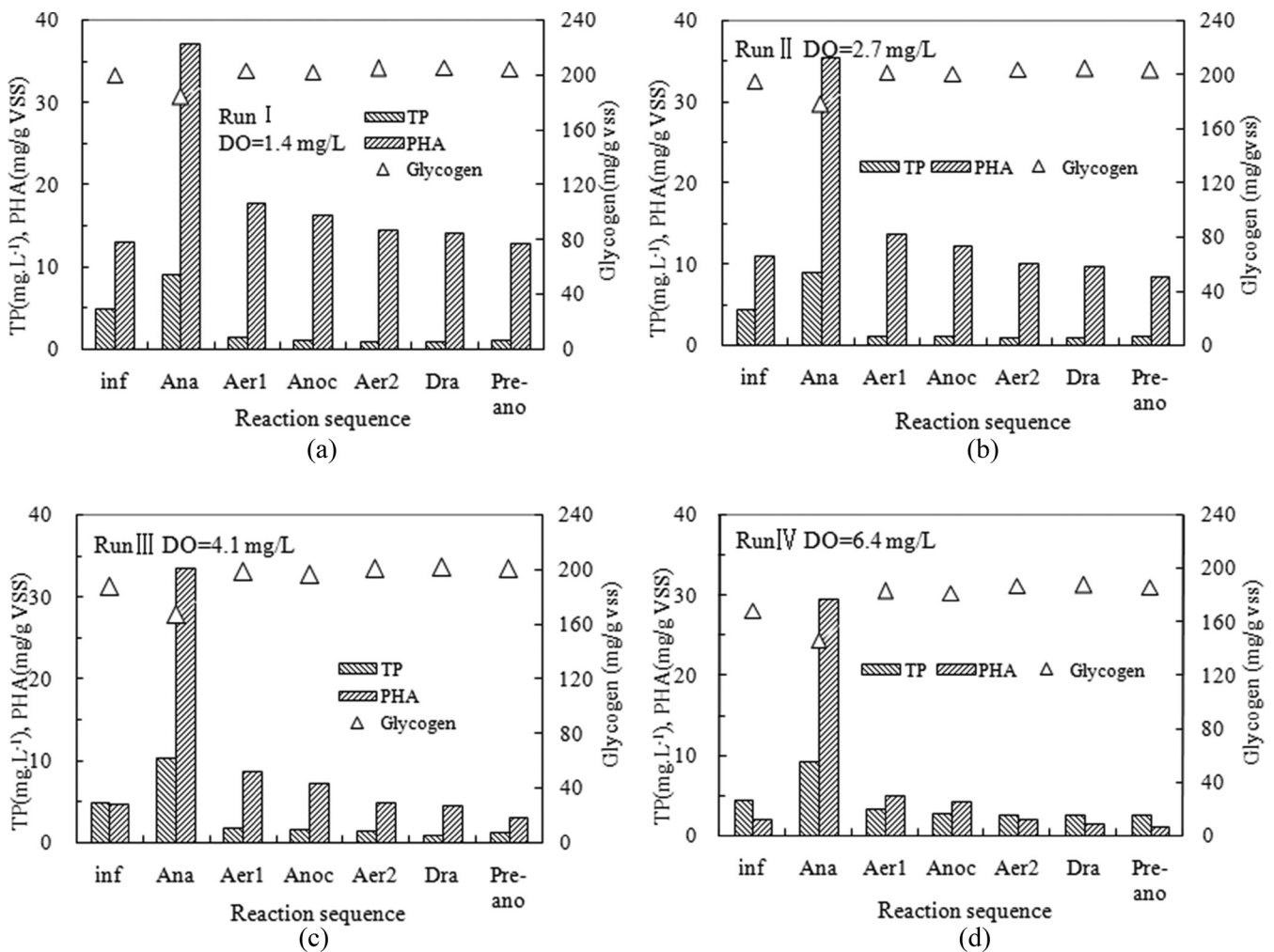


Figure 8. TP removal characteristics in one cycle of SBR under different aeration rates. Note: inf: influent, Ana: anaerobic, Aer1: aerobic1, Anoc: anoxic, Aer2: aerobic2, Dra: drainage, Pro-ano: pre-anoxic.

Table 1. The Characteristics of Phosphorus Release and Uptake, PHA Composition and Decomposition Under Different Aeration Conditions.

Run or References	Anaerobic Phosphate Release Amount, mg.L ⁻¹	Aerobic Phosphorus Accumulation Amount, mg.L ⁻¹	Anoxic Phosphorus Accumulation Amount, mg.L ⁻¹	Anaerobic Phosphate Release PO ₄ ³⁻ -P. (kg VSS.d) ⁻¹	Aerobic Phosphate Uptake Rate, kg PO ₄ ³⁻ -P. (kg VSS.d) ⁻¹	Anoxic Phosphate Uptake Rate, kg PO ₄ ³⁻ -P. (kg VSS.d) ⁻¹	Anaerobic PHA Synthesis Rate, mg-PHA. (mg-vss.d) ⁻¹	Aerobic PHA Consumption Rate, mg-PHA. (mg-vss.d) ⁻¹	Anoxic PHA Consumption Rate mg-PHA. (mg-vss.d) ⁻¹
Run I	6.07	7.66	0.38	0.083	0.045	0.009	0.290	0.100	0.030
Run II	6.14	7.78	0.12	0.085	0.046	0.003	0.288	0.110	0.030
Run III	7.21	8.50	0.14	0.093	0.047	0.003	0.343	0.125	0.032
Run IV	6.79	7.04	0.17	0.084	0.038	0.004	0.420	0.160	0.028
Ref. [2]	7.52	7.93	1.11	0.065	0.052	0.014	0.375	0.292	0.125
Ref. [1] ^a	17.1	19.5	0	0.158	0.090	0	0.297	0.12	0
Ref. [1] ^b	19.8	21.8	0	0.198	0.145	0	0.258	0.079	0

^aLow sludge concentration condition.

^bHigh sludge concentration condition.

rus removal efficiency were lower than the results in previous study [1,2], while the glycogen content in the sludge was much higher than the previous reporting values [1,2]. Thus, it can be speculated that GAOs were much richer than PAOs [23], but need to be further investigated.

The glycogen content showed a decreasing trend in the anoxic phase, which agreed with the results of Matt Winkler *et al.* [1]. On the contrary, Lv *et al.* [2] reported that the glycogen content increased under the anoxic conditions. In the aerobic 2 phase, phosphorus uptake amount was much smaller than that in the aerobic 1 phase, which might be attributed to the large consumption of PHAs. All the above may be the main characteristics of phosphorus removal in the multiple post-denitrification process.

Based on the above results and analysis, it can be seen that anaerobic phosphorus release rate was not affected by aeration rate or DO, but allowed higher biomass growth at the expense of lower PHB production, and consequently lower phosphate removal. Therefore, taking both phosphorus removal performance and energy saving into consideration, DO concentration in the aerobic1 phase should be kept at 4.1 mg.L⁻¹ during this multiple post-denitrification process; otherwise the phosphorus removal performance would be affected. The optimized TP removal was obtained in Run III or IV.

CONCLUSIONS

1. When the aeration rate was in the range of 15~40 L.h⁻¹, COD removal performances was not affected by aeration rates or DO concentrations, and effluent COD concentrations could meet the effluent limit for Grade 1A sewage treatment plants in China (GB18918-2002).
2. In the multiple post-denitrification process, with the increase of aeration rate in the range of 15~40 L.h⁻¹, TN removal performance increased first and then decreased, but SND occurred ineffectively to some extent. Under the excessive aeration, TN removal performance was inhibited. The optimized TN removal was obtained in Run IV, in which DO concentration in the aerobic1 was about 2.7 mg.L⁻¹.
3. In the multiple post-denitrification process, with the increase of aeration rate in the range of 15~40 L.h⁻¹, TP removal performance increased first and then decreased. The anaerobic phosphorus release would be not affected by excessive aeration condi-

tion, but the aerobic PHA consumption rate and the phosphorus uptake rate presented increasing and decreasing trends respectively under excessive aeration condition. The optimized TP removal was obtained in Run IV, in which DO concentration in the aerobic1 was kept at about 4.1 mg.L⁻¹ (35 L.h⁻¹).

ACKNOWLEDGEMENTS

This study was financially supported by Optional subjects of Shenzhen Water (Group) Co., Ltd, subjects of Habitat and Environment Committee of Shenzhen China, the National Science Foundation of China (No.51174090) and the scientific research project of Hunan Provincial Education Department (No.15C0556).

REFERENCES

4. Matt Winkler, E. R. C., Brinkman, C. K., "Advancing Post-anoxic Denitrification for Biological Nutrient removal". *Water Research*, Vol. 45, No. 18, 2011, pp. 6119–6130. <http://dx.doi.org/10.1016/j.watres.2011.09.006>
5. Juan, L., Chen, Y. G., Guo, We. G., "Biological Nitrogen and Phosphorus Removal in the Anaerobic-Aerobic-Anoxic-Aerobic-Anoxic-Aerobic Sequencing Batch Reactors. *China Environmental Science*, Vol. 29, No. 4, 2008, pp. 937–941.
6. Wong, P. Y., Cheng, K. Y., Kaksonen, A. H., Sutton, D. C., Ginige, M. P., "A Novel Post Denitrification Configuration For Phosphorus Recovery Using Polyphosphate Accumulating Organisms[J]". *Water Research*, Vol. 47, No. 17, 2013, pp. 6488–6495. <http://dx.doi.org/10.1016/j.watres.2013.08.023>
7. Vocks, M., Adam, C., Lesjean, B., Gnirss, R., Kraume, M., "Enhanced Post-denitrification without Addition of an External Carbon Source in Membrane Bioreactors". *Water Research*, Vol. 39, No. 14, 2005, pp. 3360–3368. <http://dx.doi.org/10.1016/j.watres.2005.05.049>
8. Chung, C. M., Cho, K. W., Kim, Y. J., Yamamoto, K., Chung, T. H., "Enhanced Biological Nitrogen Removal in MLE Combined with Post-denitrification Process and EF clarifier". *Bioprocess Biosyst Eng*, Vol. 35, No. 4, 2012, pp. 503–511. <http://dx.doi.org/10.1007/s00449-011-0623-y>
9. Chen, H., Wang, D., Li, X., Yang, Q., Luo, K., "Effect of dissolved oxygen on biological phosphorus removal induced by aerobic/extended-idle regime". *Biochemical Engineering Journal*. Vol. 21, No. 9, 2014, pp. 27–35. <http://dx.doi.org/10.1016/j.bej.2014.03.004>
10. Amand, L., Carlsson, B., "Optimal Aeration Control in a Nitrifying Activated Sludge process". *Water Research*, Vol. 46, No. 7, 2012, pp. 2101–2110. <http://dx.doi.org/10.1016/j.watres.2012.01.023>
11. Fernandez, F. J., Castro, M. C., Rodrigo, M. A., Canizares, P., "Reduction of Aeration Costs by Tuning a Multi-set point on/off Controller: A Case Study". *Control Engineering Practice*, Vol. 19, No. 10, 2011, pp.1231–1237. <http://dx.doi.org/10.1016/j.conengprac.2011.07.003>
12. Liu, Y., Shi, H., Xia, L., Shi, H., Shen, T., "Study of Operational Conditions of Simultaneous Nitrification and Denitrification in a Carousel Oxidation Ditch for Domestic Wastewater Treatment". *Biore-source Technology*, Vol.101, No. 3, 2010, pp. 901–906. <http://dx.doi.org/10.1016/j.biortech.2009.09.015>
13. Deng, R. J., Zhang, J. S., Qu, Z. J., Lu, W., "Study on the Enhanced Bio-denitrification in a Full-scale WWTP with MSBR process". *Advanced Materials Research*, Vol. 610-613, No. 1, 2013, pp. 1551–1555.
14. Brdjanovic, D., Slamet, A., van Loosdrecht, M. C. M., Hooijmans, C. M., Alaerts, G. S., Heijnen, J. J., *et al.*, "Impact of Excessive Aeration on Biological Phosphorus Removal from Wastewater". *Water Re-*

- search, Vol. 32, No. 1, 1998, pp. 200–208. [http://dx.doi.org/10.1016/S0043-1354\(97\)00183-8](http://dx.doi.org/10.1016/S0043-1354(97)00183-8)
15. Wang, X. L., Wang, S. Y., Yong, M., Peng, Y., “Anoxic Biological Phosphorus Removal and Effect of Excessive Aeration on Biological Phosphorus Removal in A²O process”. *Journal of Chemical Industry and Engineering*, Vol. 56, No. 8, 2005, pp. 1565–1570.
 16. Peng, Y., Wang, X., Li, B., “Anoxic Biological Phosphorus Uptake and the Effect of Excessive Aeration on Biological Phosphorus Removal in the A²O process”. *Desalination*, Vol. 189, No. 1, 2006, pp. 155–164. <http://dx.doi.org/10.1016/j.desal.2005.06.023>
 17. Debik, E., Manav, N., “Sequence Optimization in a Sequencing Batch Reactor for Biological Nutrient Removal from Domestic Wastewater”. *Bioprocess Biosystem Engineering*, Vol. 33, No. 12, 2010, pp. 533–540. <http://dx.doi.org/10.1007/s00449-009-0366-1>
 18. Clescerl, L. S., Greenberg, A. E., Eaton, A. D., 1998. *Standard Methods for the Examination of Water and Wastewater*. Washington, DC, PA: American Public Health Association.
 19. Takabatake, H., Satoh, H., Mino, T., Matsuo, T., “PHA (polyhydroxy-alkanoate) Production Potential of Activated Sludge Treating Wastewater”. *Water Science and Technology*, Vol. 45, No. 12, 2002, pp. 119–126.
 20. Third, K. A., Burnett, N., Cord-Ruwisch, R., “Simultaneous Nitrification and Denitrification Using Stored Substrate (PHB) as the Electron Donor in an SBR”. *Biotechnology and Bioengineering*, Vol. 83, No. 6, 2003, pp. 706–720. <http://dx.doi.org/10.1002/bit.10708>
 21. Crocetti, G. R., Banfield, J. F., Keller, J., *et al.*, “Glycogen-accumulating Organisms in Laboratory -scale and Full-scale Wastewater Treatment Processes”. *Microbiology-SGM*, Vol. 148, No. Part 1, 2002, pp. 3353–3364.
 22. Henze, M., Gujer, W., Mino, T., Matsuo, T., Wentzel, M. C., “Activated Sludge Model2d”. *Water Science and Technology*, Vol. 39, No. 98, 1999, pp. 165–182. [http://dx.doi.org/10.1016/S0273-1223\(98\)00829-4](http://dx.doi.org/10.1016/S0273-1223(98)00829-4)
 23. Wu, C., Peng, Y., Chun-Liwanb, Wang, S., “Performance and Microbial Population Variation in a Plug-flow A²O Process Treating Domestic Wastewater with Low C/N ratio”. *J. Chem Technol Biotechnol*. Vol. 86, No. 3, 2011, pp. 461–467. <http://dx.doi.org/10.1002/jctb.2539>
 24. Jin, W., Wei, J., Zhan, Q., *et al.*, “Performance and Mechanism of Excess Sludge Reduction in an OSA (Oxic-Settling-Anaerobic) Process”. *Environmental Science*, Vol. 29, No. 3, 2008, pp. 726–732.
 25. Wu, C. Y., Peng, Y. Z., Wang, S. Y., Li, X. L., Wang, R. D., “Effect of Sludge Retention Time on Nitrite Accumulation in Real-time Control Biological Nitrogen Removal Sequencing Batch Reactor”. *Chinese Journal of Chemical Engineering*, Vol. 3, No. 3, 2011, pp. 512–517. [http://dx.doi.org/10.1016/S1004-9541\(11\)60014-1](http://dx.doi.org/10.1016/S1004-9541(11)60014-1)
 26. Wu, C., Peng, Y., Li, X., Wang, S. Y., “Effect of Carbon Source on Biological Nitrogen and Phosphorus Removal in an Anaerobic-Anoxic-Oxic (A²O) Process”. *Journal of Environmental Engineering*, Vol. 136, No. 11, 2010, pp. 1248–1254. [http://dx.doi.org/10.1061/\(ASCE\)EE.1943-7870.0000262](http://dx.doi.org/10.1061/(ASCE)EE.1943-7870.0000262)
 27. Holman, J. B., Wareham, D. G., “COD, Ammonia and Dissolved Oxygen Time Profile in the Simultaneous Nitrification/Denitrification Process”. *J. Biochemical Engineering*, Vol. 22, No. 2, 2005, pp. 125–133. <http://dx.doi.org/10.1016/j.bej.2004.09.001>
 28. Zhang, D. J., Lu, P. L., Long, T. R., *et al.*, “The Integration of Methanogenesis with Simultaneous Nitrification and Denitrification in a Membrane Bioreactor”. *Process Biochem*, Vol. 44, No. 9, 2005, pp. 541–547. <http://dx.doi.org/10.1016/j.procbio.2003.11.043>
 29. Yoo, H., Ahn, K. H., Lee, H. J., Lee, K. H., Kwak, Y. J., Song, K. G., “Nitrogen Removal from Synthetic Wastewater by Simultaneous Nitrification and Denitrification via Nitrite in an Intermittently Aerated Reactor”. *Water Research*, Vol. 33, No. 1, 1999, pp. 145–154. [http://dx.doi.org/10.1016/S0043-1354\(98\)00159-6](http://dx.doi.org/10.1016/S0043-1354(98)00159-6)
 30. Bean, J. J., Hendriks, A., van Loosdrecht, M. C. M., Morgentot E., Wilderer, P. A., Heijnen, J. J., “Aerobic Granulation in a Sequencing Batch Reactor”. *Water Research*, Vol. 33, No. 10, 1999, pp. 2283–2290. [http://dx.doi.org/10.1016/S0043-1354\(98\)00463-1](http://dx.doi.org/10.1016/S0043-1354(98)00463-1)
 31. Wu, C., Peng, Y., Xiao-Ling, Li, E. A., “Effect of Carbon Source on Biological Nitrogen and Phosphorus Removal in an Anaerobic-Anoxic-Oxic (A²O) Process”. *Environmental Engineering*, Vol. 12, No. 1, 2010, pp. 1248–1254. [http://dx.doi.org/10.1061/\(ASCE\)EE.1943-7870.0000262](http://dx.doi.org/10.1061/(ASCE)EE.1943-7870.0000262)
 32. Ge, S., Peng, Y., Wang, S., *et al.*, “Enhanced Nutrient Removal in a Modified Step Feed Process Treating Municipal Wastewater with Different Inflow Distribution Ratios and Nutrient Ratios”. *Bioresour Technol*, Vol. 101, No. 23, 2010, pp. 9012–9019. <http://dx.doi.org/10.1016/j.biortech.2010.06.151>
 33. Fan, J., Vanrolleghem, P. A., Lu, S., “A Kinetic Modeling for Carbon Metabolism in Sequencing Batch Reactor under Multiple Aerobic/Anoxic Conditions”. *Applied Microbiology and Biotechnology*, Vol. 96, No. 1, 2012, pp. 241–252. <http://dx.doi.org/10.1007/s00253-011-3729-x>
 34. Takabatake, H., Satoh, H., Mino, T., Matsuo, T., “PHA (polyhydroxy-alkanoate) Production Potential of Activated Sludge Treating Wastewater”. *Water Science and Technology*, Vol. 45, No. 12, 2002, pp. 119–126.
 35. Third, K. A., Newland, M., Cord-Ruwisch, R., “The Effect of Dissolved Oxygen on PHB Accumulation in Activated Sludge cultures”. *Biotechnology and Bioengineering*, Vol. 82, No. 2, 2003, pp. 238–250. <http://dx.doi.org/10.1002/bit.10564>

Analyses of Polycyclic Aromatic Hydrocarbon in Aerosol of a Lead-zinc Concentrator

AI GUANG-HUA^{1,2,*} and LIU YAN-FEI¹

¹Faculty of Resource & Environmental Engineering, Jiangxi University of Science & Technology, Ganzhou, Jiangxi 341000, China

²Jiangxi Key Laboratory of Mining Engineering, Ganzhou, Jiangxi 341000, China

ABSTRACT: Detecting the concentration of polycyclic aromatic hydrocarbon (PAHs) in aerosol, e.g., PM_{2.5} and PM₁₀, is important for monitoring and possibly improving air quality. To fully understand the concentration distribution of polycyclic aromatic hydrocarbon in aerosol, five sampling locations were selected. A carefully designed experiment was carried out to determine the concentration of polycyclic aromatic hydrocarbon in aerosol samples, using gas chromatography-mass spectrometry (GC-MS). It is found that the concentration of Benzo(a)pyrene, which has strong carcinogenicity, is 1.03~23.35 ng/m³ and 0.24~18.75 ng/m³ in PM₁₀, PM_{2.5}. The average values were 5.07 ng/m³ and 3.91 ng/m³, indicating a serious concern for the air quality. Such level of Benzo(a)pyrene poses threat to the surrounding environment, especially, to the workers health. Results from this study are important and can be used by decision makers for better monitor.

INTRODUCTION

FOR the close relationship between PM₁₀, PM_{2.5} and human health, all countries are actively conducting research on it. In our country, a large number of flotation reagents are used in mine every year. During the mineral processing process, under effect of aeration, mechanical agitation and bubble blowing, some harmful and poisonous flotation reagents, for example PAHs and various volatile flotation reagents, carry all kinds of fine particles that generate during crushing and grinding process to form the aerosol of various particle sizes, which pollute the environment and endanger human health [1–8]. In particular, PAHs has a strong carcinogenic and mutagenic toxicity. Additionally, when the poisonous reagents were used in mineral processing operation, they would cause complex pollutants and secondary pollution. In the literature, there are many studies related to visible pollution such as slag and waste water. Only few focused on air pollution [9–17].

With the purpose to understand the distribution of PAHs in aerosol PM₁₀ and PM_{2.5} that generated in one lead-zinc ore processing factory, provide reference in further research, normalize registration system of flotation reagents and supply basis for ambient air monitoring in these factories, from June to October

in 2008, we set five sampling points in workshop of lead-zinc ore processing factory, collected PM₁₀ and PM_{2.5} samples, then used Soxhlet extraction, K-D concentration and nitrogen-blowing concentration methods to conduct preprocess the samples, and finally measured the PAHs content in samples with GC-MS, so as to make clear of detailed distribution of PAHs in aerosols generating in these factories.

MATERIALS AND METHODS

Materials

Five sampling locations namely 1, 2, 3, 4, and 5 were selected in a dressing plant to monitor air quality during the period 2008.6 to 2008.10. Flotation reagents contained collector, inhibitor, foamer and regulators were added to the selected points. The content of the mineral processing reagents is the highest at location 4, followed by 2, 1 and 3. Mining chemicals are the lowest at location 5. Samples were collected during 9:00 ~ 17:00 for 2 consecutive days. In the end, seven PM₁₀ samples and seven PM_{2.5} samples were collected for each sampling location.

Main instruments and Chemical reagents used are listed in the following PM₁₀ sampler (from Wuhan Tianhong Instrument Factory), PM_{2.5} sampler (from USA ANDERSON company), GC-MS instrument (from An Jetta Company).

*Author to whom correspondence should be addressed.
E-mail: guanghua_ai@126.com

Methods

Blowing nitrogen, soxhlet extraction, and Kuderna-Danish (K-D) methods were used to enrichment and preconcentration samples, GC-MS method was used to analyse polycyclic aromatic hydrocarbons [18–21].

Each samples is set agent blank sample, transportation space and laboratory space. The recovery of each PAHs is more than 75%, which conformance to the requirements of the recovery rate of monitoring.

Test Flow Chart

The main process of the test is that determined the solid particles concentration by weight method, then pretreatment and preconcentration the samples by soxhelt extration, K-D concentration and blowing nitrogen concentration method, at last analyzed the samples by GC-MS. The main process are shown in Figure 1.

Results

Comparison of Pollution Levels Among Different Sampling Sites

The average concentration value of PM10, PM2.5 are shown in Table 1. The PM10, PM2.5 concentration

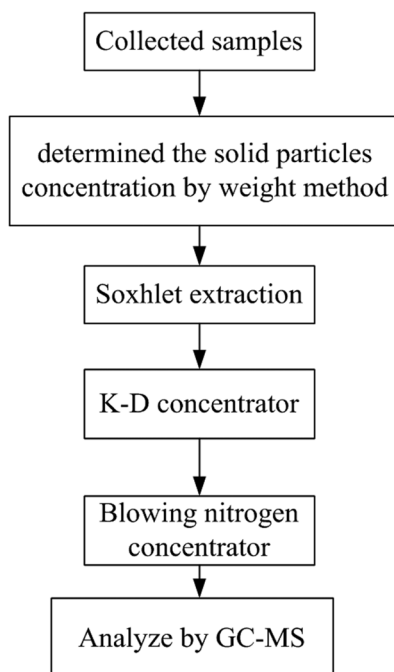


Figure 1. Main process of the test.

Table 1. The Average Concentration of PM10, PM2.5 In Each Points.

Sampling Points	1	2	3	4	5	Average
PM10 concentration ($\mu\text{g}/\text{m}^3$)	215.6	307.2	226.3	309.5	168.0	245.3
PM2.5 concentration ($\mu\text{g}/\text{m}^3$)	178.8	231.7	173.4	237.1	127.4	189.68

of the five sampling locations are shown in Table 2, indicating a serious pollution at this area.

PM10 was 82.8% than the maximum allowable concentration determined by the China air quality standards (GB3095-1996), while, PM2.5 was 97.1% higher than the USEPA standard (currently no standard for PM2.5 in China). In worst cases, PM10 and PM2.5 was 5.57 times and 3.02 times of its maximum allowable concentration, respectively. All the concentration of PM2.5 were high than the standard besides 5 sampling points. At ore dressing plant, the pollution of PM10, PM2.5 is more serious, especially the fine particle pollution.

Linear regression analysis of the concentration of PM2.5 and PM10, we found that they have strong linear correlation, the results are shown in Figure 2.

As we can see in the Figure 2, the concentration of PM2.5 have a strong linear relationship. Because PM2.5 particle is smaller than PM10 particles, it can be inhaled into the lungs more easily, then entered the blood circulation system of human body, which will cause great damage to human's healthy. So we should strength the monitoring of PM2.5.

Various Indicators of All the Sampling Points

Detection of the 16 typical PAHs in the 35 samples of PM10 and 35 samples of PM2.5, and the results are shown in Table 2.

At the five monitoring points, the mean value of the PAHs concentration in PM10 is $33.31\text{ng}/\text{m}^3$ and the mean value of the PAHs concentration in PM2.5 is $25.93\text{ng}/\text{m}^3$. That the larger amount of beneficiation reagent at sampling points, the larger PAHs (ΣPAHS) were detected. The variance of the ΣPAHS of PM10 and PM2.5 in the 5 sampling points were analyzed to examine if there were significant difference, letting α equal to 5%. The F value of PM10 samples was 2.37, which is less than 2.69, corresponding to $F_{0.05}(4, 30)$. The F value of PM2.5 samples of is 2.57, which is less than 2.69, corresponding to $F_{0.05}(4, 25)$. This shows that the sampling location has no significant influence

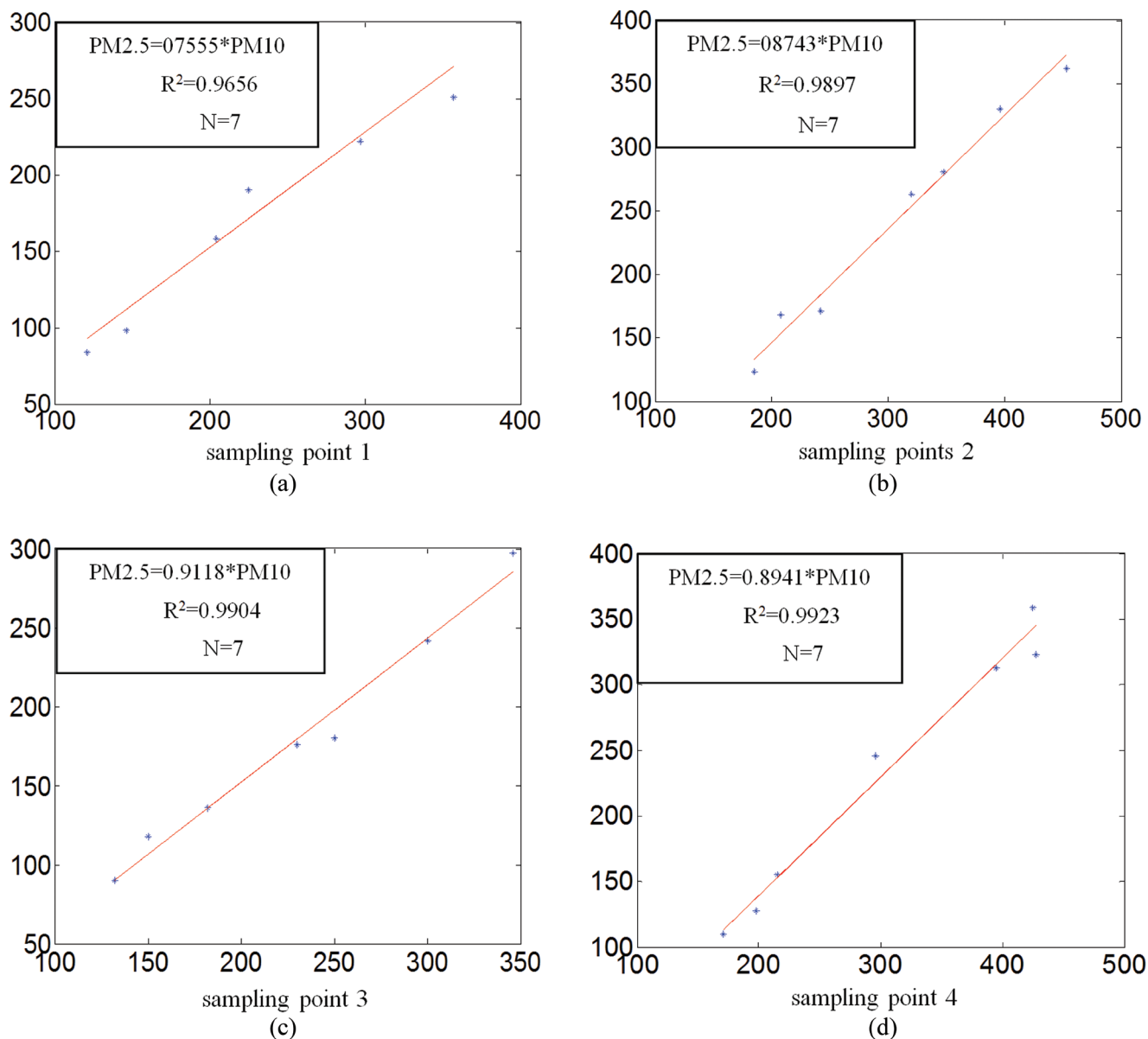


Figure 3. Linear regression analysis of the PM_{2.5} and PM₁₀.

on the results, the results approximately equal. The analysis results are shown in Table 3.

From Table III we can get that, The BaPE/BaPY ratio of PM₁₀ is range from 1.43 to 2.68, that ratios of PM_{2.5} is range from 1.44 to 5.45, and the average BaPE/BaPY ratio of PM₁₀, PM_{2.5} is 1.707 and 1.830, respectively. It is found that PAHs besides BAP in PM₁₀ and PM_{2.5}, to be equivalent to contribute 71% and 83% respectively of BAP equivalent carcinogenic concentration.

The percentage of the PAHs is that 4 ring PAHs are the primary, followed by 5 to 6 ring PAHs and 2 to 3 ring PAHs. According to the literature, the reason that high-ring PAHs are dominated is primary due to

incomplete combustion of fossil fuels. There is few motor vehicle such as cars in the concentrator, so the emissions of high-ring PAHs from motor is relatively less. At the same time, it can't be release from smelters and chemical plant, because there were no that plants around at all. The only source of PAHs is beneficiation reagents. The PHAs volatilized from beneficiation reagents in the process of ore dressing and adsorption on the solid particles.

It is generally recognized that, Benzo-a-pyrene (BAP) is representative of carcinogenic PAHs. The concentration of BAP has a strong linear relationship with that the PAHs total concentration. It is generally that the PAHs's total concentration rise with the in-

Table 2. Inspection of Various PAHs on Aerosol (PM10, PM2.5) in a Ore Dressing Plant.

Sample	Item	Concentration of PAHs (ng/m ³)															
		NAP	ACY	ACE	FLU	PILE	ANT	PYR	BKF	CHR	BAA	BBF	BKF	BAP	INP	DAH	BGP
PM10	Maximum	13.60	3.37	2.82	1.53	4.81	3.07	9.76	7.54	16.24	15.72	27.05	29.72	23.35	12.07	12.83	28.65
	Minimum	0.68	0.02	0.03	0.03	0.21	0.11	0.31	0.23	0.64	0.82	0.31	1.01	1.03	0.52	0.43	0.05
	Average	3.76	0.49	0.85	0.39	1.41	0.39	2.82	1.96	2.94	4.54	6.65	5.86	5.07	2.88	3.16	6.14
PM2.5	Maximum	8.07	2.71	1.77	1.23	4.93	0.71	6.46	8.08	12.14	12.07	18.43	17.06	18.75	9.07	10.13	20.38
	Minimum	0.48	0.02	0.07	0.05	0.06	0.02	0.38	0.21	0.11	0.51	0.32	0.61	0.24	0.24	0.33	0.03
	Average	2.65	0.42	0.39	0.32	1.11	0.36	2.01	1.85	2.25	3.39	4.81	4.20	3.91	2.39	2.75	4.76

crease of the BAP concentration, so we can describe the PAHs in aerosol of Ore dressing plant by the concentration of BAP in PM2.5 and PM10. Average concentration of BAP in PM10 is 5.07 ng/m³, while is it 3.91 ng/m³ in PM2.5. Although the concentrations of all sampling points meet the national standards, the concentration of BAP could still be a concern to the quality of the air.

The Correlation Analysis of Total PAHs of PM2.5 and PM10

The relationship of total PAHs of PM2.5 and PM10 at the five sampling points was shown in Table 4, regression equation for Σ PAHs of PM10 and PM2.5 is the following: Σ PAHs_{PM2.5} = 0.847 Σ PAHs_{PM10} - 42.063. For sampling point 1, Regression equation is PM2.5 = PM10 * 0.7787 - 0.944, correlation coefficient (R^2) is 0.9910; for sampling point 2, Regression equation

is PM2.5 = PM10 * 0.8338 - 2.832, R^2 is 0.9930; for sampling point 3 is PM2.5 = PM10 * 0.8052 - 2.2851, R^2 is 0.9963; for sampling point 4 is PM2.5 = PM10 * 0.7234 + 2.8194, R^2 is 0.9963; for sampling point 5 is PM2.5 = PM10 * 0.8071 - 0.9638, R^2 is 0.9967. Regression equation for PM2.5 and PM10 of the 35 samples is the following: PM2.5 = 0.2207 + 0.757 * PM10, R^2 is 0.9947; all of this indicating significant linear correlation between them and PAHs adsorbed on fine particles (PM2.5) is more than that adsorbed on coarse particles (PM10), PM2.5 can be inhaled into human body more easily, so more toxic PAHs will be inhaled into lung, which will cause great harm to human body.

DISCUSSION

In this study, 5 sample locations were identified for a dressing plant. Among the 16 typical PAHs concentra-

Table 3. The Concentration of Pahs on Aerosol of Each Sampling Points (PM10, PM2.5).

Sampling Points		PM10 (ng/m ³)				PM2.5 (ng/m ³)			
		Σ PAH	BaPE	BaPY	BaPE/BaPY	Σ PAH	BaPE	BaPY	BaPE/BaPY
Points 1	Maximum	101.43	17.26	11.85	1.70	80.51	13.49	9.21	1.99
	Minimum	11.67	1.54	1.03	1.45	8.73	1.16	0.77	1.46
	Average	44.80	7.60	4.78	1.61	33.94	5.88	3.49	1.72
Points 2	Maximum	100.28	12.77	7.33	2.68	79.37	12.38	5.06	2.57
	Minimum	15.12	1.70	1.14	1.45	12.52	1.43	0.95	1.51
	Average	46.48	7.48	4.34	1.84	35.97	6.26	3.37	1.87
Points 3	Maximum	90.02	13.48	8.69	2.18	72.94	11.50	7.05	5.45
	Minimum	12.59	1.88	1.21	1.43	7.89	1.30	0.24	1.47
	Average	39.33	6.73	4.09	1.74	29.38	5.01	3.02	2.18
Points 4	Maximum	200.47	36.96	23.35	1.69	124.86	28.76	18.75	2.09
	Minimum	20.99	2.90	1.71	1.45	16.97	2.23	1.07	1.44
	Average	82.80	13.59	8.75	1.60	62.72	10.72	6.90	1.69
Points 5	Maximum	73.96	12.03	6.04	2.21	61.2	10.60	6.02	2.50
	Minimum	10.31	2.96	1.35	1.44	7.66	1.18	1.03	1.44
	Average	33.31	5.85	3.39	1.71	25.93	4.73	2.79	1.73

Note: In this table, BaPE represent Benzo [a] pyrene equivalent concentration of carcinogenic, BaPY represent the concentration of Benzo [a] pyrene.

Table 4. The Correlation Analysis of Total PAHs of PM_{2.5} and PM₁₀.

Sampling Points	ΣPAHs of PM ₁₀ (ng/m ³)	ΣPAHs of PM _{2.5} (ng/m ³)	ΣPAHs of PM _{2.5} /ΣPAHs of PM ₁₀ (ng/m ³)
1 Point	313.58	237.57	0.758
2 Point	325.35	251.79	0.774
3 Point	275.28	205.67	0.747
4 Point	579.70	439.07	0.757
5 Point	233.2	181.48	0.778

tion, in PM₁₀ samples, the minimum is ACY concentrations, the highest is BKF concentration; in PM_{2.5} samples, the minimum is the ANT concentration, the highest is concentration of BAP. BAP concentration in PM₁₀ maximum value is 1.03 ng/m³ and minimum value is 23.35 ng/m³, while the range of BAP concentration in PM_{2.5} is 0.24 ng/m³ to 18.75 ng/m³. The average of BAP in PM₁₀ and PM 2.5 is 5.07 ng/m³, 3.91 ng/m³ respectively. The average ratio of BaPE/BaPY in PM₁₀ and PM_{2.5} is 1.707 and 1.830 respectively. PAHs in PM₁₀ and PM_{2.5} contributed 71% and 83%, respectively, equivalent of BAP in terms of carcinogenic induced toxicity.

ACKNOWLEDGMENT

The study was supported by the National Natural Science Foundation of China (No.51564014), we are gratefully acknowledged for the funding.

REFERENCES

- Wang, J., Chen, Z.M. and Chen, B.L., "Adsorption of Polycyclic Aromatic Hydrocarbons by Graphene and Graphene Oxide Nanosheets," *Environmental Science & Technology*, Vol. 48, No. 9, 2014, pp. 4817–4825. <http://dx.doi.org/10.1021/es405227u>
- Luan, H.L. and Yao, W., "Mine chemical pollution problems and their combined pollution debates," *Mining and Metallurgy*, Vol. 11, 2002, pp. 265–268.
- Sun, R., "The distribution of polycyclic aromatic hydrocarbons of atmospheric particles in Tianjin," *Environmental Sciences*, Vol. 13, 2000, pp. 4–17.
- Karaca, G. and Tasdemir, Y., "Polycyclic Aromatic Hydrocarbons (PAHs) Removal Applications in the Industrial Treatment Sludge using UV and TiO₂," *Journal of Residuals Science & Technology*, Vol. 11, No. 2, 2014, pp. 65–70.
- Ollivon, D, Blanchoud, H., Motelay-Massei, A. and Garban B., "Atmospheric deposition of PAHs to an urban site, Paris, France," *Atmospheric Environment*, Vol. 36, No. 17, 2002, pp. 2891–2900. [http://dx.doi.org/10.1016/S1352-2310\(02\)00089-4](http://dx.doi.org/10.1016/S1352-2310(02)00089-4)
- Brown, J.R., Field, A.R., Goldstone, M.E., Lester, J.N. and Perry, R., "Polycyclic aromatic hydrocarbons in central London air during 1991 and 1992," *Science of the Total Environment*, Vol. 177, No. 1–3, 1996, pp.73–84. [http://dx.doi.org/10.1016/0048-9697\(95\)04866-9](http://dx.doi.org/10.1016/0048-9697(95)04866-9)
- Gyula, K., Zita, V.P., Gábor, R. and József, H., "Distribution of polycyclic aromatic hydrocarbons on atmospheric aerosol particles of different sizes," *Atmospheric Research*, Vol. 46, No. 3–4, 1998, pp. 253–261. [http://dx.doi.org/10.1016/S0169-8095\(97\)00067-7](http://dx.doi.org/10.1016/S0169-8095(97)00067-7)
- Dungan, R.S., "Polycyclic aromatic hydrocarbons and phenolics in ferrous and non-ferrous waste foundry sands," *Journal of Residuals Science & Technology*, Vol. 3, No. 4, 2006, pp. 203–209.
- McCow, S.R. and Sun, Q.R., Vartiainen, M., Hong, Y.S., Yao, Y.L., Fister, T., Yao, R.Q. and Kamens, R.M., "Effect of composition and State of organic components on polycyclic aromatic hydrocarbon decay in atmospheric aerosol," *Environmental Science and Technology*, Vol. 28, No. 12, 1994, pp. 2147–2153. <http://dx.doi.org/10.1021/es00061a024>
- Freeman, D.J. and Cattell, F.C.R., "Woodburning as a source of atmospheric polycyclic aromatic hydrocarbons," *Environmental Science and Technology*, Vol. 24, No. 10, 1990, pp. 1581–1585. <http://dx.doi.org/10.1021/es00080a019>
- Graves, A.L., Boyd, W.A. and Williams, P.L., "Using Transgenic *Caenorhabditis elegans* in Soil Toxicity Testing," *Archives of Environmental Contamination and Toxicology*, Vol. 48, No. 4, 2005, pp. 490–494. <http://dx.doi.org/10.1007/s00244-004-0031-2>
- Xia, X.H., Yang, Z.F., Wang, R. and Meng, L.H., "Contamination of Oxygen-Consuming Organics in the Yellow River of China," *Environmental Monitoring and Assessment*, Vol. 110, No. 1–3, 2005, pp. 185–202. <http://dx.doi.org/10.1007/s10661-005-7863-8>
- Yeates, G.W., "Nematodes as soil indicators: functional and biodiversity aspects," *Biology and Fertility of Soils*, Vol. 37, No. 4, 2003, pp. 199–210.
- Liu, M., Cheng, S.B., Ou, D.N., Hou, L.J., Gao, L., Wang, L.L. and Xie, Y.S., "Characterization, identification of road dust PAHs in central Shanghai areas, China," *Atmospheric Environment*, Vol. 41, No. 38, 2007, pp. 8785–8795. <http://dx.doi.org/10.1016/j.atmosenv.2007.07.059>
- Cincinelli, A., Bubba, M.D., Martellini, T., Gambaro, A. and Lepri, L., "Gas-particle concentration and distribution of *n*-alkanes and polycyclic aromatic hydrocarbons in the atmosphere of Prato (Italy)," *Chemosphere*, Vol. 68, No. 3, 2007, pp. 472–478. <http://dx.doi.org/10.1016/j.chemosphere.2006.12.089>
- Li, J., Zhang, G., Li, X.D., Qi, S.H., Liu, G.Q. and Peng, X.Z., "Source seasonality of polycyclic aromatic hydrocarbons (PAHs) in a subtropical city, Guangzhou, South China," *Science of The Total Environment*, Vol. 355, No. 1–3, 2006, pp. 145–155. <http://dx.doi.org/10.1016/j.scitotenv.2005.02.042>
- Hansen, A.M., Raaschou, N.O. and Knudsen, L.E., "Urinary 1-hydroxypyrene in children living in city and rural residences in Denmark," *Science of The Total Environment*. Vol. 347, No. 1–3, 2005, pp. 98–105. <http://dx.doi.org/10.1016/j.scitotenv.2004.12.037>
- Wenlin, H., Samuel, P., James, G., *et al.*, "Levels of 1-hydroxypyrene and other monohydroxy polycyclic aromatic hydrocarbons in children: A study based on U.S. reference range values," *Toxicology Letters*. Vol. 163, No. 1, 2006, pp. 10–19. <http://dx.doi.org/10.1016/j.toxlet.2005.08.003>
- Kurt, S., Robert, B. and Yann, G., Beatrice, S., Fatiha, E. G., and Vincent, C., "Carcinogenicity of polycyclic aromatic hydrocarbons," *The Lancet Oncology*, Vol. 6, No. 12, 2005, pp. 931–932. [http://dx.doi.org/10.1016/S1470-2045\(05\)70458-7](http://dx.doi.org/10.1016/S1470-2045(05)70458-7)
- Manoli, E., Kouras, A. and Samara C., "Profile analysis of ambient and source emitted particle-bound polycyclic aromatic hydrocarbons from three sites in northern Greece," *Chemosphere*, Vol. 56, No. 9, 2004, pp. 867–878. <http://dx.doi.org/10.1016/j.chemosphere.2004.03.013>
- Kurt, S., Robert, B., Yann, G., *et al.*, "Carcinogenicity of polycyclic aromatic hydrocarbons," *The Lancet Oncology*, vol. 6, No. 12, 2005, pp. 931–932. [http://dx.doi.org/10.1016/S1470-2045\(05\)70458-7](http://dx.doi.org/10.1016/S1470-2045(05)70458-7)

Detection of Pesticide Residues in Mulberry Leaves Using Vis-Nir Hyperspectral Imaging Technology

SUN JUN^{1,2,3,*}, JIANG SHUYING², ZHANG MEIXIA², MAO HANPING¹, WU XIAOHONG² and LI QINGLIN¹

¹Jiangsu Provincial Key Laboratory of Modern Agricultural Equipment and Technology, Jiangsu University, Zhenjiang 212013, China

²School of Electrical and Information Engineering, Jiangsu University, Zhenjiang 212013, China

³Key Laboratory of Agricultural Information Service Technology, Ministry of Agriculture, Beijing 100081, China

ABSTRACT: Nonstandard use of pesticides often causes poisoning incidents of silk-worm, which is a serious threat to the development of sericulture industry. In view of this, it is very urgent to study new non-destructive testing methods that can detect pesticide residues in mulberry leaves rapidly and accurately. In this paper, six groups of mulberry leaves (144 mulberry leaves in total), on which chlorpyrifos pesticide of six different concentrations had been sprayed respectively, were chosen as experimental samples, and their hyperspectral images in 390–1050 nm were acquired by hyperspectral imaging devices. The region of interest from hyperspectral image was selected, and five sensitive wavelengths including 561.25, 680.86, 706.58, 714.32, and 724.66 nm were determined by correlation coefficients between pesticides residues and spectral reflectances. Further, based on multiple linear regression (MLR) and support vector regression (SVR), the prediction models of pesticide residues in mulberry leaves were established respectively to fit the experimental data. The results showed that the root mean square error (RMSE) and coefficient of determination (R²) of prediction set of MLR model were 47.165 and 0.637 respectively, and those of prediction set of SVR model were 27.719 and 0.874 respectively. Therefore, hyperspectral imaging technology together with SVR prediction model could accurately detect the pesticide residues in mulberry leaves.

INTRODUCTION

WITH the growth of global climate and the expansion of mulberry area in recent years, pests and diseases of mulberry become increasingly serious. In order to prevent pests and diseases, a large amount of pesticides are sprayed onto mulberry. Notably, although the application of pesticides is effective to decrease pests and diseases of mulberry and increase productivity of mulberry leaves, the abuse of chemical pesticides easily leads to pesticides residues in leaves that exceed the maximum allowed residue levels. Once the *bombyx mori linnaeus* eats mulberry leaves with pesticides, it is very likely to be poisoned. Consequently, pesticides residue has become a serious threat to the development of sericulture industry. Therefore, it is of vital importance to detect pesticides residues in mulberry leaves. Nowadays, the most common methods for detecting pesticide residues are gas chromatography (GC) [1–2], liquid chromatography (HPLC) [3–4], but they are expensive, time consuming, and destruc-

tive [4]. In view of this, the research of rapid, cheap, and non-destructive detecting methods is fairly significant for the sericulture industry so as to reduce *bombyx mori linnaeus* poisoning incidents and thus ensure enthusiasm for production of *bombyx mori linnaeus* breeders. Several non-destructive testing methods [5] for pesticide residues have been studied, such as near-infrared spectroscopy [6–9], fluorescence spectroscopy [10–11] and Raman spectroscopy method [12]. However, the above methods tend to lose important information due to their strong randomness and large errors.

Hyperspectral imaging technology [13] with ultra-high resolution multi-band is an emerging technology in the field of detecting pesticide residues. Due to the fact that it can detect pesticide residues quickly without destroying the sample, it has attracted extensive attention from scholars around the world. Several research achievements have been reported on the detection of pesticide residues in farm products. Sanchez M. T. *et al.* [9], who selected peppers as research subjects, investigated the feasibility of detecting pesticide residues by near-infrared reflectance, but merely analyzed the presence or absence of pesticide residues in peppers.

*Author to whom correspondence should be addressed.
Email: sun2000jun@ujs.edu.cn

Xue L. *et al.* [13] quantitatively detected pesticide residues in fruit surface by hyperspectral imaging technology, but only pesticide residues of high concentrations could be detected accurately. So far, no methods that can nondestructively predict pesticide residues in mulberry leaves by hyperspectral imaging technology have been reported. In order to make up for this vacancy, in this paper, mulberry leaves with pesticides of different concentrations were selected as research objects, and prediction models were established to predict pesticide residues combined with hyperspectral imaging technology.

MATERIALS AND METHODS

Sample Preparation

Chlorpyrifos EC with 40% active composition, one common organophosphorus pesticide used in mulberry fields, was selected as the experimental pesticide. Firstly, chlorpyrifos solutions (acetone was the solvent) of six different concentrations (2 mg/ml, 4 mg/ml, 6 mg/ml, 10 mg/ml, 12 mg/ml and 14 mg/ml) were prepared. Then, 24 mulberry trees in similar growing trend were selected and divided into six groups. Thirdly, the chlorpyrifos pesticide of each concentration above was correspondingly sprayed on each group of mulberry trees, respectively. Finally, after 48 h, 24 mulberry leaves were picked from each group of mulberry trees in the same two positions (a total of 144 mulberry leaves) and placed in plastic bags with 144 labels numbered from 1–144. The prepared samples of mulberry leaves were collected immediately.

Quantitative Detection Using GC

Sample Extraction and Purification

Hyperspectral images of all samples were collected in ascending numerical order. Then, each sample was sequentially extracted and purified respectively for quantitative detection by GC. The sample could be extracted through the following steps. The mulberry leave was cut into pieces, and 25 g (accurate to 0.1 mg) mulberry leave was placed into a beaker containing 50 mL chromatographic pure acetonitrile. After oscillation for 1 h, the mixture in the beaker was filtered to 100 mL volumetric cylinder with stopper filled with 5 g NaCl (superior grade pure). Then, the cylinder was covered with stopper and shaken vigorously for 1 min. At room temperature, acetonitrile and water phases

were layered after the cylinder was placed for 10 min. Further purification could be achieved by the following steps. Firstly, 10 mL acetonitrile in the upper was accurately transferred into concentrated 25 mL volumetric flask by the pipette, and the extract in flask was dried by evaporation on a water bath pot at a temperature of about 40°C. Secondly, the tributyl phosphate solution of 0.05 mg/ml (acetone was the solvent) was set as an internal standard solution, and 1 ml internal standard solution was added into flask. Thirdly, the mixture in the flask was diluted to 10 mL using acetone. Finally, the mixture of the third step was filtered into vial through an organic solvent microfiltration membrane of 13 mm * 0.2 µm.

Chromatographic Conditions

The Agilent (USA) model 7890A gas chromatograph equipped with FID and FPD was chosen to quantitatively detect pesticide residues of samples, and the capillary column (HP-5: 5%-Phenyl-methylpolysiloxane, 30 m * 0.53 * 1.0 µm) was used as the chromatographic column. The temperature elevation program was set as follows: inlet temperature: 210°C; detector temperature: 300°C; oven temperature: 120°C hold 2 min rise to 200°C at 16°C/min and hold 2 min, then to 240°C at 8°C/min. The gas conditions were as follows: the velocity of flow of high purity nitrogen (N₂) was 25 ml/min, the velocity of flow of high purity hydrogen (H₂) was 30 ml/min, the velocity of flow of air was 400 ml/min, and the velocity of flow of septum purge was 3 ml/min. The injection volume was 1 µl in a 20:1 split ratio.

Establishment of the Standard Curve

Internal standard method can eliminate errors caused by external outside interference, which can be used to detect pesticide residues in mulberry leaves. The five standard solutions (acetone was the solvent) were prepared as follows: chlorpyrifos standard solutions (purity > 95%) of five concentrations, including 0.02, 0.05, 0.1, 0.2 and 0.4 mg/ml, were prepared, and then 1 ml internal standard solution at a concentration of 0.05 mg/ml was added to each standard solution. The retention time of acetone, tributyl phosphate and chlorpyrifos was 0.496 min, 2.898 min, and 4.996 min respectively, as can be seen from Figure 1.

In Figure 2, concentration of solutions (*X*) was set as horizontal axis, and ratio of peak area (*Y*) (chlorpyrifos: tributyl phosphate) was set as vertical axis. The

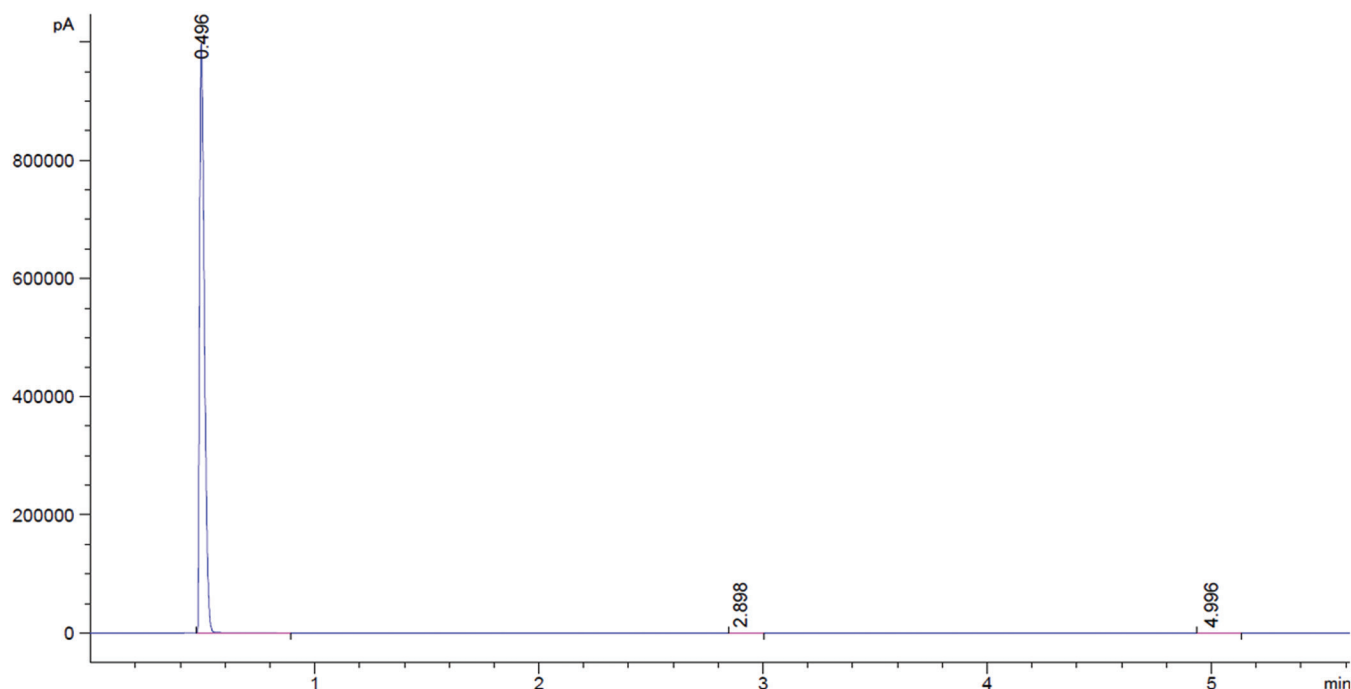


Figure 1. Chromatogram of the standard mixed solution.

standard curve was plotted based on experimental data measured by GC which were marked in red dots. As can be seen, the functional relationship ($Y = 7.528X - 0.0936$) between concentration and ratio of peak area was linear correlation, and the correlation coefficient was 0.9999.

Determination Using GC

The 144 sample solutions after extraction and purification were analyzed using GC, and Figure 3 shows a representative chromatogram of sample solution. The ingredient with retention time of 0.495 min was set as acetone, that with retention time of 2.908 min was tributyl phosphate and that with retention time of 4.992 min was chlorpyrifos, which accorded with analysis of GC. The chemical values of chlorpyrifos residues in 144 mulberry leaves were calculated by the standard curve above, and the minimum, maximum, mean and standard deviation were listed in Table 1.

Collection of the Spectrum Data

Hyperspectral images of mulberry leaves were obtained by hyperspectral image acquisition system (Im-Spector V10E, Spectral Imaging Ltd., Oulu, Finland). The hyperspectral image acquisition system should be black and white calibrated and its parameters should be reasonably set before acquiring images. The exposure

time was set to 20 ms, the moving speed of electronically controlled displacement units was set to 1.25 mm/s, and the image resolution was set as 672×512 pixels. As shown in Figure 4, the average hyperspectral data were collected from region of interest (ROI) marked by the red solid square of $64 \text{ pixels} \times 64 \text{ pixels}$ on the hyperspectral image. The ROI could be part of leaf or the entire leaf, and the selection of ROI is very important for subsequent model. In this paper, the region in middle of the right half of the leaf without wrinkles,

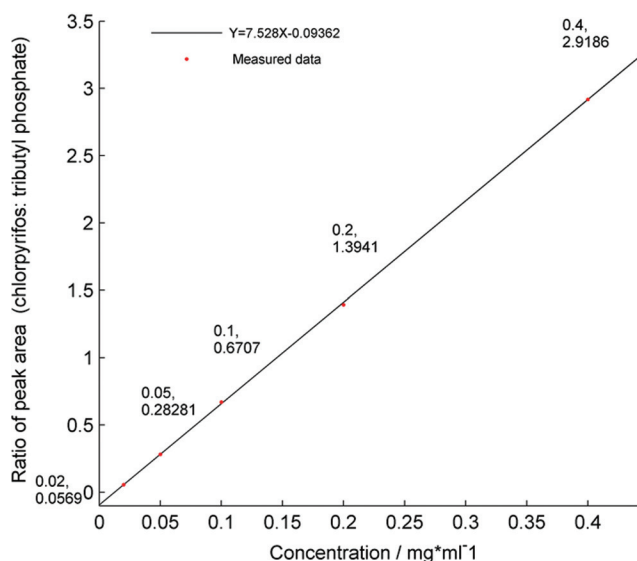


Figure 2. The standard curve.

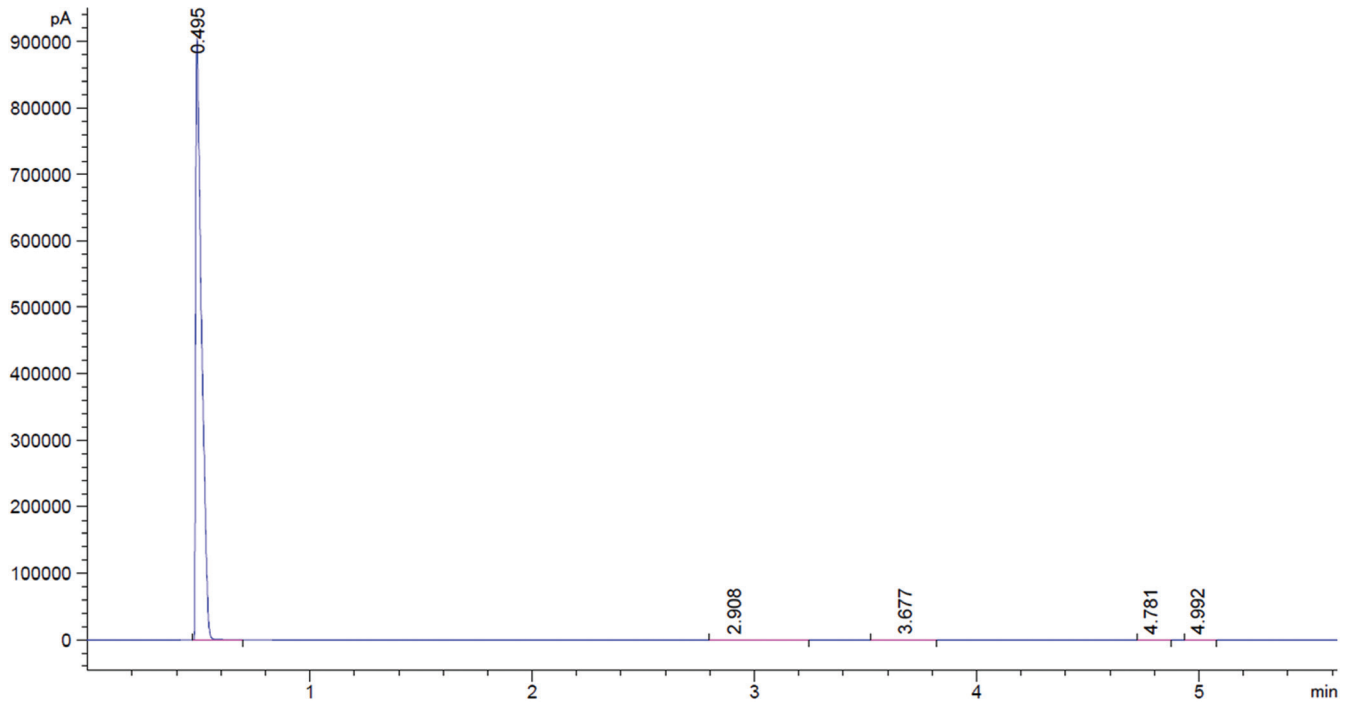


Figure 3. Chromatogram of the sample solution.

which was away from the main stem, was selected as the ROI. Due to the lower noise ratio at the beginning and ending of wavebands, 20 bands at the head and tail bands were excluded respectively. Thus, one spectral curve could be extracted from the corresponding ROI in the 450–1000 nm (a total of 472 bands). In the same way, 144 spectral curves could be extracted from the 144 corresponding ROIs.

Pretreatment of the Spectrum Data

Hyperspectral data are not only interfered easily with outside factors but also influenced by instrument noise and random errors, which may seriously reduce the accuracy of the model. In this paper, SG smoothing polynomial fitting [14] and orthogonal signal correction (OSC) method [15] were used to preprocess hyperspectral data, which could remove noise spectra and retain the valid data. As shown in Figure 5, spectrum curves of the 144 samples are neatly arranged without glitches.

Correlation Analysis of the Spectrum Data

In the region of 400–780 nm wavelength, chlorophyll is the main factor affecting leaf reflectance, whereas in 780–1050 nm there is significant correlation between cell structure and spectral reflectance. Recently, several studies have reported that pesticides residues have great influences on physiological and biochemical parameters [16–17] of greenery plants (such as chlorophyll, soluble polysaccharides and soluble proteins). Therefore, it is reasonable to deduce that there is close correlation between pesticides residues and spectral reflectance. The relationship between pesticide residues and spectral reflectance values in the 415–1023 nm wavelength region can be found by MATLAB software [18], and the correlation curves are drawn in Figure 6. As can be seen, some particular valleys and peaks appear on the curve, because the strong absorption of chlorophyll can lead to valley absorption in the 550–575 nm, the 705–710 nm and the 720–730 nm wavelength regions, but reflection peak in the 670–609 nm wavelength region. All correlation coefficients of the particular valleys are larger than -0.74 and that of peak value is -0.613 . Here, the wavelengths of 561.25, 680.86, 706.58, 714.32 and 724.66 nm marked by red stars in Figure 6 are selected as sensitive wavelengths to build prediction models.

Table 1. Chemical Values of Chlorpyrifos Residues of Samples.

Samples	Minimum ($\mu\text{g}/\text{kg}$)	Maximum ($\mu\text{g}/\text{kg}$)	Mean ($\mu\text{g}/\text{kg}$)	Standard Deviation
144	42.4757	244.6744	129.7373	75.70856

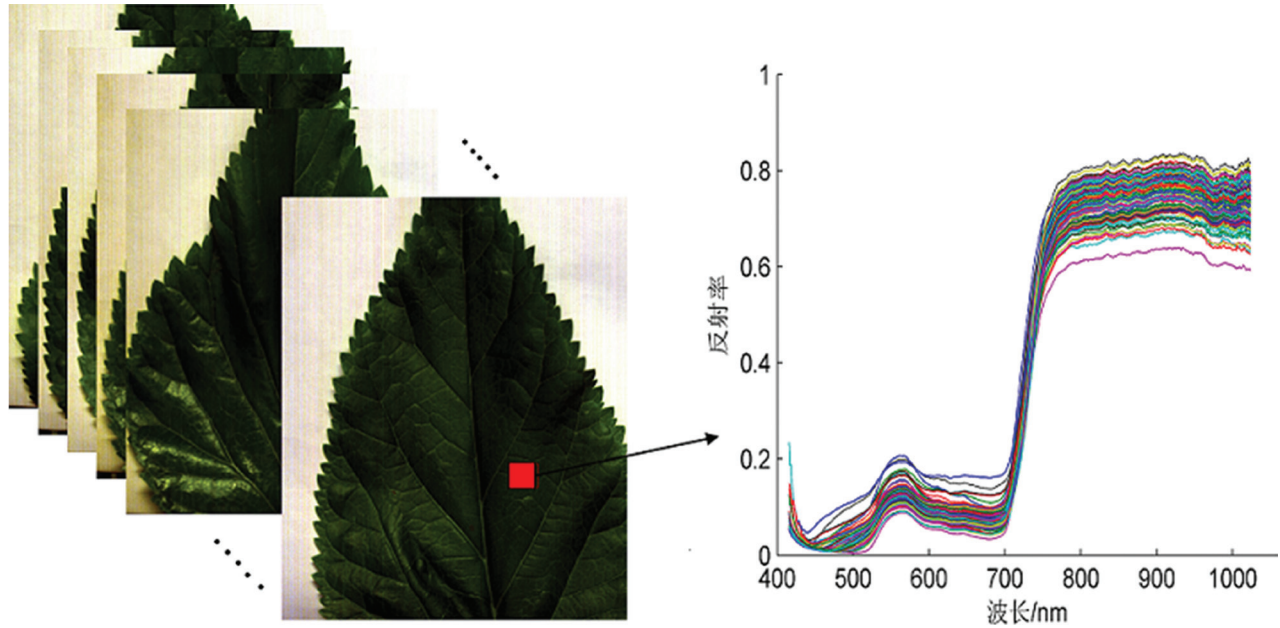


Figure 4. Diagram of spectral data extraction and reflectance spectral curve of mulberry leaves.

RESULTS AND DISCUSSION

Calibration Set and Prediction Set

In order to predict the pesticide residues, the spectral data and corresponding chemical values of 144 mulberry leaves samples were divided into calibration set and prediction set. Two thirds of spectral data and corresponding chemical values randomly were set as the calibration set, and the remaining were the prediction set.

Establishment of Predictive Models

Recently, multiple linear regression (MLR) [19] and

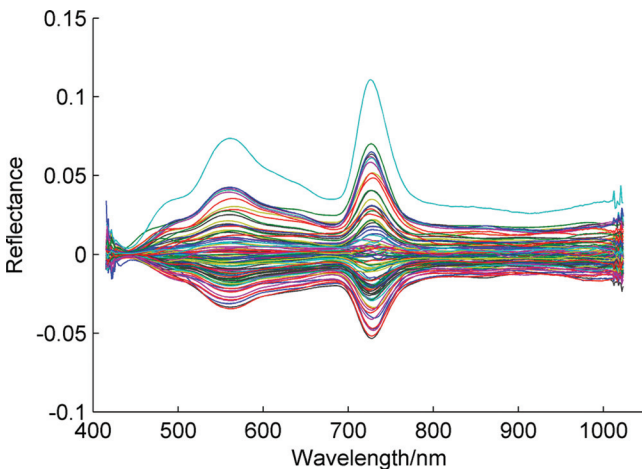


Figure 5. Reflectance spectral curve using GC smoothing and OSC.

support vector regression (SVR) [20–24] have been widely used as correction methods in many fields. Therefore, in this paper, MLR and SVR were used to detect chlorpyrifos residues in mulberry leaves. The spectral data of the 5 sensitive wavelengths which had been reprocessed using SG and OSC were set as the inputs of MLR and SVR. The predictions of calibration set and prediction set by MLR and SVR are shown in Figure 7 and Figure 8 respectively.

It can be seen from Figure 7 that the prediction model of MLR cannot predict chlorpyrifos residues in mulberry leaves, according to the coefficient of deter-

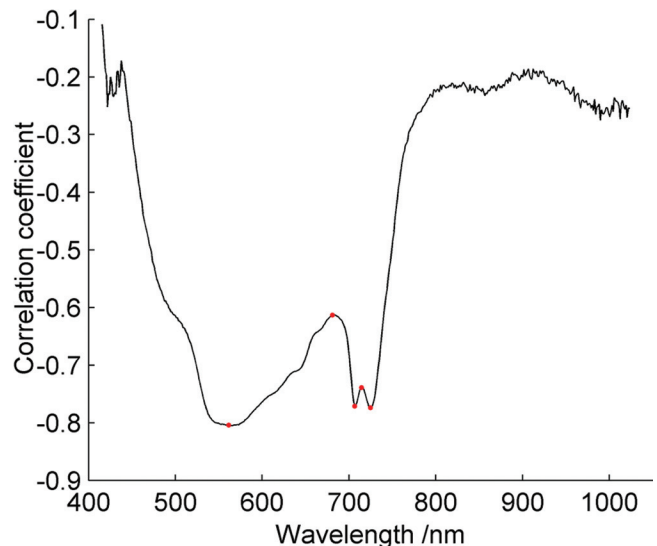


Figure 6. Correlation between pesticides residues and spectral reflectance.

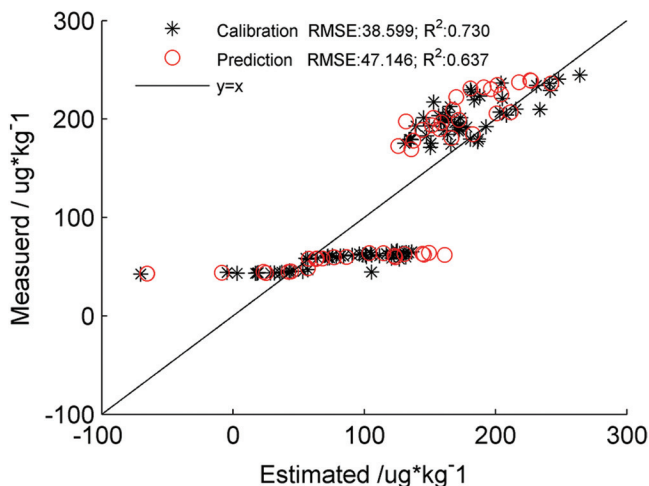


Figure 7. Scatter plots of MLR prediction model.

mination (R^2) and root mean square error (RMSE) of calibration set or prediction set. Moreover, the dispersion degree of residual scatters under the low concentration, as the reference of the straight line ($y = x$), is more serious than that under high concentration. That is to say, it is more difficult to accurately detect chlorpyrifos residues of low concentration relative to those of high concentration.

In contrast, as Figure 8 shows, predictions by SVR fit well with chemical values by GC, according to the R^2 and RMSE of both calibration set and prediction set. More importantly, chlorpyrifos residues under low concentration can be predicted using prediction model of SVR. Therefore, chlorpyrifos residues in mulberry leaves can be accurately predicted using hyperspectral imaging technology combined with preprocessing methods of GC and OSC, and the SVR prediction model. Similarly, other residues in other plants can be detected by the idea above.

CONCLUSIONS

The hyperspectral images of mulberry leaves with chlorpyrifos residues were collected using hyperspectral imaging technology and the chemical values of chlorpyrifos residues were accurately detected by GC. Then, the average spectral data were extracted from ROI on hyperspectral images using ENVI software and further preprocessed using SG smoothing method and OSC method. Ultimately, using the spectral data in five sensitive wavelengths as the inputs, two prediction models of MLR and SVR were established to predict chlorpyrifos residues in mulberry leaves. By comparison of the two models, the results of SVR model were

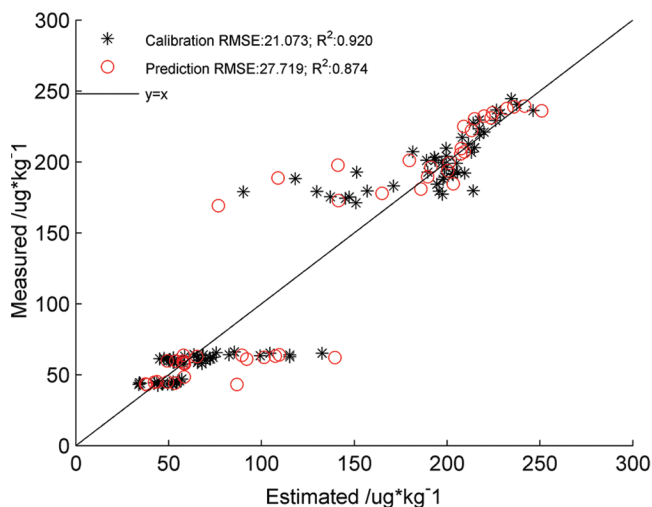


Figure 8. Scatter plots of SVR prediction model.

better than those of MLR model in respect of accurate prediction. Therefore, hyperspectral images technology combined with stoichiometry is a feasible method to non-destructively predict chlorpyrifos residues in mulberry leaves.

ACKNOWLEDGEMENTS

This work is supported by the National Natural Science Foundation of China (No. 31471413, 31401286), the Key Laboratory of Modern Agricultural Equipment and Technology of Jiangsu University (NZ201306), the Priority Academic Program Development of Jiangsu Higher Education Institutions (PAPD), China Postdoctoral Science Foundation Funded Project (2014M561594), Six Talent Peaks Project in Jiangsu Province (ZBZZ-019), the Natural Science Foundation of Jiangsu Province (BK20140550), and the Open Fund Project of Key Laboratory of Agricultural Information Service Technology, Ministry of Agriculture (2014-AIST-03).

REFERENCES

1. Malhat, F.M., Haggag, M.N., Loutfy, N.M., Osman, M.A.M., and Ahmed, M.T., "Residues of Organochlorine and Synthetic Pyrethroid Pesticides in Honey an Indicator of Ambient Environment, a Pilot Study", *Chemosphere*, Vol. 120, 2015, pp. 475–461. <http://dx.doi.org/10.1016/j.chemosphere.2014.08.032>
2. Li, Y.F., Qiao, L.Q., Li, F.W., Ding, Y., Yang, Z.J., and Wang, M.L., "Determination of Multiple Pesticides in Fruits and Vegetables Using a Modified Quick, Easy, Cheap, Effective, Rugged and Safe Method with Magnetic Nanoparticles and Gas Chromatography Tandem Mass Spectrometry", *Journal of Chromatography A*, Vol. 1361, No. 26, 2014, pp. 77–87. <http://dx.doi.org/10.1016/j.chroma.2014.08.011>
3. Carlos, R. B., Luis, A. A., Diego, A. A., Héctor, A. C., and Eddie, S., "Evaluation of Pesticide Residues in Open Field and Greenhouse Tomatoes from Colombia", *Food Control*, Vol. 2, No. 30, 2013, pp. 400–403.

4. Emilia, F., and Anna, S., "Application of a Truly One-point Calibration for Pesticide Residue Control by Liquid Chromatography–mass Spectrometry", *Journal of Chromatography B*, Vol. 2, No. 901, 2012, pp. 107–114.
5. Aghamir-Baha, S., and Ormeci, B., "Determination of Optimum Polymer Dose using UV-vis Spectrophotometry and its Comparison to Filtration Based Tests", *Journal of Residuals science & Technology*, Vol. 11, No. 3, 2014, pp. 71–76.
6. Lourdes, S. C., Antonio, J. G-J, Victor, O. S., and Francisco, P. R., "Feasibility of Using NIR Spectroscopy to Detect Herbicide Residues in Intact Olives", *Food Control*, Vol. 2, No. 30, 2013, pp. 504–509.
7. Didier, B., Thierry, W., Magalie, L. J., Raphaël, A., Luc, R., and Bernard, G. B., "Determination of Soil Content in Chlordecone (organochlorine pesticide) Using Near Infrared Reflectance Spectroscopy (NIRS)", *Environmental Pollution*, 11(157): Vol. 11, No. 157, 2009, pp. 3120–3125.
8. De, L.M., Terouzi, W., Kzaiber, F., G., Ioele, Oussama, A., Ragno, G., "Classification of Moroccan Olive Cultivars by Linear Discriminant Analysis Applied to ATR–FTIR Spectra of Endocarps", *International Journal of Food Science and Technology*, Vol. 47, No. 6, 2012, pp. 1286–1292. <http://dx.doi.org/10.1111/j.1365-2621.2012.02972.x>
9. Sanchez, M. T., Katherine, F. R., Jose, E. G., Varo, A. G., and Marin, D. P., "Measurement of Pesticide Residues in Peppers by Near-infrared Reflectance Spectroscopy", *Pest Management Science*, 66: Vol. 66, 2010, pp. 580–586.
10. Nicolas, F., Marc, T., Catherine, G., Stéphane, M., Roland, R., and Madeleine, G., "Identification and Quantification of Known Polycyclic Aromatic Hydrocarbons and Pesticides in Complex Mixtures Using Fluorescence", *Chemosphere*, No. 107, 2014, pp. 344–353. <http://dx.doi.org/10.1016/j.chemosphere.2013.12.087>
11. Rubio, L., Ortiza, M.C., and Sarabiab, L.A., "Identification and Quantification of Carbamate Pesticides in Dried Lime Tree Flowers by Means of Excitation-emission Molecular Fluorescence and Parallel Factor Analysis When Quenching Effect Exists", *Analytica Chimica Acta*, Vol. 11, No. 820, 2014, pp. 9–22. <http://dx.doi.org/10.1016/j.aca.2014.02.008>
12. Dhakal, S., Li, Y.Y., Peng, Y.K., Chao, K.L., Qin, J.W., and Guo, L.H., "Prototype Instrument Development for Non-destructive Detection of Pesticide Residue in Apple Surface Using Raman Technology", *Journal of Food Engineering*, Vol. 2, No. 123, 2014, pp. 94–103. <http://dx.doi.org/10.1016/j.jfoodeng.2013.09.025>
13. Xue, L., Li, J., and Liu, M., "Detecting Pesticide Residue on Navel Orange Surface by Using Hyperspectral Imaging", *Acta Optica Sinica*, Vol. 28, No. 12, 2008, pp. 2277–2280. <http://dx.doi.org/10.3788/AOS20082812.2277>
14. Du, S., Du, Y., and Wu, Xi., "The Surface Smoothing Methods for Three-dimensional Fluorescence Spectrometry Based on Savitzky-Golay polynomial Smoothing", *Spectroscopy and Spectral Analysis*, Vol. 2, No. 31, 2011, pp. 440–443.
15. Zolghamein, J., Shariatmanesh, T., and Babaei, Al., "Simultaneous Determination of Propanil and Monalide by Modified Glassy Carbon Electrode with Nickel Oxide Nanoparticles, Using Partial Least Squares Modified by Orthogonal Signal Correction and Wavelet Packet Transform", *Sensors and Actuators, B: Chemical*, Vol. 7, No. 197, 2014, pp. 326–333. <http://dx.doi.org/10.1016/j.snb.2014.03.003>
16. Sun, L., and Cheng, L., "Analysis of Spectral Response of Vegetation Leaf Biochemical Components", *Spectroscopy and Spectral Analysis*, Vol. 30, No. 11, 2010, pp. 3031–3025.
17. Buszewski, B., and Michel, M., "Quantitative Structure-retention Relationship Studies as an Analytical Tool in the Determination and Modeling of Pesticide Residues in Plant Organisms", *Journal of AOAC International*, Vol. 6, No. 93, 2010, pp. 1703–1714.
18. An, A., Qi, L.C., and Zhang, H.C., "The Analysis of Impact Factors for Dissolved Oxygen Concentration in Wastewater Treatment System Using an Adaptive Modeling Method", *Journal of Residuals science & Technology*, Vol. 12, No.1, 2015, pp.25-30.
19. Nelson, J. D.B., Damper, R. I., Gunn, S. R., and Guo, B., "Signal Theory for SVM Kernel Design with Application to Parameter Estimation and Sequence Kernels", *Neurocomputing*, Vol. 72, No. 1–3, 2008, pp. 15–22. <http://dx.doi.org/10.1016/j.neucom.2008.01.034>
20. Bazi, Y., and Melgani, F., "Toward an Optimal SVM Classification System for Hyperspectral Remote Sensing Images", *IEEE Transactions on Geoscience and Remote Sensing*, Vol. 44, No. 11, 2006, pp. 3374–3385. <http://dx.doi.org/10.1109/TGRS.2006.880628>
21. Alireza, F., and Naader, A., "Determination of Diphenylamine Residue in Fruit Samples Using spectrofluorimetry and multivariate analysis", *Spectrofluorimetry and Multivariate Analysis*, Vol. 1, No. 54, 2013, pp. 6–12.
22. Yuxia, F., Keqiang, L., Barbara, A. Rasco, and Huang, Y., "Determination of Carbaryl Pesticide in Fuji Apples Using Surface-enhanced Raman Spectroscopy Coupled with Multivariate Analysis", *LWT-Food Science and Technology*, Vol. 1, No. 60, 2015, pp. 352–357.
23. Zahra, D., Hassan, G., and Elahe, K., "Support Vector Regression Based QSPR for the Prediction of Retention Time of Pesticide Residues in Gas Chromatography–mass Spectroscopy", *Microchemical Journal*, Vol.1, No. 106, 2013, pp. 51–60.
24. Demura, C., Métails, B., Canlet, C., Tremblay-Franco, M., Gautier, R., Blas-Y-Estrada, F., Sommer, C., and Gamet-Payrastre, L., "Dietary Exposure to a Low Dose of Pesticides Alone or as a Mixture: The Biological Metabolic Fingerprint and Impact on Hematopoiesis", *Toxicology*, Vol. 2, No. 308, 2013, pp. 74–87. <http://dx.doi.org/10.1016/j.tox.2013.03.004>

The Remediation of Petroleum Contaminated Soils Using Microwave Irradiation: A Laboratory Study

HUAYI JIANG, MEIYING LI*, HONGYUAN QI and YULONG WANG
School of Petroleum Engineering, Xi'an Shiyou University, Xi'an 710065, China

ABSTRACT: A laboratory study was conducted to remediate petroleum contaminated soils using microwave irradiation, and the traditional method of electric heating was also used for comparison purpose. The feasibility of the microwave irradiation method was evaluated in aspects of the reaction time, petroleum removal efficiency and energy consumption level. Meanwhile, the impacts of microwave irradiation mode and soil conditions on petroleum removal efficiency were also investigated, with a thermodynamic model of soils specifically developed. The results showed that microwave irradiation was better than the traditional heating method in remediating petroleum contaminated soils with less energy consumed. Also, microwave irradiation time, microwave power, soil moisture content and soil petroleum content had all imposed significant impacts on the remediation efficiency, and the results obtained from the model were basically consistent with the experiment results. Therefore, the findings from this study are of significance in real-world applications of microwave irradiation for the remediation of petroleum contaminated soils.

INTRODUCTION

According to relevant statistics, approximately 8 million tons of petroleum annually finds its way into the environment worldwide, and it is not surprising that serious oil pollution incidents could be found in numerous chemical plants and petroleum refineries. However, it is extremely difficult to separate petroleum residuals from soils by means of evaporation, leaching or biodegradation within a short time as petroleum is characterized by high viscosity and complex composition, and petroleum residuals have caused serious harm to human beings and the surrounding environment [1].

Currently, available techniques for the remediation of petroleum contaminated soils are mainly of four types worldwide, namely, physical remediation, chemical remediation, biological remediation and integration remediation, however, most of these techniques are time-consuming, single target oriented and non-manipulable with side effects, thereby, it is imperative to find a soil remediation method that could be widely applicable, time-efficient, economically feasible, and flexibly operable [2,3].

Due to its unique heating efficiency and involving mechanisms, microwave technique has caught the attention of the various industry in recent years [4]. Tian

Meng, Wang Peng have used microwave radiation to treat a single pollutant, although few studies have been performed on petroleum contaminated soils [5,6]. In this study, microwave is used to treat petroleum contaminated soils, and involving mechanisms are then investigated. The results have important practical significance for the remediation and improvement of petroleum contaminated soils.

EXPERIMENTAL APPARATUS

A MAS-II microwave system for microwave synthesis and extraction under atmospheric pressure, including an electronic analytic balance, a moisture tester, a KDM electronic temperature-adjustable heating set, an electric drying oven (Model 101), a moisture separator, a condenser pipe, beakers, glass rods, measuring cylinders, and three-necked round-bottomed flasks.

Reagents: acetonitrile, a mixture of acetone: n-hexane (1:1), petroleum ether (fraction of 60-90) and distilled water.

EXPERIMENTAL PROCEDURE

Preparation of Petroleum Contaminated Soils

Collection and Characterization of Soil Samples. Approximately 15 kg soils without petroleum con-

*Author to whom correspondence should be addressed.
Email: 583955495@qq.com, Tel: +86 13484532011

tamination were collected at 10 cm below the ground. The soil samples from Xi'An is sandy loam, and cosmid content is about 25%, the sand content about 38%. The soil had a pH of 8.39, an organic matter content of 1.22%, a calcium carbonate content of 3.83%, and a total nitrogen content of 0.11%.

Pre-treatment and Storage of Soil Samples. The soil samples were air-dried and protected from contamination. Non-soil substances were removed, and the soils were passed through a sieve. Appropriate amounts of acetonitrile and acetone:*n*-hexane (1:1) were added to the soils to extract organics so that they would not interfere with subsequent experiments. After organic extraction, the soils were oven-dried at 60°C and stored in a bottle.

Preparation of Petroleum Contaminated Soils. Contaminated soils with various petroleum content were prepared by adding the appropriate amount of petroleum and *n*-hexane [7]. The soils were allowed to stand for a week before use.

Calculation of Petroleum Removal Efficiency

Petroleum removal efficiency was calculated as the ratio of petroleum mass difference before and after heating to petroleum mass before heating:

$$C = \frac{W \times M\% - Q}{W \times M} \times 100\% \quad (1)$$

where C is petroleum removal efficiency, W is soil mass, M is soil petroleum content, and Q is the mass of petroleum left in the soils after heating.

Microwave Treatment

50 g of petroleum contaminated soils were weighted and put in a microwave device before the microwave

treatment started. The heating process ended when the temperature rose to the set temperature. With heating time and water output recorded, petroleum removal efficiency could then be calculated.

RESULTS AND ANALYSES

A Comparison of Microwave Treatment and Traditional Electric Heating Treatment

Table 1 shows petroleum removal efficiency of soils (10% petroleum content) with either microwave irradiation or traditional electric heating treatment.

Heating soils to 100°C using microwave irradiation method would consume energy of 54 kJ (power \times time = 800 W \times 67.5 s), whereas heating soils to 180°C would consume energy of 232 kJ. It was assumed that 100% of the thermal energy from the electric heating set had been used to heat the contaminated soils without any loss. As can be seen from Table 1, it took less time for the microwave method to treat soils with higher petroleum removal efficiency and lower energy consumption. This might be because microwave irradiation treatment is a heating method at the molecular level so that soil samples are uniformly and simultaneously heated from the inside out. As a result, soil temperatures could rise quickly, and this process could even accelerate the evaporation rate of the contaminants.

Effects of Soil Moisture Content on Petroleum Removal Efficiency Using Microwave Irradiation Method

Five soil samples with moisture content ranging from 5–30% were treated with microwave irradiation method in order to evaluate the effects of soil moisture content on petroleum removal efficiency. The soils contained 10% petroleum. For the microwave irradiation

Table 1. Petroleum Removal Efficiency of Soils (10% petroleum content) with Either Microwave Irradiation or Traditional Electric Heating Treatment.

Treatment Method	Soil Weight (g)	Petroleum Content (%)	Temperature (°C)	Moisture Content (%)	Power (W)	Time (s)	Petroleum Removal Efficiency (%)
Electric heating	50	10	100	10	270	360	6
Electric heating	50	10	100	10	270	420	8
Electric heating	50	10	180	10	270	156	52
Electric heating	50	10	180	10	270	168	48
Microwave heating	50	10	100	10	800	650	45
Microwave heating	50	10	100	10	800	700	48
Microwave heating	50	10	180	10	800	300	76
Microwave heating	50	10	180	10	800	280	78

Table 2. Effects of Soil Moisture Content (%) on Petroleum Removal Efficiency (%).

Soil Weight (g)	Oil Content (%)	Temperature (°C)	Moisture Content (%)	Power (W)	Time (s)	Petroleum Removal Efficiency (%)
50	10	127	5	800	300	71
50	10	135	5	800	300	72
50	10	130	5	800	300	71
50	10	132	5	800	300	74
50	10	171	10	800	300	73
50	10	179	10	800	300	75
50	10	176	10	800	300	78
50	10	178	10	800	300	78
50	10	152	15	800	300	58
50	10	159	15	800	300	59
50	10	157	15	800	300	62
50	10	160	15	800	300	61
50	10	129	20	800	300	57
50	10	123	20	800	307	57
50	10	127	20	800	300	54
50	10	121	20	800	300	56
50	10	157	25	800	300	70
50	10	160	25	800	300	72
50	10	166	25	800	300	70
50	10	161	25	800	300	68

tion treatment, the power was 800 W, and the treatment time was 300 s.

Changes of soil temperature with time could be described by the following equation[8]:

$$\frac{T - T_0}{t} = \frac{0.556 \times 10^{-10} \varepsilon_{eff}'' f E^2}{\rho C_p} \quad (2)$$

Where t is microwave heating time, T is soil temperature after microwave heating, T_0 is soil temperature before heating, ε_{eff}'' is the effective dielectric loss factor of the soil, f is the working frequency of microwave, E is the electric field intensity, C_p is soil specific heat, and ρ is soil density.

Analysis: due to effects of soil moisture content, the dielectric loss factor of water is high, whereas it is relatively low for petroleum contaminated soils. An increase in soil moisture content could lead to an increase in the effective dielectric loss factor of the soil system, which in turn would raise the heating ability of microwaves [9]. Additionally, water has a larger specific heat capacity than soils. An increase in soil moisture content could lead to an increase in the specific heat capacity of the soil system, which in turn would weaken the heating ability of microwaves. As shown in Figure 1, an increase in soil moisture content, soil temperature and petroleum removal efficiency would increase and decrease, respectively.

The expected result is in the same with experimented, soil moisture can effectively enhance the remediation efficiency of petroleum contaminated soils when microwave irradiation method is applied.

Effects of Microwave Treatment Time on Petroleum Removal Efficiency

Fifty grams of soils with 10% moisture and 10% petroleum content were used when the microwave treatment time varying in the range of 180–600 s in order

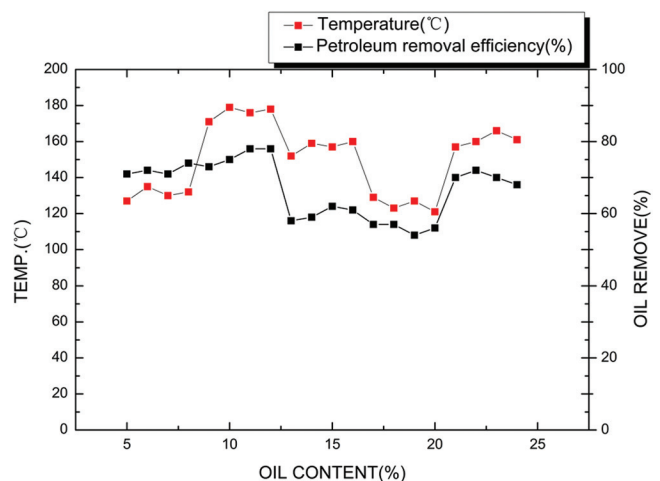


Figure 1. Changes of soil temperature (°C) and petroleum removal efficiency (%) with soil moisture content (%).

Table 3. Effects of Microwave Treatment Time (s) on Petroleum Removal Efficiency (%).

Soil Weight (g)	Petroleum Content (%)	Soil Moisture (%)	Temperature (°C)	Power (W)	Time (s)	Petroleum Removal Efficiency (%)
50	10	10	137	800	180	60
50	10	10	136	800	180	61
50	10	10	134	800	180	59
50	10	10	137	800	180	60
50	10	10	171	800	300	76
50	10	10	182	800	300	73
50	10	10	177	800	300	76
50	10	10	174	800	300	79
50	10	10	218	800	480	79
50	10	10	223	800	480	75
50	10	10	225	800	480	73
50	10	10	218	800	480	81
50	10	10	245	800	600	92
50	10	10	254	800	600	91
50	10	10	251	800	600	90
50	10	10	250	800	600	87

to evaluate the effects of treatment time on petroleum removal efficiency and soil temperature.

The expectation: When soil temperature rose to approximately 189°C, and petroleum removal efficiency increased rapidly. The flask was filled with fog, and it was assumed that pollutants were removed by evaporation and thermal desorption process during this period. After then, petroleum removal efficiency slowed down during the temperature was about 220, indicating that it required more energy to remove residual pollutants from soils. When the temperature rose to 250°C, and pollutants were removed from soils mainly through thermal decomposition process.

The expectation is right, As shown in Figure 2, the dif-

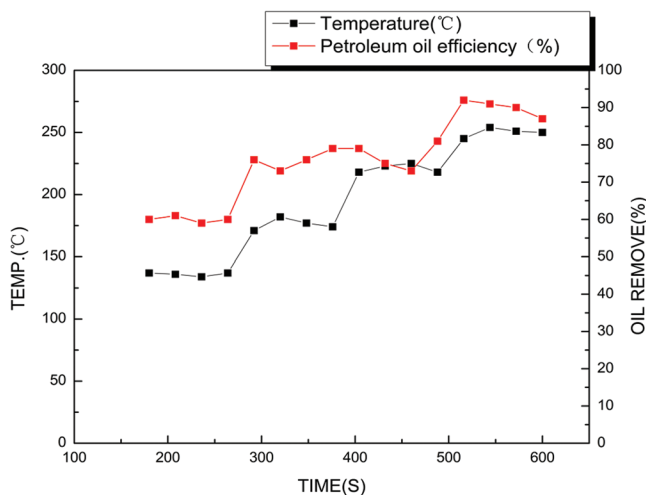


Figure 2. Changes of soil temperature (°C) and petroleum removal efficiency (%) with varying microwave heating time (s).

ferent petroleum removal efficiency achieved by different treatment in terms of heating time showed that petroleum removal efficiency became relatively stable after 300 s of heating treatment.

Effects of Microwave Power on Petroleum Removal Efficiency

Seven 50-g soil samples with 10% moisture and 10% petroleum content were microwave heated for 300 s at various levels of microwave power in order to investigate the effects of microwave power on petroleum removal efficiency.

The expectation: a higher soil temperature and petroleum removal efficiency were achieved at a higher level of microwave power.

The expected result is in the same with experimented. As shown in Figure 3, for the same treatment time of 5 min, a petroleum removal efficiency of 44% was achieved when the heating power was 300 W, whereas a petroleum removal efficiency of 78% was achieved when the power was 900 W. This was because electric field intensity became stronger with an increase in microwave power. Therefore, an increase in microwave power could help to increase petroleum removal efficiency.

Effects of Soil Initial Petroleum Content on Petroleum Removal Efficiency

Five soil samples of 10% moisture content and

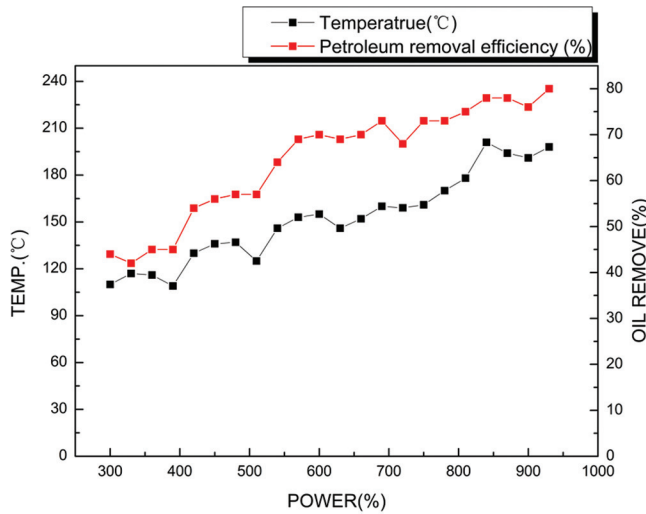


Figure 3. Changes of soil temperature (°C) and petroleum removal efficiency (%) with various levels of microwave power (W).

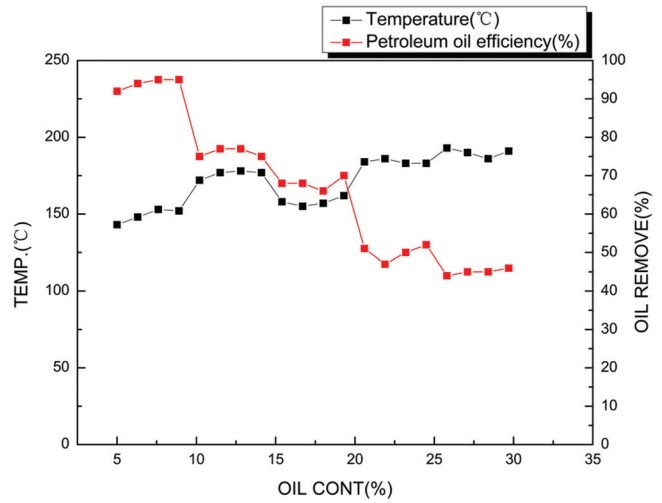


Figure 4. Changes of soil temperature (°C) and petroleum removal efficiency (%) with varying initial petroleum content (%).

various petroleum contents were treated for 300 s with microwave heating at a power of 800 W in order to evaluate the effects of initial petroleum content on petroleum removal efficiency and soil temperature.

The expectation: during which period water was heated, gasified and evaporated, and most of the light petroleum was removed when soils had low petroleum content. By contrast, subsequent heating could not

raise the temperature to the boiling temperature of pollutants, and thus these pollutants could not escape from soils.

As shown in Figure 4, changes of soil temperature and petroleum removal efficiency displayed similar trends when initial petroleum content varied between 5–20%, but displayed opposite trends when initial petroleum content varied between 20–30%. The reason

Table 4. Effects of Microwave Power (w) on Petroleum Removal Efficiency (%).

Soil Weight (g)	Petroleum Content (%)	Soil Moistue Content (%)	Temperature (°C)	Power (W)	Time (s)	Petroleum Removal Efficiency (%)
50	10	10	110	300	300	44
50	10	10	117	300	300	42
50	10	10	116	300	300	45
50	10	10	109	300	300	45
50	10	10	130	400	300	54
50	10	10	136	400	300	56
50	10	10	137	400	300	57
50	10	10	125	400	300	57
50	10	10	146	500	300	64
50	10	10	153	500	300	69
50	10	10	155	500	300	70
50	10	10	146	500	300	69
50	10	10	152	600	300	70
50	10	10	160	600	300	73
50	10	10	159	600	300	68
50	10	10	161	600	300	73
50	10	10	170	700	300	73
50	10	10	178	800	300	75
50	10	10	201	900	300	78
50	10	10	194	900	300	78
50	10	10	191	900	300	76
50	10	10	198	900	300	80

Table 5. Effects of Soil Initial Petroleum Content (%) on Petroleum Removal Efficiency (%).

Soil Weight (g)	Petroleum Content (%)	Moisture Content (%)	Temperature (°C)	Power (W)	Time (s)	Petroleum Removal Efficiency (%)
50	5	10	143	800	300	92
50	5	10	148	800	300	94
50	5	10	153	800	300	95
50	5	10	152	800	300	95
50	10	10	172	800	300	75
50	10	10	177	800	300	77
50	10	10	178	800	300	77
50	10	10	177	800	300	75
50	20	10	158	800	300	68
50	20	10	155	800	300	68
50	20	10	157	800	300	66
50	20	10	162	800	300	70
50	25	10	184	800	300	51
50	25	10	186	800	300	47
50	25	10	183	800	300	50
50	25	10	183	800	300	52
50	30	10	193	800	300	44
50	30	10	190	800	300	45
50	30	10	186	800	300	45
50	30	10	191	800	300	46

was because after 90 s of microwave heating, soil temperature rose to approximately 100°C.

This explains why when other conditions remained the same, high petroleum removal efficiency was achieved in soils with low petroleum content, whereas low petroleum removal efficiency was achieved in soils with high petroleum content.

THEORETICAL STUDY OF THE REMEDIATION OF PETROLEUM CONTAMINATED SOILS USING MICROWAVE HEATING METHOD

A numerical model was developed to calculate the distribution patterns of temperatures during three phases of the soil system. Results from both modeling and experiments were combined to provide insights regarding the mechanism of the change of soil temperature.

The Development of A Thermodynamic Model

A representative elemental volume (REV) was taken from petroleum contaminated soils. The REV consisted of the solid phase (i.e., soil particles), the petroleum phase and the water phase, with the latter two uniformly distributed within the former one. Also, the electric field was uniformly distributed.

Basic Assumptions

- The petroleum phase in each REV has the same interior temperature of t_1 .
- The water phase has the same interior temperature of t_2 .
- The solid phase has the same interior temperature of t_3 .
- The particles of the solid phase, water phase and petroleum phase are spheres with radii of r_3 , r_2 and r_1 , respectively, and the particle volume content of the petroleum phase is f .
- No heat convection occurs between the soil phase and the water phase.
- The heat transfer coefficient between the particles of the petroleum phase and the solid phase is h_1 , and that between the water phase and the solid phase is h_2 .

For particles in the petroleum phase, heat balance in any one time intervals of microwave irradiation is as follows according to the energy conservation law:

Energy flows into the particles in the petroleum phase during time $d\tau$ is 0.

Energy produced by microwave towards particles in the petroleum phase during time $d\tau$ is $Q = P_1 V_1 d\tau$.

Energy flows out of the particles in the petroleum phase during time $d\tau$ is $h_1(t_1 - t_3)A_1 d\tau$.

The increment of the energy accumulated by the particles in the petroleum phase during time $d\tau$ is $\rho_1 c_1 V_1 (dt_1/d\tau) d\tau = \rho_1 c_1 V_1 dt_1$.

According to the energy conservation law $P_1 V_1 d\tau - h_1(t_1 - t_3)A_1 d\tau = \rho_1 c_1 V_1 dt_1$.

We have the following equation for the petroleum phase:

$$P_1 V_1 - h_1(t_1 - t_3)A_1 = \rho_1 c_1 V_1 \frac{dt_1}{d\tau} \quad (3)$$

Similarly, we have the following equation for the water phase:

$$P_2 V_2 - h_2(t_2 - t_3)A_2 = \rho_2 c_2 V_2 \frac{dt_2}{d\tau} \quad (4)$$

For particles in the solid phase, as the boundaries are thermal insulated and thus do not transmit heat outwards, we have the following heat balance according to the energy conservation law:

The energy flows into the particles of the solid phase during time $d\tau$ is

$$h_1(t_1 - t_3)A_1 d\tau + h_2(t_2 - t_3)A_2 d\tau \quad (5)$$

The energy flows out of the particles of the solid phase during time $d\tau$ is 0.

The increment of the energy accumulated by the particles in the solid phase during time $d\tau$ is

$$\rho_3 c_3 V_3 \frac{dt_3}{d\tau} d\tau = \rho_3 c_3 V_3 dt_3 \quad (6)$$

According to the energy conservation law

$$h_1(t_1 - t_3)A_1 + h_2(t_2 - t_3)A_2 = \rho_3 c_3 V_3 \frac{dt_3}{d\tau} \quad (7)$$

With the assumption that the initial temperature of the solid phase is, the water phase and the petroleum phase is t_0 , then $t_1|_{\tau=0} = t_2|_{\tau=0} = t_3|_{\tau=0} = t_0$, and we have the following equation set:

$$\begin{cases} \frac{dt_1}{d\tau} = -b_1 t_1 + b_1 t_3 + a_1 \\ \frac{dt_2}{d\tau} = -b_2 t_2 + b_2 t_3 + a_2 \\ \frac{dt_3}{d\tau} = b_{31} t_1 + b_{32} t_2 - b_{31} t_3 - b_{32} t_3 \end{cases} \quad (8)$$

Where ρ_1, ρ_2 and ρ_3 are densities of the three phases, C_1, C_2 and C_3 are specific heat capacities, P_1, P_2 and P_3 are microwave loss power densities of the particles in the three phases, and V_1, V_2 and V_3 are particle volumes of the three phases. $P_1 = (1/2)\omega\epsilon_0\epsilon_1''|E_1|^2$ where ϵ_0 is the dielectric constant in vacuum and calculated as $\epsilon_0 = 8.854 \times 10^{-12}(f/m)$.

$\epsilon_1'', \epsilon_2''$, and ϵ_3'' are the dielectric losses of the three phases, ω is microwave frequency, and E_1, E_2 and E_3 are electric field intensities in the particles of the three phases.

Parameter Selection

Oil density $\rho_1 = 840 \text{ kg/m}^3$ [10], water density $\rho_2 = 1000 \text{ kg/m}^3$, soil density $\rho_3 = 1500 \text{ kg/m}^3$, petroleum specific heat capacity $c_1 = 2100 \text{ J/(kg}\cdot\text{k)}$, water specific heat capacity $c_2 = 4200 \text{ J/(kg}\cdot\text{k)}$, and soil specific heat capacity $c_3 = 1460 \text{ J/(kg}\cdot\text{k)}$. For a REV, its volume in the petroleum phase: $V_1 = (4/3)\pi r_1^3$ where $r_1 = 5 \times 10^{-5} \text{ m}$ [11], in the water phase: $V_2 = (4/3)\pi r_2^3$ where generally $r_2 = 5 \times 10^{-5} \text{ m} \sim 5 \times 10^{-7} \text{ m}$ and the value $5 \times 10^{-6} \text{ m}$ is taken in this study, and in the solid phase: $V_2 = (V_1/f) - V_1 - V_2$ whereas the percentage of petroleum particle volume in the total volume and takes a value between 0.05–0.30. The microwave loss power density in the petroleum phase $P_1 = (1/2)\omega\epsilon_0\epsilon_1''|E_1|^2$ where microwave frequency $\omega = 2.45 \times 10^9 \text{ Hz}$ [12]. The dielectric loss (ϵ_1'') of dehydrated petroleum at 2400 MHz was measured to be 0.004, the loss power density $P_2 = (1/2)\omega\epsilon_0\epsilon_2''|E_2|^2$ where $\epsilon_0 = 8.854 \times 10^{-12} (f/m)$ and $\epsilon_2'' = 29$ [13], field intensity distribution in the heating cabinet under various heating powers is $E = 1.5 \times 10^5 \text{ v/m}$ where $\epsilon_1 = 2.2$ and $\epsilon_2 = 80$ [13]. The electric field intensity of the soil particle solid phase under microwave irradiation is $E_0 = (\epsilon/\epsilon_0)E$ where $\epsilon_1 = 2.7$ and $\epsilon_2 = 16$, the electric field intensity of petroleum under microwave irradiation is $E_1 = [(3\epsilon_0)/(2\epsilon_0 + \epsilon_1)]E_0$, the electric field intensity of water drops under microwave irradiation is $E_2 = [(3\epsilon_0)/(2\epsilon_0 + \epsilon_2)]E_0$, the average heat transfer coefficients of petroleum and water are $h_1 = 0.65 \text{ w/m}^2\text{k}$ and $h_2 = 1000 \text{ w/m}^2\text{k}$, respectively [14].

Temperature Distribution and Experimental Validation of the Calculation Results

Matlab programming was used to solve Equation (8). In the experiment, the temperature measured by infrared was a macroscopic temperature of soil samples, and could be considered as the temperature of the

petroleum inside an REV. The measured temperature was compared with the temperature calculated from the model. When soil petroleum content f was 0.3, the calculated temperature distribution of the petroleum phase after simplification of the programming results was:

$$t_1 = 0.8017 \times t - \frac{4.448 \times 10^{-9}}{e^{254.2 \times t}} - \frac{43.55}{e^{0.05287 \times t}} + 53.55 \quad (8)$$

The calculated values of temperature based on the thermodynamic model agreed well with the measured values. The small discrepancies were caused by the errors in the fit parameters during modeling process. As the dielectric properties of the petroleum phase differed greatly from those of the water phase, selective heating occurred during the process of microwave heating. As a result, soils were locally over-heated and non-uniformly heated, consistent with the nonuniform color distribution of soil samples after microwave treatment.

BASIC CONCLUSIONS

Compared with traditional heating method, microwave heating is fast with higher heating efficiency. Meanwhile, uniform heating can be achieved by microwave heating method, and no marked chemical changes, such as high-temperature pyrolysis, would occur. Therefore, pollutants could be more effectively recycled, and unnecessary energy loss could be effectively reduced.

In the empirical study of the remediation of petroleum contaminated soils using microwave method, pollutants were removed mainly through processes such as steam distillation, evaporation, thermal desorption and thermal decomposition induced by microwave treatment.

Water is a strong microwave absorbent. When it is added to soils, it could effectively enhance the heating effect of microwave treatment on soils and the remediation efficiency.

In response to the fact that the dielectric constant of soils is small, substances such as water, graphite, granular activated carbon and magnetic nanoparticles

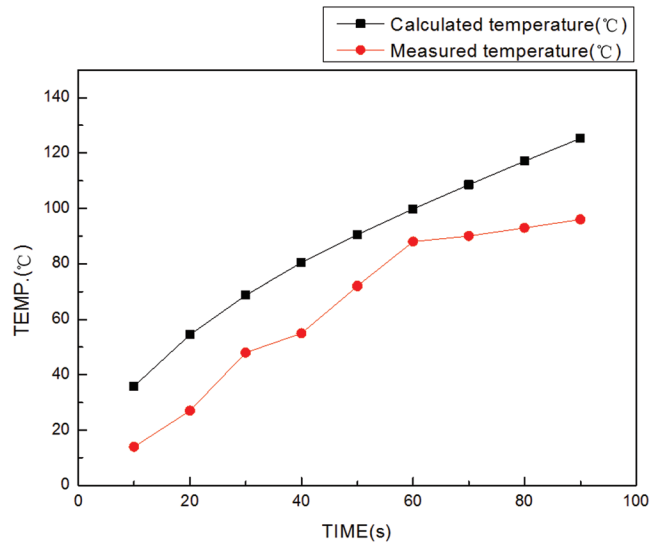


Figure 5. Distribution of calculated temperature (°C) and measured temperature (°C) in the petroleum phase when $f = 0.3$.

could be added to enhance the absorption ability of contaminated soils.

Petroleum removal efficiency would decrease with an increase in petroleum content of soil samples. When petroleum content is 5%, the average petroleum removal efficiency could be up to 94% after 300 s of microwave treatment at a power of 800 W.

With the extending of microwave heating time, the remediation efficiency could be enhanced to some extent. However, after the threshold of 360 s heating time, further extending of the heating time would not bring in big changes in terms of petroleum removal efficiency.

When microwave power is increased, the electric field intensity of microwave would increase, and the heating effect would also be enhanced. As a result, pollutants could be effectively removed from soils. Therefore, petroleum removal efficiency increases with an increase in the level of microwave power.

For 50 g petroleum contaminated soils with a moisture content of 10% and a petroleum content of 5%, maximum remediation efficiency is achieved when the treatment time is 300 s and microwave power is set to 800 W.

Calculated temperatures based on thermodynamic

Table 6. Calculated and Measured Values of Temperature (°C) in the Petroleum Phase when $f = 0.3$.

	Time (s)								
	10	20	30	40	50	60	70	80	90
Calculated Temperature (°C)	35.9	54.5	68.7	80.4	90.5	99.8	108.6	117.1	125.3
Measured Temperature (°C)	14	27	48	55	72	88	90	93	96

numerical model match with measured values, validating the mechanism proposed for the explanation of changes in soil temperatures.

REFERENCES

1. Zhang, H.H, Cui, H.M., Liu, C., Li, T.X., Chen, L.Y., Qi, H.B. and Li, F., "Treatment on oily sludge with ultrasonic and microwave," *Petroleum Huagong*, Vol. 35, No. 9, 1997, pp. 62–75.
2. Ye, M., "Application of modern biological treatment on oil-contaminated soil remediation," *Private Science and Technology*, Vol. 9, No. 9, 2011, pp.164–164.
3. Svanström, M., Bertanza, G., Laera, G., Heimersson, S., Canato, M. and Tomei, M.C., "Technical, economic and environmental assessment of wastewater and sludge management solutions designed to overcome common issue," *Journal of residuals science & Technology*, Vol. 11, No. 1, 2014, pp. 15–20.
4. Yamaki, T, Abe, Y, Kaneko, A, Segawa, T and Kawaguchi, K, "The criteria of flushing phenomena under microwave heating," *Journal of Nuclear Science & Technology*, Vol. 52, No. 2, 2014, pp. 241–250. <http://dx.doi.org/10.1080/00223131.2014.946567>
5. Wang P., "Coal desulfuration using microwave: Research status and future direction," *Coal Mining Modernization*, Vol. 1. No. 1, 2014, pp. 85–87.
6. Tian, M., Yuan, S.H. and Lu, X.H., "Studies on the remediation of HCB contaminated soil with microwave induced by MnO₂", *Environmental Protection Science*, Vol. 32, No. 2, 2006, pp. 241–250.
7. Amellal, N., Portal, J.M. and Berthelin, J., "Effect of soil structure on the bioavailability of polycyclic aromatic hydrocarbons within aggregates of contaminated soil", *Applied Geochemistry*, Vol. 16, No. 1, 2001, pp. 1611–1619. [http://dx.doi.org/10.1016/S0883-2927\(01\)00034-8](http://dx.doi.org/10.1016/S0883-2927(01)00034-8)
8. Clark, D.E., Folz, D.C. and West, J.K., "Processing materials with microwave energy," *Materials Science and Engineering: A*, Vol. 287, No.2, 2000, pp. 153–158. [http://dx.doi.org/10.1016/S0921-5093\(00\)00768-1](http://dx.doi.org/10.1016/S0921-5093(00)00768-1)
9. Jiang, H.Y. 2004. *Treating Hyperviscous and Hypercoagulate Oil Using Microwave*, Chengdu, Sichuan: Southwest Petroleum University Publications.
10. Incropera, F. P. (Translator: Lu Dayou). 1987. *Introduction to Heat Transfer*, Beijing, China: Astronautic Publishing House.
11. Yang, X.H. and Zhang, G.Z. 1996. *Oil Pipeline Design and Management*, Dongying, Shandong: University of Petroleum Press.
12. Zhang, Z.T. and Zhong, R.Q. 1988. *Introduction to Microwave Heating Technology*, Beijing, China: Higher Education Press.
13. Liu, H.L., "Microwave dehydration technology," *Oilfield Ground Engineering*, Vol. 11, NO. 4, 1992, pp. 22–25.
14. Wang Y.. 2002. Mechanism of Viscosity Reduction of Thickened Oil Using Microwave, Beijing, China: Graduate School of Chinese Academy of Sciences (Institute of Electronics).

Removal of Toxic Organic Pollutants from Coke Plant Wastewater by UV-Fenton

YANGYANG LIANG, SUQIN LI* and BIN LI

School of Metallurgical and Ecological Engineering, University of Science and Technology Beijing, Beijing 100083, China

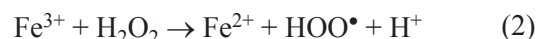
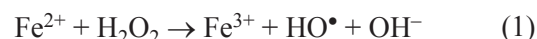
ABSTRACT: Coke plant wastewater containing lots of toxic organic pollutants should be treated before being discharged into the environment. It is challenging to treat toxic and refractory compounds using conventional methods. In this study, a UV-Fenton technology was investigated. When the initial COD, NH₃-N concentration and SS of wastewater were 5080 mg/L, 329.9 mg/L, and 847.7 mg/L, results showed that the removal rate of COD, NH₃-N and SS were 88.0%, 58.4% and 99.2% respectively under the optimal reaction conditions. Under the identified optimal condition, H₂O₂ concentration is 75 mmol/L, the concentration ratio of H₂O₂ and Fe²⁺ is 3:1, and original pH is 4 within 30 min. GC-MS analysis, revealed that organic substances such as indole and quinoline were degraded effectually.

INTRODUCTION

WASTEWATER from coke plants is often produced from coke refining, high-temperature carbonization, purification and by-product recovery processes. It is a kind of poisonous and harmful wastewater with a high concentration of refractory organic matter [1]. It has a complicated composition, mainly including phenol and phenol derivatives (about 60 %), benzene and its derivatives and quinolines as well as other polycyclic or heterocyclic organic compounds. Those compounds have an inhibitory effect on microorganism growth and are recalcitrant to degradation. Meanwhile, they could cause deactivation of human cell by tissue necrosis, and can post treats to crops, water and aquatic life. It is challenging to meet the requirements of emission standard of pollutants for coking chemical industry GB16171-2012 by conventional processes which has aroused people's concern.

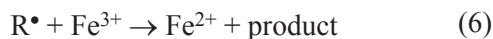
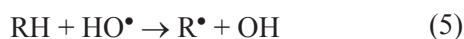
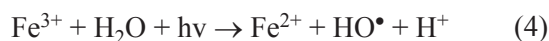
Wastewater treatment processes for coke plants can be divided into three levels [2]. The first processes mainly include solvent extraction steam cycle to remove oil or phenol from high phenol concentration waste water; Secondary treatment methods are mainly biochemical treatment; Tertiary treatment methods include flocculation, activated carbon adsorption, ozone oxidation, etc. Biological treatment is the most costly but effective method in treating coke plant wastewater.

ter. However, toxicity and inhibition effects of phenols compounds to microorganisms often limit the removal efficiency of organic pollutants [3]. Advanced Oxidation Process (AOPs) is a kind of new technology treating persistent organic pollutants, it can be used in the area of wastewater treatment and sludge minimization [4]. The reaction is essentially using highly reactive hydroxyl free radical (HO•) to oxidize refractory organic pollutants in wastewater and finally degrade them into non-toxic or low toxicity of small molecules. Such organic pollutants could be even degraded into carbon dioxide and water [5]. In traditional Fenton reaction processes, Fe²⁺ can be oxidized into Fe³⁺ by hydrogen peroxide and hydroxyl free radicals could be produced. Additionally, Fe³⁺ could be reduced into Fe²⁺, as shown in Equations (1) and (2).



In the presence of catalyst on the surface, the certain wavelength ultraviolet light can catalytic oxidation of organic pollutants in wastewater and oxidative degradation of the organic matter [6]. Under the irradiation of ultraviolet light whose wavelength is less than 300 nm, H₂O₂ can produce hydroxyl radicals and convert Fe²⁺ to Fe³⁺ efficiently. At the same time, Fe³⁺ can also produce hydroxyl radicals with the irradiation of ultraviolet. The main reactions in Fenton with ultraviolet light irradiation are shown in Equations (3) and (4).

*Author to whom correspondence should be addressed.
Suqin Li, No.30 Xueyuan Road, Haidian District, Beijing, China; 100083;
E-mail: lisuqin@metall.ustb.edu.cn; Tel: +86 10 82376226



The generated hydroxyl radicals could oxidize organic pollutants (RH) in waste water and produce new radical (R^\bullet), which could be oxidized by Fe^{3+} to generate carbon dioxide and water [7].

In this study, UV-Fenton technology is used to dispose coke plant wastewater before biochemical treatment. The effects of various factors for the treatment processes are also discussed.

METHODS

The Raw Materials

Wastewater samples were obtained from coking plant of Chengde Iron & Steel Company, Hebei, China. Water quality parameters of wastewater samples and reagents used in the experiments are shown in Table 1 and Table 2.

Experimental Setup

The optical experimental setup was self-designed with low pressure mercury lamp which was put into a water proof tube made by quartz glass with good UV transmittance. The reactor is tubular which was made by organic glass with bottom aeration. Low pressure mercury lamp was immersed into water to cool down. The parameters are shown in Table 3 and Figure 1.

Because coke plant wastewater is of high turbidity and it is difficult for the light to penetrate through it, wastewater samples were diluted 10 times and poured into the reactor with a certain amount of Fenton reagents and reacted under the irradiation of ultraviolet light through air mixing for a certain time. The pH was then adjusted to form iron ion precipitation settling down. The main factors such as H_2O_2 concentration, reagent ratio, reaction time, pH and ultraviolet light illumination were investigated in experiments.

Table 1. Quality Parameters of Raw Wastewater.

Parameters	pH	Turbidity (NTU)	Ammonia Nitrogen (mg/L)	COD (mg/L)
Value	6.8	847.7	3.29	5080

Table 2. Reagents Used in the Experiments.

Reagents	Molecular Formula	Molecular Weight	Content (%)
Hydrogen peroxide	H_2O_2	34.02	30
Ferrous sulfate	$\text{FeSO}_4 \cdot \text{H}_2\text{O}$	278.02	≥ 99.0
Sulfuric acid	H_2SO_4	98.08	95.0~98.0
Sodium hydroxide	NaOH	40.00	≥ 96.0

RESULTS AND DISCUSSION

Effect of H_2O_2 Concentration

The effect of initial H_2O_2 concentration on the degradation of coke plant wastewater was studied under a constant ratio between H_2O_2 and Fe^{2+} .

The initial concentration of H_2O_2 is a very important parameter. As shown in Figure 2, removal rates of COD and ammonium nitrogen increased with increasing H_2O_2 concentration from 10–75 mmol/L, but decreased when the H_2O_2 concentration exceeded 75 mmol/L. The optimal removal rate for COD and $\text{NH}_3\text{-N}$ is 78.7% and 58.4%, respectively. Hydroxyl radicals were generated from Fenton under ultraviolet light irradiation, which could be used to degrade organic molecules. A chain reaction could be triggered to consume organic molecules completely. Under a constant intensity of ultraviolet light, a higher dosage of Fenton produced more hydroxyl radicals, resulting in a higher removal rate of COD and ammonium nitrogen. The treatment effect, therefore, improved with increasing H_2O_2 concentration. However, in the excess of Fenton,

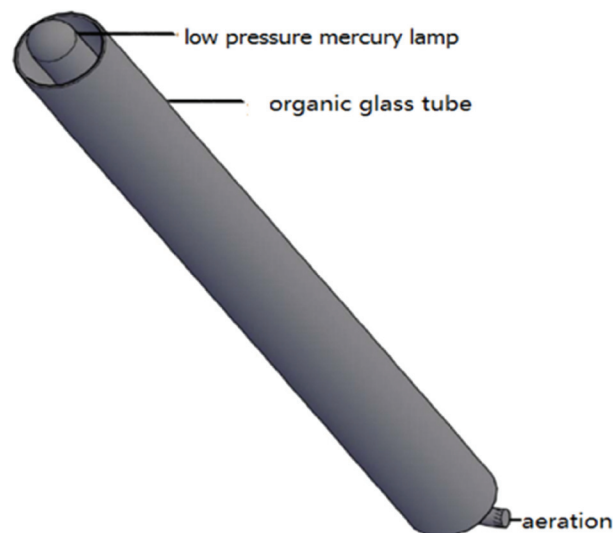


Figure 1. Schematic diagram of low pressure mercury lamps reactor.

Table 3. Parameters of Low Pressure Mercury Lamp.

Irradiation Intensity of 1 Meter (W)	Power (W)	Wavelength (nm)	Voltage (V)	Current (mA)	Pipe Diameter (mm)	Type	Manufacturer
66	25	253.7	82	350	16	TUV25W4P-SE	Philips

hydroxyl radicals were consumed by H_2O_2 to form hydroperoxyl radical, resulting in lower oxidation capability of O_2 [8,9].

Effect of Reagent Ratio

The reagent ratio on the degradation of organic pollutants is also very important. As shown in Figure 3, when the ratio of H_2O_2 and Fe^{2+} concentration was 3:1, treatment effect was the best. Removal rate of COD and $\text{NH}_3\text{-N}$ was 81.6% and 7.21%, respectively.

The main reaction of UV-Fenton is that Fe^{2+} initiates and promotes the decomposition of H_2O_2 , forming hydroxyl free radicals to react with organic matters and degrade them into small inorganic species. The concentration of Fe^{2+} determines the conversion rate of H_2O_2 to hydroxyl free radicals. When the ratio of H_2O_2 and Fe^{2+} was higher, low concentration of ferrous ion could not induce the formation of enough hydroxyl free radicals. In addition, after the pH was adjusted, H_2O_2 could generate oxygen and influence the treatment effect. While the ratio of H_2O_2 and Fe^{2+} was lower, overmuch ferrous ion quickly catalyzed hydrogen peroxide and produced a large number of hydroxyl radicals reacting with each other. Excessive Fe^{2+} ions also consumed hydroxyl radicals, being unfavorable to degradation of organic pollutants in coke plant wastewater [10].

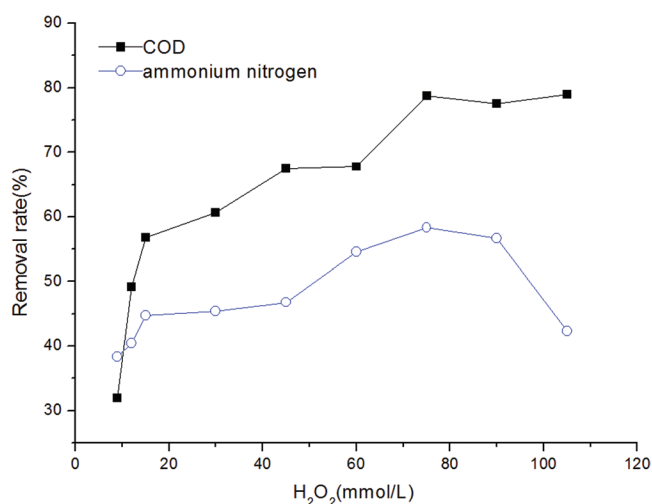


Figure 2. Effect of H_2O_2 on the degradation of coke plant wastewater.

Effect of pH

Effect of pH on the degradation of organic pollutants was shown in Figure 4.

The influence of pH of the solution on UV-Fenton system is complex. It affects the activity of both oxidant and substrate. H_2O_2 can capture proton from the solution to form H_3O_2^+ which is unfavorable to be activated by Fe^{2+} at a low pH. Under such conditions, $\text{Fe}(\text{OOH})^{2+}$ could be generated to react with H_2O_2 slowly to reduce the generation of $\cdot\text{OH}$. When pH of solution was higher than 4, Fe^{2+} could form complex compound. Some Fe^{3+} ions generated by Fenton reactions were easily precipitated as $\text{Fe}(\text{OH})_3$ [11]. Preventing it from reduction into Fe^{2+} could remarkably affect the formation of $\cdot\text{OH}$. H_2O_2 was unstable in alkaline solutions and could be easily decomposed to oxygen and water. Thus, the most suitable pH condition in UV-Fenton system was 4 when Fe^{2+} mainly existed in the form of $\text{Fe}(\text{OH})_2$. Under such conditions, $\text{Fe}(\text{OH})_2$ could react much faster with H_2O_2 than Fe^{2+} [12]. COD removal rate was 85%. By adjusting the pH to 6 after the reaction, removal rate of COD could be increased to 88%. Because iron ions reacted with water molecules and hydroxyl ions, complex iron compounds and flocculation were formed and the suspended solid particles were settled down, resulting in clean water in the outlet.

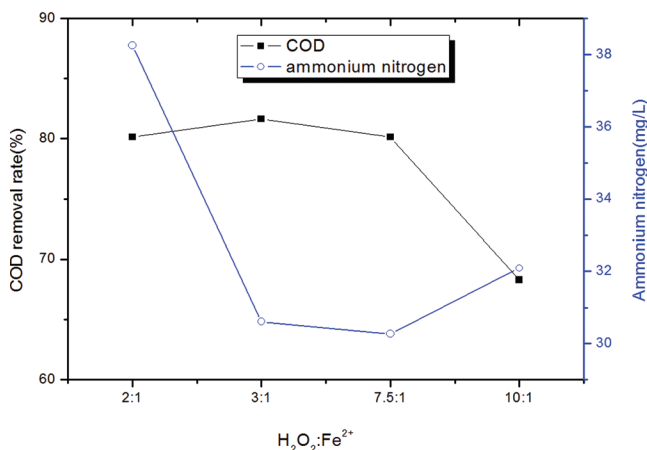


Figure 3. Effect of reagent ratio on the degradation of organic pollutants.

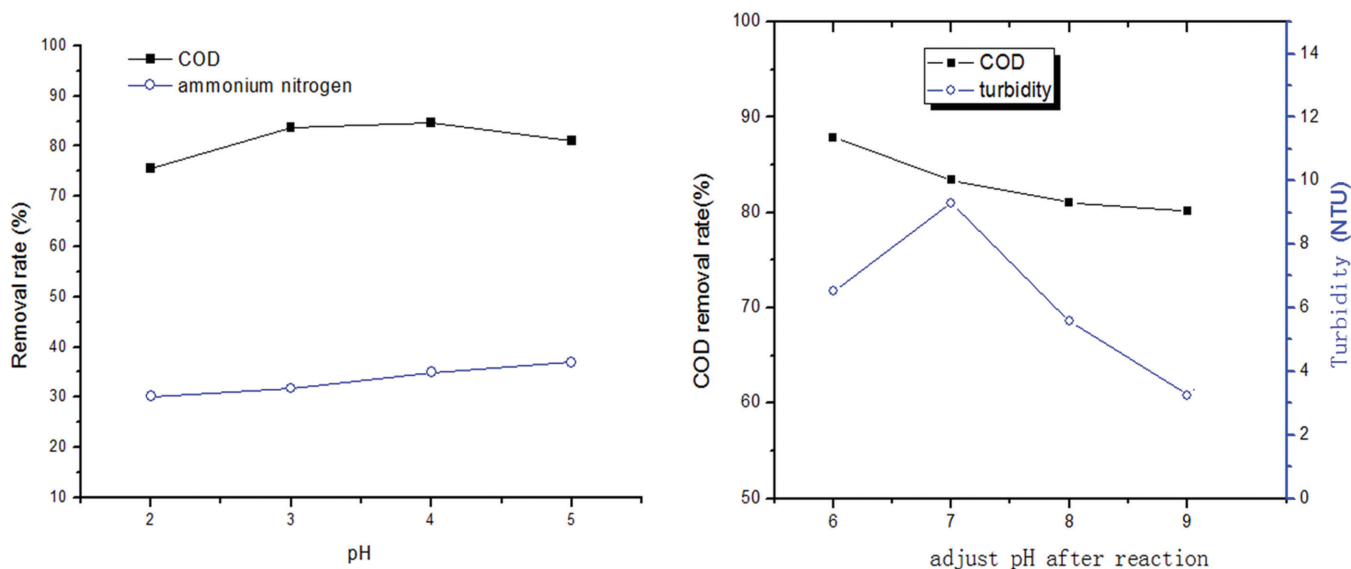


Figure 4. Effect of pH on the degradation of organic pollutants.

Effect of Reaction Time

Experimental results indicated that the reaction was very fast in UV-Fenton process at first. However, it increased slowly after 5 min, as shown in Figure 5.

When the reaction time reached 30 min, removal rates of $\text{NH}_3\text{-N}$ and COD were 31.9% and 79.7%, because the concentration of reagent and pollutants in wastewater was matching in the process of reaction. In addition, sufficient stirring and abundant $\cdot\text{OH}$ could lead to a strong degradation effect in a shorter time. However some intermediate products created in the processes were hard to be oxidized by $\cdot\text{OH}$. Hence, the removal rate of organic pollutants decreased gradually.

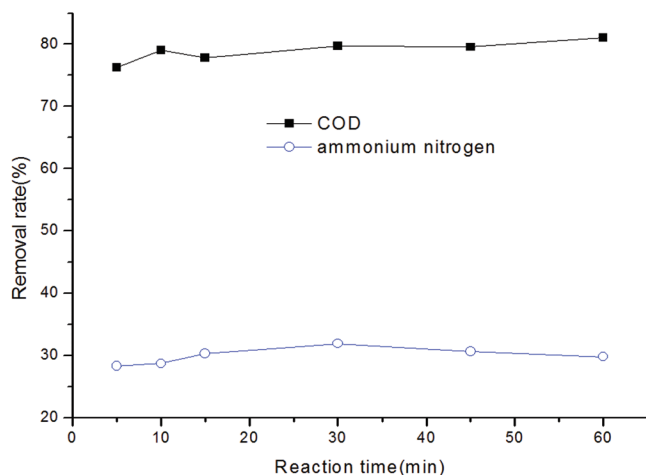


Figure 5. Effect of reaction time on the degradation of organic pollutants.

Effect of Ultraviolet Light Illumination

Results indicate that ultraviolet light affected the efficiency of pollutant degradation and improved the utilization rate of Fenton reagent, as shown in Figure 6. COD removal rate improved from 81.1–88.2% at dosage of reagents of 120 mmol/L.

The speed of reducing Fe^{3+} to Fe^{2+} was very slow, and limited the reaction rate. It limited the reduction of Fe^{3+} to Fe^{2+} . Hence, Fe^{2+} concentration in the solution was getting lower and lower. On the contrary, Fe^{3+} gradually accumulated, and the amount of Fe^{2+} needed to be increased to make efficient reaction. Combining Fenton reagent with ultraviolet light can promote the decomposition of hydrogen peroxide and induce the

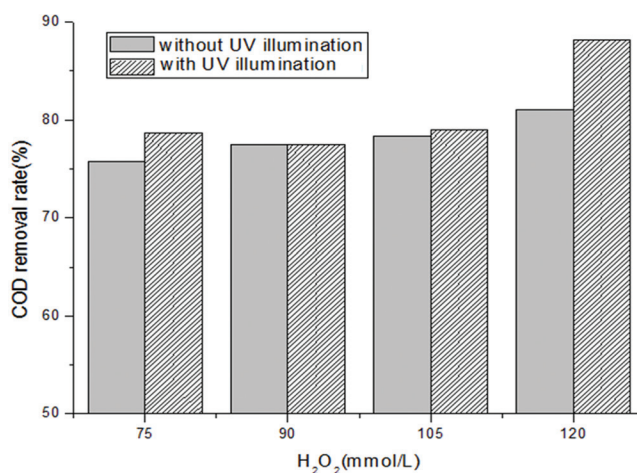


Figure 6. Effect of illumination on the degradation of organic pollutants.

reduction of ferric. During such processes, two types of hydroxyl radicals were produced for each hydrogen peroxide to reduce Fe^{3+} to Fe^{2+} . Therefore, the oxidation efficiencies of organic pollutants were increased [12]. In addition, some iron complex compounds were generated in the processes of photochemical reactions. It can also generate hydroxyl free radicals. A portion of organic matters were degraded under the irradiation of ultraviolet light.

Identification by GC-MS

The composition of coke plant wastewater before biochemical treatment was complex. The main organic matters contained phenol, benzene, pyrrole, naphthalene, imidazole, and carbazole. As shown in Table 4, main organic compounds were 3-methyl phenol ($\text{C}_7\text{H}_8\text{O}$), quinoline ($\text{C}_9\text{H}_7\text{N}$), phenol ($\text{C}_6\text{H}_6\text{O}$), indole ($\text{C}_8\text{H}_7\text{N}$), 2, 4-dimethyl phenol ($\text{C}_8\text{H}_{10}\text{O}$), 2-methyl phenol, butylated hydroxytoluene ($\text{C}_{15}\text{H}_{24}\text{O}$), as identified using GC-MS analysis.

After treated by UV-Fenton, most of the organic pollutants such as phenols, indoles and quinolines were

removed, as shown in Table 5. Only a small amount of butylated hydroxytoluenes, phenols, and docosanes were identified. Phenols, indoles and quinolines could hardly be detected. A small amount of chain alkanes were generated and part of the benzene ring was broken to produce some new substances.

CONCLUSIONS

The composition of coke plant wastewater is complex. Biodegradation of refractory organics, such as phenol substance, quinoline ($\text{C}_9\text{H}_7\text{N}$), indole ($\text{C}_8\text{H}_7\text{N}$), and butylated hydroxytoluene ($\text{C}_{15}\text{H}_{24}\text{O}$) were detected. Using UV—Fenton method, when the initial concentration of COD and $\text{NH}_3\text{-N}$ was 5080 mg/L and 329.9 mg/L, the removal rate was 88.0% and 58.4% respectively under the optimal condition. Under the optimal condition, the H_2O_2 concentration was 75 mmol/L; the ratio of H_2O_2 and Fe^{2+} ratio was 3:1; pH was 4 and the reaction duration was 30 min. Based on GC-MS analysis, lots of organic substances such as indole and quinoline were degraded effectively. UV—Fenton, as one of effective methods, can be used in advanced treatment for coke plant wastewater.

ACKNOWLEDGEMENTS

This study was financially supported by National Natural Science Foundation (51174031).

REFERENCES

- Zhang W, Wei C., Feng C, Yan B, Li N, Peng P, Fu J., "Coke plant wastewater treatment plant as a source of polycyclic aromatic hydrocarbons (PAHs) to the atmosphere and health-risk assessment for workers", *Science of the Total Environment*, Vol. 432, 2012, pp. 396–403. <http://dx.doi.org/10.1016/j.scitotenv.2012.06.010>
- Tiehm A, Kohnagel I., Neis U., "Removal of chlorinated pollutants by a combination of ultrasound and biodegradation", *Water Science and Technology*, Vol. 43, No. 2, 2001, pp. 297–303.
- Liu Q., Lu X., Liu J., "UV-Fenton preoxidation for phenolic wastewater biodegradability enhancement", *Henan, China, ICEEE* 1, 2010, pp. 185–191.
- Kaynak, G. Erden; Filibeli, "Assessment of Fenton Process as a Minimization Technique for Biological Sludge: Effects on Anaerobic Sludge Bioprocessing", *Journal of Residuals Science & Technology*, Vol. 5, No. 3, 2008, pp. 151–160.
- Sadik, W.A., El-Demerdash, A.M., Nashed, A.W., "UV-Induced decolorization of indophenol by heterogeneous advanced oxidation processes", *Polymer-Plastics Technology and Engineering*, Vol. 43, No. 6, 2004, pp. 1649–1655. <http://dx.doi.org/10.1081/PPT-200039991>
- Jemenez-Becerril, Jaime, Cesar Gonzalez-Juarez, Julio, Contreras-Bustos, Roberto, "Penetrant Liquid Waste Degradation by Radiocatalysis", *Journal of Residuals Science & Technology*, Vol. 10, No. 4, 2013, pp. 171–177.

Table 4. The Main Composition of the Raw Coke Plant Wastewater.

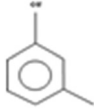
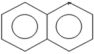
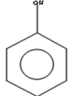
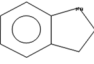
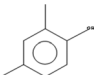
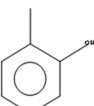
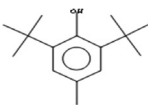
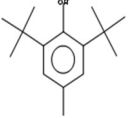
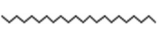
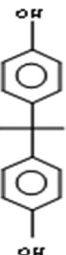
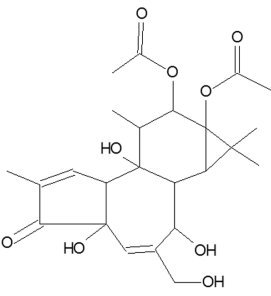
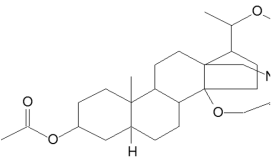
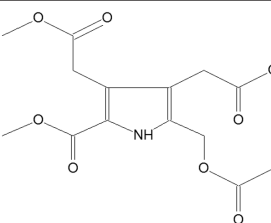
Molecular Structure	Content (%)	Formula	Compound	Number
	20.49	$\text{C}_7\text{H}_8\text{O}$	Phenol, 3-methyl-	1
	19.01	$\text{C}_9\text{H}_7\text{N}$	Quinoline	2
	16.56	$\text{C}_6\text{H}_6\text{O}$	Phenol	3
	12.25	$\text{C}_8\text{H}_7\text{N}$	Indole	4
	9.03	$\text{C}_8\text{H}_{10}\text{O}$	Phenol, 2,4-dimethyl-	5
	8.19	$\text{C}_7\text{H}_8\text{O}$	Phenol, 2-methyl-	6
	5.09	$\text{C}_{15}\text{H}_{24}\text{O}$	Butylated Hydroxytoluene	7

Table 4. The Constituents of Coke Plant Wastewater After Treatment by UV-Fenton.

Molecular Structure	Content (%)	Formula	Compound	Number
	40.65	C ₁₅ H ₂₄ O	ButylatedHydroxytoluene	1
	6.02	C ₂₂ H ₄₆	Docosane	2
	5.05	C ₁₅ H ₁₆ O ₂	Phenol, 4,4'-(1-methylethylidene)bis-	3
	3.79	C ₂₄ H ₃₂ O ₉	5H-Cyclopropa[3,4]benz[1,2-e]azulen-5-one, 9,9a-bis(acetyloxy)-1,1a,1b,2,4a,7a,7b,8,9,9a-decahydro-2,4a,7b-trihydroxy-3-(hydroxymethyl)-1,1,6,8-tetramethyl-	4
	3.49	C ₂₈ H ₄₃ NO ₆	(5á)Pregnane-3,20á-diol, 14á,18á-[4-methyl-3-oxo-(1-oxa-4-azabutane-1,4-diy)]-, diacetate	5
	3.46	C ₁₅ H ₁₉ NO ₈	1h-Pyrrole-3,4-diacetic acid, 2-acetoxymethyl-5-methoxycarbonyl-, dimethyl ester	6

- Leong S. K., Bashah N. A. A., "Kinetic Study on COD Removal of Palm Oil Refinery Effluent by UV-Fenton", *APCBEE Procedia*, Vol. 3, 2012, pp. 6–10. <http://dx.doi.org/10.1016/j.apcbee.2012.06.037>
- Chang M. W., Chung C. C., Chen J. M., Chen T. S., "Dye decomposition kinetics by UV/H₂O₂: Initial rate analysis by effective kinetic modeling methodology", *Chemical Engineering Science*, Vol. 65, 2010 pp. 135–140. <http://dx.doi.org/10.1016/j.ces.2009.01.056>
- Vassileva P., Dimitrinka V., "Investigation on natural and pretreated Bulgarian clinoptilolite for ammonium ions removal from aqueous solutions", *Journal of Hazardous Materials*, Vol. 170, 2009, pp. 948–953. <http://dx.doi.org/10.1016/j.jhazmat.2009.05.062>
- Tang H., Xiang Q., Lei M., Yan J., Zhu L., Zou J., "Efficient degradation of perfluorooctanoic acid by UV-Fenton process", *Chemical Engineering Journal*, Vol. 184, 2012, pp. 156–162. <http://dx.doi.org/10.1016/j.cej.2012.01.020>
- Utset B., Garcia J., Casado J., Domènech X., Peral J., "Replacement of H₂O₂ by O₂ in Fenton and photo-Fenton reactions", *Chemosphere*, Vol. 41, No. 11, 2000, pp. 87–92. [http://dx.doi.org/10.1016/s0045-6535\(00\)00011-4](http://dx.doi.org/10.1016/s0045-6535(00)00011-4)
- Pignatello J J, Oliveros E, MacKay A., "Advanced oxidation processes for organic contaminant destruction based on the Fenton reaction and related chemistry", *Critical Reviews in Environmental Science and Technology*, Vol. 36, No. 1, 2006, pp. 1–84. <http://dx.doi.org/10.1080/10643380500326564>

The Strength and Durability Studies of Cement Mortar Blended with Solar PV Cells

SUNG-CHING CHEN¹, RAN HUANG¹, HUI-MI HSU^{2,*} and LI-WEI TENG³

¹Department of Harbor and River Engineering, National Taiwan Ocean University, Keelung 202, Taiwan

²Center for Sustainable Development, National Ilan University, Yilan 260, Taiwan

³Department of Civil Engineering, National Ilan University, Yilan 260, Taiwan

ABSTRACT: In this article we demonstrated the study of strength and durability of cement paste blended with waste solar PV cells. In order to investigate the corresponding performance of both strength and durability due to the sustainable use of solar PV panels in cement-based composite, in which the cement was replaced with amorphous PV powders from discarded solar PV panels with a high proportion of silicon dioxide. The conclusions were made on effect of this cement replacement. The use of ground solar cells for various properties of cement-based composite was investigated, and as a result, we identified the factors affecting the strength and durability for those of cement mortar specimens which had predefined and made in laboratory. As a summary, using solar PV cells as the cement replacement did not perform well from a strength perspective while it did give a better performance of durability.

INTRODUCTION

ALKALI-ACTIVATION of slag, fly ash and other alumino-silicate materials have been fully studied for a long time [1–3]. Compared with conventional Portland cement-based composites, these materials may provide better durability in chemically aggressive environment [4], high compressive strength [5,6], lower basic creep [7], or environmental benefits [3]. The main purpose of this paper aims at the properties of alkali-activated materials in solar PV cells. None comprehensive study has been performed in this subject, even though a few attempts or related studies [8–12] could be found.

Solar panels now provide a safe, reliable, cost-effective, and eco-friendly solution for both distributed and centralized energy generation. It's expected that solar panel and its products will be a huge technological advancement in the coming time. Even now, solar power has become the fastest growing renewable energy, but with a great number of end-of-life panels being generated; it is quite important to start thinking ahead how to take care of the recycling of end-of-life panels. In many countries, the implementation of the take-back and recycling scheme has been financed from the green

viewpoint. Now, we may need to not just reduce in component incineration in favor of an increased volume of recycled panels, but also recover their values from those end-of-life panels by putting more efforts on recycling or sustainability researches.

Since solar power is the energy that is collected from the heat that the sun exerts, special gadgets such as a solar panel and a couple of other things are needed in order to collect solar power so that it can be converted into usable energy. A solar panel, also known as photovoltaic (PV) panel, is an assemblage of solar cells that convert sunlight into electricity and it is the most important part of any solar electric energy system. Solar panels contain many PV cells to produce electricity by light. Most Solar panels which are made up of the chemical property silicon comprise two layers which are linked to each other by an accumulating circuitry, and its lower layer is made of polymer. These two layers are chemically treated so that it becomes reversed electrically. Under sunlight, the lower layer's electrons move up by the accumulating circuit and assemble with the ones in the upper layer through an external circuit then to provide power to a system attaching to the panel.

For a standard solar PV panel (nearly 90% of all solar panels installed), the core components such as silicon, silver, aluminum and glass are all recyclable and all of which comprise over 90% of the weight of

*Author to whom correspondence should be addressed.
Email: hmhsu@niu.edu.tw

a standard solar PV panel. There is insufficient understanding in current literature on solar cells, not those extruded aluminum frames and glass. Therefore, it's realized that the solar recycling process should be attempted on the solar cells, comprised primarily of silicon, silver and aluminum. The process usually requires the solar cells to be ground into chips, flakes or powders. At this point, it is usually mixed with a lot of impurities. As a result, this solar cycling process is usually down streamed. In other words, instead of turning solar cells into new ones, the material is better used as feedstock for other manufacturing processes. For example, they can be utilized in the production of products like concrete. There, the main purpose of this study is to investigate the use of ground solar cells only for the cement-based composite.

THE PV COMPONENTS

For a standard solar PV cell, chemically analyzing the ground powder on its components, it revealed those of compounds as shown in Table 1, the maximum one is silicon dioxide (silica), 75.9%. Meanwhile, toxicity characteristic leaching procedure (TCLP) employed as an analytical method to find toxic chemicals in the powder indicated no those heavy metals as listed in Table 2.

TEST SPECIMENS

In order to investigate the influence of the fineness of solar PV panels, the cement was replaced with amorphous PV powders from discarded solar PV panels with a high proportion of silicon dioxide. A ball mill was used in grinding (or mixing) solar PV cells to two sizes of powders with an average diameter of 75 μm (No. 200) and 45 μm (No. 325) respectively to be prepared.

Table 1. Analysis for Components.

Component*	(%)	Component**	(mg/kg)
SiO ₂	75.9	Ag	5000
Na ₂ O	8.5	Pb	Not Detected
CaO	6.2	Cr	Not Detected
Fe ₂ O ₃	0.3	Cd	Not Detected
Al ₂ O ₃	0.1	Zn	Not Detected
MgO	2.9	Cu	Not Detected
SO ₃	2.4	Ni	Not Detected
K ₂ O	0.0		

*By XRF.

**By FLAA.

Table 2. TCLP Analysis.

Metal	(mg/L)
Pb	Not Detected
Cr	Not Detected
Cd	Not Detected
Zn	Not Detected
Cu	Not Detected
Ni	Not Detected

A total of 18 test specimens were made in a lab. Each specimen was denoted as shown in Table 3 by 2 characters and 1 number in a row, in which the first character A (B) represents a water-cement ratio of 0.35 (0.55), the second character A (B) represents a No. 200 (325) sieve, and the last number represents amount of replaced cement in terms of weight %, 0%, 5%, 10%, 15%, or 20%.

THE SLUMP TESTS

A slump test is majorly used to measure the workability of each freshly mixed cement mortar. Table 4 and Table 5 list the slumps for two different of water-cement ratios, respectively. In general, the larger the water-cement ratio the higher the slump will be. This is the case as shown in the difference between Tables 4 and 5. Furthermore, the slump is clearly related to both the fineness of PV powders and the cement replacement. The larger slump the higher fineness will be

Table 3. Mortar Mix of Test Specimens (Unit: kg/m³).

Mix	w/c	Water	Cement	PV Powder	Sand
AA0	0.35	197	563	0	1448
AA5	0.35	197	535	28	1448
AA10	0.35	197	507	56	1448
AA15	0.35	197	479	84	1448
AA20	0.35	197	450	113	1448
AB5	0.35	197	535	28	1448
AB10	0.35	197	507	56	1448
AB15	0.35	197	479	84	1448
AB20	0.35	197	450	113	1448
BA0	0.55	278	505	0	1389
BA5	0.55	278	480	25	1389
BA10	0.55	278	455	51	1389
BA15	0.55	278	429	76	1389
BA20	0.55	278	404	101	1389
BB5	0.55	278	480	25	1389
BB10	0.55	278	455	51	1389
BB15	0.55	278	429	76	1389
BB20	0.55	278	404	101	1389

Table 4. Slump of Mix Under w/c= 0.35 (Unit: cm).

Mix	Slump	Mix	Slump	Difference	(mg/L)
AA0	12.8	–	–	–	
AA5	11.9 (–7%)	AB5	13.23 (3%)	10%	
AA10	10.93 (–15%)	AB10	11.67 (–9%)	6%	↑
AA15	11.13 (–13%)	AB15	11.63 (–9%)	4%	
AA20	11.47 (–10%)	AB20	11.73 (–8%)	2%	
		→			increase

and quantitatively, especially it only exhibits the larger increase with the lower cement replacement volumes.

Besides, the higher the slump, the more workable the concrete will be. On the other hands, the higher the slump, the weaker the mortar mix will be. The additional ingredients in modern concrete mixes make it impossible to determine concrete quality from slump, however. Nevertheless, low slump values in traditional mixes generally mean higher quality concrete. Thus, the slump still plays an important role to be a symbolic representation of concrete quality.

THE COMPRESSIVE STRENGTHS

The concrete compressive strengths in age 7 or 28 days were obtained and tabulated in Tables 6 to 9 depending on the combination of the water-cement ratio and sieve No. Comparing to the control specimens, these tables show that there were only 5 specimens as denoted in diagonal slash marks, which obtained the larger concrete compressive strengths increase on both cases (7 or 28 days).

THE WATER ABSORPTION

The amount of water absorption is determined by the gain in weight of a dry specimen on immersion in water under specified conditions, test resulting obtained and tabulated in Tables 10–13 depending on the combination of the water-cement ratio and sieve No. Water absorption obviously increases as the amount of

Table 5. Slump of Mix Under w/c= 0.55 (Unit: cm).

Mix	Slump	Mix	Slump	Difference	(mg/L)
AA0	21.47	–	–	–	
AA5	21.6 (1%)	AB5	24.00 (12%)	11%	
AA10	23.6 (10%)	AB10	24.93 (6%)	4%	↑
AA15	22.03 (3%)	AB15	22.77 (6%)	3%	
AA20	22.30 (4%)	AB20	21.53 (0%)	–4%	
		→			increase

Table 6. Compressive Strength (w/c = 0.35 & No. 200).

Mix	Compressive Strength (MPa)	
	7 Days	28 Days
AA0	46.7	59.9
AA5	52.2 (12%)	64.8 (8%)
AA10	49.3 (6%)	60.5 (1%)
AA15	45.8 (–2%)	59.4 (–1%)
AA20	43.1 (–8%)	59.0 (–2%)

Table 7. Compressive Strength (w/c = 0.35 & No. 325).

Mix	Compressive Strength (MPa)	
	7 Days	28 Days
AB0	46.7	59.9
AB5	51.4 (10%)	62.8 (5%)
AB10	49.7 (6%)	63.3 (6%)
AB15	44.0 (–6%)	63.1 (5%)
AB20	44.2 (–5%)	58.4 (–3%)

Table 8. Compressive Strength (w/c = 0.55 & No. 200).

Mix	Compressive Strength (MPa)	
	7 Days	28 Days
BA0	35.4	44.3
BA5	31.1 (–12%)	40.7 (–8%)
BA10	30.7 (–13%)	43.1 (–3%)
BA15	29.2 (–18%)	45.7 (3%)
BA20	28.7 (–19%)	42.2 (–5%)

Table 9. Compressive Strength (w/c = 0.55 & No. 325).

Mix	Compressive Strength (MPa)	
	7 Days	28 Days
BB0	35.4	44.3
BB5	37.3 (5%)	48.7 (10%)
BB10	33.4 (–6%)	43.3 (–2%)
BB15	31.8 (–10%)	33.6 (–24%)
BB20	25.8 (–27%)	43.7 (–1%)

Table 10. The Water Absorption (w/c = 0.35 & No. 200).

Mix No.	Absorption (%)		
	7 Days	28 Days	
AA0	0.060	0.051	increase
AA5	0.058 (-3%)	0.047 (-8%)	
AA10	0.054 (-10%)	0.045 (-12%)	↑
AA15	0.06 (0%)	0.041 (-20%)	
AA20	0.058 (-3%)	0.041 (-20%)	

Table 11. The Water Absorption (w/c = 0.35 & No. 325).

Mix No.	Absorption (%)		
	7 Days	28 Days	
AA0	0.060	0.051	increase
AB5	0.057 (-5%)	0.038 (-25%)	
AB10	0.058 (-3%)	0.032 (-37%)	↑
AB15	0.058 (-3%)	0.028 (-45%)	
AB20	0.058 (-3%)	0.026 (-49%)	

Table 12. The Water Absorption (w/c = 0.55 & No. 200).

Mix No.	Absorption (%)		
	7 Days	28 Days	
BA0	0.08	0.074	increase
BA5	0.089 (11%)	0.076 (3%)	
BA10	0.094 (18%)	0.079 (7%)	↑
BA15	0.092 (15%)	0.072 (-3%)	
BA20	0.095 (19%)	0.07 (-5%)	

Table 13. The Water Absorption (w/c = 0.55 & No. 325).

Mix No.	Absorption (%)		
	7 Days	28 Days	
BA0	0.08	0.074	increase
BB5	0.089 (11%)	0.083 (12%)	
BB10	0.09 (13%)	0.081 (9%)	↑
BB15	0.08 (0%)	0.076 (3%)	
BB20	0.089 (11%)	0.08 (8%)	

porosity increases there must be voids (pores) for the water to be absorbed in or enter into the body of the specimen. The results reveal that large w/c ratio and high fineness exhibit lower water absorption or less porosity, which also applies to the more cement replacement as indicated in these tables.

THE SULPHATE RESISTANCE

The anti-sulphate ability was investigated by examining the performance for putting those specimens in sulfate environment, which experienced dry-wet cycles in sodium sulfate solution. The parameter, loss ratio of weight, was investigated to express the durability performance of specimens. Thru 5 cycles of repeating tests, results were obtained and tabulated in Tables 14–17 depending on the combination of the water-cement ratio and sieve No.

As we found out in these tables, w/c = 0.35 & No. 325 was the worst case. On the contrary, w/c = 0.55 & No. 325 was the best one. Both cases had the same sieve No (fineness) with different w/c ratios. In other words, the anti-sulphate ability was more sensitive on the water-cement ratio rather than fineness. Besides, for the sulphate resistance the 20% of the cement replacement should be the best choice even though it varied quite sharply at only one case, namely w/c = 0.55, No. 200.

CONCLUSIONS

In this article we demonstrated the study of strength and durability of cement mortars blended with waste solar PV cells. The conclusions were made on effect of this cement replacement. The use of ground solar cells on the various properties of cement-based composite was investigated.

The slump is clearly related to both the fineness of PV powders and the cement replacement. The larger slump the higher fineness will be and quantitatively, especially it only exhibits the larger increase with the lower cement replacement volumes. Observing a large cement replacement to 20% under w/c = 0.35, the slump is almost unaffected by the fineness of PV powders, while the non-affection applies to both the fineness of PV powders and the cement replacement for the same situation but under w/c = 0.55. Using concrete additives should substantially increase the density, strength and ability to sculpt, texture and trowel the concrete. In other words, the observation may provide an adjustment among the slump, fineness, cement replacement and the water-cement ratio.

Table 14. The Sulphate Resistance by Weight Loss (w/c = 0.35 & No. 200).

Mix No.	Cycle 1 (%)	Cycle 2 (%)	Cycle 3 (%)	Cycle 4 (%)	Cycle 5 (%)
AA0	0.000	-0.015	-0.024	-0.037	-0.024
AA5	0.000	-0.017	-0.022	-0.035	-0.022
AA10	0.000	-0.015	-0.020	-0.031	-0.024
AA15	0.000	-0.018	-0.024	-0.033	-0.020
AA20	0.000	-0.015	-0.027	-0.042	-0.035

Table 15. The Sulphate Resistance by Weight Loss (w/c = 0.35 & No. 325).

Mix No.	Cycle 1 (%)	Cycle 2 (%)	Cycle 3 (%)	Cycle 4 (%)	Cycle 5 (%)
AA0	0.000	-0.015	-0.024	-0.037	-0.024
AB5	0.000	-0.015	-0.013	-0.017	-0.006
AB10	0.000	-0.013	-0.013	-0.013	-0.007
AB15	0.000	-0.015	-0.015	-0.022	-0.013
AB20	0.000	-0.013	-0.018	-0.020	-0.013

Table 16. The Sulphate Resistance by Weight Loss (w/c = 0.55 & No.200).

Mix No.	Cycle 1 (%)	Cycle 2 (%)	Cycle 3 (%)	Cycle 4 (%)	Cycle 5 (%)
BA0	0.000	-0.021	0.000	-0.011	-0.030
BA5	0.000	-0.018	-0.005	-0.011	-0.032
BA10	0.000	-0.011	-0.007	-0.007	-0.025
BA15	0.000	-0.005	-0.002	-0.002	-0.023
BA20	0.000	-0.009	-0.007	-0.007	-0.016

Table 17. The Sulphate Resistance by Weight Loss (w/c = 0.55 & No.325).

Mix No.	Cycle 1 (%)	Cycle 2 (%)	Cycle 3 (%)	Cycle 4 (%)	Cycle 5 (%)
BA0	0.000	-0.021	0.000	-0.011	-0.030
BB5	0.000	-0.021	-0.028	-0.035	-0.046
BB10	0.000	-0.018	-0.021	-0.032	-0.050
BB15	0.000	-0.016	-0.016	-0.028	-0.021
BB20	0.000	-0.021	-0.010	-0.088	-0.121

The concrete compressive strengths in age 7 or 28 days were obtained, comparing to the control specimens, 5 of 18 specimens obtained the larger concrete compressive strengths increase on both cases. In other words, using solar PV cells as the cement replacement did not perform well from a strength perspective.

The water absorption reveal that large w/c ratio and high fineness exhibit lower water absorption or less porosity, which also applies to the more cement replacement as indicated in these tests.

As far as the anti-sulphate ability is concerned, w/c = 0.35 & No. 325 was the worst case; on the contrary, w/c = 0.55 & No. 325 was the best one. Both cases had the same sieve No (fineness) with different w/c ratios. In other words, the anti-sulphate ability is more sensitive on the water-cement ratio rather than fineness. Besides, for the sulphate resistance the 20% of the cement replacement should be the best choice even though it varied quite sharply at only one case, namely w/c = 0.55, No. 200.

In the following study, we may use alkali activator to improve the activity of alkali-activated materials in solar PV cells so as to replace Portland cement as binder in concrete. A high-pH environment is generated by using sodium silicate and sodium hydroxide as alkali-activator to excite the binding characteristics of possible alkali-activated materials in solar PV cells.

REFERENCES

1. F. Pacheco-Torgal, J. Castro-Gomes, S. and Jalali, "A review: Part 1. Historical background, terminology, reaction mechanisms and hydration products", *Constr. Build. Mater.* 22(7), 2008, pp.1305–1314. <http://dx.doi.org/10.1016/j.conbuildmat.2007.10.015>
2. P. Duxson, A. Fernández-Jiménez, J. Provis, G. Lukey, A. Palomo, and J. van Deventer, "Geopolymer technology: the current state of the art", *Asian J. Mater. Sci.*, Vol. 42(9), 2007, pp.2917–2933. <http://dx.doi.org/10.1007/s10853-006-0637-z>
3. J. Provisand, J. van Deventer. 2009, *Geopolymers: structures, processing, properties and industrial applications*, Woodhead Publishing Ltd. <http://dx.doi.org/10.1533/9781845696382>
4. A. Fernández-Jiménez, I. García-Lodeiro, and A. Palomo, "Durability of Alkali-Activated Fly Ash Cementitious Materials", *J. Mater. Sci.*, Vol. 42, 2007, pp. 3055–65. <http://dx.doi.org/10.1007/s10853-006-0584-8>
5. M. Komljenović, Z. Bašćarević, and V. Bradić, "Mechanical and microstructural properties of alkali-activated fly ash geopolymers", *J. Hazard. Mater.*, Vol. 181, 2010, pp. 35–42. <http://dx.doi.org/10.1016/j.jhazmat.2010.04.064>
6. S.A. Bernal, MejíaR. De Gutiérrez, A.L. Pedraza, J.L. Provis, E.D. Rodríguez, and S. Delvasto, "Effect of binder content on the performance of alkali-activated slag concretes", *Cem. Concr. Res.*, Vol. 41, 2011, pp. 1–8. <http://dx.doi.org/10.1016/j.cemconres.2010.08.017>
7. S.E. Wallahand B.V. Rangan, "Low-calcium fly ash-based geopolymer concrete: long term properties", Research report GC2, Curtin University of Technology, Perth, Australia.

8. L.W. Teng, R. Huang, H.M. Hsu, A. Cheng, J.R. Chang and P.H. Yu, "Strength Quality Research of Cement Mortar Blended with Solar PV Cells", *Adv. Mater. Res.* Vol. 1025–1026, 2014, pp. 1025–1030. <http://dx.doi.org/10.4028/www.scientific.net/AMR.1025-1026.1025>
9. S.C. Chen, R. Huang, H.M. Hsu, L.W. Teng and Y.P. Lai, "Durability Quality Research of Cement Mortar Containing Solar PV Cells", *Adv. Mater. Res.* Vol. 1025–1026, 2014, pp. 1020–1024. <http://dx.doi.org/10.4028/www.scientific.net/AMR.1025-1026.1020>
10. S.C. Chen, R. Huang, H.M. Hsu, J.R. Chang and L.W. Teng, "Strength-Quality Research of Concrete Blended with Solar PV Cells", *Adv. Mater. Res.* Vol. 1061–1062, 2014, pp. 392–395. <http://dx.doi.org/10.4028/www.scientific.net/AMR.1061-1062.392>
11. T.Y. Qi, G.R. Feng, Y.J. Zhang, J. Guo and Y.X. Guo, "Effects of Fly Ash Content on Properties of Cement Paste Backfilling", *J. of Residuals Science & Technology*, Vol. 12, No. 3, 2015, pp. 133–141. <http://dx.doi.org/10.12783/issn.1544-8053/12/3/3>
12. J.Y. Sun, Y.N. Yang and M. Zheng, "Double Consolidation Technology for the Stabilization of Heavy Metal Ions in the Fly Ash Generated by the Incineration of Municipal Solid Waste", *J. of Residuals Science & Technology*, Vol. 12, Supplement 1, 2015, pp. 31–37.

Separating and Recycling of Fe, Cu, Zn from Dumped Copper Slag by Microwave Irradiation Assisted Carbothermic Method

YALONG LIAO*, JUAN ZHOU and FEIRONG HUANG

Faculty of Metallurgical & Energy Engineering, Kunming University of Science & Technology, Kunming 650093, China

ABSTRACT: Iron, copper and zinc were separated and recycled from dumped copper slag using a carbothermic method in the presence of microwave irradiation. Iron in the form of fayalite and magnetite in the slag was reduced to metal iron while zinc was evaporated and captured as zinc oxide powder. Results indicated that metallization rate of iron could reach 91.38~93.45 wt% and zinc recovery efficiency was 90.5 wt% when the new methodology was employed, and that reaction temperature was 100°C lower compared to that of traditional processes, reaction time of the new process was decreased by 90 min.

INTRODUCTION

MILLIONS of tons of dump copper slag quenched with water in metallurgical plant were dumped each year, which not only employed lots of land resources but also caused serious environmental problems [1–3]. Additionally it was proved that copper slag is a source of valuable metals including iron, copper, and zinc. Recovering metals from metallurgical residues, therefore, have become increasingly important. However, mineralogical structure and the size of phase particulate within copper slag could be influenced by many factors such as separation processes, instruments and cooling methods [4–7]. Slow cooling often results in crystallization of slag constituent, and forms a great many different mineral phases. On the contrary, fast cooling results in an amorphous and homogeneous case with respect to metal distribution. When copper slag is cooled with water, there are usually crystalline liking fayalites along with other silicates and vitreous. The content of iron in vitreous is nearly the same as that in fayalite. Due to fine mineral dissemination, complex mineralogical composition, and especially the fact that iron in the slag is mainly in fayalite (Fe_2SiO_4) and vitreous, recovering those valuable constituents such as iron, copper and zinc by traditional approaches is very challenging.

Numerous methodologies for recovering metals from slag produced in copper smelters were reported in

the literature. Such methods mainly focus on flotation separation [8], leaching [9–12], reducing [13], roasting [14,15], and pyrometallurgical impoverishment [16–19]. Progresses have been made for both product quality and recovery efficiency. Most of the raw materials of copper slag used in these investigations, however, were often from converter furnace slag or brass melting slag which contained high grading Cu, Co, and/or Ni. The grade of Cu in these kinds of slag was greater than 3.5 wt%, and most of copper mineralogical phase in the slag was sulphide. Some studies demonstrated that dump copper slag was applied in several domains including architecture industry, cement manufacture, road construction, and civil engineering, etc [20–22]. However, few studies focused on recovery or utilization of valuable metals in the dump copper slag quenched with water.

Though there are numerous valuable metals in dump copper slag, recovery of copper has drawn increasing attention. It is difficult to recycle copper or zinc in the slag due to the fact that iron could limit and influence the efficiency of copper recovery. It is therefore reasonable to recycle iron before recovering other valuable metals. The aim of this study is to exam reduction of ferrous in the form of ferrous compounds such as fayalite, magnetite and ferrous oxide in the slag with Cu 0.93 wt%, Zn 1.14 wt%, and Fe 39.82 wt%. The carbothermic processes assisted with microwave irradiation was adopted to first reduce FeO in the form of fayalite Fe_2SiO_4 and Fe_2O_3 to recover Fe. Accordingly zinc silicates in the slag were reduced to zinc metal which volatilized in fume. The product from the carbo-

*Author to whom correspondence should be addressed.
E-mail: liaoylsy@163.com; Tel: 86-871-65198154

ermic reduction was further used to separate Cu from iron using magnetic separation and gravity separation processes.

EXPERIMENT

Materials and Instrument

Instruments in this study are listed below: Rod pulverizer (Kunming University of science & technology), Vacuum filters, electrothermal blast drying box (GZX-9030-MBE, Shanghai medical equipment Co. Ltd), microwave furnace (Kunming University of science & technology), thermocouple (NK-130), digital temperature meter (XMT-1300), X-ray diffraction meter (XRD) (Bruker, Germany), and Electrical resistance furnace SX2-10-13 (Yifeng Shanghai, China).

Materials are listed as follows: copper slag (Produced in a smelter, Yunnan Province China), calcium oxide (chemical grade, CaO > 99 wt%), anthracite (fixed carbon 76.4 wt%), and binder.

Mineralogical Composition Analysis

The characterization methods using electro microscope, electro probe and X-ray diffraction (XRD) were employed in this study. Powder samples of copper slag and reduction products were analyzed by XRD technique using BRUKER D8ADVADCE (Germany) apparatus with a detection limit of 3 wt%.

Reduction Procedure

All the materials used in experiment such as copper slag, calcium oxide, and anthracite were grounded to particle sizes, 80 wt% of which were screened through 0.074 mm sieve. 100 g copper slag, a certain amount of anthracite coal and calcium oxide was put in a mortar for grinding. After fully mixed, it was added with binder to pellet in the form of balls with a diameter of about 1 cm. The pellets were then dried at 120°C for 2 h. The dried pellets were treated further with two different methods. One was placed in the microwave oven equipped with thermocouple to heat up to a specified temperature and kept for some time. For comparison, the other one was placed in electrical resistance furnace (SX2-10-13) for reacting for some time at specified temperature. The samples were removed from the oven when its temperature was below 400°C. It was cooled down to room temperature before further analysis of the components and recovery efficiency.

Table 1. The Composition of Copper Smelting Slag.

Item	T _{Fe}	MgO	CaO	SiO ₂	Al ₂ O ₃	Cu	Zn	S
Content %	39.82	1.32	3.06	34.90	3.66	0.936	1.14	0.31

Zinc silicates and zinc oxide in the slag were reduced to zinc violating in fume which could be captured as zinc oxide powder. The reductive product was pulverized to a particle size with diameter of 0.045 mm. Cu was then separated from iron by means of magnetic separation and recycled by gravity separation process.

RESULTS AND DISCUSSION

Composition and Structure of Raw Material

Copper slag was analyzed with optical sheet identification, x-ray diffraction analysis, manual panning, electron microscope and electron microprobe analysis. Results of chemical composition and mineralogical composition and distribution of iron in the dump copper slag were displayed in Table 1 and Table 2. There were lots of valuable metals in dump copper slag such as copper, zinc and iron, with relatively high percentage of iron in it. The grade of copper in the slag was 0.936 wt %, while iron was 39.82 wt%, and zinc was 1.14 wt%, as shown in Table 1.

From Table 2, it could be found that the slag was a mixture of multiple metals in mineralogy phases. The main composition was vitreous phase and fayalite. As for iron, two kinds of iron were found in copper slag. On the one hand, crystal phases such as magnetite, fayalite, and bornite exist. On the other hand, atoms of such metals were distributed in the vitreous phase. The proportion of Fe in the form of fayalite accounted for 43.82 wt% and it was 45.29 wt% for the form of vitreous. Magnetite was 10.46 wt% and bornite only accounted for 0.42 wt%.

Characterization of Reduction Products

Metallization rates in different method were dis-

Table 2. Distribution of Iron Composition of Slag.

Items	Proportion, %	Fe Content, %	Fe Distribution, %
Bornite	1.0	17.0	0.42
Magnetite	7.0	60.0	10.46
Fayalite	44.5	39.5	43.82
Vitreous	46.0	39.5	45.29
Total	98.5		99.99

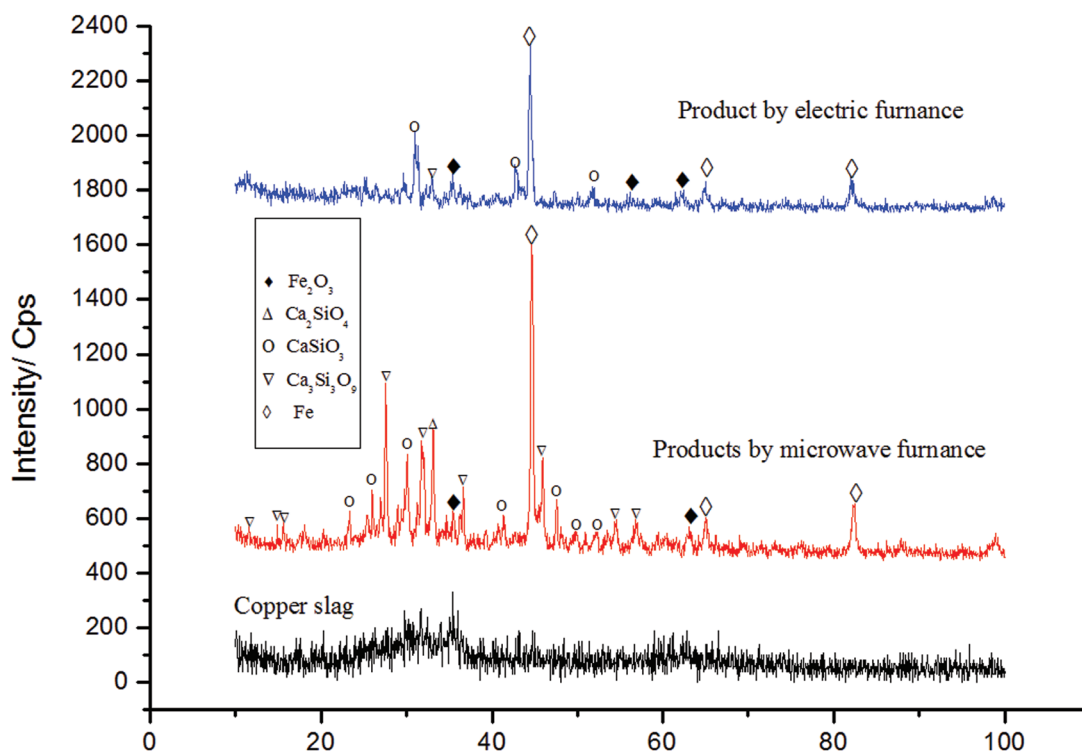


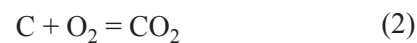
Figure 1. XRD pattern of products and raw material.

played in Table 3. Metallization rate of iron accounted for 88.26 wt% for the traditional carbothermic method, but it was 92.46 wt% when reduced by microwave-assisted carbothermic method. Both reaction temperature and reaction duration were decreased substantially when microwave irradiation was adopted.

Figure 1 shows the X-ray diffraction graphs of raw material and reduction products. It could be found that copper slag before reduction was in vitreous phase, fayalite and vitreous phase. It could also be found that most of the iron was in metal iron in the reduction products and most of SiO_2 in the reduction products combined with CaO to form calcium silicate. There was little ferrous oxide in the products by microwave-assisted method compared to the reduction products by electric furnace. Accordingly the intensity of metal iron and calcium silicates by microwave-assisted reduction was more outstanding than that of the corresponding substance by electric furnace.

The mechanism of iron recovery from copper slag

could be described in the following chemical reactions:



Under the condition of high temperature, iron olivine (Fe_2SiO_4) in the slag could react with calcium oxide [see Equation (1)]. Equation (2) shows that portion of carbon reacts with oxygen in the air to form carbon dioxide at low temperature. Equation (3) shows that carbon dioxide generated in Equation (2) could react with carbon to form carbon monoxide at a temperature that is higher than 980°C . This denotes that carbon monoxide is the main constituent in the atmosphere of the process when temperature is more than 980°C . As carbon monoxide has strong reductive properties, iron

Table 3. The Iron Metallization Rate by Different Method.

No.	Experimental Parameters						Metallization Rate, %
	Furnace	Slag, g	C, g	CaO, g	Temp., $^\circ\text{C}$	Time, min	
1	SX2-10-13	100	30	20	1200	240	88.20
2	Micr. Furnace	100	30	20	1100	90	92.46

oxide (FeO) could be converted to metallic iron (Fe) as shown in Equation (4).

Microwave heating is a type of molecule inner heating since it causes vibration between molecules to produce energy. It can heat the material from both inside and outside, where temperature was uniform. Additionally, carbon has good capacity of microwave absorption. Therefore while carbothermic reduction with microwave irradiation was employed to reconstruct mineralogy in the copper slag and reduce ferrous compounds to metal iron, microwave irradiation served at least two functions. One was the catalyst of the chemical reductive reaction. The other was to accelerate the increase of temperature by eliminating heat transfer restrictions which were required in traditional recovery method.

Orthogonal Conditions Experimental

Based on the mechanism of iron recovery from copper slag [Equations (1)–(4)], several factors, e.g., temperature, time and reactants, could influence the proficiency of the process. Therefore orthogonal experiments considering four affecting factors and three different levels were carried out. Oxidation calcium, anthracite, reaction temperature and reaction time were the four affecting factors adopted in the process, as shown in Table 4; orthogonal experimental results are shown in Table 5.

From Table 5 it can be found that both anthracite and reaction temperature have great influences on metallization efficiency. The optimal conditions for recovering iron metals from copper slag in the carbon-thermal reduction process assisted by microwave irradiation

Table 4. Different Factors Influencing Reaction.

Items	C, g	CaO	Temp., °C	Time, min.
Level one	10	10	1000	30
Level two	20	20	1100	90
Level three	30	30	1200	150

were 30 g of anthracite, 20 g of calcium oxide at the temperature of 1100°C, for 90 min.

Experiment Results under the Optimizing Conditions

According to the optimal conditions determined by orthogonal experiments several experiments were carried out to verify such conditions. 100 g of copper slag, 30 g of anthracite and 20 g of calcium oxide were mixed with blinder to pellet in the form of balls with a diameter of about 1cm. The dried mixture pellet was placed in a microwave oven to reduce at 1100°C for 90 min. Compared to the result of microwave oven samples, the same constituent were placed in the electro-resistance furnace to reduce at 1200°C for 240 min. The metallization rate of iron in each experiment was displayed in Table 6.

Table 6 indicated that iron metallization rate ranges between 91.38 wt% and 93.45 wt% under the conditions determined by orthogonal experiments. On the contrary, metallization rate was between reached 87.80 wt% and 88.48 wt% when copper slag was reduced in electro-resistance furnace even under higher reaction temperature and longer residue time.

Table 5. Results of Orthogonal Conditions Experimental.

No.	Experimental Parameters					Metallization Rate, %
	Copper Slag, g	C, g	CaO, g	Temp., °C	Time, min	
1	100	10	10	1000	30	51.13
2	100	10	20	1100	90	80.86
3	100	10	30	1200	150	67.29
4	100	20	10	1100	150	77.23
5	100	20	20	1200	30	88.92
6	100	20	30	1000	90	66.97
7	100	30	10	1200	90	86.81
8	100	30	20	1000	150	70.07
9	100	30	30	1100	30	90.26
Level One Average		66.43	71.72	62.72	76.77	
Level Two Average		77.71	79.95	82.77	78.21	
Level Three Average		82.23	74.84	81.00	71.53	
Range		15.80	7.23	20.05	6.68	

Range = highest average – lowest average.

Table 6. Results of Optimizing Conditions Experiment.

No.	Experimental Parameters					Metallization Rate, %	Comment
	Copper Slag, g	C, g	CaO, g	Temp., °C	Time, min		
1	100	30	20	1100	90	92.38	Microwave
2	100	30	20	1100	90	91.56	Microwave
3	100	30	20	1100	90	92.80	Microwave
4	100	30	20	1100	90	91.38	Microwave
5	100	30	20	1100	90	92.15	Microwave
6	100	30	20	1100	90	93.26	Microwave
7	100	30	20	1100	90	92.70	Microwave
8	100	30	20	1100	90	91.85	Microwave
9	100	30	20	1100	90	93.10	Microwave
10	100	30	20	1100	90	93.45	Microwave
11	100	30	20	1200	240	87.98	Traditional
12	100	30	20	1200	240	88.25	Traditional
13	100	30	20	1200	240	88.35	Traditional
14	100	30	20	1200	240	87.82	Traditional
15	100	30	20	1200	240	88.48	Traditional
16	100	30	20	1200	240	88.32	Traditional
17	100	30	20	1200	240	88.25	Traditional
18	100	30	20	1200	240	88.35	Traditional
19	100	30	20	1200	240	87.80	Traditional
20	100	30	20	1200	240	88.40	Traditional

Zinc Recycling

Zinc silicates in copper slag were reduced to metallic zinc and evaporated in the fume. The metallic zinc was captured as zinc oxide product while the copper slag pellets were reduced by carbothermic method. All of zinc oxide were collected and tested during carbothermic method mentioned in Table 6. While 1000 g copper slag was disposed assisted by microwave irradiation, 15.8 g zinc oxide product with 91.2 wt% of ZnO was obtained. Zinc recycling efficiency reached 90.5 wt%. Accordingly, 1000 g copper slag was disposed by traditional carbothermic reduction, where 17.2 g zinc oxide product with ZnO 74.6 wt% was obtained. Zinc recycling efficiency was 80.6 wt% under such conditions.

CONCLUSIONS

Results from experiments and analyses in this study show that: first, microwave irradiation could heat samples mixed with anthracite coal, copper slag and calcium oxide; second, microwave irradiation served as a catalyst in the recovery processes, and the reaction duration for reducing the ferrous compounds in copper slag could be decreased by 90 min; finally, the optimal conditions for iron recovery from copper slag using

microwave-assisted carbothermic method were described as follows. For each 100 g of copper slag, 30 g of anthracite and 20 g of calcium oxide should be used. The reaction temperature was 1100°C and reaction duration was 90 min. Under such conditions metallization ratio of iron could reach 91.38~93.45 wt%. Sponge iron derived from separating the product of carbothermic reduction assisted by microwave irradiation could be used directly for steelmaking and zinc oxide powder with 91.2 wt% of ZnO could be obtained. Additionally, copper concentrate could be obtained after magnetic separation and floating separation. Separation tailings could further be used as cement raw materials.

ACKNOWLEDGEMENTS

This work was financially supported by National Natural Science Foundation of China (Coded as number 21266011, and 21566017) and the pre-investigation fund jointed by Jinchuan group Co., Ltd and Kunming University of Science & Technology (Coded as number 4201252011).

REFERENCES

1. Zhang C., Wang Y. M., Zhang Z. L., Wang D. Y., Luo C. Z., and Xu F., "Health risk assessment of heavy metals and As in vegetable and soil system in Chongqing, southwest of China", *Journal of Residual*

- Science & Technology*, Vol. 12, No. 4, 2015, pp. 231–240. <http://dx.doi.org/10.12783/issn.1544-8053/12/4/6>
2. Wei L. D., “Study on migration and pollution in shallow groundwater near a slag field”, *Journal of Residuals Science & Technology*, Vol. 12, No. 4, 2015, pp. 191–197. <http://dx.doi.org/10.12783/issn.1544-8053/12/4/1>
 3. Tolaymat T., Al-Abed S. R., and Jegadeesan G., “Impact of bioreactor landfill leachate quality on As, Cd, Pb and Zn leaching from mine residues”, *Journal of Residual Science & Technology*, Vol. 6, No. 2, 2009, pp. 89–96.
 4. Mawaja K., Mukongo T., Mbaya R. K., and Mochubele E. A., “Effect of annealing treatment on the crystallisation and leaching of dumped base metal smelter slags”, *Journal of Hazardous Materials*, Vol. 183, No. 1-3, 2010, pp. 294–300. <http://dx.doi.org/10.1016/j.jhazmat.2010.07.023>
 5. González-Castanedo Y., Moreno T., Fernández-Camacho R., Sánchez de la Campa A. M., Alastuey A., Querol X., and Rosa J. D. L., “Size distribution and chemical composition of particulate matter stack emissions in and around a copper smelter”, *Atmospheric Environment*, Vol. 98, 2014, pp. 271–282. <http://dx.doi.org/10.1016/j.atmosenv.2014.08.057>
 6. Rozendaal A., and Horn R., “Textural, mineralogical and chemical characteristics of copper reverberatory furnace smelter slag of the Okiep Copper District, South Africa”, *Minerals Engineering*, Vol. 52, 2013, pp. 184–190. <http://dx.doi.org/10.1016/j.mineng.2013.06.020>
 7. Ettler V., Johan Z., Křibek B., Šebek O., and Mihaljevič, M., “Mineralogy and environmental stability of slags from the Tsumeb smelter, Namibia”, *Applied Geochemistry*, Vol. 24, No. 1, 2009, pp. 1–15. <http://dx.doi.org/10.1016/j.apgeochem.2008.10.003>
 8. Muravyov M. I., Fomchenko N. V., Usoltsev A. V., Vasilyev E. A., and Kondratěva T. F., “Leaching of copper and zinc from copper converter slag flotation tailings using H₂SO₄ and biologically generated Fe₂(SO₄)₃”, *Hydrometallurgy*, Vol. 119–120, 2012, pp. 40–46. <http://dx.doi.org/10.1016/j.hydromet.2012.03.001>
 9. Basir S. M. A., and Rabah M. A., “Hydrometallurgical recovery of metal values from brass melting slag”, *Hydrometallurgy*, Vol. 53, 1999, pp. 31–44. [http://dx.doi.org/10.1016/S0304-386X\(99\)00030-4](http://dx.doi.org/10.1016/S0304-386X(99)00030-4)
 10. Herrerros O., Quiroz R., Manzano E., Bou C., and Vinals J., “Copper extraction from reverberatory and flash furnace slags by chlorine leaching”, *Hydrometallurgy*, Vol. 49, 1998, pp. 87–101. [http://dx.doi.org/10.1016/S0304-386X\(98\)00010-3](http://dx.doi.org/10.1016/S0304-386X(98)00010-3)
 11. Zhang Y., Man R. L., Ni W. D., and Wang H., “Selective leaching of base metals from copper smelter slag”, *Hydrometallurgy*, Vol. 103, 2010, pp. 25–29. <http://dx.doi.org/10.1016/j.hydromet.2010.02.009>
 12. Li Y. J., Perederiy I., and Papangelakis V. G., “Cleaning of waste smelter slags and recovery of valuable metals by pressure oxidative leaching”, *Journal of Hazardous Materials*, Vol. 152, No. 2, 2008, pp. 607–615. <http://dx.doi.org/10.1016/j.jhazmat.2007.07.052>
 13. Zhai X. J., Li N. J., Zhang X., Fu Y., and Jiang L., “Recovery of cobalt from converter slag of Chambishi Copper Smelter using reduction smelting process”, *Trans. Nonferrous Met. Soc. China*, Vol. 21, No. 9, 2011, pp. 2117–2121. [http://dx.doi.org/10.1016/S1003-6326\(11\)60982-5](http://dx.doi.org/10.1016/S1003-6326(11)60982-5)
 14. Ziyadanogullari B., “Recovery of copper and cobalt from concentrate and converter slag”, *Sep. Sci. Technol.*, Vol. 35, 2000, pp. 1963–1971. <http://dx.doi.org/10.1081/SS-100100630>
 15. Altundogan H. S., and Tumen F., “Metal recovery from copper converter slag by roasting with ferric sulphate”, *Hydrometallurgy*, Vol. 44, 1997, pp. 261–267. [http://dx.doi.org/10.1016/S0304-386X\(96\)00038-2](http://dx.doi.org/10.1016/S0304-386X(96)00038-2)
 16. Arslana C., and Arslan F., “Recovery of copper, cobalt, and zinc from copper smelter and converter slags”, *Hydrometallurgy*, Vol. 67, 2002, pp. 1–7. [http://dx.doi.org/10.1016/S0304-386X\(02\)00139-1](http://dx.doi.org/10.1016/S0304-386X(02)00139-1)
 17. Jalkanen H., Vehvilainen J., and Poijarvi J., “Copper in Solidified copper smelter slags”, *Scand. J. of Metall.*, Vol. 32, 2003 pp. 65–70. <http://dx.doi.org/10.1034/j.1600-0692.2003.00536.x>
 18. Yuce I. O., Sahin F. C., and Sirin B., Addemir A.O., “A reduction study of copper slag in a DC arc furnace”, *Scand. J. of Metall.*, Vol. 28, 1999, pp. 93–99.
 19. Zhang L. N., Zhang L., Wang M. Y., and Sui Z. T., “Research on selective reducing impoverishment process of copper slag”, *Nonferr. Met.*, Vol. 57, 2005, pp. 44–47(in Chinese).
 20. Wu W., Zhang W. D., and Ma G. W., “Optimum content of copper slag as a fine aggregate in high strength concrete”, *Materials and Design*, Vol. 31, 2010, pp. 2878–2883(in Chinese). <http://dx.doi.org/10.1016/j.matdes.2009.12.037>
 21. Shi C. J., Meyer C., and Behnood A., “Utilization of copper slag in cement and concrete, Resources”, *Conservation and Recycling*, Vol. 52, 2008, pp. 1115–1120. <http://dx.doi.org/10.1016/j.resconrec.2008.06.008>
 22. Alp I., Deveci H., and Söngün H., “Utilization of flotation wastes of copper slag as raw material in cement production”, *Journal of Hazardous Materials*, Vol. 159, 2008, pp. 390–395. <http://dx.doi.org/10.1016/j.jhazmat.2008.02.056>

Research on the Feces-Bearing Capacity of the Farmland in Anhui Province of China

CAILIN ZHANG¹, XIAOLONG CHEN¹, DONGFU FAN², TONGQIAN KANG² and SHUYUN YANG^{1,2,*}

¹*School of Resources and Environment, Anhui Agricultural University, 130 West Changjiang Road, Hefei 230036, Anhui, China*
²*Hefei Scientific Observing and Experimental Station of Agro-Environment, Ministry of Agriculture, P.R. China, Hefei 230036, China*

ABSTRACT: Anhui is a typical province with rich produced agriculture in the south of China, which is economically typical among those less developed provinces in the central and western regions of China. Therefore, study on the feces loads of farmland in the province is significant for guidance of the central and western regions. This study investigated the fecal pollution loads of farmland resulting from farming of Anhui Province. The results indicated that the average annual livestock feces exertion was 59.59 million tons during 2006–2010, which was equivalent to 282,000 tons of N and 111,500 tons of P. And the results for human feces of rural residents were 23.84 million tons, 143,000 tons and 48,600 tons, respectively. The five-year average loads of feces, feces-derived N and P loads were 20.20 thm^{-2} , 102.91 kg hm^{-2} and 38.76 kg hm^{-2} , respectively. There were respectively 22.1%, 13.0% and 63.6% of the total counties exceeding the corresponding loads bearing limits of feces, N and P. The average P loads of the whole province surpassed the limit for 10.7%. In conclusion, the loads of feces and N of farmland were high, and some areas were in pollution of feces and N, while most areas were in pollution of P, which must be controlled as soon as possible.

INTRODUCTION

FECES has become one of main non-point sources of rural pollution because the return to farmland aggravates the nitrogen (N) and phosphorus (P) loads of the farmland, most of which is over-fertilized in China (including Anhui Province) [1–5]. It was reported that there will be a large increase of feces amount in the following 15 years [6,7]. According to the past research, the rural non-point pollution source was a critical factor for water pollution, as over 850 out of 1200 major rivers investigated were affected and there was not any fish or shrimps in 2400 km of river [8,9]. Viewing from feces pollution on farmland in different regions, it aggravated gradually from the northwest to the southeast [1]. There were two categories of researches on the livestock feces pollution in China. The macroscopic research was normally done over the province, while the microscopic research focused on small watershed and pollution controls [1,10–15]. Several methods have been developed to study this area, but the integrated models similar to the decision support system regard-

ing the capacity of waste loads in the Arroyo Colorado River watershed were rarely used [16].

Anhui Province is a typical agricultural province located within 600 km of the Shanghai economic circle, and the livestock and poultry breeding is an important part of the local economy. In addition, many livestock industries may be transferred to the province as the escalation of the industrial relocation in the Yangtze River Delta regions, because Anhui Province is rich in agricultural products, economically less developed and close to the Yangtze River Delta. Therefore, feces pollution can't be ignored since it may result in further farmland pollution [17,18]. Anhui has a rural population of 53.63 million (2012) accounting for 7.95% of the country's total rural population of China [19]. According to the investigations, most human feces was applied to fields, in addition to the livestock feces. Therefore, effects of human feces were also considered in this study.

At present, the unified national feces, nitrogen and phosphorus threshold criteria for farmland have not been set up yet. The standards put forward by domestic and foreign researchers vary greatly. Shanghai Academy of Agricultural Sciences put forward the standards of the livestock feces loads for rural farmland

*Author to whom correspondence should be addressed.
E-mail: yangshy@ahau.edu.cn

in Shanghai suburbs [20]. Some scholars believed that the bearing capacity of livestock feces for farmland is 30 t hm^{-2} [21]. Zhaoliang Zhu found that nitrogen application over 150–180 kg could cause environmental pollution [22]. According to the European Union (EU) specifications, the annual fecal nitrogen application limit is 170 kg hm^{-2} , otherwise, nitrate leaching would occur [23].

In this paper, based on the data of rural population, livestock breeding and farmland of counties from 2006–2010, the feces excretion amount, total nitrogen (TN), total phosphorus (TP) and farmland loads of feces, N and P were estimated by the county level, and the environmental impacts of feces application on the farmland were analyzed with reference to feces, N and P limit. Results of the feces output and farmland loads should have practical significance for the control of non-point source of agricultural pollution and drawing up plans of livestock and poultry development.

MATERIALS AND METHODS

Basic Data

The rural population, livestock and poultry breeding, farmland areas and related information came from “Anhui Statistical Yearbook” of 2007–2011 [24]. According to the characteristics of Anhui Province, the pigs, draft cattle, beef cattle, cows, horses, sheep, donkeys, mules, chicken, hens, ducks, geese, rabbits and human beings were researched. Comparison study of the present economic level in the rural areas of Anhui indicated that it was close to that of Shanghai City in 1980s. Therefore, feces parameters of Shanghai rural residents at that period were adopted in this article (Table 1) [25].

Anhui has 114 county-level units. In the article, districts under various municipalities were merged into county-level areas since most municipal areas are rather small, which may affect the comparability of different areas. For example, the total area of Tongling City, including five districts, is only 1083 km^2 . So it was considered as one county-level region. After merging, there were 77 county-level regions with similar areas.

Calculation Parameters

There are no national standards for the daily feces excretion amount of different livestock and poultry in China at present. In this paper, the feces excretion parameters were the average data of previously published

Table 1. Feces Excretion Parameters, Nutritional Contents (TN, TP) of Different Livestock and Poultry.

Varieties	Feces Excretion	
	Parameters	TN (%) TP (%)
Draft cattle	10.10 ta^{-1}	0.351 0.082
Beef cattle	7.70 ta^{-1}	0.351 0.082
Cow	19.40 ta^{-1}	0.351 0.082
Horse	5.90 ta^{-1}	0.378 0.077
Donkeys and mules	5.00 ta^{-1}	0.378 0.077
Pig	1.93 ta^{-1}	0.238 0.074
Sheep	0.87 ta^{-1}	1.014 0.216
Broiler chicken	36.50 kga^{-1}	1.032 0.413
Laying hen	53.30 kga^{-1}	1.032 0.413
Duck and goose	39.00 kga^{-1}	0.625 0.290
Rabbits	41.40 kga^{-1}	0.874 0.297
Human being	127.75 kga^{-1}	0.600 0.204

Note: N and P contents of duck and goose were averaged.

work. Feces and nutrition amounts were estimated based on the parameters and the corresponding TP and TN contents of livestock and human feces (Table 1) [12,14,21,26,27].

Estimation Method

The method to estimate the annual feces amount of a county was as follows: using the following formula to calculate certain livestock (human beings) feces excretion amount first [21]:

$$Q = B * T * X \quad (1)$$

where Q is annual feces excretion amount, B is feeding amount (population amount), T is calculation period and X is excretion parameter. Then, all livestock and human feces amounts were summed up.

The method to estimate the pure nutrition amount in feces of a county was as follows: calculating the nutrition amount in the feces of an animal first with the following formula:

$$A = Q * c \quad (2)$$

where A is the nutrition amount, Q is the feces exertion amount and c is the nutrition contents in the feces of an animal per unit mass. Then, all the nutrition amounts were summed up.

RESULTS AND DISCUSSION

Feces Exertion Amount and the Contents of TN and TP in Anhui Province during 2006–2010

The results of the total feces amount (TF) and the

corresponding TN and TP amounts in Anhui Province during 2006–2010 were estimated by the livestock and poultry feeding, feces excretion parameters and P, N contents.

The average annual total feces excretion of livestock and poultry during 2006–2010 was 59.59 million tons, with a compound annual increase of 7.97%, which was equivalent to 282,000 tons of average TN and 111,500 tons of average TP, respectively. The feces excretion, TN, TP of Anhui within these 5 years presented relatively slow upward trend, which was in correspondence to the livestock and poultry breeding increase (Figure 1).

The feces excretion of rural residents was changed from 23.56–24.04 million tons in the 5 years, with a rate of annual change less than or equal to 1.83%. The five-year average feces excretion was 23.84 million tons, which was equivalent to 40% of the livestock feces. Converted TN and TP of the five-year average were 143,000 and 48,600 tons, respectively, about half of which was from livestock. This result showed that the rural human feces amount was necessary to be considered in the study of farmland feces loads due to its large production. Meanwhile, human feces amount was approximately a constant. Thus, livestock feces was the priority of the study on farmland feces loads.

The average annual TN and TP of human and livestock feces were 425,000 and 160,100 tons in these 5 years, respectively, which were equivalent to 83.17% and 65.25% of N and P fertilizer applications in Anhui Province during this period. Therefore, rational and effective application of feces to farmland is beneficial

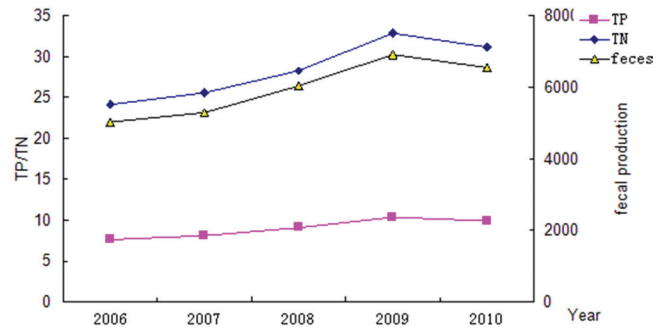


Figure 1. TF, TN and TP in Anhui Province during 2006–2010 except for human feces.

for both fecal pollution solvation and the reduction of chemical fertilizer application.

Farmland Feces Loads of Various Counties in Anhui Province during 2006–2010

The provincial average livestock feces loads of farmland during 2006–2010 was 14.43 thm^{-2} [Figure 2(a)]. Shexian, Jixi, Xiuning and Taihu exceeded the application standards (30 thm^{-2}) and Shexian was the highest (54.76 thm^{-2}). Only the loads of 37 counties were lower than 15 thm^{-2} . The south and west areas of Anhui Province had higher loads since the farmland was smaller, or the industry or tourism was the leading industry. The counties in the north of the Huaihe River and the east of the province had loads lower than 15 thm^{-2} , suggesting these areas had potentials to enlarge the livestock scales.

The average farmland feces loads of the province

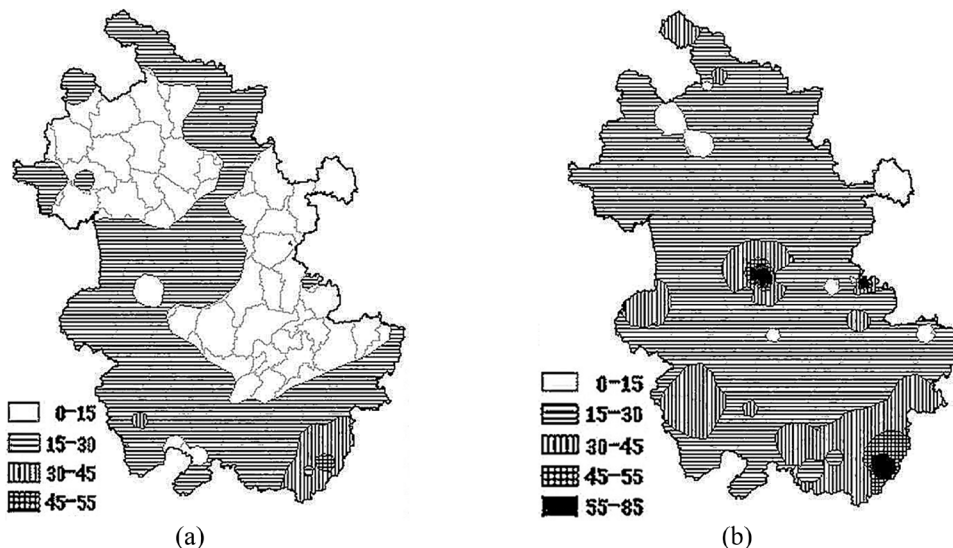


Figure 2. Average farmland feces loads of various counties in Anhui Province during 2006–2010. (a) Five-year average farmland feces loads of livestock and poultry; (b) five-year average farmland loads including human feces, livestock and poultry feces.

was 20.20 thm^{-2} after addition of human feces [Figure 2(b)]. Hefei was the highest of 85.07 thm^{-2} . 17 counties or 22.1% of the total counties including Shexian and Ma'anshan exceeded 30 thm^{-2} , in which there were more than 4 counties exceeding 30 thm^{-2} without consideration of human feces. Only 8 counties including Lujiang were lower than 15 thm^{-2} , and less than 37 counties considered only farmland livestock and poultry feces. These results indicated that human feces played a critical role in farmland feces contaminations, and the results would be seriously distorted if only livestock and poultry feces were considered.

Farmland N Loads of Various Counties in Anhui Province during 2006–2010

The pure nitrogen loads converted from livestock feces of Anhui Province was 68.27 kghm^{-2} on average during 2006–2010 [Figure 3(a)], in which Shexian was the highest of 180.11 kghm^{-2} and exceeded the EU standards of 170 kghm^{-2} . Meanwhile, Ningguo and Dangshan exceeded 150 kghm^{-2} . The results of nitrogen loads were not always the same as that of the livestock feces loads because the nitrogen contents of feces varied with different livestock species, which also varied greatly in different counties. For example, Ningguo fed mainly poultry with higher fecal nitrogen contents, and the nitrogen loads converted from the feces was 167.73 kghm^{-2} , ranking in the second place in the province, though its livestock feces loads was not high. Livestock industry of Xiuning was mainly pig feeding. Though its feces loads was higher than that of

Ningguo, its nitrogen loads was lower (111.12 kghm^{-2}) due to the low nitrogen contents of pig feces. The more concentrated the livestock industries were, the more concentrated the distribution of feces tended to be. The counties with high N loads were wholly polluted, while there was only spot pollution in the counties with low N loads.

The average farmland feces N loads was 102.91 kghm^{-2} after addition of human feces [Figure 3(b)]. Hefei (503.14 kghm^{-2}) and Ma'anshan (398.79 kghm^{-2}) ranked in the first two places, and far exceeded the average local N fertilizer application (173.33 kghm^{-2} and $-125.88 \text{ kghm}^{-2}$). Besides, another 8 counties, such as Shexian and so on, exceeded the EU standards. The N loads of 10 counties including Shitai were about $150\text{--}170 \text{ kghm}^{-2}$. 20 counties were in pollution, accounting for 26% of the total counties, indicating that the farmland feces N pollution was serious.

Farmland P Loads of Various Counties in Anhui Province during 2006–2010

Phosphorus has poor mobility and is easy to be accumulated in the soil. Therefore, both the phosphorus contents from feces application and the phosphorus level of soil should be considered when appraising the environmental effect of feces phosphorus. The pure phosphorus contents from feces application should not exceed 35 kghm^{-2} , otherwise, the surplus phosphorus will enter the surface runoff through leaching which will cause water eutrophication [28,29].

The average farmland P loads converted from live-

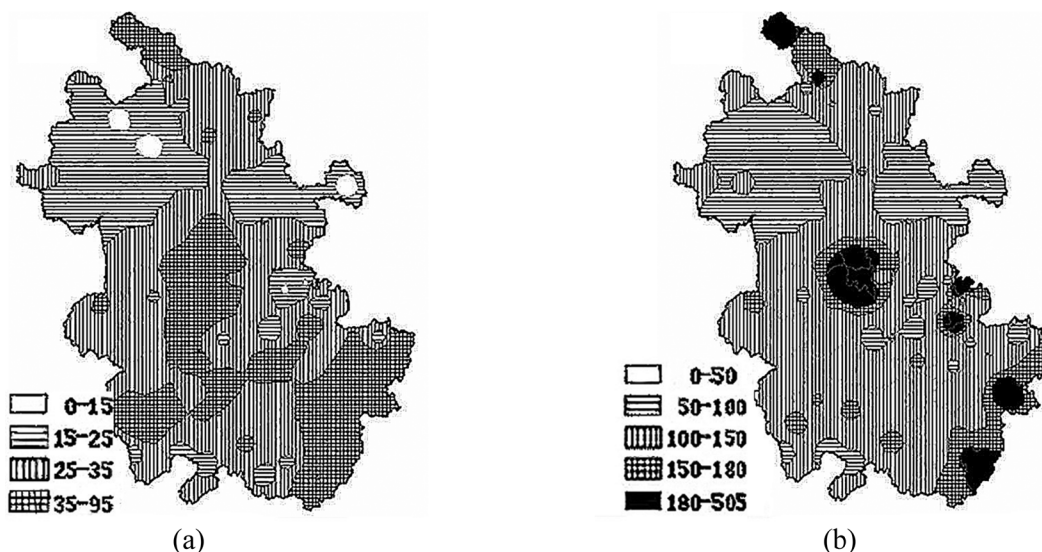


Figure 3. Average farmland feces N loads of various counties in Anhui Province from 2006–2010. (a) The average farmland feces N loads of livestock and poultry feces; (b) the average farmland feces N loads of human feces, livestock and poultry feces.

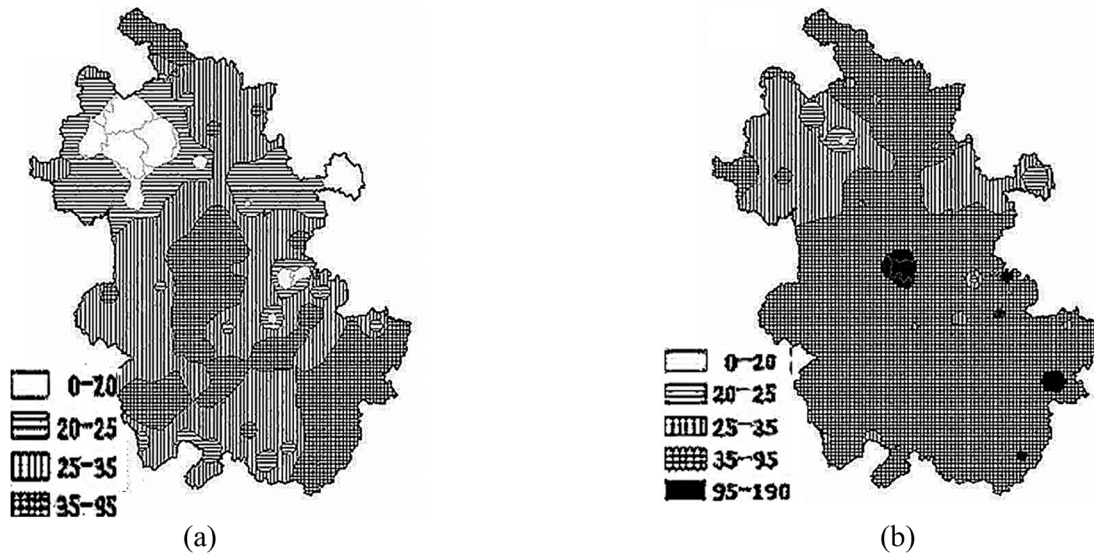


Figure 4. Average farmland feces P loads of various counties in Anhui Province from 2006–2010. (a) The average farmland feces P loads of livestock and poultry feces; (b) the average farmland feces P loads of human feces, livestock and poultry feces.

stock feces was 26.99 kg hm^{-2} from 2006–2010 [Figure 4(a)], which was close to the limit of 35 kg hm^{-2} . Ningguo was 94.68 kg hm^{-2} , ranking in the first place of the counties and equal to 2.71 times of the limit. 28 counties, such as Shexian and so on exceeded the limit, where had higher P loads of farmland from livestock feces.

The average farmland feces P loads was 38.76 kg hm^{-2} after addition of human feces in 2006–2010, which exceeded the limit of 35 kg hm^{-2} , indicating the farmland was overloaded [Figure 4(b)]. Some areas might be in serious P pollution if uneven feces distribution was taken into consideration. Counties ranking in the first two places were still Hefei and Ma'anshan, with P loads of $189.91 \text{ kg hm}^{-2}$ and $140.64 \text{ kg hm}^{-2}$, respectively, which were far exceeding the average local P fertilizer application (18.61 kg hm^{-2} and 9.90 kg hm^{-2}). In addition, Ningguo and other 46 counties were more than 35 kg hm^{-2} . Generally, feces application caused overload of P to farmland in the province, and 66.3% of the total counties were in pollution. Areas polluted by P were larger than those by N.

DISCUSSION

The feces loads of farmlands in the whole province were in high levels and there were prevalent fecal contamination. There is a fast expansion in the livestock and poultry industry in the future owing to the huge consumer market for animal food. Livestock in Anhui Province will keep rapid increase as excess food offers adequate feed source for livestock farming, resulting in plenty of livestock feces exertion. But if failed

to take measures to make the livestock feces harmless and resourceful, the feces will aggressively affect the healthy farming development, pollute the near farmland, water bodies and threaten the ecological environment seriously. The paper, aimed at working out the present situation of feces pollution, N pollution and P pollution in Anhui Province to provide scientific basis for the development of pollution control measures, and making reasonable plan and scientific decisions. The related pollution control measures need to be further researched.

Affected by the livestock feed varieties, breeding periods and seasons, weather, management levels and other factors [24,28], there is a certain error between the estimated feces amount and actual feces exertion. According to the factual investigation of Anhui Province, the buffaloes were considered as draft cattle and the yellow cattle were considered as beef cattle. However, a few yellow cattle were used as draft cattle before their slaughter, resulting in lower feces estimation as the excretion parameter is larger when yellow cattle were considered as draft cattle than that of beef cattle. The raising numbers of ducks and geese were calculated by means of the poultry numbers minus chicken numbers, a small amount of poultry less than geese and ducks in volume and emission were counted into the amount of geese and ducks, resulting in larger feces estimation of ducks and geese.

CONCLUSION

The average annual total livestock feces exertion

was 59.59 million tons from 2006 to 2010, equivalent to 282,000 tons of N and 111,500 tons of P. The average annual total human feces exertion was 23.84 million tons, equivalent to 143,000 tons of N and 48,600 tons of P. The human feces and its N and P were 28.6%, 28.3% and 25.4% of the total statistic feces respectively. Most feces was applied to farmland in its original form and had great environmental impacts on the farmlands. To study the environmental effects of feces in Anhui Province, rural human feces must be taken into consideration.

The average farmland feces loads of the province was 20.20 thm^{-2} in the five years. 17 counties out of 77 exceeded the limit of 30 thm^{-2} , with Hefei at the highest of 85.07 thm^{-2} . Human feces pollution played an important role in feces pollution of the whole province. Feces loads was in high levels and there were prevalent feces contaminations over the province.

The average farmland N and P loads of livestock feces in the 5 years were 68.27 kghm^{-2} and 26.99 kghm^{-2} , respectively, with only the N loads of Shexian surpassing the EU limit of 170 kghm^{-2} while 29 counties exceeding the P load limit of 35 kghm^{-2} . This showed there were great differences in the farmland bearing capacities, and N and P pollution risks from the feces were also different. In addition, different livestock species resulted in different farmland N and P loads and feces loads. The N loads of the counties mainly engaged in poultry exertion were higher than those of pig exertion.

The average annual N and P loads in the five years were 102.91 kghm^{-2} and 38.76 kghm^{-2} respectively after taking into account of human feces. The average N loads of the province was equal to 60.5% of the EU limit. There were 10 counties and cities exceeding the EU limit, with Hefei and Ma'anshan over the local average nitrogen fertilizer applications. The average P loads of the whole province was more than the limit, with 49 counties surpassing the limit, accounting for 63.6% of the total counties. The P loads of Hefei and Ma'anshan were the highest.

ACKNOWLEDGEMENTS

I deeply appreciate teacher Yang, my supervisor, for his consistent and illuminating instruction. He walked me through the process of the writing. Without his constant encouragement and guidance, the paper wouldn't have reached the present form. Meanwhile, I would like to express my gratitude to China clean development mechanism fund (CDMFUND), who funded us to finish the work.

AUTHOR CONTRIBUTIONS

These authors contributed to the conception of the study, analysis and manuscript preparation, data analyses and manuscript writing and the analysis with constructive discussions. Teacher Yang guided the entire work.

NOTES

The authors declare no competing financial interest.

REFERENCES

- Chaney, R., Filcheva, E., Green, C., *et al.*, "Zn deficiency promotes Cd accumulation by lettuce from biosolids amended soils with high Cd: Zn ratio", *J. Journal of Residuals Science & Technology*, Vol. 3, No. 2, 2006, pp. 79–85.
- Zhang, X., Dong, Y., Wang, H., *et al.*, "Spatial and temporal variation in farmland load of livestock feces in Jiangsu Province", *J. Scientia Geographica Sinica*, Vol. 27, No. 4, 2007, pp. 597–601.
- Rastghalam, Z., Hoodaji, M., Javanmard, H. R., "Influence of Humic Acid and Superabsorbent Usage on Lead Phytoextraction from Contaminated Soil by *Brassica napus L.*", *J. Journal of Residuals Science & Technology*, Vol. 9, No. 1, 2012, pp. 21–27.
- Chen, Y., Zhao, H., Xie, Z., *et al.*, "Heavy Metal Pollution Characteristics in the Kaili Coal Mining Region, Guizhou Province, China", *J. Journal of Residuals Science & Technology*, Vol. 12, Suppl. 1, 2015, pp. s123–s131. <http://dx.doi.org/10.12783/issn.1544-8053/12/S1/18>
- Wei, H., Hu, D., Cheng, X., *et al.*, "Residual Levels of Organochlorine Pesticides and Heavy Metals in the Guanzhong Region of the Weihe Basin, North-western China", *J. Journal of Residuals Science & Technology*, Vol. 12, No. 1, 2015, pp. 31–36. <http://dx.doi.org/10.12783/issn.2376-578X/12/1/5>
- Zhang, F., Wang, J., Zhang, W., *et al.*, "Nutrient use efficiencies of major cereal crops in China and measures for improvement", *J. Acta Pedologica Sinica*, Vol. 45, No. 5, 2009, pp. 915–924.
- Fischer, G., Ermolieva, T. and Sun L. X., "Environmental pressure from intensification of livestock and crop exertion in China: Plausible trends towards 2030", *Catsei Project Report*, 2010, pp.1–29.
- Wang, F., Zhang, L. and Pei, Z., "Current situation of fowls breeding in Huangpi district and its control countermeasures", *J. Environ. Sci. Technol.*, Vol. 32, No. 6, 2009, pp. 545–549.
- Schaffner, M., Bader, H.P. and Scheidegger, R., "Modeling the contribution of pig farming to pollution of the Thachin River", *J. Clean Technol. Envir.*, Vol. 4, No. 12, 2010, pp. 407–425. <http://dx.doi.org/10.1007/s10098-009-0255-y>
- Hoar, B. R., Atwill, E. R. and Farver, T. B., "Estimating maximum possible environmental loading amount of *cryptosporidium partum* attributable to adult beef cattle", *J. Quant. Microbiol.*, Vol. 2, No. 1, 2000, pp. 21–36. <http://dx.doi.org/10.1023/A:1010044012356>
- Peng, L. and Wang, D., "Estimation of annual quantity of total excretion from livestock and poultry in Chongqing municipality", *J. Transactions of the CSAE*, Vol. 20, No. 1, 2004, pp. 288–292.
- Zhang, K. and Gao, H. 2004. *Livestock and poultry breeding industry pollutant treatment and disposal*, Beijing, Chemical Industry Press.
- Mallin, M. A. and Cahoon, L. B., "Industrialized animal reduction is a major source of nutrient and microbial pollution to aquatic ecosystems", *J. Population and Environment*, Vol. 24, No.5, 2003, pp. 369–385. <http://dx.doi.org/10.1023/A:1023690824045>
- Su, Y., Zheng, D. and Lin, W., "A study on the prevention and control of pollution in domestic animal and poultry farming in Fujian Province", *J. Fujian Geography*, Vol. 19, No. 3, 2004, pp. 1–4.

15. Liu, P., Chen, Z. and Xu, S., "Waste loading and treatment strategies on the excreta of domestic animals in the Yangtze Delta", *J. Resources and Environment in the Yangtze River Basin*, Vol. 11, No. 5, 2002, pp. 456–460.
16. Hernandez, E. A. and Uddameri, V., "An assessment of optimal waste load allocation and assimilation characteristics in the Arroyo Colorado River watershed, TX along the US–Mexico border", *J. Clean Technol. Envir.*, Vol. 4, No. 15, 2013, pp. 617–631. <http://dx.doi.org/10.1007/s10098-012-0546-6>
17. Anhui agriculture committee, "The general situation of agricultural industrialization of Anhui province". <http://www.ahny.gov.cn/info.asp?typeid=139>. (In Chinese)
18. The 42nd government office of Anhui province. "The twelfth Five-Year Plan for animal husbandry development of Anhui province", 2010. http://wenku.baidu.com/link?url=yXOVkv4CkcukRJ4_VvZkCsx4x-3YgWTit-mtkthz6cr8mbIeIR9u-6eztBGEelvGvZ_EkrKxLejI1DF-BudlEUR5RMzoBEgWdCzlfmaU7ySxa###. (In Chinese)
19. Anhui province bureau of statistics. 2013. "Anhui statistical yearbook 2013", Beijing, China Statistics Press. http://www.ahnj.gov.cn/tjj/web/tjn_view.jsp?_index=1#. (In Chinese)
20. Zhang, Y., Hong, H., Zeng, Y., *et al.*, "Discussion on ecological environment problems and countermeasures based on Livestock and poultry breeding of jiulong river estuary basin", *J. Chongqing Environmental Science*, Vol. 25, No. 7, 2003, pp. 29–34.
21. Yang, C. 2002. "The scale of livestock and poultry breeding pollution investigation and prevention countermeasures", Beijing, China Environmental Science Press.
22. Zhu, Z., "Loss of fertilizer N from plants-soil system and the strategies and techniques for its reduction", *J. Soil and Environmental Sciences*, Vol. 9, No. 1, 2000, pp. 1–6.
23. Wang, F., Ma, W., Dou, Z., *et al.*, "The estimation of the production amount of animal manure and its environmental effect in China", *J. China Environment Science*, Vol. 26, No. 5, 2006, pp. 614–617.
24. Anhui province bureau of statistics. 2007–2011. Anhui statistical yearbook 2007–2011, Beijing, China Statistics Press. http://www.ahnj.gov.cn/tjj/web/tjn_view.jsp?_index=1. (In Chinese)
25. Xu, Z., Wang, J. and Zhuang, X., "Human feces and urine nitrogen emissions and model research", *J. Journal of Anhui Agricultural Sciences*, Vol. 37, No. 33, 2009, pp. 16510–16512.
26. Wang, X. 1999. Livestock manure, Shanghai, Shanghai Jiao Tong University Press.
27. Xin, Z., "Status of poultry and animal feces pollution to the environment and its technology to explore", *J. Chinese Qinghai Journal of Animal and Veterinary Sciences*, Vol. 4, 2004, pp. 35–37.
28. Yang, F., Yang, S. and Zhu, Y., *et al.*, "Analysis on livestock and poultry exertion and nitrogen pollution load of cultivated land during last 30 years in China", *J. Transactions of the Chinese Society of Agricultural Engineering*, Vol. 29, No. 5, 2013, pp. 1–11.
29. Oenema, O., Van L. E., Plette S., *et al.*, "Environmental effects of manure policy options in the Netherlands", *J. Water Sci. Technol.*, Vol. 49, No. 3, 2004, pp. 101–108.
30. The national agricultural technology extension service center. 1999. China organic fertilizer nutrients, Beijing, China Agriculture Press. http://baike.baidu.com/link?url=tNn4qSEpfQgAyJOTcD1ugrNZNgTCWBaXnw5mG1OUArGLOaGUGd3I407B7_pJLJ-n0RsJ1nxYexRy-xOehgXKx_. (In Chinese)

Facile Synthesis of $\text{Fe}_3\text{O}_4\text{-N-}[(3\text{-Trimethoxysilyl)propyl}]$ ethylenediamine Triaceticacid Trisodium Salt and Adsorption of Sr^{2+}

YAOQIANG HU^{1,2}, CHAOMING QUAN^{1,2}, MIN GUO¹, XIUSHEN YE^{1,*} and ZHIJIAN WU¹

¹Qinghai Institute of Salt Lakes, Chinese Academy of Sciences, Xining 810008, China

²University of Chinese Academy of Sciences, Beijing 100049, China

ABSTRACT: $\text{Fe}_3\text{O}_4\text{-N-}[(3\text{-Trimethoxysilyl)propyl}]$ ethylenediamine triaceticacid trisodium ($\text{Fe}_3\text{O}_4\text{-TMS}$) has been synthesized by TMS adsorb to the surface of Fe_3O_4 . Energy dispersive spectrometer (EDS) was used to characterize $\text{Fe}_3\text{O}_4\text{-TMS}$. The results of EDS indicate that TMS is modified on the surface of Fe_3O_4 successfully. The effects of initial concentration, pH, and coexist ions on the equilibrium adsorption capacities of strontium ion were investigated comprehensively. Removal of Sr^{2+} could reach 100% when initial concentration of Sr^{2+} is 1.0 mmol/L. The effect of pH conforms to S curve. Equation of the curve is $q_{\text{Sr}} = 0.08104 - 0.09012/(1 + \exp((\text{pH} - 2.92707)/0.2995))$. Correlation coefficient is equal to 0.9987. Sodium and calcium ions suppress the adsorption of strontium ion. Complexation and ion exchange maybe main adsorption mechanism.

INTRODUCTION

As a radioactive isotope of strontium, ^{90}Sr is one of the fission products of uranium [1]. So nuclear waste contains lots of ^{90}Sr . ^{90}Sr could launch β rays, and its half-life reaches 28.6 years [2,3]. ^{90}Sr with its long half-life is considered to be the critical isotope tend to be strongly retained within the living organisms such as bones [4]. Therefore ^{90}Sr is a contamination that must be removed. Treatment of liquid radioactive waste quite often involves the application of several methods such as filtration, precipitation, sorption, ion exchange and membrane separation to meet the requirements for the release of decontaminated effluents into the environment [5–11]. Adsorption has become one of the most commonly used separation methods due to its simplicity, selectivity and efficiency [12,13]. However, many other interfering elements in the nuclear waste such as ^{137}Cs and ^{40}K are also problems [3]. Further, concentration of Sr is unusually enriched in oil-field brines of Qaidam Basin, China and have excellent potential for development and utilization in future [14]. A problem arose when separates strontium from oil-field brines. A number of interfering elements such as sodium, potassium and magnesium, especially

calcium, due to their similar chemical behavior, affect the separation of strontium seriously [3].

Ethylene diamine tetraacetic acid (EDTA) has a strong complexation with strontium ion. TMS and EDTA have same functional groups (carboxyl). So it is highly likely that TMS has a strong complexation with strontium ion. TMS is not easy to form gel itself. It is easy to separate adsorbate and adsorbent when TMS is modified on the surface of Fe_3O_4 with the help of magnet. The influences of initial concentration, pH and ionic strength on the adsorption of Sr^{2+} have been investigated. Ca^{2+} has the closest size to Sr^{2+} among bivalent cations. So in addition to Na^+ the effect of Ca^{2+} on the adsorption of Sr^{2+} was also investigated. The results provide a simple method to synthesize $\text{Fe}_3\text{O}_4\text{-TMS}$ and an effective composite adsorbent for the adsorption of strontium ion.

EXPERIMENTAL

Synthesis of Fe_3O_4 and $\text{Fe}_3\text{O}_4\text{-TMS}$

Fe_3O_4 particles were prepared by co-precipitating Fe (III) and Fe (II) ions (25.0 g $\text{FeCl}_3 \cdot 6\text{H}_2\text{O}$ and 15.8 g $\text{FeCl}_2 \cdot 4\text{H}_2\text{O}$ dissolved into 150 mL H_2O) in ammonia [15]. Both $\text{FeCl}_3 \cdot 6\text{H}_2\text{O}$ and $\text{FeCl}_2 \cdot 4\text{H}_2\text{O}$ were purchased from Sinopharm Chemical Reagent Co., Ltd. 2.0 mL TMS was added into suspension of Fe_3O_4 . 1.0

*Author to whom correspondence should be addressed.
E-mail: yexs@isl.ac.cn; Tel.: +86 971 6320622; Fax: +86 971 6320622

mL 0.5 mol/L NaOH was dropped into the suspension to initiate TMS hydrolyzation. After keep stirring for 48 h, Fe₃O₄-TMS was obtained by magnetic separation. To facilitate saving, Fe₃O₄-TMS was dry and grinding.

Characterization of Fe₃O₄ and Fe₃O₄-TMS

The EDS spectra of Fe₃O₄ and Fe₃O₄-OTS were obtained with an Oxford INCA instrument (Oxford Instrument Co., Ltd., UK).

Analytical Method

The concentrations of metal ions were determined by an ICS-1100 ionic chromatograph (Dionex Corporation). An IonPac[®] CG12A guard column (4 × 50 mm), an IonPac[®] CS12A separation column (4 × 250 mm), a CSRS 300 suppressor (4 mm) and a DS6 heated conductivity detector were employed. 0.4 mL of the sample solution was diluted to 10 mL. Twenty-five μL of this diluted solution was injected into the ionic chromatograph. The eluent was 20 mmol L⁻¹ methanesulfonic acid solution at a flow rate of 1.0 mL min⁻¹ at 30°C.

Adsorption Experiments

In equilibrium adsorption experiments, the effects of initial concentration, solution pH and coexist ions were investigated. For each experiment, an exact amount of Fe₃O₄-TMS and 25 mL SrCl₂ solution at certain concentration and pH were shaking by a SHA-C shaking water bath (Changzhou Guohua Co., Ltd.) with a shaking speed of 100 rpm for 8 h. Fe₃O₄-TMS and solution were separated by magnet.

The adsorption capacity of metal ions onto Fe₃O₄-TMS was calculated by the following equation:

$$q = \frac{V(C_0 - C)}{m} \quad (1)$$

where q (mmol g⁻¹) is the adsorption capacity of metal ions onto the Fe₃O₄-TMS, V (L) the volume of the solution, m (g) is the dry weight of Fe₃O₄-TMS and C_0 and C (mmol L⁻¹) are the metal ion concentrations before and after adsorption, respectively. When the equilibrium solution concentration C_e was used instead of C , the equilibrium adsorption capacity q_e was obtained.

The distribution coefficient (D) and the separation

factor (β) were calculated according to the following two equations:

$$D = \frac{q_e}{C_e} \quad (2)$$

$$\beta_C^S = \frac{D_{Sr}}{D_{Ca}} \quad (3)$$

RESULTS AND DISCUSSION

EDS Characterization of Fe₃O₄-TMS

As shown in Table 1, compared with Fe₃O₄, sodium and silicon, characteristic element of TMS were detected by EDS. Atomic content of carbon may be a background noise in Table 1. Carbon content also improves to a certain degree. It indicated that TMS was modified to the surface of Fe₃O₄ successfully.

Adsorption Equilibrium Time

Figure 1 shows adsorption of Sr²⁺ occurs rapidly in the first 1 h, after which the adsorption capacity changes slowly. It needs 2 h to reach equilibrium. According to the adsorption kinetic results, the adsorption time was fixed at 8 h for the following adsorption experiments to make sure that all the adsorption experiments reach equilibrium.

For the adsorption of methylene blue on activated carbon, the equilibrium was found to achieve within 30 min [16]. For the adsorption of neutral red by Fe₃O₄ hollow nanospheres, 1 h was needed to reach equilibrium [17]. But the equilibrium time of strontium ion adsorption by molecularly imprinted hybrid gel was more than 10 h long [18]. The time of equilibrium adsorption of titanosilicates adsorb is about 50 min [19].

Table 1. Elemental Compositions of Fe₃O₄ and Fe₃O₄-TMS.

Element	Fe ₃ O ₄		Fe ₃ O ₄ -TMS	
	Weight %	Atomic %	Weight %	Atomic %
C	3.82	9.23	4.90	10.65
O	31.20	56.68	37.58	61.36
Na			0.95	1.08
Si			0.72	0.67
Cl	0.877	0.71	0.38	0.28
Fe	64.12	33.37	55.47	25.95
Totals	100.00	100.00	100.00	100.00

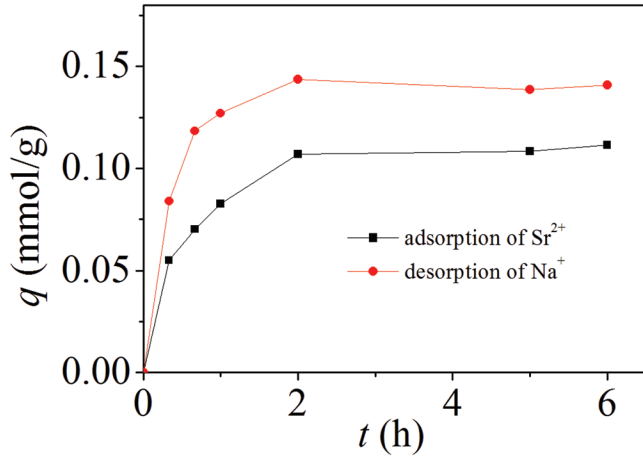


Figure 1. Adsorption kinetic curves..

The equilibrium time of antimony silicate adsorb Sr^{2+} within 30 min [20]. The equilibrium time of TMS adsorb Sr^{2+} is in intermediate stage.

Effect of Initial Concentration

Initial concentration has little impact on the adsorption of Sr^{2+} in the range of 1–6 mmol/L (Figure 2). Percent of Sr^{2+} removal reach 100% when initial concentration of Sr^{2+} is 1 mmol/L (Table 2). It shows that TMS has a strong affinity for Sr^{2+} . When initial concentration continues increase, the adsorption capacity of Sr^{2+} almost do not increase. Maybe it is because adsorption sites reach saturation. In general, the adsorption capacity of Sr^{2+} increases with the increase of initial concentration [21,22]. However, compared to the selected concentration range in this paper, the concentration ranges they choose are narrow.

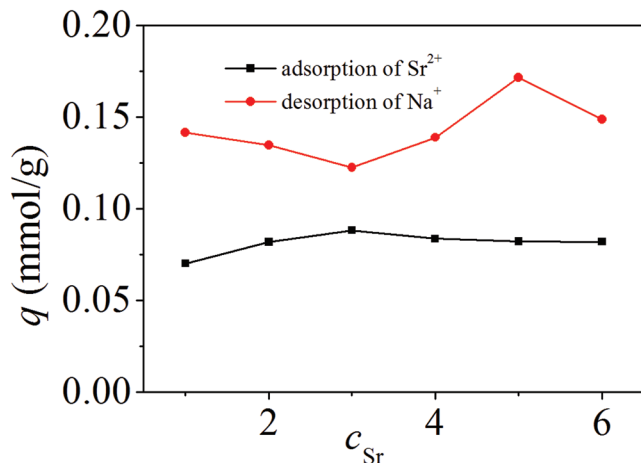


Figure 2. Effect of initial concentration on the equilibrium adsorption capacity.

Table 2. Percents of Sr^{2+} Removal in Different Initial Concentrations.

Initial Concentration	Sr^{2+} Removal %
1	100
2	52.13
3	36.81
4	26.59
5	20.71
6	17.00

Effect of pH

As shown in Figure 3, the adsorption capacity of Sr^{2+} increases with the increase of pH in acid solution. Variation tendency conforms to Type S curve. Equation of the curve is $q_{\text{Sr}} = 0.08104 - 0.09012 / (1 + \exp((\text{pH} - 2.92707)/0.2995))$. Its correlation coefficient reaches 0.9987. When pH is lower than 2.3, $\text{Fe}_3\text{O}_4\text{-TMS}$ can not adsorb Sr^{2+} . This regularity has been reported in the adsorption of Pb(II) on diatomite and adsorption of Cd(II) onto goethite [23,24]. The adsorption capacity increases abruptly at pH 2.3–3.5, and maintains a high level at pH > 3.5. Wallace inferred that the protonation of specific sorption sites on adsorbent surfaces could prevent the electrostatic (outer-sphere) adsorption of Sr^{2+} in low pH values solution [25,26].

Effect of Coexist Ions

Concentrations of Sr^{2+} maintain at 3 mmol/L in this batch of adsorption experiments. When concentration of Na^+ increases from 3–60 mmol/L, the adsorption capacity of Sr^{2+} increases first and then decreases slightly

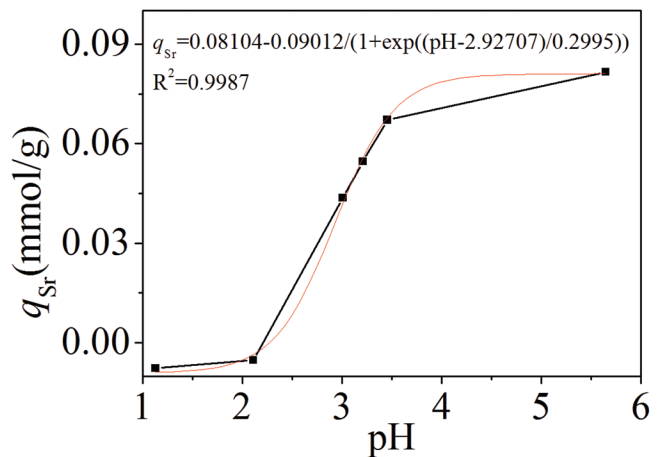


Figure 3. Effect of initial solution pH on the equilibrium adsorption capacity.

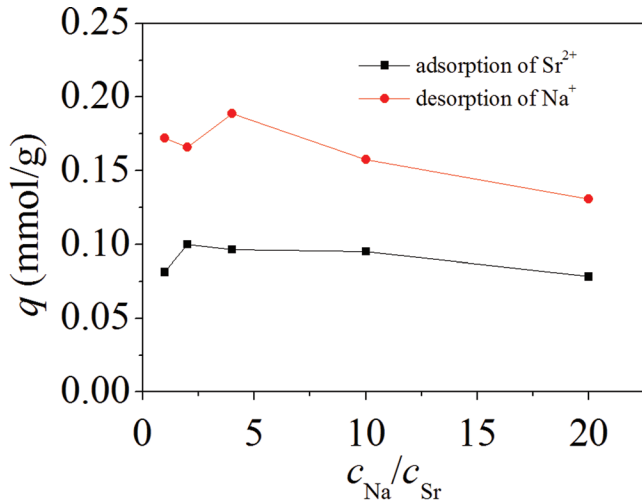


Figure 4. Effect of Na^+ on the equilibrium adsorption capacity of Sr^{2+} .

(Figure 4). The adsorption capacity of Sr^{2+} still keeps at a high capacity when the concentration of Na^+ is 60 mmol/L. However, Ca^{2+} has a bigger influence on the adsorption of Sr^{2+} than Na^+ (Figure 5). The adsorption capacity of Sr^{2+} decreases with the concentration of Ca^{2+} increase. The adsorption capacity of Ca^{2+} increases with the concentration of Ca^{2+} increase. When the concentration of Ca^{2+} is greater than 12 mmol/L, the adsorption capacities of Sr^{2+} and Ca^{2+} decrease. The corresponding desorption capacities of Na^+ also decrease. The maximum separation factor is obtained when the concentration of Ca^{2+} is 30 mmol/L (Table 3).

Adsorption Mechanism

Na^+ is released in the process of adsorption (Figure

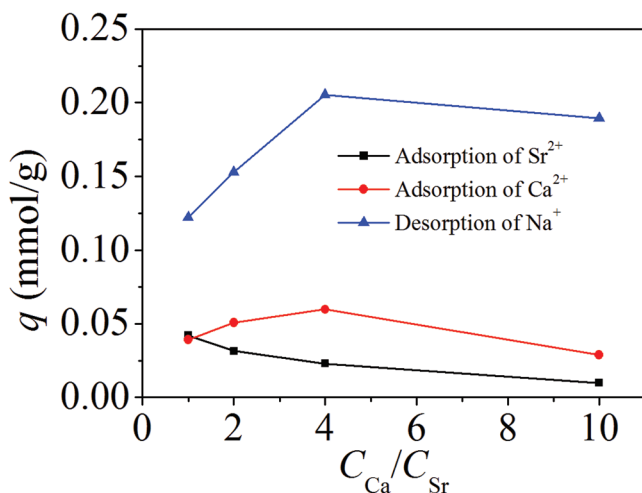


Figure 5. Effect of Ca^{2+} on the equilibrium adsorption capacity of Sr^{2+} .

Table 3. Distribution Coefficient and Separation Factor Influenced by $C_{\text{Ca}}/C_{\text{Sr}}$

$C_{\text{Ca}}/C_{\text{Sr}}$	D_{Sr}	D^{Ca}	β^{S_c}
1	0.4133	0.3720	1.11
2	0.2957	0.2302	1.28
3	0.2044	0.1282	1.59
4	0.0845	0.0245	3.45

2). It means that ion exchange maybe a kind of adsorption mechanism of TMS adsorb Sr^{2+} . But the ratio of Sr^{2+} adsorption and Na^+ desorption is not equal to 1:2. TMS has plenty of carboxyl. Calcium alginate also carries plenty of carboxyl like TMS [27]. It has a great potential for the removal of strontium [28–30]. Carboxyl has strong binding forces with strontium and calcium. These forces include complexation and electrostatic attraction. Complexation is the main adsorption mechanism for calcium alginate. Judged from the structure of TMS and adsorption results, complexation and ion exchange maybe the main adsorption mechanism as shown in Figure 6.

CONCLUSIONS

In this paper, Fe_3O_4 -TMS has been synthesized by TMS adsorb to the surface of Fe_3O_4 . The results of EDS indicate that TMS is modified to the surface of Fe_3O_4 successfully. Fe_3O_4 -TMS shows a great potential on strontium adsorption. 2 h is needed to reach equilibrium. The adsorption capacity of strontium increases rapidly between pH 2.3 and 3.5, and keeps at a high level between 3.5 and 5.6. Calcium has a bigger influence on strontium than sodium. Fe_3O_4 -TMS hardly adsorbs strontium when concentration of calcium reaches 30 mmol/L. Judged from the structure of TMS and adsorption results, complexation and ion exchange maybe the main adsorption mechanism.

ACKNOWLEDGEMENTS

This work was financially supported by National Natural Science Foundation of China (51403229, 21401209, U1407114), the Foundation of Youth Innovation Promotion Association, CAS (Y310031024), the Foundation of Knowledge Innovation Program of CAS (KZCX2-EW-QN309), Natural Science Foundation of Qinghai Province (2013-Z-706, 2015-ZJ-933Q), and the West Light Foundation of CAS.

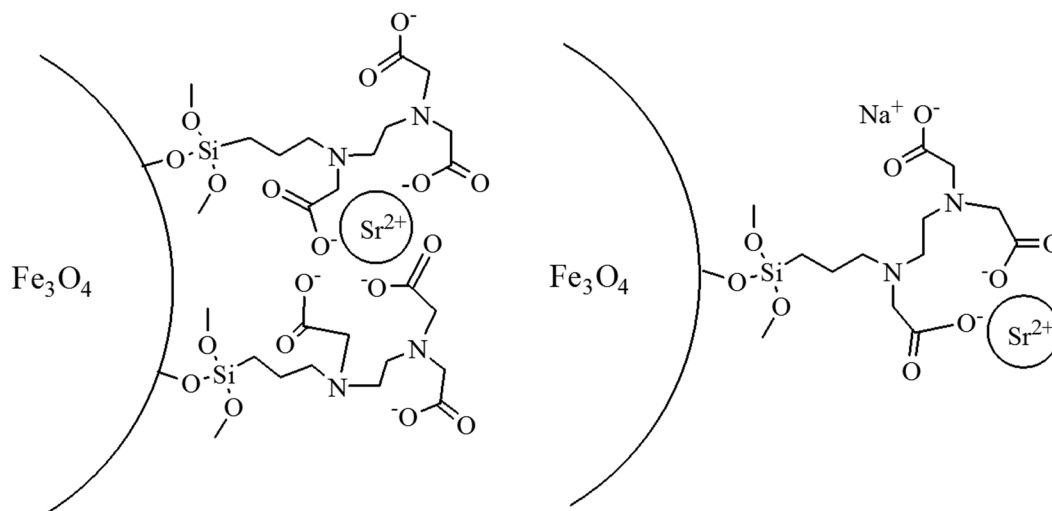


Figure 6. Adsorption mechanism of Sr^{2+} .

REFERENCES

- Isnard, H., Aubert, M., Blanchet, P., Brennetot, R., Chartier, F., Geertsen, V., Manuguerra, F., "Determination of $^{90}\text{Sr}/^{238}\text{U}$ ratio by double isotope dilution inductively coupled plasma mass spectrometer with multiple collection in spent nuclear fuel samples with in situ $^{90}\text{Sr}/^{90}\text{Zr}$ separation in a collision-reaction cell", *Spectrochim. Acta B*, Vol. 61, No. 2, 2006, pp. 150–156. <http://dx.doi.org/10.1016/j.sab.2005.12.003>
- Ji, Y. Q., Hu, Y. T., Tian, Q., Shao, X. Z., Li, J. Y., Safarikova, M., Safarik, I., "Biosorption of Strontium Ions by Magnetically Modified Yeast Cells", *Separ. Sci. Technol.*, Vol. 45, No. 10, 2010, pp. 1499–1504. <http://dx.doi.org/10.1080/01496391003705664>
- Grahek, Z., Eskinja, I., Kosutic, K., Lulic, S., Kvastek, K., "Isolation of radioactive strontium from natural samples: separation of strontium from alkaline and alkaline earth elements by means of mixed solvent anion exchange", *Anal. Chim. Acta*, Vol. 379, No. 1–2, 1999, pp. 107–119. [http://dx.doi.org/10.1016/S0003-2670\(98\)00655-2](http://dx.doi.org/10.1016/S0003-2670(98)00655-2)
- Synhaeve, N., Wade-Gueye, N. M., Musilli, S., Stefani, J., Grandcolas, L., Gruel, G., Soudi, M., Dublineau, I., Bertho, J. M., "Chronic exposure to low concentrations of strontium 90 affects bone physiology but not the hematopoietic system in mice", *J. Appl. Toxicol.*, Vol. 34, No. 1, 2014, pp. 76–86. <http://dx.doi.org/10.1002/jat.2834>
- Rao, S. V. S., Paul, B., Lal, K. B., Narasimhan, S. V., Ahmed, J., "Effective removal of cesium and strontium from radioactive wastes using chemical treatment followed by ultra filtration", *J. Radioanal. Nucl. Ch.*, Vol. No. 2, 246, 2000, pp. 413–418.
- Luo, X., Zhang, G., Wang, X., Gu, P., "Research on a pellet co-precipitation micro-filtration process for the treatment of liquid waste containing strontium", *J. Radioanal. Nucl. Chem.*, Vol. 298, No. 2, 2013, pp. 931–939. <http://dx.doi.org/10.1007/s10967-013-2495-x>
- Kubota, T., Fukutani, S., Ohta, T., Mahara, Y., "Removal of radioactive cesium, strontium, and iodine from natural waters using bentonite, zeolite, and activated carbon", *J. Radioanal. Nucl. Chem.*, Vol. 296, No. 2, 2013, pp. 981–984. <http://dx.doi.org/10.1007/s10967-012-2068-4>
- Duff, M. C., Hunter, D. B., Hobbs, D. T., Fink, S., Dai, D. Z., Bradley, J. P., "Mechanisms of Strontium and Uranium Removal from High-Level Radioactive Waste Simulant Solutions by the Sorbent Monosodium Titanate", *Environ. Sci. Technol.*, Vol. 38, No. 19, 2004, pp. 5201–5207. <http://dx.doi.org/10.1021/es035415+>
- Valsala, T. P., Joseph, A., Sonar, N. L., Sonavane, M. S., Shah, J. G., Raj, K., Venugopal, V., "Separation of strontium from low level radioactive waste solutions using hydrous manganese dioxide composite materials", *J. Nucl. Mater.*, Vol. 404, No. 2, 2010, pp. 138–143. <http://dx.doi.org/10.1016/j.jnucmat.2010.07.017>
- Banerjee, D. M., Rao, A., Samanta, S. K., "Evaluation of Amberlite IRC—718 Chelating Ion Exchange Resin in Loading – Elution – Regeneration Cycles for the Separation and Recovery of Strontium from Alkaline Radioactive Waste", *Solvent Extr. Ion Exc.*, Vol. 26, No. 6, 2008, pp. 687–698. <http://dx.doi.org/10.1080/07366290802437608>
- Raut, D. R., Mohapatra, P. K., Manchanda, V. K., "A highly efficient supported liquid membrane system for selective strontium separation leading to radioactive waste remediation", *J. Membrane Sci.*, Vol. 390–391, 2012, pp. 76–83. <http://dx.doi.org/10.1016/j.memsci.2011.11.015>
- Fan, X. D., Zhang, X. K., "Adsorption of Heavy Metals by Adsorbents from Food Waste Residue", *J. Residuals Sci. Tech.*, Vol. 12, S1, 2015, pp. S155–S158. <http://dx.doi.org/10.12783/issn.1544-8053/12/S1/22>
- Wu, Q. Q., Liu, G. Q., Zheng, X. L., Ren, J. G., "Screening of Heavy Metal Tolerant Microbes in Sludge and Removal Capability of Lead", *J. Residuals Sci. Tech.*, Vol. 12, No. 2, 2015, pp. 85–91. <http://dx.doi.org/10.12783/issn.1544-8053/12/2/7>
- Tan, H., Rao, W., Ma, H., Chen, J., Li, T., "Hydrogen, oxygen, helium and strontium isotopic constraints on the formation of oilfield waters in the western Qaidam Basin, China", *J. Asian Earth Sci.*, Vol. 40, No. 2, 2011, pp. 651–660. <http://dx.doi.org/10.1016/j.jseas.2010.10.018>
- Liu, H., Qing, B., Ye, X., Li, Q., Lee, K., Wu, Z., "Boron adsorption by composite magnetic particles", *Chem. Eng. J.*, Vol. 151, No. 1–3, 2009, pp. 235–240. <http://dx.doi.org/10.1016/j.cej.2009.03.001>
- Vargas, A. M. M., Cazetta, A. L., Kunita, M. H., Silva, T. L., Almeida, V. C., "Adsorption of methylene blue on activated carbon produced from flamboyant pods (*Delonix regia*): Study of adsorption isotherms and kinetic models", *Chem. Eng. J.*, Vol. 168, No. 2, 2011, pp. 722–730. <http://dx.doi.org/10.1016/j.cej.2011.01.067>
- Iram, M. Guo, C. Guan, Y. Ishfaq, A., Liu, H., "Adsorption and magnetic removal of neutral red dye from aqueous solution using Fe_3O_4 hollow nanospheres", *J. Hazard. Mater.*, Vol. 181, No. 1–3, 2010, pp. 1039–1050. <http://dx.doi.org/10.1016/j.jhazmat.2010.05.119>
- Li, Q., Liu, H., Liu, T., Guo, M., Qing, B., Ye, X., Wu, Z., "Strontium and calcium ion adsorption by molecularly imprinted hybrid gel", *Chem. Eng. J.*, Vol. 157, No. 2–3, 2010, pp. 401–407. <http://dx.doi.org/10.1016/j.cej.2009.11.029>
- Oleksienko, O., Levchuk, I., Sitarz, M., Meleshevych, S., Strelko, V., Sillanpaa, M., "Removal of strontium (Sr^{2+}) from aqueous solutions with titanosilicates obtained by the sol-gel method", *J. Colloid Interf. Sci.*, Vol. 438, 2015, pp. 159–168. <http://dx.doi.org/10.1016/j.jcis.2014.09.075>
- Zhang, L., Wei, J., Zhao, X., Li, F., Jiang, F., "Adsorption characteristics of strontium on synthesized antimony silicate", *Chem. Eng. J.*, Vol. 277, 2015, pp. 378–387. <http://dx.doi.org/10.1016/j.cej.2015.04.145>
- Ahmadpour, A., Zabihi, M., Tahmasbi M., Bastami, T. R., "Effect of adsorbents and chemical treatments on the removal of strontium from

- aqueous solutions”, *J. Hazard. Mater.*, Vol. 182, No. 1–3, 2010, pp. 552–556. <http://dx.doi.org/10.1016/j.jhazmat.2010.06.067>
22. Inan, S., Altas, Y., “Adsorption of Strontium from Acidic Waste Solution by Mn-Zr Mixed Hydrous Oxide Prepared by Co-Precipitation”, *Separ. Sci. Technol.*, Vol. 45, No. 2, 2010, pp. 269–276. <http://dx.doi.org/10.1080/01496390903409666>
23. Sheng, G., Wang, S., Hu, J., Lu, Y., Li, J., Dong, Y., Wang, X., “Adsorption of Pb(II) on diatomite as affected via aqueous solution chemistry and temperature”, *Colloid. Surface. A*, Vol. 339, No. 1-3, 2009, pp. 159–166. <http://dx.doi.org/10.1016/j.colsurfa.2009.02.016>
24. Lackovic, K., Angove, M. J., Wells, J. D., Johnson, B. B., “Modeling the adsorption of Cd(II) onto goethite in the presence of citric acid”, *J. Colloid Interf. Sci.*, Vol. 269, No. 1, 2004, pp. 37–45. <http://dx.doi.org/10.1016/j.jcis.2003.08.041>
25. Wallace, S. H., Shaw, S., Morris, K., Small, J. S., Fuller A. J., Burke, I. T., “Effect of groundwater pH and ionic strength on strontium sorption in aquifer sediments: Implications for ⁹⁰Sr mobility at contaminated nuclear sites”, *Appl. Geochem.*, Vol. 27, No. 8, 2012, pp. 1482–1491. <http://dx.doi.org/10.1016/j.apgeochem.2012.04.007>
26. Veglio, F., Esposito, A., Reverberi, A. P., “Copper adsorption on calcium alginate beads: equilibrium pH-related models”, *Hydrometallurgy*, Vol. 65, No.1, 2002, pp. 43–57. [http://dx.doi.org/10.1016/S0304-386X\(02\)00064-6](http://dx.doi.org/10.1016/S0304-386X(02)00064-6)
27. Gok, C., Gerstmann, U., Aytas, S., “Biosorption of radiostrontium by alginate beads: application of isotherm models and thermodynamic studies”, *J. Radioanal. Nucl. Chem.*, Vol. 295, No. 1, 2013, pp. 777–788. <http://dx.doi.org/10.1007/s10967-012-1838-3>
28. Fuks, L., Oszczak, A., Gniazdowska, E., Sternik D., “Calcium alginate and chitosan as potential sorbents for strontium radionuclide”, *J. Radioanal. Nucl. Chem.*, Vol. 304, No. 1, 2015, pp. 15–20. <http://dx.doi.org/10.1007/s10967-014-3698-5>
29. Idota, Y., Harada, H., Tomono, T., Morimoto, K., Kobayashi, S., Kakimoto, C., Miyajima, C., Kasahara, F., Ogihara, T., “Alginate Enhances Excretion and Reduces Absorption of Strontium and Cesium in Rats”, *Biol. Pharm. Bull.*, Vol. 36, NO. 3, 2013, pp. 485–491. <http://dx.doi.org/10.1248/bpb.b12-00899>
30. Moreira, A. P. D., Sader, M. S., Soares G. D. A., Leao, M. H. M. R., “Strontium Incorporation on Microspheres of Alginate/ β -tricalcium Phosphate as Delivery Matrices”, *Mater. Res.*, Vol. 17, No. 4, 2014, pp. 967–973. <http://dx.doi.org/10.1590/S1516-14392014005000095>

Characteristics of Mercury Emissions from a Coal-fired Power Plant

LIU QI-ZHEN¹, SUN YI¹, BAI YONG^{2,*}, XU XIAO-YU¹, TIAN YING-MING² and LU JINMEI³

¹Shanghai Environmental Monitoring Center 200030, China

²Shanghai HuaChuan Environment Technology Corp. 200232, China

³Department of Engineering and Safety, UiT The Arctic University of Norway 9037, Tromsø, Norway

ABSTRACT: Coal-fired power plant is one of the important mercury emission sources in the world. In order to understand the characteristics of mercury emission from the coal-fired power plants in Shanghai area, a series of measurement data was collected on a continuous basis to evaluate the mercury emissions speciation profiles, and the mercury emissions factors as well. The whole-process mercury emissions data in 2012 was also obtained with the manual sampling method. The results show that (1) the ratio of the mercury balances in the two units were 75.6% and 87.8%, respectively; (2) the existing air pollutant control devices in the two power plants showed certain mercury removal capability, and the average mercury removal efficiencies from dust collector plus Wet-FGD was more than 50%; (3) the average mercury content in the mixed coal 73 $\mu\text{g}/\text{kg}$, which ranged from 40 to 102 $\mu\text{g}/\text{kg}$. The annual average emission concentration of Hg^{2+} in #1 Unit was close to that in #4 Unit. However, the emission concentration of Hg^0 in #4 Unit was 2.62 $\mu\text{g}/\text{Nm}^3$, two times higher than that in #1 Unit. The Hg^0 was removed by the Fabric Filter, whose efficiency was two times more than the ESPs. (4) In the coal-fired power plants, the mercury emission was greatly impacted by coal types, APCD.

INTRODUCTION

MERCURY emission from anthropogenic sources is a global environmental pollution problem. According to the recent global inventory, about 65% of emission came from stationary fuel combustion in 2000. Geographically, Asia accounts for about 54% of the emission, and China is the largest Hg emitting country. As the largest coal producer and consumer in the world, the amount of Hg released from China has been increasing rapidly in recent years [1–2]. Meanwhile, human health risk caused by Hg are getting more and more attention [3–4]. Researches show that the main source of mercury emission to the atmosphere is fossil fuel burning, especially coal combustion. In the U.S., recent estimates attribute 56% of all anthropogenic Hg emissions to stationary combustion sources and 87% of all Hg emissions from stationary combustion sources to Coal-fired power plants. Coal-fired power plants are the largest mercury emission source in the world [5–8]. Mercury emission to the atmosphere accounts for 60%, or even more of the total mercury emission

from Coal-fired power plants [9]. Wang *et al.* devoted themselves to the inventory of mercury emissions from anthropogenic activities in China.

In the inventory, many uncertainties still remain in our knowledge of primary anthropogenic releases of mercury to the atmosphere in China. Specifically, there are lacking actual measurements of Hg emission rates, Hg species profiles from Chinese combustors and the capture of Hg in Chinese emission control devices [10]. There are even higher uncertainties for the speciation profiles. Hence, there has been increasing needs to characterize the Hg emissions from coal-fired power plants in China [11–12]. A total of 124 onsite tests of coal-fired power plants were selected from existing literature to characterize mercury behavior so as to calculate mercury emission factor in the world, among which 29 tests were conducted in China [13]. In these 29 tests, the mercury measurement method is 30B, or Ontario Hydro Method but it lacks of continuous data to evaluate the mercury emissions speciation profiles and the mercury emissions factor.

The most important factors affecting mercury emissions are the mercury content of coal and the mercury removal efficiency of APCD (air pollutant control devices). At present, the power plants were equipped with

*Author to whom correspondence should be addressed.
E-mail: bai.yong@huachuantech.com

the high efficiency dust collector and the Wet-FGD for the very low pollutant emission limit. Power plants will also burn many kinds of coal together to gain good economic benefit and meet the emission limit. In this paper, we used the traditional manual sample test methods, and Tekran 3300 Hg-CEMs to study the mercury balances and the synergistic effect of the dust collectors and FGD facilities for mercury removal. We estimated the mercury emission Characteristics in coal-fired power plants in Shanghai area with one year continuous data from the Tekran 3300 Hg-CEMs. The objective is to grasp the mercury emission speciation profiles in the coal-fired power plants and the relationship between mercury emissions and the existing APCD in Shanghai area.

MATERIALS and METHODS

The Information of the Two Coal-Fired Power Plants

Units #1 and #4 are coal-fired power plants in Shanghai area, which were selected as the research objects. They are 300 MW units. The existing APCD are listed in the Table 1.

The Sample and Test Methods

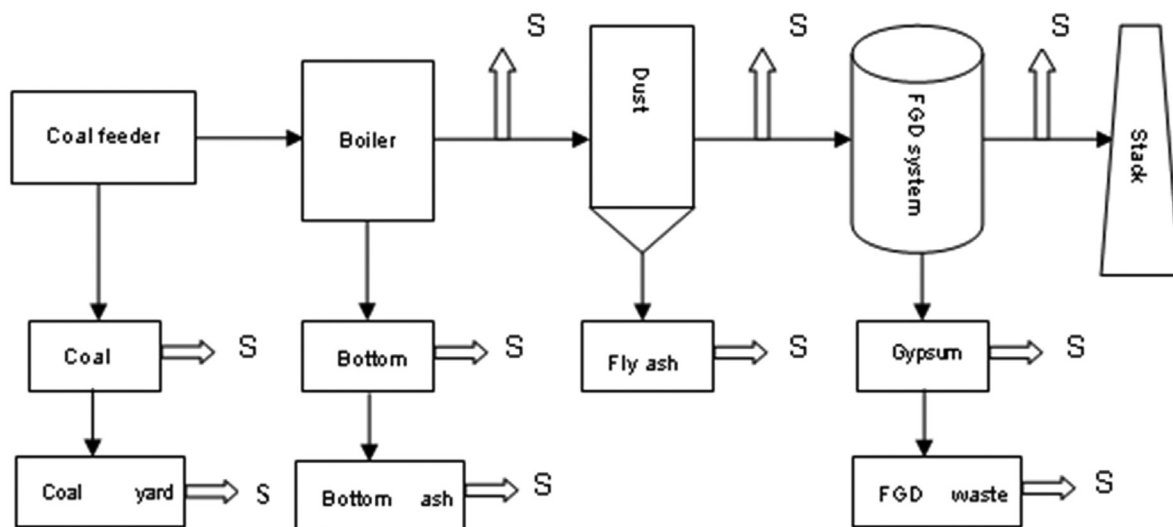
The sampling locations are shown in Figure 1. The mercury emission from the coal fired power plant is

Table 1. The Details of The Existing APCD.

Name	SCR	Dust Collector	Desulfurization	GGH
#1	NO	ESPs	Wet-FGD	YES
#4	NO	Fabric Filters	Wet-FGD	YES

from the mercury containing coal. APCD will affect the mercury emission, some of which will exist in the bottom ash, fly ash, gypsum and waste water. The rest will be emitted with the flue gas.

In one sampling cycle, we calculate the mercury mass distribution after the different APCD to get the mercury transform regulation. Gaseous mercury sampling was conducted simultaneously at the inlet of the dust collector, inlet of the Wet-FGD (outlet of the dust collector) and outlet of the Wet-FGD. In the other sampling cycle, two paired samples were running at the same sampling points for gaseous mercury (USEPA Method 30B). At the same time, about ten pieces of solid samples were collected from the raw coal [Method of the mercury in raw coal is Determination of Mercury in Coal (GB/T 16659-2008)], bottom ash, fly ash, gypsum (USEPA Method 7473), waste water [Method of mercury in waste water is atomic fluorophotometry method in Air and Waste Gas Monitor Analysis (4th Edition)], and record the flue gas flow, the hourly consumptions or outputs of various solid samples. All the data is used to calculate the mercury balances. The two Tekran 3300 Hg-CEMs were installed at the inlet of the stacks, which monitor the mercury emissions online.



S - sampling point

Figure 1. The sample points we're composed of raw coal, bottom ash, inlet of the dust collector, fly ash, outlet of the dust collector, outlet of the Wet-FGD, gypsum, and waste water. The sample points are from raw coal to mercury emissions in the stack, which can track the mercury transfer and emission rule.

RESULT AND DISCUSSION

The Mercury Balances

In the two power plants, the average mercury content was 73 $\mu\text{g}/\text{kg}$ in raw coal, which is lower than the average mercury mass concentration 220 $\mu\text{g}/\text{kg}$ in China [14]. The mercury mass concentration varied greatly from 40–102 $\mu\text{g}/\text{kg}$. It is very close to Shuxiao Wang’s result in 2010, which tested a mercury mass concentration range from 17–385 $\mu\text{g}/\text{kg}$ in six power plants [15]. After the burning of raw coal at the

high temperature in combustion zone of boilers, the Hg in coal releases into the exhaust gas as elemental mercury (Hg^0) vapor. With the existence of Cl, Br, SO_2 and particles in flu gas, part of the Hg^0 is oxidized into Hg^{2+} either by gas phase oxidation or catalytic oxidation due to thermo-chemical processes [16–17]. Less than 1% Hg was removed by the bottom ash, and about 41.82–53.4% Hg was adsorbed by the fly ash and removed by the dust collector, and about 17.26–39.96% Hg was removed by Wet-FGD, the remaining mercury emitted to the atmosphere. In Figure 2, it can be seen from the mercury balances and distribution in the two

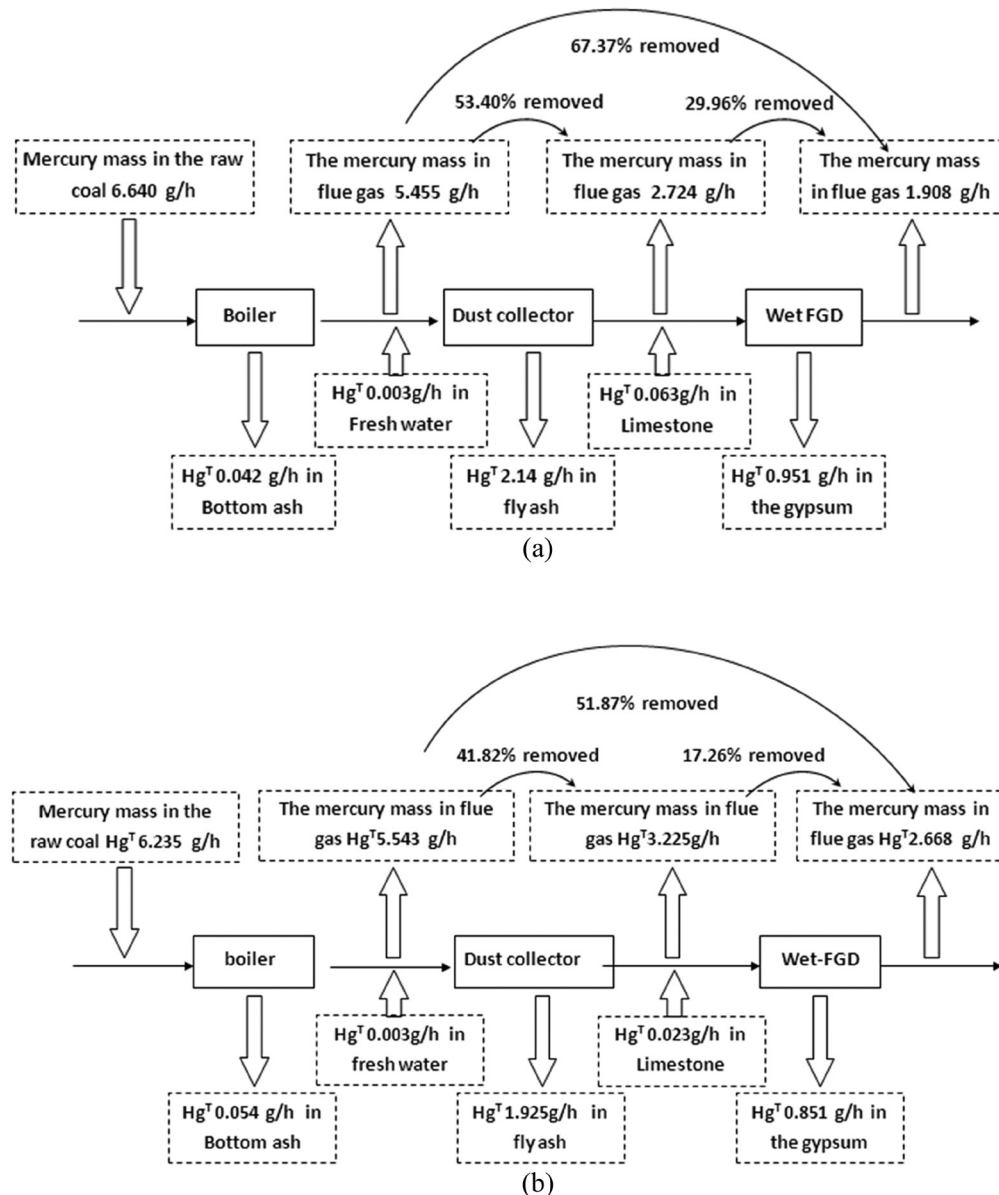


Figure 2. The characteristics of the mercury emissions are complex in the power industry. The influential factors include coal type, boiler type, combustion type, dust collectors, Wet-FGD system and so on. We can see the mercury transferred after each equipment in the two power plants. The mercury emission mass reduced about 17% after the boiler. There are two reasons. Firstly, mercury content is an average value from all kinds of coals in power plants. However, the coal burning is not an fixed proportion. Secondly, there are ratio measure errors after the boiler.

power plants, the existing APCD had certain mercury removal capability, average mercury removal efficiencies of dust collector plus Wet-FGD was more than 50%.

The mercury balances in the two units were 75.6% and 87.8% respectively. The two results were within the acceptable error range of $\pm 30\%$ [18–19].

Annual Characteristic of the Mercury Emissions

In Figure 3 and Table 2, the average total gaseous mercury emission concentration was not high. It was $1.34 \mu\text{g}/\text{Nm}^3$ in the 1# Unit, but $3.01 \mu\text{g}/\text{Nm}^3$ in the 4# Unit, which was two times more than that in the #1 unit. We found that the percentage of the average element mercury concentration was very high in the total gaseous mercury emission, 1# unit 72%, 4# unit 87%. The oxidized mercury concentration was rather low, but the average concentration was very close to each other.

In Table 2, the element mercury emission was $2.62 \mu\text{g}/\text{Nm}^3$ in the #4 unit, two times more than that from #1 unit $0.96 \mu\text{g}/\text{Nm}^3$. There was no big difference in the coal types used in the two Units. The difference was the dust collector, Fabric Filters with ESPs. In the #1 Unit, the Fabric Filters collects the particles in the flue gas, and some unburned carbon was also collected. The fine particles and the unburned carbon build up on the surface of the Fabric Filters and absorb the element mercury extensively [20–21].

Table 2. The Mercury Emission Average Concentration in One Year.

Name	Total Mercury ($\mu\text{g}/\text{Nm}^3$)	Element Mercury ($\mu\text{g}/\text{Nm}^3$)	Oxidized Mercury ($\mu\text{g}/\text{Nm}^3$)
#1	1.34 (100%)	0.96 (72%)	0.38 (28%)
#4	3.01(100%)	2.62 (87%)	0.39 (13%)

The annual average Hg^{2+} emission from #1 Unit and Unit #4 were $0.38 \mu\text{g}/\text{m}^3$ and $0.39 \mu\text{g}/\text{m}^3$ respectively. This means that the Wet-FGD systems have effect on the removal of Hg^{2+} . The Wet-FGD systems mainly remove Hg^{2+} by means of the scrubber solution. As the Hg^{2+} is soluble in water, when gaseous Hg^{2+} is dissolved in the Wet-FGD scrubber solution. Hg^{2+} reacts with the sulfate, which will produce insoluble mercury sulfate and deposit in the slurry. Thus the Hg^{2+} can be removed. That is why the Wet-FGD systems have efficiency of Hg^{2+} . However, in these two units, the annual average Hg^{2+} concentration is not very low. The EGU Mercury Speciation Profiles for the Clean Air Mercury Rule project list mercury speciation profile data of the power plant. The average Hg^{2+} concentration after Wet-FGD normally lower than $0.1 \mu\text{g}/\text{m}^3$, with the exception of one power plant which had a Hg^{2+} concentration of $0.32 \mu\text{g}/\text{m}^3$ [22]. We can make sure that the Wet-FGD can remove the Hg^{2+} , but there exists some unknown conditions which will affect the Hg^{2+} removal efficiency.

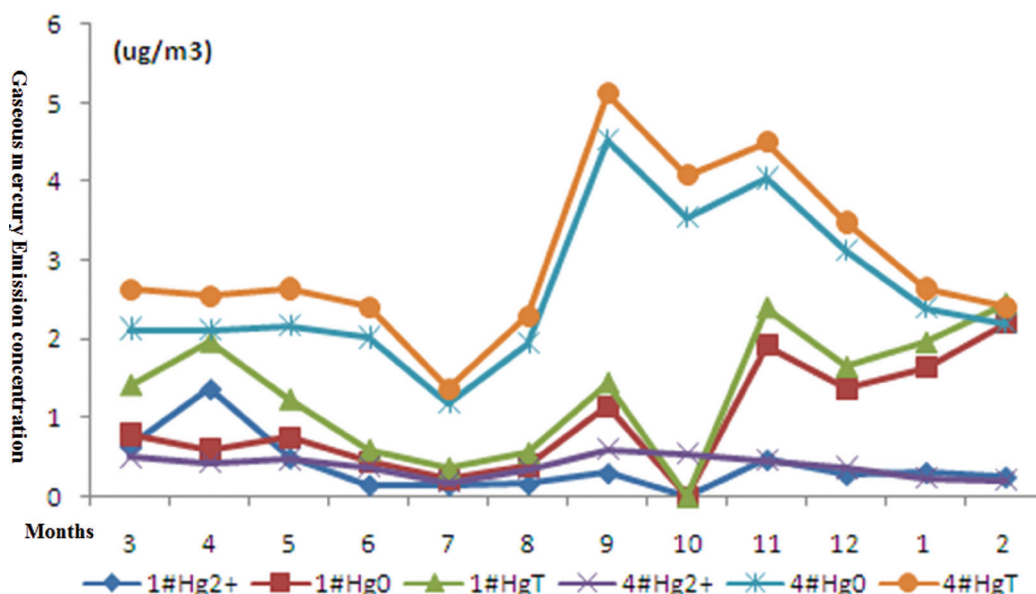


Figure 3. The annual operating data of the Tekran 3300 Hg-CEMs from March 2012 to February 2013. Tekran 3300 Hg-CEMs is an online system. It monitors the mercury emissions and calculates the average mercury emission concentration, which is converted with 6% oxygen.

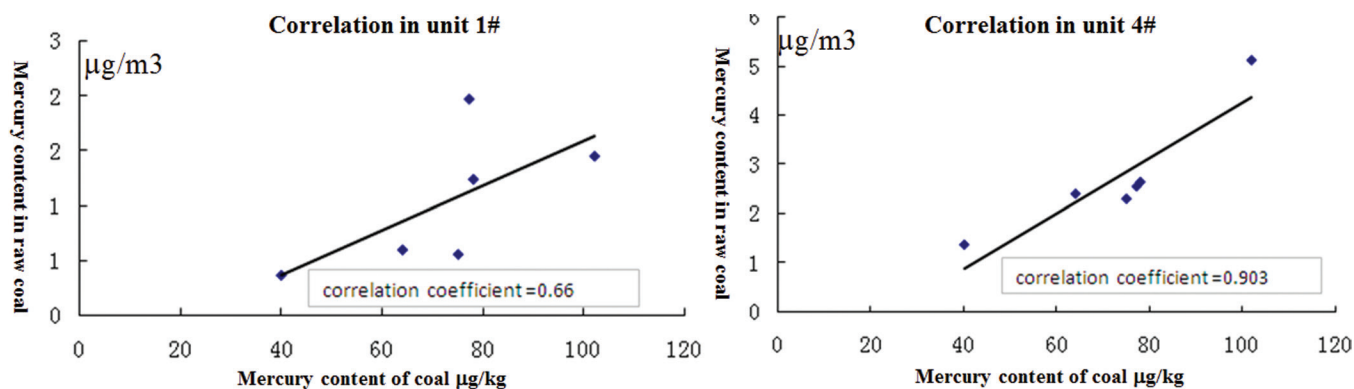


Figure 4. Correlations between mercury content of coal and total mercury emission concentration in flue gas.

Impact of Coal Types

We sampled the raw coal in the two power plants from April to September in 2012. The data shows the average mercury content in raw coal in the power plant was 73 µg/kg (Figure 4). Moreover, the mercury content varied in the different coal types in power plants. The average mercury content is lignite 0.221 mg/kg (range from 0.102–0.309 mg/kg), bituminous coal 0.045 mg/kg (range from 0.00–0.213 mg/kg), subbituminous coal 0.132 mg/kg (range from 0.019–0.532 mg/kg), anthracite coal 0.196 mg/kg (range from 0.085–0.437 mg/kg). The Halogen content varied in different coal types in the power plant. The average Halogen content are lignite Cl 238 mg/kg, Br 74 mg/kg, bituminous coal (0.045 mg/kg), subbituminous coal (0.132 mg/kg), anthracite coal (0.196 mg/kg) (Department of Environmental Science and Engineering Tsinghua University, Reducing mercury emissions from coal combustion in the energy sector United Nations Environment Program).

At present, the coal-fired power plants in China often burn many kinds of coal together to get a good economic benefit, and the mercury emissions are in positive correlations with the mercury content in the coal. As the coal type changes, the mercury emissions will change too. This is because mercury content in the raw coal changes substantially from 40 to 102 µg/kg. There is much difference in the correlation coefficient between mercury content of coal and total mercury emission concentration in flue gas in unit 1# and unit 4# (Figure 4). In the unit 4 that uses ESP for dust collection, the correlation is 0.903, which is much higher than that in unit 1#, which uses Fabric Filter for dust collection. As mentioned before, fabric filter capture mercury in a more efficient way due to unburned carbon. The percentage of unburned carbon changes in different mixed coals and different fire modes. Prob-

ably, this is the reason of low correlation. In the unit 4# with EPS for dust collection, the mercury emission concentration affects greatly by mercury content in the raw coal.

CONCLUSIONS

The data collected in the whole-process mercury emissions in 2012 in two coal-fired power plants with the manual sampling showed that: (1) the ratio of the mercury balances in the two units were 75.6% and 87.8% respectively; (2) the existing air pollutant control devices in the two power plants had certain mercury removal capability, and the mercury removal efficiency of dust collector plus Wet-FGD was more than 50% on average; (3) In the unit 4#, ESP for dust collection, mercury content of coal and total mercury emission concentration in flue gas is high correlation.

To better understand the characteristic of Hg emissions from coal-fired power plants in China, there is a need to collect long time continuous data to evaluate the mercury emissions speciation profiles and the mercury emissions factor. The long time Hg-CEM data showed that: (1) The annual average emission concentration of Hg²⁺ in #1 Unit was close to that in the #4 Unit. However, the emission concentration of Hg⁰ in #4 Unit was 2.62 µg/Nm³, two times more than that in #1 Unit. The Hg⁰ was removed by the Fabric Filter, whose efficiency was two times more than the ESPs. (2) In the coal-fired power plants, coal types along with APCD have a significant influence on the mercury emissions. In 1999, the coal-fired power plants in China were seldom equipped with flue gas purification devices. But nowadays they have high efficiency dust collector and Wet-FGD. At present, the coal-fired power plants in China often burn many kinds of coal in order to get a good

economic benefit, and the average mercury content in the mixed coal in the two power plants is 73 $\mu\text{g}/\text{kg}$ (40–102 $\mu\text{g}/\text{kg}$). This is one of the two reasons for lower mercury emissions in two power plants.

ACKNOWLEDGEMENTS

This work was funded by the China EPA National Department Public Benefit Research Foundation (No. 201209050). We would like to acknowledge Doctor Liu Xin and Doctor Zhang Kun for their assistance in paper proofreading.

REFERENCES

- Pacyna, E.G., Pacyna, J.M., Steenhuisen, F., and Wilson, S. 2006. "Global anthropogenic mercury emission inventory for 2000", *Atmos. Environ.*, Vol. 40, No. 22, pp. 4048–4063. <http://dx.doi.org/10.1016/j.atmosenv.2006.03.041>
- Pirrone, N., Mason, R., et al. 2009. *Mercury Fate and Transport in the Global Atmosphere: Emissions, Measurements and Models*, USA, PA: Springer
- Jia, J.L., et al. "Human Health Risk Assessment of Harmful Trace Elements in Coal Gasification Residues", *Journal of Residuals Science & Technology*, No. 12, 2015, pp. 97–103. <http://dx.doi.org/10.12783/issn.1544-8053/12/S1/15>
- Chen, Y., et al. "Heavy Metal Pollution Characteristics in the Kaili Coal Mining Region, Guizhou Province, China", *Journal of Residuals Science & Technology*, No. 12, 2015, pp. 123–130. <http://dx.doi.org/10.12783/issn.1544-8053/12/S1/18>
- Wu, D. and Zhang, S.Q., "Comments on Prevention Measures and Regulation of Mercury Pollution Overseas", *Environmental Protection*, No. 5B, 2007, pp. 72–76.
- Report on global atmospheric mercury assessment: Sources, emissions and transport, 2009, Geneva, UNEP.
- Nriagu, J.Q. and Paeyna, J.M., "Quantitative assessment of worldwide contaminant ion of air, water and soil by trace metals", *Nature*, No. 333, 1988, pp. 134–139. <http://dx.doi.org/10.1038/333134a0>
- Ambrose, J. L., Gratz, L. E., Jaffe, D. A., et al. "Mercury Emission Ratios from Coal-Fired Power Plants in the Southeastern U.S. during NOMADSS", *Environmental Science & Technology*, No. 49, 2015, pp. 10389–10397. <http://dx.doi.org/10.1021/acs.est.5b01755>
- Zhang, L. and Wang, M.H., "Environmental mercury contamination in China: sources and impacts", *Environment International*, No. 33, 2007, pp. 108–121. <http://dx.doi.org/10.1016/j.envint.2006.06.022>
- Wu, Y., Streets, D.G., Wang, S.X., Hao, J.M., et al. "Uncertainties in estimating mercury emissions from coal-fired power plants in China", *Atmos. Chem. Phys.*, No. 10, 2010, pp. 2937–2947.
- Niksa, S., and Fujiwara, N., "Predicting complete Hg speciation along coal-fired utility exhaust systems", *EPRI-DOE-EPAA & WMA combined utility air pollution control symposium: The MEGA symposium*, No. 45, 2004, Washington DC, USA.
- Clack, H., "Mercury capture within coal-fired power plant electrostatic precipitators model evaluation", *Environmental Science and Technology*, No. 43, 2009, pp. 1460–1466. <http://dx.doi.org/10.1021/es8015183>
- Reducing mercury emissions from coal combustion in the energy sector, United Nations Environment Program, 2011, China, Tsinghua University.
- Wang, Q.C., Shen, W.G. and Ma, Z.W., "Estimation of Mercury Emission from Coal Combustion in China", *Environ. Sci. Technol.* No. 34, 2000, pp. 2711–2713. <http://dx.doi.org/10.1021/es990774j>
- Wang, S.X., Zhang, L., Li, G.H., Wu, Y., Hao, J.M., et al., "Mercury emission and speciation of coal-fired power plants in China", *Atmospheric Chemistry and Physics*, No. 10, 2010, pp. 1183–1192. <http://dx.doi.org/10.5194/acp-10-1183-2010>
- Meij, R., Vredendregt, L. H. J., and Winkel, H. "The fate and behavior of mercury in coal-fired power plants", *Journal of Air Waste Management*, No. 52, 2002, pp. 912–917. <http://dx.doi.org/10.1080/10473289.2002.10470833>
- Galbreath, K. C. and Zygarrlicke, C. J., "Mercury transformations in coal combustion flue gas", *Fuel Process. Technology.*, No. 65, 2000, pp. 289–310.
- Takahisa, Y. and Kazuo, A., "Mercury emissions from a coal fired power plant in Japan", *The Science of the Total Environment*, Vol. 259, No. 1, 2000, pp. 97–103.
- Yu, L.X., Qu, Y.J., Jia, J., et al., "Study and Analysis of Mercury Migration and Transformation from Coal-fired Power Plants Based on Field Tests", *Environmental Science & Technology*, Vol. 37 No. 120, 2014, pp. 463–466.
- Wang, Q., Duan, Y.F., Wu, C.J., et al. "Research on Mercury Removal Characteristics of Desulphurization System of Coal-fired Power Plants", *Boiler Technology*, Vol. 39, No.1, 2008, pp. 69–75.
- Xu, W., Wang, J., Wang, W., "Preliminary Investigation on the Effects of Dust Removal and Desulfurization of Coal-fired Generated Flue Gas on Removal of Different Formations of Mercury", *East China Electric Power*, Vol. 38, No. 1, 2010, pp. 47–50.
- David, B. and Shelly, J., "Mercury Speciation Profiles for the Clean Air Mercury Rule". 2011, US EPA.

Extraction of Aluminum from Coal Fly Ash by Alkali Activation with Microwave Heating

NENGSHENG LIU¹, JINHUI PENG¹, LIBO ZHANG¹, SHIXING WANG¹, SHAOJUN HUANG² and SUFANG HE^{2,*}

¹Faculty of Metallurgical and Energy Engineering, Kunming University of Science and Technology, Kunming 650093, P. R. China

²Research Center for Analysis and Measurement, Kunming University of Science and Technology, Kunming 650093, P. R. China

ABSTRACT: Recovering aluminum from coal fly ash (CFA) is a practical option for its value-added utilization. The alkali activation of CFA with Na_2CO_3 was carried out using two heating methods: the conventional heating (CH) and microwave heating (MWH). Compared to CH, MWH enhanced the atomic diffusion and mass transportation in the CFA- Na_2CO_3 mixture, accelerated the decomposition of mullite and the formation of the soluble Al-containing materials, thus greatly reducing the sintering temperature and dramatically shortening the activation reaction time. Under the moderate activation condition in MWH (700°C and 20 min), the aluminum extraction could reach 95.52% or more.

INTRODUCTION

COAL FLY ASH (CFA), a well-known industrial by-product, is increasingly spewed out mainly from coal-fired power plants, and also partly from the smelting, and chemical industries [1,2]. Currently, the annual generation of CFA is estimated more than 750 million tons all over the world [1–4]. In China, the annual generation is still increasing and anticipated to reach 580 million tons by 2015 [4], due to the rapid growth of industries. At present, the utilization of CFA is mainly concentrated in some low and medium value applications such as concrete production [4], soil amelioration [4–7], ceramic industry [8–10], mineral filler [11] and so on. Moreover, the utilization rate is very low [1,4], and so a large proportion of CFA is generally dumped in lands without further treatments [1,4], which not only results in the occupancy of vast lands, but also causes serious pollution of soil, water, air and even organism [1,4,12,13]. Therefore, the efficient, safe and high value disposal of CFA is highly desired.

Extracting aluminum from CFA is a practical option since CFA contains about 10–55% (by mass) of Al_2O_3 [14–18]. Especially, high-aluminum CFA (40–50%) has been found in southern Inner Mongolia, northern Shanxi and the Shaanxi province of China [4,19–20]. The proven high-alumina coal reserve in Inner Mongo-

lia is approximately 50 billion tons [4]. So, it is estimated that about 15 billion tons of high-alumina CFA will be produced, namely, about 5 billion tons of alumina can be recovered [4]. This huge number is equivalent to 12 billion tons of bauxite, which is the 3.2 times as abundant as the proven bauxite resources in China [4]. These are especially important for China since it depends so much on the import of bauxite [4], mainly from Indonesia and Australia, to meet the demand for alumina. Therefore, several newly revised regulations have been issued by the state and local government to encourage the recovery of alumina from this high-alumina CFA and then the comprehensive utilization [4,19].

CFA mainly consists of mullite, quartz and other amorphous phases [1,20]. As the major form of aluminum in CFA, the mullite is very stable and generally considered a non-reactive reactive matter [1,20–21]. Owing to these, it is a stiff task to efficiently extract aluminum from CFA via the conventional Bayer Process and direct acid leaching method only after a vigorous treatment through some methods [1,20,22–24]. The alkali activation of CFA, namely, the CFA is mixed with certain alkaline activators (such as NaOH , Na_2CO_3 , Lime and calcium oxide), then calcined at high temperature (1000–1200°C) [25–26], has been extensively used to motivate the reactivity of CFA to improve the aluminum extraction [1,25,27–28]. Although some competitive development and improved aluminum extraction have been achieved with the help of this acti-

*Author to whom correspondence should be addressed.
E-mail: shuca1983@163.com; Tel.: +86-871-65113973; Fax: +86-871-65111617

vation [1,27–28], the large amounts of additive and the high energy consumption are still the major obstacles hindering the large-scale applications [1,19,27–28]. To solve these problems, the improvement of heating efficiency is essential.

In light of these, the advance and development of microwave technology open up new opportunities. Generally speaking, microwave heating (MWH) is a process that can couple electromagnetic field with materials to convert into thermal energy [19,29]. It is widely accepted that MWH can enhance the diffusion and mass transportation in solids [30–32], thus lowering the energy barrier of reaction. Owing to these, MWH has many advantages, including lower energy consumption, a faster heating rate and less processing time [19,33–36], and been frequently applied in the processes of energy-saving sintering [19,37–39].

The MWH was therefore introduced into the Na_2CO_3 -activation system of high-aluminum CFA (obtained from Inner Mongolia) in the present study, and then followed by the leaching with dilute hydrochloric acid. The effect of activation temperature and holding time on the extraction efficiency of alumina were studied in detail. To highlight the superiority of MWH, the conventional heating (CH) with the muffle furnace was also used for Na_2CO_3 -activation system. Many analysis techniques such as TG-DSC, XRD, XRF and SEM were used to follow the changes in the physic-chemical properties of CFA before and after the Na_2CO_3 -activation.

EXPERIMENTAL

Materials and Instruments

CFA samples used in this study were obtained from the coal-fired power plant in Inner Mongolia, China. The hydrochloric acid (HCl, Shanghai reagent Factory) and sodium carbonate (Na_2CO_3 , Shanghai reagent Factory) are analytical grade reagents.

The microwave furnace [37], equipped with a single-mode continuous controllable power, was used for MWH. A microwave frequency of 2.45 GHz was applied and the output power is controlled within the maximum of 2 kW. The activation temperature was measured with thermocouple, and controlled by varying the input microwave power. For comparison, the muffle furnace (YFX12/16Q-YC, Y-feng, China), was also used for CH experiments. Water bath magnetic stirrer (DF-101S, YUHUA, China) was used in the leaching process.

Processing Procedure

CFA samples were firstly dried at 70°C for 2 h to eliminate the effect of relative humidity, and then mixed with Na_2CO_3 (the weight ratio of Na_2CO_3 /CFA was 1:1). This mixture was soaked with a little of de-ionized water, and then cured at room temperature for 2 h. After these, the muffle furnace or the microwave furnace was used to roast the mixture. Then, the grinded mixture was leached with HCl of 6 mol/L at 363 K for 60 min, using the Solid/Liquid ratio of 1:10. Finally, The Al concentration of leaching solution was analyzed by ICP-OES (Prodigy, Leeman, USA). The extraction efficiency was expressed by the following formula:

$$\eta = \frac{m_F(\text{Al}_2\text{O}_3)}{m_{ACFA}(\text{Al}_2\text{O}_3)} \times 100\% \quad (1)$$

$$= \frac{C(\text{Al}^{3+})V(F) \cdot \frac{102}{54}}{m_{ACFA}(\text{Al}_2\text{O}_3)} \times 100\%$$

Where η is the extraction efficiency of aluminum, $m_F(\text{Al}_2\text{O}_3)$ denotes the mass of Al_2O_3 in leaching solution, $m_{SCFA}(\text{Al}_2\text{O}_3)$ denotes the mass of Al_2O_3 in activation coal fly ash before leaching, $C(\text{Al}^{3+})$ is the Alumina concentration in leaching solution, and $V(F)$ denote the volume of leaching solution.

Analysis

The phase analysis was carried out on an automated power X-ray diffractometer (TTRAX III, RIGAKU, Japan) with Cu Ka radiation, at 40 kV and 700 mA. The scan ranged from 10° to 90° at the speed of 10°/min.

TG-DSC was carried out in a Simultaneous thermal analyzer (STA 449 F3 Jupiter, NETZSCH, Germany) in an argon atmosphere. The sample loading was 10 mg and the heating rate was 5°C/min.

Chemical composition of CFA was analyzed by X-ray fluorescence analyzer (1800, SHIMADZU, Japan), at 40 kV and 95 mA, with the prt of 8 ml/min.

Particle size distribution of CFA raw material was analyzed by Laser particle size analyzer (Rise-2002, RISE, China).

RESULTS AND DISCUSSION

The Physic-chemical Properties of Raw CFA

CFA is one of the most complex materials [4,41].

The insight into the chemical and mineralogical properties of CFA is critical for the extraction of alumina.

The chemical composition of CFA measured by XRF showed that the weight contents of SiO_2 , Al_2O_3 , Fe_2O_3 and CaO were 37.47%, 46.22%, 5.05% and 3.17%, respectively, indicating that this CFA is a kind of high-alumina ones.

The XRD pattern of the raw CFA (Figure 1) exhibited that only strong peaks assigned to $\text{Al}_6\text{Si}_2\text{O}_{13}$ (mullite) and SiO_2 (quartz and amorphous silica) had been detected by XRD. No other phase had been found.

The particle size distribution of CFA was also investigated. $D_5 = 3.47 \mu\text{m}$, $D_{10} = 4.47 \mu\text{m}$, $D_{25} = 7.68 \mu\text{m}$, $D_{50} = 15.80 \mu\text{m}$, $D_{75} = 27.14 \mu\text{m}$, $D_{90} = 38.93 \mu\text{m}$, $D_{99} = 61.10 \mu\text{m}$, the max calculus distribution was got at the size of $20.71 \mu\text{m}$. This particle size distribution is beneficial to alkali activation reaction.

Thermal Treatment of CFA- Na_2CO_3 Mixture

The thermal treatment of the CFA- Na_2CO_3 mixture was investigated by TG-DSC analysis, and the corresponding TG-DSC curves were showed in Figure 2. Two main steps of mass loss could be found. The first mass loss of 4.8% at 60–130°C region, accompanied with an endothermic peak centered at 80°C in DSC profile, was ascribed due to the removal of adsorbed

water [1,41]. The second mass loss of 21.6% occurred in the temperature range of 550–920°C, correspondingly, there appeared a series of exothermic and endothermic peaks in the DSC curve. It was reported that only an exothermic peak. due to the combustion of unburnt carbon in CFA [1,42], could be found in the this temperature range. Therefore, these complicated peaks indicated that very complicated reactions might take place between CFA and Na_2CO_3 [1,42], which were in favor of the decomposition of mullite and then the improvement of alumina extraction in the following acid-leaching [1].

As well, the capability of the CFA- Na_2CO_3 mixture to absorb microwave energy was studied in detail. As Figure 2 shown, the temperature-rise process of the CFA- Na_2CO_3 mixture in microwave field could be divided into two stages: 18–400°C and 400–900°C. The average heating rate was 40.6°C/min in the first stage, and then rapidly increased to 249.5°C/min in the second stage. These phenomena could be explained as follow. As known from XRD result, mullite, quartz and amorphous silica were the main phase of CFA. The microwave energy was adsorbed firstly by the amorphous silica due to the selective heating of microwave [19,43], since quartz is microwave transparent, and the microwave absorption capacity of amorphous silica is much better than those of mullite and Na_2CO_3 [19,43].

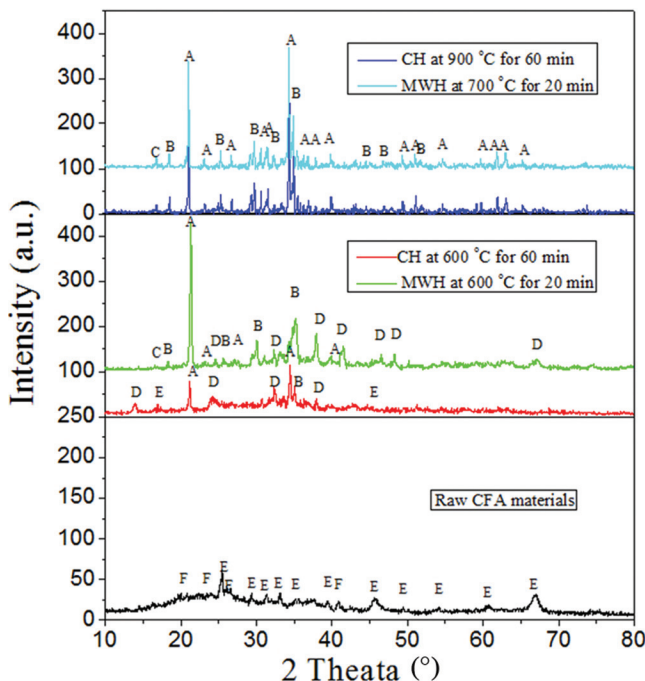


Figure 1. XRD patterns of sintered CFA under different conditions. A: NaAlSiO_4 ; B: Na_2SiO_3 ; C: Al_2O_3 ; D: Na_2CO_3 ; E: $\text{Al}_6\text{Si}_2\text{O}_{13}$; F: SiO_2 .

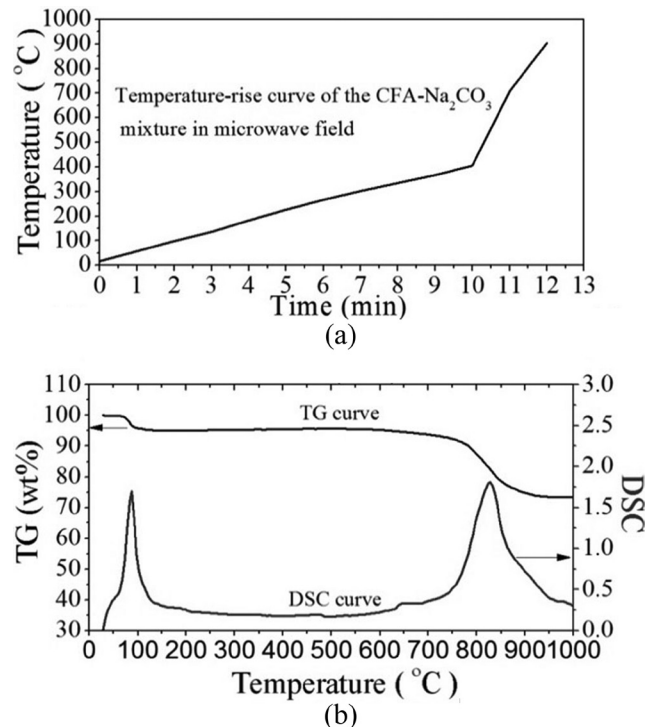


Figure 2. TG-DSC and temperature-rise curves of the CFA- Na_2CO_3 mixture in microwave.

After heating the mixture to 400°C, the amorphous silica reacted with mullite and Na_2CO_3 to form a new material, which has a stronger microwave absorption capacity [19]. These might contribute to the great increase of the heating rate in the second stage, which in turn accelerated the activation of CFA.

Alkali Activation of CFA with MWH and CH

Heating temperature is one of the most important parameters since the low temperature may result in the incomplete activation of CFA and then the reduced extraction efficiency, while the high temperature may

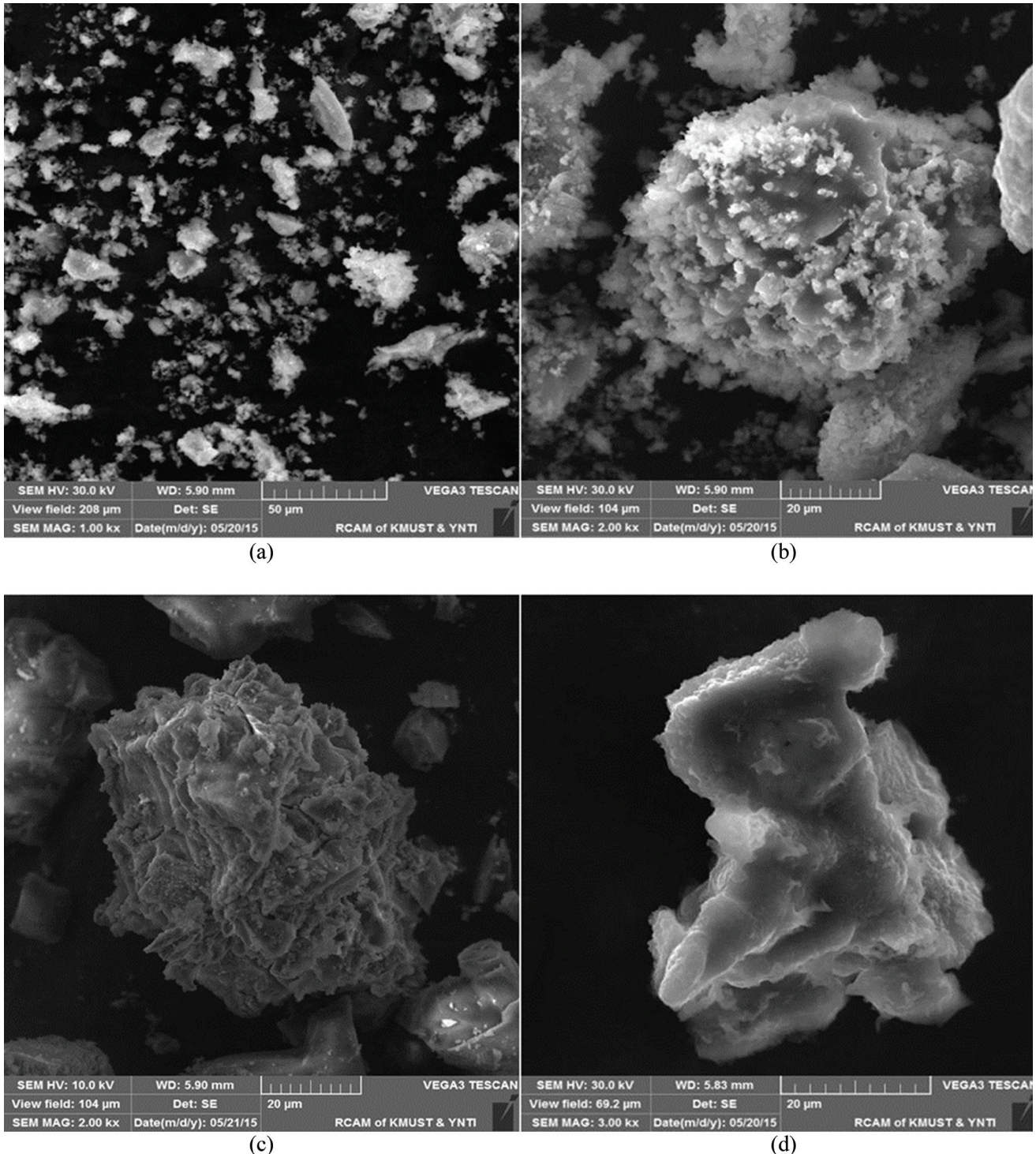


Figure 3. SEM images of CFA- Na_2CO_3 mixture sintered under different conditions. (a) and (b): heated at 600°C for 90 min by CH; (c) and (d): heated at 600°C for 20 min by MWH.

lead to the high energy consumption. To obtain the appropriate heating temperature, several alkali activation experiments were performed within the temperature range of 600–1000°C. Correspondingly, the heating time for CH and MWH was 60 min and 20 min, respectively. As expected, the aluminum extraction efficiency increased with temperature for both MWH and CH. Moreover, the aluminum extraction efficiencies of MWH were much higher than those of CH, especially for the lower temperature. For example, 71.34%, 95.52%, 96.42%, 96.87% and 97.06% were obtained at temperature of 600°C, 700°C, 800°C, 900°C, 1000°C, respectively, under MWH, compared to 33.28%, 48.63%, 71.71%, 95.10%, 96.11% under CH, respectively. The results showed the overwhelming advantage of MWH with respect to CH.

Considering the great difference in aluminum extraction efficiency at 600°C by the two methods, the changes of CFA in the phase and morphology were studied.

As seen from Figure 1, Na_2CO_3 and NaAlSiO_4 are the main phase after activation of CFA by Na_2CO_3 using MWH at 600°C, while NaAlSiO_4 , Na_2CO_3 and $\text{Al}_6\text{Si}_2\text{O}_{13}$ (mullite) could be identified under CH at 600°C. Clearly, the amount of NaAlSiO_4 was much higher for MWH. It could be concluded easily that MWH was much more beneficial to the decomposition of mullite to extract more alumina.

Important information could be also obtained from the SEM results, as depicted in Figure 3. Obviously, a considerable difference in morphology was observed over CFA- Na_2CO_3 mixture, activated by CH and MWH, respectively. After activation with CH [Figure 3(a) and 3(b)], the mixture mainly consisted of isolated particles with the irregular shape, and no significant fused phase could be found. Moreover, a lot of small particles attached diffusely over the surface of the mixture [Figure 3(b)], implying the incomplete activation of CFA. On the contrary, after activation with MWH [Figures 3 (c) and 3(d)], the fused phase was seen noticeably, indicating the thorough reaction between CFA and Na_2CO_3 [19]. These might be due to the fact that microwave enhanced the atomic diffusion and mass transportation in the mixture, and improved the heating efficiency, thus promoting the efficient activation reactions and increasing aluminum extraction efficiency.

Also, in view of the similar aluminum extraction efficiency obtained at 900°C by CH and at 700°C by MWH, the crystalline structure of the mixture on the above two conditions was further studied. As Figure 1

shown, NaAlSiO_4 , Na_2SiO_3 and Al_2O_3 could be identified for the both samples, accompanied with the disappearance of Na_2CO_3 and mullite. The similar crystalline structure implied that MWH had the much higher heating efficiency than CH.

The effects of duration time on aluminum extraction efficiencies were investigated by changing duration time at 900°C for CH and 700°C for MWH, respectively. For MWH, the alumina extraction efficiency increased from 78.51–95.52% as the duration time increased from 5 min to 20 min, then, it reached a plateau as the duration time was 20 min and 30 min. Similar phenomenon was observed for CH, the alumina extraction efficiency rapidly increased from 58.42–95.10% with the duration time from 10 min to 60 min, followed by a plateau within the time range of 60–100 min. Clearly, the very efficient activation reaction between Na_2CO_3 and CFA could be achieved in the short time when MWH was used.

Figure 4 showed the XRD patterns of Na_2CO_3 -CFA mixture after activation by MWH with different time. No diffraction peak assigned to Na_2CO_3 and $\text{Al}_6\text{Si}_2\text{O}_{13}$ (mullite) could be seen, suggesting the complete decomposition of mullite even when very short duration time (5 min) was used. The diffraction peaks corresponded to the soluble NaAlSiO_4 were clearly visible,

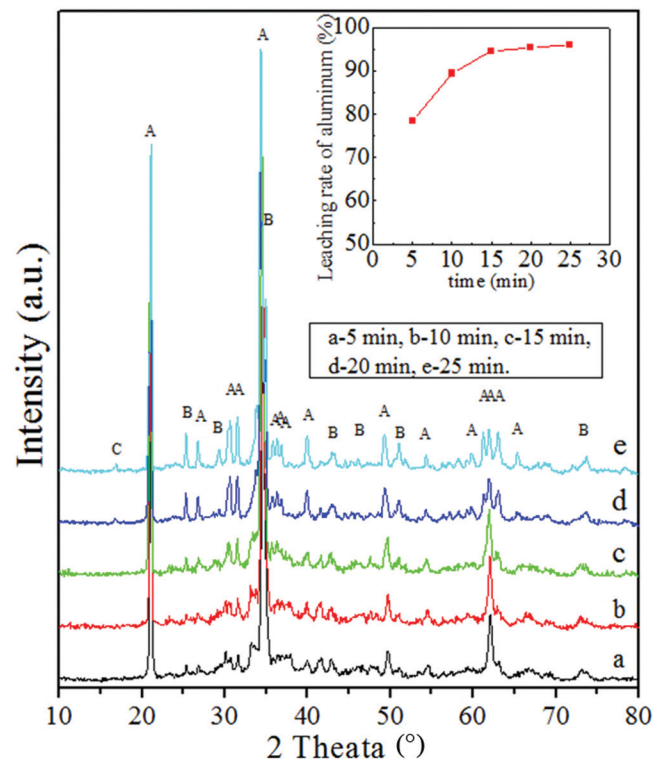


Figure 4. XRD patterns of CFA- Na_2CO_3 mixture sintered with different time by MWH. A: NaAlSiO_4 ; B: Na_2SiO_3 ; C: Al_2O_3 .

moreover, the intensities of these peaks increased with the duration time, implying the more amount of NaAlSiO₄ with increased duration time. These findings were consistent with the above Al leaching results. Additionally, a small amount of Al₂O₃ formed after activation with duration time above 20 min. These XRD results further confirmed the efficient activation of CFA by Na₂CO₃ with MWH in the short time.

CONCLUSIONS

The comparative study of the MWH and CH for activation of CFA by Na₂CO₃ was carried out in this paper. According to the experimental and characterization results, a high aluminum extraction efficiency (> 95.52%) and the complete decomposition of mullite into NaAlSiO₄, Na₂SiO₃ and Al₂O₃ could be achieved at a moderate temperature (700°C) in short time (20 min) when MWH was used; as for CH, a much higher temperature (900°C) and longer time (60 min) were needed to successfully activate the CFA to obtain the equivalent aluminum extraction. These could be due to the fact that MWH, compared to CH, improved the heating efficiency, enhanced the atomic diffusion and mass transportation in the CFA-Na₂CO₃ mixture, accelerated the decomposition of mullite and the formation of the soluble Al-containing materials. Therefore, MWH is a promising technique for the activation of CFA to recovery aluminium.

ACKNOWLEDGEMENTS

This work was supported by the Natural Science Foundation of China (Grant No. 21367015, 51363012 and U1402233).

REFERENCES

- Guo, Y.X., Li, Y.Y., Cheng, F.Q., Wang M., Wang, X.M., "Role of additives in improved thermal activation of coal fly ash for alumina extraction", *Fuel Processing Technology*, Vol. 110, No. 2, 2013, pp. 114–121. <http://dx.doi.org/10.1016/j.fuproc.2012.12.003>
- Ahmaruzzaman, M., "A review on the utilization of fly ash", *Progress Energy Combustion Science*, Vol. 36, No. 3, 2010, pp. 327–363. <http://dx.doi.org/10.1016/j.peccs.2009.11.003>
- Blissett, R.S., Rowson, N.A., "A review of the multi-component utilisation of coal fly ash", *Fuel*, Vol. 97, No. 7, 2013, pp. 1–23.
- Yao, Z.T., Xia, M.S. Sarker, P.K., Chen, T., "A review of the alumina recovery from coal fly ash, with a focus in China", *Fuel*, Vol. 120, No. 3, 2014, pp. 74–85. <http://dx.doi.org/10.1016/j.fuel.2013.12.003>
- Manoharan, V., Yunusaa, I.A.M., Loganathan, P., Lawrie, R., Skilbeck, C.G., Burchett, M.D., Murray, B.R., Eamus, D., "Assessments of Class F fly ashes for amelioration of soil acidity and their influence on growth and uptake of Mo and Se by canola", *Fuel*, Vol. 89, No. 11, 2010, pp. 3498–504. <http://dx.doi.org/10.1016/j.fuel.2010.06.028>
- Lee, H., Ha, H.S., Lee, C.H., Lee, Y.B., Kim, P.J., "Fly ash effect on improving soil properties and rice productivity in Korean paddy soils", *Bioresource Technology*, Vol. 33, No. 33, 1982, pp. 249–256.
- Matsi, T., Keramidis, V.Z., "Fly ash application on two acid soils and its effect on soil salinity, pH, B, P and on ryegrass growth and composition", *Environmental Pollution*, Vol. 104, No. 1, 1999, pp. 107–112. [http://dx.doi.org/10.1016/S0269-7491\(98\)00145-6](http://dx.doi.org/10.1016/S0269-7491(98)00145-6)
- Erol, M., Küçükbayrak, S., Ersoy-Meriçboyu, A., "Characterization of sintered coal fly ashes", *Fuel*, Vol. 87, No. 7, 2008, pp. 1334–1340. <http://dx.doi.org/10.1016/j.fuel.2007.07.002>
- Yao, Z.T., Tan, S.H., Xia, M.S., Ye, Y., Li, J.H., "Synthesis, characterization and sintering behaviour of indialite ceramic from fly ash", *Waste Management Research*, Vol. 29, No. 10, 2011, pp. 1090–1097. <http://dx.doi.org/10.1177/0734242X10378329>
- Erol, M., Küçükbayrak, S., Ersoy-Meriçboyu, A., "Comparison of the properties of glass, glass-ceramic and ceramic materials produced from coal fly ash", *J. Hazardous Materials*, Vol. 153, 2008, pp. 418–425. <http://dx.doi.org/10.1016/j.jhazmat.2007.08.071>
- Nayak, N., Panda, C.R., "Aluminium extraction and leaching characteristics of Talcher Therna I: Power Station fly ash with sulphuric acid", *Fuel*, Vol. 89, No. 1, 2010, pp. 53–58. <http://dx.doi.org/10.1016/j.fuel.2009.07.019>
- Sočo, E., Kalemkiewicz, J., "Investigations on Cr mobility from coal fly ash", *Fuel*, Vol. 88, No. 8, 2009, pp. 1513–1519. <http://dx.doi.org/10.1016/j.fuel.2009.02.021>
- Wu, C.Y., Yu, H.F., Zhang, H.F., "Extraction of aluminum by pressure acid-leaching method from coal fly ash", *Transactions Nonferrous Metals Society China*, Vol. 22, No. 9, 2012, pp. 2282–2288. [http://dx.doi.org/10.1016/S1003-6326\(11\)61461-1](http://dx.doi.org/10.1016/S1003-6326(11)61461-1)
- Wu, Y.S., Xu, P., Chen, J., Li, L.S., Li, M.C., "Effect of Temperature on Phase and Alumina Extraction Efficiency of the Product from Sintering Coal Fly Ash with Ammonium Sulfate", *Chinese J. Chemical Engineering*, Vol. 22, No. s11-12, 2014, pp. 1363–1367.
- Vassilev, S.V., Vassileva, C.G., "A new approach for the classification of coal fly ashes based on their origin, composition, properties, and behavior", *Fuel*, Vol. 86, No. 10-11, 2007, pp. 1490–1512. <http://dx.doi.org/10.1016/j.fuel.2006.11.020>
- Blissett, R.S., Rowson, N.A., "A review of the multi-component utilisation of coal fly ash", *Fuel*, Vol. 97, No. 7, 2012, pp. 1–23. <http://dx.doi.org/10.1016/j.fuel.2012.03.024>
- Bai, G., Qiao, Y., Shen, B., Chen, S., "Thermal decomposition of coal fly ash by concentrated sulfuric acid and alumina extraction process based on it", *Fuel Processing Technology*, Vol. 92, No. 6, 2011, pp. 1213–1219. <http://dx.doi.org/10.1016/j.fuproc.2011.01.017>
- Iyer, R., "The surface chemistry of leaching coal fly ash", *J. Hazardous Materials*, Vol. 93, No. 3, 2002, pp. 321–329. [http://dx.doi.org/10.1016/S0304-3894\(02\)00049-3](http://dx.doi.org/10.1016/S0304-3894(02)00049-3)
- Zhang, Z.Y., Qiao, X.C., Yu, J.G., "Aluminum release from microwave-assisted reaction of coal fly ash with calcium carbonate", *Fuel Processing Technology*, Vol. 134, 2015, pp. 303–309. <http://dx.doi.org/10.1016/j.fuproc.2014.12.050>
- Li, H.Q., Hui, J.B., Wang, C.Y., Bao, W.Y., Sun, Z.H., "Extraction of alumina from coal fly ash by mixed-alkaline hydrothermal method, Hydrometallurgy", Vol. 147-148, No. 8, 2014, pp. 183–187. <http://dx.doi.org/10.1016/j.hydromet.2014.05.012>
- Izquierdo, M., Querol, X., "Leaching behaviour of elements from coal combustion fly ash: An overview", *International J. Coal Geology*, Vol. 94, No. 3, 2012, pp. 54–66. <http://dx.doi.org/10.1016/j.coal.2011.10.006>
- Dudas, M.J., "Long-term leachability of selected elements from fly ash", *Environmental Science Technology*, Vol. 15, No. 7, 1981, pp. 840–843. <http://dx.doi.org/10.1021/es00089a013>
- Park, H.C., Park, Y.J., Stevens, R., "Synthesis of alumina from high purity alum derived from coal fly ash", *Materials Science Engineering*, Vol. A 367, No. 1-2, 2004, pp. 166–170.
- Kelmers, A.D., Canon, R.M., Egan, B.Z., Felker, L.K., Gilliam, T.M., Jones, G., Owen, G.D., Seeley, F.G., Watson, J.S., "Chemistry of the direct acid leach, calcsinter, and pressure digestion-acid leach methods

- for the recovery of alumina from fly ash”, *Resources Conservation*, Vol. 9, 1982, pp. 271–279. [http://dx.doi.org/10.1016/0166-3097\(82\)90081-5](http://dx.doi.org/10.1016/0166-3097(82)90081-5)
25. Criado, M., Fernández-Jiménez, A., Palomo, A., “Alkali activation of fly ash. Part III: Effect of curing conditions on reaction and its graphical description”, *Fuel*, Vol. 89, No. 11, 2010, pp. 3185–3192. <http://dx.doi.org/10.1016/j.fuel.2010.03.051>
26. Palomo, A., Gtutzeck, M.W., Blanco, M.T., “Alkali-activated fly ashes: a cement for the future”, *Cement Concrete Research*, Vol. 29, No. 8, 1999, pp. 1323–1329. [http://dx.doi.org/10.1016/S0008-8846\(98\)00243-9](http://dx.doi.org/10.1016/S0008-8846(98)00243-9)
27. Matjie, R.H., Bunt, J.R., van Heerden, J.H.P., “Extraction of alumina from coal fly ash generated from a selected low rank bituminous South African coal”, *Minerals Engineering*, Vol. 18, No. 3, 2005, pp. 299–310. <http://dx.doi.org/10.1016/j.mineng.2004.06.013>
28. Gabler Jr., R.C., Stoll, R.L., “Extraction of leachable metals and recovery of alumina from utility coal ash”, *Resources Conservation*, Vol. 9, No. 1–4, 2013, pp. 131–142.
29. Oghbaei, M., Mirzaee, O., “Microwave versus conventional sintering: a review of fundamentals, advantages and applications”, *J. Alloys Compounds*, Vol. 494, No. 1–2, 2010, pp. 175–189. <http://dx.doi.org/10.1016/j.jallcom.2010.01.068>
30. Janny, M.A., Kimrey, H.D., Allen, W.R., Kiggans, J.O., “Enhanced diffusion in sapphire during microwave heating”. *J. Materials Science*, Vol. 32, No. 32, 1997, pp. 1347–1355. <http://dx.doi.org/10.1023/A:1018568909719>
31. Freeman, S.A., Booske, J.H., Cooper, R.F., “Microwave field enhancement of charge transport in sodium chloride”, *Physical Review Letters*, Vol. 74, No. 11, 1995, pp. 2042–2045. <http://dx.doi.org/10.1103/PhysRevLett.74.2042>
32. Booske, J.H., Cooper, R.F., Freeman, S.A., Rybakov, K.I., Semenov, V.E., “Microwave ponderomotive forces in solid-state ionic plasmas”, *Physics Plasmas*, Vol. 5, No. 5, 1998, pp. 1664–1670. <http://dx.doi.org/10.1063/1.872835>
33. Panneerselvam, M., Rao, K.J., “Novel microwave method for the synthesis and sintering of mullite from kaolinite”, *Chemistry Materials*, Vol. 15, No. 11, 2003, pp. 2247–2252. <http://dx.doi.org/10.1021/cm0301423>
34. Ebadzadeh, T., “Effect of mechanical activation and microwave heating on synthesis and sintering of nano-structured mullite”, *J. Alloys Compounds*, Vol. 489, No. 1, 2010, pp. 125–129. <http://dx.doi.org/10.1016/j.jallcom.2009.09.030>
35. Fang, Y., Cheng, J.P., Agrawal, D.K., “Effect of powder reactivity on microwave sintering of alumina”, *Materials Letters*, Vol. 58, No. 3–4, 2004, pp. 498–501. [http://dx.doi.org/10.1016/S0167-577X\(03\)00533-0](http://dx.doi.org/10.1016/S0167-577X(03)00533-0)
36. Fujitsu, S., Ikegami, M., Hayashi, T., “Sintering of partially stabilized zirconia by microwave heating using ZnO-MnO₂-Al₂O₃ plates in a domestic microwave oven”, *J. American Ceramic Society*, Vol. 83, No. 8, 2000, pp. 2085–2087. <http://dx.doi.org/10.1111/j.1151-2916.2000.tb01517.x>
37. Ye, Q.X., Zhu, H.B., Zhang, L.B., Ma, J., Zhou, L., Liu, P., Chen, J., Chen, G., Peng, J.H., “Preparation of reduced iron powder using combined distribution of wood-charcoal by microwave heating”, *J. Alloys Compounds*, Vol. 613, No. 10, 2014, pp. 102–106. <http://dx.doi.org/10.1016/j.jallcom.2014.06.016>
38. Samouhos, M., Taxiarchoua, M., Tsakiridis, P.E., Potiriadis, K., “Greek ‘red mud’ residue: A study of microwave reductive roasting followed by magnetic separation for a metallic iron recovery process”, *J. Hazardous Materials*, Vol. 254–255, 2013, pp. 193–205. <http://dx.doi.org/10.1016/j.jhazmat.2013.03.059>
39. Amankwah, R.K., Pickles, C.A., “Microwave roasting of a carbonaceous sulphidic gold concentrate”, *Minerals Engineering*, Vol. 22, No. 13, 2009, pp. 1095–1101. <http://dx.doi.org/10.1016/j.mineng.2009.02.012>
40. Vassilev, S.V., Vassileva, C.G., “Methods for characterization of composition of fly ashes from coal-fired power stations: A critical overview”, *Energy Fuel*, Vol. 19, No. 3, 2005, pp. 1084–98. <http://dx.doi.org/10.1021/ef049694d>
41. Yang, N., Hai, W. 2001. *The Handbook of Inorganic Metalloid Materials Atlas*, Wuhan, Wuhan University of Technology Press.
42. Payá, J., Monzó, J., Borrachero, M.V., Perris, E., Amahjour, F., “Thermogravimetric methods for determining carbon content in fly ashes”, *Cement Concrete Research*, Vol. 28, No. 5, 1998, pp. 675–686. [http://dx.doi.org/10.1016/S0008-8846\(98\)00030-1](http://dx.doi.org/10.1016/S0008-8846(98)00030-1)
43. Zhang, Z.Y., Qiao, X.C., Yu, J.G., “Microwave selective heating-enhanced reaction rates for mullite preparation from kaolinite”, *RSC Advances*, Vol. 4, No. 6, 2013, pp. 2640–2647. <http://dx.doi.org/10.1039/C3RA43767A>

Effects of Two kinds of Herbage Crops on the Removal of High Molecular Weight Polycyclic Aromatic Hydrocarbons in Sludge

FENG SHENG-DONG¹, WANG WEI¹, SHI WEI¹, ZHANG XUE², JIA HAI-BIN¹, ZHANG XUE-NA¹, LI YU-LING, CHANG RUI-XUE³ and YANG ZHI-XIN^{1,*}

¹Key Laboratory for Farmland Eco-Environment, Hebei Province and College of Resource and Environmental Sciences, Agricultural University of Hebei, Baoding - 0710001, P.R.China.

²Agricultural University of Hebei Bohai Campus, Baoding - 0710001, P.R.China.

³College of Agricultural Resources and Environmental Sciences, China Agricultural University, Beijing 100193, P.R.China

ABSTRACT: The purpose of this study was to compare the effects of two herbage crops (awnless brome and alfalfa) on the removal of high molecular weight polycyclic aromatic hydrocarbons (HMW-PAHs) in sludge, including 9 PAHs. The results showed that Awnless brome and alfalfa had similar removal percentages for the total Σ 9 HMW-PAHs in the sludge, which were 85.75% and 85.08%, respectively. However, these two plants were different in the removal percentages of individual PAHs, for example, awnless brome had higher removal percentages for the 4-ring compounds (Pyr, BaA, Chry, BbF and BKF), while alfalfa showed higher removal percentages for the 5-ring and 6-ring compounds (BaP, DbA, Bghip and InP). The activities of catalase and polyphenol oxidase in the sludge planted with alfalfa were significantly higher than those in the sludge with awnless brome, while the activities of dehydrogenase in these two kinds of sludge were opposite. In conclusion, awnless brome and alfalfa could be directly used for the remediation of HMW-PAHs-polluted sludge, and awnless brome inclined to degrade the HMW-PAHs with 4 rings, while alfalfa tended to degrade the HMW-PAHs with 5 and 6 rings.

1. INTRODUCTION

WITH rising treatment rate of urban sewage, the residual sludge is rapidly increasing. Higher PAHs content in industrial wastewater sludge was found, some of which even reached 2000 mg/kg [1]. PAHs have strong carcinogenic effect, so that many countries have listed PAHs in the blacklist of priority pollutants, in which high molecular weight PAHs (HMW-PAHs) were more poisonous and risky in the environment than low molecular weight PAHs. In the applied process of agricultural sludge, the PAHs in the sludge endanger the safety of farm field [2]. Therefore, reduction of PAHs in the sewage sludge to a safe level is particularly urgent in China. However, the most widely used removal approach of sludge PAHs is concentration-digestion-dehydration-compost or landfill process [3], and the PAHs in the sludge cannot be effectively removed, especially the HMW-

PAHs are more difficult to degrade. Numerous studies have shown that some plants can be used to repair the PAHs-contaminated soil [4], whereas the efficacy varies greatly among plant species [5]. Phytoremediation has shown promise as a potentially effective and low-cost treatment option. However, there were only a few reports about using plants to degrade PAHs in sludge ecosystem [6]. We had shown in a previous study that alfalfa and awnless brome (Smooth brome grass) have stronger resistance to the PAHs-polluted sludge [7,8]. The objective of this study was to explore the abilities of awnless brome and alfalfa to degrade HMW-PAHs in the sludge. The changing rules of enzyme activities in the sludge planted with these two grasses were discussed in order to understand their potential mechanism of phytoremediation on PAHs.

2. MATERIALS AND METHODS

2.1. Materials

Sludge was taken from domestic wastewater treat-

*Author to whom correspondence should be addressed.
E-mail: yangzhixin@126.com

ment plant in Baoding, China. The sludge was then air-dried and sieved through a 2 mm mesh to remove rocks. The nutrient levels of the sludge were 23.47 g·kg⁻¹ of total N, 0.6993 g·kg⁻¹ of available P and 3.8634 g·kg⁻¹ of available K. The seeds of awnless brome and alfalfa were purchased from Jingjingyuan Seed Company.

2.2. Experimental Design

The measured initial total HMW-PAHs concentration in the sludge was measured as 1235.83 µg·kg⁻¹, including 9 PAHs as follows: pyrene (Pyr) (181.94 µg·kg⁻¹), chrysene (Chry) (223.65 µg·kg⁻¹), benzo[a]anthracene (BaA) (85.34 µg·kg⁻¹), benzo[b]fluoranthene (BbF) (62.95 µg·kg⁻¹), benzo[k]fluoranthene (BkF) (240.43 µg·kg⁻¹), benzo[a]pyrene (BaP) (60.45 µg·kg⁻¹), dibenzo[a,h]anthracene (DbA) (43.84 µg·kg⁻¹), benzo[ghi]perylene (BghiP) (80.19 µg·kg⁻¹) and indeno[1, 2, 3-cd]pyrene (InP) (257.02 µg·kg⁻¹). Then, the air-dried and sieved sludge were packed into greenhouse pots (1.5 kg dry weight per sludge pot), which was 15 × 20 cm (diameter × height) in size. These pots were then moved to the greenhouse of Agriculture University of Hebei in China and kept for 7 days at 60% of field water capacity before transplanting seedlings. The temperature of the greenhouse was 20–23°C in the day and 17–19°C in the night.

Alfalfa and awnless brome were chosen as the plant species in the study. Seeds of each plant were germinated and grown on moist perlite in growth chambers and the seedlings were transplanted to the greenhouse pots after 10–15 days of germination. Six seedlings of alfalfa or awnless brome in each pot were transplanted. Treatments in this trial were set as follows: (1) sludge without plants (CK); (2) sludge with alfalfa (AS); (3) sludge with awnless brome (BS). Each treatment was performed in triplicate. Seedling transplanting date was considered as the starting time of the experiment. After five months of plant growth, the sludge and plants were sampled. The planted and unplanted sludge were carefully collected, homogenized and each sludge sample was divided into two parts, one of which was placed in a small plastic bag at 4°C was used immediately for enzyme activities analysis. And the second was air-dried at room temperature under ventilated and near-dark conditions, ground, and then sieved through 1-mm mesh. The shoots of the plants were harvested, washed in tap water followed by distilled water, then freeze-dried. Dry sludges and shoots of the plants samples were stored in polyethylene Ziploc bags at 4°C in the dark prior to PAHs analysis.

2.3. Plant and Sludge Analysis

2.3.1. PAHs Analysis of the Plants and Sludge

Sample extraction: sludge (20 g) and plant samples (15 g)s were extracted for 16 h with an extraction solvent of hexane and acetone (50:50, v/v) in a Soxhlet apparatus. After reducing these extracts to 1 mL through rotary evaporation as well as nitrogen pressure blowing at 60°C, and then silica chromatography columns were used to purify the samples. The final fraction of 1 mL was transferred to a 2 mL vial capped with a Teflon-lined septum ready for PAH analysis using 7890A-5975C (Agilent, USA) equipped with a Agilent HP-5MS chromatographic column [7,9]. All detectable PAHs concentrations were reported as µg·kg⁻¹ (dry wt.).

All samples were subjected to strict quality control procedures. 20 µl (10 µg/ml) P-Terphenyl-d14 and 20 µl (10 µg / ml) 4-bromo-2-fluoro-biphenyl are added in the sludge sample prior to the extraction, which is used to evaluate the recovery efficiency of experimental analysis. The chrysene-d12 and perylene-d12 added in the study are used as internal standards for HMW-PAH analysis, which each of 5 µl (40 ng/µl) is added in 1ml extract solution [11]. Statistical significance was evaluated using SPSS version 10.0 with one-way analysis of variance (ANOVA) and least significant difference (LSD) tests for comparison of treatment means with $P < 0.05$.

2.3.2. Analysis of the Enzyme Activities in the Sludge

Urease (UR) activity was measured as described by Kandeler and Gerber [10]. The activity was expressed as micrograms of hydrolyzed substrate per hour at 30°C by 1 g of dried sludge. Catalase (CAT) activity was measured with the standard method, potassium permanganate titration [11]. One unit of catalase activity decomposed 1.0 µmole H₂O₂ per minute (pH 7.0, 25°C). The polyphenol oxidase (PPO) activity was measured by the method described by Kunwar and Khan [12]. The amount of purpurogallin formed was estimated by measuring the absorbance at 420 nm. The activity was expressed as per minute per gram of soil fresh weigh. Dehydrogenase (DH) assays were performed using soluble tetrazolium salt (TTC) as an artificial acceptor [13], and the activity was defined as micromoles of substrates transformed per hour at 30°C by 1 g of dried sludge.

2.4. Calculation

2.4.1. Final Removal Percentage of the PAHs in the Sludge

Removal percentage = (Initial PAHs concentration of sludge – PAHs residual concentration of sludge after five months of plant growth)/ Initial PAHs concentration of sludge × 100 %

2.4.2. Accumulation Contribution Percentage of the Plant Shoots

Accumulation Contribution percentage = (HMW-PAHs content in plant shoots of each pot × dry weight of plant shoots in each pot) / [(Initial PAHs concentration of sludge – PAHs residual concentration of sludge after five months of plant growth) × dry weight of sludge in each pot] × 100 %.

3. RESULTS AND DISCUSSION

3.1. HMW-PAHs Accumulation in Alfalfa and Awnless Brome Shoots

After five months growth, the HMW-PAHs accumulated in the alfalfa and the awnless brome shoots were presented in Table 1. The total amounts of 9 HMW-PAHs that accumulated in the alfalfa biomass were significantly higher than that in the awnless brome. However, the contents of respective HMW-PAHs that accumulated in the two plants were significantly different. Higher concentrations of Pyr, BaA, Chry were observed in the shoots of alfalfa than those in the awnless brome shoots, while higher concentrations of BbF, BkF, BaP, DbA were observed in the shoots of awnless brome. In addition, the concentrations of BghiP and InP in the shoots of alfalfa and the awnless brome were not significantly different. The percentages of respective HMW-PAHs were significantly different in the alfalfa by LSD test, which were in the order of Pyr (84.2%)

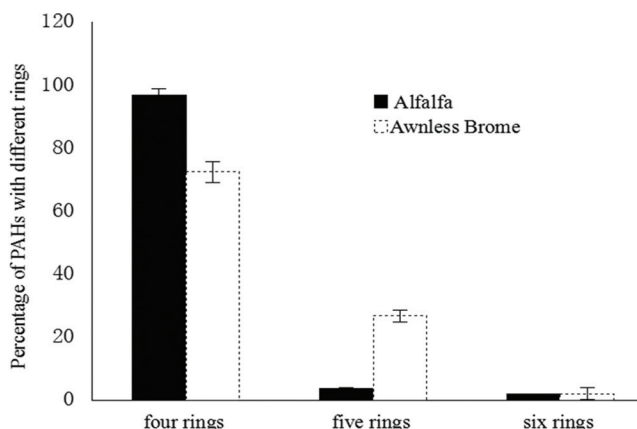


Figure 1. Percentage of PAHs with different rings to Σ9 PAHs in Alfalfa and Awnless Brome.

> Chry (7.21%) > BaA (3.84%) > BkF ≈ BaP (1.33%, 1.47%) > BbF ≈ DbA ≈ BghiP ≈ InP (0.54 ~ 0.59%). Similarly, those in the awnless brome were also significantly different, but were in the order of Pyr (55.2%) > DbA (22.32%) > Chry (9.84%) > BkF ≈ BaP (3.36%, 3.41%) > BaA (2.2%) > BbF (1.77%) > BghiP ≈ InP (0.95%). The results showed that pyrene was the most easily to be absorbed by the two plants among all these HMW-PAHs. Moreover, great variations of the HMW-PAHs concentrations in the shoots were observed between the two plants, which should be resulted from the plant properties.

As shown in Figure 1, alfalfa shoot contained a higher percentage of 4-ring PAHs (96.9%) than awnless brome (72.4%), while awnless brome contained a higher portion of 5-ring PAHs (26.7%) than alfalfa, whereas the bioaccumulation of 6-ring PAHs was lower than 1% in both plants. For both alfalfa and awnless brome shoots, the bioaccumulation decreased with the increasing aromatic ring-numbers, which was in consistent with the results from Michael H. *et al.* (2009) [14]. Moreover, identification of the HMW-PAHs in the shoots indicated that the PAHs must have been actively translocated from the sludge to the shoots, especially for the 4-ring PAHs.

Table 1. The Contents of HMW-PAHs and Percentages of Respective HMW-PAHs in the Total Σ9 PAHs in the Awnless Brome and Alfalfa.

HMW-PAH Type	Pyr	BaA	Chry	BbF	BkF	BaP	DbA	BghiP	InP	Sum
PAHs content in alfalfa (µg/kg)	156.04	7.11	13.37	1.10	2.46	2.73	1.02	1.00	1.00	185.83
The percentage of each PAH in alfalfa (%)	84.20a	3.84c	7.21b	0.59e	1.33d	1.47d	0.55e	0.54e	0.54e	
PAHs content in awnlessbrome (ug/kg)	58.08	2.32	10.36	1.86	3.54	3.59	23.49	1.00	1.00	105.24
The percentage of each PAH in awnless brome (%)	55.2a	2.20e	9.84c	1.77f	3.36d	3.41d	22.32b	0.95g	0.95g	

Notes: Values in each row followed with different capital letters (a, b, c, e, d and g) indicated significant differences among the percentages of respective HMW-PAHs in the total Σ9 PAHs (p < 0.05).

Table 2. The Contents of PAHs in All Treatments After Five Months of Plant Growth ($\mu\text{g}/\text{kg}$).

Treatments	Pyr	BaA	Chry	BbF	BkF	BaP	DbA	BghiP	InP	$\Sigma 9$ PAHs
CK	100.07a	85.04a	210.23a	62.32a	187.54a	56.22a	32.26a	58.54a	179.91a	972.13a
AS	47.42b	8.88b	33.51b	13.97b	32.02b	14.98b	1.00c	19.88c	12.70c	184.36b
BS	21.14c	5.56b	22.69c	10.44b	23.01b	18.77b	11.08b	30.58b	32.79b	176.05b

Notes: Values in each column followed with different capital letters (a, b and c) indicated significant differences among the percentages of respective HMW-PAHs contents ($p < 0.05$).

3.2. Removal Percentages of HMW-PAHs from the Sludge by Awnless Brome and Alfalfa

After five months of plant growth, the concentrations of each PAH in AS and BS treatments were significantly lower than those in CK (Table 2). So, significantly higher PAH degradation percentage were found in treatments with plant growth (Figure 2). These results agreed with the conclusion of Cui [15]. Overall, there was a similar removal percentage for the sum of $\Sigma 9$ HMW-PAHs from the sludge, which were 85.08% of the total PAHs removed by the alfalfa and 85.75% by the awnless brome. The removal percentage of the awnless brome was just 0.67% higher than that of the alfalfa (Figure 2).

Compared the removal percentages of respective HMW-PAHs between the two plants (Figure 2), for the 4-ring compounds, 88.38% of Pyr, 93.49% of BaA, 89.86% of Chry, 83.42% of BbF, and 90.43% of BkF was respectively removed from the sludge planted with awnless brome after 5 months, which was respectively 14.44%, 3.89%, 4.842%, 5.61%, 3.75% higher than alfalfa. For the 5-ring PAHs, the removal percentages of BaP and DbA by awnless brome was 68.95% and 74.72%, which was 6.27% and 23.0% lower than those by alfalfa respectively. The removal percentages were

respectively 61.87% and 87.24% for the 6-ring PAHs, BghiP and InP by awnless brome, which was 13.34% and 7.82% lower than alfalfa (Figure 2). Overall, awnless brome treatments had a 6.7% higher removal percentages for the total 4-ring PAHs than alfalfa, while the removal percentages for the total 5-ring and 6-ring PAHs by alfalfa were 13.3% and 9.1% higher than awnless brome, respectively.

Although the accumulation of HMW-PAHs in the two plant tissues was obvious, the PAHs amounts extracted from each plant only accounted for 0.075% and 0.20% of the total removal amounts of $\Sigma 9$ HMW-PAHs by alfalfa and awnless brome, respectively (Table 3). However, despite the fact that the total content of $\Sigma 9$ HMW-PAHs that accumulated in alfalfa was significantly higher than that in the awnless brome, the contribution ratio of awnless brome uptake to sludge PAHs removal amount was larger than alfalfa because of its higher dry weight biomass after 5 months of growth. For each HMW-PAH, awnless brome also had a higher accumulation contribution percentage compared with alfalfa. The contribution percentage of DbA absorbed by awnless brome from the sludge was the highest among all the HMW-PAHs, which was up to 1.45%. All these results suggested that the accumulation of HMW-PAHs in the plant tissues was negligible

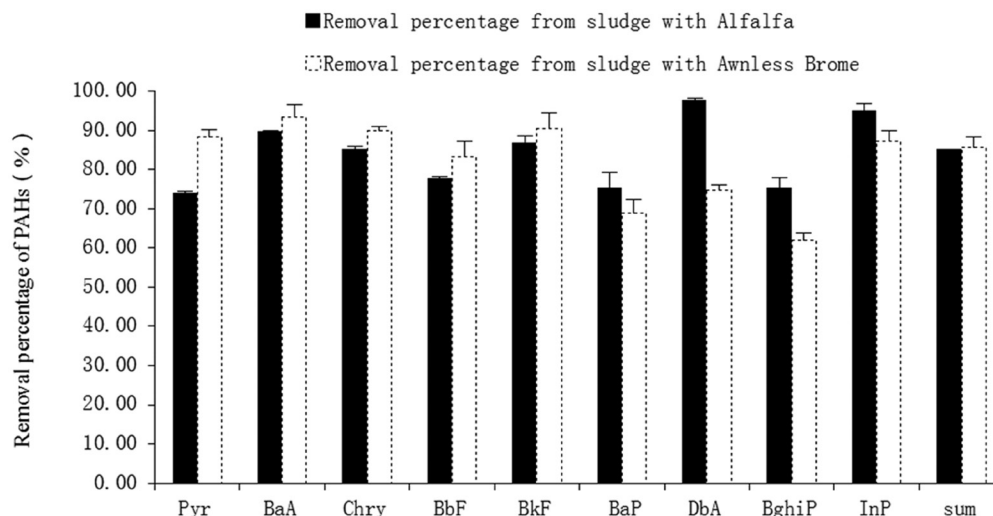


Figure 2. The removal percentage of Single PAH and Sum of $\Sigma 9$ PAHs. Averages and standard errors of three replicates are shown.

Table 3. Contributions of Plant Accumulation to the Sludge HMW-PAHs Removal Amounts (%).

Type	Pyr	BaA	Chry	BbF	BkF	BaP	DbA	BghiP	InP	Sum
Alfalfa	0.493	0.039	0.030	0.010	0.005	0.025	0.010	0.007	0.002	0.075
Awnless Brome	0.732	0.059	0.104	0.072	0.033	0.175	1.453	0.041	0.009	0.210

to the total remediation. These results agreed with the conclusion of Gao [16], who concluded that enhanced dissipation of PAHs in planted soil was mainly because of the plant-promoted biodegradation, but the contribution of plant uptake and accumulation was negligible. Plants may contribute to the biodegradation of organic compounds through increasing the microbial numbers [17], promoting the microbial activity [18] and modifying the microbial community in the rhizosphere [18], and thus cause the massive input of easily degradable organic substances, the improvement of physical and chemical soil conditions, and increased humidity and adsorption of pollutants in the rhizosphere. The plant-promoted biodegradation of HMW-PAHs in the sludge should be the comprehensive results of the above factors in this study.

3.3. The Changing Rules of Enzyme Activities in the Sludge

To find out the reasons causing the difference of HMW-PAHs degradation percentages in the sludge with the two plant treatments, microbial extra-cellular enzyme activity was monitored at the end of the experiment (Table 4). Results showed that significant differences were observed for the activities of PPO and CAT between awnless brome and alfalfa planted sludge. The activities of PPO (2.80) in the alfalfa planted sludge were significantly higher than the awnless brome planted sludge (1.62), whereas the activity of DH (12.15) was lower significantly than awnless brome (22.13). However, there was no significant difference for the UR and CAT activities between the awnless brome and alfalfa treatments.

The difference in the removal of different HMW-PAHs may be caused by the different activities of enzymes in the rhizospheric areas. The removal percent-

ages of awnless brome for PAHs with 4 rings were obviously higher than alfalfa, which may be related to DH whose activity was significantly higher in the sludge at the presence of awnless brome. In addition, DH typically occurs in all intact, viable microbial cells, and is usually related to the presence of viable microorganisms and their oxidative capability [13]. Therefore, it was speculated that awnless brome might excrete some biochemical substances under the stress of HMW-PAHs with four-rings, change rhizosphere environment and the structure of microbial populations, stimulate DH activities significantly in the rhizosphere which is in favor of 4-ring HMW-PAH dissipation. Strong correlations between hydrocarbon removal and dehydrogenase activity are frequently observed in soil condition [19]. Lee *et al.* [20] found that there was a negative correlation between dehydrogenase activity and the contents of phenanthrene and pyrene in soil condition. However, a positive correlation between dehydrogenase activity and the contents of PAHs has also been observed in soil condition [21]. The opposite results in the PAHs contaminated soil might be attributed to the difference of their root exudation.

In this study, alfalfa had 13.3% and 9.1% higher removal percentages for the PAHs with 5 and 6 rings than awnless brome, respectively. The activities of PPO in the presence of alfalfa were higher than those in the presence of awnless brome. PPO are very important oxidoreductase in soils, which can catalyze the degradation and transformation processes of aromatic compounds [22] and might be related to the degradation of 5- and 6-ring PAHs. UR and CAT were not significantly different between these two kinds of plants, indicating the effect of this enzyme on the sludge HMW-PAHs degradation was not different in the two plant treatments. At present, there have been a lot of research on the phytoremediation of soil PAHs pollu-

Table 4. Enzyme Activities of Sludge in the Different Treatments.

Treatments	Urease (UR)	Dehydrogenase (DH)	Polyphenol Oxidase (PPO)	Catalase (CAT)
CK	100.07a	58.54a	179.91a	972.13a
AS	47.42b	19.88c	12.70c	184.36b
BS	21.14c	30.58b	32.79b	176.05b

Note: Values in each column followed with different capital letters (a, b and c) indicated significant differences among different treatments. CAT units: $\mu\text{g TPF g}^{-1}$ sludge, UR units: $0.1\text{N KMnO}_4 \text{ mL mL}^{-1}$ sludge (20 min), DH units: $\text{mg NH}_4^+ \text{ g}^{-1}$ sludge (24 h), PPO units: $\text{mg Purple purple theogallin g}^{-1}$ sludge (2 h).

tion, but few were about the PAHs phytoremediation in sludge. There are great differences in the physical and chemical properties between soil and sludge, so the plant repair mechanism for the sludge PAHs needs further study because of the complexity of the sludge compositions.

4. CONCLUSIONS

Both of awnless brome and alfalfa could be directly used for the remediation of HMW-PAHs-polluted sludge. Awnless brome cultivation had greater potential to degrade four-ring PAHs from the sludge, while alfalfa was better for the degradation of five-ring and six-ring PAHs from the sludge. Two plants did uptake the HMW-PAHs into the plant parts but the contribution percentages of plant accumulation to the total remediation were negligible. The activities of PPO and CAT in the sludge with alfalfa were higher than those in the sludge with awnless brome, while it was opposite for DH, which might correspond to the difference of the removal percentages between the two plants. Furthermore, based on the removal percentages of the two plants, the better way may be awnless brome and alfalfa intercropping, for which further studies should be carried out in the future. Further research work is also required to elucidate the relationship between specific enzymes activities and the degradation of HMW-PAHs in sludge.

5. ACKNOWLEDGEMENTS

This work was financially supported by the National High Technology Research and Development Program of China (863 Program) (2012AA101403-3) and Project of Education Department of Hebei Province (Z2013058).

6. REFERENCE

1. Wild, S. R., Berrow, M. L., Jones, K. C., "The persistence of polynuclear aromatic hydrocarbons (PAHs) in sewage sludge amended agricultural soils.[J]". *Environmental Pollution*, Vol. 72, No. 2, 1991, pp. 141–157. [http://dx.doi.org/10.1016/0269-7491\(91\)90064-4](http://dx.doi.org/10.1016/0269-7491(91)90064-4)
2. Zhao Jinbao, Cui Yubo, Sun Hongjie, Wang Jie. "The review of phytoremediation in the polycyclic aromatic hydrocarbons polluted sludge". *Liaoning Chemical Industry*, Vol. 39, No. 12, 2010, pp. 1250–1253.
3. J. Bieñ, T. Kamizela, M. Kowalczyk. "The Effectiveness of Acid Fermentation of Sonicated Primary Sludge". *Journal of Residuals Science & Technology*, Vol. 12, No. 1, 2015, pp. 1–8. <http://dx.doi.org/10.12783/issn.2376-578X/12/1/1>
4. Gao Y Z, Ling W T, Zhu L Z, *et al.* "Ryegrass-Accelerating Degradation of Polycyclic Aromatic Hydrocarbons(PAHs) in Soils[J]". *Journal of Agro-environmental Science*, Vol. 24, No. 3, 2005, pp. 498–502.
5. Cao Shengxian. 2009. "The analysis of mechanisms and efficiencies of the removal and remediation of phenanthrene and pyrene in soil by several plants[D]". Chong Qing in China: Southwest University.
6. Cui, Y. B., Sun, H. J., Ran, C. Q., *et al.* "Comparison of PAHs distribution in stabilized sludge by sludge drying bed and reed bed.[J]". *Environmental Science*, Vol. 34, No. 3, 2013, pp. 1161–1165.
7. Chang Rui-xue, Zhao Ou-ya, LI Yu-Ling, Yang Zhi-xin, Feng Sheng-dong. "Studies Herbage Plants on Effectiveness of PAHs Remediation in Different Sludge and Iron Mine Tailings Combination[J]". *Journal of Soil and Water Conversation*, Vol. 28, No. 5, 2014, pp. 1–7.
8. Wang Wei, Feng Sheng-dong, Yang Zhi-xin *et al.* "Effect of different sludge-soil combination on PAHs remediation under smooth bromegrass-sludge system[J]". *Acta Prataculturae Sinica*, Vol. 24, No. 2, 2015, pp. 148–160.
9. Sardar, K., Lin, A., Shuzhen, Z., *et al.* "Accumulation of polycyclic aromatic hydrocarbons and heavy metals in lettuce grown in the soils contaminated with long-term wastewater irrigation.[J]". *Journal of Hazardous Materials*, Vol. 152, No. 2, 2008, pp. 506–515. <http://dx.doi.org/10.1016/j.jhazmat.2007.07.014>
10. Kandeler, E., Gerber, H., "Short-term Assay of Substrate Urease Activity Using Colorimetric Determination of Ammonium[J]". *Biology & Fertility of Soils*, Vol. 6, No. 1, 1988, pp. 68–72. <http://dx.doi.org/10.1007/BF00257924>
11. Cohen, G., Dembiec, D., Marcus J., "Measurement of catalase activity in tissue extracts.[J]". *Analytical Biochemistry*, Vol. 34, No. 1, 1970, pp. 30–38. [http://dx.doi.org/10.1016/0003-2697\(70\)90083-7](http://dx.doi.org/10.1016/0003-2697(70)90083-7)
12. K.B. Kunwar, P.A. Khan. Peroxidase and polyphenol oxidase in excised ragi (*Eleusine corocana* cv PR202) leaves during senescence. *Indian J. Exp. Biol.*, Vol. 25, 1982, pp. 412–416.
13. Trevors, J. T., "Dehydrogenase activity in soil: A comparison between the INT and TTC assay[J]". *Soil Biology & Biochemistry*. Vol. 16, No. 6, 1984, pp. 673–674. [http://dx.doi.org/10.1016/0038-0717\(84\)90090-7](http://dx.doi.org/10.1016/0038-0717(84)90090-7)
14. Huesemann, M. H., Hausmann, T. S., Fortman, T. J., *et al.* "In situ phytoremediation of PAH- and PCB-contaminated marine sediments with eelgrass (*Zostera marina*). Ecol Eng[J]". *Ecological Engineering*, Vol. 35, No. 10, 2009, pp. 1395–1404. <http://dx.doi.org/10.1016/j.ecoeng.2009.05.011>
15. Yubo Cui, Wanjun Zhang, Hongjie Sun *et al.* "Polycyclic Aromatic Hydrocarbon Accumulation in Phragmites australis Grown on Constructed Wetland for Sludge Stabilization[J]". *Journal of Residuals Science & Technology*, Vol. 12, 2015, pp. 215–219. <http://dx.doi.org/10.12783/issn.1544-8053/12/4/4>
16. Y. Gao, L. Zhu, "Plant uptake, accumulation and translocation of phenanthrene and pyrene in soils[J]". *Chemosphere*, Vol. 55, No. 9, 2004, pp. 1169–1178. <http://dx.doi.org/10.1016/j.chemosphere.2004.01.037>
17. P. Binet, J.M. Portal, C. Leyval, "Application of GC-MS to the study of anthracene disappearance in the rhizosphere of ryegrass[J]". *Organic Geochemistry*, Vol. 32, No. 2, 2001, pp. 217–222. [http://dx.doi.org/10.1016/S0146-6380\(00\)00168-6](http://dx.doi.org/10.1016/S0146-6380(00)00168-6)
18. E.J. Joner, S.C. Corgié, N. Amellal, C. Leyval, "Nutritional constraints to degradation of polycyclic aromatic hydrocarbons in a simulated rhizosphere[J]". *Soil Biology & Biochemistry*, Vol. 34, No. 6, 2002, pp. 859–864. [http://dx.doi.org/10.1016/S0038-0717\(02\)00018-4](http://dx.doi.org/10.1016/S0038-0717(02)00018-4)
19. Margesin, A. Zimmerbauer, F. Schinner, "Monitoring of bioremediation by soil biological activities[J]". *Chemosphere*, Vol. 40, No. 4, 2000, pp. 339–346. [http://dx.doi.org/10.1016/S0045-6535\(99\)00218-0](http://dx.doi.org/10.1016/S0045-6535(99)00218-0)
20. S.H. Lee, W.S. Lee, C.H. Lee, J.G. Kim, "Degradation of phenanthrene and pyrene in rhizosphere of grasses and legumes [J]". *Journal of Hazardous Materials*, Vol. 153, No. 1-2, 2008, pp. 892–898. <http://dx.doi.org/10.1016/j.jhazmat.2007.09.041>
21. G. Gramms, K.D. Voigt, B. Kirshe, "Oxidoreductase enzymes liberated by plant roots and their effects on soil humic material[J]". *Chemosphere*, Vol. 38, No. 7, 1999, pp. 1481–1494. [http://dx.doi.org/10.1016/S0045-6535\(98\)00369-5](http://dx.doi.org/10.1016/S0045-6535(98)00369-5)
22. Ruuska, S. A., Andrews, T. J., Badger, M. R., *et al.* "The Role of Chloroplast Electron Transport and Metabolites in Modulating Rubisco Activity in Tobacco. Insights from Transgenic Plants with Reduced Amounts of Cytochrome b/f Complex or Glyceraldehyde 3-Phosphate Dehydrogenase[J]". *Plant Physiology*, Vol. 122, No. 2, 2000, pp. 491–504. <http://dx.doi.org/10.1104/pp.122.2.491>

Study on Anaerobic Digestion of Kitchen Waste for Biogas Production

FENG LEI¹, GAO YUAN¹, KOU WEI^{2,*}, LI RUNDONG¹, YU MEILING², SHAO LIJIE² and WANG XIAOMING²

¹Liaoning Province Clean Energy Key Laboratory, Shenyang Aerospace University, Shenyang Daoyi Street No.37, Shenyang, China 110136

²Liaoning Institute of Energy Resources, 65# Yingquan St, Yingkou, Liaoning, China 115003

ABSTRACT: The effect of initial total solid (TS) concentrations on the volume percent of methane and TAN contents from the anaerobic digestion of kitchen waste was studied in this paper by setting the initial TS as 4 wt%, 5 wt%, 6 wt%, 7 wt%. The inflection points of the cumulative biogas productions curve of different initial TS concentration took place at day 8, 19 day, 17 day, 15 day, 9, 20 day, respectively. The concentrations of methane generally rose firstly and then declined except that two different peaks (71.54% and 64.31%) of the methane volume percent were observed in day 15 and day 25 respectively under the condition of initial TS mass fraction of 4 wt%. The maximum methane volume percent under the condition of initial TS mass fraction of 5 wt%, 6 wt%, and 7 wt% was 76.7%, 73.93%, and 74.32% respectively in day 20. The TAN contents increased with the reaction time under the influence of varied initial TS contents. When the initial TS content was 4 wt%, 5 wt%, 6 wt%, and 7 wt%, the accumulated total ammonia nitrogen (TAN) content in day 30 was 1830, 2659, 2647, and 3040 mg/L respectively.

INTRODUCTION

THE municipal solid waste (MSW) has surpassed 490 million tons with economic development and urbanization in recent years in China [1]. Kitchen waste accounts for 40–60% of MSW [2]. In particular, in some large cities of China, the output of kitchen waste exceeds 1500 tons per day [3]. Other than raising swines [4,5], the kitchen waste was treated, together with other household wastes, with landfill, composting and other pathways, which not only occupies vast valuable land but also pollutes the surroundings [6–8]. Based on the nature of kitchen waste, anaerobic digestion technology has advantages on kitchen waste treatment, such as harmless disposal and co-production of clean biogas [9,10].

The anaerobic process has been investigated under mesophilic conditions [11,12]. The first step of the anaerobic degradation, the hydrolysis, is considered to be the rate-limiting step [13]. Xing Wang et al analyzed the factors influencing methane production from anaerobic digestion of kitchen waste with the response surface method. Substrate concentration had the biggest influence on anaerobic digestion among the three

parameters (substrate concentration, ratio between inoculum and substrate, and concentration of calcium ions) [14]. TAN, as an inhibiting factor, was mainly generated from the decomposition of protein and other nitrogenous organic matter. Due to the lack of autotrophic inorganic-nitrogen-consuming microorganisms in anaerobic digestion systems, the generated TAN can not be further converted [15,16], causing the accumulation of TAN. Deficiencies in ammonia nitrogen have been shown to cause low methane yields due to low microbial activity and buffering capacity [17], while excessive ammonia nitrogen may inhibit biogas production [18]. If put different quantitative material in the same volume reactor, the higher material quality, the higher the concentration of TAN. Biogas production is related to the VS or TS, some scholars believe that biogas production is the highest when TS = 4 wt%, but some studies have shown that biogas production is the highest when TS = 13 wt% [19–21]. Ensiling of crops, excess sludge and cattle dung were used in the above paper. The material in this research was kitchen waste. During the actual operations, favorable factors for the anaerobic digestion system should be paid full attentions to. For example, pH is between 6.8–7.2, The best temperature is 37°C, every day stirring was performed, and the carbon and nitrogen ratio (C/N) is proper [22]. For instance, a few reinforcements or techniques could

*Author to whom correspondence should be addressed.
E-mail: fl_iceee@163.com; Tel: 024-89723608; Fax: 024-89724558

be adopted to ensure the activity of methane-producing bacteria, in order to achieve a higher gas production and a smooth anaerobic digestion process, such as, inoculum domestication, there are many types of anaerobic bacteria cultivation methods, the most important is to create anaerobic environment, by adding reducing agent to the medium, or removal the free oxygen in environment by adopting the method of physical and chemical, in order to reduce the redox potential. Followed by the reactor insulation, make the system temperature stable, with little fluctuation. Different biogas production occurred under the condition of different initial material and experiment condition [23–25]. So this article selected the TS concentration was 4–7 wt% as the main line, to explore the effect to the biogas production of the low TS for kitchen waste. The effect of initial TS concentrations on the volume percent of methane and TAN contents from the anaerobic digestion of kitchen waste which was fundamental scientific finding was studied in this paper.

MATERIALS AND METHOD

Materials and Their Characteristics

The kitchen waste was derived from the Canteen of Shenyang Aerospace University in China, and cut into particulates with a diameter of 10 mm. The mid-temperature (37°C) domesticated inoculated sludge was obtained from a waste water treatment plant in north Shenyang. Mass fractions of TS and volatile solid (VS) in the kitchen waste were 23.31 wt% and 92.84 wt%, respectively. Mass fractions of TS and VS in the inoculated sludge were 11.95 wt% and 78.05 wt%, respectively. The C/N ratio of the raw material was 21.38.

Table 1. The Kitchen Waste and Inoculated Sludge Parameter.

Raw Material	TS (wt%)	VS/TS (wt%)
Kitchen waste	23.31	92.84
Inoculated sludge	11.95	78.05

And VS was calculated on the base of TS. The kitchen waste and inoculated sludge parameter were shown in Table 1.

Experimental Apparatus

The experimental apparatus contained a self-designed anaerobic fermentation reactor, which was shown as Figure 1. Two wide-mouthed 1 L bottles acted as a gas collecting bottle and a water collecting bottle. Total volume of the reactor was 1.1 L and work volume was 1 L. The bottleneck was sealed with a rubber stopper and sealant. The apparatus was placed in airtight and anaerobic environment. The fermentation reactor was heated with a thermostat water bath.

Experimental Method and Equipment

In this study, the initial mass fraction of TS was separately set as 4 wt%, 5 wt%, 6 wt%, and 7 wt%. Experiments were repeated for three times. The Initial kitchen waste weight and the inoculated sludge volume were shown in Table 2, and add water to the reactor to the level (1 L). The fermentation reactor was filled with 1 L of sample and was cultured at 37°C for 30 days in the water bath. The fermentation liquor was withdrawn with a syringe, of which the pH was measured with a digital pH meter per day. The fermentation liquor was

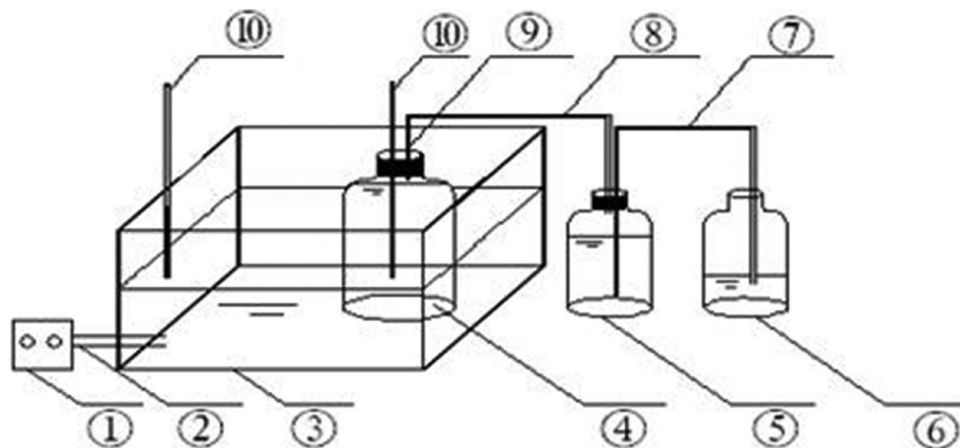


Figure 1. Experimental apparatus of anaerobic digestion. 1–controller, 2–heated rod, 3–water bath, 4–reactor, 5–collecting bottle, 6–water collecting bottle, 7–exhalent siphon, 8–airway, 9–test tube, 10–thermometer.

Table 2. The Initial Kitchen Waste Weight and the Inoculated Sludge Volume.

Initial TS Weight Content (%)	Initial Kitchen Waste Weight (g)	Inoculated Sludge Volume (mL)
4	17.8	300
5	60.7	300
6	103.6	300
7	146.5	300

then returned into the reactor. The ideal value pH of fermented liquid is 7. During the anaerobic process, the pH of fermented liquid was below 7. When the pH was less than 6.8, pH was increased to 7.0 with the addition of NaHCO_3 solution at about 5 P.M. whose pH was 9. Volume of NaHCO_3 solution injected was calculated and added according to the rule above. Stirring were performed twice a day. One was after the pH adjust, the other was at about 9 A.M.. The production of biogas was determined once per day by its displacement of water. Biogas production of the sequencing batch reactor was further revised with the production of control group where only inoculum was added without any substrates. Simultaneously, the pH of fermentation liquor, total ammonia nitrogen (TAN) concentrations and other parameters were monitored at intervals during the sequencing-batch anaerobic digestion process. Measuring total ammonia nitrogen value once two days before the 12 days, then test the value every three days, testing the volume percent of methane every two days in the first ten days, and then testing that every five days. TS and VS were determined by using the drying method at 103–105°C and 600°C, respectively. The TAN concentration was measured by spectrophotometry with a HI96700 TAN determinator, whose method was ASTM D1426-93, Nessler. Composition of the biogas was determined by a gas detector (GT901 CH_4 -IR). To make the data accurate, We connect the biogas bag port to the receiving detecting instrument sensors tightly. Total organic carbon was checked by potassium dichromate volumetric-external heating method, total nitrogen was measured by kjeldahl determination. The ratio of total organic carbon and total nitrogen was the C/N value.

RESULTS AND DISCUSSION

Analysis of Biogas Production and Composition from Anaerobic Digestion of Kitchen Waste

Daily and cumulative biogas productions per gram of VS were depicted in Figure 2. Under different TS

concentrations, the total biogas productions were significantly different.

In detail, with an initial TS concentration of 4 wt%, the biogas production in the first day was up to $106.75 \text{ mL}\cdot\text{g}^{-1} \text{ VS}$. In day 29, the biogas production was zero and the reaction was complete terminated. The daily biogas production was dramatically reduced day by day in the first four days. The daily biogas production was relatively stable from day 5 to day 19, and biogas production peaks were observed at day 8 ($17.40 \text{ mL}\cdot\text{g}^{-1} \text{ VS}$), day 14 ($15.06 \text{ mL}\cdot\text{g}^{-1} \text{ VS}$), and day 18 ($15.58 \text{ mL}\cdot\text{g}^{-1} \text{ VS}$). In the remaining time, the daily biogas production was also stable in the range of 4.68 to $0.26 \text{ mL}\cdot\text{g}^{-1} \text{ VS}$.

The percentage cumulative biogas productions in the first several days accounted for the total amount was shown in the Table 3.

For initial TS concentration of 4 wt%, from day 1 to day 7, the daily gas production was high and exhibited a significant convex curve. However, from day 8 to day 18, the cumulative biogas productions curve accorded with the characteristics of a concave function and the gas production was low. Finally, from day 19 to day 30, the slope of the curve was almost zero, indicating that the gas production was zero.

When the initial TS content was 5 wt%, the daily gas production in day 3 reached a maximum of $71.74 \text{ mL}\cdot\text{g}^{-1} \text{ VS}$ and a minimum of $0.21 \text{ mL}\cdot\text{g}^{-1} \text{ VS}$ in day 30. The daily gas production was significantly decreased from day 3 to day 9. Three maximums of 20.93, 14.17, and $10.54 \text{ mL}\cdot\text{g}^{-1} \text{ VS}$ were reached in day 10, 12, and 18. In the remaining time, the daily gas production was stable and low (8.07 – $0.21 \text{ mL}\cdot\text{g}^{-1} \text{ VS}$).

For initial TS concentration of 5 wt%, In terms of the convexity and concavity, the curve from day 1 to day 6 was evidently convex with high daily gas productions, whereas the curve from day 7 to day 20 was concave with low daily gas productions. The cumulative biogas productions was a constant from day 21 to day 30 and thus the daily gas production was almost zero.

Table 3. The Percentage Cumulative Biogas Productions in the First Several Days Accounted for the Total Amount.

Initial TS Weight Content (%)	The Number of the First Several Days	The Percentage (%)
4	4	60.60
5	6	61.50
6	7	49.50
7	5	27.5

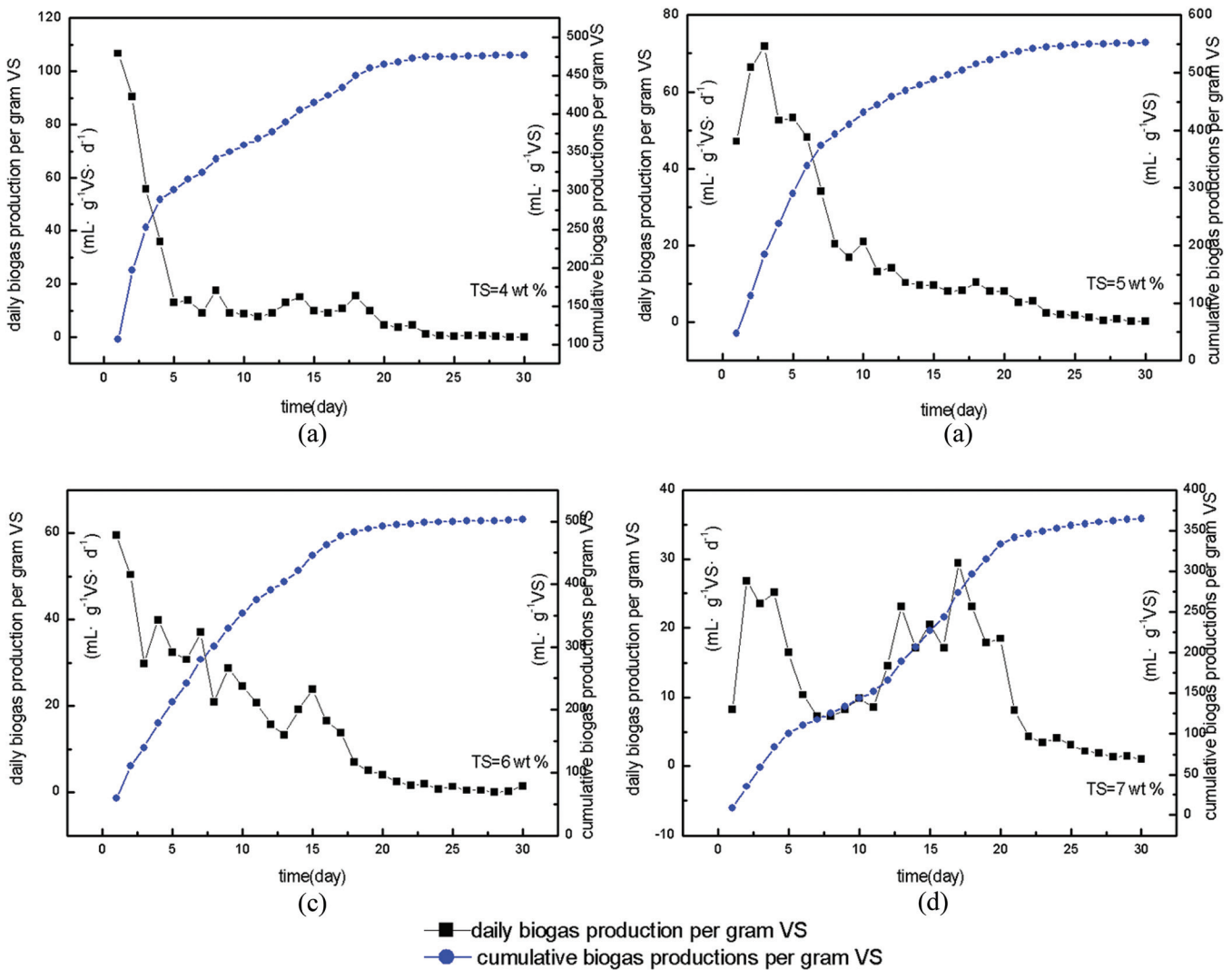


Figure 2. Daily biogas production and cumulative biogas productions under the condition of different initial TS content.

Under the condition of initial TS mass fraction of 6 wt%, the daily gas production reached a maximum of $59.55 \text{ mL}\cdot\text{g}^{-1} \text{ VS}$ in the first day. The minimum of $0.045 \text{ mL}\cdot\text{g}^{-1} \text{ VS}$ was observed in day 28. A small increase occurred in the last two days. In comparison, under this condition of initial TS mass fraction, the gas production fluctuated evidently. Four peaks of 39.83, 37.02, 28.77, and 23.77 $\text{mL}\cdot\text{g}^{-1} \text{ VS}$ were observed in day 4, 7, 9, and 15 respectively. In the remaining time, the daily gas production was relatively stable but low ($6.91\text{--}0.04 \text{ mL}\cdot\text{g}^{-1} \text{ VS}$).

For initial TS concentration of 6 wt%, from day 1 to day 7, the curve was obviously convex and the daily gas production was high. From day 8 to day 17, the curve exhibited a concave function and daily gas production was low. Finally, the daily gas production was almost zero from day 18 to day 30.

When the initial TS content was 7 wt%, the maxi-

imum daily gas production was $29.40 \text{ mL}\cdot\text{g}^{-1} \text{ VS}$ in day 17 and the minimum daily gas production was $1.041 \text{ mL}\cdot\text{g}^{-1} \text{ VS}$ in day 30. The gas production fluctuated more violently under this condition of TS content. Six maximums of 26.85, 25.24, 9.94, 23.19, 29.40, and 18.52 $\text{mL}\cdot\text{g}^{-1} \text{ VS}$ were observed in day 2, 4, 10, 13, 17, and 20 respectively. The gas production was stable in the remaining time with a daily gas production of $6.91\text{--}0.04 \text{ mL}\cdot\text{g}^{-1} \text{ VS}$.

For initial TS concentration of 7 wt%, the curve of cumulative biogas production from day 1 to day 5 was convex and daily gas productions were high. In contrast, the curve day 6 to day 15 was concave and daily gas productions were low. However, from day 16 to day 20 the daily gas production was significantly increased. The daily gas production was almost zero from day 21 to day 30.

Under the conditions of 4 wt%, 5 wt%, 6 wt%, and 7

Table 3. Contributions of Plant Accumulation to the Sludge HMW-PAHs Removal Amounts (%).

Type	Pyr	BaA	Chry	BbF	BkF	BaP	DbA	BghiP	InP	Sum
Alfalfa	0.493	0.039	0.030	0.010	0.005	0.025	0.010	0.007	0.002	0.075
Awnless Brome	0.732	0.059	0.104	0.072	0.033	0.175	1.453	0.041	0.009	0.210

wt% of TS, cumulative biogas productions was 476.36, 551.10, 502.76, 364.26. Initial TS content 5 wt % had the highest value comparing with the initial TS content was 4 wt%, 6 wt% and 7 wt%, it was 13.56 %, 8.77%, 33.90% higher, respectively. In the literature different biogas production occurred under the condition of different initial material and experiment condition [22–24]. The inflection points of the cumulative biogas productions curve were observed at day 8–19, day 17, day 15, and day 9–20. Hence, these points are also critical for the anaerobic digestion of kitchen waste for biogas production.

Composition of Biogas from Kitchen Waste Anaerobic Digestion

The plot of volume percent of methane versus time is depicted in Figure 3. Most of the volume percent of methane rose in the first place and then declined except that when the initial TS mass fraction was 4 wt%, two different peaks (71.54% and 64.31% in day 15 and 25) were observed respectively. Under the condition of initial TS mass fraction of 5 wt %, the volume percent of methane reached a maximum of 76.7% in day 20, which is also the maximum in the entire process. When the initial TS mass fraction was 6 wt% and 7 wt%, the volume percent of methane reached a maxi-

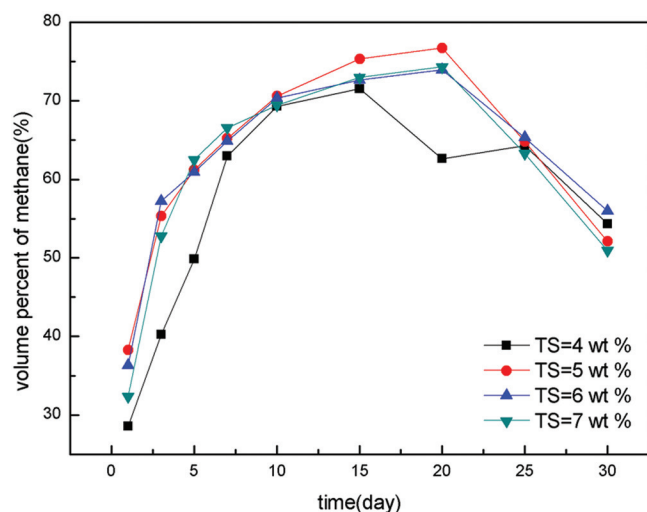


Figure 3. Volume percent of methane under the influence of different initial contents of solids.

um of 73.93% and 74.32% respectively in day 20. The volume percent of methane reached a maximum in day 15 to day 20 and the fraction gradually reduced afterwards.

Dependence of TAN Concentration on TS Content

The range of C:N which was proper for microorganism growth was 20–30, and the optimal value was 25 [26]. Herein, the C:N ratio of the raw material was 21.38, and hence it was expected that little ammonia (inhibitor) was produced. Evolution of TAN contents under the influence of different initial contents of solids is illustrated in Figure 4. The maximum TAN content is only 3040 mg·L among all these experiments. Consequently, the gas production was hardly depressed. Sung and Liu [27] and Procházka *et al.* [28] they have demonstrated that higher TAN concentrations (> 4000 mg·L) could cause obvious inhibition of methanogenesis. Whereas, Sawayama *et al.* [29] and Lauterbock *et al.* [30] observed the inhibition when the TAN concentration exceeds 6000 mg NH₄-N·L. So ammonia nitrogen inhibition did not exist in this experiment.

In Figure 4, the TAN contents increased with the reaction time regardless of the initial TS concentration. When the initial TS mass fraction was 4 wt%, 5 wt%,

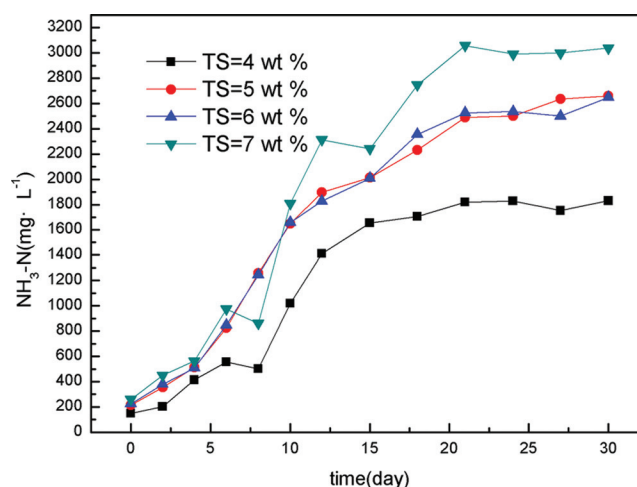


Figure 4. Evolution of TAN contents under the influence of different initial contents of solids.

6 wt%, and 7 wt%, the content of accumulated TAN in day 30 was 1830, 2659, 2647, and 3040 mg·L respectively. Specially, when the initial TS mass fraction was 7 wt%, the TAN content decreased dramatically in day 8 and then increased. Such a phenomenon was also observed from day 15 to day 20.

CONCLUSION

1. Initial TS content 5 wt% had the highest value comparing with the initial TS content was 4 wt%, 6 wt% and 7 wt%, it was 13.56%, 8.77%, 33.90% higher, respectively. Under the conditions of 4 wt%, 5 wt%, 6 wt%, and 7 wt% of initial TS content, the inflection points of the cumulative biogas productions curve took place at day 8, 19 day, 17 day, 15 day, 9, 20 day, respectively.
2. Each of the methane volume percent decreased after their corresponding peaks under the condition of initial TS mass fraction of 5 wt%, 6 wt%, and 7 wt%, two peaks occurred during the experiment process of initial TS mass fraction of 4 wt%.
3. The TAN contents increased with the reaction time under the influence of varied initial TS contents. When the initial TS content was 4 wt%, 5 wt%, 6 wt%, and 7 wt%.

ACKNOWLEDGEMENTS

This work was supported by the Cultivation Plan for Youth Agricultural Science and Technology Innovative Talents of Liaoning Province support. (No. 2014016)

REFERENCE

1. Fu, J., Han, X. K. and Li, G., "Exploration on Municipal Solid Waste Classification and Organic Wastes Disposal Methods", *China Resources Comprehensive Utilization*, Vol. 32, No. 2, 2015, pp. 30–33.
2. Ni, M., Leung, D. Y. C. and Leung, M. K. H., "An overview of hydrogen production from biomass", *Fuel Processing Technology*, Vol. 87, No. 5, 2006, pp. 461–472. <http://dx.doi.org/10.1016/j.fuproc.2005.11.003>
3. Zhang, L. and Jahng, D., "Long-term anaerobic digestion of food waste stabilized by trace elements", *Waste Management*, Vol. 32, No. 8, 2012, pp. 1509–1515. <http://dx.doi.org/10.1016/j.wasman.2012.03.015>
4. Ribbens, S., Dewulf, J., Koenen, F., Mintiens, K., Sadeleer, L., Kruif, A. and Maes, D., "A survey on biosecurity and management practices in Belgian pig herds", *Preventive Veterinary Medicine*, Vol. 83, No. 3–4, 2008, pp. 228–241. <http://dx.doi.org/10.1016/j.prevetmed.2007.07.009>
5. Yang, S. Y., Ji, K. S., Baik, Y. H., Kwak, W. S. and McCaskey, T. A., "Lactic acid fermentation of food waste for swine feed", *Bioresource Technology*, Vol. 97, No. 15, 2006, pp. 1858–1864.
6. Manfredi, S. and Pant, R., "Improving the environmental performance of bio-waste management with life cycle thinking (LCT) and life cycle assessment (LCA)", *International Journal of Life Cycle Assessment*, Vol. 18, No. 1, 2012, pp. 285–291.
7. Hanc, A., Szakva, J. and Svehla, P., "Effect of composting on the mobility of arsenic, chromium and nickel contained in kitchen and garden waste", *Bioresource Technology*, Vol. 126, No. 6, 2011, pp. 444–452.
8. Emilia, D. B., Jan, D. B., Jadwiga, J. and Ryszard, S., "Monitoring of municipal waste generated in the city of Warsaw", *Waste Management Research*, Vol. 30, No. 8, 2012, pp. 772–780.
9. Tauseef, S. M., Abbasi, T. and Abbasi, S. A., "Energy recovery from wastewaters with high-rate anaerobic digesters", *Renewable and Sustainable Energy Reviews*, Vol. 19, No. 1, 2013, pp. 704–741. <http://dx.doi.org/10.1016/j.rser.2012.11.056>
10. Ismail, M. N., Tinia, I. M. and Rozita, O., "Production of biogas from solid organic wastes through anaerobic digestion: a review", *Applied Microbiology and Biotechnology*, Vol. 95, No. 2, 2012, pp. 321–329. <http://dx.doi.org/10.1007/s00253-012-4152-7>
11. Feng, L., Kou, H. L., Zhang, X. D. and Li, R. D., "The research of corrected first order kinetics on hydrolysis and biogas generation in batch anaerobic digestion", *Journal of Residuals Science & Technology*, Vol. 12, No. 4, 2015, pp. 249–255. <http://dx.doi.org/10.12783/issn.1544-8053/12/4/8>
12. Kim, M., Ahn, Y. H. and Speece, R.E., "Comparative process stability and efficiency of anaerobic digestion; mesophilic vs thermophilic", *Water Research*, Vol. 36, No. 17, 2002, pp. 4369–4385. [http://dx.doi.org/10.1016/S0043-1354\(02\)00147-1](http://dx.doi.org/10.1016/S0043-1354(02)00147-1)
13. Recktenwald, M., Dey, E. S. and Norrlof, O., "Improvement of Industrial-scale Anaerobic Digestion by Enzymes Combined with Chemical Treatment", *Journal of Residuals Science & Technology*, Vol. 12, No. 4, 2015, pp. 205–214. <http://dx.doi.org/10.12783/issn.1544-8053/12/4/3>
14. Wang, X. H. P., Liu, Zhang, L. Y. and Peng, X.F. "Optimization of Methane Fermentation of Kitchen Waste Using Response Surface Methodology", *China Biogas*, Vol. 32, No. 5, 2014, pp. 22–28.
15. Ulundag, D. S., Demirer, G. N., Frear, C. and Chen, S., "Anaerobic digestion of dairy manure with enhanced ammonia removal", *Journal of Environment Management*, Vol. 86, No. 1, 2008, pp. 193–200. <http://dx.doi.org/10.1016/j.jenvman.2006.12.002>
16. Jiang, J.G., Wang, Y., Sui, J. C. and Wu, S. Y., "Variations of the ammonia concentration of high solid anaerobic digestion technology for organic waste", *China Environmental Science*, Vol. 27, No. 6, 2007, pp. 721–726.
17. Prochazka, J., Dolejs, P., Maca, J. and Dohanyos, M., "Stability and inhibition of anaerobic processes caused by insufficiency or excess of ammonia nitrogen", *Appl Microbiol Biotechnol*, Vol. 93, No. 1, 2012, pp. 439–447. <http://dx.doi.org/10.1007/s00253-011-3625-4>
18. Chen, Y., Cheng, J.J. and Creamer, K.S., "Inhibition of anaerobic digestion process: a review", *Bioresour Technol*, Vol. 99, No. 10, 2008, pp. 4044–4064. <http://dx.doi.org/10.1016/j.biortech.2007.01.057>
19. Kreuger, E., Nges, I. A. and Björnsson, L., "Ensiling of crops for biogas production: effects on methane yield and total solids determination [J]", *Biotechnology for Biofuels*, Vol. 4, No. 24, 2011, pp. 44. <http://dx.doi.org/10.1186/1754-6834-4-44>
20. Liu, X. L., Wang, M. M., Hu, X. J. and Song, Y. H., "Effect of Total Solids Content on the Biogas Production and Phosphorus Release from Excess Sludge[J]", *Advanced Materials Research*, Vol. 1010-1012, No. 1010-1012, 2014, pp. 1006–1009. <http://dx.doi.org/10.4028/www.scientific.net/AMR.1010-1012.1006>
21. Mathad, R., Palled, V., Desai, S. R., Lokesh, and Shirwal, S., "Performance of cattle dung at different total solids in prototype digesters for biogas production[J]", *International Journal of Agricultural Engineering*, Vol. 6, No. 2, 2013, pp. 431–433.
22. Yen, H. W. and Chiu, C. H., "The influences of aerobic-dark and anaerobic-light cultivation on CoQ (10) production by Rhodospirillum rubrum in the submerged fermenter", *Enzyme and Microbial Technology*, Vol. 41, No. 5, 2007, pp. 600–604. <http://dx.doi.org/10.1016/j.enzmictec.2007.05.005>
23. Chen, X. G., Rowena, T. R. and Zhang, R. H., "Anaerobic digestion of food wastes for biogas production", *Int J Agric & Biol Eng*, Vol. 3, No. 4, 2010, pp. 61–72.
24. Eastman, J. A. and Ferguson, J. F., "Solubilization of particulate organics carbon during the acid phase of anaerobic digestion". *Journal Water Pollution Control Federation*, Vol. 53, No. 3, 1981, pp. 352–366
25. Linke, B., "Kinetic study of thermophilic anaerobic digestion of

- solid wastes from potato processing". *Biomass and Bioenergy*, Vol. 30, No. 10, 2006, pp. 892–896. <http://dx.doi.org/10.1016/j.biombioe.2006.02.001>
26. Yen, H. W. and Chiu, C. H., "The influences of aerobic-dark and anaerobic-light cultivation on CoQ (10) production by *Rhodobacter sphaeroides* in the submerged fermenter". *Enzyme and Microbial Technology*, Vol. 41, No. 5, 2007, pp. 600–604. <http://dx.doi.org/10.1016/j.enzmictec.2007.05.005>
27. Sung, S. and Liu, T., "Ammonia inhibition on thermophilic anaerobic digestion". *Chemosphere* Vol. 53, No. 1, 2003. pp. 43–52. [http://dx.doi.org/10.1016/S0045-6535\(03\)00434-X](http://dx.doi.org/10.1016/S0045-6535(03)00434-X)
28. Procházka, J., Dolejš, P., MácA, J. and Dohányos, M., "Stability and inhibition of anaerobic processes caused by insufficiency or excess of ammonia nitrogen". *Applied Microbiology and Biotechnology*, Vol. 93, No. 1, 2012, pp. 439–447. <http://dx.doi.org/10.1007/s00253-011-3625-4>
29. Sawayama, S., Tada, C., Tsukahara, K. and Yagishita, T., "Effect of ammonium addition on methanogenic community in a fluidized bed anaerobic digestion", *Journal of Bioscience and Bioengineering*, Vol. 97, No. 1, 2004, pp. 65–70. [http://dx.doi.org/10.1016/S1389-1723\(04\)70167-X](http://dx.doi.org/10.1016/S1389-1723(04)70167-X)
30. Lauterbock, B., Ortner, M., Haider, R. and Fuchs, W., "Counteracting ammonia inhibition in anaerobic digestion by removal with a hollow fiber membrane contactor", *Water Research*, Vol. 46, No. 15, 2012, pp. 4861–4869. <http://dx.doi.org/10.1016/j.watres.2012.05.022>

GUIDE TO AUTHORS

1. Manuscripts shall be sent electronically to the Editor-in-Chief, Dr. P. Brent Duncan at pduncan@unt.edu using Microsoft Word in an IBM/PC format. If electronic submission is not possible, three paper copies of double-spaced manuscripts may be sent to Dr. P. Brent Duncan, (Editor of the *Journal of Residuals Science & Technology*, University of North Texas, Biology Building, Rm 210, 1510 Chestnut St., Denton, TX 76203-5017) (Tel: 940-565-4350). Manuscripts should normally be limited to the space equivalent of 6,000 words. The editor may waive this requirement in special occasions. As a guideline, each page of a double-spaced manuscript contains about 300 words. Include on the title page the names, affiliations, and addresses of all the authors, and identify one author as the corresponding author. Because communication between the editor and the authors will be electronic, the email address of the corresponding author is required. Papers under review, accepted for publication, or published elsewhere in journals are normally not accepted for publication in the *Journal of Residuals Science & Technology*. Papers published as proceedings of conferences are welcomed.
2. Article titles should be brief, followed by the author's name(s), affiliation, address, country, and postal code (zip) of author(s). Indicate to whom correspondence and proofs should be sent, including telephone and fax numbers and e-mail address.
3. Include a 100-word or less abstract and at least six keywords.
4. If electronic art files are not supplied, submit three copies of camera-ready drawings and glossy photographs. Drawings should be uniformly sized, if possible, planned for 50% reduction. Art that is sent electronically should be saved in either a .tif or .JPEG files for superior reproduction. All illustrations of any kind must be numbered and mentioned in the text. Captions for illustrations should all be typed on a separate sheet(s) and should be understandable without reference to the text.
5. DEStech uses a numbered reference system consisting of two elements: a numbered list of all references and (in the text itself) numbers in brackets that correspond to the list. At the end of your article, please supply a numbered list of all references (books, journals, web sites etc.). References on the list should be in the form given below. In the text write the number in brackets corresponding to the reference on the list. Place the number in brackets inside the final period of the sentence cited by the reference. Here is an example [2].
Journal: 1. Halpin, J. C., "article title", *J. Cellular Plastics*, Vol. 3, No. 2, 1997, pp. 432–435.
Book: 2. Kececioglu, D. B. and F.-B. Sun. 2002. *Burn-In Testing: Its Quantification and Optimization*, Lancaster, PA: DEStech Publications, Inc.
6. Tables. Number consecutively and insert closest to where first mentioned in text or type on a numbered, separate page. Please use Arabic numerals and supply a heading. Column headings should be explanatory and carry units. (See example at right.)
7. Units & Abbreviations. Metric units are preferred. English units or other equivalents should appear in parentheses if necessary.
8. Symbols. A list of symbols used and their meanings should be included.
9. Page proofs. Authors will receive page proofs by E-mail. Proof pages will be in a .PDF file, which can be read by Acrobat Reader. Corrections on proof pages should be limited to the correction of errors. Authors should print out pages that require corrections and mark the corrections on the printed pages. Pages with corrections should be returned by FAX (717-509-6100) or mail to the publisher (DEStech Publications, Inc., 439 North Duke Street, Lancaster, PA 17602, USA). If authors cannot handle proofs in a .PDF file format, please notify the Editor, Dr. P. Brent Duncan at pduncan@unt.edu.
10. Index terms. With proof pages authors will receive a form for listing key words that will appear in the index. Please fill out this form with index terms and return it.
11. Copyright Information. All original journal articles are copyrighted in the name of DEStech Publications, Inc. All original articles accepted for publication must be accompanied by a signed copyright transfer agreement available from the journal editor. Previously copyrighted material used in an article can be published with the *written* permission of the copyright holder (see #14 below).
12. Headings. Your article should be structured with unnumbered headings. Normally two headings are used as follows:
Main Subhead: DESIGN OF A MICROWAVE INSTALLATION
Secondary Subhead: Principle of the Design Method
If further subordination is required, please limit to no more than one (*Third Subhead*).
13. Equations. Number equations with Arabic numbers enclosed in parentheses at the right-hand margin. Type superscripts and subscripts clearly above or below the baseline, or mark them with a caret. Be sure that all symbols, letters, and numbers are distinguishable (e.g., "oh" or zero, one or lowercase "el," "vee" or Greek nu).
14. Permissions. The author of a paper is responsible for obtaining releases for the use of copyrighted figures, tables, or excerpts longer than 200 words used in his/her paper. Copyright releases are permissions to reprint previously copyrighted material. Releases must be obtained from the copyright holder, which is usually a publisher. Forms for copyright release will be sent by the editor to authors on request.

Table 5. Comparison of state-of-the-art matrix resins with VPSP/BMI copolymers.

Resin System	Core Temp. (DSC peak)	T _E	Char Yield, %
Epoxy (MY720)	235	250	30
Bismaleimide (H795)	282	>400	48
VPSP/Bismaleimide copolymer			
C379: H795 = 1.9	245	>400	50
C379: H795 = 1.4	285	>400	53

General: The *Journal of Residuals Science & Technology* and DEStech Publications, Inc. are not responsible for the views expressed by individual contributors in articles published in the journal.